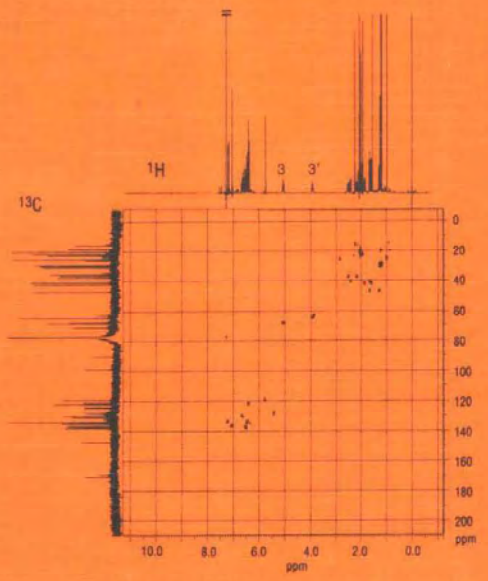
Carotenoids

Volume 1B: Spectroscopy

Edited by G. Britton
S. Liaaen-Jensen
H. Pfander



Birkhäuser

MCCORMICK 1022

Carotenoids
Volume 1B: Spectroscopy

G. Britton, S. Liaaen-Jensen, and H. Pfander (Editors)

- *Carotenoids* provides an introduction to the fundamental chemistry of these important compounds, detailed accounts of the basic methods used in carotenoid research, and critical discussions of the biochemistry, functions and applications of carotenoids. More than twenty years on from the Isler monograph of the same name, this new book series is designed to pass on a wealth of practical experience that has accumulated in recent years. The series also builds on Straub's work in *Key to Carotenoids, second Edition*.

- The first volume consists of two parts, Volume 1A covering the general methods of isolation and analysis, and Volume 1B the application of spectroscopic techniques to identification and structure elucidation. Topics in Volume 1B include: the electronic structure of carotenoids, UV/visible, infrared, resonance Raman and NMR spectroscopy, circular dichroism, mass spectrometry, X-ray crystallography, and a combined approach to the identification and structure elucidation of carotenoids.

- All written by leading experts, the chapters provide not only up-to-date information on specialized topics for experienced carotenoid researchers but, especially, practical guidance to workers in nutrition and medicine, food science, biotechnology, plant physiology, photosynthesis, and taxonomy, who wish to venture into this field.

ISBN 3-7643-2909-2
ISBN 0-8176-2909-2

9 783764 329099

Carotenoids

Volume 1B: Spectroscopy

Edited by G. Britton
S. Liaaen-Jensen
H. Pfander

江苏工业学院图书馆
藏书章

Birkhäuser Verlag
Basel · Boston · Berlin

International Editorial Advisory Board

K. Bernhard, F. Hoffmann-La Roche and Co. Ltd., Switzerland
C. H. Eugster, University of Zürich, Switzerland
H. A. Frank, University of Connecticut, USA
M. Ito, Kobe Women's College of Pharmacy, Japan
H. Mayer, F. Hoffmann-La Roche and Co. Ltd., Switzerland
J. Paust, BASF AG, Germany
K. Schiedt, F. Hoffmann-La Roche and Co. Ltd., Switzerland
B. C. L. Weedon, University of Nottingham, U.K.

List of Contributors

Susanne Back
Reserca AB
S-118 84 Stockholm
Sweden

Kurt Bernhard
F. Hoffmann-La Roche and Co. Ltd.
Department of Vitamins and Fine Chemicals
Grenzacherstrasse
CH-4002 Basel
Switzerland

George Britton
Department of Biochemistry
The University of Liverpool
P. O. Box 147
Liverpool L69 3BX
United Kingdom

Richard Buchecker
Roche Liquid Crystals Research and Development
F. Hoffmann-La Roche and Co. Ltd.
Grenzacherstrasse
CH-4002 Basel
Switzerland

Gerhard Englert
Department of Pharmaceutical Research
F. Hoffmann-La Roche and Co. Ltd.
Grenzacherstrasse
CH-4002 Basel
Switzerland

Curt R. Enzell
Tibbles
Hangvar
S-620 34 Lärbro
Sweden

Mireille Grosjean
Department of Pharmaceutical Research
F. Hoffmann-La Roche and Co. Ltd.
Grenzacherstrasse
CH-4002 Basel
Switzerland

Bryan E. Kohler
Department of Chemistry
University of California
Riverside
California 92521
USA

Yasushi Koyama
Faculty of Science
Kwansei Gakuin University
Uegahara
Nishinomiya 662
Japan

Synnøve Liaaen-Jensen
Organic Chemistry Laboratories
University of Trondheim
Norwegian Institute of Technology
N-7034 Trondheim-NTH
Norway

XIV

Frode Mo
University of Trondheim
Norwegian Institute of Technology
Department of Physics
N-7034 Trondheim-NTH
Norway

Klaus Noack
Department of Pharmaceutical Research
F. Hoffmann-La Roche and Co. Ltd.
Grenzacherstrasse
CH-4002 Basel
Switzerland

Preface to Volume 1B

The informed use of a range of spectroscopic methods is essential to modern analysis and structure elucidation. The application of such techniques including X-ray diffraction for the identification and structure elucidation of carotenoids is surveyed in Volume 1B. The use of spectroscopic methods for studying the location and functioning of carotenoids *in vivo* has not been covered in detail.

For all spectroscopic methods a sound understanding of the basic principles is imperative. References are therefore given to suitable general books and reviews. UV/Visible light absorption spectroscopy is a basic analytical method used by all carotenoid workers. The treatment of this technique, with more details of basic principles and procedures and structural correlations, reflects this wider use. Other physical techniques are generally more specialized and require expert knowledge and experience for many applications. A more specialized treatment is therefore given. However, major emphasis is placed throughout on practical guidance for interpretation of spectra, and on tabulated data such as NMR assignments and MS fragmentations for carotenoid end groups, identification of functional groups by IR and identification of chromophores by UV/Vis spectroscopy.

George Britton
Synnøve Liaaen-Jensen
Hanspeter Pfander

Editors' Notes on the Use of these Books: Vol. 1B

The *Carotenoids* books are planned to be used with the *Key to Carotenoids*, Second Edition. Throughout the series, whenever a known, natural carotenoid is mentioned, its number in the *Key to Carotenoids* or the *Appendix* (Vol. 1A, Chapter 8) is given in bold print. Other compounds, including purely synthetic carotenoids, that do not appear in the *Key* are numbered separately, in italics, in sequence for each Chapter, and their formulae are shown. Note that the *Key* numbers given are those in the Second Edition of the *Key to Carotenoids* (1987). The numbering of compounds in the original *Key to Carotenoids* (1976) and the list in the 1971 Isler *Carotenoids* book is different.

There is substantial cross-referencing between Volume 1A and 1B, which constitute two parts of a single volume and are intended to be used together.

Trivial names

The IUPAC semi-systematic names for all known naturally occurring carotenoids are given in the *Key to Carotenoids*, 2nd Edition, and in the Appendix (Vol. 1A, Chapter 8). Trivial names for many carotenoids are, however, well-established and convenient, so the practice of using these trivial names rather than the often cumbersome IUPAC semi-systematic names will, in general, be maintained in this series. An important exception is the naming of those compounds which bear the trivial name '(prefix)-carotene'. To avoid confusion caused by the use of Greek-letter prefixes that do not correspond to the series of prefixes used to designate end groups in the IUPAC system (*e.g.* 'γ-carotene' does not contain γ end groups) the old names α-carotene, β-carotene, γ-carotene, δ-carotene and ε-carotene are abandoned according to the IUPAC recommendation, and replaced by β,ε-carotene, β,β-carotene, β,ψ-carotene, ε,ψ-carotene and ε,ε-carotene, respectively.

References

Selective key references for major papers and review articles are given, rather than comprehensive lists of original literature sources.

Indexing

The indexes have been prepared primarily to aid the use of these books as general information and practical guides. No author index or index of biological sources of carotenoids is given. For information on individual carotenoids the *Key to Carotenoids*, which gives the trivial and semi-systematic names of each carotenoid, and references to its occurrence, isolation, spectroscopic properties, synthesis, *etc.* should be used.

The Index should be used together with the List of Contents to direct the reader to particular concepts, definitions, phenomena, techniques and procedures during the practical use of the books.

Contents

Chapter 1
Electronic Structure of Carotenoids
Bryan E. Kohler 1
A. Introduction 1
B. Overview of Carotenoid Electronic Structure 2
C. The Electronic Structure of Linear Polyenes 3
1. Identification of the S_1 and S_2 states 3
2. Systematics of S_1 and S_2 energies in polyenes and carotenoids 6
3. Simple model for calculating S_1 and S_2 energies 3
D. Electronic Structure and *cis-trans* Photoisomerization 8
E. Electronic Structure and UV/Vis Spectra 9
References 12

Chapter 2
UV/Visible Spectroscopy
George Britton 13
A. Introduction 13
B. Instrumentation 14
1. Spectrophotometer 14
2. Cells (cuvettes) 15
C. Origin and Features of the UV/Vis Spectrum of a Carotenoid 15
1. Electronic transitions 15
2. The spectrum of a carotenoid 16
3. Spectral fine structure 16
D. Relationship between Molecular Structure and Spectroscopic Properties 17
1. General principles 17
2. The chromophore 18
3. Geometrical (*cis-trans*) isomers 20
4. Cyclic end groups 22
a) γ Ring, ε ring 22
b) β Ring 23
c) 3,4-Didehydro-β ring 24
d) 2-Nor-β ring 25
e) Aryl φ and χ rings 27
5. Acetylenic groups 27
6. Allenic groups 27
7. *Retro*-carotenoids 31
8. Carbonyl groups 31
a) Aldehydes 31
b) Acyclic ketones 34
c) Secocarotenoids 36
d) Cyclic ketones 36

e) Carboxylic acids and esters 39
9. Other functional groups 39
a) Hydroxy groups 39
b) Epoxide groups 41
E. Effects of Molecular Environment 43
1. Effect of different solvents 43
2. Effect of water 44
3. Effect of protein 44
4. Spectra at low temperature 45
F. Tests for Functional Groups on a Spectroscopic Scale 46
G. Tables of Absorption Maxima 46
H. Quantitative Spectrophotometric Analysis 56
References 62

Chapter 3
Circular Dichroism
Richard Buchecker and Klaus Noack 63
A. Introduction 63
1. Chiroptical methods for the determination of absolute configuration of carotenoids 63
2. Brief historical survey of the application of chiroptical methods to carotenoids 63
B. Theory of CD Spectra 65
1. General aspects 65
2. Importance of conformation 67
3. Conclusions: applications of CD to carotenoids 74
C. Experimental Aspects 74
D. Relationships between Structure and CD 76
1. Monochiral and homodichiral carotenoids 76
a) Carotenoids with cyclic end groups that cause inherently chiral chromophores and conservative CD spectra 76
i) Substituted β rings 76
ii) Substituted 4-keto-β rings 80
iii) 5,6-Epoxy-β end groups 81
iv) *Retro*-carotenoids 82
b) Carotenoids containing chiral cyclic end groups that induce chirality and cause non-conservative CD spectra 83
i) ε Rings 83
ii) γ End groups 87
iii) Saturated cyclic end groups with two or three hydroxy groups 87
iv) 5,8-Epoxides (furanoids) 88
v) Allenic end groups 89
vi) Five-membered rings 90
vii) 3,6-Epoxides 90
c) Acyclic carotenoids 91
i) Acyclic end groups bearing oxygen functions at C-1, or at C-1 and C-2 91

ii) Acyclic C_{45} and C_{50} carotenoids 92
2. Heterodichiral carotenoids 93
3. Modifications of the polyene chain 97
a) Geometrical isomerism 97
i) Carotenoids with conservative spectra 97
ii) Carotenoids that exhibit non-conservative spectra 99
b) Other modifications 100
4. Some special investigations 105
References 114

Chapter 4
Infrared Spectroscopy
Kurt Bernhard and Mireille Grosjean 117
A. Principles, Scope and Limitations 117
B. Practical Aspects 118
1. Instrumentation 118
2. Infrared Spectrophotometers 118
3. Sampling 119
a) Solutions 119
b) Mulls 119
c) KBr discs 119
C. Interpretation of IR Spectra 120
1. General features 120
2. Infrared spectra of selected carotenoids 120
a) Alkanes (perhydrocarotenes) 121
b) Alkenes 121
c) Geometrical isomers 122
d) Alkynes, allenes and arenes. 122
e) Alcohols and ethers 123
f) Aldehydes and ketones 123
g) Esters and carboxylic acids 123
h) Sulphates 124
References 134

Chapter 5
Resonance Raman Spectroscopy
Yasushi Koyama 135
A. Introduction 135
1. Principles of resonance Raman spectroscopy 135
2. Scope and limitations of resonance Raman spectroscopy 135
B. Experimental Procedures 137
1. Instrumentation 137
2. Sample preparation 138
3. Raman measurements 138
a) Carotenoids free in solution 139

b) Carotenoids bound *in situ* 139
C. Raman Intensities: Dependence of Resonance Raman Intensity on Excitation Energy 139
1. Resonance Raman excitation profile for all-*E*-β,β-carotene in solution 139
2. Selective detection of resonance Raman scattering from a carotenoid in intact cells of a phototrophic bacterium 141
D. Raman Frequencies: Normal Modes of Vibration 143
1. The C=C stretching frequency that reflects the bond order 143
2. Key Raman lines of *cis-trans* geometrical configurations 143
E. Applications of Resonance Raman Spectroscopy in the Carotenoid Field 146
References 146

Chapter 6
NMR Spectroscopy
Gerhard Englert 147
A. Introduction 147
B. Experimental Aspects 148
1. Measuring frequency 148
2. Sensitivity 151
a) Pulsed Fourier-transform (FT) spectroscopy 151
b) ^{1}H-NMR 152
c) ^{13}C-NMR 153
d) ^{17}O-NMR 156
e) Spin-lattice relaxation time T_1 157
i) ^{13}C-NMR 157
ii) ^{1}H-NMR 159
f) Spin-spin relaxation time T_2 159
C. Chemical Shifts of End Groups 161
1. ^{1}H-NMR 161
2. ^{13}C-NMR 185
D. Chemical Shifts and Spin Couplings of Carotenoids 199
1. ^{1}H-NMR 199
2. ^{13}C-NMR 211
E. Carotenoid *Cis*-Isomers 220
1. ^{1}H-NMR 220
2. ^{13}C-NMR 223
F. Experimental Techniques 225
1. ^{1}H-NMR 225
a) Homonuclear decoupling 225
b) Double-INDOR-Difference (DID) 225
c) Nuclear Overhauser effect (NOE) 230
i) Longitudinal NOE 230
ii) Transverse or rotating-frame NOE (ROE) 231

d) Total correlation spectroscopy (TOCSY, or HOHAHA) 236
e) Homonuclear ^1H, ^1H-correlated 2D spectroscopy (COSY) 239
i) Regular cross peaks 242
ii) Folded cross peaks 245
2. ^{13}C-NMR 247
a) ^1H-decoupled ^{13}C-NMR 247
b) ^1H-coupled ^{13}C-NMR 247
c) Distortionless enhancement by polarization transfer (DEPT) 249
d) ^1H, ^{13}C-Correlated 2D spectroscopy (hetero-COSY) 251
i) ^{13}C-Detected ^1H, ^{13}C-COSY 251
ii) ^1H-Detected ^1H, ^{13}C-COSY 252
G. Experimental 258
H. Concluding Remarks 259
References 259

Chapter 7
Mass Spectrometry
Curt R. Enzell and Susanne Back 261
A. Introduction 261
B. Ionization Techniques 262
1. Electron impact 262
2. Fast atom bombardment 262
3. Chemical ionization 265
4. Particle desorption 271
C. Tandem Mass Spectrometry 271
1. Linked scanning 271
2. MIKE Scanning 273
D. Combined Chromatography-Mass Spectrometry 274
1. GC-MS and LC-MS 274
2. SFC-MS 274
E. Elimination of In-Chain Units 277
1. Mechanisms for the major reactions 277
2. Intensity ratio of the $[M-92]^{+\cdot}$ and $[M-106]^{+\cdot}$ peaks 280
a) Regular carotenoids 280
b) Acyclic C_{50} carotenoids 283
c) Aromatic carotenoids 283
d) Oxocarotenoids 283
e) Carotenoids substituted at C-20 285
f) Acyclic carotenoids with fewer than 11 conjugated double bonds 285
g) *Retro*-carotenoids 286
h) Irregular carotenoids 287
3. Other reactions 287
a) Formation of $[M-78]^{+\cdot}$, $[M-79]^{+}$, and $[M-80]^{+\cdot}$ ions 287
b) 5,6-Epoxides and 5,8-epoxides 288

c) Acyclic 7,8-dihydrocarotenoids and 7,8,11,12-tetrahydrocarotenoids 289
d) Acetylenic carotenoids 291
e) Allenic carotenoids 291
F. Elimination Reactions of Terminal Groups 291
1. Acyclic end groups 302
2. Cyclic end groups 306
G. Carotenoid Conjugates 313
1. Fatty acid and retinoic acid esters 313
2. Sulphates 313
3. Glycosides 314
H. Conclusions 317
References 317

Chapter 8
X-Ray Crystallographic Studies
Frode Mo 321
A. Introduction 321
B. Experimental 321
1. X-ray diffraction and determination of structure 321
2. Determination of absolute configuration 323
C. Studies of Carotenoid Structure 325
1. Structural studies before 1970 325
2. Structural studies after 1970 327
a) Carotenoids and apocarotenoids 327
b) The carotenoid chain 331
D. Structures of Degraded Carotenoids, Synthons and Analogues 334
E. Concluding Remarks 338
References 340

Chapter 9
Combined Approach: Identification and Structure Elucidation of Carotenoids
Synnøve Liaaen-Jensen 343
A. Introduction 343
B. Polarity: Evidence from Chromatography 343
C. Spectroscopic Data 344
1. Key information provided 344
a) UV/Vis spectra 344
b) Mass spectra 345
c) ^{1}H-NMR and ^{13}C-NMR spectra 345
d) IR spectra 345
e) CD spectra 345
D. Chemical Derivatization 346
1. Key information obtained 346
E. Recommended Procedure 347

1. Identification 347
2. Structure elucidation 347
F. Examples of Structure Elucidation 348
1. Decaprenoxanthin (C_{50}) 348
2. Actinioerythrin (C_{38}) 349
3. Prasinoxanthin (C_{40}) 351
5. Bastaxanthin (carotenoid sulphate) 351
5. P457 (glycoside) 352
References 354

Index 355

Carotenoids
Volume 1 B: Spectroscopy
© 1995 Birkhäuser Verlag Basel

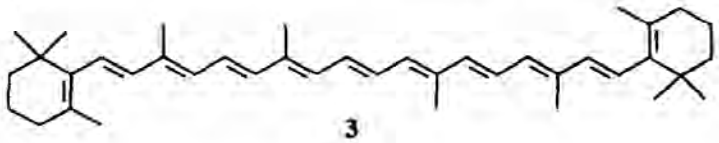
Chapter 1
Electronic Structure of Carotenoids

Bryan E. Kohler

A. Introduction

The carotenoids play an obvious role as pigments that give many natural objects their pleasing colours. They have even more important roles as initiators and mediators of photochemistry in processes that range from photosynthesis to vision. There are several other chromophores that absorb light in the visible and near-ultraviolet regions of the spectrum, but the electronic structure of linear polyene chains is qualitatively distinct from that of other conjugated hydrocarbons such as, for example, the polyacenes. The aim of this Chapter is to communicate the picture of the electronic structure of linear polyenes that has emerged over the past 20 years. Although much of this work has concentrated on short-chain polyenes as models, it nevertheless provides a basis for understanding the spectroscopic and photochemical properties of carotenoids.

In 1972 it was discovered that the excited state responsible for the longest wavelength strong absorption band in diphenyloctatetraene was not the lowest-energy excited singlet state [1]. A previously undetected excited singlet state at lower energy rationalized fluorescence properties that had been thought to be anomalous (Fig. 1), so it was conjectured that all linear polyenes, the carotenoids included, would have a similar hidden low-lying excited singlet state [2-4]. This is now known to be true. An important goal of this Chapter is to describe this relatively newly discovered S_1 state in terms of simple molecular orbital concepts. This is critically important; since virtually all photoprocesses in linear polyenes originate in the lowest-energy excited singlet state, the importance of correctly identifying and characterizing that state cannot be overemphasized. The revised state ordering given in Fig. 1 accounts for a number of observations previously considered curious, including the provocative lack of fluorescence of β,β-carotene (3).



3

In the discussion that follows, some basic properties of linear conjugated molecules are reviewed, such as delocalized π-electrons, bond-length alternation, isomers and conformers. A brief outline of the simple molecular orbital concepts that apply to these molecules provides a background for the UV/Vis spectroscopy of the carotenoids.

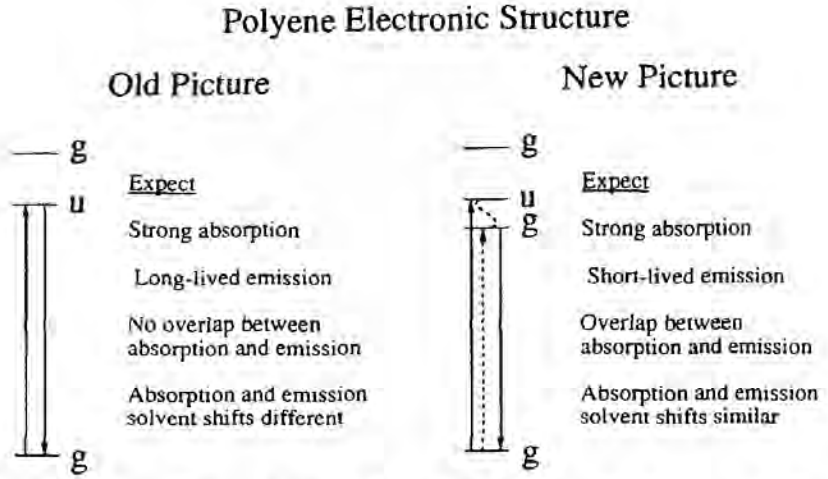


Fig. 1. Energy level diagrams for linear polyenes. The old and new pictures are presented. The expectations for the new picture correspond to what is observed, those of the old picture do not.

B. Overview of Carotenoid Electronic Structure

The key structural element of carotenoids is the conjugated polyene backbone. It is the delocalization of π-electrons along this backbone that gives carotenoids their characteristic electronic spectra and is largely responsible for the photophysical and photochemical properties of these molecules, including *cis-trans* photoisomerization.

The atoms in an unsubstituted linear polyene are arranged in a planar zigzag chain, with the formal repeating unit –CH=CH–. There is pronounced bond-length alternation. The length of a formal C–C single bond (1.45 Å) is shorter than that in a normal alkane (1.53 Å), although the length of a formal C=C double bond (1.34 Å) is the same as that in ethylene (1.336 Å). The shortening of the single bonds is consistent with delocalization of the π-electrons, that is that they are able to move along the polyene chain.

Carotenoids are methyl-substituted polyenes which have the formal repeating unit –CH=CH–CCH_3=CH–. Alternatively, they may be considered as linear polyenes in which every fourth hydrogen atom (or fifth in the central part of the molecule) has been replaced by a methyl group. X-Ray crystallography has shown that the structural consequences of this methyl substitution are relatively minor; the C–C and C=C bond lengths are nearly the same as in the unsubstituted polyenes. The C=C–C bond angles in the linear polyenes are all very close to 125°. In the carotenoids the C=C–C bond angle is also 125° if the carbon at the apex is not

methyl substituted, but averages 117° if this carbon is methyl substituted. This presumably reflects steric crowding which gives a slight bow and a barely perceptible helical twist to the zigzag backbone of the carotenoids.

The barriers to rotation about the formal double bonds in a polyene or carotenoid are sufficiently large for double-bond *cis* and *trans* isomers to be isolated as independent, distinct compounds. This is not true of s-*cis* and s-*trans* conformers.

The differences in excitation energies for *cis* and *trans* isomers of a given molecule are small compared to the change in excitation energy that is associated with adding or subtracting a conjugated double bond. The basic electronic structure is, therefore, almost independent of isomeric form.

C. The Electronic Structure of Linear Polyenes

1. Identification of the S_1 and S_2 states

The main objective in this Section is to describe the molecular orbital character of the S_1 and S_2 states of polyenes. It is useful to review briefly the essentials of a description of the electronic structure of a conjugated polyene chain by the simplest of molecular orbital theories, Hückel theory [5, 6], in order to define terms that will be used in the discussion of spectra that follows. Further details may be found in standard texts [6] or in review articles [7, 8].

Because it accounts for the excitation energy and the intensity of the lowest-energy strong absorption band of linear polyenes, the description of the π-electron states that is given by Hückel theory can be considered to be very successful. On the other hand, Hückel theory may be considered to have a serious weakness, because it incorrectly predicts that the excited state responsible for this absorption is S_1, the lowest-energy excited singlet state (as will be seen below, it is not S_1, it is S_2). However, LCAO-MO (linear combination of atomic orbitals-molecular orbital) theory at the Hückel level is well known and the new state ordering may be described efficiently in terms of linear combinations of Hückel configurations.

Because it is so well established, the electronic structure of the simplest conjugated model compound, butadiene, will be described. In simple Hückel theory only those electrons are considered that are not used in making the σ-bonded framework of sp^2-hybridized carbons (Fig. 2). The problem is to find for these electrons the linear combinations of the atomic orbitals (2p orbitals that are perpendicular to the plane of the zigzag chain; also called 2p-π orbitals) that are solutions of the Schrödinger equation for the molecule. A linear polyene with n double bonds will have 2n 2p-π atomic orbitals which will lead to 2n linearly independent molecular orbitals. Hückel theory, which is a set of approximations for the molecular Schrödinger equation, generates a closed-form general solution for molecular orbital energies and gives the atomic orbital coefficients for a given molecular orbital for a polyene with an arbitrary number of double bonds in conjugation [6]. The molecular orbitals for butadiene (n = 2) are sketched in Fig. 3.

An electronic configuration is defined as a particular assignment of the 2n π-electrons to molecular orbitals. At this level of treatment, the energy of a given configuration is simply the

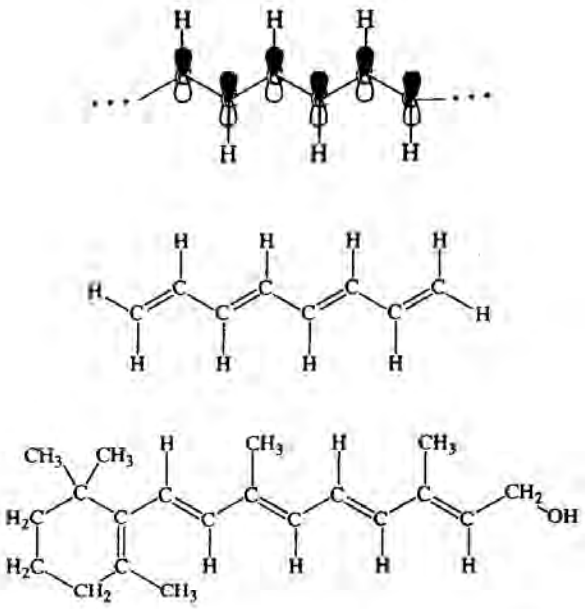


Fig. 2. Conjugated linear chains. At the top is sketched the sp^2 hybridized chain, together with the 2p-π atomic orbitals on which the delocalized π-molecular orbitals are based. Below this are shown the valence-bond representations of an unsubstituted linear polyene (octatetraene, middle) and a substituted polyene of the carotenoid type (retinol, bottom).

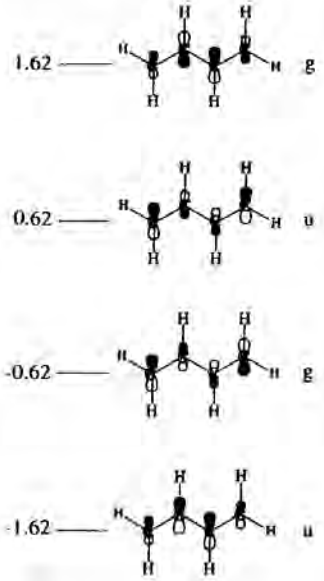


Fig. 3. Molecular orbitals of butadiene. The energy-ordered π-electron molecular orbitals, showing symmetry labels to the right and energies in units of |β|, the magnitude of the Hückel resonance integral, to the left. The size and relative sign of the atomic orbital are proportional to the orbital coefficient.

sum of the energies of the occupied molecular orbitals. It is common to associate molecular states with single configurations although, as will be seen later, this can lead to errors. Figure 4 introduces the key configurations necessary for understanding carotenoid electronic structure. In the minimum-energy or ground-state configuration (1^1A_g) all the bonding molecular orbitals are doubly occupied. The lowest-energy excited configuration (1^1B_u) is generated from the ground-state configuration by promoting one electron from the highest-energy occupied molecular orbital (HOMO) to the lowest-energy unoccupied molecular orbital (LUMO). Other single electron promotions and multiple electron promotions are possible, and all lead to higher-energy configurations. Analogous configurations obtain for all linear polyenes; the addition of each double bond just adds one doubly-occupied bonding molecular orbital at the bottom and one empty antibonding molecular orbital at the top and changes the orbital energies.

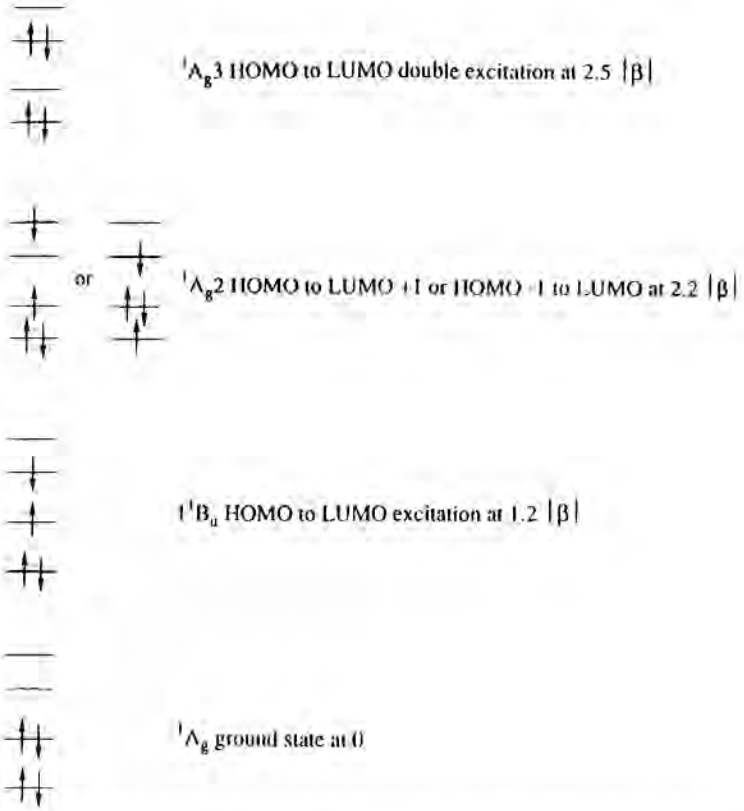


Fig. 4. Orbital occupation and energy in units of |β| for the key configurations of butadiene.

The agreement between this theoretical model and low-resolution spectroscopic experiments is excellent. With a proper choice of the energy of the Hückel resonance integral, β, the predicted energy of the HOMO to LUMO excitation and the intensity of the associated transition are close to the observations for the lowest-energy strong absorption ($1^1A_g \rightarrow 1^1B_u$)

for a large number of compounds. If different resonance integrals are used for the formal single and double bonds, the correspondence between calculated and measured excitation energies can be made exact for entire homologous series [8].

While LCAO-MO theory can provide a convincing interpretation of the low-resolution absorption spectra in terms of the $1^1A_g \rightarrow 1^1B_u$ transition, there are aspects of the fluorescence spectra that are at variance with the theoretical picture.

i) The fluorescence and absorption spectra have little overlap. This is most striking when some vibrational fine structure is present. If absorption and emission involved the same excited state, the lowest-energy peak in the absorption spectrum and the highest-energy peak in the emission spectrum should coincide.

ii) Calculations predict a very short radiative lifetime (1 to 2 ns). In fact, fluorescence lifetimes are often much longer (100 ns for octatetraene in *n*-hexane [9]).

iii) The solvent-shift behaviour of the absorption and fluorescence spectra of a given molecule are different. The strong absorption band shifts by approximately 10^4 cm^{-1} to lower energy for unit change in $(\eta^2-1)/(\eta^2+2)$, where η is the refractive index for the solvent; changing solvent has little effect on the fluorescence. If these spectra involved the same excited state, the solvent shifts would be similar.

The discrepancy seen under high-resolution conditions clearly shows that the absorption and emission spectra are associated with different excited states. The implication is that, although the 1^1B_u state is responsible for the strong absorption band, there is another extremely weakly-absorbing excited state that lies lower in energy than this.

Since all polyene π-electron states have either B_u or A_g symmetry, the weakness of the fluorescence excitation spectrum, and the strong increase in intensity as excitation energies approach the 1^1B_u origin, suggest that this lower-energy state is an A_g state. This assignment has been confirmed by 2-photon excitation spectroscopy [10].

It is clear, therefore, that the appealingly simple LCAO-MO model for the electronic structure of linear polyenes is incompatible with the experimental observation that the state generated from the ground configuration by the promotion of a single electron from the HOMO to the LUMO is not the lowest-energy excited singlet. The fundamental problem arises because an approximation is used in which the inter-electron repulsion energy is treated by considering that one electron interacts with an averaged charge cloud generated by all the other electrons. In other words, one of the basic assumptions of molecular orbital theory is invalidated because the π-electrons in linear polyenes move in a highly correlated way. For a summary of the subsequent theoretical work, the interested reader is referred to recent reviews [3, 7].

2. Systematics of S_1 and S_2 energies in polyenes and carotenoids

For several homologous series of model compounds, the measured 2^1A_g and 1^1B_u excitation energies are well fitted by the empirical relationship $n = A+B/n$ where n is the number of conjugated double bonds. A more satisfying and economical analysis is one where the effect of a given substituent ($\delta n_{substituent}$) is assumed to change the conjugation length from n to an

effective length $n_{eff} = n+\delta n_{substituent}$. With this formalism, the 2^1A_g and 1^1B_u 0–0 excitation energies of a number of different homologous series, including a series of β,β-carotene (3) homologues, can be put onto the same universal curve, as is seen in Fig. 5.

The 2^1A_g and 1^1B_u 0–0 excitation energies can be estimated reliably for a wide variety of linear polyenes in solution in *n*-alkanes. It is also useful to be able to correct these estimates for the effects of solvent environment. To within a few hundred cm^{-1} the 1^1B_u excitation energy obeys the relationship

$$\nu = \nu_o + (\eta^2-1)/(\eta^2+1) \times 10^4 \text{ cm}^{-1}$$

where η is the refractive index of the solvent, whereas the 2^1A_g energy is nearly independent of solvent environment. The universal curves given in Fig. 5 and this simple estimate of the effects of solvent environment give reasonable estimates for the S_1 and S_2 energies of a large variety of linear polyenes.

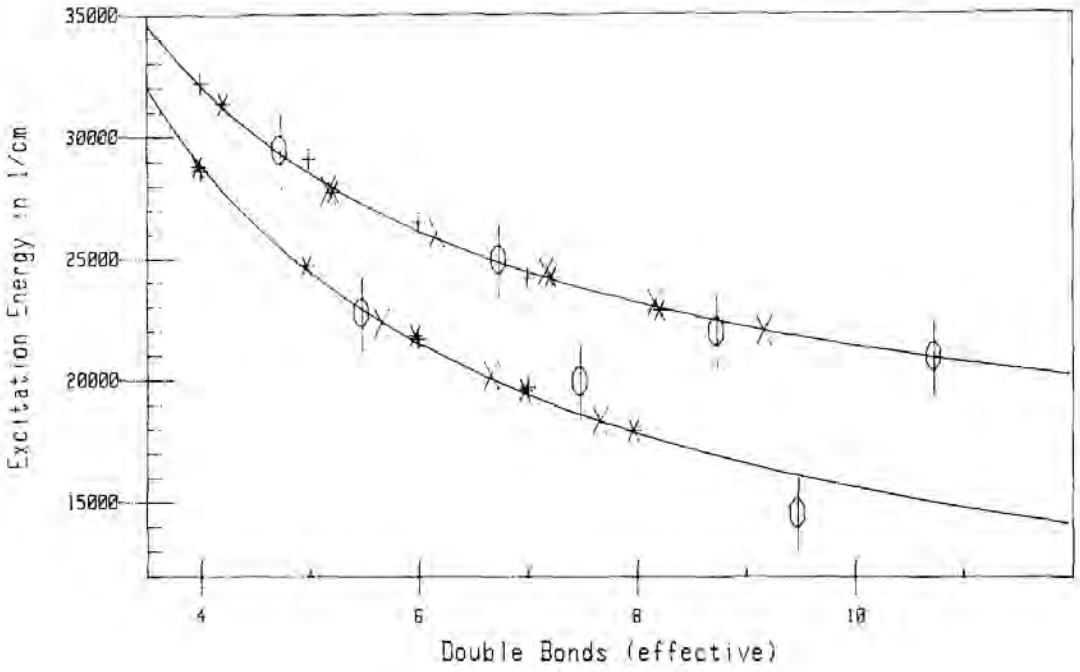


Fig. 5. Universal curves for 2^1A_g and 1^1B_u excitation energies versus the effective number of conjugated double bonds. The line for 1^1B_u energy (upper curve) is $\upsilon = 14250\ cm^{-1} + 71000\ cm^{-1}/n_{eff}$; the line for 2^1A_g energy (lower curve) is $\upsilon = 6800\ cm^{-1} + 88300\ cm^{-1}/n_{eff}$. There are 18 experimental points on the upper curve: 9 plotted as * and x for unsubstituted and alkyl-substituted polyenes, respectively, ($n_{eff} = n$); 5 plotted as + for diphenylpolyenes ($n_{eff} = n + 3.2$) and 4 plotted as ϕ for β,β-carotene homologues ($n_{eff} = n - 0.3$). There are 14 experimental points on the lower curve: 8 plotted as * and x for unsubstituted and alkyl-substituted polyenes, respectively, ($n_{eff} = n$); 3 plotted as + for diphenylpolyenes ($n_{eff} = n + 1.7$) and 3 plotted as ϕ for β,β-carotene oligomers ($n_{eff} = n + 0.5$).

3. Simple model for calculating S_1 and S_2 energies

The demonstration [11] that the correct order of excited singlet states of polyenes could only be obtained by paying explicit attention to electron–electron interaction has been reinforced by a number of subsequent theoretical studies [12-15]. An interpretative theoretical model, based upon the solution of a quadratic equation involving two Hückel energies and a mixing parameter that is dependent on chain length, allows all the twentyfive 2^1A_g and 1^1B_u excitation energies that have so far been obtained in high-resolution experiments to be reproduced with a root-mean-square deviation of only 160 cm^{-1} [8]. This picture of the 2^1Ag state is satisfyingly simple; it is a superposition of the $^1Ag2$ and $^1Ag3$ configurations shown in Fig. 4.

D. Electronic Structure and *Cis-Trans* Photoisomerization

Geometrical (*cis-trans*) isomerization is a characteristic photochemical property of the carotenoids, and has been explored quite thoroughly [16]. Modern research in this area is now directed towards understanding the phenomenon in terms of the underlying electronic structure.

The two fundamental questions to be answered are: (i) in what electronic state does the photoisomerization originate and, (ii) in what ways do the chemical properties of this state differ from those of the ground state? Increasingly, this information is summarized in terms of potential-energy surfaces, *i.e.* plots of the energies of the relevant electronic states *versus* nuclear configuration or molecular geometry.

A large body of empirical evidence supports the argument that, at least in the case of photoisomerization of carotenes, photochemistry is initiated in the manifold of excited singlet states. In solutions at room temperature, vibrational relaxation and internal conversion within a given spin manifold are expected to be much faster than the rate of photochemical transformation, so it would be anticipated that carotenoid photoisomerization originates in the S_1 state. Thus, the discovery that S_1 is not the state responsible for the lowest-energy strong absorption band of linear polyenes has profound implications for understanding photoisomerization of carotenoids.

The direct determination of the photochemically relevant features of the potential-energy surface of the polyene 2^1A_g state is at an early stage. The picture for octatetraene is quite complete and is described in a recent review article [17]. For octatetraene the 2^1A_g potential-energy surface has a well defined minimum for each isomer at a geometry that does not differ substantially from the equilibrium geometry in the ground state. Specifically, a strongly twisted equilibrium geometry for the excited state is ruled out.

The thermodynamic barrier to isomerization on the 2^1A_g potential-energy surface is astonishingly low, approximately 1 $kcal.mol^{-1}$ [17, 18]. While it is not yet known whether the surprisingly low isomerization barriers seen in the S_1 state of octatetraene are characteristic of all linear polyenes and carotenoids, this is the most reasonable expectation.

E. Electronic Structure and UV/Vis Spectra

As might be anticipated from the similarities in electronic structure, the electronic absorption spectrum of a given carotenoid closely resembles that of the unsubstituted polyene with the same number of conjugated double bonds. The principal differences, namely a 10 to 30 nm shift of the lowest-energy strong absorption band to longer wavelength and decreased vibrational fine structure, reflect small perturbations of the basic polyene electronic structure by the methyl substituents. Although *cis* and *trans* isomers may often be distinguished on the basis of their UV/Vis absorption spectra, the most important spectral differences seen with isomers are related not to excitation energies but to the relative intensities of higher-energy absorption bands ('*cis*-peaks') [16, 19].

As discussed above, it is now clear that the lowest excited state of linear polyenes, including carotenoids, is the 2^1A_g state. It is also well established, however, that the origin of the main absorption band is the strongly allowed $1^1A_g \rightarrow 1^1B_u$ transition. The shapes of electronic absorption and fluorescence bands derive from the vibrational levels that are associated with the initial and final electronic states, as is shown in cartoon form in Fig. 6.

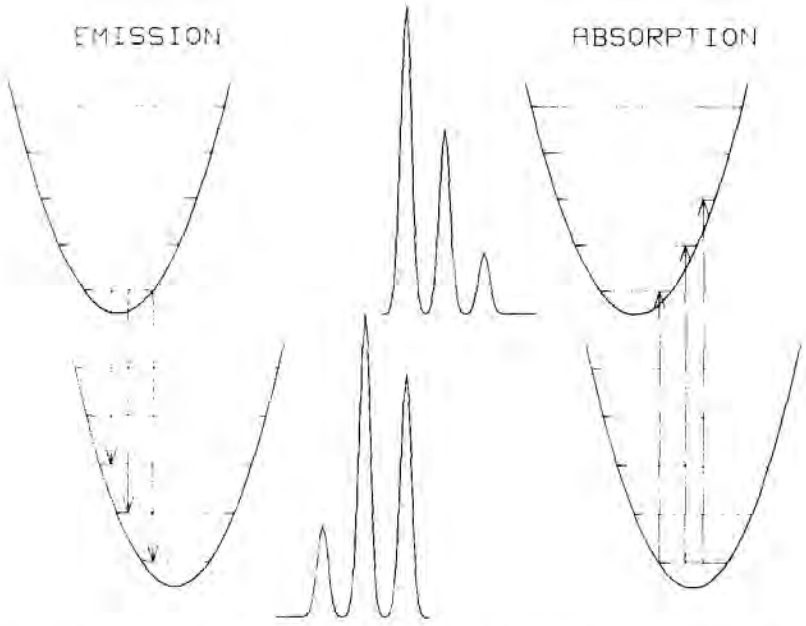


Fig. 6. Vibrational fine structure in absorption and fluorescence spectra. Electronic energy as a function of conformation is the potential energy function for nuclear motion. As indicated, minimum energy conformations are usually different in different electronic states. Absorption fine-structure intervals (upper spectrum) are determined by excited-state vibrational frequencies; emission fine-structure intervals (lower spectrum) are determined by ground-state vibrational frequencies. The intensity of a fine-structure component is proportional to the squared overlap of the ground-state and excited-state vibrational functions.

Detailed discussions of vibrational fine structure in UV/Vis spectra can be found in standard texts [20]. The typical three-peaked shape of the main absorption band of linear polyenes (*e.g.* acyclic carotenoids) arises from transitions from the lowest vibrational level of the electronic ground state to the lowest vibrational levels of the electronic excited state. Broadening of these peaks because of rotational levels and inhomogeneity leads to overlap and loss of the distinct three-peaked shape. Three kinds of inhomogeneity cause this vibrational fine structure to be almost completely absent in spectra of many carotenoids measured as solutions at room temperature. First, there is inhomogeneity of initial-state energy, introduced by thermal population of excited vibrational levels in the ground state. Second, there is environmental inhomogeneity. The random structure in a liquid means that each solute molecule sees a different microenvironment and, thus, experiences a different solvent shift of its excitation energy. Third, for linear-chain molecules such as the carotenoids, there is also inhomogeneity with respect to molecular conformation, since a large number of s-*cis* conformers may be populated. All these sources of spectral broadening are significantly decreased on going from a room-temperature solution to a low-temperature, solid-state environment. Although this introduces some experimental complexity, the added information is worthwhile.

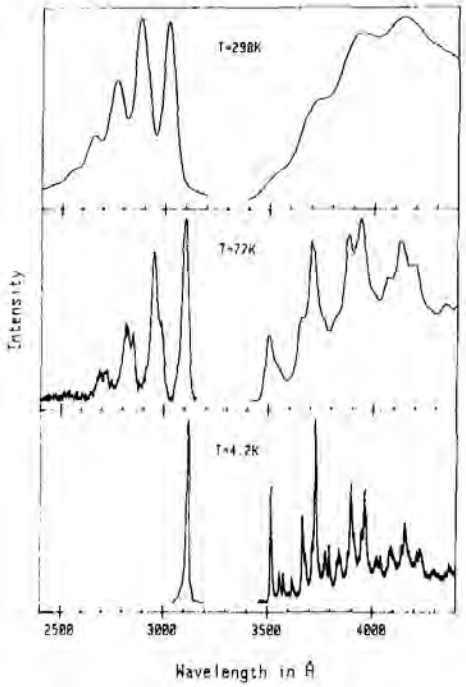


Fig. 7. Absorption and fluorescence for an *n*-octane solution of all-*trans* octatetraene at different temperatures (room temperature at the top, 77K in the centre and 4.2K at the bottom). For each pair of spectra, absorption is at the left, fluorescence at the right. As resolution is increased it becomes clear that absorption and fluorescence involve different excited states.

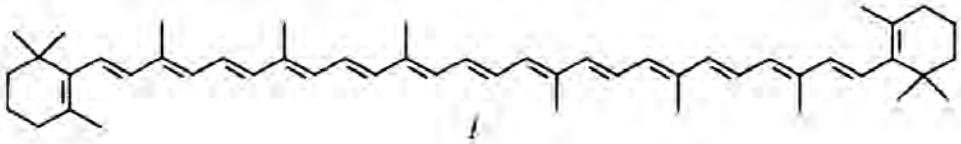
The top part of Fig. 7 shows the absorption spectrum measured for a solution of octatetraene in *n*-octane, at room temperature. Because of the simplicity of the molecule and the fact that the isomeric composition is more than 90% all-*trans*, the characteristic polyene absorption band already shows some vibrational fine structure. As is easily seen in the low-temperature spectra, most of the vibronic intensity involves the C=C and C–C stretch modes whose frequencies in the ground state are *ca.* 1600 cm^{-1} and 1200 cm^{-1}, respectively. Because, at room temperature, the absorption bands are broader than the difference between the C=C and C–C vibrational frequencies, these peaks are not resolved and an apparent spacing of *ca.* 1300 cm^{-1} is seen. As this solution is cooled to 77K (liquid nitrogen temperature), the octane becomes polycrystalline. The lower temperature and the fact that, in the octane crystals, the molecular environment of the octatetraene guest molecules is extremely homogeneous, significantly increase the resolution of the absorption and fluorescence spectra, as seen in the middle part of Fig. 7. To obtain a totally resolved spectrum, all that remains is to lower the temperature to 4.2K (liquid He). The resulting spectra are shown in the bottom part of Fig. 7.

These trends in excitation energies can also provide insight into other matters such as, for example, why the absorption spectra of short carotenoid analogues show no vibrational fine structure while those of longer species such as lycopene (**31**) do. The diminution of vibrational fine structure in cyclic carotenoids such as β,β-carotene (**3**) can be attributed quantitatively to conformational heterogeneity that is caused by the β ring. The key concept here is that effective conjugation length depends on molecular geometry. For two double bonds to be conjugated (that is, to share π-electrons), they must be coplanar. Because extension of conjugation decreases π-electron energy (resonance stabilization) and because other contributions to the energy are relatively insensitive to the angle of twist about an essentially single bond, unsubstituted polyene chains are planar in their equilibrium or lowest-energy conformation. However, if the polyene chain terminates with a β ring, non-bonded repulsions between the methyl groups on the ring and the hydrogen atom on the carbon at the end of the first double bond in the chain (C-8) are introduced, which are largest at the planar conformation. Thus, the total energy as a function of twist about the ring–chain single bond (C-6,7) has two principal contributions, namely one that is minimized at the planar conformation and one that is minimized at the perpendicular conformation. In consequence, the ground-state energy does not strongly depend on twist about the ring–chain bond; this means that, in solution at room temperature, a broad range of conformations will exist. As pointed out above, the excitation energy for the lowest-energy strong absorption band depends strongly on the number of conjugated double bonds, n, going as (71 200 cm^{-1})/n. If the effective value of n is distributed, that is, has a range δn, the excitation energy will be spread over a range (71 200 cm^{-1})δn/n^2; the shorter the chain the greater the range. Analysis of the spectra of lycopene (**31**), β,ψ-carotene (**12**), β,β-carotene (**3**) and the C_{50} analogue decapreno-β,β-carotene (*1*) gives δn = 0.25 per β ring, which accounts quantitatively for the presence of fine structure in the spectra of the long carotenoids containing the β ring and the lack of fine structure in the shorter ones [21].

At least for polyenes with 3 to 8 double bonds in conjugation, under ordinary solution conditions, the lowest-energy intense absorption band of a polyene chromophore is associated with the $S_0 \rightarrow S_2$ transition (the $1^1A_g \rightarrow 1^1B_u$ transition) and the relaxed fluorescence comes from the $S_0 \leftarrow S_1$ transition ($1^1A_g \leftarrow 2^1A_g$). Exceptions to this rule are expected to occur as the

conjugated polyene chain becomes long and the energy separation between S_2 and S_1 approaches the energy separation between S_1 and S_0.

High-resolution spectra have not yet been measured for a series of carotenoids though, recently, spectroscopic studies have been reported [22] for a homologous series referred to as 'mini-carotenes' (β,β-carotene, **3**, analogues with 5 to 9 conjugated double bonds in the polyene chain). Although the estimates of 0–0 excitation energies from their low-resolution spectra are necessarily approximate, the data fit nicely on the universal curve (Fig. 5) when it is assumed that $n_{effective}$ for a carotenoid with two terminal β rings differs from the formal number of conjugated double bonds by +0.5 for the 2^1A_g state and by –0.3 for the 1^1B_u state.



1

References

[1] B. S. Hudson and B. E. Kohler, *Chem. Phys. Lett.*, **14**, 299 (1972).
[2] B. S. Hudson and B. E. Kohler, *J. Chem. Phys.*, **59**, 4984 (1973).
[3] B. S. Hudson, B. E. Kohler and K. Schulten, *Excited States*, **6**, 1 (1982).
[4] B. E. Kohler, *Biophys. Struct. Mech.*, **3**, 101 (1977).
[5] E. Hückel, *Z. Physik*, **70**, 204 (1931); **76**, 628 (1932).
[6] L. Salem, *The Molecular Orbital Theory of Conjugated Systems*, Benjamin, Reading, Massachusetts (1966).
[7] D. Baeriswyl, D. K. Campbell and S. Mazumdar, in *Conducting Polymers* (ed. H. Kiess), p. 7, Springer (1992).
[8] B. E. Kohler, *J. Chem. Phys.*, **93**, 5838 (1990).
[9] J. R. Ackerman, D. Huppert, B. E. Kohler and P. M. Rentzepis, *J. Chem. Phys.*, **77**, 3967 (1982).
[10] M. F. Granville, G. R. Holtom and B. E. Kohler, *J. Chem. Phys.*, **72**, 4671 (1980).
[11] K. Schulten and M. Karplus, *Chem. Phys. Lett.*, **14**, 305 (1972).
[12] S. N. Dixit and S. Mazumdar, *Phys. Rev. B*, **29**, 1824 (1984).
[13] Z. Soos and S. Ramasesha, *Phys. Rev. B*, **29**, 5410 (1984).
[14] D. Baeriswyl and K. Maki, *Phys. Rev. B*, **31**, 6633 (1985).
[15] I. Ohmine, M. Karplus and K. Schulten, *J. Chem. Phys.*, **68**, 2298 (1978).
[16] L. Zechmeister, Cis-Trans *Isomeric Carotenoids, Vitamins A, and Arylpolyenes*, Springer, Vienna (1962).
[17] B. E. Kohler, *Chem. Rev.*, **93**, 41 (1993).
[18] J. R. Ackerman and B. E. Kohler, *J. Amer. Chem. Soc.*, **106**, 3681 (1984).
[19] J. Dale, *Acta Chem. Scand.*, **8**, 1235 (1954).
[20] J. M. Hollas, *Modern Spectroscopy, 2nd Edition*, Wiley, New York (1992).
[21] R. Hemley and B. E. Kohler, *Biophys. J.*, **20**, 377 (1977).
[22] P. O. Andersson, T. Gillbro, A. E. Asato and R. S. H. Liu, *J. Luminescence*, **51**, 11 (1992).

Carotenoids
Volume 1 B: Spectroscopy
© 1995 Birkhäuser Verlag Basel

Chapter 2
UV/Visible Spectroscopy

George Britton

A. Introduction

Because of their long conjugated double-bond system, the carotenoids show strong main absorption bands in the visible or, in some cases, UV region. The positions of the absorption maxima and the shape or fine structure of the UV/visible (UV/Vis) spectrum are characteristic. Light-absorption properties, together with information derived from chromatographic behaviour, have long provided one of the first criteria for identification or structural characterization of carotenoids [1]. The UV/Vis spectrum gives information about the chromophore of the molecule, but tells nothing about functional groups except conjugated carbonyl groups that form part of the chromophore. The term 'chromophore' refers to the conjugated, unsaturated part of the molecule, containing delocalized π-electrons, which is responsible for the absorption of light in the visible region (Chapter 1).

Carotenoids in solution generally obey the Beer-Lambert law, so accurate quantitative analysis can be achieved by spectrophotometric methods (see Vol. 1A, Chapter 5).

Comprehensive tables listing the absorption maxima and absorption coefficients of carotenoids have been included in many publications [2-4] and are widely used. The injudicious use of such tables, without some knowledge and understanding of the relationship between structural features and spectral properties, can, however, lead to erroneous conclusions, particularly if solvent effects and the importance of spectral shape are overlooked. The light-absorption properties of a carotenoid are also dependent on the medium. Thus the absorption spectrum of a carotenoid *in vivo* may be affected by interactions with proteins, lipids, *etc.*, and may therefore differ significantly from the spectrum of that carotenoid in organic solvent.

In this Chapter, exhaustive tabulated data for all known carotenoids will not be given. Tables are included, but the main emphasis is placed on the relationship between structure and spectroscopic properties, as a guide to the identification of the chromophore of a carotenoid.

B. Instrumentation

1. Spectrophotometer

Some kind of UV/Vis spectrophotometer is part of the basic equipment of any chemistry, biochemistry or biology laboratory. Modern, advanced instruments are computer-controlled and have sophisticated data-handling systems with visual-display screen and printer/plotter. Older instruments with a built-in or added-on chart recorder are reliable, however, and give good results, though they require manual calibration to ensure accuracy of wavelength and absorbance readings. Even if no recording spectrophotometer is available, a spectrum of acceptable quality can be obtained by manual plotting.

The essential components of a spectrophotometer are as follows:

i) *Light source.* The usual source for work in the UV region (180 to 400 nm) is a deuterium arc lamp, and, for work in the visible region above 400 nm, a tungsten-filament, tungsten-halogen, or quartz-iodine lamp.

ii) *Means of dispersing the light into its component wavelengths.* In conventional instruments this is achieved by means of a prism or, preferably, a diffraction grating, as the dispersing element, with an arrangement of slits to ensure that the range of wavelengths falling on the sample is as narrow as possible (*e.g. ca.* 1 nm). A set of optical components (slits, mirrors *etc.*) and mechanical devices allows the wavelength of the light falling on the sample to be varied with time, *i.e.* the spectrum to be scanned.

iii) *Detector.* After passing through the sample, the essentially monochromatic light is received by the detector, which is usually some kind of electron photomultiplier tube, that monitors the intensity of the transmitted light at each wavelength. The variation in the intensity of the light transmitted (or absorbed), as a function of wavelength, generates the absorption spectrum.

The most satisfactory and most commonly used spectrophotometers are double-beam instruments, in which two light beams are generated and pass simultaneously through the sample cell and the reference cell. The difference in intensity between these two transmitted beams represents the light absorbed by the sample.

Simple single-beam spectrophotometers in which a single light beam is directed through a single sample can also be used. For quantitative work with these instruments a zero calibration must be performed by re-setting the absorbance to zero with a reference cell containing only solvent in the light beam, before the sample cell is introduced into the light beam and its absorbance read.

Recently, an alternative spectrophotometer design has been introduced. This is based on photodiode-array detection and has proved powerful in HPLC (Vol. 1A, Chapter 6, Part IV). In this case, light of the whole spectral range falls upon the sample, and the transmitted light is then dispersed. Light of all wavelengths falls upon the photodiode array simultaneously, but the array is positioned so that each diode receives a very narrow waveband. The responses of all the photodiodes are collected simultaneously, so a complete spectrum can be recorded in a very short time (milliseconds).

2. Cells (cuvettes)

Nearly all spectrophotometers are designed to accommodate normally a cell of 1 cm pathlength. Open-top, rectangular cells, with lid, are the most commonly used, but microcells, in which the total volume is reduced without decreasing the working area or pathlength, are useful for small samples. For work entirely in the visible region, glass cells can be used, but glass does not transmit below 300 nm and cannot be used in the UV region. Fused natural quartz or fused synthetic silica cells then have to be used. Disposable plastic cells should never be used with organic solvents.

C. Origin and Features of the UV/Vis Spectrum of a Carotenoid

1. Electronic transitions

Organic molecules have the fundamental property of being able to absorb light in the UV or visible wavelength range. The absorption of this light energy produces a higher-energy or excited state of the molecule. The energy absorbed (E) is equal to the difference between the energy of the excited state produced (E_1) and that of the unexcited, ground-state molecule (E_0). Thus, $E = E_1 - E_0$ and is inversely proportional to the wavelength of the light absorbed, by the expression $E = hc/\lambda$.

The transitions involved are electronic transitions. In the case of carotenoids, the relevant transition is a $\pi \rightarrow \pi^*$ transition, in which one of the bonding π-electrons of the conjugated double-bond system is promoted to a previously unoccupied π^* antibonding orbital. For such a conjugated system, in which the π-electrons are highly delocalized, the excited state is of comparatively low energy. The energy required to bring about the transition is therefore relatively small and corresponds to light in the visible region.

The relationship between electronic structure or configuration and the UV/Vis light absorption properties of carotenoids has been discussed in Chapter 1. The transition responsible for the main absorption band is that between the electronic ground state (1^1A_g) and the second excited state (1^1B_u), which involves a change in symmetry from a g state to a u state and is therefore strongly allowed. Transitions from the ground state to higher electronic states are also possible, provided they obey the symmetry selection rules. These higher energy transitions give rise to absorption bands in the UV region which are usually weak, but are observed particularly in the spectra of long-chromophore compounds.

When the symmetry properties of a carotenoid change, absorption bands that are usually not detected may become a significant feature of the spectrum, as the transitions that produce them become allowed. This is particularly important in the case of *cis* isomers. For all-*trans* compounds, the electronic structure has a centre of symmetry, and the ground state is a g state, so transitions to a higher g state are forbidden. When one double bond becomes *cis*, the original symmetry is lost, and transition to a higher excited g state becomes allowed. This gives rise to an absorption band in the UV region, known as the *cis*-band or *cis*-peak. The usefulness of this absorption band for structural studies is discussed in Section D.3.

2. The spectrum of a carotenoid

The most important feature of the absorption spectrum of a carotenoid is the main absorption band in the visible region. Several pieces of important information can be obtained from the spectrum. First, the position of the main absorption band, specified by λ_{max}, the wavelength of maximum absorption, provides structural information because it is determined by the chromophore of the molecule. Secondly, the intensity of absorption, expressed as the absorbance, A, is related to the structure and to the concentration of carotenoid in the sample, and thus provides the basis for quantitative analysis. Thirdly, for reasons outlined in Chapter 1, with most carotenoids the spectrum appears not as a single band but shows three more-or-less distinct peaks. This effect, known as (vibrational) fine structure, is seen to different extents with different carotenoids and provides an important diagnostic element.

The position or the intensity of the main absorption band of a carotenoid can be influenced by a number of factors such as a change in the molecular environment of the carotenoid molecule. The following terms are used to describe these effects:

bathochromic shift: displacement of λ_{max} to longer wavelength
hypsochromic shift: displacement of λ_{max} to shorter wavelength
hyperchromic effect: an effect which causes an increase in absorbance
hypochromic effect: an effect which causes a decrease in absorbance

3. Spectral fine structure

Because the overall shape or fine structure of the spectrum of a carotenoid conveys information about the structure of the chromophore, it is useful to compare spectra with respect to their shape as well as the positions of the absorption maxima. It is usually not convenient to present all spectra as diagrams, but a numerical notation, %III/II, describing fine structure, has proved useful [5]. In this notation, the base-line or zero value is taken as the minimum between the two peaks, the peak height of the longest-wavelength absorption band is designated as III, that of the middle absorption band (usually λ_{max}) as II (Fig. 1). Spectral fine structure is then expressed as the ratio of the peak heights III/II, as a percentage. In a few cases, notably ζ-carotene (**38**), III > II, so the value of %III/II may be slightly greater than 100. For conjugated ketocarotenoids such as canthaxanthin (**380**), which give a simple, rounded spectrum with no fine structure, neither peak heights III and II, nor a minimum between them, can be defined, so the %III/II value is 0.

An indication of the relationship between spectral fine structure and %III/II can be obtained from the spectra illustrated in Figures later in this Chapter. Thus β,β-carotene (**3**), lycopene (**31**) and β,ψ-carotene (**12**) give %III/II values of 25, 65, and 40, respectively (see Fig. 5) and lutein, in ethanol, gives a value of 60% (Fig. 7).

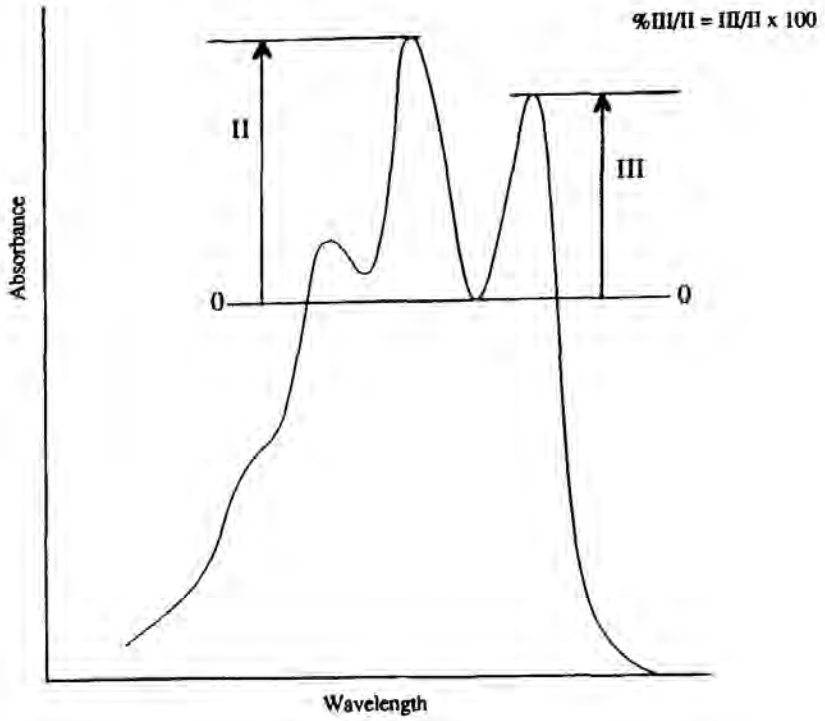


Fig. 1. Spectral fine structure. Calculation of %III/II for a carotenoid [5].

D. Relationship between Molecular Structure and Spectroscopic Properties

1. General principles

Almost all carotenoids absorb light in the 400 to 500 nm wavelength range. Differences between the spectra of individual carotenoids can be substantial, however, both in the positions of the λ_{max} and in the degree of vibrational fine structure. These differences, often subtle, are of vital importance in the identification and characterization of carotenoids. A thorough understanding of the relationships between molecular structure and light absorption properties of carotenoids is therefore essential. It is stressed strongly that the UV/Vis spectrum alone is not sufficient to characterize a carotenoid, but merely provides information about the chromophore. Most substituent groups do not affect the spectrum. Thus, as an

example, β,β-carotene (**3**) and its several hydroxy derivatives such as zeaxanthin (**119**) have the same chromophore and therefore identical spectra. Similarly the overall carbon skeleton of the carotenoid is not an important factor. Thus carotenoids with a C_{30} skeleton or a C_{50} skeleton have spectra similar to that of the conventional C_{40} carotenoid with the same chromophore, *e.g.* tunaxanthin (**149**, C_{40}) and decaprenoxanthin (**448**, C_{50}) have virtually identical spectra, as do neurosporene (**34**, C_{40}) and its C_{30} analogue 4,4'-diaponeurosporene (**515**).

Additional information about polarity and the presence of functional groups is needed before the constitution of a carotenoid can be established. Attention is drawn again to the recommended minimum criteria for identification listed in Chapter 9 and Vol. 1A, Chapter 5.

In the discussion that follows, the effects of various structural features on the absorption spectra of carotenoids are discussed. These effects are illustrated by well-known examples but they apply to any carotenoids with that structural feature. If the principles are understood and followed, it should be possible to deduce the probable chromophore of an unknown carotenoid by examination of its UV/Vis spectrum. The reader is strongly encouraged to take this approach rather than look through comprehensive tables of data in the hope of finding a match.

2. The chromophore

The structural feature which determines the spectral properties of the carotenoids is the chromophore of conjugated double bonds. As the length of the chromophore increases, it becomes easier to promote one of the bonding π-electrons to the excited state. The energy of the excited state and the energy required to bring about the transition are reduced, *i.e.* the absorption occurs at longer wavelength. This effect is illustrated nicely by the λ_{max} values, determined in hexane, for the series of all-*E* acyclic compounds with increasing number of conjugated double bonds (c.d.b.) (Table 1).

As the length of the chromophore increases, the effect of further increases on the λ_{max} becomes smaller. The extension by two double bonds on going from phytoene to phytofluene causes an increase of 62 nm in λ_{max}, whereas the increase by two double bonds from neurosporene to lycopene leads to an increase of only 30 nm. The theoretical maximum for a linear polyene of infinite length has been calculated to be only 608 nm [1].

The positioning of the lateral methyl groups relative to the chromophore does have a small effect on the spectrum. The λ_{max} of the 'symmetrical' and 'unsymmetrical' forms of ζ-carotene (tetrahydrolycopenes **38** and **37**, respectively) differ by approximately 5 nm. With the longer chromophore compounds spirilloxanthin (**166**) and 3,4-didehydrolycopene (**30**), which have a tridecaene chromophore located symmetrically and unsymmetrically, respectively, the difference in λ_{max} is smaller (Table 2).

Spectral fine structure is also affected as chain length increases. At first, the degree of fine structure, which is small for phytoene, increases through phytofluene and ζ-carotene and then decreases again as the chromophore is extended further.

Table 1. Absorption maxima (λ_{max}) for acyclic carotenoids with different lengths of the polyene chromophore.

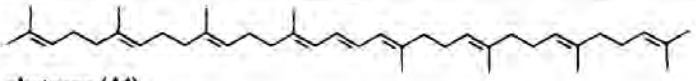
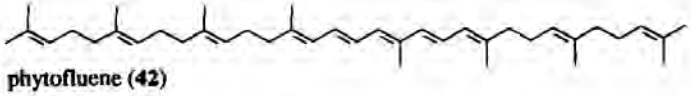
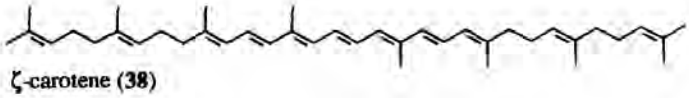
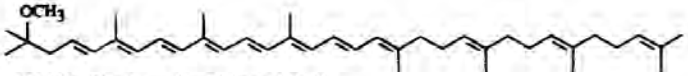
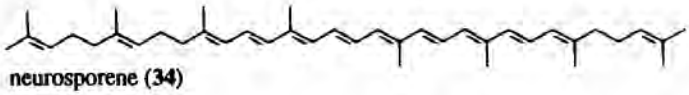
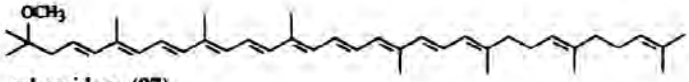
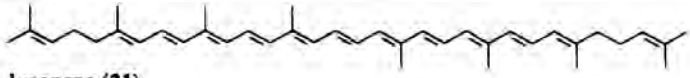
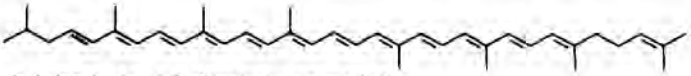
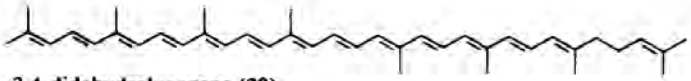
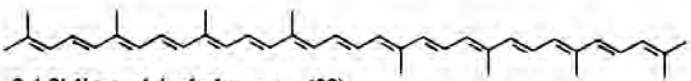
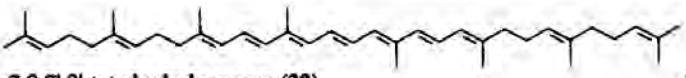
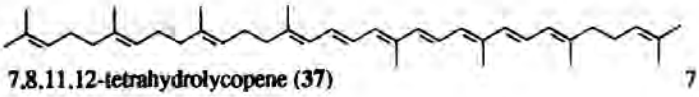
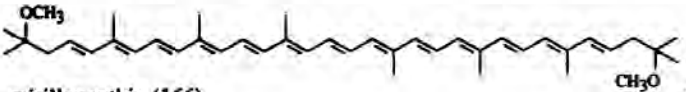
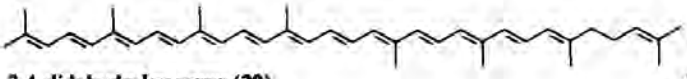
Carotenoid	c.d.b.	λ_{max} nm (hexane)		
 phytoene (**44**)	3	276	286	297
 phytofluene (**42**)	5	331	348	367
 ζ-carotene (**38**)	7	378	400	425
 11',12'-dihydrospheroidene (**101**)	8	392	413	439
 neurosporene (**34**)	9	415	440	468
 spheroidene (**97**)	10	427	454	486
 lycopene (**31**)	11	444	470	502
 3,4-didehydro-1,2-dihydrolycopene (**32**)	12	457	483	518
 3,4-didehydrolycopene (**30**)	13	465	492	527
 3,4,3',4'-tetradehydrolycopene (**29**)	15	480	510	540

Table 2. Comparison of λ_{max} values for acyclic carotenoids with symmetrically and unsymmetrically positioned chromophores.

Carotenoid	c.d.b.	λ_{max} nm (hexane)		
 7,8,7',8'-tetrahydrolycopene (38)	7	378	400	425
 7,8,11,12-tetrahydrolycopene (37)	7	374	395	420
 spirilloxanthin (166)	13	466	494	529
 3,4-didehydrolycopene (30)	13	465	492	527

3. Geometrical (*cis-trans*) isomers

The absorption spectra of most *cis* isomers are fairly similar to those of the all-*trans* isomer, but there are small differences that are seen consistently and are diagnostic for structural assignment [6]:

i) a small hypsochromic shift in λ_{max} (usually only 2 to 6 nm for mono-*cis*)
ii) a significant hypochromic effect
iii) a reduction in vibrational fine structure
iv) the appearance of a new absorption band, the *cis*-peak (B), at a characteristic position about 142 nm below the longest-wavelength absorption maximum (III) in the spectrum of the all-*trans* compound, when measured in hexane.

In the case of the biosynthetic intermediate phytoene (**44**), which has a chromophore of only 3 c.d.b. and absorbs in the UV region, a *cis*-peak is not seen for the 15*Z* isomer, which has λ_{max} only 1 nm to shorter wavelength then the all-*E* form, with reduced fine structure. As the length of the chromophore increases, differences of several nm are seen in the λ_{max} of different geometrical isomers.

The development of the *cis*-peak is illustrated by β,β-carotene (Fig. 2). For the all-*trans* form, the main absorption band ($1^1A_g \rightarrow 1^1B_u$) is very intense. When a peripheral double

bond becomes *cis* (the 9-*cis* isomer), the intensity of this main band decreases as a weak *cis*-band (the *cis*-peak) appears at 340 nm, corresponding to the transition to a higher energy level g state. The 15-*cis* isomer, in which the *cis* double bond is in the centre of the molecule, shows maximum bending of the chromophore and a well developed *cis*-band, with corresponding decrease in intensity of the main absorption band.

In practical terms, the intensity of the *cis*-band is greater as the *cis* double bond is nearer to the centre of the molecule. This provides an indication of the possible location of a *cis* double bond in a carotenoid molecule, but this empirical assignment must always be proved rigorously by NMR spectroscopy (Chapter 6).

A double *cis*-peak, *i.e.* with two maxima, is characteristic of an aliphatic or monocyclic chromophore. In a symmetrical di-*cis* carotenoid, the centre of symmetry may be restored, so that the *cis* band again becomes a weak feature.

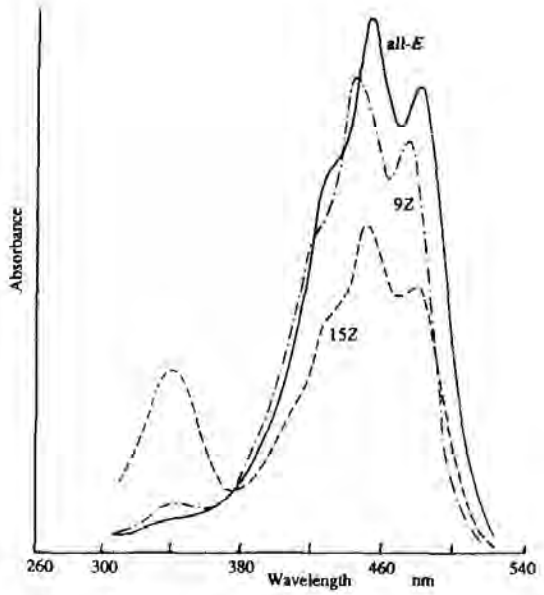


Fig. 2. Comparison of the absorption spectra of geometrical isomers of β,β-carotene, in hexane.

For di-*cis* and poly-*cis* carotenoids, a large hypsochromic shift in the main absorption band may be seen. Prolycopene (7Z,9Z,7'Z,9'Z-lycopene, **31**), for example, has λ_{max} at 414, 436, 463 nm, in contrast to 444, 470, 502 nm for all-*E*-lycopene, and the spectral fine structure is also greatly reduced (Fig. 3).

The relative intensity of a *cis*-peak can be designated by a numerical notation similar to the %III/II notation used to indicate spectral fine structure [5, 7]. The intensity or absorbance of the *cis*-peak (band B) is expressed as a percentage of the absorbance of the middle main absorption band, II, which is usually λ_{max}. The relative intensity of the *cis*-peak is expressed as $\%A_B/A_{II}$ or $\% D_B/D_{II}$ (Fig. 4).

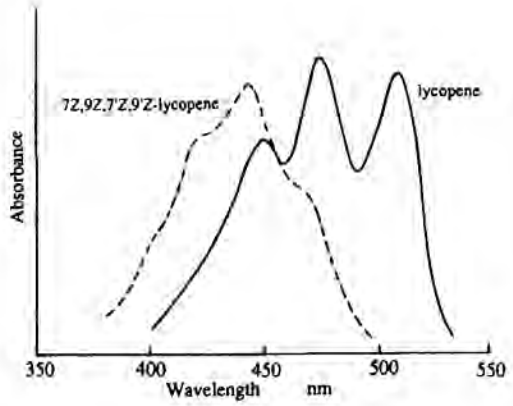


Fig. 3. Absorption spectra of lycopene (**31**) and its 7Z, 9Z, 7'Z, 9'Z isomer, prolycopene, in hexane.

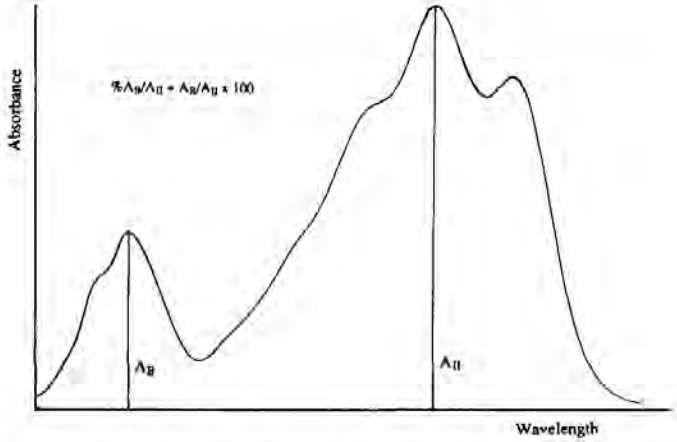


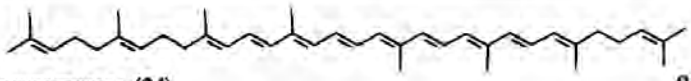
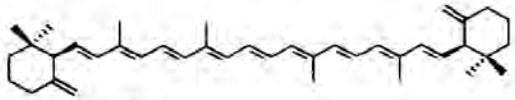
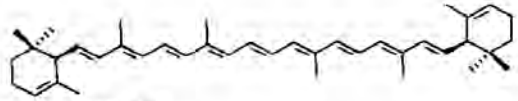
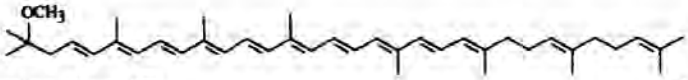
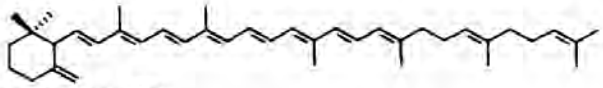
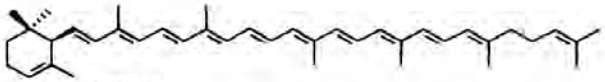
Fig. 4. Expression of the relative intensity of a *cis*-peak as $\%A_B/A_{II}$.

4. Cyclic end groups

a) γ Ring, ε ring.

In the γ and ε end groups, the ring double bond is isolated, *i.e.* is not conjugated with the main polyene chain. In γ,γ-carotene (**15**) and ε,ε-carotene (**20**), therefore, the chromophore is simply the central acyclic nonaene chain, and the spectra of these compounds are similar to that of the acyclic nonaene carotenoid, neurosporene (**34**). Slight differences (1 to 2 nm) may be seen because of the different disposition of the lateral methyl groups on the polyene chromophore. Similarly, a γ ring or an ε ring at one end of the molecule leaves a conjugated decaene chromophore. ε,ψ-Carotene (**21**), for example, has a spectrum similar to that of the acyclic decaene compound spheroidene (**97**) (Table 3).

Table 3. Effect of γ rings and ε rings on λ_{max} of carotenoids.

Carotenoid	c.d.b.	λ_{max} nm (hexane)		
 neurosporene (**34**)	9	415	440	468
 γ,γ-carotene (**15**)	9	414	439	468
 ε,ε-carotene (**20**)	9	416	440	470
 spheroidene (**97**)	10	427	454	486
 γ,ψ-carotene (**17**)	10	429	455	487
 ε,ψ-carotene (**21**)	10	421	456	489

b) β Ring

The effect of cyclization to form the β ring is illustrated in Fig. 5, which compares the spectra of lycopene (**31**), β,ψ-carotene (**12**), and β,β-carotene (**3**). All these compounds have a chromophore of nominally 11 conjugated double bonds, since the endocyclic C-5,6 double bond is formally in conjugation with the polyene chain. For the endocyclic C-5,6 double bond to be fully effective in the conjugated chromophore, it would have to adopt coplanarity with the main polyene chain. This is clearly not the case. Because of steric hindrance, particularly between the methyl substituent at C-5 of the ring and the hydrogen atom at C-8 of the chain, such coplanarity cannot be achieved and the molecule adopts a preferred conformation in which the ring and consequently the C-5,6 double bond are twisted

substantially out of plane (see Vol. 1A, Chapter 3). Orbital overlap is therefore considerably reduced and the contribution of the ring double bond to the effective chromophore is small (see Chapter 1). Two main effects on the spectra are apparent.

i) The degree of spectral fine structure is much reduced in the β-ring compounds.

ii) The λ_{max} of the β-ring carotenoids are at shorter wavelengths than those of the acyclic carotenoid with the same number of conjugated double bonds in the chromophore. A β-ring double bond increases the λ_{max} by only around 5 nm (Table 4).

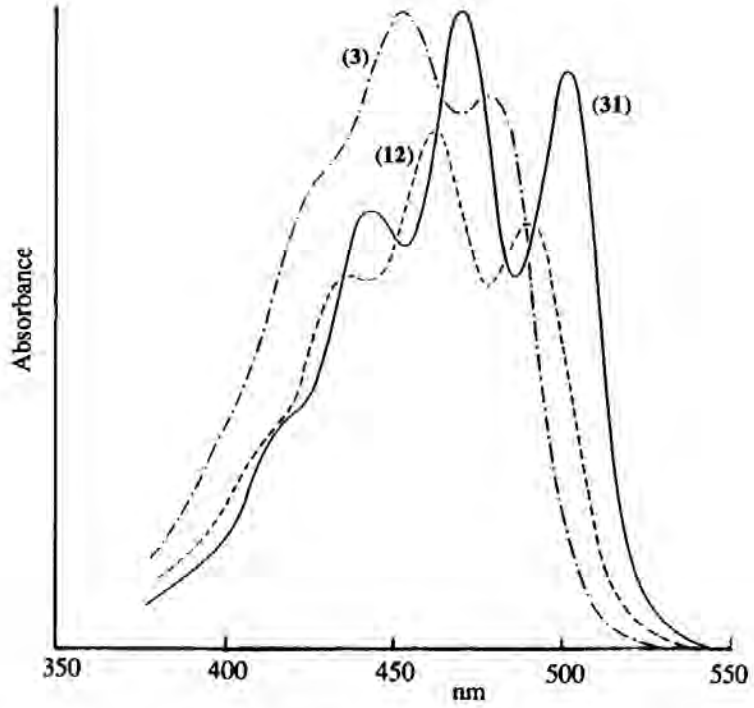


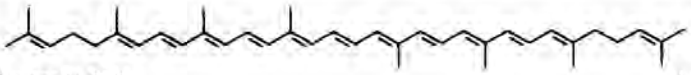
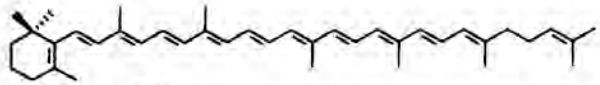
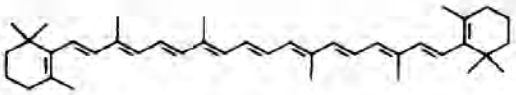
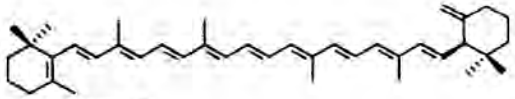
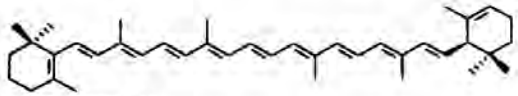
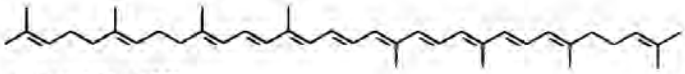
Fig. 5. Effect of β rings on λ_{max} and spectral fine structure: absorption spectra of β,β-carotene (3), β,ψ-carotene (21) and ψ,ψ-carotene (lycopene, 31), in hexane.

β,γ-Carotene (5) and β,ε-carotene (7), in which the double bond of the second ring does not constitute part of the chromophore, have a monocyclic chromophore (β ring plus 9 c.d.b.) and λ_{max} similar to those of a monocyclic compound with the same chromophore.

c) 3,4-Didehydro-β ring

An additional double bond in the 3,4-position of the β ring formally extends conjugation, and increases λ_{max} by about 10 nm, in hexane. Spectral fine structure is reduced (Table 5).

Table 4. Effect of β rings on λ_{max} of carotenoids.

Carotenoid	c.d.b.	λ_{max} nm (hexane)		
 lycopene (31)	11	444	470	502
 β,ψ-carotene (12)	β + 10	435	461	490
 β,β-carotene (3)	β + 9 + β	425	450	478
 β,γ-carotene (5)	β + 9	420	445	472
 β,ε-carotene (7)	β + 9	421	445	473
 neurosporene (34)	9	415	440	470

d) 2-Nor-β ring

Although the chromophore is formally the same, the main absorption maximum of 2,2'-dinor-zeaxanthin (*1*) is bathochromically shifted by 15 to 20 nm from that of zeaxanthin (β,β-carotene-3,3'-diol, **119**) itself (Table 6). This effect is attributed to the reduced steric crowding and greater planarity of the cyclopentene rings.

Table 5. Effect of 3,4-didehydro-β rings on λ_{max} of carotenoids.

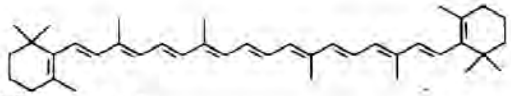
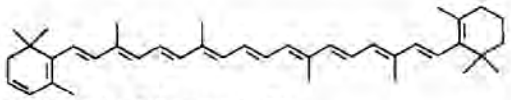
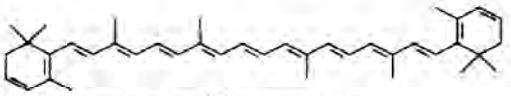
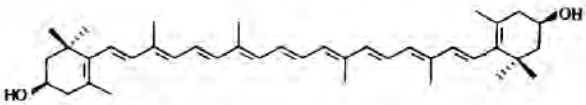
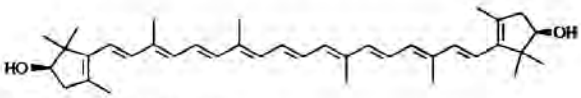
Carotenoid	λ_{max} nm (hexane)		
 β,β-carotene (3)	425	450	478
 3,4-didehydro-β,β-carotene (2)		461	
 3,4,3',4'-tetradehydro-β,β-carotene (1)		471	

Table 6. Comparison of λ_{max} of a β,β type carotenoid and its 2,2'-dinor derivative.

Carotenoid	λ_{max} nm (ethanol)		
 zeaxanthin (119)	425	450	478
 2,2'-dinor-zeaxanthin (1)	442	466	497

e) Aryl ϕ and χ rings

With the 1,2,5-trimethylphenyl (ϕ) end group, steric hindrance between the C-1 and C-5 methyl substituents and the C-8 hydrogen atom of the chain prevents the ring and chain from attaining coplanarity. The contribution of a ϕ end group to the spectrum is identical to that of a β ring. Thus chlorobactene (ϕ,ψ-carotene, **27**) and β,ψ-carotene (**12**) have almost identical spectra (Table 7).

In the 1,2,3-trimethylphenyl (χ) end group, steric hindrance by a C-5 methyl substituent is removed, and a higher degree of coplanarity is attained. The spectra of renierapurpurin (χ,χ-carotene, **28**) and lycopene (ψ,ψ-carotene, **31**) are similar (Table 7).

5. Acetylenic groups

Replacement of one of the double bonds of a polyene chromophore by an acetylenic group is expected to result in a spectral shift of 15 to 20 nm to shorter wavelength. This is found for the synthetic compounds 15,15'-didehydro-β,β-carotene (*2*) and 15,15'-didehydrolycopene (*3*), which have an acetylenic group in the centre of the chromophore (Table 8).

All the known naturally occurring acetylenic carotenoids, however, have cyclic end groups, and the triple bond is located in the 7,8-position. In the 7,8-didehydro-β end group, the steric strain normally imposed by interference between the C-5 methyl substituent and the C-8 hydrogen atom, which causes a reduction in λ_{max}, is no longer present. The two opposing effects on the spectrum balance, so the spectra of zeaxanthin (**119**) and its monoacetylenic and diacetylenic analogues diatoxanthin (**118**) and alloxanthin (**117**) are similar (Table 8).

Acetylenic (7,8-didehydro) derivatives of some arylcarotenes also occur naturally. The introduction of a triple bond at C-7,8 of the ϕ end group again leads to the relief of steric strain, and this balances the effect of the acetylenic group on the spectrum, *cf.* isorenieratene (**24**) and 7,8-didehydroisorenieratene (**23**). In the case of the χ end group, this steric strain would not exist, so the hypsochromic effect of the C-7,8 triple bond would be seen. Carotenoids of this structural type have not yet been isolated.

6. Allenic groups

Several natural xanthophylls, *e.g.* neoxanthin (**234**) and fucoxanthin (**369**), have an allenic group in the C-6,7,8 position. In an allene the π-orbitals of the two double bonds are perpendicular to each other. The C-7,8 double bond is coplanar with the polyene chain and forms a part of the chromophore. The C-6,7 double bond, however, is in a different plane and makes no contribution. Neoxanthin (**234**) therefore has a spectrum similar to that of a conjugated nonaene (as in violaxanthin, **259**), though at slightly shorter wavelengths and with slightly reduced fine structure (Table 9). An allenic group in any other part of the polyene chain would produce a carotenoid with two separate, perpendicular, shorter chromophores to the two sides of the allenic carbon atom.

Table 7. Effect of aryl end groups on λ_{max} of carotenoids.

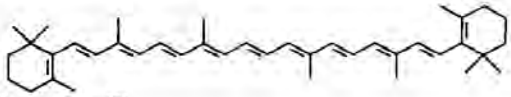
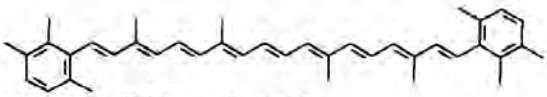
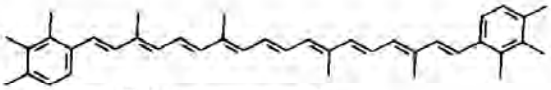
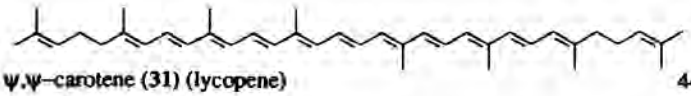
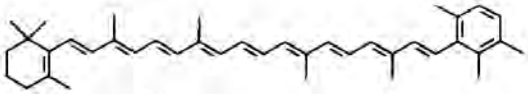
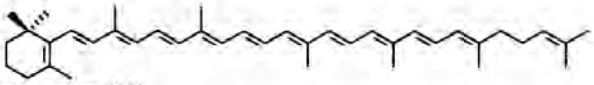
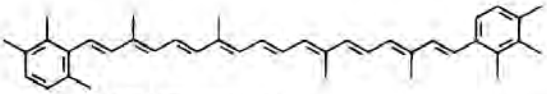
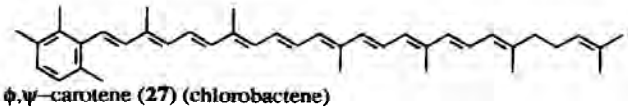
Carotenoid	λ_{max} nm (hexane)		
 β,β-carotene (3)	425	450	478
 ϕ,ϕ-carotene (24) (isorenieratene)	426	448	475
 χ,χ-carotene (28) (renierapurpurin)	442	468	500
 ψ,ψ–carotene (31) (lycopene)	444	470	502
 β,ϕ-carotene (9) (β-isorenieratene)	426	449	476
 β,ψ-carotene (12)	435	461	490
 ϕ,χ-carotene (26) (renieratene)	437	460	491
 ϕ,ψ–carotene (27) (chlorobactene)	435	461	491

Table 8. Effect of acetylenic groups on λ_{max} of carotenoids.

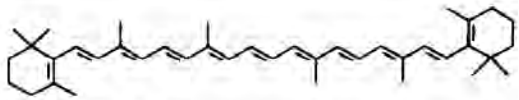
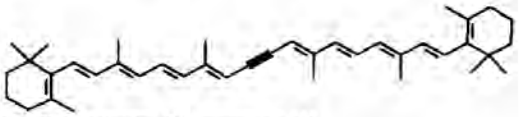
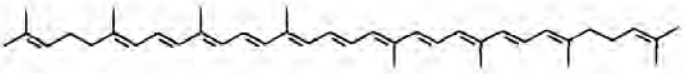
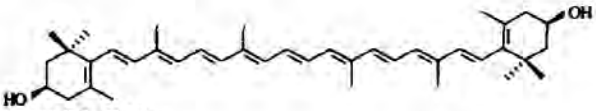
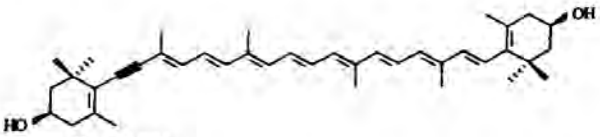
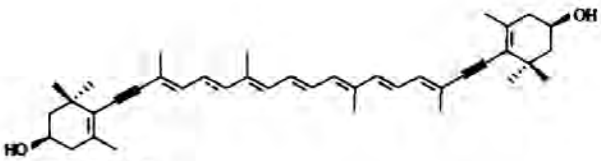
Carotenoid	λ_{max} nm (hexane or ethanol)		
 β,β-carotene (3)	425	450	478
 15,15'-didehydro-β,β-carotene (2)		431	458
 lycopene (31)	444	470	502
 15,15'-didehydrolycopene (3)		453	484
 zeaxanthin (119)	425	450	478
 diatoxanthin (118)	424	449	477
 alloxanthin (117)	424	450	479

Table 9. Effect of allenic groups on λ_{max} of carotenoids.

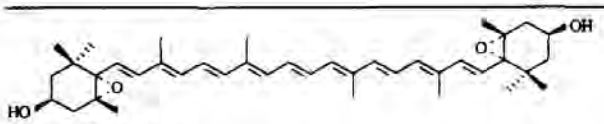
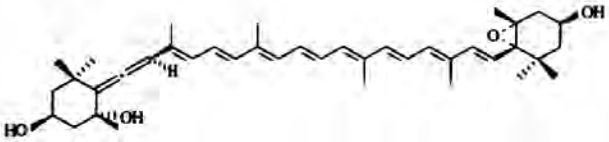
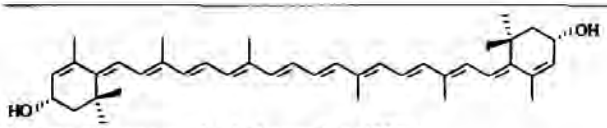
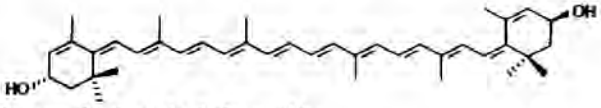
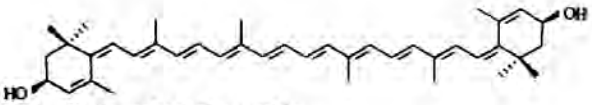
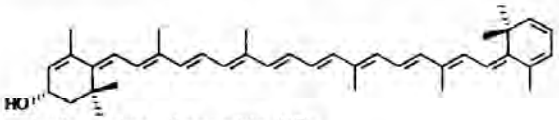
Carotenoid	λ_{max} nm (ethanol)		
 violaxanthin (**259**)	419	440	470
 neoxanthin (**234**)	415	439	467

Table 10. Comparison of λ_{max} values of some *retro*-carotenoids.

Carotenoid	λ_{max} nm (ethanol)		
 6-*trans*, 6'-*trans* -eschscholtzxanthin (**180**)	448	474	505
 6-*trans*, 6'-*cis*-eschscholtzxanthin	442	466	498
 6-*cis*, 6'-*cis*-eschscholtzxanthin	434	456	488
 anhydroeschscholtzxanthin (**47**)	474	497	530

7. *Retro*-carotenoids

An acyclic *retro*-carotenoid would simply exhibit a spectrum characteristic of the number of double bonds in the chromophore. In the known naturally occurring *retro*-carotenoids, the conjugated double-bond system extends into cyclic end groups. In *retro*-dehydro-β,β-carotene (**48**) and its 3,3'-dihydroxy derivative eschscholtzxanthin (**180**), the ring and chain are linked directly by a double bond at C-6,7. This reduces the flexibility of the molecule, so that the ring-chain conformation is more nearly planar. The spectra of these compounds, which formally have 12 conjugated double bonds, are similar in λ_{max} and fine structure to that of lycopene (**31**), which has an acyclic undecaene chromophore.

The 6-*cis* and 6-*trans* isomers of these *retro*-compounds are stable and can be isolated. The λ_{max} of the 6,6'-di-*cis* compounds are about 20 nm lower than those of the 6,6'-di-*trans* form. An additional C-2,3 double bond in the ring, as in anhydroeschscholtzxanthin (**47**), extends the chromophore, and λ_{max} occur at longer wavelength (Table 10).

8. Carbonyl groups

An isolated carbonyl group which is not in conjugation with the main chromophore generally makes no contribution to the spectrum of a carotenoid. A carbonyl group in conjugation with the main polyene chain of a carotenoid formally extends the chromophore. This results in a spectral shift to longer wavelength, usually accompanied by loss of spectral fine structure.

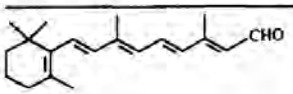
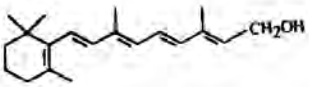
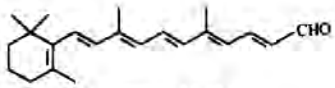
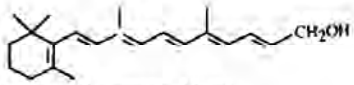
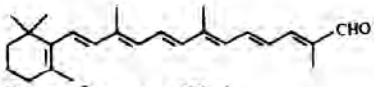
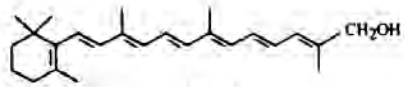
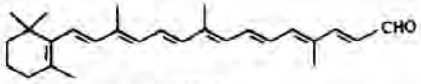
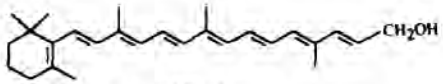
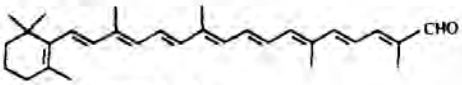
When determined in ethanol, the spectra of most carotenoids containing carbonyl groups have virtually no fine structure and exhibit only a single, broad, rounded peak, from which λ_{max} is difficult to determine accurately. In some non-polar solvents, especially petrol or hexane, some spectral fine structure may be retained. Peridinin (**558**) provides a particularly striking example of this effect.

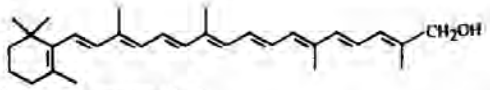
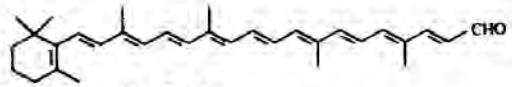
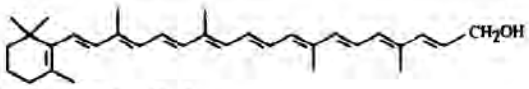
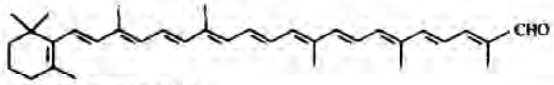
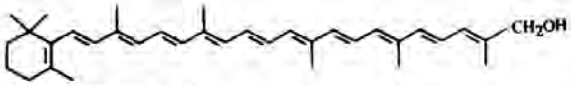
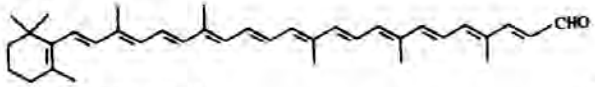
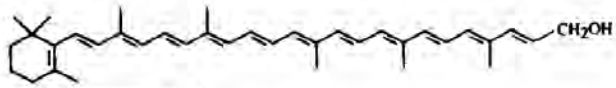
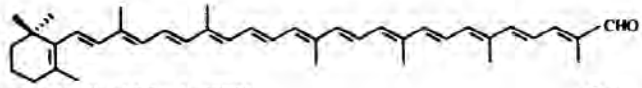
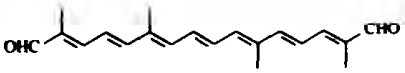
a) Aldehydes

A terminal conjugated aldehyde group effectively extends the chromophore and leads to an increase in λ_{max} of 25 to 30 nm. This effect is illustrated well by comparing the λ_{max} of an apocarotenal and the corresponding apocarotenol. The increase is greater for shorter chain compounds (Table 11). The short-chain monoaldehydes generally show considerable spectral fine structure, but the fine structure decreases as the chain length increases. The C_{20} acyclic dialdehyde crocetindial (**536**) exhibits very pronounced fine structure (%III/II = 118).

The cross-conjugated side-chain aldehyde group in rhodopin-20-al (**277**) and related compounds has a similar effect to a terminal aldehyde group, and causes an increase of about 28 nm in λ_{max} compared with the corresponding alcohol.

Table 11. Effect of aldehyde groups on λ_{max} of carotenoids.

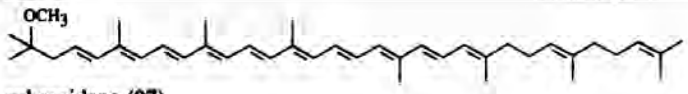
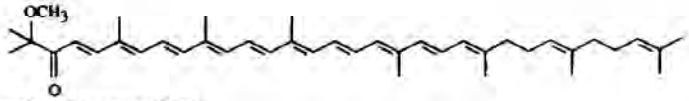
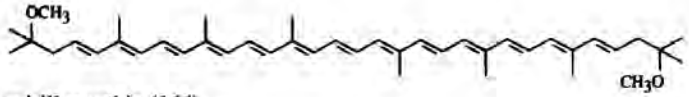
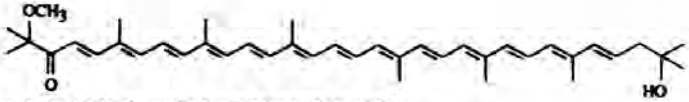
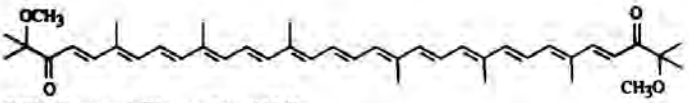
Compound	chain	c.d.b.	λ_{max} nm (ethanol)		
 retinal	C_{20}	4		370	
 retinol				326	
 14'-apo-β-caroten-14'-al	C_{22}	5		392	
 14'-apo-β-caroten-14'-ol			340	355	375
 12'-apo-β-caroten-12'-al	C_{25}	6		413	
 12'-apo-β-caroten-12'-ol			358	380	408
 10'-apo-β-caroten-10'-al	C_{27}	7		434	
 10'-apo-β-caroten-10'-ol			386	408	432
 8'-apo-β-caroten-8'-al	C_{30}	8		452	

Compound	chain	c.d.b.	λ_{max} nm (ethanol)		
 8'-apo-β-caroten-8'-ol	C_{30}	8	405	430	460
 6'-apo-β-caroten-6'-al	C_{32}	9		473	
 6'-apo-β-caroten-6'-ol			422	446	474
 4'-apo-β-caroten-4'-al	C_{35}	10		485	
 4'-apo-β-caroten-4'-ol			436	462	491
 2'-apo-β-caroten-2'-al	C_{37}	11		498	
 2'-apo-β-caroten-2'-ol			447	473	503
 torularhodinaldehyde (271)	C_{40}	12		507	
 torularhodinol			454	484	514
 crocetindial (536)	C_{20}	7	410	433	459

b) Acyclic ketones

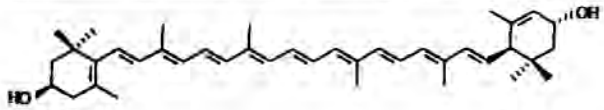
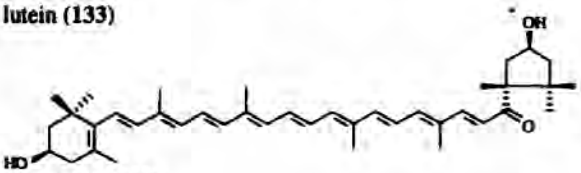
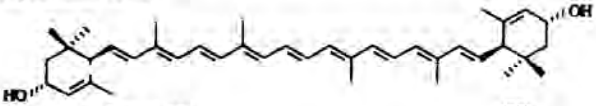
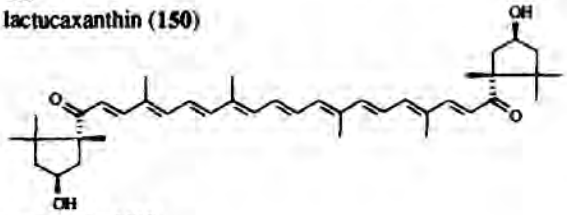
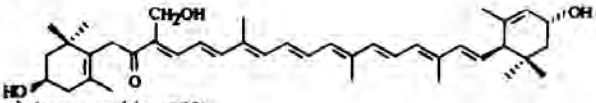
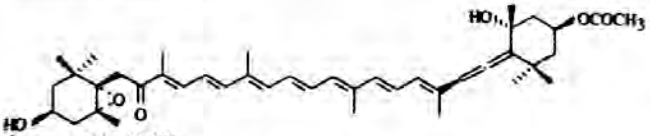
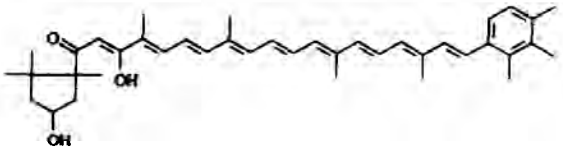
Extension of an acyclic chromophore by a conjugated keto group increases λ_{max} by about 30 nm, *e.g.* spheroidene (**97**) and spheroidenone (**319**). The increase in λ_{max} becomes smaller as the length of the conjugated polyene chain increases. The effect of a second conjugated keto group is also smaller, *cf.* spirilloxanthin (**166**) and the related 2-keto and 2,2'-diketo compounds **342** and **416** (Table 12).

Table 12. Effect of keto groups on λ_{max} of acyclic carotenoids.

Carotenoid	λ_{max} nm (hexane)		
 spheroidene (**97**)	429	454	486
 spheroidenone (**319**)	(460)	485	(515)
 spirilloxanthin (**166**)	465	491	526
 2-keto-1'-O-demethylspirilloxanthin (**342**)	488	516	550
 2,2'-diketospirilloxanthin (**416**)	498	528	560

A similar effect is seen with carotenoids that have cyclic end groups but, in the linear part of the molecule, contain a conjugated keto group which forms part of the chromophore. The effect of one or two keto groups at C-6 (C-6') in the carotenoids with ε end groups is illustrated by comparing the spectra of capsanthin (**335**) and capsorubin (**413**) with those of lutein (**133**) and lactucaxanthin (**150**), respectively (Table 13).

Table 13. Effect of keto groups on λ_{max} of dicyclic carotenoids: (a) keto group located in the acyclic polyene chain.

Carotenoid	position of keto group	λ_{max} nm (ethanol)		
 lutein (133)	-	422	445	474
 capsanthin (335)	C-6'		476	
 lactucaxanthin (150)	-	419	440	470
 capsorubin (413)	C-6, C-6'		481	
 siphonaxanthin (350)	C-8		453	
 fucoxanthin (369)	C-8	426	449	475
 trikentriorhodin (341)	C-6		473	

Similar extension of the chromophore and increase in λ_{max} is seen with cyclic carotenoids that contain a conjugated keto group at C-8, *e.g.* siphonaxanthin (**350**) and fucoxanthin (**369**). In more complicated cases, *e.g.* trikentriorhodin (**341**), the presence of a keto group at C-8 and a hydroxy group at C-6 produces a β-hydroxyketone structure, and internal hydrogen bonding significantly alters the spectrum (Table 13).

c) Secocarotenoids

In the secocarotenoids, only the C-6 keto group that is in conjugation with the polyene chain has an effect on the spectrum. Thus semi-β-carotenone (**559**) has λ_{max} at 487 nm (in hexane), an increase of 40 nm from that of a simple chromophore of 9 acyclic conjugated double bonds plus one β ring. A second 5,6-seco-β end group, *i.e.* a second conjugated keto group, has a much smaller effect; β-carotenone (**562**) has λ_{max} at approximately 490 nm.

d) Cyclic ketones

The presence of a conjugated keto group at C-4 of a β ring increases λ_{max} by approximately 10 nm, the actual value being somewhat dependent on solvent. The effect of a second 4-keto-β ring is approximately the same as the first (Fig. 6).

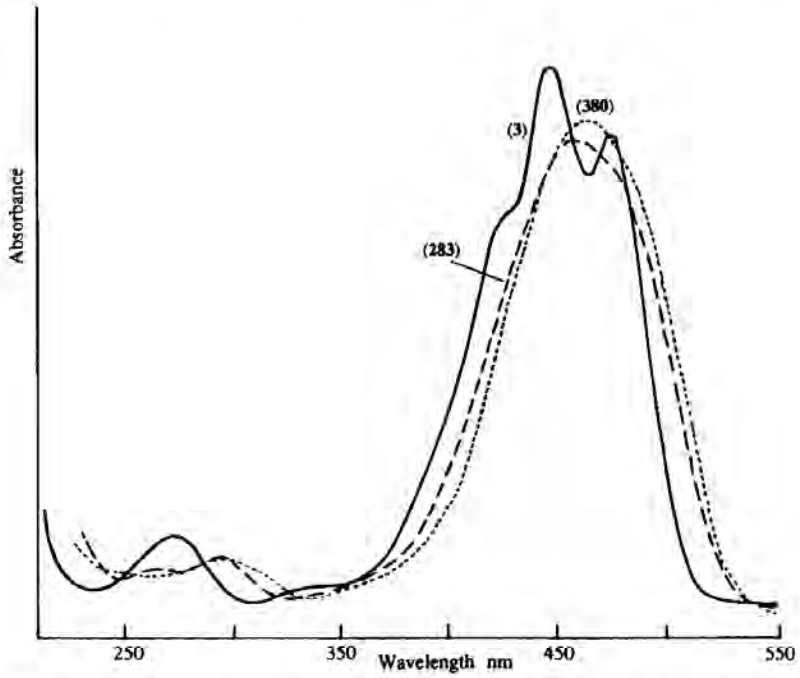
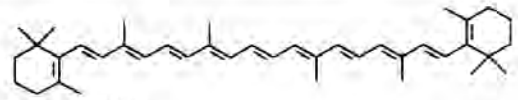
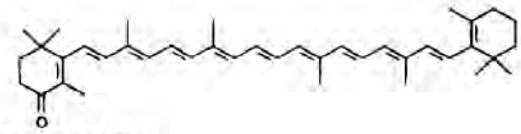
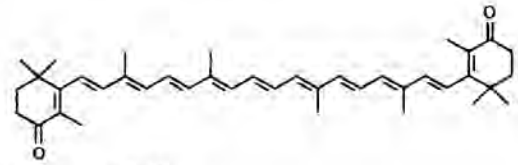
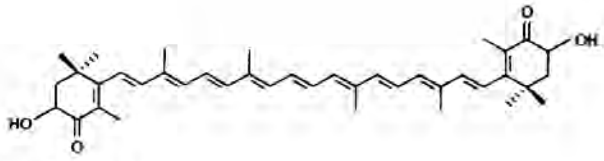
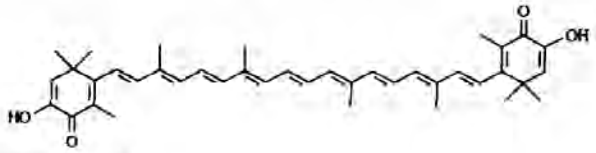
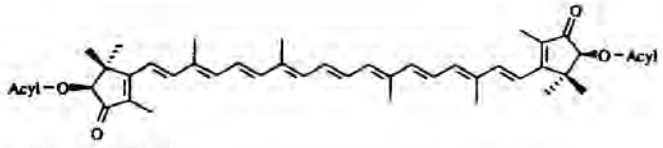
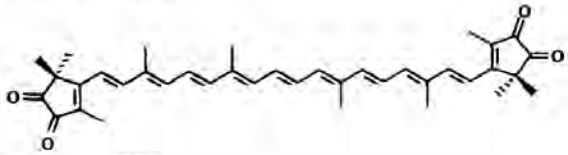
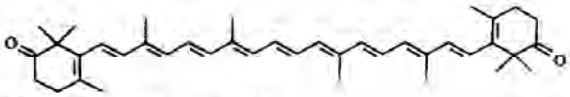
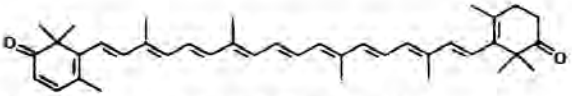
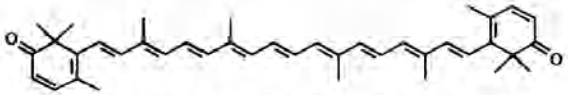
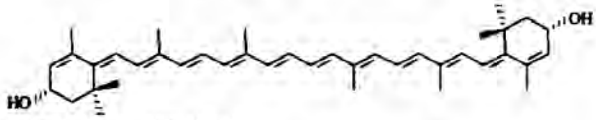
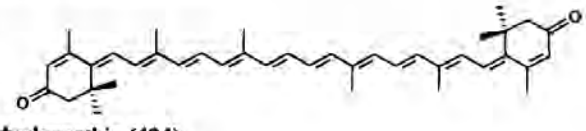


Fig. 6. Effect of conjugated keto groups on the absorption spectra of β-ring carotenoids: (a) β,β-carotene (**3**), (b) echinenone (**283**), (c) canthaxanthin (**380**), in ethanol.

Table 14. Effect of keto groups on λ_{max} of dicyclic carotenoids: (b) keto group located in the cyclic end group.

Carotenoid	λ_{max} nm (ethanol or hexane)		
 β,β-carotene (3)	425	450	478
 echinenone (283)		461	
 canthaxanthin (380)		474	
 astaxanthin (403)		478	
 astacene (398)		478	

Carotenoid	λ_{max} nm (ethanol or hexane)		
 actinioerythrin (**552**)		497	
 violerythrin (**553**)		562	
 β,β-carotene-2,2'-dione (**379**)	425	450	478
 3,4-didehydro-β,β-carotene-2,2'-dione (**378**)		472	
 3,4,3',4'-tetradehydro-β,β-carotene-2,2'-dione (**377**)		490	
 eschscholtzxanthin (**180**)	448	474	505
 rhodoxanthin (**424**)		490	520

The additional C-2,3 double bond in the diosphenol end groups of astacene (**398**) makes little spectral contribution, so the spectra of astaxanthin (**406**) and astacene are similar. The corresponding five-membered ring 2-nor derivatives, however, exist exclusively in the 3,4-diketo form, and absorb at very long wavelengths, *e.g.* violerythrin (**553**) at 556 nm (in acetone) (Table 14).

A keto group at C-2 of a β ring is not conjugated and therefore has no effect on the absorption spectrum (*cf.* β,β-carotene, **3** and β,β-carotene-2,2'-dione, **379**). An additional double bond at C-3,4 renders the keto group in conjugation with the extended polyene system. 3,4,3',4'-Tetradehydro-β,β-carotene-2,2'-dione (**377**) absorbs at much longer wavelength (Table 14).

The addition of a conjugated keto group in the ring of a *retro*-carotenoid also leads to an increase in λ_{max} and reduction in fine structure, *cf.* rhodoxanthin (**424**) and eschscholtzxanthin (**180**) (Table 14).

e) Carboxylic acids and esters

The bathochromic effect of a carboxylic acid group or its ester is smaller than that of an aldehyde, as illustrated by torularhodin (**428**) and its methyl ester in comparison with torularhodinaldehyde (**271**) and the parent hydrocarbon torulene (**11**). As expected, with carotenoid dicarboxylic acids and their esters, *e.g.* crocetin (**538**) and bixin (**533**), the further extension of the chromophore causes a large increase in λ_{max} (Table 15).

The lactone (olide) group in carotenoids such as peridinin (**558**) and pyrrhoxanthin (**556**), formally a cross-conjugated system, also causes a substantial increase in λ_{max} and decrease in fine structure (Table 15).

9. Other functional groups

a) Hydroxy groups

Functional groups and other structural modifications which do not change the chromophore of the molecule do not have any effect on the spectrum. Thus β,β-carotene (**3**) and its many derivatives that contain one or more hydroxy groups in the 2, 3 or 4 positions all have virtually identical spectra (Table 16). It is therefore not possible to distinguish between positional isomers such as zeaxanthin (**119**), isozeaxanthin (**129**) and β,β-carotene-2,2'-diol (**113-115**) from their UV/Vis spectra alone.

In neutral conditions, the phenolic hydroxy groups in dihydroxyisorenieratene (**161**) have little effect on the spectrum but, in basic conditions, ionization causes a substantial bathochromic shift.

Table 15. Effect of carboxylic groups and their esters on λ_{max} of carotenoids.

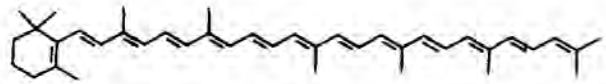
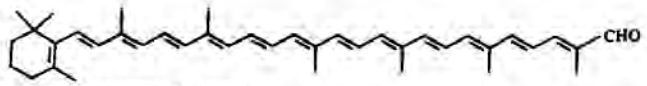
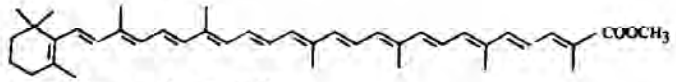
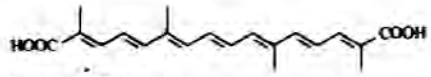
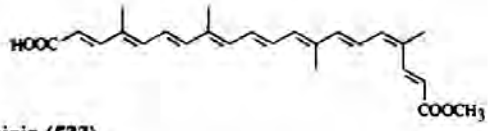
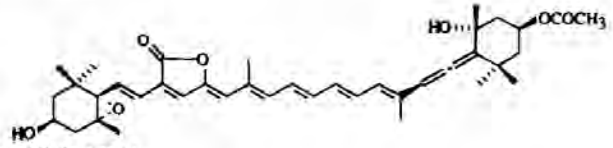
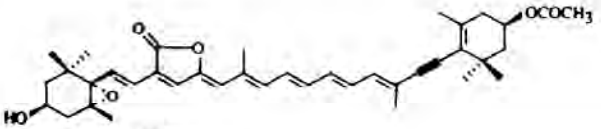
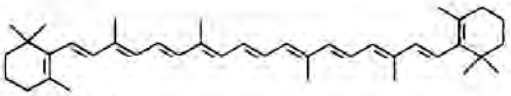
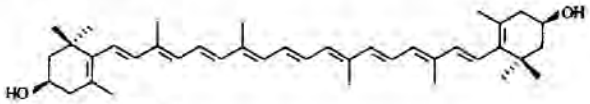
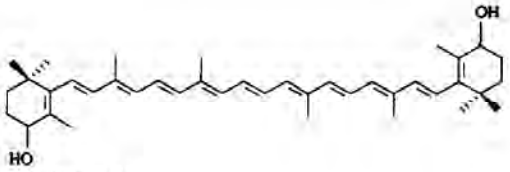
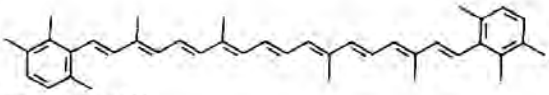
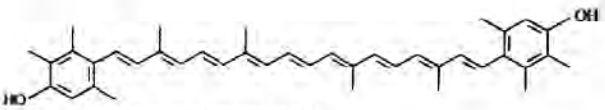
Carotenoid	λ_{max} nm (hexane or ethanol)		
 torulene (11)	451	485	517
 torularhodinaldehyde (271)		505	535
 torularhodin (428)		491	523
 torularhodin methyl ester (429)	469	495	525
 crocetin (538)	401	423	447
 bixin (533)	433	457	490
 peridinin (558)		455	485
 pyrrhoxanthin (556)		459	488

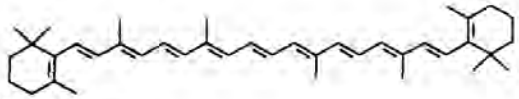
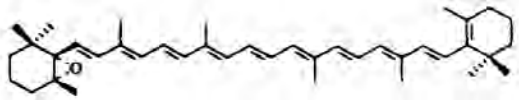
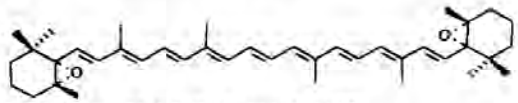
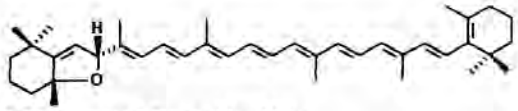
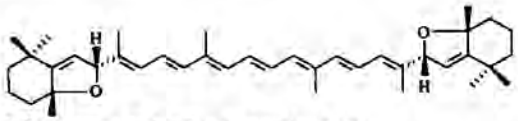
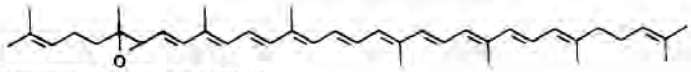
Table 16. Effect of hydroxy groups on λ_{max} of carotenoids.

Carotenoid	λ_{max} nm (ethanol)		
 β,β-carotene (3)	425	450	478
 zeaxanthin (119)	425	450	478
 isozeaxanthin (124)	425	450	478
 isorenieratene (24)	426	448	475
 3,3'-dihydroxyisorenieratene (161)	427	449	476

b) Epoxide groups

The addition of an epoxy group to a double bond removes that double bond from the chromophore. The 5,6-epoxide of lycopene (**222**) therefore has a spectrum like that of the decaene-chromophore carotenoid spheroidene (**97**), and the 5,6:5',6'-diepoxide of β,β-carotene has a simple linear nonaene chromophore and a spectrum close to that of ε,ε-carotene (**20**) (Table 17).

Table 17. Effect of epoxy groups on λ_{max} of carotenoids.

Carotenoid	λ_{max} nm (ethanol)		
 β,β-carotene (3)	425	450	478
 β,β-carotene-5,6-epoxide (213)	423	445	474
 β,β-carotene-5,6:5',6'-diepoxide (257)	417	440	468
 β,β-carotene-5,8-epoxide (239)	407	428	452
 β,β-carotene-5,8:5',8'-diepoxide (265)	380	400	425
 lycopene (31)	444	470	502
 lycopene-5,6-epoxide (222)	428	455	487

The corresponding 5,8-epoxides (furanoids) of β-ring carotenoids have even shorter chromophores. β,β-Carotene-5,8:5',8'-diepoxide has the characteristic spectrum of a heptaene (Table 17).

In the acyclic 1,2-epoxides, such as lycopene-1,2-epoxide (**217**) and the cyclic 3,6-epoxides such as cycloviolaxanthin (**259.2**), the presence of the epoxide group does not alter the chromophore and therefore has no effect on the spectrum.

Epoxidation of a double bond in the polyene chain breaks the conjugation at that position. In-chain epoxides therefore have two separated chromophores and show the characteristic absorption of both parts.

E. Effects of Molecular Environment

1. Effect of different solvents

The energy of the $1^1A_g \rightarrow 1^1B_u$ transition that gives rise to the main absorption band of carotenoids is dependent on the refractive index of the solvent. The spectral shift depends on the polarizability rather than the polarity of the solvent, and the frequency shifts to lower energy, *i.e.* a spectral shift to longer wavelength, as the refractive index of the solvent increases.

In practical terms, this means that λ_{max} values for any carotenoid are similar in petrol, hexane, diethyl ether, ethanol, methanol and acetonitrile. In other solvents, a pronounced and consistent bathochromic shift may be seen (Table 18).

Table 18. *Bathochromic effect of different solvents on λ_{max} of carotenoids.*

Solvent	Approx. bathochromic shift (nm)
hexane	0
light petroleum	0
ethanol	0
diethyl ether	0
acetonitrile	0
acetone	2-6
chloroform	10-20
dichloromethane	10-20
benzene	18-24
toluene	18-24
pyridine	18-24
carbon disulphide	30-40

For identification of a carotenoid chromophore, the spectra (λ_{max} and fine structure) of unknown and standard must be shown to be identical to each other in at least two different solvents.

Because of these solvent effects, care must be exercised when deducing structural information about a carotenoid from its absorption spectrum determined on-line during HPLC, especially if dichloromethane or any other solvent that causes a bathochromic shift is a component of the mobile phase.

2. Effect of water

Water can have a major effect on the spectra of carotenoids in water-miscible solvents. When the water content is high (30 to 50% in most cases), a marked decrease is seen in the intensity of the usual main absorption band as this is replaced by a new, intense peak, usually in the near UV region *e.g.* at 354 nm for lycopene (**31**), 370 nm for lutein (**133**), 380 nm for zeaxanthin (**119**), and 401 nm for violaxanthin (**259**). This peak is usually comparatively narrow and displays no fine structure (Fig. 7).

The new main absorption band may be accompanied by another, weak band at longer wavelength (*e.g. ca.* 520 nm for lutein). The effect is attributed to exciton interactions between closely adjacent chromophores as the hydrophobic carotenoid molecules aggregate in the presence of water.

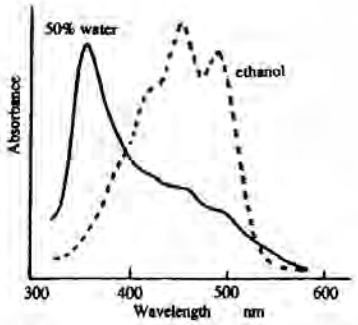


Fig. 7. Effect of high concentrations of water on the absorption spectrum of lutein (**133**) in ethanol.

3. Effect of protein

When carotenoids are associated with lipoproteins, the carotenoid is normally located in a lipid environment. Even in an aqueous medium the carotenoid spectrum is not greatly changed from that in organic solution; a small bathochromic shift of *ca.* 10 nm is common.

Specific interactions with protein, such as occur in the blue or purple carotenoproteins (Vol. 1A, Chapter 7, Example 12), cause a very large bathochromic shift in λ_{max} (up to *ca.* 150 nm), usually with no alteration in the spectral bandwidth or fine structure (Fig. 8).

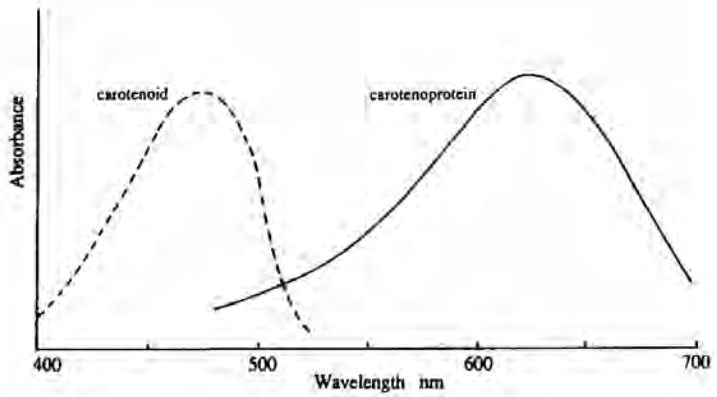


Fig. 8. Absorption spectra of astaxanthin and its complex with protein, α-crustacyanin, in phosphate buffer, pH 7.

4. Spectra at low temperature

The appearance of the UV/Vis spectrum of a carotenoid can change substantially at low temperature, when conformational interconversions become frozen and the molecule exists in one preferred conformation. The low-temperature spectra of a number of carotenoids, including β,β-carotene (**3**), lycopene (**31**), echinenone (**283**) and canthaxanthin (**380**) in EPA (*i.e.* diethyl ether/isopentane/ethanol, 5:5:2) have been recorded [7]. Two major effects are seen on cooling, namely a bathochromic shift, usually of 10 to 40 nm, and an increase in spectral fine structure, often with the appearance of new absorption bands. The total area under the spectral curve does not change significantly.

The changes seen are particularly noticeable for the carotenoids containing conjugated carbonyl groups. Thus, at 77°K, rhodopin-20-al (**277**), which at room temperature shows no spectral fine structure, has a three-banded spectrum similar in shape to the room-temperature spectrum of rhodopin (**93**) and lycopene (**31**) (Fig. 9) [8].

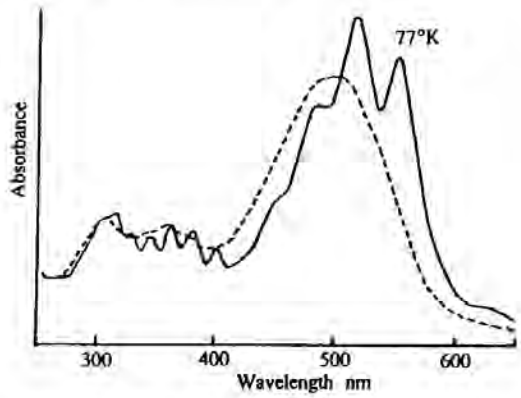


Fig. 9. Absorption spectra of rhodopin-20-al (**277**) at 25°C and at 77°K, in EPA [7, 8].

F. Tests for Functional Groups on a Spectroscopic Scale

Some tests for particular functional groups in a carotenoid are conveniently carried out in a spectrophotometer cuvette and monitored for diagnostic changes in the spectrum. The two must useful tests are those for 5,6-epoxides and for aldehyde and keto groups. Details of the reactions are given in Vol. 1A, Chapter 4.

Test for carotenoid 5,6-epoxides
The spectrum of the carotenoid is determined, in ethanol. One drop of dilute acid, *e.g.* 0.1*M* HCl, is added and the spectrum is determined again. Carotenoids with one 5,6-epoxy group show a hypsochromic shift of 20 nm, those with two such groups a shift of 40 nm.

Test for aldehydes or ketones
The spectrum of the carotenoid is determined, in ethanol. A small amount of solid sodium borohydride is added and the spectrum is determined again after 30 s, 5 min and 30 min. Reduction of a conjugated carbonyl group to the corresponding alcohol results in a hypsochromic shift of 15 to 30 nm and an increase in fine structure. Aldehydes react rapidly (usually within 30 s) whereas ketones may take 20 to 30 min for complete reduction.

G. Tables of Absorption Maxima

Values for λ_{max} for some of the most frequently encountered carotenoids, determined in a variety of solvents, are given in Table 19. In most cases the data have been extracted from the extensive tables that are given in several review articles [2-4, 9, 10], or have been determined in the author's laboratory. References to UV/Vis data for all known naturally occurring carotenoids are given in the *Key to Carotenoids* [11] and in Vol. 1A, Chapter 8.

It is common to see, in different publications, variations of 2 to 3 nm in λ_{max} for the same carotenoid in the same solvent, especially when the lack of fine structure makes the accurate estimation of λ_{max} difficult. Also, in many publications, no indication of fine structure is given. It is therefore emphasized again that it is dangerous simply to rely on matching recorded spectra with tabulated data without a thorough understanding of the relationships between structure and light absorption properties. Whenever possible, the spectrum of the compound under investigation should be compared directly with that of an authentic standard determined under the same conditions and in approximately the same concentration. Spectra of unknown and standard should be identical in both λ_{max} and fine structure, in at least two different solvents.

In publications, when UV/Vis data for carotenoids are reported, it is highly desirable to indicate fine structure, as %III/II, as well as giving λ_{max} values.

Table 19. UV/Vis spectroscopic data for a range of carotenoids. Solvents: A, acetone; B, benzene; C, chloroform; Et_2O, diethyl ether; EtOH, ethanol; H, hexane; P, light petroleum (b.p. 40-60°C); Pyr, pyridine.

Carotenoid	λ_{max} nm			%III/II	Solvent
Actinioerythrin (**552**)	480	508	538		A
	470	496	529		P
Adonirubin (**391**)		479		0	C
		478		0	EtOH
		466		0	H
Adonixanthin (**328**)		465		0	EtOH
		460		0	P
[Similar spectrum: idoxanthin (**349**)]					
Aleuriaxanthin (**81**)	440	463	493		A
	434	460	491		P
Alloxanthin (**117**)	430	453	483		A
	438	463	493		B
	436	460	489		C
	427	450	478	30	EtOH
	423	450	479	32	H, P
Anhydrorhodovibrin (**91**)	459	488	522		A
	471	499	533		B, C
	454	483	514	68	EtOH
	454	482	515		P
[Similar spectrum: rhodovibrin (**167**)]					
Antheraxanthin (**231**)	430	456	484		C
	422	444	472	55	EtOH
	422	445	472	60	H, P

[Similar spectrum: β,β-carotene-5,6-epoxide (**213**); β-cryptoxanthin-5,6-epoxide (**224**)]

Table 19. continued

Carotenoid	λ_{max} nm			%III/II	Solvent
Astacene (398)		482		0	A
		494		0	C
		478		0	EtOH
		473		0	P
Astaxanthin (404-406)		480		0	A
		485		0	B, C
		478		0	EtOH
		468		0	P
Auroxanthin (267-270)	381	402	427	101	A
	385	413	438		C
	380	400	425	102	EtOH, P
[Similar spectrum: aurochrome (265)]					
Azafrin (504)		426	447		C
	385	408	431		EtOH
		409			P
Bacterioruberin (456)	468	498	532		A
	475	506	544		C
	464	494	528		P
[Similar spectrum: bisanhydrobacterioruberin (453)]					
Bixin (533)	433	470	502		C
	429	457	484		EtOH
	432	456	490		P
Canthaxanthin (380)		484		0	B
		482		0	C
		474		0	EtOH
		466		0	P
Capsanthin (335)	460	483	518		B
		476			EtOH
	450	475	505		P

Table 19. continued

Carotenoid	λ_{max} nm			%III/II	Solvent
Capsorubin (413)	460	489	523		B
	445	479	510		P
β,β-Carotene (3)	429	452	478	15	A
	435	462	487		B
	435	461	485		C
		450	476	25	EtOH
	425	450	477	25	H, P
β,ε-Carotene (7)	424	448	476	55	A
	432	456	485		B
	433	457	484		C
	423	444	473		EtOH
	422	445	473	55	H, P
[Similar spectrum: β,γ-carotene (5)]					
β,ψ-Carotene (12)	439	461	491		A
	447	447	510		B
	446	475	509		C
	440	460	489	35	EtOH
	437	462	494	40	H, P
ε,ε-Carotene (20)	425	451	482		B
	417	440	470	85	EtOH
	416	440	470	90	P
[Similar spectrum: γ,γ-carotene (15)]					
ε,ψ-Carotene (21)	440	470	503		C
	431	456	489	85	P
ζ-Carotene (38)	377	399	425		EtOH
(7,8,7',8'-tetrahydrolycopene)	378	400	425	103	H, P
ζ-Carotene ('unsymmetrical') (37) (7,8,11,12-tetrahydrolycopene)	374	395	420	95	H, P

Table 19. continued

Carotenoid	λ_{max} nm			%III/II	Solvent
β-Carotenone (562)	453	486	522		B
	460	490	522		C
	448	480	512	5	EtOH
Chlorobactene (27)	450	476	508		B
	435	461	491	40	P
Chrysanthemaxanthin/		432	461		B
flavoxanthin (249, 248)		430	459		C
	400	421	448	75	EtOH
		421	450		P
Crocetin (538)	413	435	462		C
	401	423	447		EtOH
	400	422	450		P
Crocetindial (536)	422	445	473		B
	408	430	458	115	P
Crocoxanthin (59)	432	458	488		B
	430	454	482		C
	423	447	477	65	EtOH
	422	445	475	70	H
[*Similar spectrum: monadoxanthin* (132)]					
α-Cryptoxanthin/zeinoxanthin (60, 62)	433	459	488		B
	435	459	487		C
	423	446	473	60	EtOH
	421	445	475	60	H
β-Cryptoxanthin (55)	435	463	489		B
	435	459	485		C
	428	450	478	27	EtOH
	425	449	476	25	P
[Similar spectrum: β,β-carotene-2-ol (51, 52); isocryptoxanthin (57)]					

Table 19. continued

Carotenoid	λ_{max} nm			%III/II	Solvent
Diadinoxanthin (**230**)	428	449	479	70	A
	432	455	482		C
	424	445	474	60	EtOH
	421	445	475	60	H
Diatoxanthin (**118**)	432	454	481	30	A
		463	492		B
	433	458	486		C
	425	449	475	25	EtOH
		448	476	30	H
7,8-Didehydroastaxanthin (**402**)		474		0	EtOH
	478	495	522		Pyr
Echinenone (**283**)		460		0	A
		470			B
		471			C
		461		0	EtOH
		458	482		P
[Similar spectrum: hydroxyechinenones (**293-296**)]					
Eschscholtzxanthin (**180**)	458	485	516		B
	446	472	503		EtOH
	444	472	502		H
Fucoxanthin (**369**)	420	443	467	5	A
	431	461	485		B
		460	478		C
	426	449	475		EtOH
	425	446	473	5	P
Isorenieratene (**24**)	443	465	493		B
	438	460	495		C
	426	448	475		P

Table 19. continued

Carotenoid	λ_{max} nm			%III/II	Solvent
Lactucaxanthin (**150**)	420	440	471		A
	423	451	481		B
	424	439	468	85	EtOH
[Similar spectrum: tunaxanthins (**149-159**); decaprenoxanthin (**447**); mactraxanthin (**212**); sarcinaxanthin (**441**)]					
Lutein (**133**)	432	458	487		B
	435	458	485		C
	422	445	474	60	EtOH
	421	445	474	60	P
[Similar spectrum: loroxanthin (**196**)]					
Lutein-5,6-epoxide (**232**)	429	455	485		B
	433	453	483		C
	420	441	470	85	EtOH
	420	440	470	85	H, P
Lycopene (**31**)	448	474	505		A
	455	487	522		B
	458	484	518		C
	446	472	503	65	EtOH
	444	470	502	65	P
[Similar spectrum: lycophyll (**179**); lycoxanthin (**109**); rhodopin (**93**)]					
Mutatoxanthin (**245**)		439	468		B
		437	468		C
	409	427	457	50	EtOH
	407	426	456	45	P
[Similar spectrum: mutatochrome (**239**)]					
Mytiloxanthin (**353**)		480		0	B
		470		0	EtOH

Table 19. continued

Carotenoid	λ_{max} nm			%III/II	Solvent
Myxoxanthophyll (193)	450	478	510	60	A
	462	488	522	50	B
	460	488	522		C
	448	473	503	65	EtOH
Neochrome (250)	398	421	448	75	A
	408	434	460		B
	401	424	451		EtOH
Neoxanthin (234)/dinoxanthin (235)	416	440	470	85	A
	426	453	483		B
	423	448	476		C
	415	439	467	80	EtOH
	416	438	467	87	P
Neurosporaxanthin (463)		472		0	A, H
		486			B
Neurosporene (34)	424	451	480		C
	416	440	470		EtOH, H
	414	439	467	100	P
Okenone (317)	465	487	518		A
	460	484	516	5	P
Oscillaxanthin (208)	470	499	534	60	A
	480	510	548		C
	468	492	526	60	EtOH
Peridinin (558)		468			A, B
		475			EtOH
		455	485		P
Phytoene (44)	276	286	297	10	H, P
Phytofluene (42)	331	348	367	90	H, P
Plectaniaxanthin (146)	454	478	509		A
	445	471	502		P

Table 19. continued

Carotenoid	λ_{max} nm			%III/II	Solvent
Prasinoxanthin (359)		461			C
		450	466		EtOH
Pyrrhoxanthin (556)		458			A
		468	494		B
	439	453	480	25	Et_2O
		459	487	30	H
Renierapurpurin (28)	464	487	519		B
Renieratene (26)	457	476	507		B
Rhodoxanthin (424)	474	504	542		B
	482	510	546		C
		496	538		EtOH
	456	487	521		P
Rubixanthin (72)	439	474	509		C
	433	463	496	40	EtOH
	434	460	490		P
Semi-α-carotenone (560)		480	500		C
	438	462	490		H
Semi-β-carotenone (559)	458	486	518		B
		487	519		C
	440	467	495		H
Siphonaxanthin (350)		466			C
		452			EtOH
		446	468		P
Spheroidene (97)	441	468	502		B
	440	466	500		C
	429	454	486	80	EtOH
	427	454	486		P

Table 19. continued

Carotenoid	λ_{max} nm			%III/II	Solvent
[Similar spectrum: hydroxyspheroidene (172)]					
Spheroidenone (319)	445	484	505		A
		499			C
		488			EtOH
	460	483	515	0	P
[Similar spectrum: hydroxyspheroidenone (343)]					
Spirilloxanthin (166)	479	510	546		B
	475	505	543		C
	465	492	526	62	EtOH, P
Torularhodin (428)	485	519	557		B
	483	515	554		C
	463	495	532		EtOH
	467	501	537		P
Torulene (11)	470	503	541		B
	467	501	537		C
	456	486	520		EtOH
	454	480	514		P
Uriolide (430)		448	472	11	A
		448	472	35	H
Vaucheriaxanthin (238)	420	441	467		A
	426	451	480		C
	420	442	470	80	EtOH
Violaxanthin (259)	427	453	483		B
	426	449	478		C
	419	440	470	95	EtOH
	416	440	465	98	P
Violerythrin (553)		556		0	A

Table 19. continued

Carotenoid	λ_{max} nm			%III/II	Solvent
α-Zeacarotene (**22**)	398	421	449		H
β-Zeacarotene (**13**)	406	428	454		EtOH
					H, P
Zeaxanthin (**119**)	430	452	479		A
	440	463	491		B
	433	462	493		C
	428	450	478	26	EtOH
	424	449	476	25	P

[Similar spectrum: β,β-carotene-2,2'-diol (**113-115**); isozeaxanthin (**129**); caloxanthin (**182**); nostoxanthin (**196**); crustaxanthin (**197**); C.p. 450 (**439**)]

H. Quantitative Spectrophotometric Analysis

Carotenoids in solution obey the Beer-Lambert law, *i.e.* their absorbance (= extinction, optical density) is linearly proportional to the concentration. Spectrophotometric methods are therefore used for the routine quantitative analysis of carotenoids. The practical details of this quantitative analysis and the methods of calculation used are given in Vol. 1A, Chapter 5.

The quantitative analysis is dependent on the availability of accurate standard values, as absorption coefficients. Published values for the specific absorption coefficient, $A^{1\%}_{1cm}$, defined as the theoretical absorbance of a 1% solution, *i.e.* 1 g in 100 ml, in a cell of 1 cm pathlength, and the molar absorption coefficient or molar absorptivity, ε_{mol}, defined as the theoretical absorbance of a solution of 1 *M* concentration, are given in Table 20. Again these values are largely taken from tables compiled in other review articles [2-4, 9, 10]. It must be realized, however, that the accurate determination of these coefficients is not easy. The normal procedure involves weighing a small quantity of carotenoid, typically 1 to 2 mg, with an accuracy of ±0.001 mg. This requires an accurate and sensitive balance and it is essential that the carotenoid sample is absolutely pure and free from all contaminants, including residual solvent. It can also be difficult to achieve complete solution of a carotenoid in the desired solvent. Because of these difficulties, there may be a significant level of error or uncertainty in some of the published values. Thus, for example, $A^{1\%}_{1cm}$ values of 1940 and 2520 are given for β-zeacarotene (**13**) in hexane and light petroleum, respectively. The values should be virtually identical in these solvents. Also ε_{mol} values are expected to be the same for carotenoids with the same chromophore. This is clearly not true of some published values.

Table 20. Absorption coefficients ($A^{1\%}_{1cm}$ and ε_{mol}) for a range of carotenoids. Solvents: A, acetone; B, benzene; C, chloroform; CS_2, carbon disulphide; Cy, cyclohexane; Et_2O, diethyl ether; EtOH, ethanol; H, hexane; MeOH, methanol; P, light petroleum (b.p. 40-60°C); Pyr, pyridine.

Carotenoid	$A^{1\%}_{1cm}$	ε_{mol}	λ(nm)	Solvent
Aleuriaxanthin (**81**)	2600	143500	460	P
	2440	134700	463	A
Anhydrorhodovibrin (**91**)	2700	152800	482	P
Antheraxanthin (**231**)	2350	137200	446	EtOH
4'-Apo-β-caroten-4'-al	2500	120500	487	P
6'-Apo-β-caroten-6'-al	2120	93700	472	P
8'-Apo-β-caroten-8'-al (**482**)	2640	109800	457	P
10'-Apo-β-caroten-10'-al (**499**)	2190	82300	435	P
12'-Apo-β-caroten-12'-al (**507**)	2160	75600	414	P
Astacene (**398**)	1690	100000	498	Pyr
Astaxanthin (**403-406**)	2100	125100	470	H
Auroxanthin (**267-270**)	1850	111000	400	E
Azafrin (**504**)	2200	93700	409	P
Bacterioruberin (**456**)	2350	173900	494	P
	2540	188000	498	A
Bixin (**533**)	4200	165500	456	P
Canthaxanthin (**380**)	2200	124100	466	P
	2092	118000	480	B
Capsanthin (**335**)	2072	121000	483	B
Capsorubin (**413**)	2200	132000	489	B
β,β-Carotene (**3**)	2592	138900	450	P
	2620	140400	450	EtOH
	2396	128500	465	$CHCl_3$
	2337	125300	465	B
	2505	134300	452	Cy

Table 20. continued

Carotenoid	$A^{1\%}_{1cm}$	ε_{mol}	λ(nm)	Solvent
β,β-Carotene (3) (con'd)	2008	107600	484	CS_2
	2080	111500	449	Et_2O
β,ε-Carotene (7)	2800	150100	444	P
	2180	116800	477	CS_2
	2710	145300	445	H
β,ψ-Carotene (12)	3100	166200	462	P
	2760	147900	462	H
ε,ε-Carotene (20)	3120	167200	440	P
	2890	154900	444	Cy
	2900	155400	440	H
ε,ψ-Carotene (21)	3290	176300	456	P
ζ-Carotene (38)	2555	138000	400	H
ζ-Carotene ('unsymmetrical') (37)	2519	135500	395	H
β,β-Carotene 5,6:5',6'-diepoxide (257)	2690	152800	440	H
β,β-Carotene-5,6-epoxide (213)	2590	143000	444	H
β-Carotenone (562)	1626	97600	490	$CHCl_3$
Citranaxanthin (466)	2143	97800	463	P
Crocetin (538)	4320	141700	422	P
Crocetindial (536)	3970	117500	445	B
Cryptocapsin (303)	1972	112000	486	B
α-Cryptoxanthin/zeinoxanthin (60,62)	2636	145500	445	H
	2355	130000	459	B
β-Cryptoxanthin (55)	2386	131900	449	P
	2460	135700	450	H
Diadinoxanthin (230)	2230	129800	448	A
	2500	145500	447	EtOH
	2110	122800	447	H
	2250	130900	445	MeOH

Table 20. continued

Carotenoid	$A^{1\%}_{1cm}$	ε_{mol}	λ(nm)	Solvent
3,4-Didehydro-β,β-carotene (**2**)	2330	124400	461	P
3,4-Didehydrolycopene (**30**)	3000	160200	492	P
2,2'-Dihydroxy-β,β-carotene (**113-115**)	2060	117000	452	A
2,2'-Diketospirilloxanthin (**416**)	2000	124800	518	P
Echinenone (**283**)	2158	118700	458	P
	2110	116000	461	Cy
	2091	115000	472	B
Eschscholtzxanthin (**180**)	3269	185000	472	H
Fucoxanthin (**369**)	1060	69700	448	A
	1600	105300	449	H
	1140	75000	447	EtOH
	2036	134000	478	CS_2
2-Hydroxy-β,β-carotene (**51**)	2290	126400	452	A
2-Hydroxy-β,ε-carotene (**58**)	2330	128600	447	A
4'-Hydroxyechinenone (**296**)	2250	127300	454	P
2-Hydroxyplectaniaxanthin (**192**)	2445	142800	476	A
Hydroxyspheroidenone (**343**)	2070	120900	501	B
Isofucoxanthin (**363**)	1600	105300	453	P
Isorenieratene (**24**)	2080	109800	448	P
Isozeaxanthin (**129**)	2400	136300	450	P
Lutein (**133**)	2550	144800	445	EtOH
	2480	140900	445	Et_2O
	2600	147700	445	Et_2O
	2236	127000	458	B
	2160	122700	475	CS_2
Lutein-5,6-epoxide (**232**)	2400	140200	441	EtOH
	2800	163500	441	EtOH
	2373	138600	455	B

Table 20. continued

Carotenoid	$A^{1\%}_{1cm}$	ε_{mol}	λ(nm)	Solvent
Lycopene (31)	3450	184900	470	P
	3370	180600	487	B
Lycophyll (179)	3240	184000	508	A
Lycoxanthin (109)	3080	170000	474	A
Mutatochrome (239)	2260	124800	428	Et_2O
	1989	109800	437	B
Myxoxanthophyll (193)	2160	157700	478	A
Neochrome (250)	2270	136200	424	EtOH
Neoxanthin (234)	2470	148200	438	EtOH
	2243	134600	439	EtOH
	2245	134700	453	B
Neurosporaxanthin (463)	1715	85400	477	P
	2210	110100	486	B
Neurosporene (34)	2918	157000	440	H
Okenone (317)	2320	134100	484	P
Oscillaxanthin (208)	750	66900	490	10% Pyr /MeOH
Peridinin (558)	1340	84400	455	A
	1290	81300	467	B
	1290	81300	470	$CHCl_3$
	1450	91300	453	Et_2O
	1325	83500	472	EtOH
Physalien (126)	1340	139900	452	P
Phytoene (all-*E*) (44)	915	49800	286	H
	1250	68000	286	P
(15*Z*)	757	41200	286	H
Phytofluene (42)	1350	73200	348	P
	1577	85500	348	H
Plectaniaxanthin (146)	2505	142300	478	A

Table 20. continued

Carotenoid	$A^{1\%}_{1cm}$	ε_{mol}	λ(nm)	Solvent
Prolycopene (7Z,9Z,7'Z,9'Z-31)	1920	102900	436	P
Rhodopin (93)	2989	165600	470	P
Rhodoxanthin (424)	2500	140500	490	H
	2386	134100	491	Cy
Rubixanthin (72)	2750	151800	460	P
Saproxanthin (140)	2920	165900	479	A
Semi-α-carotenone (560)	1431	81300	500	$CHCl_3$
Semi-β-carotenone (559)	1850	105100	467	H
Sintaxanthin (473)	2588	111300	462	B
Spheroidene (97)	2785	158200	468	B
Spirilloxanthin (166)	2470	147200	510	B
Torularhodin (methyl ester) (428)	2040	115100	501	P
	2950	170500	497	P
Torularhodinaldehyde (271)	2840	155600	514	P
Torulene (11)	3240	173000	480	P
Triphasiaxanthin (561)	1654	96600	480	$CHCl_3$
Violaxanthin (259)	2550	153000	440	EtOH
	2400	144000	442	A
	2240	134400	454	B
α-Zeacarotene (22)	1850	99500	421	H
	2450	131800	421	P
β–Zeacarotene (13)	2520	135600	428	P
	1940	104400	427	H
Zeaxanthin (119)	2348	133400	449	P
	2480	140900	450	EtOH
	2540	144300	450	EtOH
	2340	132900	452	A

References

[1] W. Vetter, G. Englert, N. Rigassi and U. Schwieter, in *Carotenoids* (ed. O. Isler), p. 189, Birkhäuser, Basel (1971).
[2] B. H. Davies, in *Chemistry and Biochemistry of Plant Pigments, 2nd Edition* (ed. T. W. Goodwin), Vol. 2, p. 38, Academic Press, London and New York (1976).
[3] E. de Ritter and A. E. Purcell, in *Carotenoids as Colorants and Vitamin A Precursors* (ed. J. C. Bauernfeind), p. 815, Academic Press, New York and London (1981).
[4] G. Britton, *Meth. Enzymol.*, **111**, 113 (1985).
[5] S. Liaaen-Jensen, *Kgl. Norske Vidensk. Selsk. Skr., No. 8* (1962).
[6] L. Zechmeister, Cis-Trans *Isomeric Carotenoids, Vitamins A and Arylpolyenes*, Springer, Vienna (1962).
[7] B. Ke, F. Imsgard, H. Kjøsen and S. Liaaen-Jensen, *Biochim. Biophys. Acta*, **120**, 139 (1970).
[8] S. Liaaen-Jensen, *Pure Appl. Chem.*, **20**, 421 (1969).
[9] K. S. Rowan, *Photosynthetic Pigments of Algae*, p.112, Cambridge University Press, Cambridge (1989).
[10] K. Schmidt, A. Connor and G. Britton, in *Chemical Methods in Prokaryotic Systematics*, p. 403, Wiley, Chichester (1994).
[11] O. Straub, *Key to Carotenoids, 2nd Edition* (ed. H. Pfander), Birkhäuser, Basel (1987).

Carotenoids
Volume 1 B: Spectroscopy
© 1995 Birkhäuser Verlag Basel

Chapter 3
Circular Dichroism

Richard Buchecker and Klaus Noack

A. Introduction

1. Chiroptical methods for the determination of absolute configuration of carotenoids

The only interactions with their environment by which chiral molecules can be distinguished from their mirror images are those with a chiral environment, which can be either 'chiral' light or other chiral molecules. The interactions with chiral, *i.e.* polarized, light can be measured as rotation of the plane of linearly polarized light at discrete wavelengths (angle of rotation α) or the wavelength dependence (dispersion) of this angle of rotation (*optical rotatory dispersion, ORD*) or as the difference between the absorbance of right and left circularly polarized light as a function of wavelength (*circular dichroism spectroscopy, CD*).

Interactions with the chiral environment that is created by other chiral molecules can be used to separate optical isomers. This can be achieved by chromatography on chiral stationary phases, or by chemical reactions with other chiral molecules to produce diastereoisomers, which can be separated or distinguished by conventional (achiral) physical or chemical methods. This Chapter is concerned only with the interactions of chiral carotenoids with linearly polarized light or, more usually, with circularly polarized light.

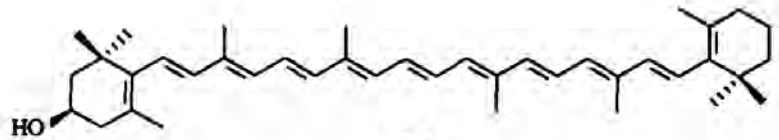
2. Brief historical survey of the application of chiroptical methods to carotenoids

Up to the 1950s, the determination of the angle of rotation of linearly polarized light at a fixed, discrete wavelength was the only chiroptical method that had been employed in carotenoid research. The strong absorption in the visible part of the spectrum made measurements at 589 nm (Na line) or at 546 nm (Hg line) very difficult; measurements with red light at 656.3 nm (Hg C line) or at 643.85 nm (Cd line) could be performed with greater confidence [1, 2]. A

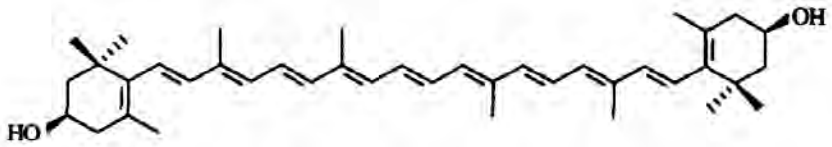
detailed summary of the use and the limitations of older measurements of optical rotation was given in 1971 [3].

When commercial equipment for the measurement of ORD became available in the 1960s, the determination of spectra on the short-wavelength side of the strong visible absorption became possible. Some empirical rules that correlate structure and spectra were proposed [4]. As, with very few exceptions, the asymmetric carbon atoms which render carotenoids chiral are located in the end groups, a convenient classification of optically active carotenoids was proposed [4]. It was observed that, to a first approximation, the effects of the two end groups in a carotenoid are additive. Three main stereochemical types of carotenoid were considered:

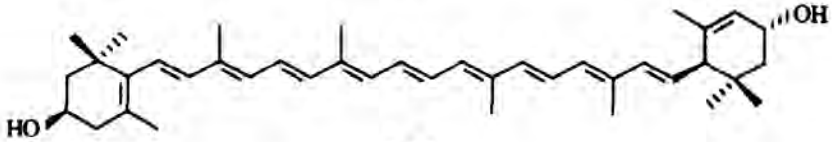
i) monochiral compounds with one chiral end group and one achiral end group, *e.g.* cryptoxanthin (**55**),
ii) homodichiral compounds with two identical chiral end groups, *e.g.* zeaxanthin (**119**),
iii) heterodichiral compounds with two nonidentical chiral end groups, *e.g.* lutein (**133**).



55



119



133

The invention of the CD spectrometer with periodic modulation of the state of polarization of circularly polarized light [5] and the commercial production of the instrument in the late 1960s then made it possible and convenient to obtain CD spectra. Both ORD and CD were rapidly adopted in carotenoid research, but ORD was very soon supplanted by CD because of the greater simplicity of the CD spectra. Today most papers that deal with chiral carotenoids report their CD spectra or at least the CD maxima.

B. Theory of CD Spectra

1. General aspects

In this Chapter, the theory of CD spectra will only be touched upon briefly. There are excellent books on the general theory of optical activity [6], but nowhere are carotenoids treated specifically.

Differential absorption of left and right circularly polarized light by any material is only possible if the product of the electric and magnetic transition dipole moments is not zero, *i.e.*

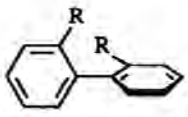
$$R = \mu \cdot m \cdot \cos(\mu, m) \neq 0$$

For liquid samples this condition can only be met by chiral molecules, *i.e.* those molecules which cannot be brought to coincidence with their mirror image by any symmetry operation. They do not possess an improper axis of rotation (rotation-reflection axis). This also implies that no symmetry planes can be present. Proper symmetry axes are, however, allowed (see books on group theory [6, 7]).

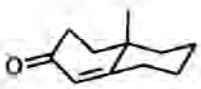
For CD to be observed upon excitation of a molecule by the absorption of circularly polarized light, the electric and the magnetic transition dipole moments must have a component parallel to each other in order to make $R \neq 0$. This condition is fulfilled when a chromophore in a chiral molecule is itself intrinsically chiral, *e.g.* hexahelicene (*1*), chiral biphenyls (*2*), non-planar conjugated ketones (*3*) and carotenoids such as zeaxanthin (**119**) with a non-planar (chirally twisted) conjugated chain. The condition is also fulfilled when a chromophore that is not intrinsically chiral is asymmetrically perturbed by a more distant chiral part of the molecule so that left and right circularly polarized light is absorbed differentially [6]. Examples of this are non-conjugated ketones such as the chiral cyclopentanone (*4*) where the keto group is in a chiral ring or 2-chlorocyclohexanone (*5*) where the keto group is in an achiral ring with asymmetrically positioned substituents, and also carotenoids such as tunaxanthin (e.g. **154**) where the chiral centres do not induce a twist of the conjugated chain



1



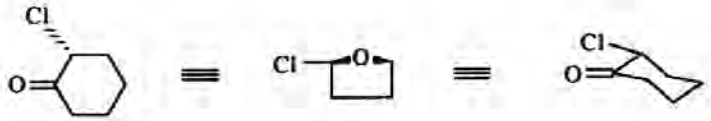
2



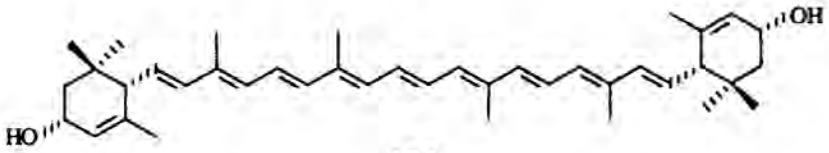
3



4



5



154

Circular dichroism is measured as the absorbance of left circularly polarized light minus that of right circularly polarized light [5].

$$\Delta A = A_{left} - A_{right}$$

and in molar units:

$$\Delta\varepsilon = (\Delta A \times MW)/(c \times d)$$

where MW = molecular weight
c = concentration in g/litre
d = cell length in cm

Another unit often used is molecular ellipticity [θ], which is, at first approximation, proportional to Δε, such that

$$\Delta\varepsilon = [\theta]/3300$$

To the authors' knowledge, in only one paper has an attempt been made to correlate the observed CD spectra with the electric and magnetic transition dipole moments that have been calculated for some model configurations of carotenoids [8], and it is now known that rather unrealistic geometrical models were used, since no conformational analysis was included. That study [8] can, however, be taken as a first attempt to show the application of theory to carotenoid CD spectra. Further work in this direction is needed.

In the practical application of CD spectra, determinations of absolute configuration are still based mainly on empirical correlations with spectra of similar molecules with established stereochemistry. A number of rules have been proposed for the classification and interpretation of the CD spectra.

i) Molecules with one or two asymmetrically substituted terminal rings which contain a double bond formally conjugated with the polyene chain give so-called conservative CD

spectra, *i.e.* spectra that consist of five or six relatively sharp maxima of alternating sign whose intensities integrate approximately to zero [8, 9].

ii) The presence of a *Z* double bond in the polyene chain of such a compound reverses all signs in the CD spectrum, compared to that of the all-*E* compound [9, 10, 11]. In the CD spectra of corresponding di-*Z* compounds, the signs are again as for the all-*E* isomer [9, 12].

iii) When a carotenoid has cyclic end groups in a half-chair conformation, it is the conformation of the ring that is of overriding importance for the CD spectrum, regardless of the type of substituents on the ring [13].

iv) The effects of the end groups are additive, *i.e.* a homodichiral carotenoid exhibits a CD spectrum with approximately twice the intensity of that of the corresponding monochiral compound [4].

v) Non-conservative CD spectra, *i.e.* spectra with no regular sign alternation, are produced by molecules that have a chirally perturbed but intrinsically achiral chromophore [8], *i.e.* molecules in which the ring end groups contain either no double bonds or double bonds that are not conjugated.

vi) The inherently chiral chromophores normally cause strong CD, the inherently achiral but chirally perturbed chromophores weaker CD.

vii) The distinction between the two classes of chromophores is, however, not always straightforward, since the effective extent of the chromophore is often ambiguous. This will be seen when specific examples are discussed below.

2. Importance of conformation

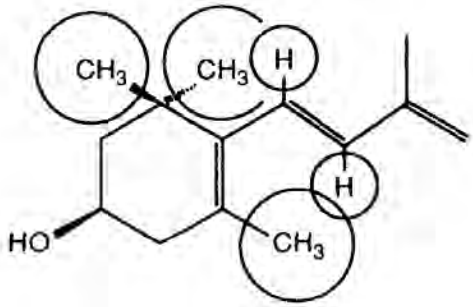


Fig. 1. Steric hindrance in the planar 6-s-*cis* form of β,β-carotene (3).

In carotenoids with a β end group, where the C-5,6 double bond of the ring is formally conjugated with the long chain of alternating single and double bonds, both the planar conformations, 6-s-*cis* and 6-s-*trans*, are strongly sterically hindered. This steric hindrance is relieved by a twist around the C-6,7 bond. The double bond in the ring is therefore not coplanar with the chain and an intrinsically asymmetric chromophore is created (Fig. 1) [9].

Most CD spectra of carotenoids exhibit strong temperature dependence. Their $\Delta\varepsilon$ values increase significantly, often by a factor of up to five, when the samples are cooled to liquid nitrogen temperature [9, 14] (Fig. 2). This is a manifestation of the presence of conformational equilibria.

In carotenoids in which the conjugated system is twisted due to steric hindrance, a conformational analysis must be made and the conformation(s) adopted in solution must be established for the CD spectra to be understood. As a general rule, the absolute configuration of a compound can only be determined from CD spectra if the conformation of the molecule is known, and *vice versa*.

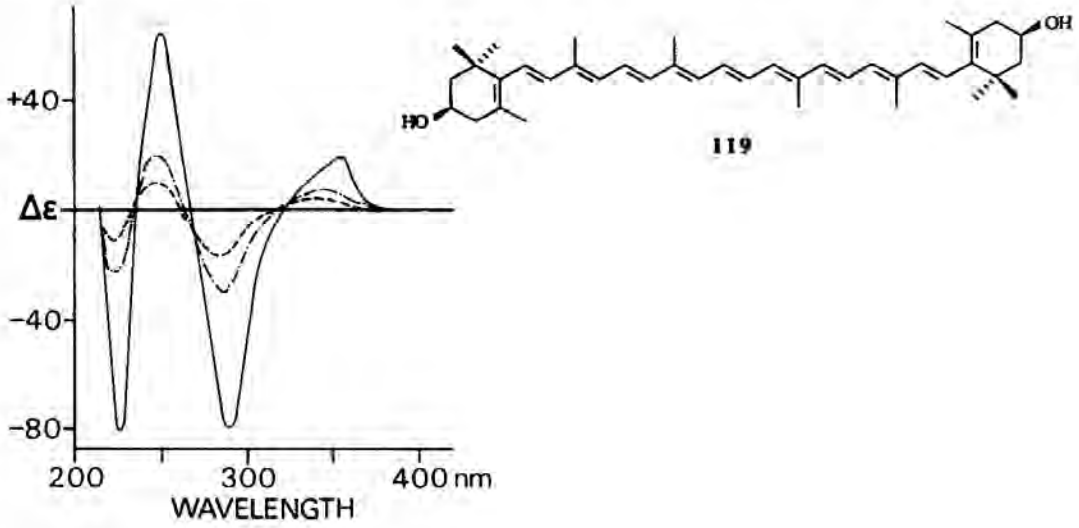


Fig. 2. Temperature dependence of the CD spectrum of (3*R*,3'*R*)-zeaxanthin (**119**) (in EPA). [14]. ----- +20°C, ····· –60°C, —— –180°C

With (3*R*,3'*R*)-zeaxanthin (**119**), as an example of this type of molecule, the twist can be in either direction from the hindered planar 6-s-*cis* form. Twisted 6-s-*trans* forms have even stronger steric hindrance (see below) and can in this case be neglected. Besides this twist of the ring with respect to the plane of the chain, the conformation of the ring itself must be taken into account. Molecular modelling with energy minimization reveals that the conformation with the hydroxy group at C-3 axial is 1.1 kcal.mol^{-1} less stable than the one with the hydroxy group equatorial [15]. The latter conformation is therefore strongly favoured.

The two possible twist forms of the ring relative to the chain, both in the strongly preferred ring conformation with the hydroxy group equatorial, are therefore not exact mirror images and have slightly different energies. Hence they are populated to a different degree. The two forms represent oppositely twisted, intrinsically chiral chromophores and hence give opposite CD spectra. Since the more stable form is always present in excess, it determines the sign of the CD spectrum if its intrinsic CD is as strong as or stronger than that of the less stable form. Its proportion in the equilibrium mixture increases as the temperature is lowered so an increase in the CD intensity is observed. In principle, for a quantitative evaluation of the temperature

dependency, both equilibria, namely the equatorial *vs.* axial orientation of the hydroxy group at C-3, and the twist around the C-6,7 single bond, must be taken into account. However, if the energy difference between the two ring conformational forms is comparatively high, *i.e.* the ring exists almost exclusively in the form with the hydroxy group equatorial, and if a distorted 6-s-*trans* form can also be neglected on energetic grounds, the problem is reduced to a simple equilibrium between the two twisted 6-s-*cis* conformations. This seems to be the case for zeaxanthin (**119**).

When the sign rules for twisted butadiene are applied to the twisted carotenoids, the signs of the CD maxima can be correlated with the helicity of the twisted chromophore [9]. The twisted carotene is considered to be analogous to the twisted butadiene, but with the two helically arranged double bonds now separated by the conjugated chain and not by only one single bond. The symmetries of the transitions are the same in the twisted butadiene and the carotenoid, but their energy is shifted to much lower values in the carotenoid.

The sign pattern of the CD spectrum of (3*R*,3'*R*)-zeaxanthin (**119**) corresponds to the conformation with left-handed (negative) helicity [9, 16] and agrees with the conformation that is found in the crystal of β,β-carotene (**3**) [17] (see Fig. 3).

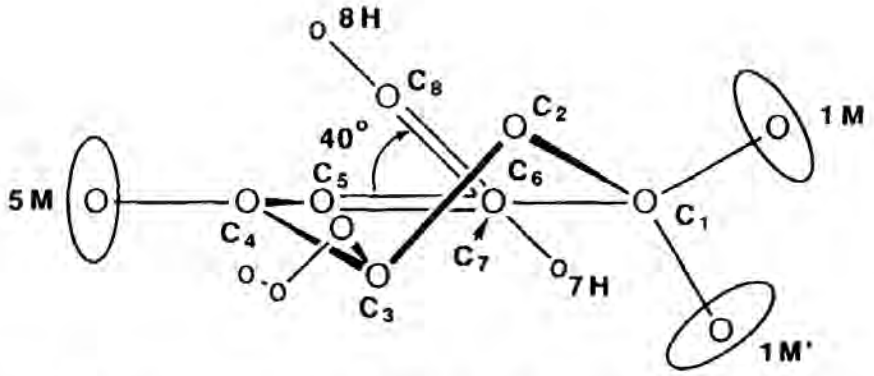


*Fig. 3. View of the 3-hydroxy-β ring from along the C-6,7 bond. The torsion angle of about 40° corresponds to the potential-energy minimum for zeaxanthin (**119**) (see Fig. 5).*

There are more complicated cases than zeaxanthin (**119**). One example is astaxanthin (**406**) where the CD maxima change sign upon cooling [9, 18] (Fig. 4). At temperatures down to −60°C, the CD maxima increase; below this, they decrease and then go through zero at about −120°C before increasing again with opposite sign. At room temperature, an energetically less favoured conformer obviously determines the CD spectrum in spite of its being present as less than 50% of the total.

This different behaviour of (3*R*,3'*R*)-zeaxanthin (**119**) and (3*S*,3'*S*)-astaxanthin (**406**) (both with the hydroxy groups at C-3 and C-3' equatorial) can be understood by comparison of their curves of potential energy *vs.* C-6,7 twist angle, obtained by application of the MOLOC forcefield [15], which show some significant differences. These potential curves are illustrated

in Figs. 5 and 6. A twist angle of 0° corresponds to the planar 6-s-*cis* form, 180° to the planar 6-s-*trans* form.

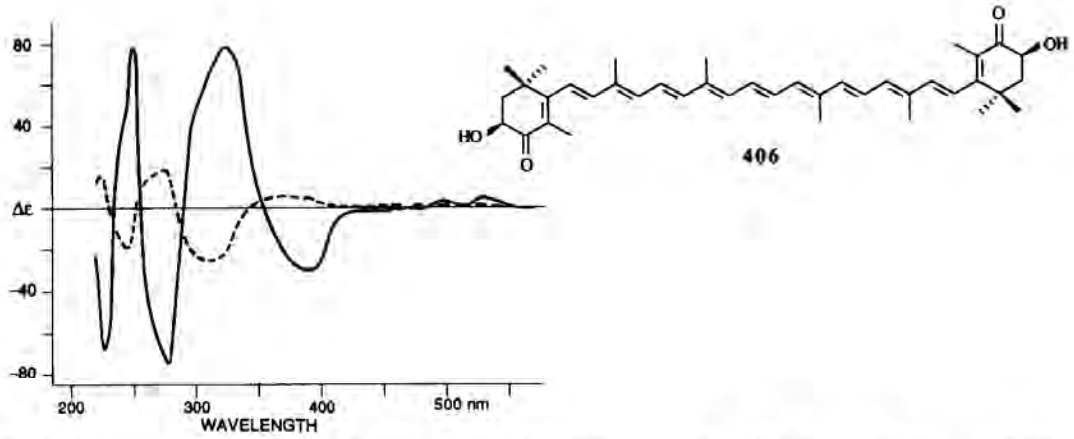


Fig. 4. Temperature dependence of the CD spectrum of (3*S*,3'*S*)-astaxanthin (**406**) diacetate [14]. ----- +20°C, —— −180°C

The curve for zeaxanthin (**119**) (Fig. 5) clearly has two strong potential-energy maxima near the two planar conformations and distinct minima of different heights at torsion angles of 40° and 320°(= −40°), which correspond to two distorted 6-s-*cis* forms, and 140° corresponding to one distorted 6-s-*trans* form. The minimum of the distorted 6-s-*trans* form is of considerably higher energy (by *ca.* 0.9 kcal.mol^{-1}) than that of the higher of the two s-*cis* forms. The energy difference between the two 6-s-*cis* conformations is about 0.4 kcal.mol^{-1} which agrees nicely with the value of 0.3 to 0.4 kcal.mol^{-1} calculated from the temperature dependence of the CD spectra [14]. In zeaxanthin (**119**), therefore, mainly the two 6-s-*cis* forms compete in the equilibrium and no sign change is to be expected in the CD spectra upon cooling. The conformation with the lower minimum agrees with the helicity determined by the C2-helicity rule.

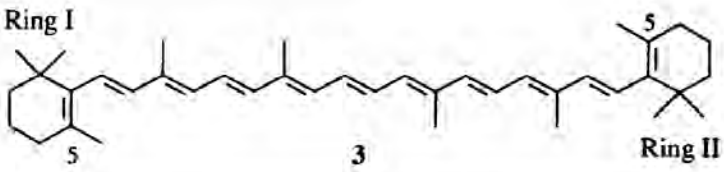
The potential energy curve of astaxanthin (**406**) (Fig. 6) again has two strong maxima for the two planar conformations and three minima at C-6,7 twist angles of *ca.* 40°, 320° (−40°) and 140°. In contrast to the case of zeaxanthin (**119**), however, the distorted 6-s-*trans* form has very nearly the same energy as one of the 6-s-*cis* forms, and the minimum of the −40° twisted s-*cis* form is about 0.6 kcal.mol^{-1} lower than that of the conformation with the +40° twist. Three conformations of similar energy content therefore compete with each other, so the temperature dependence of the CD spectra of astaxanthin is complicated.

Since the low-temperature CD maxima of (3*S*,3'*S*)-astaxanthin (**406**) have opposite signs to the low-temperature maxima of (3*R*,3'*R*)-zeaxanthin (**119**), it follows from the C2-symmetry rules that the most stable conformers are of opposite chirality [9]. This is in agreement with the X-ray structure of canthaxanthin (**380**) (as a model for astaxanthin, **406**)

which shows that, in the crystal, the twist of the chain relative to the ring is opposite to that of β,β-carotene (**3**) (as a model for zeaxanthin **119**). Canthaxanthin (**380**) and β,β-carotene (**3**) do not possess asymmetrically substituted rings and exist in two mirror-image conformations. Inspection of their potential-energy curves leads to the extrapolation that the conformers with the lowest energy in astaxanthin (**406**) and zeaxanthin (**119**) would be of the same chirality. This demonstrates the limited accuracy of such energy calculations and shows clearly the severe limitations in predicting absolute configurations from CD spectra if it is not possible to discriminate with absolute certainty between conformations that have similar energy but different chirality. Differences of < 0.3 kcal are at the limit of the method. That (3*R*,3'*R*)-zeaxanthin (**119**) and (3*S*,3'*S*)-astaxanthin (**406**) have the same absolute configuration is established beyond doubt by chemical correlations [13].

In β,β-carotene (**3**) also, two twisted 6-s-*cis* forms are in equilibrium. However, since in this optically inactive molecule the two ring conformations are mirror images (no distinction of the C-3 substituents), there are two equilibria, one between two twist forms which are mutually mirror images of each other, and the other between two symmetrical *meso* forms. This constitutes a racemic mixture (Table 1).

Table 1. Conformations in the equilibrium mixture of β,β-carotene (**3**)



3

	Conformation Ring I	Conformation Ring II	
E (1)	A, up	A, up	pair of enantiomers
E(−1)	B, down	B, down	
E (2)	A, down	A, down	pair of enantiomers
E (−2)	B, up	B, up	
M (1)	A, up	B, down	pair of identical
M (−1)	B, down	A, up	*meso* forms
M (2)	B, up	A, down	pair of identical
M (−2)	A, down	B, up	*meso* forms

Conformation A = half-chair with C (1) and C (3) above the plane C (4, 5, 6)
Conformation B = half-chair with C (1) and C (3) below the plane C (4, 5, 6)
'up' = C (5) above the plane of the chain
'down' = C (5) below the plane of the chain

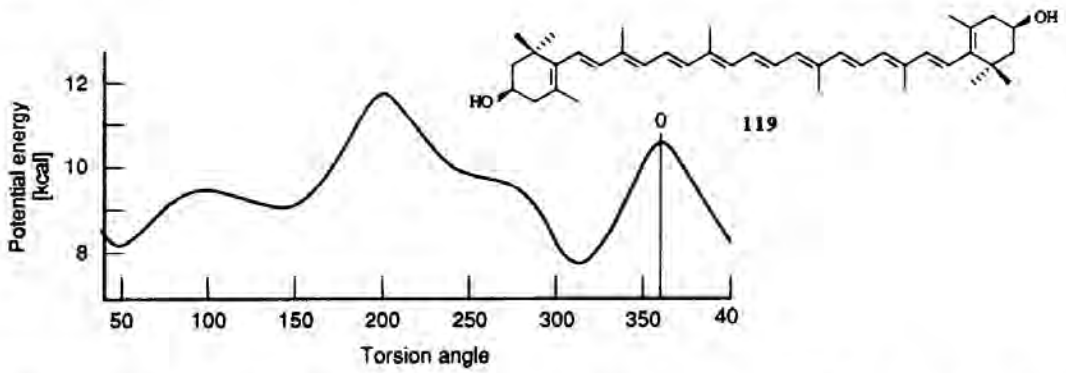


Fig. 5. Curve of potential energy *vs.* twist angle around the C-6,7 single bond of (3*R*,3'*R*)-zeaxanthin (**119**) with the hydroxy group held in an equatorial position; planar s-*cis* form = 0°.

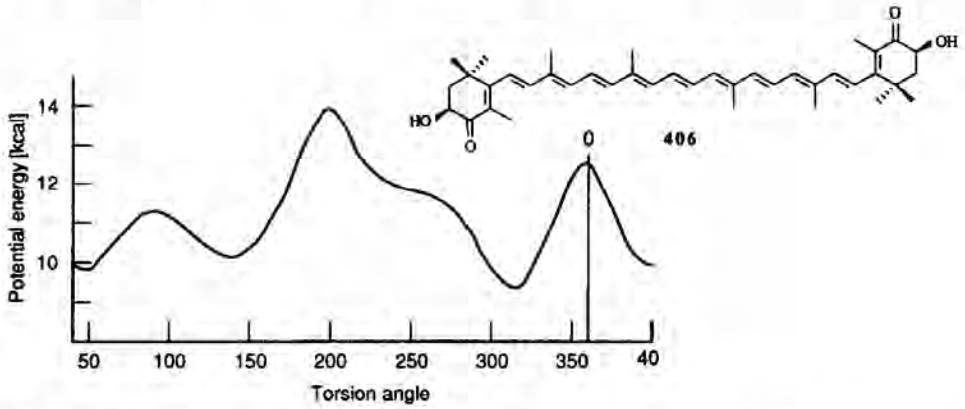


Fig. 6. Curve of potential energy *vs.* twist angle around the C-6,7 single bond of (3*S*,3'*S*)-astaxanthin (**406**) with the hydroxy group held in an equatorial position; planar s-*cis* form = 0°.

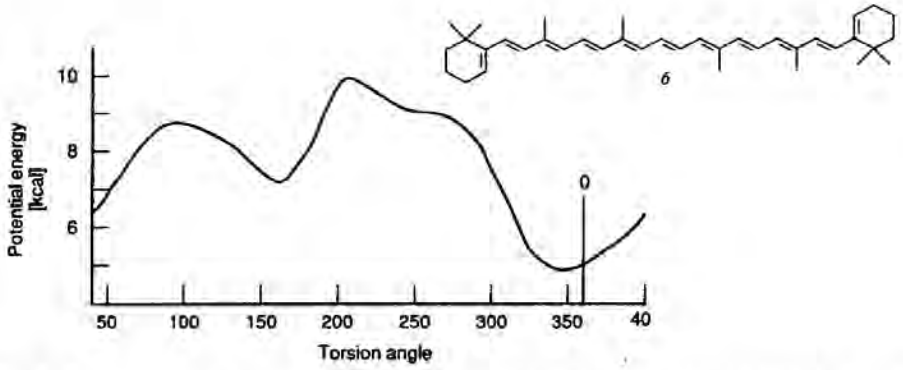
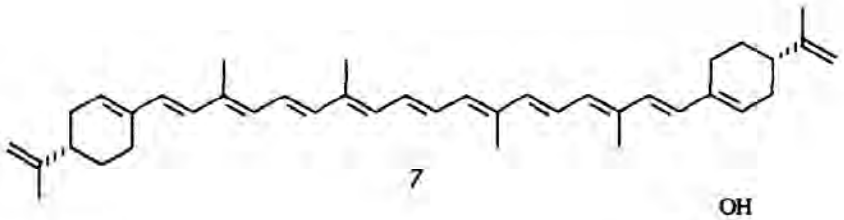
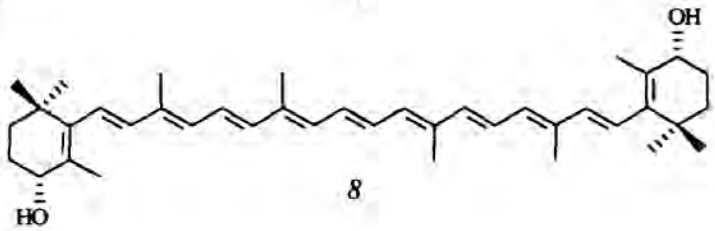


Fig. 7. Curve of potential energy *vs.* twist angle around the C-6,7 single bond of 18,18'-dinor-β,β-carotene (*6*); planar *s-cis* form = 0°.

That in zeaxanthin (**119**) and astaxanthin (**406**) the methyl group at C-5 is decisive for the conformational equilibrium is shown by the potential energy curve of the 5,5'-bisdemethyl compound 18,18'-dinor-β,β-carotene (*6*) (Fig. 7). In this molecule the almost planar 6-s-*cis* form has by far the lowest energy, more than 2 kcal.mol^{-1} lower than the distorted 6-s-*trans* form. There is only one minimum near planarity and not two as in the case of the compounds that contain a C-5 methyl group. A model compound with a somewhat similar structure (*7*) shows a different type of CD spectrum from that of zeaxanthin (**119**), and a much smaller temperature dependence, in agreement with the potential energy curve [19]. However, in this model compound, the geminal methyl groups at C-1 are also missing, so the almost planar 6-s-*trans* form has a similar energy to the almost planar 6-s-*cis* form.



7



8

Potential energy calculations reveal that, when a hydroxy group is located at C-4, the ring conformation in which this hydroxy group is equatorial is stabilized much less than when the hydroxy group is at C-3. The energy difference between the forms with pseudoequatorial and pseudoaxial hydroxyl at C-4 is only 0.2 kcal.mol^{-1}, which is near the limits of precision of the calculation. The smaller temperature dependence of the CD spectrum of (4*R*,4'*R*)-isozeaxanthin (*8*) is in agreement with this observation [20, 21].

The foregoing discussions and examples show how important it is to establish with confidence the different conformations and conformational equilibria before attempting to deduce the absolute configurations of compounds from their CD spectra.

For carotenoids in which the chiral perturbation of the planar chromophore stems from chiral centres which do not cause a chiral twist of the conjugated system, only empirical rules can be given. No comprehensive theory has been proposed for CD spectra of the different types of these carotenoid structures. In addition, non-conservative CD spectra of carotenoids often show a strong temperature dependence which reveals the importance of conformational equilibria also in compounds of this type. It is therefore recommended that the CD spectra of carotenoids be measured at different temperatures, whenever possible.

3. Conclusions: applications of CD to carotenoids

The conclusion from the foregoing discussion on theory is that determinations of absolute configuration *a priori* from the CD spectra are today only possible for carotenoids with a twisted conjugated system of double bonds, and then only when the conformations of the ring itself and of the twist of the ring in relation to the chain are known. However, when closely related molecules are compared, where the ring conformation is known and the twist of the ring with respect to the chain can be assumed to depend only on the ring conformation, it may be inferred whether these compounds have the identical or mirror-image absolute configuration; (see the examples below of 2,3-disubstituted or 4-substituted β,β-carotenes). Even in these cases, however, the similarity of the structures must be very close; zeaxanthin (**119**) and astaxanthin (**406**) are not close enough.

Further useful applications of CD spectra include establishing whether two samples of the same carotenoid compound from different sources have identical or mirror-image configurations, and determining the enantiomeric purity of a substance, if a reference spectrum is known.

By comparison of the CD spectra of compounds with known absolute configuration, the conformation, in principle, can also be determined. Conformational equilibria can be studied by the temperature dependence of CD spectra.

Further refinement of the theory should allow the calculation and interpretation of CD spectra also of carotenoids that have non-conservative CD spectra.

C. Experimental Aspects

In the UV range (*ca.* 380 to 200 nm) most carotenoids have only weak absorption but substantial CD intensity, so CD spectra can be measured in the UV without too much difficulty. This is, however, not the case in the range of the strong main visible absorption (500 to 380 nm). Here, molar absorption coefficients of >100 000 are normal and the CD is often very weak. Since for CD measurement the absorbance should not exceed 2, very thin cells and/or very dilute solutions have to be used, and consequently the measured CD signal is very weak. A low signal-to-noise ratio and slight instability of the baseline make measurement of CD in this spectral region extremely difficult. An absorbance that is too high can cause strong artifacts in the CD spectrum. It is therefore recommended that, in this wavelength range, the spectra are measured for at least two different concentrations or cell path lengths to ensure that Beer's law is followed. Because of these difficulties, very few CD spectra in the visible range have been reported in the literature. Most modern CD spectrometers, however, offer the possibility of averaging repeatedly-scanned spectra in order to improve the signal-to-noise ratio, which increases with the square root of the number of scans. Multiple scans are preferred to very long integration times (>20 sec) at each wavelength increment or to very high time constants in analogue-measuring instruments. With averaging over multiple scans, slow drift of the baseline due to temperature fluctuations or other instabilities is also averaged out. For each determination, a separate baseline obtained with the same cell should be subtracted from the

spectrum. With these possibilities it is assumed that more CD spectra in the visible range will be published in the near future.

Spectra may be reported in several ways. Information is conveyed most clearly if the actual spectral curves are illustrated. If this is not possible, tables or lists of the wavelengths and $\Delta\varepsilon$ values of all positive and negative maxima and λ values of cross points should be given, as well as solvent, cell thickness and concentration.

The CD spectra of carotenoids can be measured in any optically inactive transparent solvent. For recording spectra at low temperature a solvent with low melting point must be chosen. For temperatures down to the boiling point of liquid nitrogen, the mixture of spectroscopic grade solvents known as EPA is routinely used. The composition of EPA, by volume, is

diethyl ether (5)/isopentane (5)/ethanol (2)

For room temperature (RT) spectra, the low boiling point and high vapour pressure of this mixture may be a disadvantage since concentrations may change because of evaporation. If spectra are to be measured only at room temperature, higher-boiling solvents are preferred. Ethanol, hexane, heptane, cyclohexane, peroxide-free dioxane *etc*. can be chosen, according to the solubility of the compounds. No example is known where RT spectra in EPA differ from those in ethanol alone. Chlorinated solvents absorb in the UV and may contain traces of acid. They are therefore less desirable. The photochemical instability of many carotenoids must not be overlooked. It is therefore recommended that each spectrum is determined at least twice to make sure that the sample maintains its integrity during the measurement.

Special care is needed for low-temperature spectra. An important consideration is the solubility of the sample, which drastically diminishes at low temperature, but the choice of solvent also depends on the desired temperature range and on the melting point of the solvent. Solvent mixtures often have considerably lower melting points than pure solvents. Suitable mixtures are given in textbooks on low-temperature spectroscopy [22]. The standard mixture EPA does not crystallize but becomes very viscous at low temperature and then forms a transparent hard glass at very low temperature. Corrections have to be made for changes in concentration caused by thermal contraction which can put a high strain on the glass of the cell windows and induce a linear birefringence that results in distortions of the baseline. It is often necessary to thaw the sample and repeat the cooling, perhaps at a different rate, to obtain an acceptable baseline. Unfortunately, most commercial low-temperaure equipment uses rectangular cells which are more susceptible to strain-induced birefringence than are circular cells.

Despite its disadvantages for measurements at room temperature, EPA is still the solvent mixture that is most often used for determination of carotenoid CD. All spectra presented in the following sections were obtained for EPA solution, if no other solvent is indicated. For a better comparison, all curves from the literature have been redrawn to a suitable scale or, if no curves were published, have been plotted from numerical data.

D. Relationships between Structure and CD

1. Monochiral and homodichiral carotenoids

Monochiral and homodichiral carotenoids, by definition, possess only one chiral end group or two identical chiral end groups, respectively. They are therefore suitable examples with which to investigate the effect of a specific chiral end group on the CD spectrum of a carotenoid.

a) Carotenoids with cyclic end groups that cause inherently chiral chromophores and conservative CD spectra

i) Substituted β rings. A substituted β ring formally contributes one double bond to the chromophore. Carotenoids with inherently chiral chromophores are probably best represented by ones that contain two simple substituted β rings *e.g.* zeaxanthin (**119**). The CD of zeaxanthin (**119**) is mainly determined by two conformational equilibria, namely (i) the conformational equilibrium of the β ring itself and (ii) the conformational equilibrium between the ring and the polyene chain along the C-6,7 axis, as discussed in Section B. The strongly conservative CD spectrum of (3*R*,3'*R*)-zeaxanthin (**119**) is shown in Fig. 8.

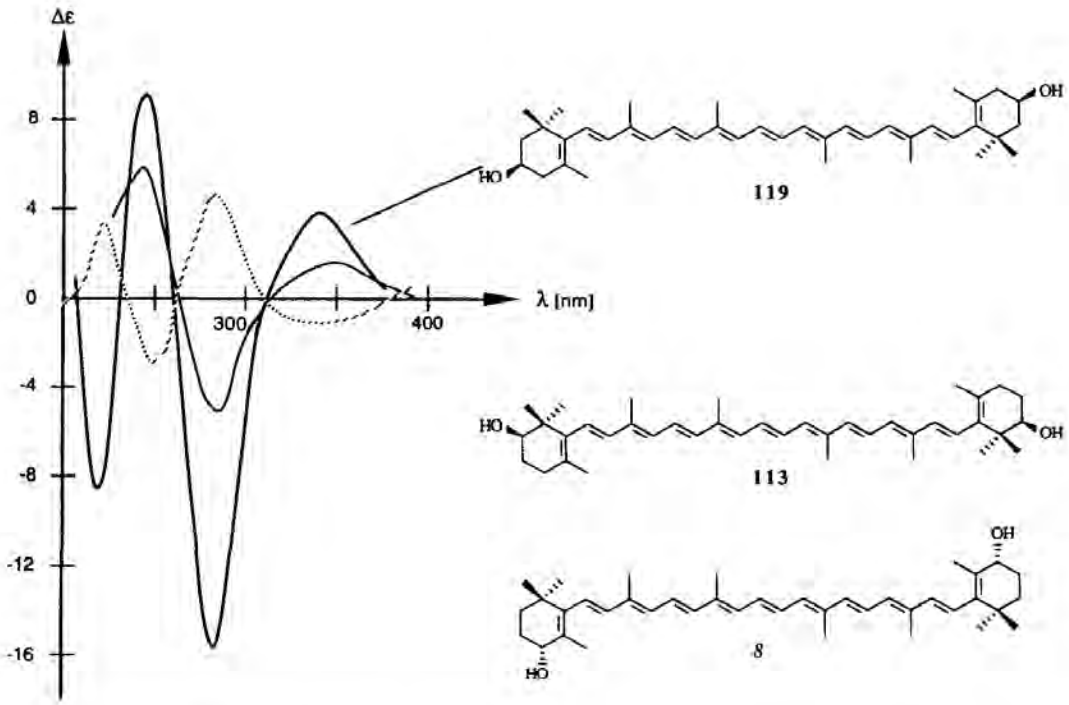
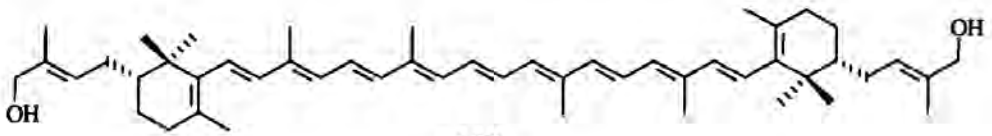


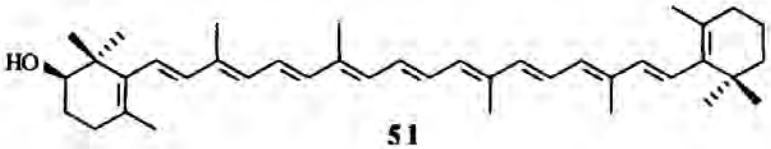
Fig. 8. CD spectra of (3*R*,3'*R*)-zeaxanthin (**119**) ——— [11], (2*R*,2'*R*)-β,β-carotene-2,2'-diol (**113**) ..... [23] and (4*R*,4'*R*)-isozeaxanthin (*8*) —— (in ethanol) [21].

Table 2. Comparison of CD spectra of carotenoids that contain chiral β rings with different substitution patterns. (Solvents: A = diethyl ether/hexane, 1:2; B = dichloromethane, EPA = diethyl ether/isopentane/ethanol, 5:5:2).

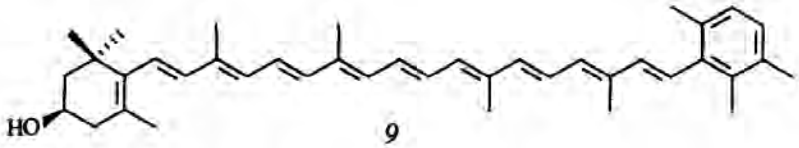
Carotenoid	Δε (λ)	Δε = 0 (nm)	Δε (λ)	Δε = 0 (nm)	Δε (λ)	Δε = 0 (nm)	Δε (λ)	Solv.	Ref.
(2*R*,2'*R*)-2,2'-Dihydroxy-β,β-carotene (**113**)	4.7 (220)		−4.4 (246)		5.9 (281)		−1.1 (340)	EPA	[24]
(2*R*,2'*R*)-C.p. 450 (**439**)	−8.6 (220)		5.0 (246)		−9.1 (284)		2.1 (341)	EPA	[25]
(3*R*,3'*R*)-Zeaxanthin (**119**)	−7.7 (225)		8.1 (251)		−14.6 (290)		3.7 (348)	B	[10]
(4*R*,4'*R*)-Isozeaxanthin (*8*)			5.8 (244)	264	−5.0 (285)	314	1.6 (349)	EtOH	[20]
(2*R*)-2-Hydroxy-β,β-carotene (**51**)	2.6 (225)		−1.6 (251)		3.1 (281)		−0.8 (334)	EPA	[31]
(3*R*)-β-Cryptoxanthin (**55**)			5.2 (248)		−7.7 (288)		1.9 (345)	C	[9]
(3*R*)-3-Hydroxy-β,ϕ-carotene (*9*)	−6.9 (217)	219	4.5 (248)	263	−8.9 (284)	312	4.6 (338)	A	[27]
(3*R*)-Rubixanthin (**72**)	−3.0 (224)	235	4.0 (251)	264	−9.1 (291)	318	2.9 (346)	EPA	[28]
(4*R*)-4-Hydroxy-β,β-carotene (*10*)		222	4.2 (242)	265	−2.7 (284)			EPA	[21]
(4*R*)-4'-Hydroxyechinenone (*11*)	−0.9 (232)	240	1.1 (252)	270	−1.8 (298)	330		EPA	[21]
(4*R*)-Isorubixanthin (*12*)		224	1.7 (252)	268	−3.0 (292)	325		EPA	[21]
(3*S*,4*S*,3'*S*,4'*S*)-Crustaxanthin (*13*)	−13.3 (222)	230	19.5 (244)	262	−24.8 (283)	308	8.5 (342)	EtOH	[29]
(3*S*,4*R*,3'*S*,4'*R*)-Crustaxanthin (*14*)	−13.2 (222)	234	10.0 (248)	258	−14.6 (281)	310	4.0 (337)	EtOH	[29]
(2*R*,3*R*,2'*R*)-Caloxanthin (**182**)	−11.9 (220)	232	8.8 (245)	261	−16.7 (282)	313	3.5 (340)	EPA	[30]
(2*R*,3*R*,2'*R*,3'*R*)-Nostoxanthin (**196**)	−10.4 (222)	231	8.8 (244)	260	−16.0 (283)	312	4.6 (337)	EPA	[30]



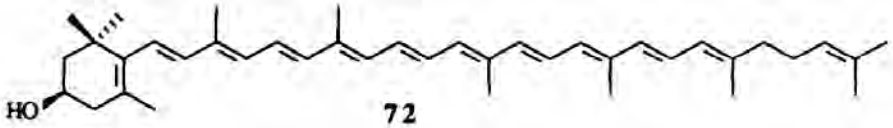
439



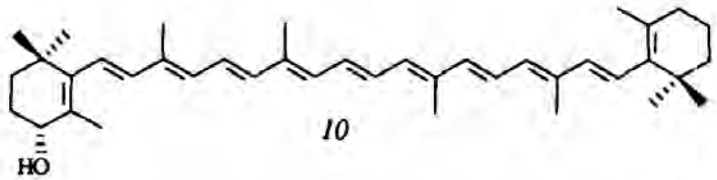
51



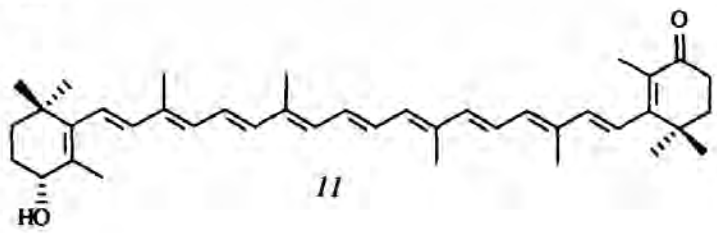
9



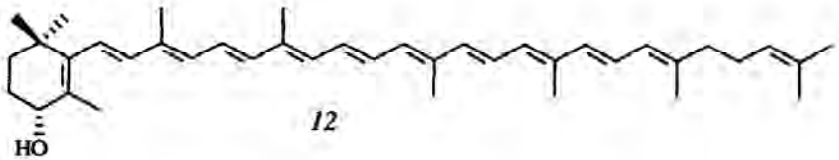
72



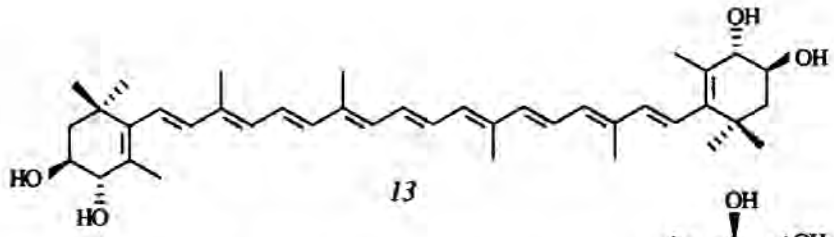
10



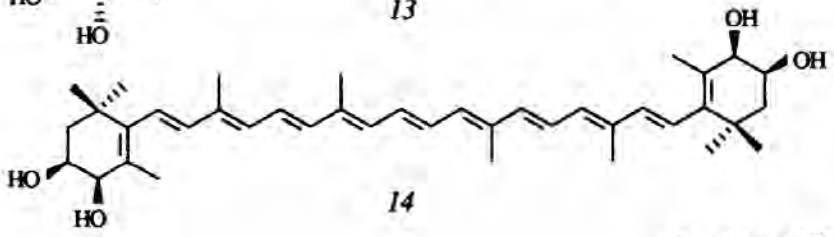
11



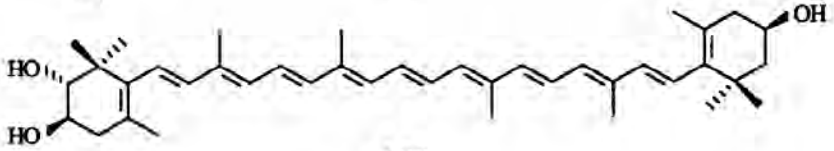
12



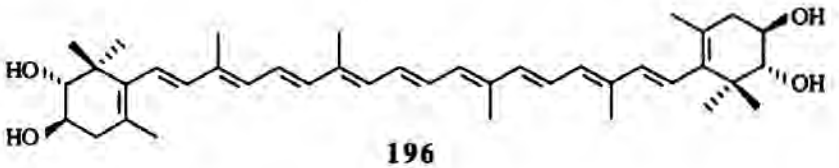
13



14



182



196

The CD spectra of β,β-type carotenoids with other substitution patterns are all of similar shape (Fig. 8 and Table 2). The nature of the substituent is of minor importance as long as it is able to stabilize a specific conformation of the ring. This is clearly demonstrated by the fact that (2*R*,2'*R*)-β,β-carotene-2,2'-diol (**113**) and C.p. 450 (**439**), which have opposite chirality, give spectra that are opposite in sign. The intensity of the spectrum of the latter compound is higher because the larger substituent stabilizes the decisive conformation to a greater degree than does the hydroxy group.

Of more importance than the nature of the substituent is its position in the ring. Substituents at C-3 stabilize the conformation most efficiently. There would be severe steric interactions between an axial substituent at C-3 and the axial methyl at C-1, so the conformation with the C-3 substituent in the equatorial position is less strained and is hence enforced. There is no appreciable steric hindrance between a substituent at C-2 and the C-1 methyl groups, so the stabilizing effect of an equatorial substituent at C-2 is much less and, as a consequence, the CD spectra are of reduced intensity. The stabilizing effect of an equatorial substituent at C-4 is also considerably smaller, because the energy difference between the ring conformations with pseudoequatorial and pseudoaxial allylic substituents is small. Surprisingly, however, the spectrum of (4*R*,4'*R*)-isozeaxanthin (*8*) has about the same intensity as that of the 2,2'-diol (**113**). There must therefore be additional unknown influences on the conformational equilibrium between ring and polyene chain.

Regarding the absolute configuration at the substituted carbon atom, it is important to note that opposite chirality of neighbouring centres stabilizes the same ring conformation. Thus, in (3*R*,3'*R*)-β,β-carotene-3,3'-diol (zeaxanthin, **119**) and (4*R*,4'*R*)-β,β-carotene-4,4'-diol (isozeaxanthin, *8*), the same conformation is stabilized by the equatorial hydroxy groups, and the CD spectra are similar. With (2*R*,2'*R*)-β,β-carotene-2,2'-diol (**113**), in which the equatorial hydroxy group stabilizes the opposite conformation, the CD spectrum is the same shape but of opposite sign. It is therefore necessary to perform at least a conformational analysis of the cyclohexene ring before the chirality at a substituted carbon atom may be inferred from the CD spectrum. For carotenoids bearing more than one substituent on the ring this analysis is sometimes rather difficult. In this situation it is essential to be sure which substituent is the dominating influence on the conformation. Comparison of the spectra of carotenoids with disubstituted β rings, listed in Table 2, demonstrates that it is always the chirality at C-3 which determines the sign of the CD. The higher intensity of the CD of (3*S*,4*S*,3'*S*,4'*S*)-crustaxanthin (*13*), with 3,4-*trans* substitution, compared with that of zeaxanthin (**119**), can be attributed to a synergism of the effects of the neighbouring substituents. A similar effect is not observed, however, with caloxanthin (**182**) or nostoxanthin (**196**) which have analogous di-equatorial 2,3-*trans* substitution. These compounds exhibit Cotton effects of the same intensity as zeaxanthin (**119**) does. It would be of interest to study the CD spectra of carotenoids with 2,4-disubstituted rings with differing relative configurations.

This general correlation between the conformation of the β ring and the sign of the CD has been called the 'conformational rule' [13, 31], and is reliable provided that only the conformation of the cyclohexene ring determines the twist angle around the C-6,7 axis.

For monochiral carotenoids with only one intrinsically chiral end group, such as β-cryptoxanthin (**55**), rubixanthin (**72**) and others, there are no fundamental differences from the above treatment. CD spectra very similar to those of the dichiral analogues, but with approximately half the intensity, are observed (Table 2). For the unsubstituted β rings of the cryptoxanthin (**55**) enantiomeric conformers, both half-chair conformations have equivalent energy and therefore an equal population is present of conformers of the unsubstituted ring with positive and negative twist angles around the C-6,7 axis. Consequently in half of the cryptoxanthin (**55**) conformers the effect of the enantiomeric 3-hydroxy-β-ring conformer that lies on the other side of the chromophore is cancelled. In rubixanthin (**72**) the C-5',6' double bond of the acyclic end group is part of the planar chromophore and therefore cannot contribute to its overall twist.

ii) Substituted 4-keto-β rings. The best representative carotenoid with this type of end group is astaxanthin (**406**). Here it is not simply a ring double bond as in zeaxanthin (**119**) but an α,β-unsaturated ketone that contributes to the intrinsically chiral carotenoid chromophore. Although, in principle, the CD type is not expected to differ from that of the simple substituted β-ring carotenoids, there is no doubt that differences in the ring geometry and in steric and electronic factors in the ring must influence the conformational equilibrium with respect to the C-6,7 axis. In addition, a bathochromic shift of the transitions is to be expected. However, from comparison of the CD spectra of (3*R*,3'*R*)-zeaxanthin (**119**) and (3*S*,3'*S*)-astaxanthin (**406**) which have the same absolute configuration (Fig. 9), the close similarity is evident. When the observed bathochromic shift is taken into consideration, the signs of the

corresponding Cotton effects are identical. This fact was not predictable. The effect is strongly temperature-dependent; drastic differences are observed at lower temperatures (see Section B.2).

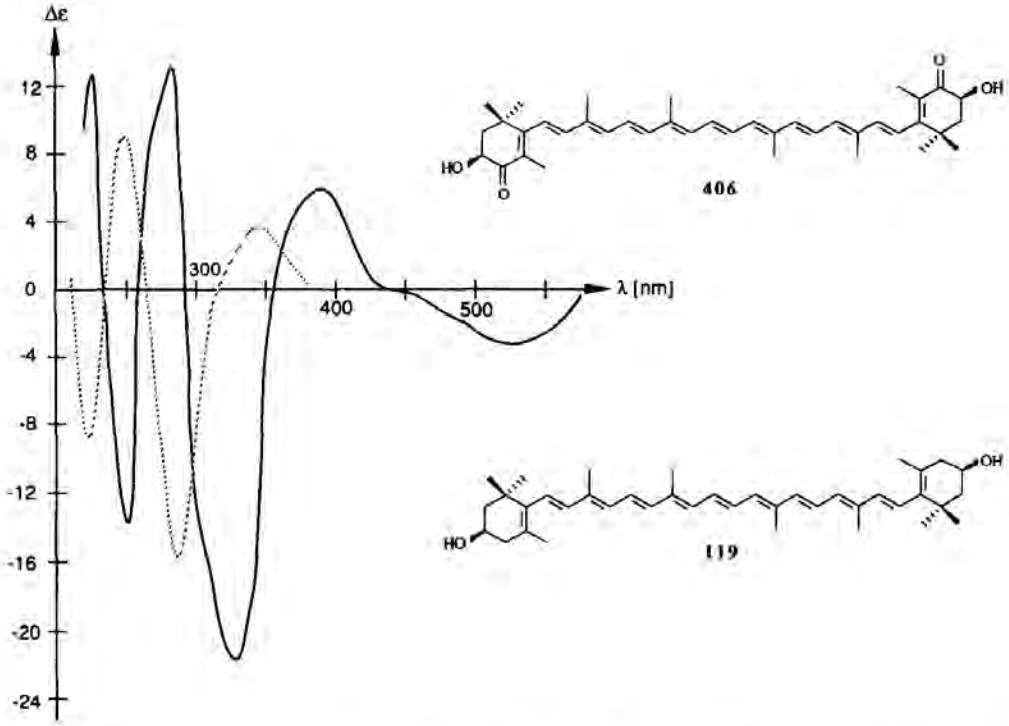


Fig. 9. CD spectra (in dichloromethane) of (3*S*,3'*S*)-astaxanthin (**406**) ——— [10] and (3*R*,3'*R*)-zeaxanthin (**119**) ..... [11].

iii) 5,6-Epoxy-β end groups. At first sight it is not obvious that replacement of the 5,6-double bond in the β ring by an epoxy group should still result in an inherently chiral chromophore. In the visible absorption spectra, epoxides absorb at shorter wavelengths than the parent carotenoids which retain the double bond. It is well known, however, that partial double-bond character is retained on formation of such three-membered rings. In fact carotenoid 5,6-epoxides do have strongly conservative CD spectra comparable to those of other substituted β types (Fig. 10). Since the epoxy group is itself stereogenic, additional chiral substitution in the ring is not necessary for this strong CD (*e.g.* 5,6:5',6'-diepoxy-5,6,5',6'-tetrahydro-β,β-carotene, *16*). The influence of additional substituents like hydroxy groups at C-3 and C-3' is rather small [*cf.* violaxanthin (**259**) and 3,3'-epiviolaxanthin (*15*)]. From CD spectra of epoxides, therefore, conclusions can only be drawn about the absolute configuration of the epoxy group.

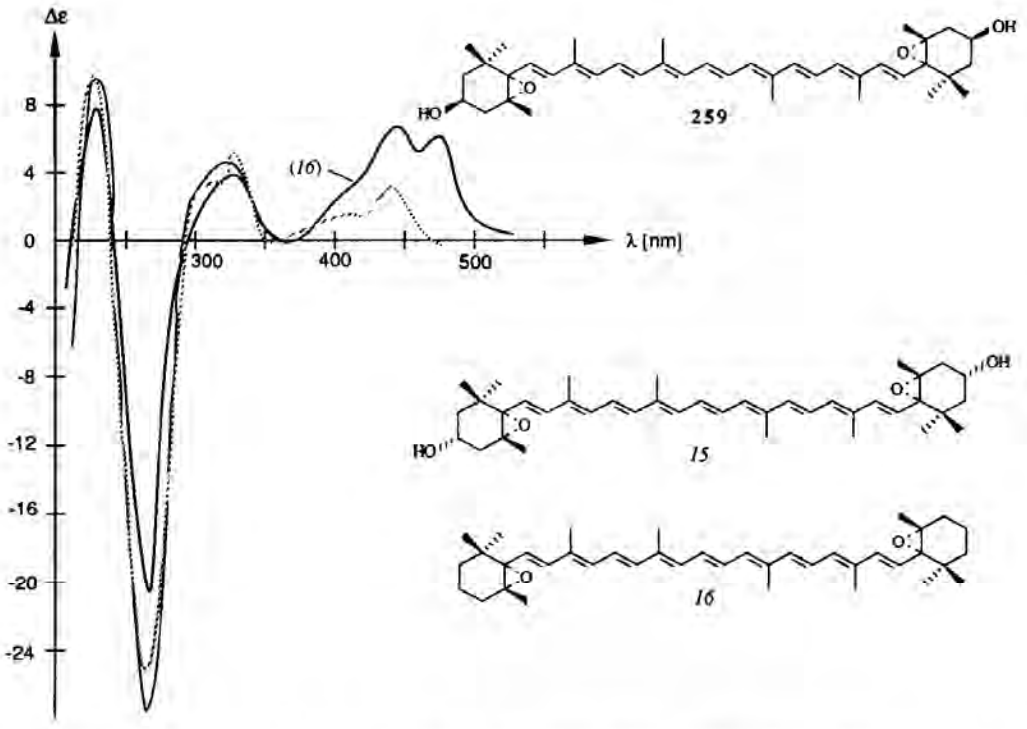
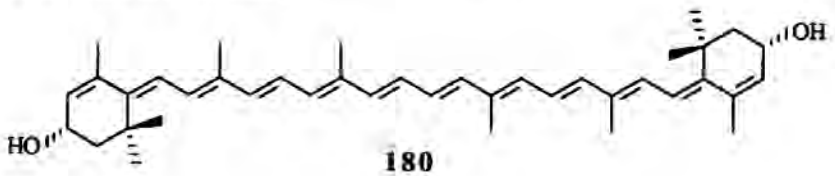


Fig. 10. CD spectra of (3*S*,5*R*,6*S*,3'*S*,5'*R*,6'*S*)-violaxanthin (**259**) (in ethanol) ——— [32], (3*R*,5*R*,6*S*,3'*R*,5'*R*,6'*S*)-epiviolaxanthin (*15*) ..... [26] and (5*R*,6*S*,5'*R*,6'*S*)-5,6:5',6'-diepoxy-β,β-carotene (*16*) ▬▬ [33].

iv) Retro-*carotenoids*. The only optically active *retro*-carotenoid encountered in Nature up to now is eschscholtzxanthin (**180**). Its CD spectrum is clearly determined by the absolute configuration at C-3 and is not altered by the formal change of the C-6,7 and C-6',7' double bonds from the *E* to the *Z* configuration [34]. Although the CD spectrum is not strictly conservative, strong (Δε up to 30) and partly alternating Cotton effects are observed. This unexpectedly high intensity strongly suggests an inherently chiral chromophore. From a conformational analysis similar to those described in Section B.2 a comparatively small twist around the C-7,8 axis is indicated as a result of steric hindrance between H-8 and the methyl groups of the ring. The C-4,5 and C-6,7 double bonds are coplanar. Thus an intrinsically chiral chromophore seems to be formed although, exceptionally, this chirality is not due to twisting between ring and chain. Cooling experiments and the synthesis of in-chain *Z* isomers would contribute to a better understanding.



180

b) Carotenoids containing chiral cyclic end groups that induce chirality and cause non-conservative CD spectra.

i) ε Rings. Carotenoids that contain ε-ring end groups owe their chirality to an asymmetric centre at C-6 next to the chromophore. This structural feature normally would be expected to lead to rather weak, non-conservative CD spectra. For ε-ring carotenoids, the spectra observed are indeed non-conservative, but they are relatively strong (Fig. 11). This implies an interaction between the polyene chromophore and the homoallylic double bond of the ring. Figure 11 and Table 3 show the CD spectra of different ε-type carotenoids. It is clear that the spectra of monochiral carotenoids [*e.g.* β,ε-carotene (**7**), ε,ψ-carotene (**21**)] are approximately only half as intense as that of the homodichiral ε,ε-carotene (**20**). Furthermore, substitution at C-3 has no influence on the sign of the Cotton effects nor on the general shape of the spectrum (*cf.* the ε,ε-carotene-3,3'-diols, the tunaxanthins **150**, **154**, **156**). Obviously such allylic C-3 substituents do not alter the spatial relationship between the ring double bond and the polyene chain. Hence the configuration of C-3' of lutein (**133**), for example, cannot be deduced from the CD spectrum.

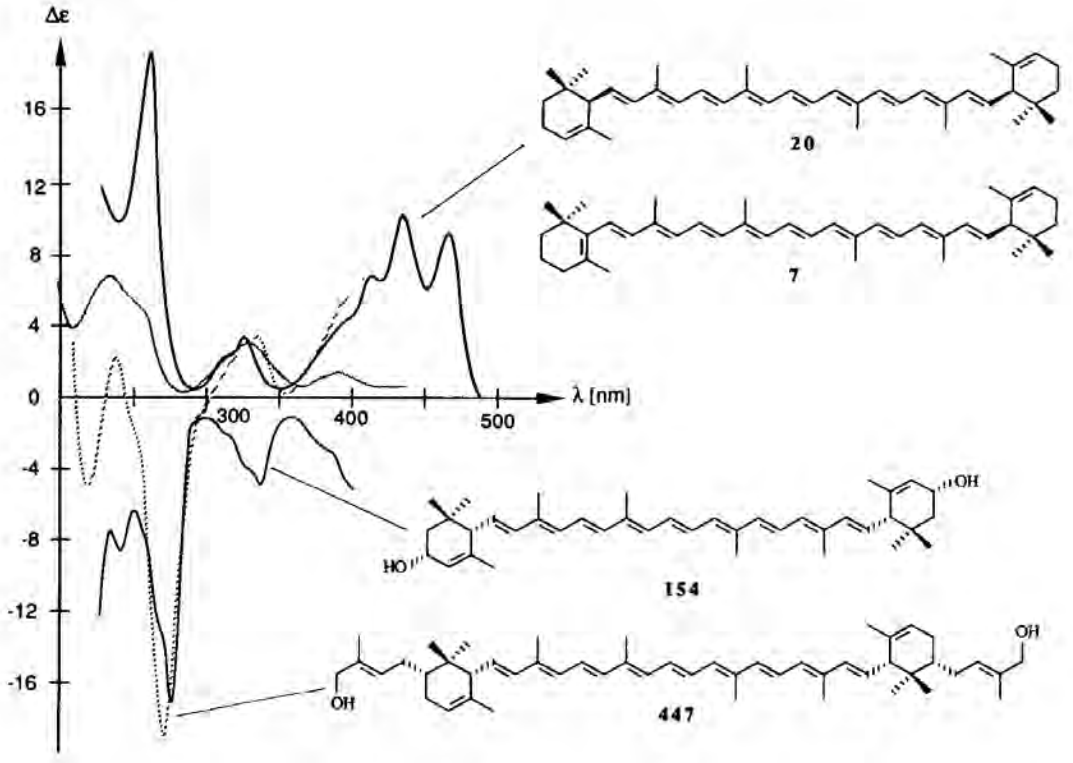


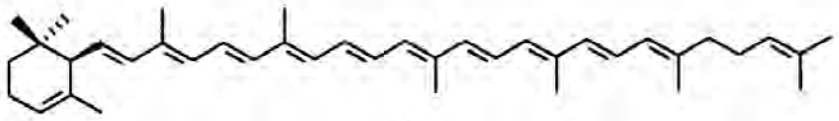
Fig. 11. CD spectra of (6*R*,6'*R*)-ε,ε-carotene (**20**) —— [35], (6*R*)-β,ε-carotene (**7**) (in dioxane) ≈≈≈ [36], (3*R*,6*S*,3'*R*,6'*S*)-tunaxanthin (chiriquixanthin B) (**154**) —— [37] and (2*R*,6*R*,2'*R*,6'*R*)-decaprenoxanthin (**447**) ////// [38].

Substituents at C-2 also seem not to alter the spectra decisively if they are *cis* to the polyene chain as, for example, in decaprenoxanthin (**447**). Substituents in a *trans* relationship, however, would be expected to distort decisively the conformational equilibrium that involves a pseudoequatorial polyene chain. In this case, dramatic changes of the spectrum are expected, depending on the nature of the substituent. Unfortunately the available spectra of the diastereoisomeric 2,2'-dimethyl-ε,ε-carotenes (*17* and *18*) are very weak and are hard to interpret.

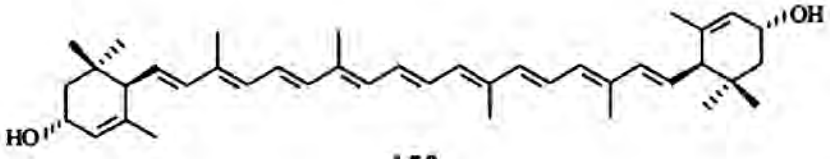
In this context, it is interesting to note that replacement of the cyclohexene C-4,5 double bond by an epoxy group does not change the general shape of the CD spectrum despite the two additional centres of chirality in each ring [35]. This does not invalidate the proposal that interaction between ring double bond and polyene chain is important, but rather confirms the double-bond character of epoxides as was outlined in Section 1.a.iii.

Table 3. Comparison of CD spectra of carotenoids incorporating chiral ε rings and of their epoxides. (Solvents: diox = dioxane; EPA = diethyl ether/isopentane/ethanol, 5:5:2).

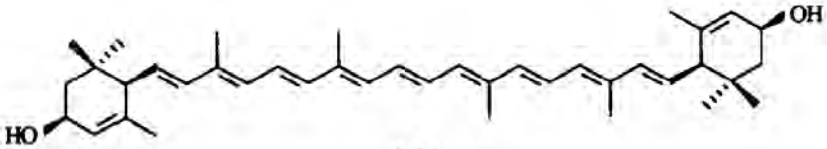
Carotenoid	Δε (λ, nm)					Solv.	Ref.
(6*R*)-ε,ψ-Carotene (**21**)	11.7 (215)	6.1 (242)		3.6 (285)	3.3 (347)	diox.	[36]
(3*R*,6*R*,3'*R*,6'*R*)-Lactucaxanthin (**150**)	4.0 (215)	7.0 (230)	17.5 (264)	1.5 (290)	2.5 (325)	EPA	[39]
(3*S*,6*R*,3'*S*,6'*R*)-Chiriquixanthin B (**154**)		8.3 (234)	18.0 (274)	0 (290)	4.8 (400)	EPA	[37]
(2*R*,6*S*,2'*R*,6'*S*)-2,2'-Dimethyl-ε,ε-carotene (*17*)		0 (238)	2.8 (260)	0 (288)	−1.8 (305) 2.4 (349)	EPA	[40]
(2*R*,6*R*,2'*R*,6'*R*)-2,2'-Dimethyl-ε,ε-carotene (*18*)	−3.6 (210)	−1.2 (235)	−4.7 (265)	−0.3 (285)	−0.9 (327)	EPA	[40]
(4*S*,5*R*,6*R*,4'*S*,5'*R*,6'*R*)-4,5:4',5'-Diepoxy-ε,ε-carotene (*19*)		0 (230)	13.6 (264)	0 (293)	−0.9 (325)	EPA	[35]
(4*R*,5*S*,6*R*,4'*R*,5'*S*,6'*R*)-4,5:4',5'-Diepoxy-ε,ε-carotene (*20*)	-3.3 (226)	0 (240)	10.1 (264)	0 (289)	−2.1 (322)	EPA	[35]



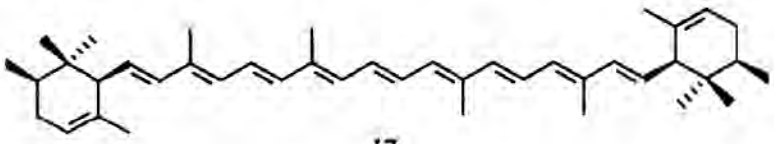
21



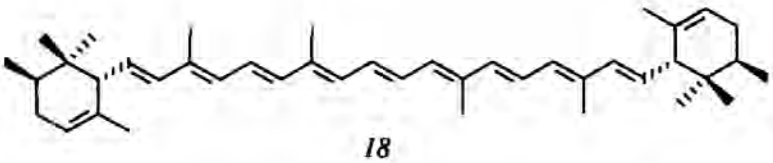
150



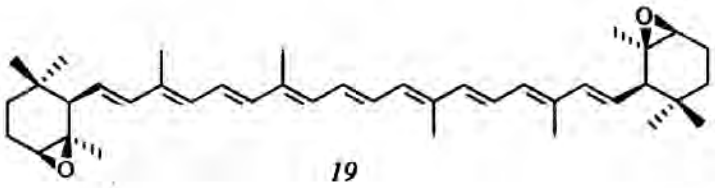
156



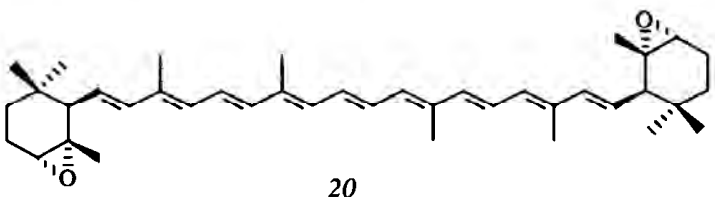
17



18



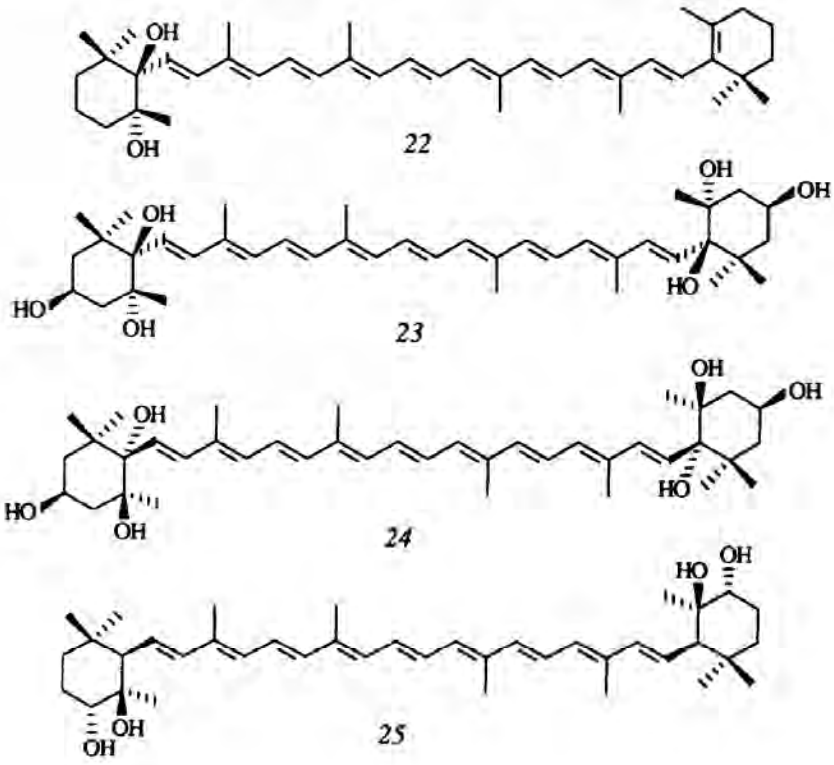
19



20

Table 4. Comparison of CD spectra of carotenoids incorporating hydroxylated dihydro rings. (Solvents: EtOH = ethanol; EPA = diethyl ether/isopentane/ethanol, 5:5:2).

Carotenoid	Δε (λ)	Δε = 0 (nm)	Δε (λ)	Δε = 0 (nm)	Δε (λ)	Δε = 0 (nm)	Δε (λ)	Solv.	Ref.
(5*R*,6*R*)-5,6-Dihydro-β,β-carotene-5,6-diol (*22*)	–0.7 (210)	217	2.0 (231)	245	–1.3 (267)		–0.1 (293) 0 (350)	EtOH	[43]
(3*S*,5*R*,6*R*,3'*S*,5'*R*,6'*R*)-5,6,5',6'-Tetrahydro-β,β-carotene-3,5,6,3',5',6'-hexol (*23*)	1.9 (224)			245	–3.6 (265)	278		EtOH	[44]
(3*S*,5*S*,6*S*,3'*S*,5'*S*,6'*S*)-5,6,5',6'-Tetrahydro-β,β-carotene-3,5,6,3',5',6'-hexol (*24*)	1.1 (215)	240			2.9 (265)			EtOH	[44]
(4*R*,5*R*,6*R*,4'*R*,5'*R*,6'*R*)-5,6,5',6'-Tetrahydro-β,β-carotene 4,5,4',5'-tetrol (*25*)	–1.4 (224)	231	1.0 (244)		2.1 (259) 3.5 (266)	289	0.7 (313) 0 (346)	EPA	[35]



ii) γ End groups. The γ end group, like the ε end group, possesses a bis-allylic chiral centre at C-6. However, due to the presence of only one sp^2-carbon in the ring, γ end groups are able to form real chair conformations, unlike β rings or ε rings. This different geometrical relationship between the exocyclic double bond and the polyene chain must also result in a different electronic interaction, if there is any such interaction at all. Consequently, CD spectra of γ-end-group carotenoids (Fig. 12) are not comparable with those of ε types. The comparatively strong Cotton effects that are observed with γ-ring carotenoids suggest, however, that at least some π–π interaction between end-group double bond and polyene chain is probable. Too few CD spectra of such carotenoids are available to allow any conclusions to be made about the influence of location and nature of different substituents in the γ ring.

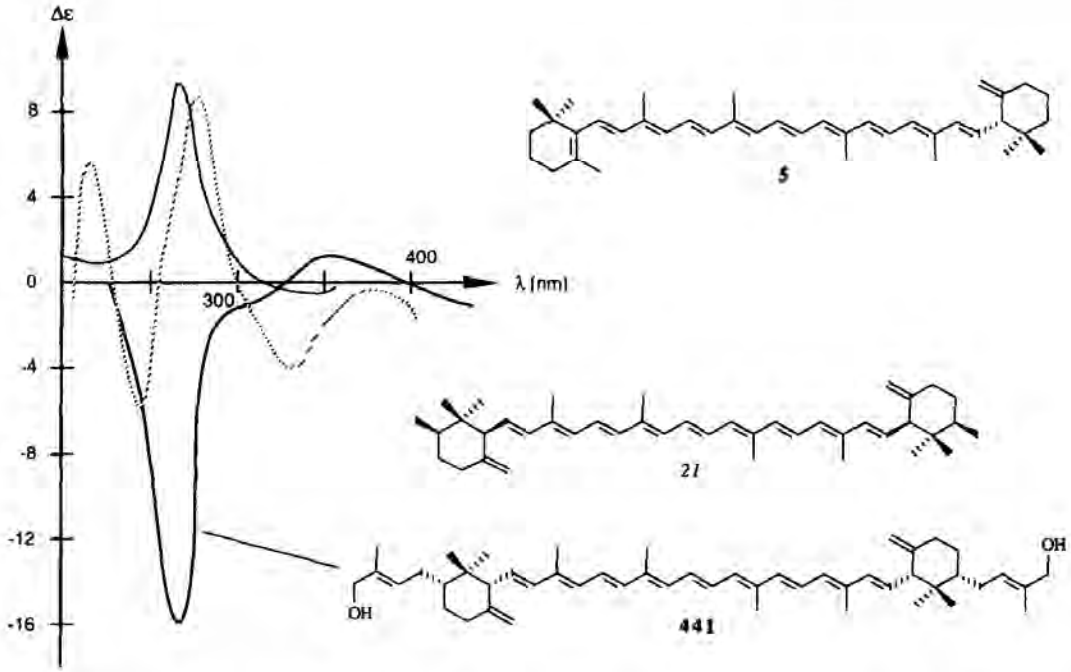


Fig. 12. CD spectra of (6'*S*)-β,γ-carotene (**5**) .... [41], (2*R*,6*R*,2'*R*,6'*R*)-sarcinaxanthin (**441**) ——— and (2*R*,6*S*,2'*R*,6'*S*)-2,2'-dimethyl-γ,γ-carotene (*21*) ——— [42].

iii) Saturated cyclic end groups with two or three hydroxy groups. Known natural carotenoids with this kind of end group include only 5,6-diols and 3,5,6-triols. The CD spectra of 5,6-diols are remarkably weaker than those of the corresponding 5,6-epoxides (Table 4) even though both bear oxygen substituents at C-5 and C-6. Obviously no inherently chiral chromophore is involved here. Comparison of the few available spectral data for monochiral and homodichiral carotenoids of this type does not allow any reliable correlation to be made between CD and the chirality of a specific centre. A similar situation would also hold for related carotenoids with 4,5-diol end groups although these have not yet been encountered in Nature.

iv) 5,8-Epoxides (furanoids). As rearrangement products of 5,6-epoxides, carotenoids with the condensed bicyclic 5,8-epoxy-5,8-dihydro-β end group are often encountered. Disregarding substituents of the six-membered ring, two C-8 epimeric forms are possible, giving 5,8-*cis* and 5,8-*trans* structures. The CD spectra of both epimers (Fig. 13) show a typical non-conservative shape with increasing intensity towards shorter wavelengths. The signs of the Cotton effects clearly are determined by the absolute configuration at C-8. This is not surprising, considering that a change of the configuration at C-5 can cause only a small chiral disturbance of the polyene chain compared to the strong direct influence of the polarized chiral centre at C-6 of the 5,6-epoxides. Furthermore, the rather rigid dihydrofuran ring is not subjected to conformational changes if the configuration at C-5 is reversed or if additional substituents are present *e.g.* at C-3 of the cyclohexane ring (*cf.* qualitative CD spectra of the C-8 epimeric auroxanthins (**267-270**) [47]).

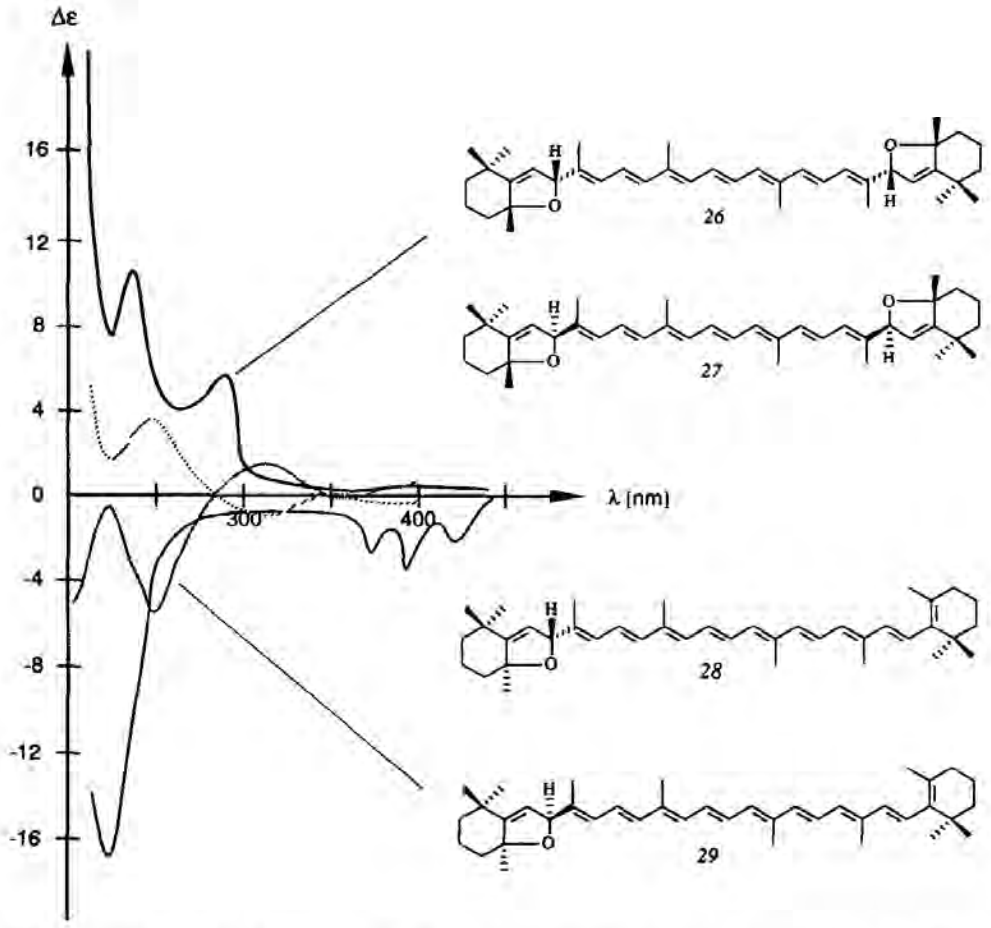
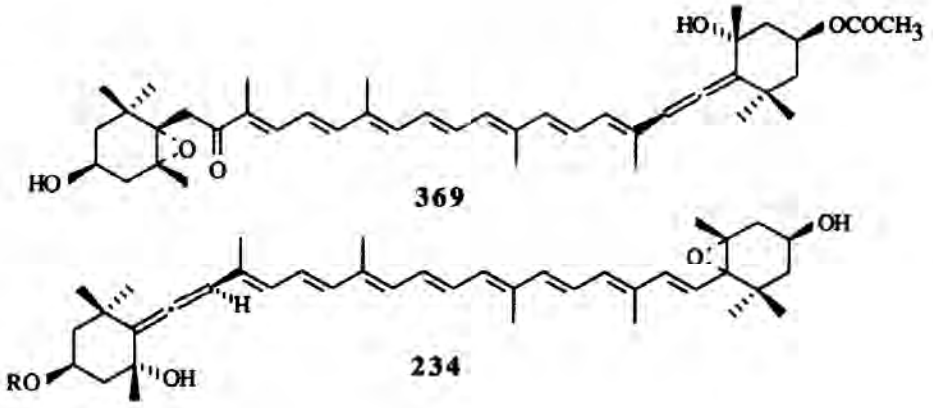


Fig. 13. CD spectra of (5*R*,8*R*,5'*R*,8'*R*)-aurochrome (*26*) ——, (5*R*,8*S*,5'*R*,8'*S*)-aurochrome (*27*) —— [45], (5*S*,8*R*)-mutatochrome (*28*) ////, and (5*S*,8*S*)-mutatochrome (*29*) ···· [46].

v) Allenic end groups. Carotenoids with allenic end groups occur in large amounts in Nature, *e.g.* neoxanthin (**234**) and fucoxanthin (**369**). This structural feature has a chiral axis and introduces axial chirality. The spectrum of the homodichiral carotenoid mimulaxanthin (**202**) (Fig. 14) shows only very weak, non-conservative CD, the origin of which is attributed to the axial chirality of the allene group and is probably not influenced by the absolute configuration of the hydroxy substituents at C-3 and C-5. However, carotenoids of this type with diastereoisomeric end groups have not yet been obtained, so a conclusion in this respect is precluded.



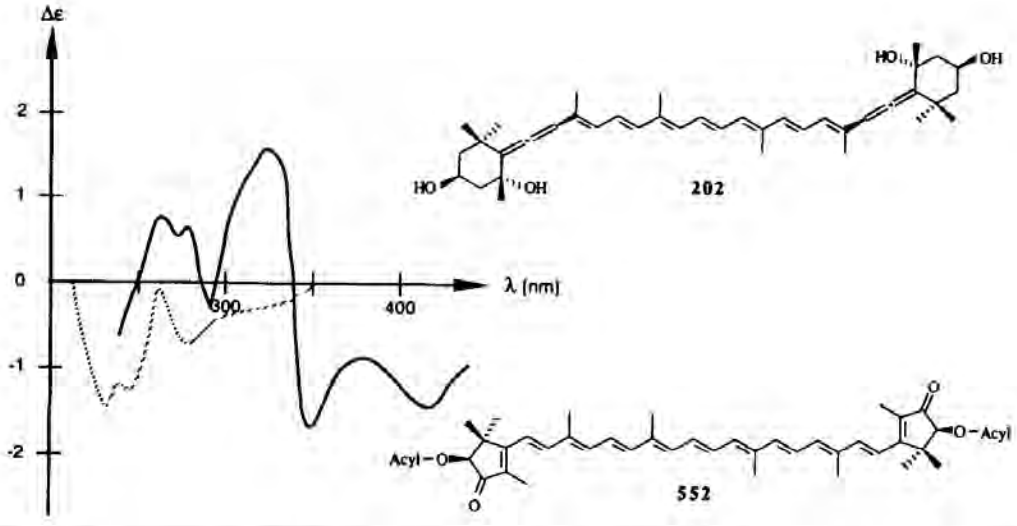


Fig. 14. CD spectra of (3*S*,5*R*,6*R*,3'*S*,5'*R*,6'*R*)-mimulaxanthin (**202**) (in hexane/ether/methanol, 10:2:1) —— [48], and (3*S*,3'*S*)-actinioerythrin (**552**) .... [49].

vi) Five-membered rings. An example of a carotenoid with a five-membered ring is actinioerythrol (**552**) which is structurally related to astaxanthin (**406**). In contrast to astaxanthin, however, only weak Cotton effects ($\Delta\varepsilon$ up to 2) of a rather non-conservative type are observed (Fig. 14). It is clearly indicated by the long wavelength of absorption and by analysis of models that there is no steric hindrance to force the ring enone system out of the plane of the main chromophore, so no inherently chiral chromophore is formed.

Capsorubin (**413**), its C-3 epimer (*30*) and a C-2 hydroxylated isomer (*31*) have been synthesized. The identity of their CD spectra is striking (Fig. 15). It therefore seems that changes of the ring conformation do not have any influence. Obviously the centres of chirality in the α-position to the keto groups (*i.e.* C-5 and C-5') are exclusively responsible for the CD. Classification of the spectral type is not clear. Regular alternation of Cotton effects is observed, but only one of the maxima is relatively strong ($\Delta\varepsilon$ up to 8).

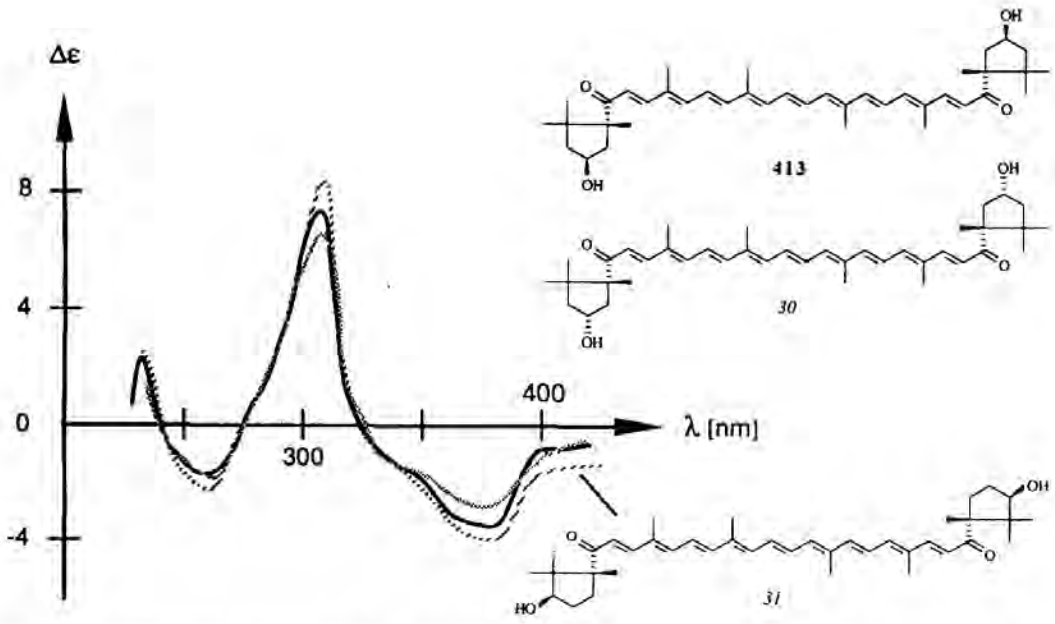


Fig. 15. CD spectra (in dioxane) of (3*S*,5*R*,3'*S*,5'*R*)-capsorubin (**413**) ———, (3*R*,5*R*,3'*R*,5'*R*)-epicapsorubin (*30*) ∞∞∞ and (2*R*,5*R*,2'*R*,5'*R*)-isocapsorubin (*31*) ⁄⁄⁄⁄ [50].

vii) 3,6-Epoxides. A few recent papers report the natural occurrence of optically active carotenoids with cyclic end groups that incorporate a C-3,6 oxygen bridge (see references in [51]). These end groups are of interest because of their rigid ring structure and the presence of a boat conformation of the cyclohexane ring. Few CD data are available for monochiral or homodichiral carotenoids or related model structures of this type [52, 53], so general conclusions are not yet possible. The spectra are weak and resemble conservative spectra.

c) Acyclic carotenoids

Acyclic end groups generally have a much higher degree of conformational flexibility than their cyclic analogues. It is therefore almost impossible to deduce which specific conformer would be of decisive importance for the CD spectrum. Some carotenoids with this kind of end group exhibit surprisingly strong Cotton effects whilst others possess almost no significant CD. Even more confusing is the observation that, in some cases, a conservative or nearly conservative type of CD is found, although it is impossible to attribute any inherently chiral chromophore to the molecule under consideration. Finally, unexpected sign changes for mono-*Z* isomers have been observed, a typical indication of an inherently chiral chromophore.

i) Acyclic end groups bearing oxygen functions at C-1, or at C-1 and C-2. 1,2-Epoxides and 1,2-glycols with identical chirality at C-2 exhibit relatively weak CD spectra of identical sign and similar general shape (Fig. 16). This is not surprising since in these two cases there is a centre of chirality with a dipole moment induced by an oxygen atom at an identical distance from the chromophore. This situation is different from that of the inherently chiral 5,6-epoxy-β ring. It is surprising, however, that the spectra of these acyclic carotenoid epoxides and glycols are close to conservative in type. This is not in accordance with the general rule that conservative spectra are only shown by inherently chiral chromophores. In addition, sign change for mono-*Z* isomers is observable, another feature which does not fit theoretical predictions.

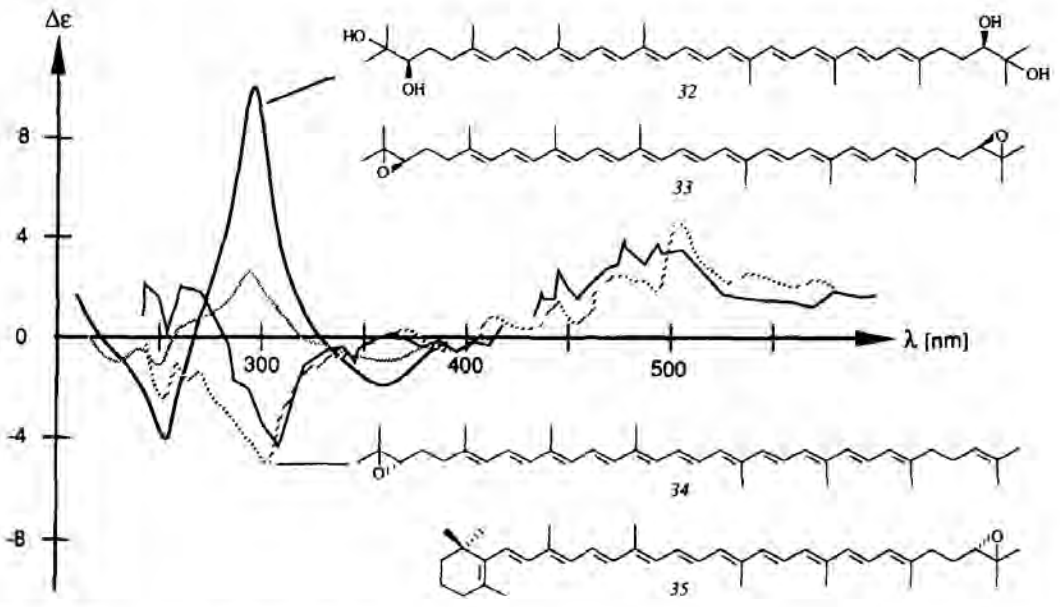
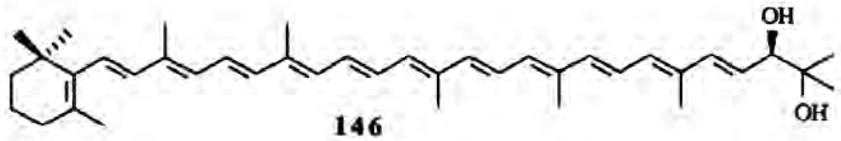


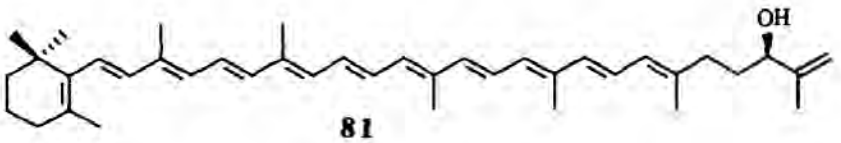
Fig. 16. CD spectra of (2*R*,2'*R*)-1,2,1',2'-tetrahydroxy-1,2,1',2'-tetrahydrolycopene (*32*) (in dichloromethane) ——— [54], (2*R*,2'*R*)-1,2:1',2'-diepoxy-1,2,1',2'-tetrahydrolycopene (*33*) »»» [54], (*S*)-1,2-epoxy-1,2-dihydrolycopene (*34*) ,,,, [55] and (*S*)-1',2'-epoxy-1',2'-dihydro-β,ψ-carotene (*35*) —— [55].

Surprisingly, plectaniaxanthin (**146**), a 1,2-glycol with a centre of chirality at C-2' in an allylic position relative to the polyene chain, exhibits only very weak Cotton effects at room temperature. The acylated derivatives, however, or the glycol itself at lower temperatures, give spectra with intensities similar to those of spectra of other 1,2-glycols (unpublished work, *cf.* also [56]). The weak CD of plectaniaxanthin (**146**), therefore, must be attributed to an unfavourable conformational equilibrium rather than to the constitution of the carotenoid. Plectaniaxanthin (**146**), however, has a monocyclic chromophore, so further comparisons with purely aliphatic 1,2-glycols may not be reliable.

Aleuriaxanthin (**81**), the last representative to be discussed, again has a hydroxy substituent attached to the chiral centre at C-2'. In contrast to the other carotenoids with this structural element, however, an isolated terminal vinylic group replaces the second hydroxy group. As with plectaniaxanthin (**146**), only very weak Cotton effects are observable, and these are not comparable to those for similar carotenoids [57, 58].



146



81

ii) Acyclic C_{45} and C_{50} carotenoids. Despite the substantially greater number of carbon atoms, carotenoids of this group are constitutionally comparable to some of the chiral 2-hydroxylated carotenoids discussed in the previous paragraph. Formally, the hydroxy group at C-2 is simply replaced by an isoprene unit. The structural differences which are of relevance for the CD are the changes in the polarity of the substituent group at the chiral centre, the larger space requirement of the C_5 units with probable implications for the conformational equilibrium, and an elongated chromophore. The observed spectra (Fig. 17) are of similar intensity to those of the corresponding 1,2-epoxides but are remarkably stronger than those found for plectaniaxanthin (**146**) and aleuriaxanthin (**81**). The spectral type has become even more conservative, a feature which is still not understood. Any explanation of this phenomenon by means of hydrogen bridges or interaction of terminal double bonds with the chromophore must be disregarded because tetradeoxybacterioruberin (*36*), which has completely saturated hydrocarbon end groups, exhibits an identical type of spectrum. The fact that sign inversion of all Cotton effects occurs upon complete saturation of the terminal double bonds adds another intriguing feature. [Note: (*R,R*)-bacterioruberin (**456**) and (*S,S*)-tetradeoxybacterioruberin (*36*) have equivalent absolute configurations].

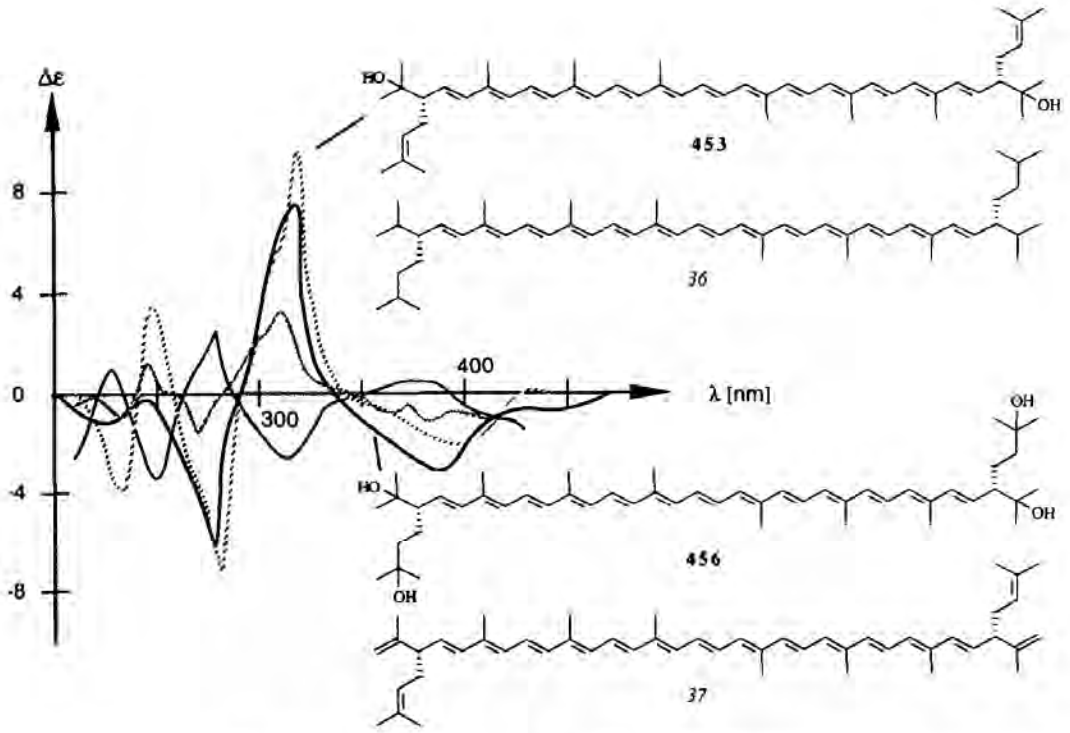


Fig. 17. CD spectra of (2*S*,2'*S*)-bisanhydrobacterioruberin (**453**) ~~~ [59], (2*R*,2'*R*)-tetradeoxybacterioruberin (*36*) —— [59], (2*S*,2'*S*)-bacterioruberin (**456**) ▬▬ [60] and (2*S*,2'*S*)-tetraanhydrobacterioruberin (*37*) ···· [59].

2. Heterodichiral carotenoids

It would be far beyond the scope of this Chapter to discuss in detail the numerous spectra that have been published of heterodichiral carotenoids, *i.e.* those that bear two different chiral end groups. The most important practical point is that the CD spectra of these compounds are, in principle, the sum of contributions derived from the spectra of the corresponding monochiral and homodichiral compounds with the individual end groups. Many examples encountered in the previous section obviously show that monochiral carotenoids exhibit the same shape of spectrum as analogous homodichiral carotenoids, but the intensity for the latter is approximately doubled. This leads to the assumptions that, in a dichiral carotenoid, the effects of the two end groups are independent and roughly additive. As was outlined earlier in Section B.1, this model is indeed correct as long as some caution is exercised.

In the following example, the application of the additivity rule is demonstrated, and some practical guidelines for applying this rule to different carotenoids are given. During this discussion, the expression 'CD effect of end group A' will be used to signify the effect of end

group A on the CD spectrum of the carotenoid under consideration. Obviously a CD spectrum cannot be assigned to an end group alone. Lutein (**133**), as a prominent representative heterodichiral carotenoid, will be used as a practical example, although its absolute configuration was originally elucidated in a different way.

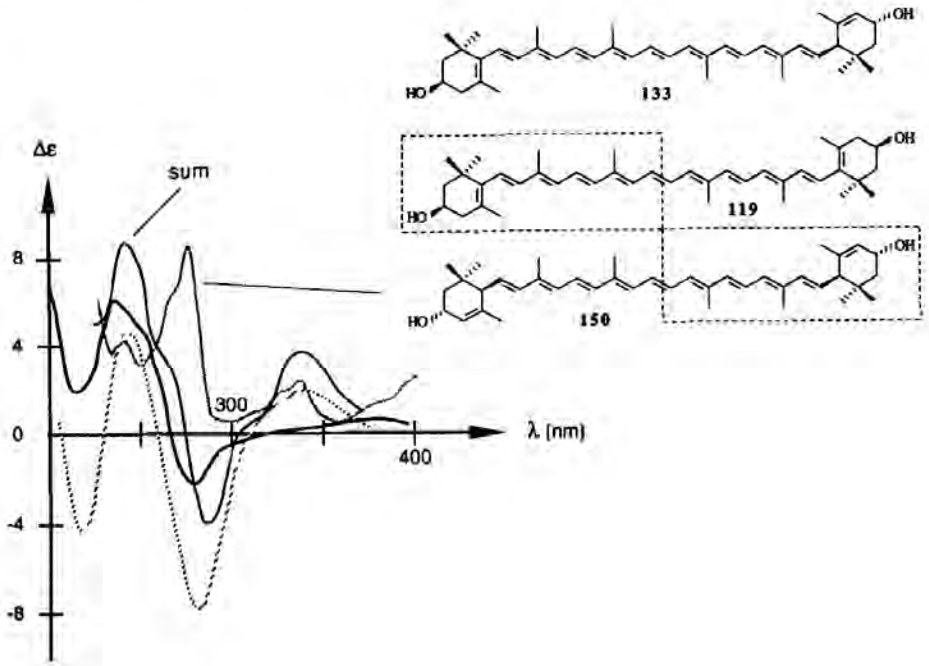


Fig. 18. CD spectra of (3*R*,6*R*,3'*R*,6'*R*)-lactucaxanthin (**150**) (1/2 intensity) ⁘⁘, (3*R*,3'*R*)-zeaxanthin (**119**) (1/2 intensity) ,,,, sum of both spectra ——, and spectrum of (3*R*,3'*R*,6'*R*)-lutein (**133**) ▬▬ [36].

The two end groups of lutein (**133**) are present also in the homodichiral carotenoids zeaxanthin (**119**) and lactucaxanthin (**150**), respectively. According to the additivity rule, addition of the CD spectra of these two compounds, but with half the intensities, should result in the CD of lutein (**133**). The addition was performed by transformation of the curves for zeaxanthin (**119**) and lactucaxanthin (**150**) into numerical values, subsequent addition of Δε values at corresponding wavelengths and then back-transformation into the resulting curve. The calculated and the measured spectra, as shown in Fig. 18, are indeed quite similar. In particular, all the minima and maxima, including signs and relative intensities, are identical. The positions of the peaks and the absolute intensities are, however, not very accurate. This is at least partly attributable to the fact that the three carotenoids involved have different chromophore lengths and hence different absorption maxima. For verification of the result, two similar additions, one with the CD of the enantiomer of zeaxanthin (**121**) and one with the CD of the enantiomer of lactucaxanthin (**159**) were also performed. This transformation should lead to a set of mirror-image spectra which are clearly distinguishable from the previous type.

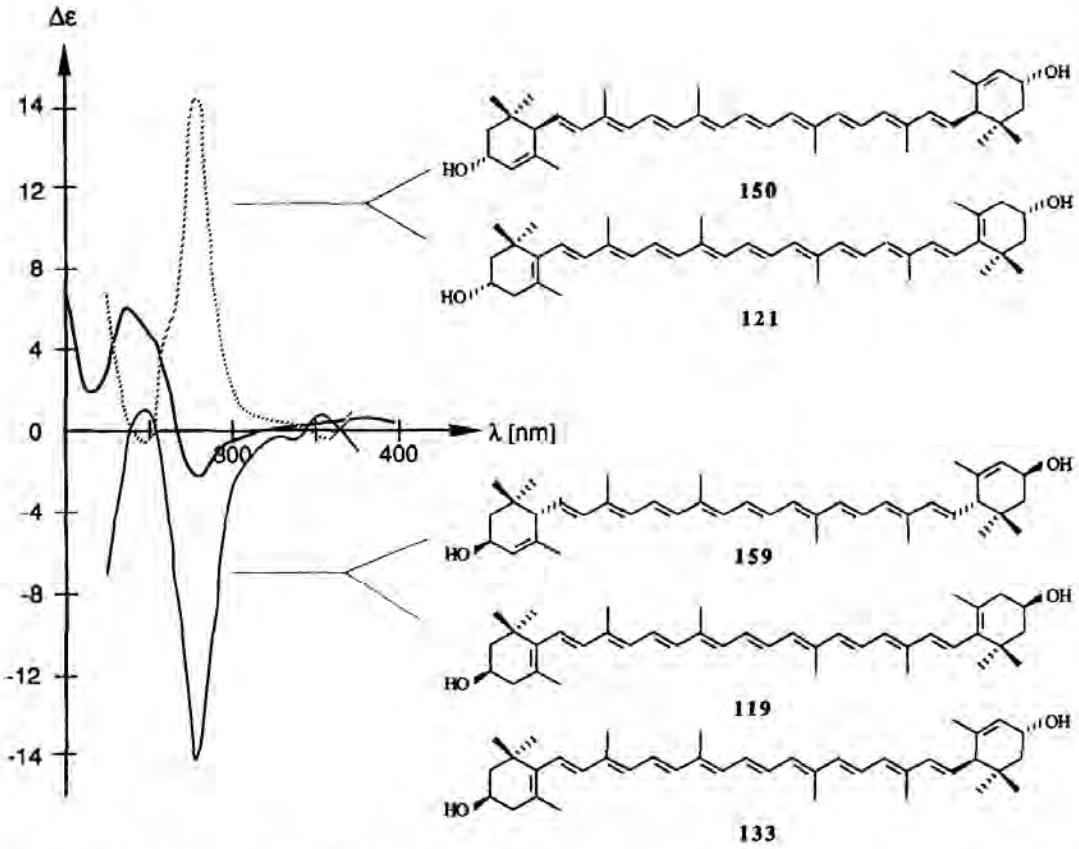
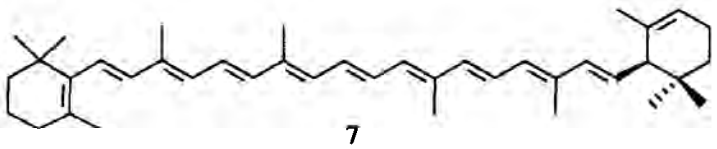
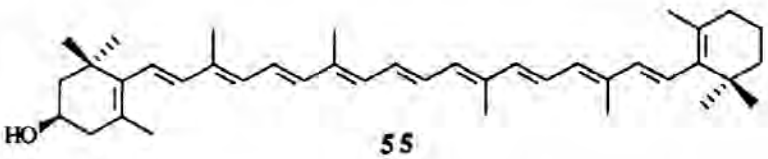


Fig. 19. Calculated CD spectra of 1/2 (3*R*,6*R*,3'*R*,6'*R*)-lactucaxanthin (**150**) + 1/2 (3*S*,3'*S*)-zeaxanthin (**121**) ...., 1/2 (3*S*,6*S*,3'*S*,6'*S*)-lactucaxanthin (**159**) + 1/2 (3*R*,3'*R*)-zeaxanthin (**119**) ———, and recorded spectrum of (3*R*,3'*R*,6'*R*)-lutein (**133**) ▬▬ [36].

The result is shown in Fig. 19. Both spectra clearly differ from that of lutein (**133**). If the chirality of lutein (**133**) were unknown, the absolute configuration at C-3 and C-6' could now be concluded with reasonable reliability. As was explained in Section D.1.b., the correlation would not allow any conclusion about the configuration at C-3'. Thus similar results would have been obtained by addition of the spectra of (6'*R*)-β,ε-carotene (**7**) and (3*R*)-β-cryptoxanthin (**55**) despite the absence of a 3'-hydroxy group in β,ε-carotene (**7**).



7



55

In order to compute the CD spectrum of a heterodichiral carotenoid by addition of the effects of its end groups a series of rules should be observed.

i) The CD contributions derived from the effects of the two end groups to be added should be of comparable intensity. Discrepancies are especially significant when strong conservative and weak non-conservative spectra are to be added. In this case, the results are not reliable, due to inaccuracies of wavelength and intensities in the available measured values.

ii) The end-group CD contributions used for addition should, whenever possible, originate from carotenoids that have identical chromophores, preferably the same chromophore as the target molecule. The position and sometimes even the intensity of a Cotton effect are dependent on the type and length of the chromophore. Generally, longer chromophores cause a bathochromic shift of CD maxima and minima, *i.e.* towards longer wavelength. In such cases it can be difficult to decide which Cotton effects should be added. If the spectral shifts are identifiable unequivocally, *e.g.* by comparison with related spectra, addition is sometimes possible simply by correction for the shifts prior to the addition. Sometimes small shift differences do not change the general shape of the resulting spectrum decisively. An example of this, lutein (**133**), was presented above. In such cases, correct conclusions can be reached without prior shift corrections. This shift sensitivity can easily be checked by comparing the spectra obtained with and without corrections.

iii) Spectral contributions obtained at significantly different temperatures cannot be added, because of the usually strong temperature-dependence of CD spectra. It is therefore also obvious that, for comparison with the calculated spectrum, the spectrum of the target carotenoid should be determined at the same temperature.

iv) The additivity rule has only been applied to all-*trans* carotenoids and nothing is known about its validity for *cis* polyenes. If the CD of a *trans* carotenoid has to be calculated, the spectral contributions must also originate from all-*trans* carotenoids. This requirement is sometimes difficult to fulfil, especially when only small, non-crystalline samples are available. From the strong changes that can be observed, mainly in conservative spectra, upon change of the polyene geometry, it is obvious that disregarding this requirement would lead to highly unreliable results.

v) In most cases it is possible to use measurements performed in different solvents. It has been shown that solvent dependence of CD, in the range of solvents generally used, is rather small.

vi) To check the result, it is valuable to perform the addition also by using the CD of a carotenoid with the enantiomeric end group. Results are only considered reliable if there is a clear difference between the two calculated spectra and if the measured spectrum of

the target compound is clearly similar to one of them. In cases where spectra with relatively weak intensities are involved, reliable assignments are sometimes rather difficult. It is then recommended that the additions and comparisons are performed with spectra measured at the temperature of liquid nitrogen. Then the intensities are normally considerably larger and the spectral contributions used in the calculations are more characteristic.

It must be stressed that comparison of calculated with measured spectra normally does not give any information about relative configurations of two or more substituents in the same ring. The relative configurations can, however, often be deduced from ^{1}H-NMR spectra (Chapter 6). It is essential to know unambiguously which chiral elements in an end group are really decisive for the CD. The result of the addition can consequently give information only about the chirality of these decisive elements and not about other chiral elements in the end group.

Finally, in a few cases, the CD spectra of carotenoids that contain end groups which are not represented in any known monochiral or homodichiral carotenoid have been calculated by an inverse application of the additivity rule. Thus, in a carotenoid consisting of one end group, A, which has a known effect on the CD and a second end group, B, for which the effect on the CD is unknown, the effect contributed by end group B can be calculated by subtracting the contribution attributed to end group A from the observed CD of carotenoid A–B. The result can then be used for further correlations.

Detailed examples of stereochemical correlations by means of the additivity rule are given in the literature, *e.g.* [61].

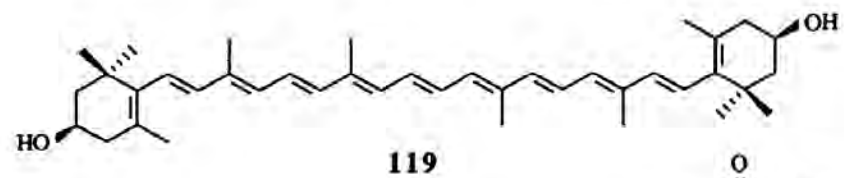
3. Modifications of the polyene chain

All CD spectra that have been discussed in Section D.1-2 were of carotenoids with a simple, all-*trans* polyene chain. There are, however, many natural carotenoids in which the polyene chain exhibits some additional features like triple bonds, cross-conjugation or oxygen substituents. In addition, *E*/*Z* isomerism of one or more double bonds is a feature that is often encountered. All these modifications influence the CD spectra.

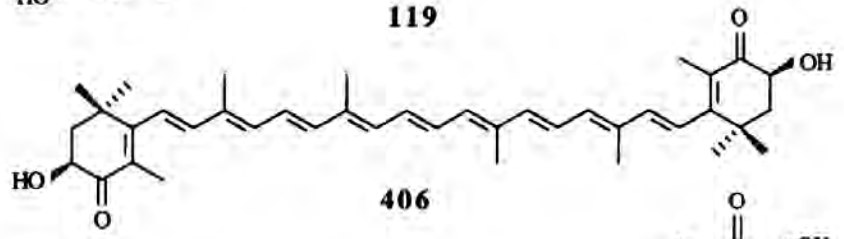
a) Geometrical isomerism

i) Carotenoids with conservative spectra. There have been few publications of CD spectra of *cis* isomers of carotenoids. As early as 1939, however, it was observed that geometrical isomerization of optically active carotenoids can have a strong influence on the optical rotation [62].

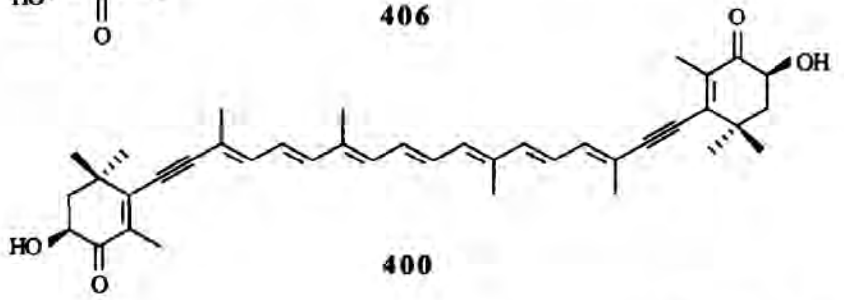
For carotenoids that show conservative CD spectra, the influence of *cis*/*trans* isomerism has already been mentioned several times above. Such carotenoids with an odd number of *cis* double bonds have spectra that are opposite in sign to the spectrum of the all-*trans* isomer, whereas those with an even number of *cis* double bonds exhibit CD with the same signs as the all-*trans* compound. This has been verified on several occasions for isomers of (3*R*,3'*R*)-zeaxanthin (**119**) [9,11,12],(3*S*,3'*S*)-astaxanthin (**406**) and its esters [10,14,18],7,8,7',8'-



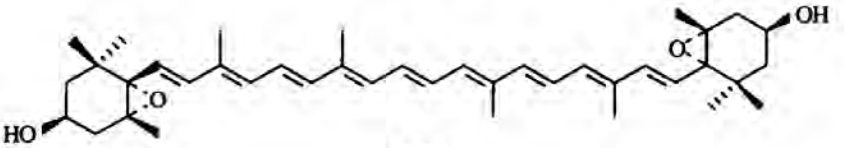
119



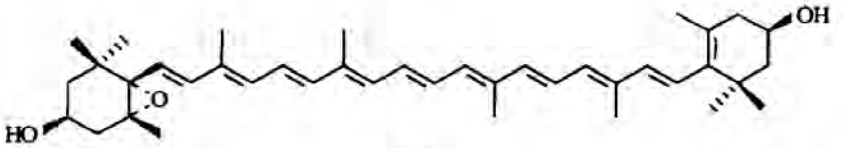
406



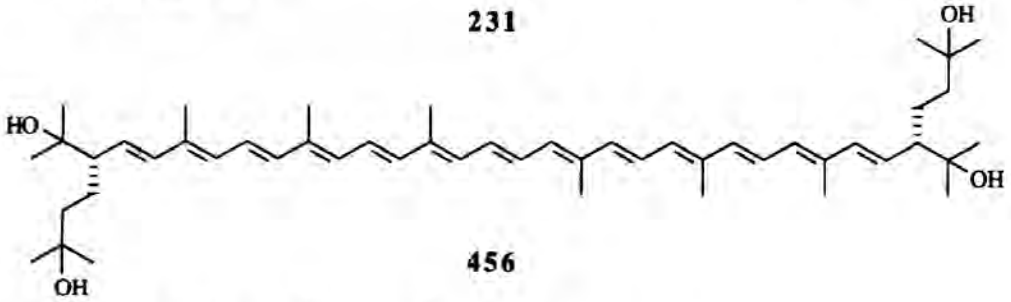
400



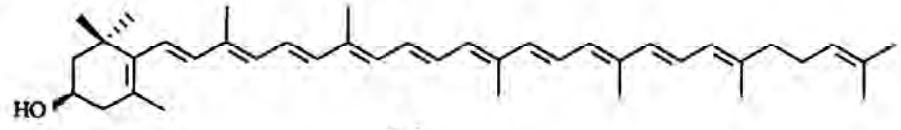
259



231



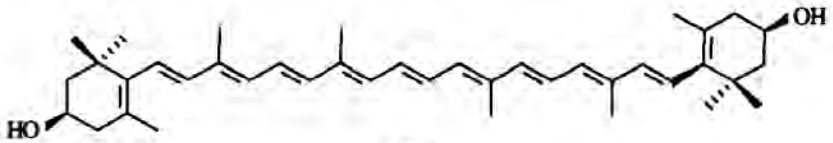
456



72

tetradehydroastaxanthin (**400**) and its 9Z and 9Z,9'Z isomers [9], violaxanthin (**259**) [26,32], antheraxanthin (**231**) [63], and (2*S*,2'*S*)-bacterioruberin (**456**) [64]. The rule is also valid for the monochiral rubixanthin (**72**) [19]. It is thought that this sign inversion is due to the 90° tilt of the C2-symmetry axis upon introduction of a *cis* double bond in the chain [9, 14]. Although the signs of the CD peaks are inverted, the spectra are not exact mirror images. The relative intensities of the bands are considerably altered. In the CD spectrum, the first UV peak, at the position of the *cis*-peak of the absorption spectrum, becomes considerably more intense in the mono-*cis* isomers that have the *cis* double bond near the middle of the chain. The influence of the position of the *cis* double bond in the chain has been studied [12, 14] for mono-*cis* isomers and a number of poly-*cis* isomers of zeaxanthin (**119**). The strongly hindered 7Z and 7Z,7'Z isomers are special and show a rather complicated CD pattern and also a complicated temperature dependence, due to several simultaneous conformational equilibria. The sign inversion does not occur in the longest wavelength CD peak under the main absorption but only in the UV bands between *ca.* 400 and 200 nm; no theoretical explanation could be offered for this observation [12].

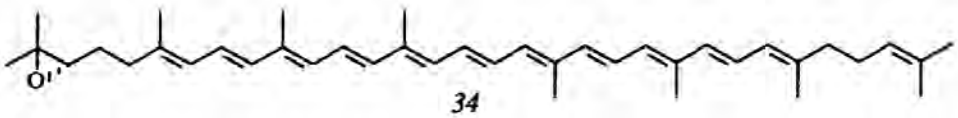
ii) Carotenoids that exhibit non-conservative spectra. The case of *cis* isomers of carotenoids that give non-conservative CD spectra is poorly understood; few examples can be found in the literature. At room temperature, the CD spectra of lutein (**133**) and 3'-epilutein (**137**) are on the borderline of conservative and non-conservative types [14]. The low-temperature spectra are approximately conservative and show the same sign inversion as the spectra of the zeaxanthin (**119**) isomers; only the peak in the UV region at the wavelength of the *cis*-peak in the absorption spectrum is an exception for all-*E*-lutein (**133**). The CD spectra of the *cis* isomers of lutein are more conservative than that of all-*E*-lutein [11, 14, 65]. The bands in the visible range are again irregular, as for zeaxanthin (**119**) [14].



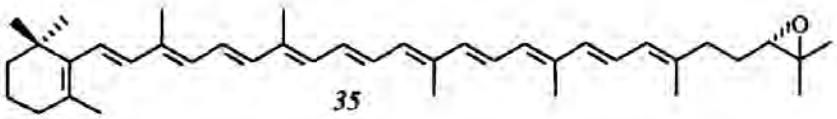
137

Similar results are given by the all-*E* and the 5Z and 7Z isomers of 1,2-epoxy-1,2-dihydrolycopene (*34*), the all-*E* and 7'Z isomers of 1',2'-epoxy-1',2'-dihydro-β,ψ-carotene (*35*), and the all-*E* and several mono-*Z* isomers of capsanthin (**335**) [66]. Especially at low temperature, these compounds show 'conservative-like' CD spectra which invert sign upon geometrical isomerization, but again only in the UV part of the spectra [54, 55].

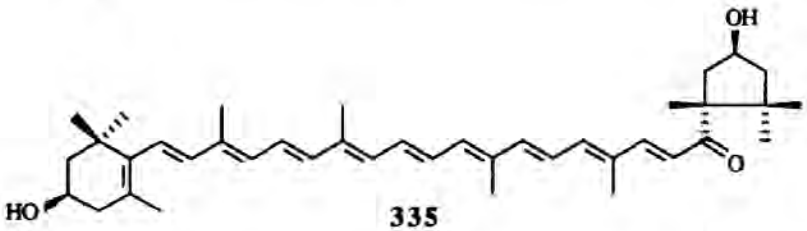
Isomers of fucoxanthin (**369**) provide another example of borderline conservative/non-conservative spectra. Recently, *cis* isomers of fucoxanthin (**369**) have been isolated and characterized by ^{1}H-NMR spectroscopy. The CD spectra of the all-*E* and three mono-*Z* isomers were published. The CD of the all-*E* isomer is clearly not conservative; those of the 13Z and the 9'Z isomers resemble conservative spectra, whereas that of the 13'Z isomer does not. Some sign inversions were observed, however [67].



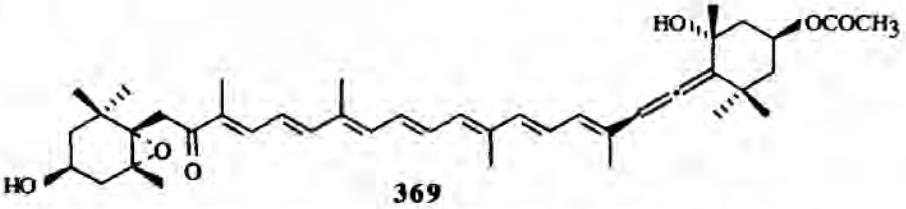
34



35

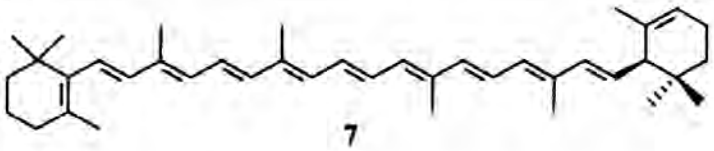


335



369

The only example of CD spectra of *cis* isomers of carotenoids that have truly non-conservative spectra is the pair of all-*E*- and 11'Z-β,ε-carotene (**7**), for which there is clearly no sign inversion [68].

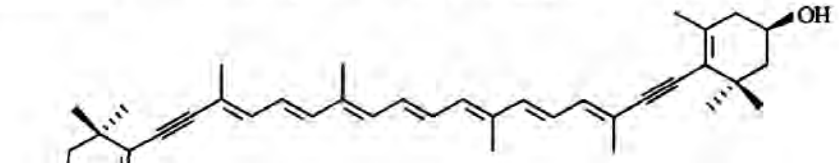


7

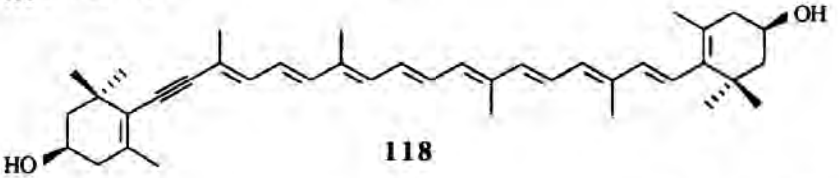
b) Other modifications

In a relatively large number of the carotenoids that are found in Nature, allenic or acetylenic groups replace one or two double bonds of the polyene chain. Since allenes, attached to the ring, are chiral, they are considered as part of the end group in Section D.1.b. Central triple bonds at C-15,15' are often introduced during the total synthesis of carotenoids, and CD spectra of many such intermediates have been published. In this Chapter, however, interest will be focused only on naturally occurring acetylenic carotenoids where the triple bond is located next to the ring, *i.e.* at C-7 and/or C-7'. There are only very small differences between the UV/Vis absorption spectra of the acetylenic carotenoids and their pure polyene analogues. In the CD, however, dramatic changes arise when terminal double bonds are replaced by triple bonds. Comparison of the CD spectra of zeaxanthin (**119**), diatoxanthin (**118**) and alloxanthin

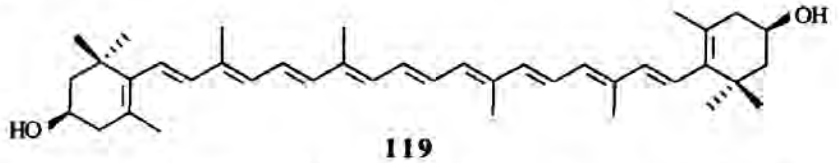
(**117**), compounds which have the same end groups but 0, 1, and 2 triple bonds, respectively, shows a drastic successive decrease of intensity (Fig. 20). In addition, the CD of the diacetylenic compound alloxanthin (**117**) is not typically conservative, although some sign changes are still present. The extremely weak spectrum of alloxanthin (**117**) leads to the assumption that no inherently chiral chromophore is involved. Model considerations indeed suggest that no clearly distinguishable conformations along the C-6,7 axis can be found if the double bond at C-7 is replaced by the completely symmetrical triple bond. A group which, in simple β-ring polyene carotenoids, would induce distinct conformers by steric interaction between ring and chain is now separated from the chain by the axially symmetrical triple bond. There is, therefore, no steric hindrance so no intrinsically chiral chromophore is created. Thus alloxanthin (**117**) must be classified rather as a carotenoid with an induced chiral chromophore. This view is supported by the CD of diatoxanthin (**118**). Here the same spectrum is found as for zeaxanthin (**119**), but with only half the intensity. Obviously the CD is completely dominated by the effects of the zeaxanthin-like end of the molecule. Diatoxanthin (**118**) is therefore comparable to monochiral carotenoids with one 3-hydroxy-β end group. Similar CD relationships are seen with the analogous dehydro derivatives of astaxanthin (**406**) (Fig. 21). Whilst (3*S*,3'*S*)-7,8-didehydroastaxanthin (**402**) exhibits a spectrum similar to that of astaxanthin (**406**) with similar temperature behaviour but reduced intensity, (3*S*,3'*S*)-7,8,7',8'-tetradehydroastaxanthin (**400**) has only a weak, rather non-conservative CD. At liquid nitrogen temperature, no significant increase of intensity is observed [9]. This is again evidence that conformational energy differences are negligible.



117



118



119

Another structural deviation of the polyene chain is the presence of substituents bearing oxygen atoms. Such substituents may form part of the chromophore *e.g.* in peridinin (**558**) or fucoxanthin (**369**). Comparison of the CD spectrum of the cross-conjugated compound peridinin (**558**) [70] or that of fucoxanthin (**369**), which has a terminal carbonyl group in its chromophore [67], with that of neoxanthin (**234**) [71] shows that all three are non-

conservative, with medium to weak negative Cotton effects. However the positions and relative intensities of the maxima are quite different. It is evident that strong differences in the polarization of the chromophore must have an influence on the CD. Up to now, however, no systematic investigation of such influences has been performed.

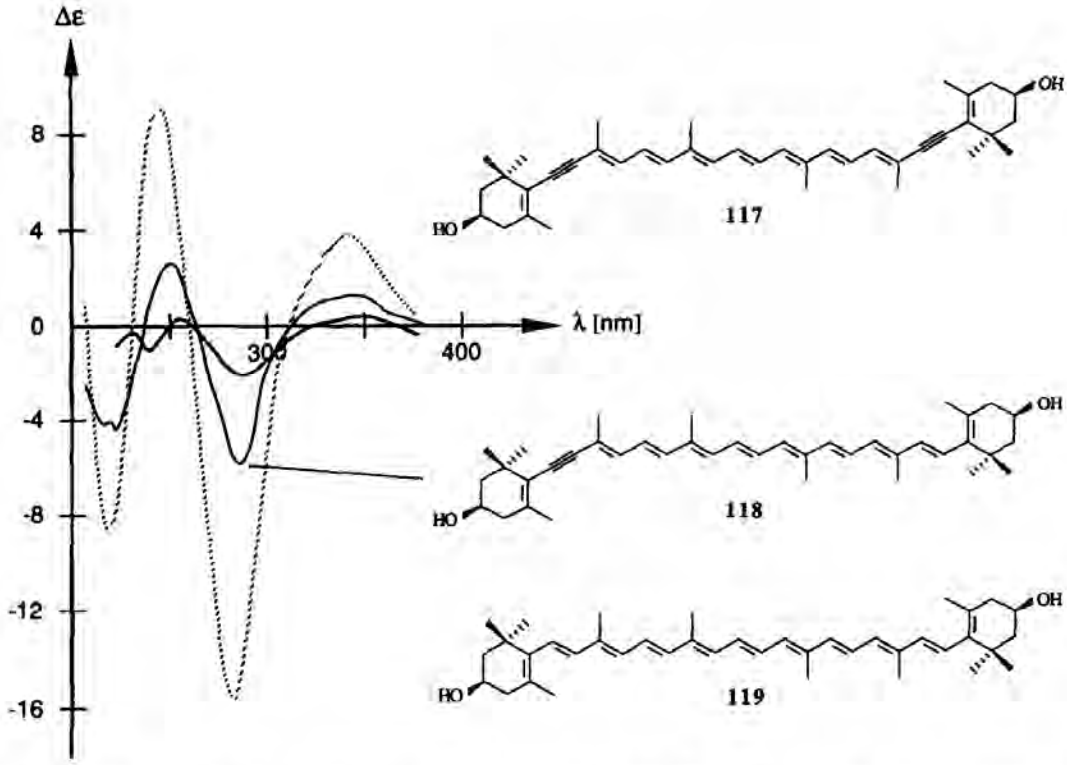


Fig. 20. CD spectra of (3*R*,3'*R*)-alloxanthin (**117**) ▬▬ [69], (3*R*,3'*R*)-diatoxanthin (**118**) —— [11] and (3*R*,3'*R*)-zeaxanthin (**119**) .... [11].

Unexpected spectral changes can arise when substituents are present which are not conjugated to the chromophore. Examples are provided by loroxanthin (**190**) [73] and 19'-hexanoyloxyfucoxanthin (**371**) [72] where one of the in-chain methyl groups bears a free or acylated hydroxy substituent, respectively. Such compounds exhibit a strong tendency for *cis/trans* isomerism at the double bond adjacent to the substituted methyl group with preference for the *cis* form (designated *E* by application of the sequence rule). Relevant CD data for pure isomers are, therefore, difficult to obtain. Comparison of the CD spectrum of carefully purified all-*trans* loroxanthin (**190**) [73] with that of its relative, lutein (**133**), which lacks the hydroxy group at C-19, still shows striking differences. The influence of such substituents on the CD is obviously much larger than expected. Possible explanations include small conformational differences or hydrogen bridges within the polyene chain, but up to now no explanation for these findings is available.

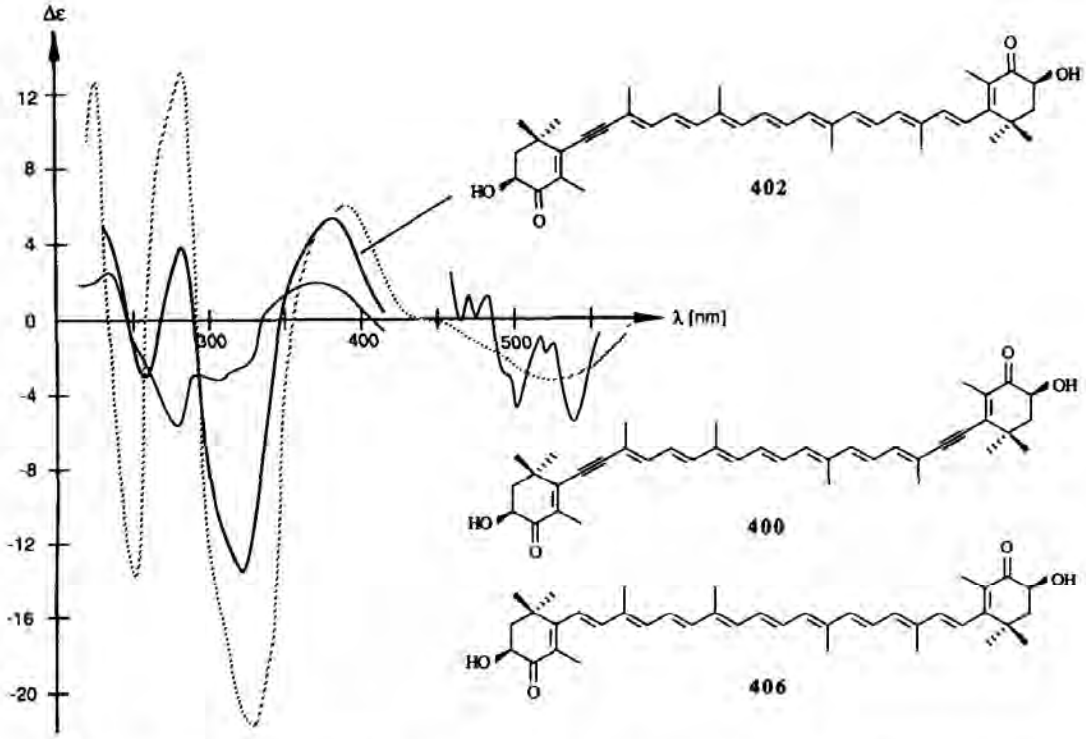
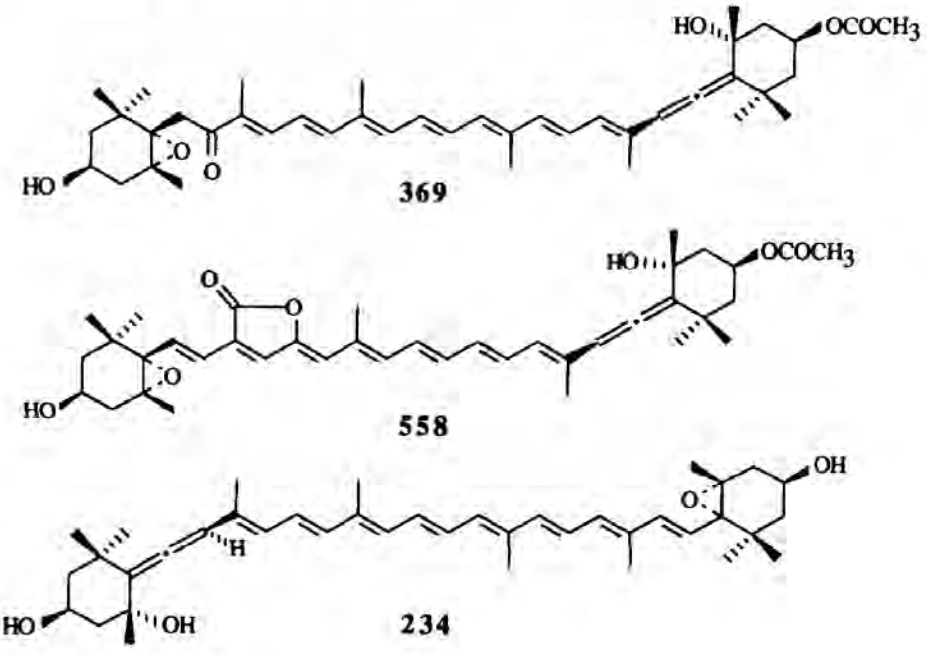
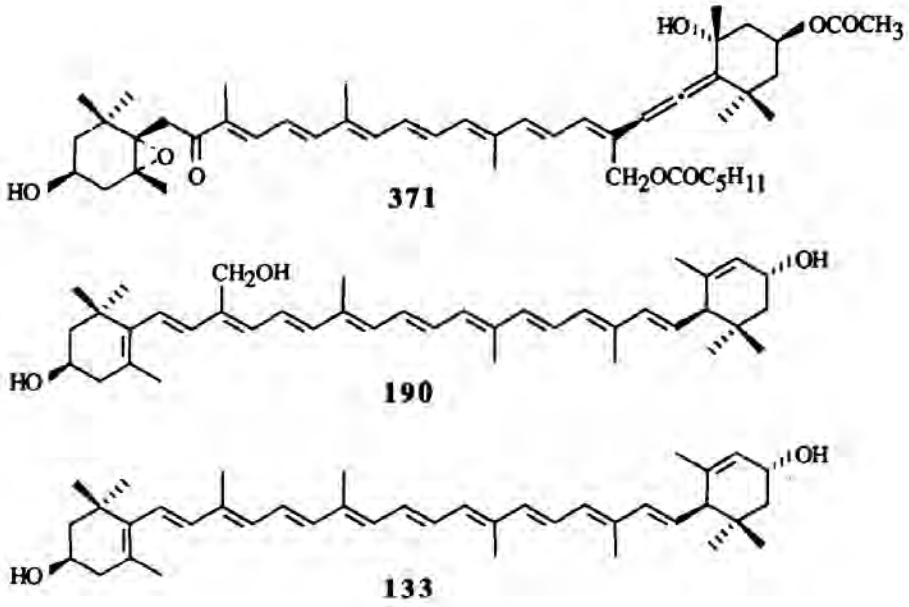


Fig. 21. CD spectra of (3*S*,3'*S*)-7,8-didehydroastaxanthin (**402**) ——— [9], (3*S*,3'*S*)-7,8,7',8'-tetradehydroastaxanthin (**400**) ——— [9] and (3*S*,3'*S*)-astaxanthin (**406**) (in dichloromethane) ...., [10].





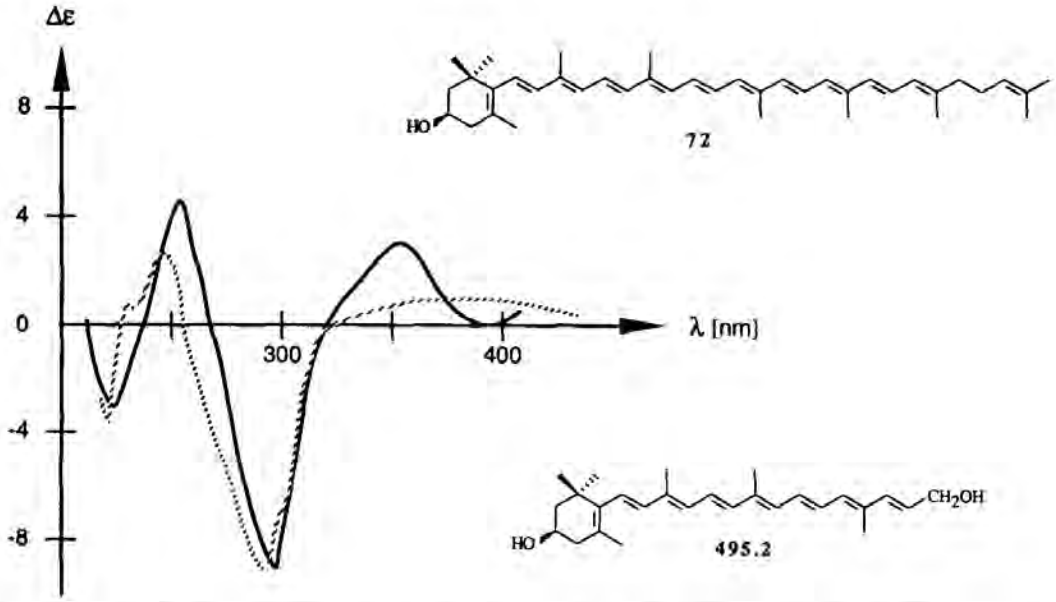


Fig. 22. CD spectra of (3*R*)-rubixanthin (**72**) ——— [28] and (3*R*)-3-hydroxy-10'-apo-β-caroten-10'-ol (**495.2**) .... [74].

Finally, some general remarks about the influence of the length of the chromophore are appropriate. To the authors' knowledge, no systematic investigation of this topic has yet been undertaken. It is known that differences of one or two conjugated double bonds cause hypsochromic shifts of 10 to 40 nm, depending on the spectral region. The general shape of the CD spectrum is usually maintained. These shifts are in accordance with the corresponding UV/Vis absorptions. In Fig. 22 the CD spectra of rubixanthin (**72**) and 10'-apo-β-carotene-3,10'-diol (**495.2**) with identical chiral rings but with a decaene and a heptaene chain, respectively, are compared. Despite the difference of three double bonds in the chromophore there is still a surprising agreement of the curves. Greater dissimilarities are to be expected, however, if carotenoids with greater differences in chromophore length are compared. Care must be exercised in such cases, as no general rules have been worked out.

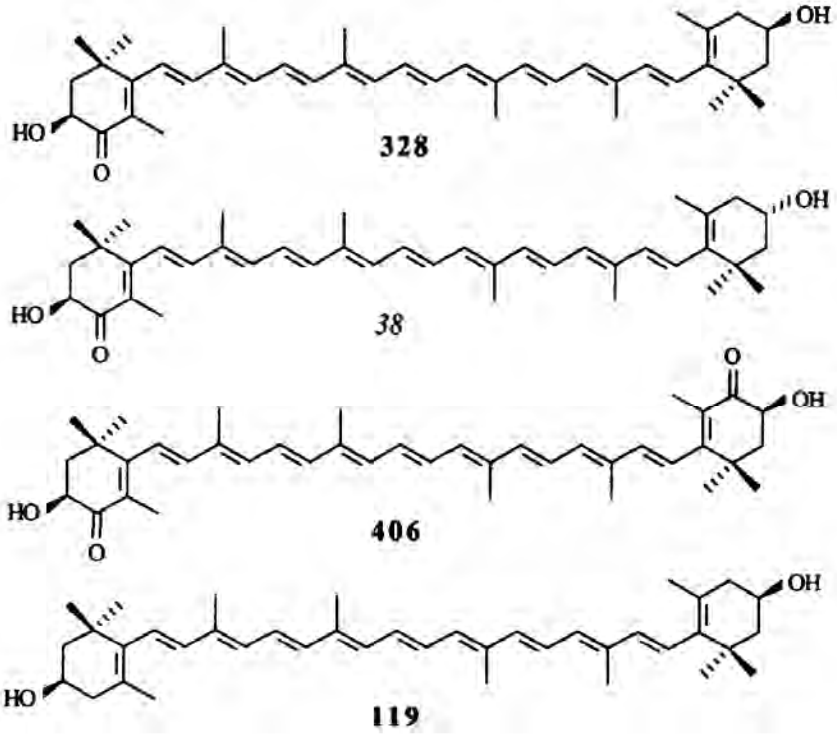
4. Some special investigations

The application of CD spectra to study conformational equilibria has been treated in Section B.2. It has been shown how important it is to know the predominant conformations at equilibrium in order to be able to assign absolute configurations from CD spectra. On the other hand, temperature-dependent and solvent-dependent CD spectra can be used for the study of con-formational equilibria [14].

Another, as yet ill understood, phenomenon should also be mentioned. Striking changes in the intensities of CD peaks have been detected when the sample concentration is varied [18]. With 9Z- and 9Z,9'Z-astaxanthin (**406**) diacetate, enormous enhancements of the peaks in the visible range have been observed. At low temperature, the overlapping maxima seem to be split into a positive and negative component, the maximum of the absorption spectrum being located at the zero crossing of these two CD maxima. This resembles the exciton splitting in the CD spectra of compounds with closely connected aromatic rings [75]. Similar observations, in this case even at room temperature, were also made for the all-*E* and several mono-*Z* isomers of bacterioruberin (**456**) (K. Noack, unpublished results, see also [64]). These observations have been explained tentatively by association phenomena at the higher concentrations, but this question certainly merits further research.

An interesting example of the application of the additivity hypothesis and of the temperature dependence is seen in the CD spectra of (3*S*,3'*R*)- and (3*S*,3'*S*)-adonixanthin (**328** and *38*, respectively) (Figs. 23, 24) in comparison with those of (3*R*,3'*R*)-zeaxanthin (**119**) and (3*S*,3'*S*)-astaxanthin (**406**) [76]. As has been shown above (Section B.2), at room temperature, the CD spectra of **119** and **406** are, apart from a wavelength shift, quite similar. At low temperature (–180°C), the CD of **119** simply intensifies, whereas that of **406** changes sign and also becomes very intense. The room temperature CD of **328** closely resembles those of **406** and **119**. At low temperature, however, it becomes weak and changes its shape substantially. With *38* it is the low-temperature spectrum which resembles the low-temperature spectrum of **406**, whereas the room-temperature spectrum is weak and quite different in shape. These observations can be explained by a superimposition of independent effects from the two halves of molecules **119** and **406**. In compound **328**, at room temperature, the two halves make contributions of the same sign to the spectra, whereas at low temperature, the effect of the

3-hydroxy-4-oxo-substituted half changes sign, as with astaxanthin (**406**). The effects of the two halves thus have opposite signs, resulting in the weak spectrum. With compound *38* it is the opposite; at room temperature there is compensation of opposite effects but, at low temperature, addition of effects with the same sign.



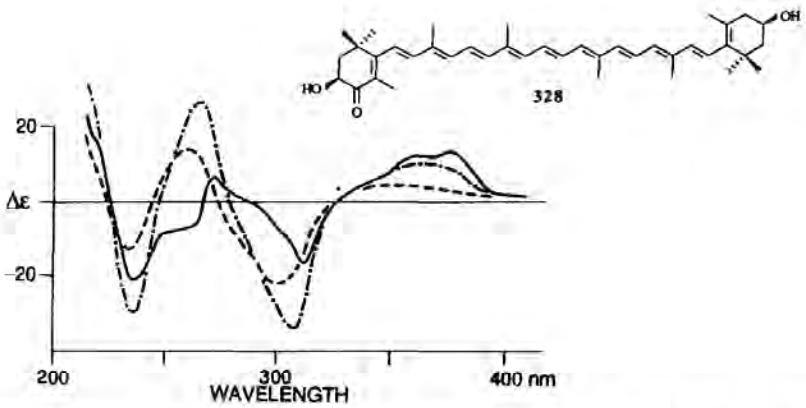


Fig. 23. Temperature dependence of CD spectrum of (3*S*,3'*R*)-adonixanthin (**328**) [76]. ----- +20°C, ---- -120°C, —— -180°C

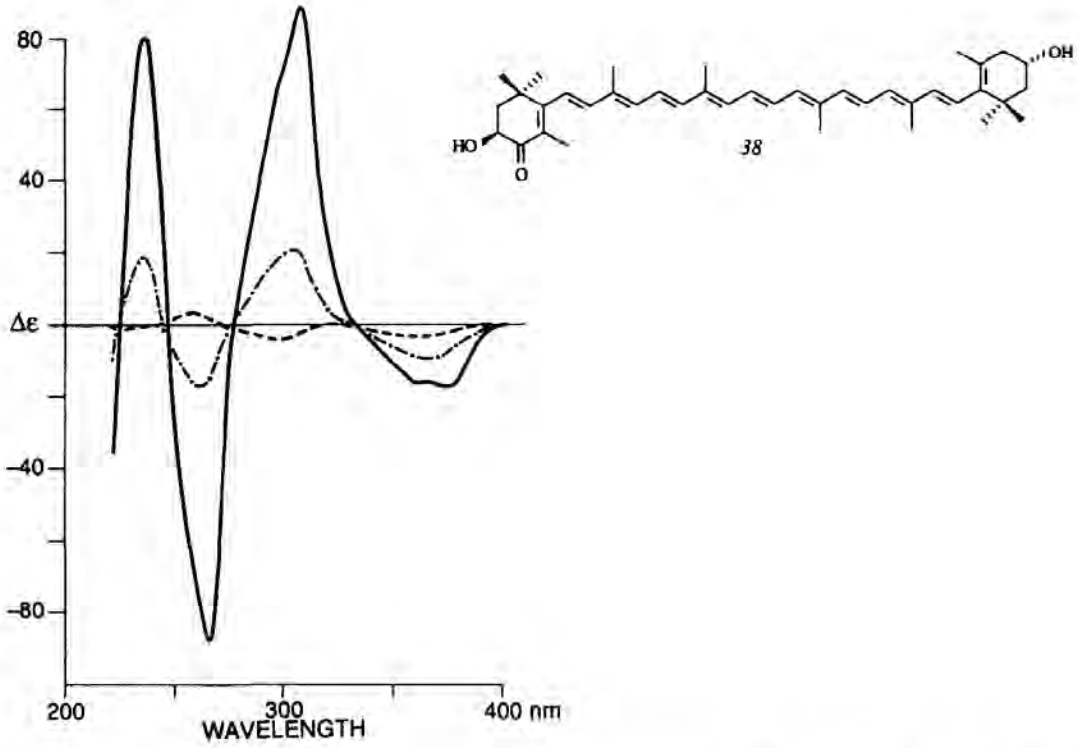
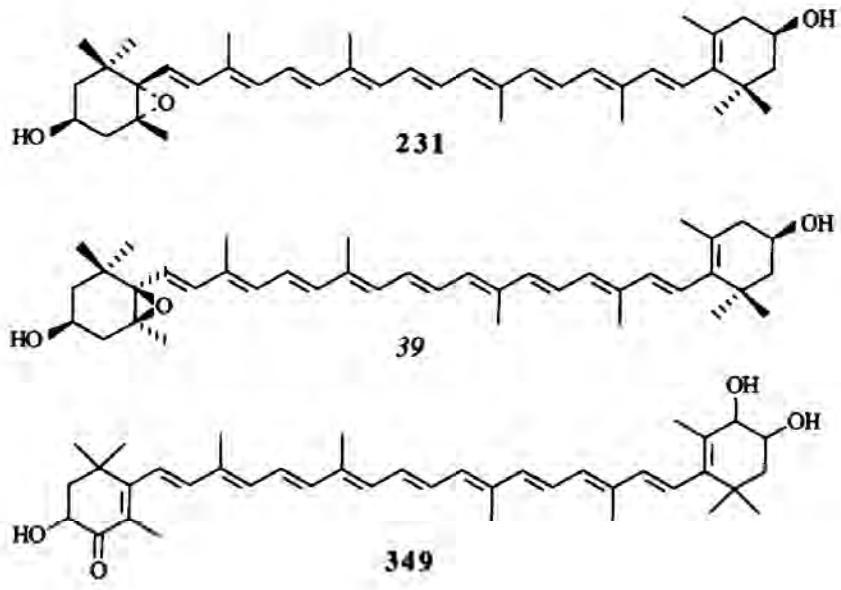


Fig. 24. Temperature dependence of CD spectrum of (3*S*,3'*S*)-adonixanthin (*38*) [76]. ---- +20°C, ---- -120°C, —— -180°C



An analogous example is the pair of all-*E*-antheraxanthin (**231**) [(3*S*,5*R*,6*S*,3'*R*)] and its synthetic isomer 'antheraxanthin B' (3*S*,5*S*,6*R*,3'*R*) (*39*) [63].

A further, though somewhat more complicated, example is given by the four diastereoisomers of idoxanthin (**349**) and their four enantiomers, which can be completely separated chromatographically as diastereoisomeric tricarbamate derivatives (see Vol.1, Chapter 7, Example) [77]. The relative configurations of the substituents on the rings were assigned by NMR spectroscopy. Figures 25 and 26 show the temperature-dependent CD spectra of all eight compounds as their carbamate derivatives (K. Noack and K. Schiedt, unpublished results). The carbamate part influences the CD spectra chiefly in the low-wavelength range, whereas the carotenoid part is mainly responsible for the spectral features in the range from 400 to about 240 nm. The intensities are, however, significantly higher for the derivatized than the underivatized compounds (Figs. 26, 27). It has been shown before that a substituent at C-4 has only a comparatively small influence on the CD spectra. With respect to the relative configurations at C-3 and C-3', the compounds can therefore be divided into two groups, the first (compounds *40-43*) with the same and the second (compounds *44-47*) with opposite absolute configurations at C-3 and C-3'. The same phenomena as seen with the diastereoisomers of adonixanthin (**328**) can also be observed with the idoxanthin (**349**) carbamates (as a first approximation, the influence of the substituent at C-4' can be neglected). Compounds *40* and *42* have very similar spectra, as do compounds *41* and *43*, but the spectra of the two pairs of compounds are almost mirror images of each other and all show the same temperature dependence. The spectra are quite strong at room temperature, do not show much change below *ca.* –60°C, and have very distinct fine structure at low temperature. The other group of compounds (*44-47*) with the opposite configuration at C-3 and C-3' show different behaviour. Their spectra are rather weak at room temperature and increase in intensity strongly on cooling. Again the two 'quasi-enantiomers' show spectra with opposite signs (the pairs *44*, *45* and *46*, *47*). This demonstrates that the carbamate part has only a secondary influence in this spectral region.

A caveat which shows the ambiguous influence of the C-4 substituent may be added at this point. The carbamate derivatives of isozeaxanthin (*8*) and 4'-hydroxyechinenone (*11*) show spectra opposite in sign to those of the underivatized carotenoids (K. Schiedt and K. Noack, unpublished results).

These case studies from the authors' laboratory where chosen as examples to illustrate how detailed studies of carotenoid CD spectra can be used to improve understanding of carotenoid structures and conformations and also to draw attention to some of the limitations of the method. The coverage has been restricted to free carotenoids in organic solution. Complexation of carotenoids with proteins or molecular ordering in micelles and membranes can induce strong optical activity in the carotenoid chromophore. Such phenomena have not been treated in this Chapter.

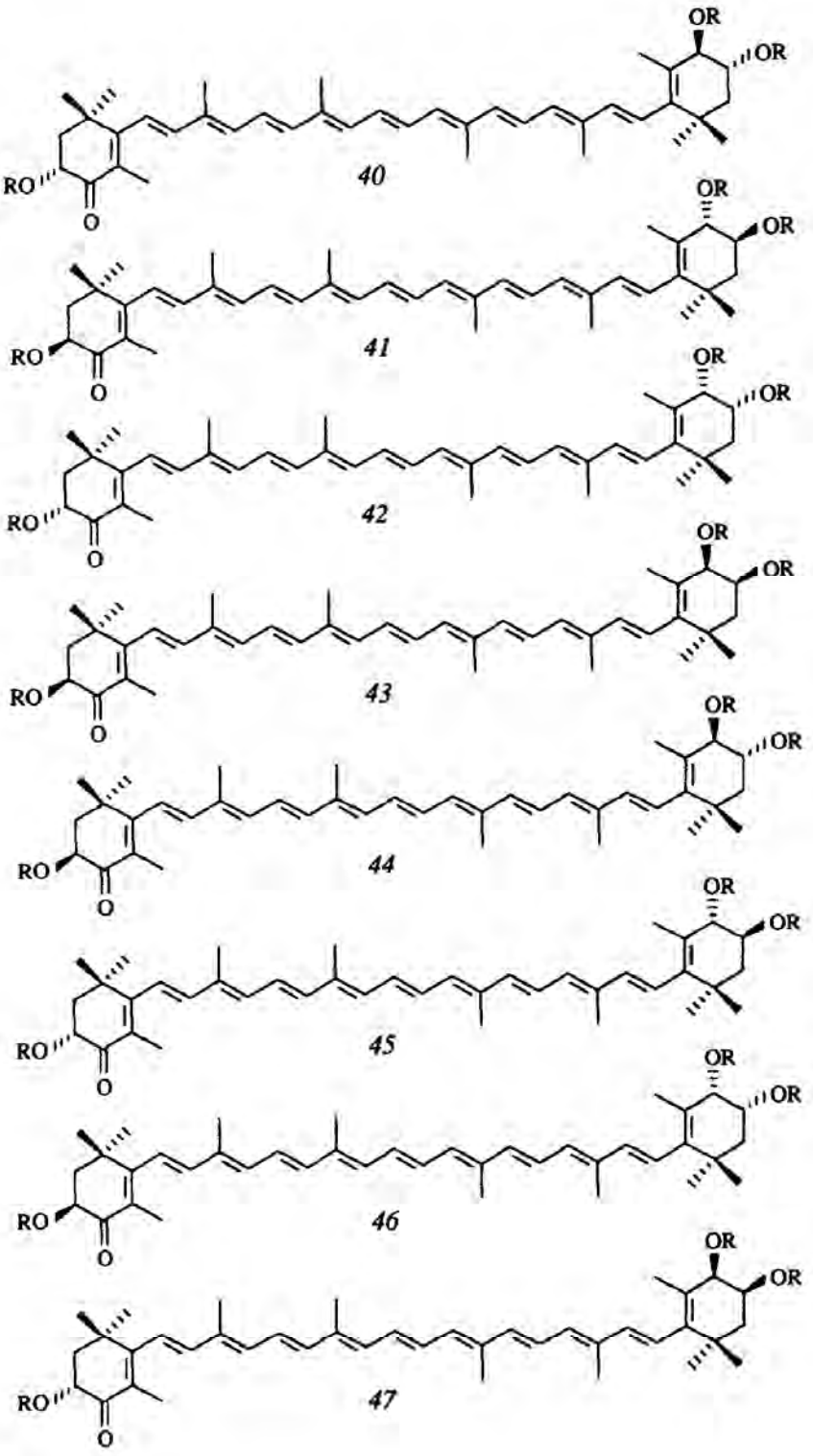

OR
OR
RO
O
40
41
42
43
44
45
46
47

Fig.25a

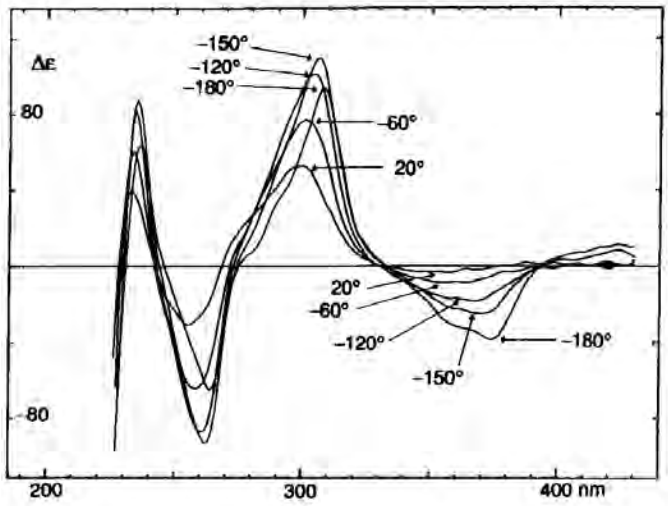


Fig.25b

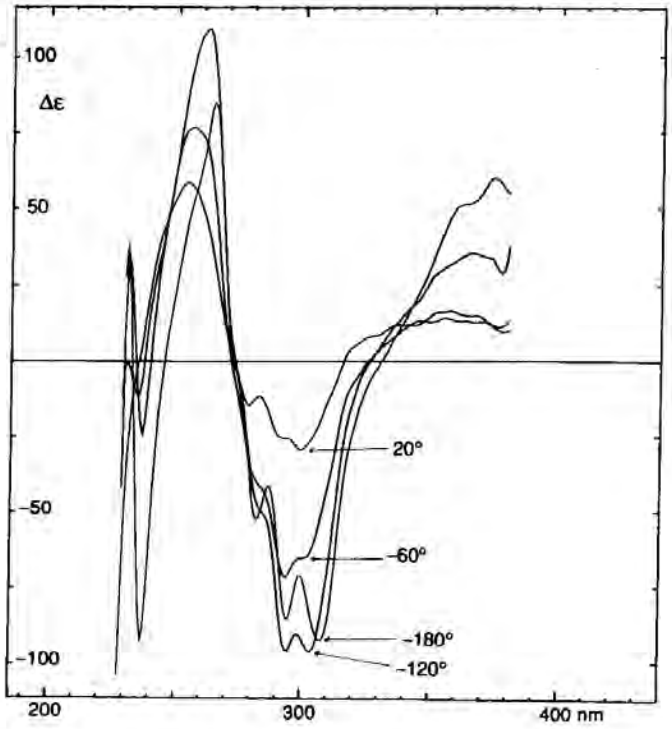


Fig. 25. Temperature-dependent CD spectra of idoxanthin (**349**) tricarbamates. a: (*40*), b: (*41*)

R =

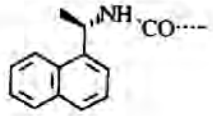


Fig.25c

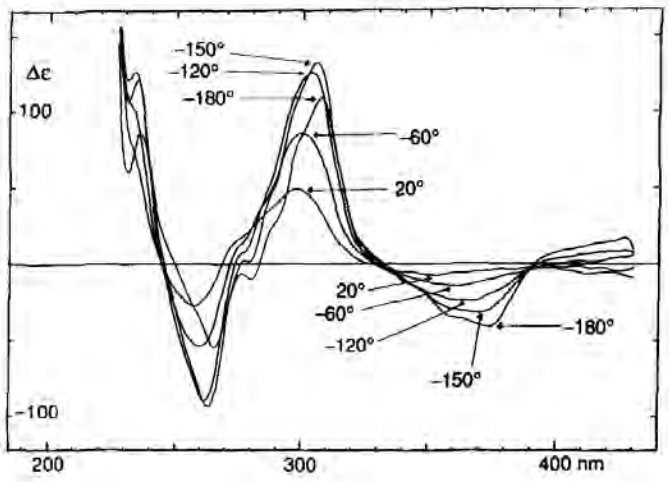


Fig.25d

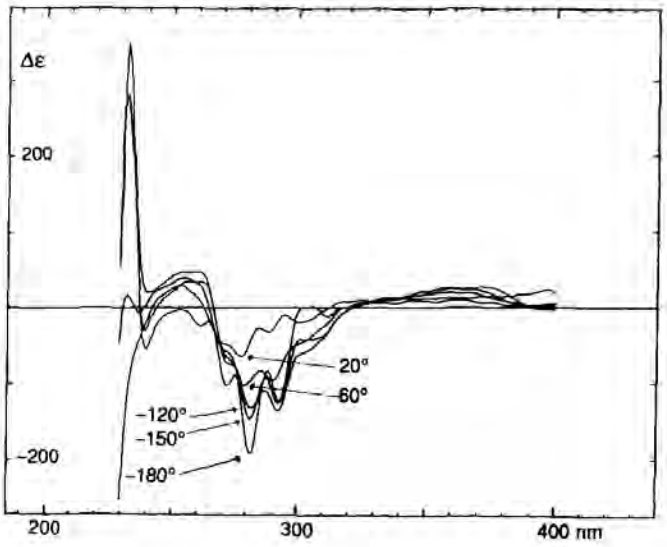


Fig. 25. Temperature-dependent CD spectra of idoxanthin (**349**) tricarbamates. c: (*42*), d: (*43*)

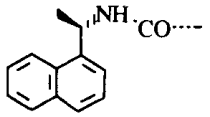
R = 

Fig.26a

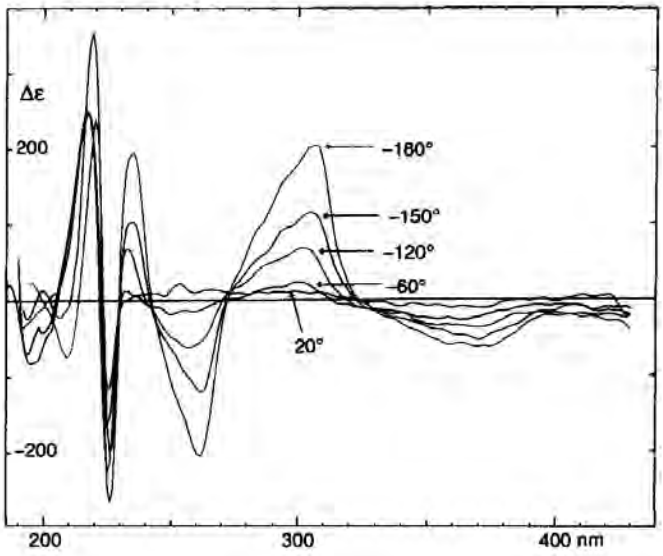


Fig.26b

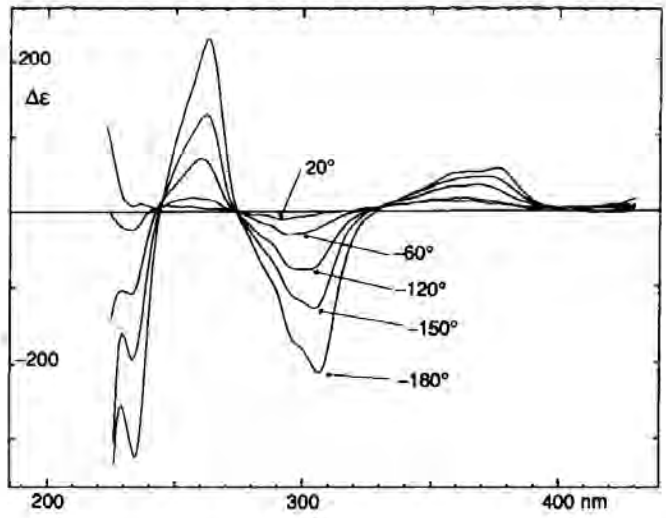


Fig. 26. Temperature-dependent CD spectra of idoxanthin (**349**) tricarbamates. a: (*44*), b: (*45*)

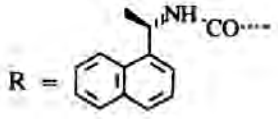


Fig.26c

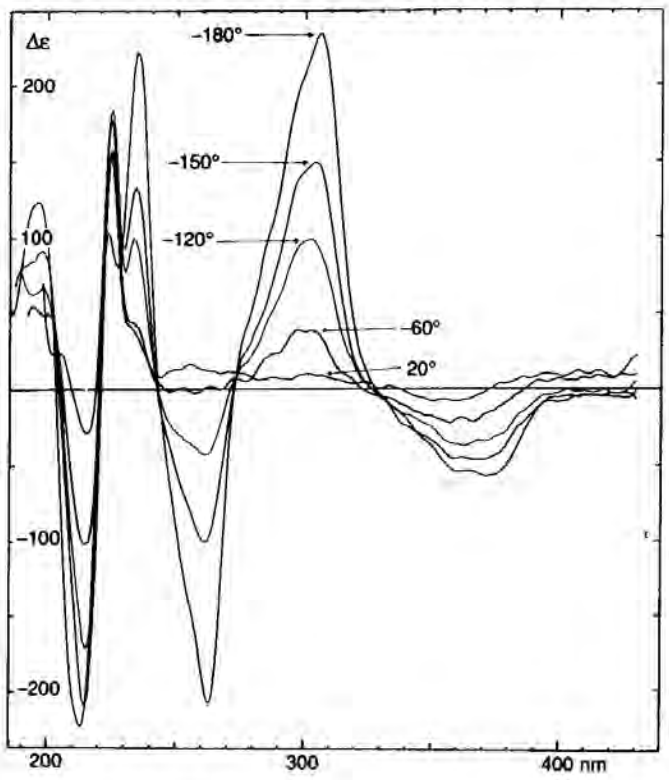


Fig.26d

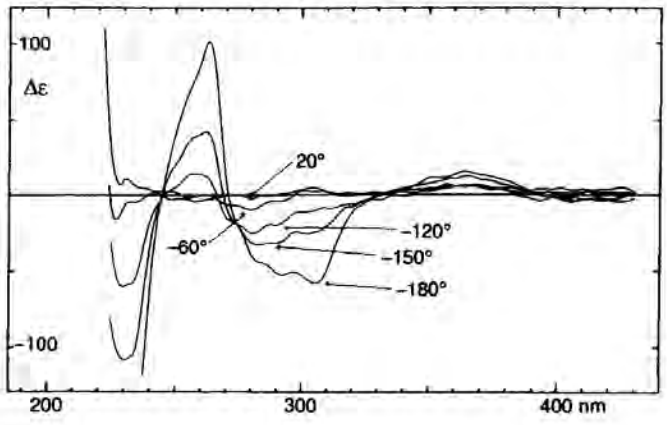
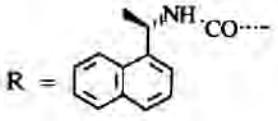


Fig. 26. Temperature-dependent CD spectra of idoxanthin (**349**) tricarbamates. c: (*46*), d: (*47*)



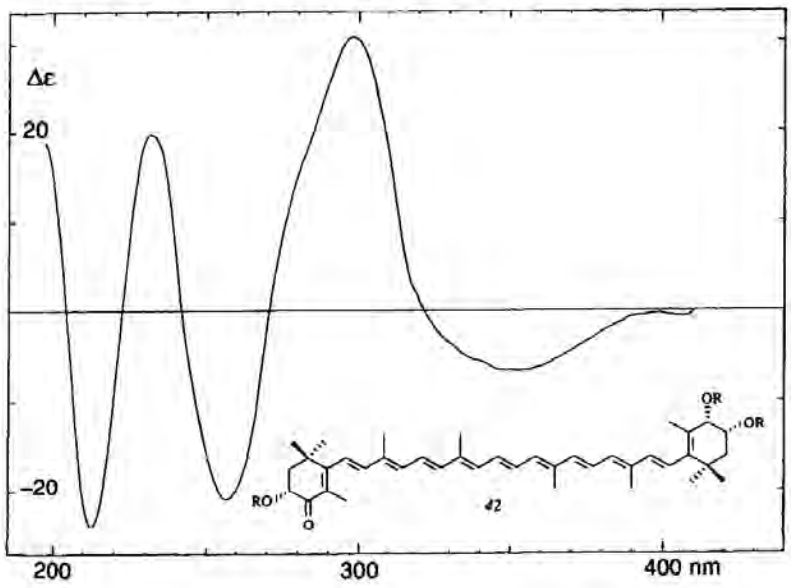


Fig. 27. CD spectrum of (3*R*,4*S*,3'*R*)-idoxanthin (*42*, R = H) at room temperature.

References

[1] R. Kuhn, A. Winterstein and E. Lederer, *Hoppe Seyler's Z. Physiol. Chem.*, **197**, 141 (1931).
[2] L. Zechmeister and P. Tuzson, *Chem. Ber.*, **62**, 2226 (1929).
[3] B. C. L. Weedon, in *Carotenoids* (ed. O. Isler), p. 267, Birkhäuser, Basel (1971).
[4] L. Bartlett, W. Klyne, W. P. Moss, P. M. Scopes, G. Galasko, A. K. Mallams and B. C. L. Weedon, *J. Chem. Soc. C.*, **1969**, 2527.
[5] L. Velluz, M. Legrand and M. Grosjean, *Optical Circular Dichroism: Principles, Measurements and Applications*, Academic Press, Weinheim and New York (1965).
[6] E. Charney, *The Molecular Basis of Optical Activity, Optical Rotatory Dispersion and Circular Dichroism*, Wiley, New York (1979).
[7] F. A. Cotton, *Chemical Applications of Group Theory, 2nd. Edition*, Wiley, New York (1971).
[8] V. Sturzenegger, R. Buchecker and G. Wagnière, *Helv. Chim. Acta*, **63**, 1074 (1980).
[9] K. Noack and A. J. Thomson, *Helv. Chim. Acta*, **62**, 1902 (1979).
[10] G. Englert, F. Kienzle and K. Noack, *Helv. Chim. Acta*, **60**, 1209 (1977).
[11] S. Hertzberg, G. Borch and S. Liaaen-Jensen, *Acta Chem. Scand.*, **B33**, 42 (1979).
[12] G. Englert, K. Noack, E. A. Broger, E. Glinz, M. Vecchi and R. Zell, *Helv. Chim. Acta*, **74**, 969 (1991).
[13] A. G. Andrewes, G. Borch, S. Liaaen-Jensen and G. Snatzke, *Acta Chem. Scand.*, **B28**, 730 (1974).
[14] K. Noack, in *Carotenoid Chemistry and Biochemistry* (ed. G. Britton and T. W. Goodwin), p. 135, Pergamon, Oxford (1982).

[15] K. Müller, H. J. Ammann, D. M. Doran, P. R. Gerber, K. Gubernator and G. Schrepfer, *Bull. Soc. Chim. Belg.*, **97**, 655, (1988).
[16] W. Klyne and V. Prelog, *Experientia*, **16**, 521 (1960).
[17] J. C. J. Bart and C. H. MacGillavry, *Acta Crystallogr.*, **B24**, 1587 (1968).
[18] K. Noack and A. J. Thomson, *Helv. Chim. Acta*, **64**, 2383 (1981).
[19] R. Buchecker, U. Marti and C. H. Eugster, *Helv. Chim. Acta*, **65**, 896 (1982).
[20] A. Haag and C. H. Eugster, *Helv. Chim. Acta*, **65** 1795 (1982).
[21] A. Haag and C. H. Eugster, *Helv. Chim. Acta*, **68**, 1897, (1985).
[22] B. Meyer, in *Low Temperature Spectroscopy: Optical Properties of Molecules in Matrices, Mixed Crystals, and Frozen Solutions*, p. 203, American Elsevier, New York (1971).
[23] A. G. Andrewes, S. Liaaen-Jensen and G. Borch, *Acta Chem. Scand.*, **B28**, 737 (1974).
[24] S. Gut, H. Wolleb and H. Pfander, *Helv. Chim. Acta*, **72**, 496 (1989).
[25] H. Wolleb and H. Pfander, *Helv. Chim. Acta*, **69**, 646 (1986).
[26] M. Acemoglu, P. Uebelhart, M. Rey and C. H. Eugster, *Helv. Chim. Acta*, **71**, 931, (1988).
[27] R. Buchecker, C. H. Eugster and C. Litchfield, *Helv. Chim. Acta*, **60**, 2780 (1977).
[28] E. Märki-Fischer, U. Marti, R. Buchecker and C. H. Eugster, *Helv. Chim. Acta*, **66**, 494 (1983).
[29] D. J. Buschor and C. H. Eugster, *Helv. Chim. Acta*, **73**, 1002 (1990).
[30] R. Buchecker, S. Liaaen-Jensen, G. Borch and H. W. Siegelman, *Phytochem.*, **15**, 1015 (1976).
[31] H. Kjøsen, N. Arpin and S. Liaaen-Jensen, *Acta Chem. Scand.*, **B26**, 3053 (1972).
[32] G. P. Moss, J. Szabolcs, G. Tóth and B. C. L. Weedon, *Acta Chim. Acad. Sci. Hung.*, **87**, 301 (1975).
[33] M. Acemoglu and C. H. Eugster, *Helv. Chim. Acta*, **67**, 184 (1984).
[34] A. G. Andrewes, G. Englert, G. Borch, H. H. Strain and S. Liaaen-Jensen, *Phytochem.*, **18**, 303 (1979).
[35] P. Uebelhart, A. Baumeler, A. Haag, R. Prevo, J. H. Bieri and C. H. Eugster, *Helv. Chim. Acta*, **69**, 816 (1986).
[36] R. Buchecker and C. H. Eugster, *Helv. Chim. Acta*, **56**, 1124 (1973).
[37] H. Mayer, in *Carotenoid Chemistry and Biochemistry* (ed. G. Britton and T. W. Goodwin), p. 55, Pergamon, Oxford (1982).
[38] M. Gerspacher and H. Pfander, *Helv. Chim. Acta*, **72**, 151 (1989).
[39] D. Siefermann-Harms, S. Hertzberg, G. Borch and S. Liaaen-Jensen, *Phytochem.*, **20**, 85 (1981).
[40] A. G. Andrewes, G. Borch and S. Liaaen-Jensen, *Acta Chem. Scand.*, **B30**, 214 (1976).
[41] M. Hallenstvet, R. Buchecker, G. Borch and S. Liaaen-Jensen, *Phytochem.*, **16**, 583 (1977).
[42] S. Hertzberg and S. Liaaen-Jensen, *Acta Chem. Scand.*, **B31**, 215 (1977).
[43] W. Eschenmoser and C. H. Eugster, *Helv. Chim. Acta*, **61**, 822 (1978).
[44] R. Buchecker, U. Marti and C. H. Eugster, *Helv. Chim. Acta*, **67**, 2043 (1984).
[45] M. Acemoglu and C. H. Eugster, *Helv. Chim. Acta*, **67**, 471 (1984).
[46] W. Eschenmoser, E. Märki-Fischer and C. H. Eugster, *Helv. Chim. Acta*, **67**, 170 (1984).
[47] E. Märki-Fischer, R. Buchecker and C. H. Eugster, *Helv. Chim. Acta*, **67**, 2143 (1984).
[48] R. Buchecker and C. H. Eugster, *Helv. Chim. Acta*, **63**, 2531 (1980).
[49] R. K. Müller, H. Mayer, K. Noack, J. J. Daly, J. D. Tauber and S. Liaaen-Jensen, *Helv. Chim. Acta*, **61**, 2881 (1978).
[50] A. Rüttimann, G. Englert, H. Mayer, G. P. Moss and B. C. L. Weedon, *Helv. Chim. Acta*, **66**, 1939 (1983).
[51] M. P. Gmünder and C. H. Eugster, *Helv. Chim. Acta*, **73**, 1954 (1990).
[52] M. P. Gmünder and C. H. Eugster, *Helv. Chim. Acta*, **73**, 2190 (1990).
[53] J. Deli, P. Molnar, G. Tóth, A. Baumeler and C. H. Eugster, *Helv. Chim. Acta*, **74**, 819 (1991).
[54] H. Meier, P. Uebelhart and C. H. Eugster *Helv. Chim. Acta*, **69**, 106 (1986).
[55] M. Kamber, H. Pfander and K. Noack, *Helv. Chim. Acta*, **67**, 968 (1984).
[56] H. Rønneberg, G. Borch, R. Buchecker, N. Arpin and S. Liaaen-Jensen, *Phytochem.*, **21**, 2087 (1982).
[57] N. Arpin, H. Rønneberg, G. W. Francis and S. Liaaen-Jensen, *Phytochem.*, **12**, 2751 (1973).
[58] W. Eschenmoser, P. Uebelhart and C. H. Eugster, *Helv. Chim. Acta*, **66**, 82 (1983).

[59] J. E. Johansen and S. Liaaen-Jensen, *Acta Chem. Scand.*, **B33**, 551 (1979).
[60] G. Borch, S. Norgård and S. Liaaen-Jensen, *Acta Chem. Scand.*, **26**, 402 (1972).
[61] H. Rønneberg, A. G. Andrewes, G. Borch, R. Berger and S. Liaaen-Jensen, *Phytochem.*, **24**, 309 (1985).
[62] L. Zechmeister, Cis-trans *Isomeric Carotenoids, Vitamins A and Arylpolyenes*, Springer-Verlag, Vienna (1962).
[63] E. Märki-Fischer, R. Buchecker, C. H. Eugster, G. Englert, K. Noack and M. Vecchi, *Helv. Chim. Acta*, **65**, 2198 (1982).
[64] R. Riesen and H. Pfander, *Abstr. 9th Int. Symp. Carotenoids*, Kyoto, 1990, P118.
[65] D. Berset and H. Pfander, *Helv. Chim. Acta*, **68**, 1149 (1985).
[66] E. Märki-Fischer and C. H. Eugster, *Helv. Chim. Acta*, **68**, 1708 (1985).
[67] J. A. Haugan, G. Englert, E. Glinz and S. Liaaen-Jensen, *Acta Chem. Scand.*, **46**, 389 (1992).
[68] H. P. Märki, Ph.D. Thesis, University of Zürich (1980).
[69] F. C. Pennington, F. T. Haxo, G. Borch and S. Liaaen-Jensen, *Biochem. Syst. Ecol.*, **13**, 215 (1985).
[70] J. E. Johansen, G. Borch and S. Liaaen-Jensen, *Phytochem.*, **19**, 441 (1980).
[71] R. Buchecker, S. Liaaen-Jensen and C. H. Eugster, *Phytochem.*, **14**, 797 (1975).
[72] S. Hertzberg, T. Mortensen, G. Borch, H. W. Siegelman and S. Liaaen-Jensen, *Phytochem.*, **16**, 587 (1977).
[73] E. Märki-Fischer, P. A. Bütikofer, R. Buchecker and C. H. Eugster, *Helv. Chim. Acta*, **66**, 1175 (1983).
[74] C. H. Eugster, in *Carotenoids: Chemistry and Biochemistry* (ed. N. I. Krinsky, M. M. Mathews-Roth and R. F. Taylor), p. 1, Plenum Press, New York (1990).
[75] N. Harada and K. Nakanishi, *Circular Dichroic Spectroscopy: Exciton Coupling in Organic Stereochemistry*, Oxford University Press, Oxford (1983).
[76] K. Noack, *Helv. Chim. Acta*, **64**, 1833 (1981).
[77] K. Schiedt, H. J. Mayer, M. Vecchi, E. Glinz and T. Storebakken, *Helv. Chim. Acta*, **71**, 881 (1988).

Carotenoids
Volume 1 B: Spectroscopy
© 1995 Birkhäuser Verlag Basel

Chapter 4

Infrared Spectroscopy

Kurt Bernhard and Mireille Grosjean

A. Principles, Scope and Limitations

Atoms in a molecule change their mutual positions in a periodic manner by stretching of the bonds and variation of bond angles. Infrared (IR) radiations enhance these vibrations to a maximum. When the frequency of the IR radiation matches the characteristic energy (frequency) of one of these vibrational modes, the energy will be absorbed. A polyatomic molecule which has many different atoms and functional groups has a great number of possible vibration modes and these give rise to many different absorption bands in the IR spectrum. Usually it is not possible to correlate all IR bands with the corresponding vibrations, but several key structural elements provide characteristic bands in the spectrum. The strength of IR spectroscopy thus lies in the qualitative identification of features of the molecular structure from absorption bands that are characteristic of certain functional groups.

For IR spectroscopy of organic molecules, including carotenoids, the wavelength range between 2.5 μm and 25 μm is of practical interest. The positions of absorption bands are normally indicated by the frequency in wavenumbers, *i.e.* the reciprocal value of the wavelength, which lies in the range between 4000 cm^{-1} (corresponding to 2.5 μm wavelength) and 400 cm^{-1} (corresponding to 25 μm).

Comparison of the IR spectrum of a purified compound with that of a standard, determined under the same conditions, provides one criterion for identification. Even with mixtures and impure samples it is possible to detect the presence of certain functional groups, *e.g.* carbonyl, sulphate. Further advantages are that the method requires only simple manipulations and gives rapid results at relatively low cost. The main disadvantage is the limited information given, especially from molecules that lack functional groups, *e.g.* carotenes [1]. Although IR spectroscopy played an important role in the elucidation of carotenoid structures in the 1950s and 1960s, and can still help to solve some difficult problems, NMR spectroscopy is now a far superior general tool for structure elucidation.

For basic information about the principles and application of IR spectroscopy, the reader should consult one of several papers, books or reviews [2-6]. Some reviews of the application

of IR spectroscopy, alone or with the complementary technique of Raman spectroscopy (Chapter 5) are also available [1, 7-12].

B. Practical Aspects

1. Instrumentation

Major advances have been made in the past 10 years by the introduction of Fourier transform (FTIR) instruments. These have several major basic advantages over the classical dispersive instrument, especially in sensitivity and accuracy. Thus an FTIR instrument will measure an IR spectrum in about one-thousandth of the time required to obtain a spectrum of the same quality with a dispersive instrument. Alternatively, for an equal investment of instrument time, the sensitivity achieved by an FTIR instrument is better by a factor of 10 to 100. In addition, the frequency scale is derived from a helium neon laser which acts as an internal reference for each scan; the frequency calibration is therefore much more accurate and has much better long-term stability.

2. Infrared Spectrophotometers

All IR spectrophotometers have a source of infrared radiation which is usually some solid material heated to incandescence by an electric current. The two most commonly used sources are the Nernst Glower, which is composed mainly of oxides of rare earths such as zirconium, yttrium and thorium, or the Globar, which is a silicon carbide rod. These sources are efficient emitters of infrared radiation and come close to the energy distribution of a theoretical black body.

The infrared energy which has passed through the sample is measured by an infrared detector. There are two basic types, namely thermal detectors, which measure the heating effects of radiation, and selective detectors, whose response depends on the wavelength.

Thermal detectors include thermocouples, bolometers and pyroelectric detectors, one example of which, the DTGS crystal (deuteriated triglycine sulphate), is well suited for FTIR spectrometers. The most important type of selective detector is the photoconductive cell which combines rapid response with high sensitivity. An example is the mercury cadmium telluride detector (MCT) which is cooled with liquid nitrogen and is used in research grade FTIR instruments.

Between the source and the detector, two basic types of device are used to separate the components of polychromatic radiation and to analyse the radiation so that intensity can be assigned for each wavelength resolution element. Monochromators, used in dispersive instruments, employ a prism or grating; grating instruments have the better resolution.

Most commercially available IR spectrophotometers now are Fourier transform instruments, equipped with a Michelson interferometer. The plot of detector response (DTGS or MCT) is a so-called interferogram which, for a polychromatic source, is the sum of all the

cosine functions corresponding to each monochromatic radiation of the IR beam. A spectrum is then generated by a Fourier transform; this laborious mathematical task is performed very quickly by computer.

3. Sampling

The transmission technique is the oldest sampling technique in optical spectroscopy and is still the most widely used, primarily because it requires only simple accessories. The sample is placed in the light beam of the spectrometer and the intensity of the incident beam is compared with the intensity transmitted by the sample.

The same relationships between transmittance or absorbance and concentration (Beer-Lambert law) apply as in UV/Vis spectrophotometry (Chapter 2).

There are several techniques for presenting the sample in order to obtain the infrared transmission spectra of solids. Those most widely used in modern work are described briefly below. Of them, the KBr disc method is preferred when a sufficient amount of crystalline sample is available. Solutions are more convenient and versatile when only small amounts of non-crystalline sample can be obtained.

a) Solutions

The sample is dissolved in a suitable solvent and the solution placed in a cell consisting of two windows of IR-transparent material separated by a spacer of suitable thickness. The applicability of the method is limited by the poor solubility of many substances and the fact that no solvent is transparent over the entire frequency range.

Recorded frequencies (wavenumbers) for a certain compound may be different in different solvents.

b) Mulls

Crystalline or powdered samples may be prepared as a suspension or mull by grinding to a uniform paste in a mixture of liquid paraffins, known as 'Nujol'. This method has the disadvantage that the aliphatic C–H stretching region is obscured.

c) KBr discs

The most commonly used procedure is to prepare a KBr disc or pellet. Potassium bromide as a matrix is transparent to IR radiation down to 400 cm^{-1}; it is, unfortunately, rather hygroscopic, so that KBr discs usually show a weak band at about 3440 cm^{-1}, and a weaker band at 1640 cm^{-1} due to absorbed water. Nevertheless, this method gives the most information over the entire mid-IR region. It is rapid, relatively inexpensive, and the spectra obtained show sharp bands and good reproducibility.

Experimental procedure: preparation of a KBr pellet (13 mm disc). About 1 mg of the sample is mixed with 300 mg of potassium bromide of high purity, then ground again for one to two minutes in an agate ball mill. The mixture is then placed into a suitable die of a hydraulic press, preferably one which can be evacuated prior to pressing. Evacuation improves the lifetime of the disc clarity. After evacuating for about two minutes, a pressure of approximately 200 bar is applied for a few seconds. The vacuum is then broken and the pressure slowly released.

A good disc has 80 to 90% transmittance in regions where the sample does not absorb.

C. Interpretation of IR Spectra

1. General features

A precise treatment of the vibrations of complex molecules is not feasible, and IR spectra can generally be interpreted only from empirical comparisons of spectra, and by extrapolations from theoretical studies of simpler molecules. Nevertheless, some useful generalizations can be derived by regarding the IR bands as arising from simple stretching and bending motions localized in individual bonds.

The two important areas of a spectrum for preliminary examination are the region above 1300 cm^{-1} and the 900-650 cm^{-1} region. The region above 1300 cm^{-1} is called the functional-group region. The characteristic stretching frequencies for important functional groups such as OH, NH, and C=O occur in this portion of the spectrum. Strong absorption bands in the 900-650 cm^{-1} region generally indicate the presence of an aromatic or heteroaromatic structure in the molecule; the strong out-of-plane C–H bending and ring-bending absorptions displayed in this portion of the spectrum can often be correlated with the substitution pattern of the aromatic system.

The intermediate portion of the spectrum, between 1300 and 900-850 cm^{-1}, is usually referred to as the 'fingerprint' region and is nearly unique for every molecular species. Bands that originate in interacting vibrational modes give this complex absorption pattern of weak to middle intensity. Intensive bands in this region of the spectrum are due principally to the C–O stretching vibration in alcohols, phenols, ethers and esters.

2. Infrared spectra of selected carotenoids

Examples have been selected to illustrate the general features of the IR spectra of carotenoids as conjugated polyenes, and also to show those IR bands that are characteristic of some specific functional groups and therefore indicate the presence of certain structural features in the carotenoid molecule. A collection of representative spectra is included at the end of this Section.

The IR spectra shown were recorded for KBr pellets and were collected at ambient temperature by means of a Nicolet 7199 FTIR spectrophotometer with the 700 SX software.

This instrument is equipped with a water-cooled Globar source, a Ge-coated KBr beam-splitter and a broad range, liquid nitrogen-cooled MCT detector. All spectra were recorded at a resolution of 2 cm^{-1} by collecting 32 interferograms and processed by means of the 700 SX software; the spectra are base-line corrected and normalized.

Band intensities are denoted in the conventional way: vs (very strong), s (strong), m (medium), w (weak).

a) Alkanes (perhydrocarotenes)

Like most organic compounds, carotenoids and their hydrogenated derivatives contain methylene and methyl groups which give rise to bands at 2950-2850 cm^{-1} (CH stretching), around 1465 cm^{-1} (CH deformation) and 1380 cm^{-1} (methyl CH deformation). Carotane (perhydro-β,β-carotene) shows a simple spectrum (Spectrum 1):

Spectrum	Compound	CH_2/CH_3 cm^{-1}	CH_2/CH_3 cm^{-1}	CH_3 cm^{-1}
1	Carotane (perhydro-β,β-carotene, *1*)	2925, 2825 s	1461 m	1380 m

(b) Alkenes

The polyene structure of most carotenoids gives rise to weak bands between 1650 and 1550 cm^{-1} (C=C stretching), and a quite strong band between 990 and 960 cm^{-1} (CH out-of-plane deformation), if at least one disubstituted *trans* double bond is present.

Spectrum	Compound	C=C cm^{-1}	CH cm^{-1}
2	Lycopene (**31**)	1629, 1559 w	960 s
3	β,β-Carotene (**3**)	1622, 1561 w	965 s
4	(6'*R*)-β,ε-Carotene (**7**)	1624, 1565 w	964 s
5	4',5'-Didehydro-4,5'-retro-β,β-carotene (**48**)	1621, 1543 w	953 s

These alkane/alkene frequencies appear in the IR spectra of all carotenoids. When other functional groups are present in the molecule, the frequencies of these additional groups are superimposed on those of the skeletal CH_2/CH_3 and C=C groups and the intensities of the latter can be modified.

c) Geometrical isomers

The presence of at least one *Z* (*cis*) double bond in a carotenoid results in the appearance of additional strong absorption in the region around 750-800 cm^{-1}, attributed to C–H out-of-plane deformation vibrations of disubstituted *Z* double bonds, *e.g.* at 775 cm^{-1} for 15*Z* carotenoids. Key IR and Raman bands have been identified as characteristic of particular *Z*-isomers of β,β-carotene [9]. Thus, IR bands at 775-780 cm^{-1} are characteristic of a 'centrally bent' (15*Z* or 13*Z*) isomer, those at 825-830 cm^{-1} characteristic of the all-*E* and 'peripherally bent' (7*Z* or 9*Z*) isomers.

d) Alkynes, allenes and arenes

A central C≡C bond in a carotenoid is expected to give an IR band near 2200-2190 cm^{-1}. Because of symmetry rules, the intensity of this band may be very weak or zero, so the absence of such a C≡C stretching band does not necessarily mean that no central C≡C group is present (Spectrum 6).

When a C≡C bond is present near the end of the carotenoid chromophore, normally a weak C≡C stretching band is seen, but this is enhanced in ketones such as 7,8,7',8'-tetradehydroastaxanthin (**400**). (Spectrum 7)

Allene groups give rise to a band of medium intensity between 2000 and 1900 cm^{-1} (Spectrum 8). The IR band at 1928 cm^{-1} proved crucial in the assignment of an allenic structure to fucoxanthin (**369**) [7]. In arenes, the sharp aromatic bands near 1600 cm^{-1} appear close to the polyene C=C stretching band and are often not distinguishable. In the case of isorenieratene (**24**) (Spectrum 9) the strong out-of-plane bending vibration of the two adjacent hydrogen atoms on the aromatic ring, appearing at 810 cm^{-1}, confirms the aromatic structure.

Spectrum	Compound	C≡C cm^{-1}	C=C=C cm^{-1}	aryl CH=CH
6	15,15'-Didehydro-β,β-carotene (*2*)	no		
7	all-*E*-(3*S*,3'*S*)-7,8,7',8'-Tetradehydroastaxanthin (**400**)	2159 s		
8	(3*S*,5*R*,6*R*)-6,7-Didehydro-5,6-dihydro-β,β-carotene-3,5-diol (*3*)		1928 m	
9	Isorenieratene (**24**)			810 m

e) Alcohols and ethers

Alcohols in the solid state have broad strong absorption near 3300-3400 cm^{-1} due to the stretching of the O–H···O bonds (Spectra 8, 10-12). In addition, the vibrations involving the stretching of the C–O single bond give rise to strong infrared bands in the region of 1000 to 1200 cm^{-1}; this is also the case for ethers (Spectrum 13).

Spectrum	Compound	OH cm^{-1}	C-O cm^{-1}
8	(3*S*,5*R*,6*R*)-6,7-Didehydro-5,6-dihydro-β,β-carotene-3,5-diol (*3*)	3426 s	1038 m
10	(3*R*,3'*R*)-Zeaxanthin (**119**)	3393 m	1042 s
11	(3*RS*, 3'*RS*)-Astaxanthin (**403**)	3489 m	1074 s
12	Astacene (**398**)	3421 m	1062 s
13	Aurochrome (**265**)		1067, 998 m

f) Aldehydes and ketones

Aliphatic aldehydes and ketones are characterized by the very strong C=O stretching frequency absorption near 1715 cm^{-1}. Conjugation results in a lowering of this frequency to between 1700 and 1600 cm^{-1} (Spectra 11, 12, 14-16). The aldehyde CH group also gives rise to two sharp but weak bands at 2900-2800 cm^{-1} and 2775-2695 cm^{-1} (Spectrum 14).

Spectrum	Compound	C=O cm^{-1}	CH (aldehyde) cm^{-1}
14	12'-Apo-β-caroten-12'-al (**507**)	1662 vs	2818, 2713 w
15	Canthaxanthin (**380**)	1657 vs	
16	β-Carotenone (**562**)	1710, 1668 vs	
11	(3*RS*, 3'*RS*)Astaxanthin (**403**)	1653 vs	
12	Astacene (**398**)	1619 vs	

g) Esters and carboxylic acids

Esters are characterized by strong absorption due to the C=O stretching frequency between 1740 and 1700 cm^{-1}. Like ethers and alcohols, they also have a C–O single bond which gives rise to strong (and often complex) bands in the region 1300-1050 cm^{-1}.

Carboxylic acids exist predominantly as the hydrogen-bonded dimer and most of them have their C=O band at 1720-1660 cm^{-1}. In addition, they are usually characterized by a strongly bonded, broad OH stretching band centring near 3000 cm^{-1} (Spectra 17, 18).

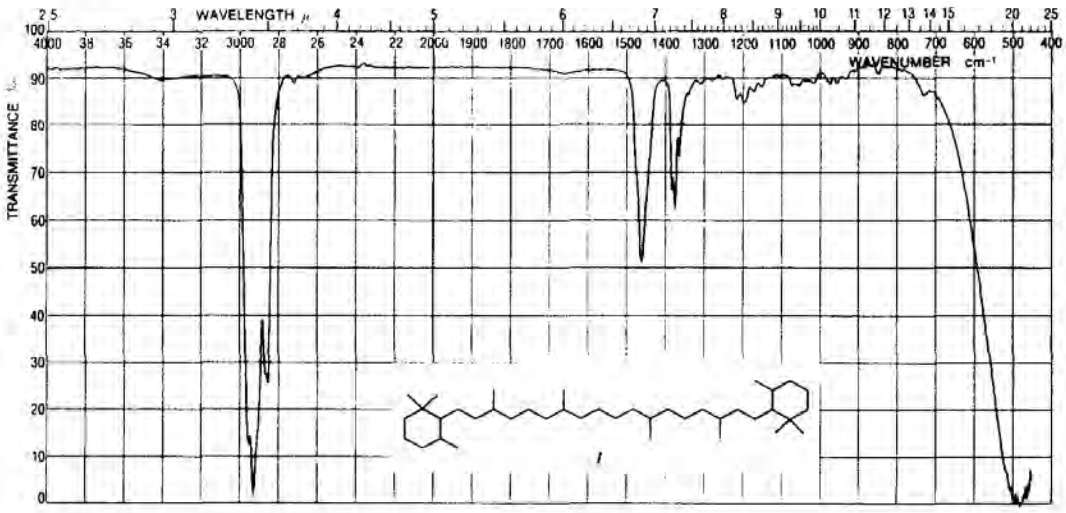
Spectrum	Compound	OH cm^{-1}	C=O cm^{-1}	C-O cm^{-1}
17	Bixin (**533**)	3300-2400 s	1716 vs	1287 s, 1159 vs
18	Crocetin (**538**)	3300-2200 s	1668 vs	1273 s, 1243 s

h) Sulphates

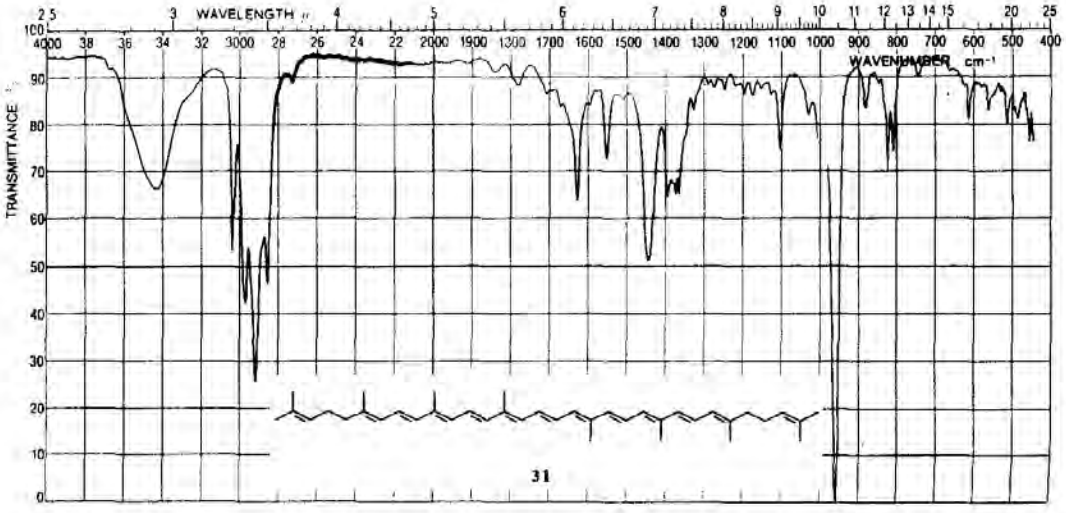
Carotenoid sulphates, *e.g.* astaxanthin (**406**) disulphate (Na salt) show strong absorption at 1240 cm^{-1} due to the SO_3 group (spectrum 19). These substances are often hygroscopic and also show an intensive OH band due to water when IR spectra are recorded in KBr.

Spectrum	Compound	OH cm^{-1}	C=O cm^{-1}	SO_3 cm^{-1}
19	Astaxanthin (**406**) 3,3'-di-sulphate di-Na salt	3439 s	1670 s	1240 vs

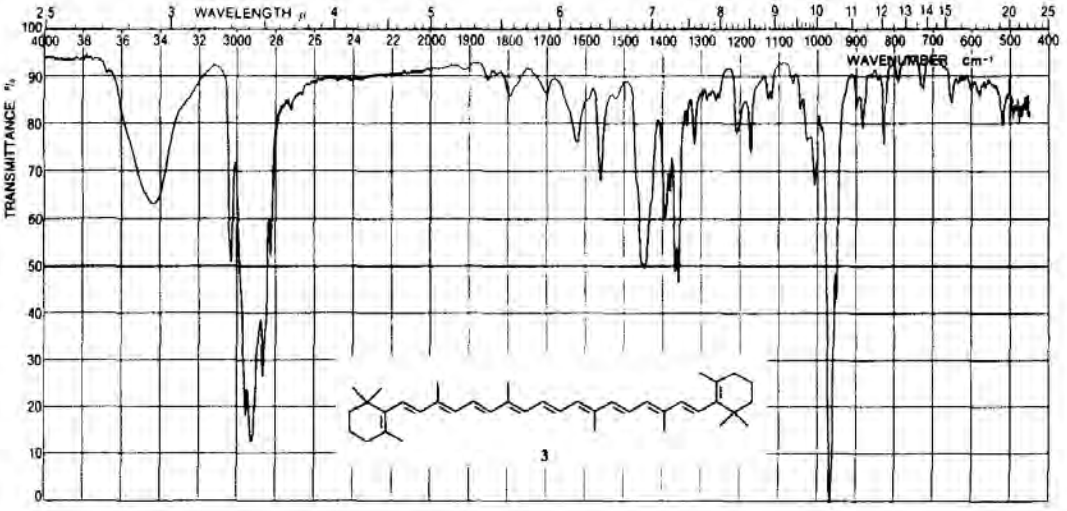
Spectrum 1



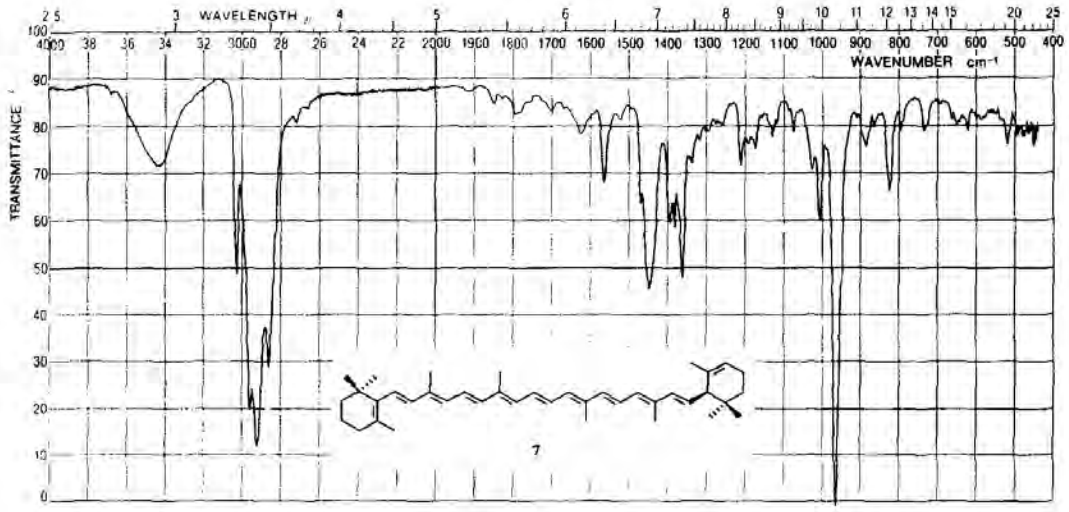
Spectrum 2



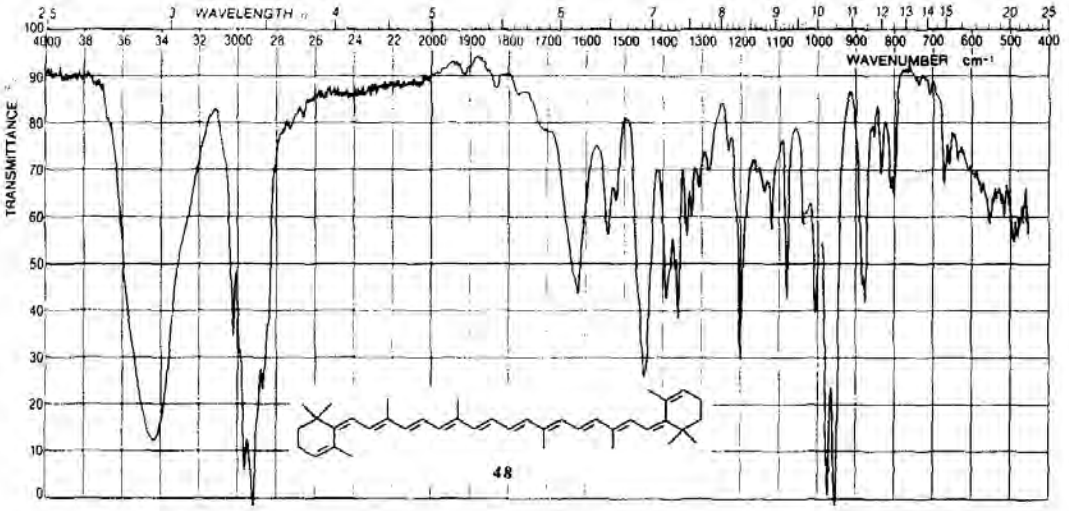
Spectrum 3



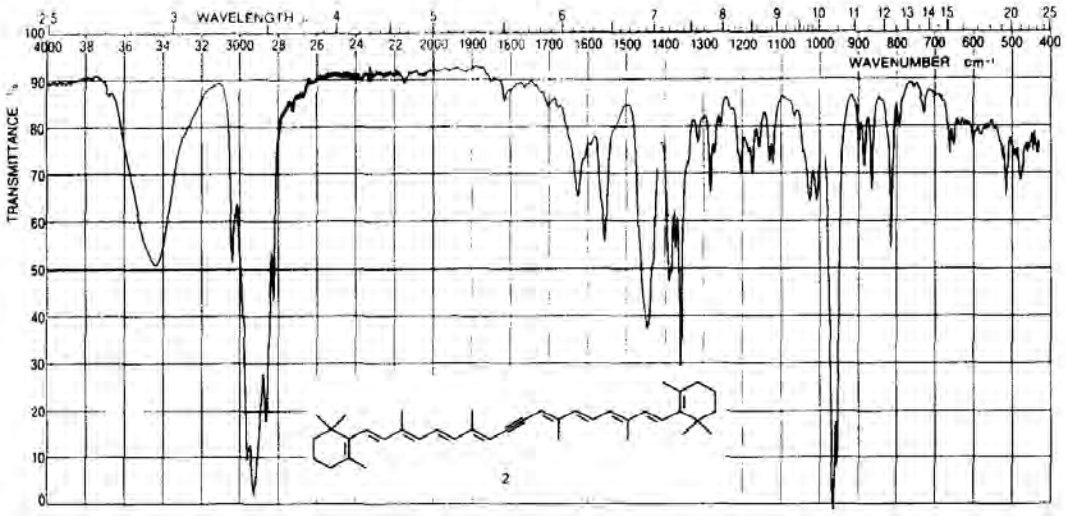
Spectrum 4



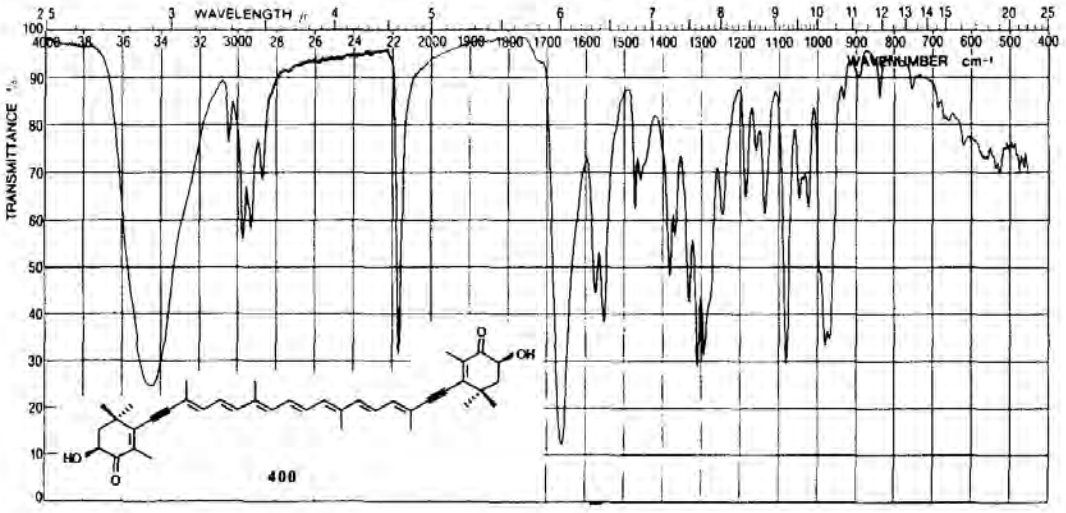
Spectrum 5



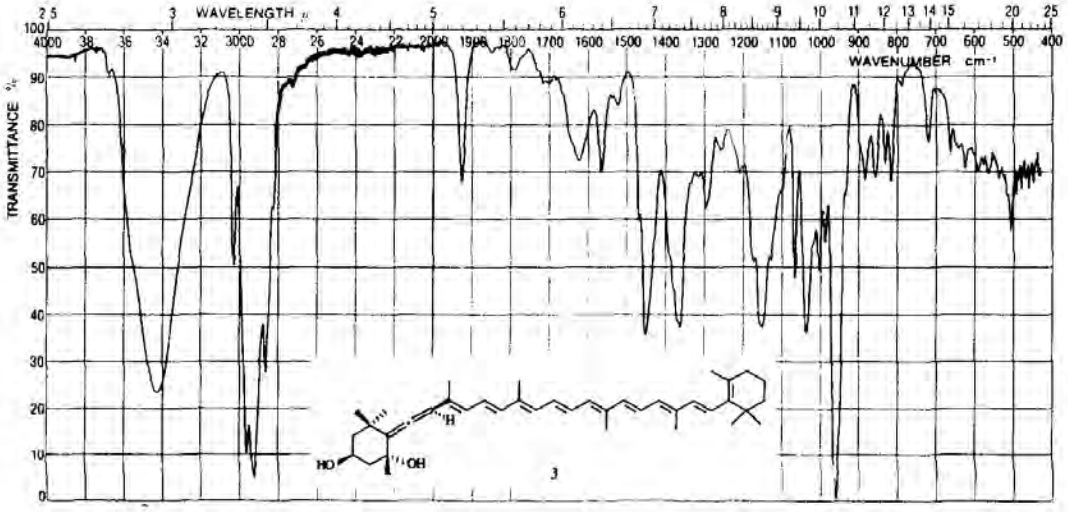
Spectrum 6



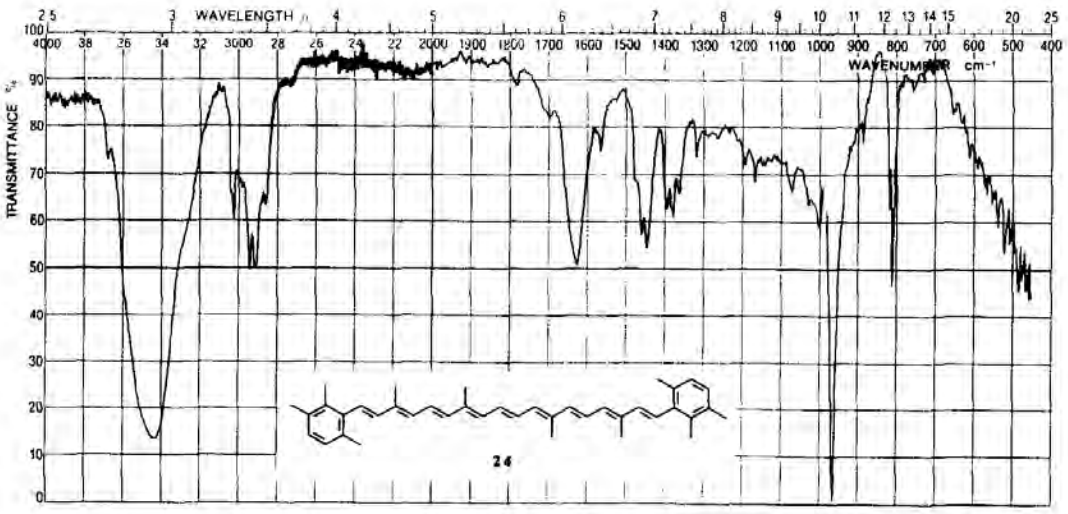
Spectrum 7



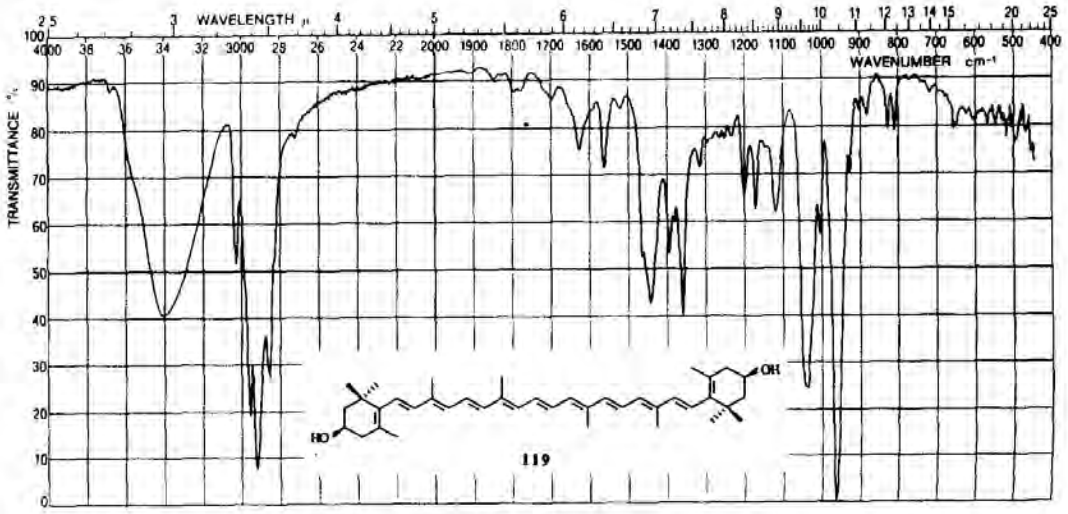
Spectrum 8



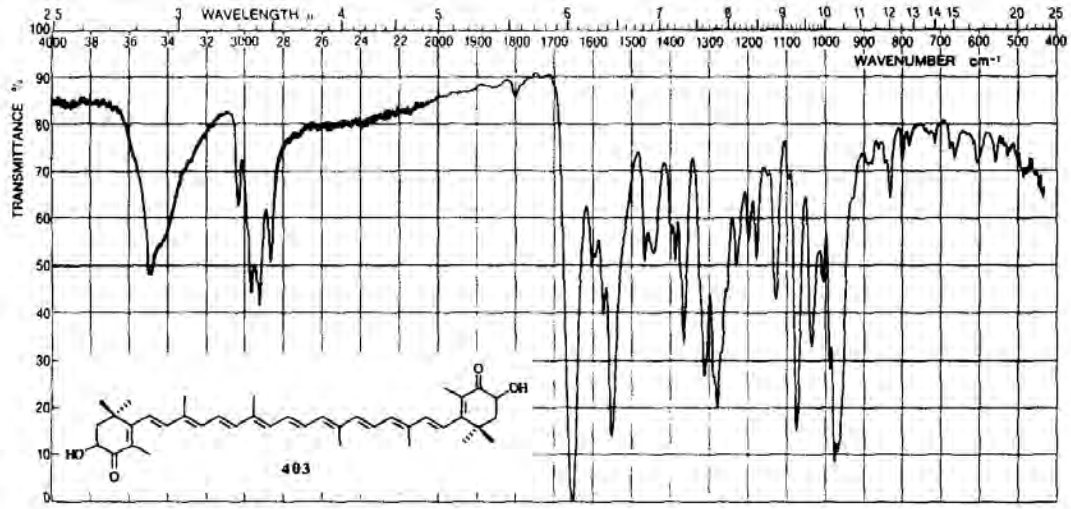
Spectrum 9



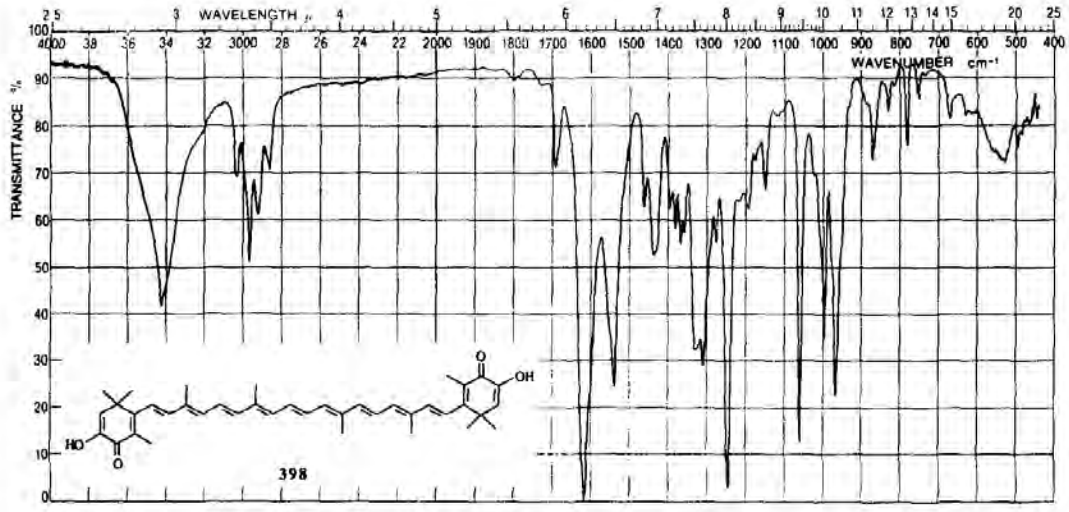
Spectrum 10



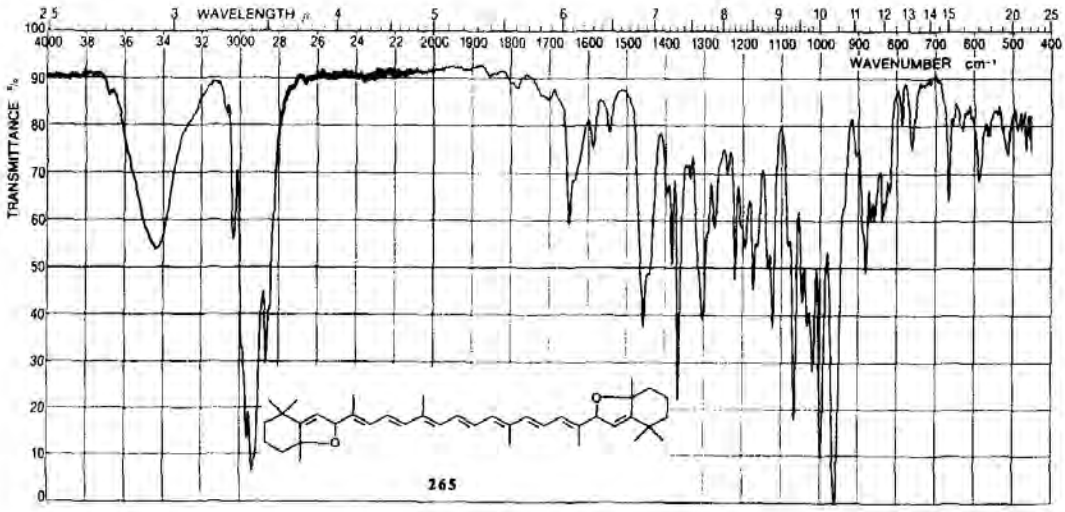
Spectrum 11



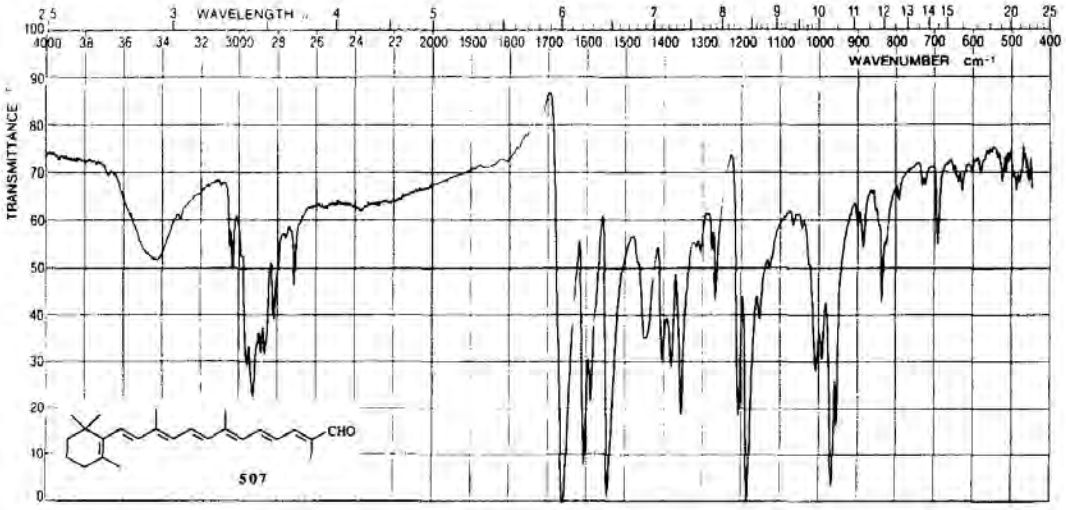
Spectrum 12



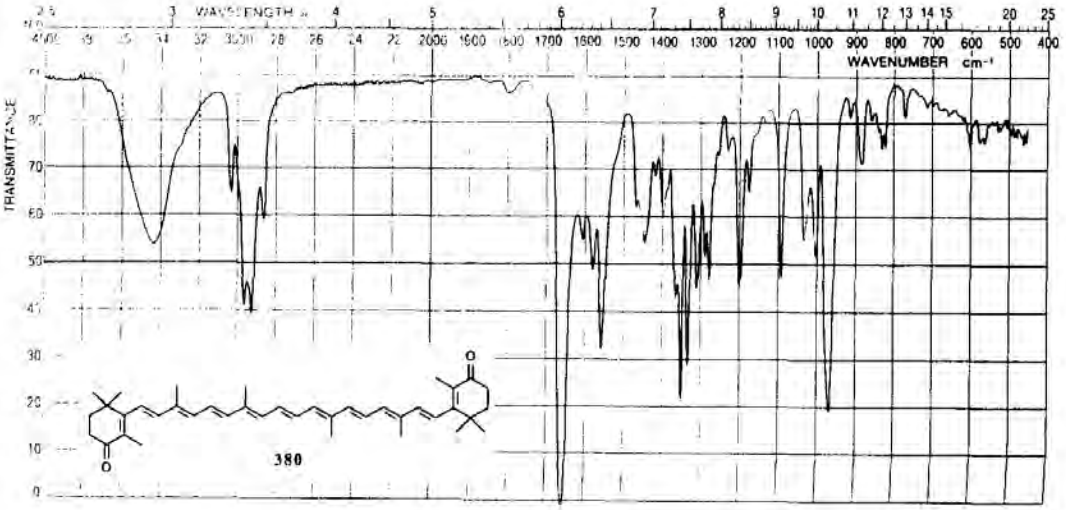
Spectrum 13



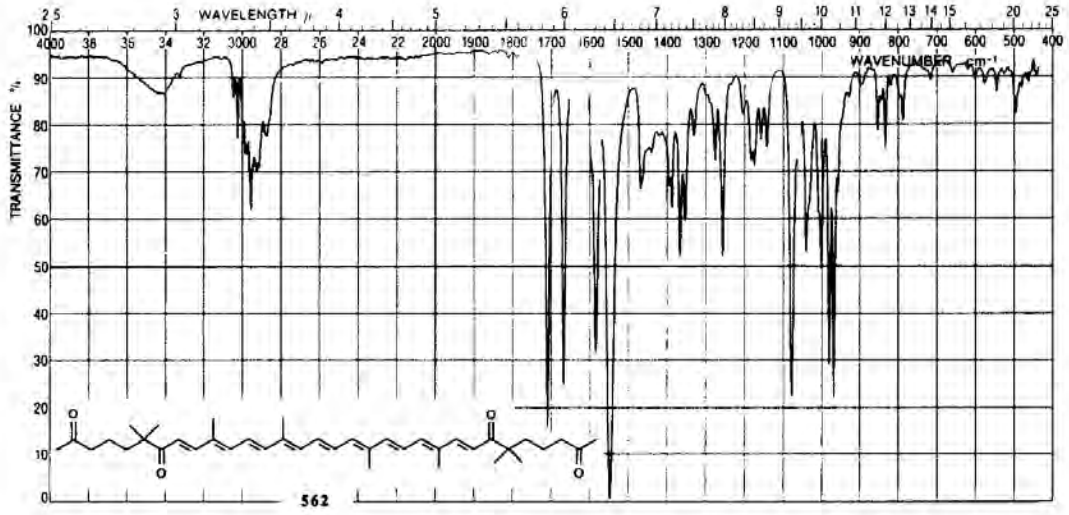
Spectrum 14



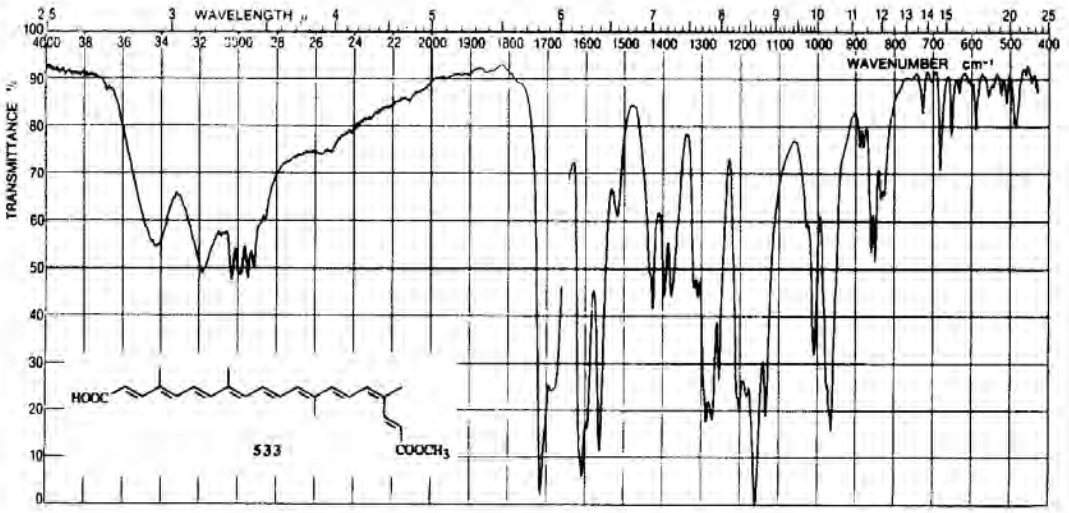
Spectrum 15



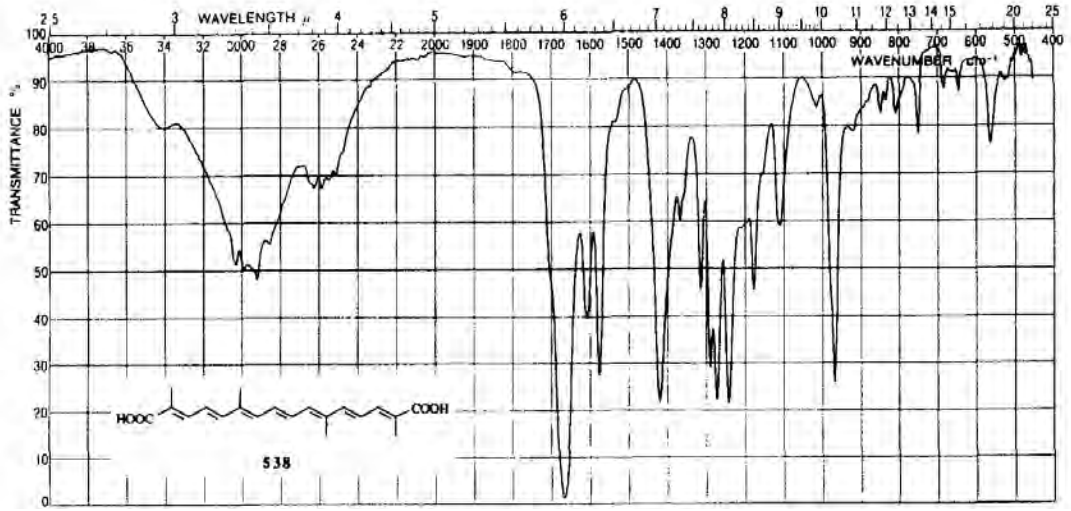
Spectrum 16



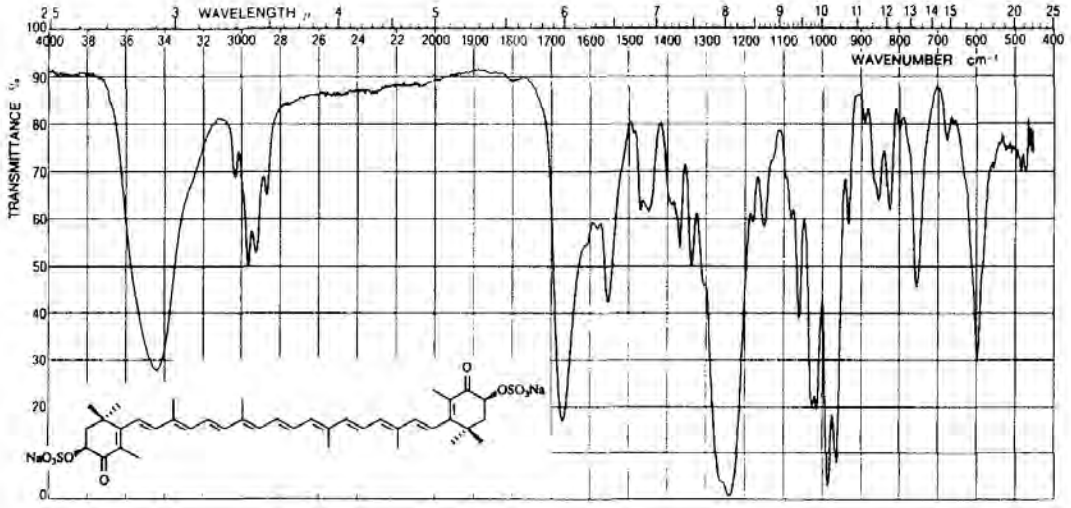
Spectrum 17



Spectrum 18



Spectrum 19



D. References

[1] U. Schwieter, H. R. Bolliger, L. H. Chopard-dit-Jean, G. Englert, M. Kofler, A. König, C. von Planta, R. Rüegg, W. Vetter and O. Isler, *Chimia*, **19**, 294 (1965).

[2] D. Lin-Vien, N. B. Colthup, W. G. Fateley and J. G. Grasselli, *The Handbook of Infrared and Raman Characteristic Frequencies of Organic Molecules*, Academic Press, New York (1991).

[3] N. B. Colthup, L. H. Daly and S. E. Wiberley, *Introduction to Infrared and Raman Spectroscopy*, Academic Press, Boston (1990).

[4] S. F. Johnston, *Chem. in Britain*, **1990**, 573.

[5] P. R. Griffiths and J. A. Hareth, *Fourier Transform Infrared Spectroscopy*, Wiley, New York (1986).

[6] C. J. Pouchert, *The Aldrich Library FT-IR Spectra, Vol. 1-3*, Aldrich Chem. Comp. Inc., Milwaukee, USA (1985).

[7] B. C. L. Weedon, *Fortschr. Chem. Org. Naturst.*, **27**, 91 (1969).

[8] G. P. Moss and B. C. L. Weedon, in *Chemistry and Biochemistry of Plant Pigments* (ed. T. W. Goodwin), Vol. 1, p. 186, Academic Press, London (1976).

[9] Y. Koyama, I. Takatsuka, M. Nakata and M. Tasumi, *J. Raman Spectrosc.*, **19**, 37 (1988).

[10] G. Britton, *Nat. Prod. Reports*, **1**, 78 (1984).

[11] G. Britton, *Nat. Prod. Reports*, **3**, 603 (1986).

[12] G. Britton, *Nat. Prod. Reports*, **6**, 373 (1989).

Carotenoids
Volume 1 B: Spectroscopy
© 1995 Birkhäuser Verlag Basel

Chapter 5

Resonance Raman Spectroscopy

Yasushi Koyama

A. Introduction

1. Principles of resonance Raman spectroscopy

Raman spectroscopy is a kind of vibrational spectroscopy that is complementary to infrared spectroscopy. When the incident light with frequency υ_0 is scattered by a molecule which is vibrating with frequency υ_1, the scattered light contains not only the component with frequency υ_0 (Rayleigh scattering) but also components with frequencies $\upsilon_0 \pm \upsilon_1$ (Raman scattering). The $(\upsilon_0 + \upsilon_1)$ component is called anti-Stokes Raman scattering; the $(\upsilon_0 - \upsilon_1)$ component is called Stokes Raman scattering. These scattering processes are shown schematically in Fig. 1. Since population of the v" = 0 vibrational level is higher than that of the v" = 1 level due to Boltzmann distribution, the Stokes Raman line is always stronger and is used for Raman measurements. Infrared absorption can be induced only when the incident light energy $h\upsilon_1$ matches the energy gap ΔE (v"= 0 → v"= 1). Raman scattering, however, can be induced by light with various values for energy $h\upsilon_0$.

Raman intensity varies depending on the frequency υ_0 of the incident light. When the light energy $h\upsilon_0$ approaches the energy gap between the electronic levels, $E_1 - E_0$, the Raman intensity is strongly enhanced. In this case the Raman process is said to be in 'pre-resonance', with the electronic transition $E_1 \leftarrow E_0$. When $h\upsilon_0$ matches the electronic energy gap, the Raman process is in 'rigorous resonance' and the Raman intensity is enhanced by as much as a factor of 10^5 in comparison with the completely off-resonance condition. Resonance Raman spectroscopy is Raman spectroscopy performed under the resonance conditions.

2. Scope and limitations of resonance Raman spectroscopy

Polyatomic molecules such as carotenoids have many vibrational degrees of freedom (3N–6, where N is the number of atoms in the molecule), and their normal vibrations, *i.e.* υ_1, υ_2, . . . υ_{3N-6}, give rise to both Raman and infrared spectra. In infrared absorption, those local

vibrations which cause large changes in the dipole moment give rise to high intensity bands (the 'finger-print' vibrations), whereas in Raman scattering it is those overall vibrations which cause large changes in the polarizability that give rise to high intensity. Therefore, Raman-active vibrations are generally structure-sensitive. Only a limited number of Raman-active vibrations can be detected under the resonance conditions, however; they must be in accord with structural changes caused by transition to the electronic state in resonance.

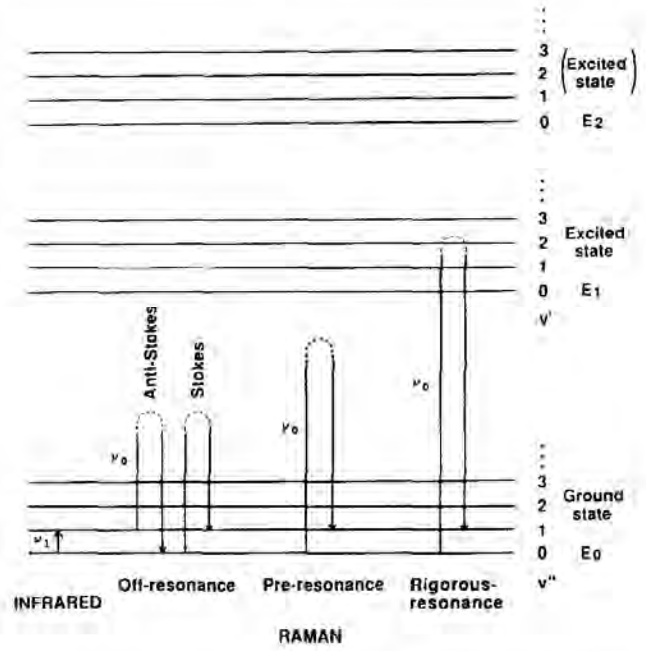


Fig. 1. Schematic representation of the processes of infrared absorption and resonance Raman scattering.

The carotenoid molecule is a strong Raman scatterer, and it is straightforward to record the resonance Raman spectrum of a carotenoid at a concentration as low as 10^{-5} M. The unique strength of resonance Raman spectroscopy is its capability of probing selectively a particular chromophore. When Raman scattering is recorded by using a probe wavelength in the 450 to 550 nm region, the pure spectrum can be obtained of a carotenoid *in situ* in a complex matrix such as a spinach leaf, orange skin or even pearls. In more detailed investigations, resonance Raman spectroscopy provides a powerful means of probing the structure of a carotenoid when this is bound to sub-cellular structures, for example in photosynthetic systems. Other pigments, which show electronic absorption bands in other spectral regions (chlorophylls, phaeophytins or quinones), as well as molecules such as peptides, lipids and carbohydrates that have no absorption in the visible region, give rise to no lines in the resonance Raman spectrum when this is recorded by excitation in the region of 450 to 550 nm (see Section C.2).

Pieces of structural information that can be obtained by resonance Raman spectroscopy include the bond order, the *cis-trans* (*Z*/*E*) configuration and the distortion of the conjugated backbone of carotenoids, which exhibit π–π^* absorption in this wavelength region. The method provides a unique opportunity to compare the structure of the conjugated backbone in the free and bound states.

Resonance Raman spectroscopy also has inherent limitations. First, it provides little information on the structures of the end groups, because Raman lines due to the vibrations in the end groups which are not conjugated to the polyene backbone are not resonance-enhanced. Secondly, quantitative analysis of carotenoids by means of resonance Raman spectroscopy is not straightforward. Resonance Raman intensity strongly depends on the resonance condition, and it is not straightforward to adjust the resonance condition for the purpose of comparison. Further, self-absorption of Raman scattering, which is frequency-dependent and concentration-dependent, always distorts the relative intensities of Raman lines to some extent.

For detailed treatment of the principles and techniques of resonance Raman spectroscopy, several specialist books are available [1-6].

B. Experimental Procedures

1. Instrumentation

An Ar^+-laser of 2 to 4W power is the most appropriate light source for resonance Raman spectroscopy of carotenoids which show the S_2 (B_u) $\leftarrow$ S_0 (A_g) absorption in the region 450 to 550 nm (see Chapter 1). This source provides eight laser lines at 457.9, 465.8, 472.7, 476.5, 488.0, 496.5, 501.7 and 514.5 nm. The 488.0 and 514.5 nm lines are very strong, and are the ones most frequently used for Raman measurements. In some cases, however, one of the other lines may provide a better resonance condition (see Section. C.1), and the 457.9 nm line is sometimes useful for reducing the background of fluorescence due to unspecified contaminants (Section B.2). An interference filter must be used to purify each laser line by removing additional natural emission lines [1] which interfere with the Raman lines, especially in the case of solid samples.

For Raman measurements, the laser beam is focused on the sample by a lens and the 90° scattering radiation is collected, focused and directed to the detector by a series of lenses, slits, gratings and mirrors.

There are two alternative methods for detection of Raman scattering; one uses a combination of a photomultiplier and a double monochrometer, the other a combination of a multichannel detector and a triple polychrometer. In both cases, removal of the stray light that originates from the Rayleigh scattering is most important, because the Raman scattering is much weaker than the Rayleigh scattering.

Photomultipliers are generally more sensitive than multichannel detectors and give high optical resolution. However, the scanning is time-consuming (10 to 40 min), and stability of the laser power during the scanning must be maintained to avoid 'distortion' of relative

intensities of the Raman lines. Many hours are required for repeated scanning, which is sometimes necessary in order to improve the signal-to-noise ratio.

Spectral resolution with the triple polychrometer–multichannel detector system is determined by the dispersion of the grating and by the dimension and number of pixels of the multichannel detector, and is generally lower than with the double monochrometer–photomultiplier system. However, Raman data can be collected all the time during irradiation, and a spectrum with extremely high signal-to-noise ratio can easily be obtained in less than 1 minute. Possible fluctuation of the laser power does not affect the relative intensity of the Raman lines. An image-intensified diode-array detector is currently the best choice of multichannel detector.

2. Sample preparation

Fluorescence is the greatest problem faced in Raman spectroscopy. Traces of contaminants can give rise to a high fluorescence background. Therefore, rigorous purity of the sample is prerequisite. It is also necessary to monitor degradation of carotenoid samples in solution, caused by irradiation with the laser beam. Contaminants such as chlorophyll, phaeophytin, phycocyanin and phycoerythrin need to be removed completely, because they are strongly fluorescent and function also as sensitizers to cause isomerization of carotenoids in the triplet state. Degradation products of carotenoids are also potential triplet sensitizers. Since the Raman spectrum of a carotenoid varies depending on the geometrical configuration (see Section D.2.) and the spectrum of an isomeric mixture gives only a broad profile with no specific structural information, isomeric purity is crucial in resonance Raman spectroscopy of a carotenoid.

Carotenoids bound to other molecular structures *in situ* are generally stable, and resistant to decomposition or isomerization caused by laser irradiation. Therefore, Raman measurements of carotenoids *in situ* are much more straightforward than those of carotenoids free in solution. For suspensions of membrane preparations or pigment-protein complexes, complete removal of free chlorophyll, phaeophytin and peptides by washing with buffer (with or without a detergent) is necessary. Selection of a non-fluorescent detergent (impurities dissolved in the detergent sometimes fluoresce) is important. Intact samples, such as living cells of phototrophic bacteria, leaves, *etc.*, should be rinsed with water; deposited impurity or detergent can be fluorescent.

3. Raman measurements

The power density of the laser beam at the sample should be kept as low as possible in any Raman measurement in order to minimize degradation of the sample; the output power of the laser should be reduced, and too tight focusing of the laser beam on the sample avoided.

The concentration of the sample solution should be kept low in order to avoid degradation of the sample by the absorbed light energy and distortion of the relative Raman

intensities by self-absorption of the Raman scattering. A carotenoid concentration of 10^{-5} to 10^{-4} M is sufficient for ordinary measurements. The volume of the sample solution depends on the Raman cell to be used: 0.3 ml for a liquid nitrogen-cooled low-temperature cell, 1 to 2 ml for a spinning cell, 3 to 5 ml for a flow cell, and 30 to 60 ml for a jet stream.

a) Carotenoids free in solution

Two alternative methods are used to minimize the effect of isomerization of carotenoids in solution. Isomerization can be avoided in a Raman cell at the temperature of liquid nitrogen. The sample solution is placed in a thin glass tube and then dipped into liquid nitrogen.

When Raman measurement at room temperature is necessary, a flow method can be used. This can be either a flow of the sample solution (1 to 10 $cm.s^{-1}$) in a glass tube or a jet of the sample solution (1 to 10 $m.s^{-1}$) ejected from a nozzle. Isomerization does take place in the laser beam, but the effect is minimized because the solution is circulated so that the isomerization products are diluted in the reservoir of solution before entering into the laser beam again.

b) Carotenoids bound *in situ*

Carotenoids bound to proteins and other structures *in situ* are much more stable, and a spinning cell can be used for suspensions of materials such as membrane preparations or pigment-protein complexes. However, the same circular portion of the solution on the spinning cell wall is irradiated repeatedly. Alternatively, a stirring cell with a small spinning magnet inside and with a magnetic stirrer outside can be used. The low-temperature cell or flow cell can be used for these samples, as for samples in solution. Living bacterial cells can be measured in the spinning or stirring Raman cell. Larger intact tissue samples can be dipped into water to prevent local heating caused by laser irradiation.

C. Raman Intensities: Dependence of Resonance Raman Intensity on Excition Energy

1. Resonance Raman excitation profile for all-*E*-β,β-carotene in solution

Figure 2a shows the resonance Raman spectra of all-*E*-β,β-carotene (**3**) in isopentane at liquid nitrogen temperature, recorded by use of five different lines of an Ar^+-laser [7]. Figure 2b shows the dependence of the intensities of the υ_1 (the C=C stretching at 1525 cm^{-1}) and the υ_2 (the C–C stretching at 1155 cm^{-1}) Raman lines (see Section D) on the energy used to excite the Raman process. Each of these relationships is called 'a resonance-Raman excitation profile'. The electronic absorption spectrum of β,β-carotene (**3**) is also shown.

The set of observed Raman spectra (Fig. 2b) shows that the absolute as well as the relative intensities of the υ_1 and υ_2 Raman lines of β,β-carotene strongly depend on the energy of excitation. Both the υ_1 and υ_2 Raman lines are strongest when excitation at 496.5 nm is

used (spectrum 4), whilst the relative intensity of the υ_2 Raman line is considerably lower than that of the υ_1 Raman line when excitation is at 465.8 nm (spectrum 2). In other words, the resonance Raman excitation profile (Fig. 2a) of the υ_1 Raman line is completely different from that of the υ_2 Raman line. The basic principles of the resonance Raman excitation profile are described elsewhere [7, 8].

Calculations show that a peak in the excitation profile can be generated every time the light energy $h\upsilon_0$ matches the energy gap between the electronic ground state ($v'' = 0$) and one of the vibrational levels ($v' = 0, 1, 2, 3, \ldots$) in the electronic excited state. The overlap integrals between the vibrational wave functions of the ground and excited electronic states determine the relative intensity of the peaks in the excitation profile. The resonance Raman excitation profile therefore provides an important piece of information about the displacement of the equilibrium position that results from excitation from the electronic ground state to the excited state in resonance.

Fig. 2a

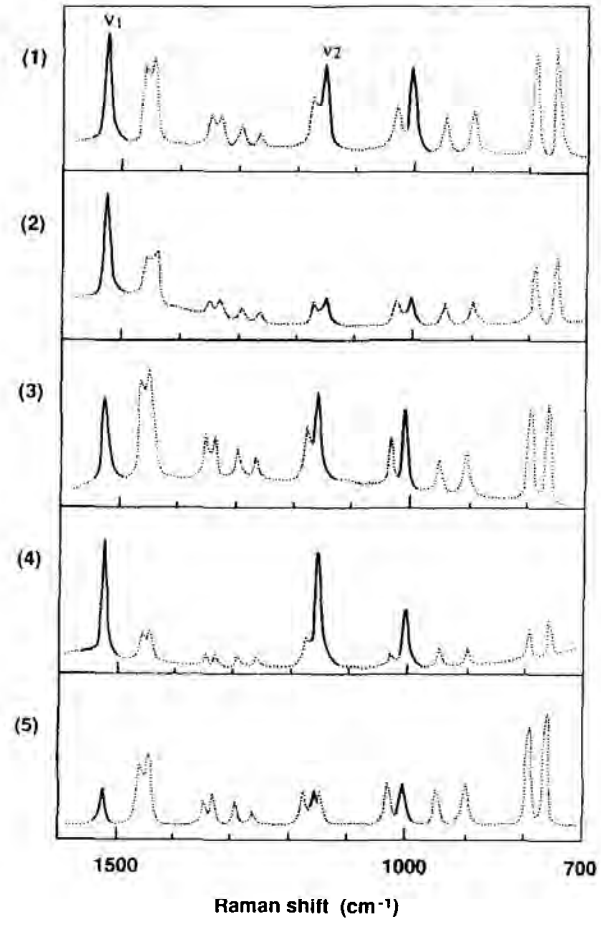


Fig. 2b

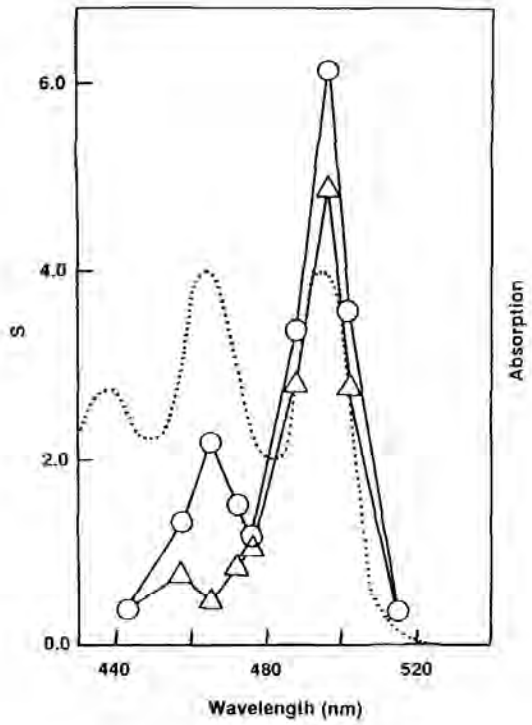
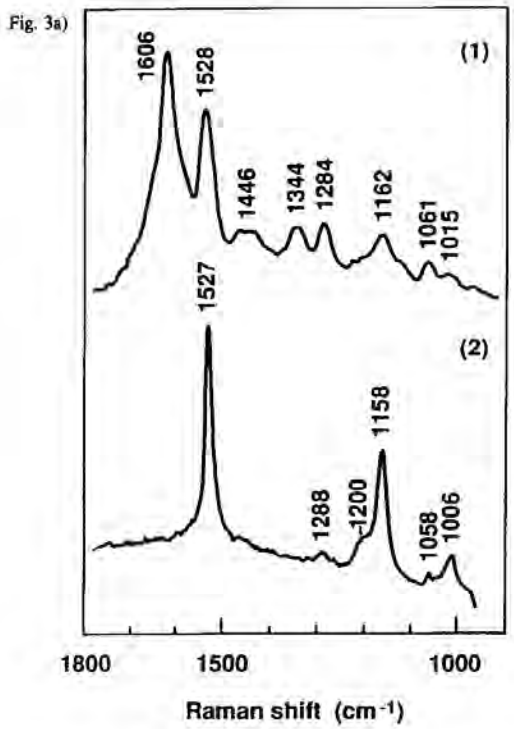


Fig. 2. Dependence of resonance Raman intensity on the excitation energy (resonance Raman excitation profile) for all-*E*-β,β-carotene (**3**) [7]: (a) the Raman spectra at (1) 457.9, (2) 465.8, (3) 476.5, (4) 496.5 and (5) 514.5 nm excitation (in isopentane at −155°C). Dotted lines indicate the Raman lines due to the solvent isopentane. (b) the resonance Raman excitation profiles for the υ_1 (o) and υ_2 (Δ) Raman lines and the electronic absorption spectrum.

2. Selective detection of resonance Raman scattering from a carotenoid in intact cells of a phototrophic bacterium

Figure 3 shows (a) the resonance Raman spectra obtained from cells of *Rhodobacter sphaeroides* G1C [9] excited by using (1) the 355 nm and (2) the 488 nm laser lines, and (b) the electronic absorption spectrum of the cells. Raman spectrum 1 shows the Raman lines of bacteriochlorophyll *a* as well as those of the carotenoid, neurosporene (**34**), whereas Raman spectrum 2 shows only the Raman lines of neurosporene (**34**) [9]. The electronic absorption spectrum shows that the 355 nm line is in resonance with both the Soret absorption of bacteriochlorophyll *a* and with the *cis*-peak of neurosporene (**34**). The unique capability of resonance Raman spectroscopy to detect the carotenoid selectively is clearly demonstrated, and the selection of the 488 nm line of an Ar^+ laser for recording a pure resonance Raman spectrum of the carotenoid is justified.



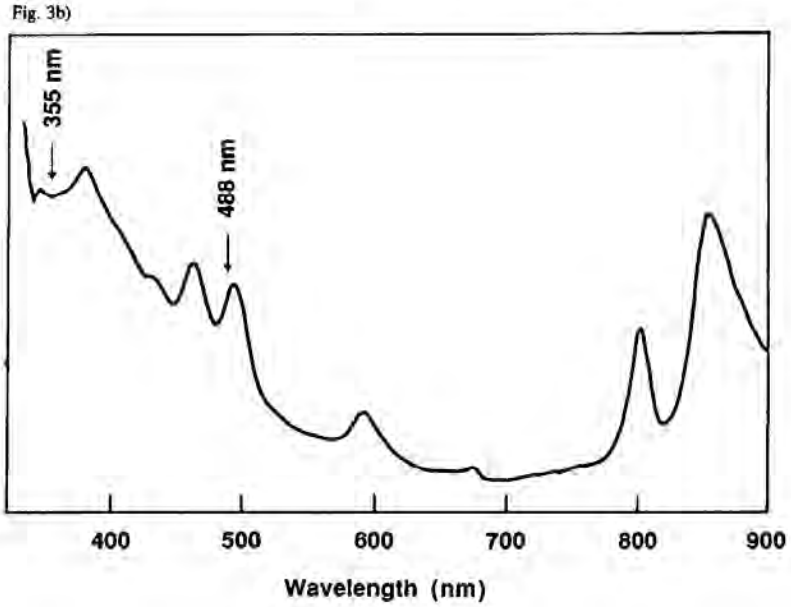


Fig. 3. Selective detection of Raman scattering from a carotenoid, neurosporene (**34**), in the intact cells of *Rhodobacter sphaeroides* G1C: (a) The resonance Raman spectra excited at (1) 355 nm and (2) 488 nm [9], and (b) the electronic absorption spectrum showing the above two different resonance conditions.

D. Raman Frequencies: Normal Modes of Vibration

In the resonance Raman process, the vibrations that are strongly resonance enhanced are those in which the displacements of atoms in the molecule are in accordance with the distortion of the molecule when the transition takes place from the electronic ground state to the excited state in resonance. For carotenoids, these vibrations include the C=C stretchings (1550 to 1500 cm^{-1}), the C–H in-plane bendings (1400 to 1100 cm^{-1}), and the C–C stretchings (1200 to 900 cm^{-1}) of the conjugated backbone, when the Raman process is in resonance with the $B_u \leftarrow A_g$ ($\pi \cdot \pi^*$) electronic transition. These unit vibrations mix with one another within each group. The resultant vibrations in each group can couple with one another to form a set of 'normal modes', because all the above vibrations take place within the same plane, *i.e.* that of the conjugated backbone. A normal mode of vibration is defined as one of the above mixed and coupled vibrations, which can be induced independently without inducing any additional vibrations. Other kinds of normal modes appear in the resonance Raman spectrum of a carotenoid. The in-plane rocking vibration of the methyl groups attached to the conjugated chain couples with the adjacent C–H in-plane bending (*ca.* 1010 cm^{-1}), and is also resonance enhanced. The C–H out-of-plane vibration coupled with the C=C torsion (*ca.* 960 cm^{-1}) can be strongly resonance enhanced when some distortion is applied around a certain C=C bond in the conjugated backbone.

Each normal mode has its own frequency, which depends on the set of force constants and also on the geometry of the molecule. The frequencies of normal modes thus provide information about bond orders and geometrical configuration of the conjugated backbone.

1. The C=C stretching frequency that reflects the bond order

The strongest Raman line which appears above 1500 cm^{-1} (denoted as υ_1 in Section C.1.) is assigned to a normal mode in which all the C=C stretchings are mixed in-phase; the C=C stretchings in the central part of the molecule make the largest contribution. Figure 4 shows the relationship between the frequency of the particular mode (here, simply called the C=C stretching) and the number of conjugated C=C bonds, for a variety of carotenoids in THF solution [10]. A rough linear relationship is seen; the lower frequency for a longer conjugated chain is definitely ascribed to its increased conjugation (decreased bond-order) in the central part and the resultant decrease in the C=C stretching force constants. This relationship may be used to assess the number of C=C bonds for an unknown carotenoid, if the all-*trans* configuration is confirmed by resonance Raman spectroscopy.

2. Key Raman lines of *cis-trans* geometrical configurations

The frequency of the C=C stretching mode depends also on the geometrical configuration of the conjugated backbone. In the case of β,β-carotene (**3**), the 'isomerization shifts' (defined as the shift of the Raman line to higher frequencies with respect to that of the all-*E* isomer) for

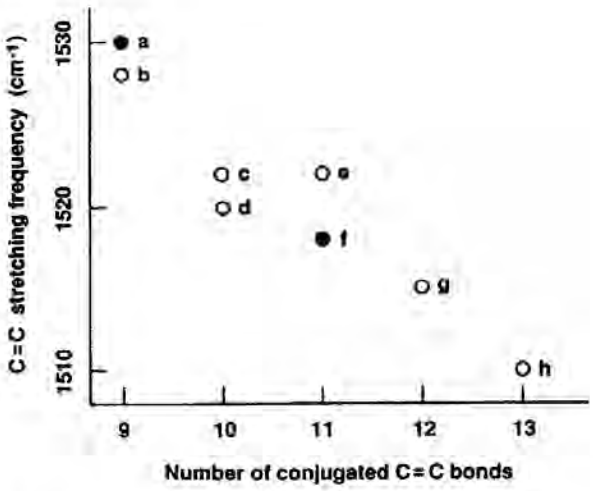


Fig. 4. Relationship between the frequency of the C=C stretching Raman line and the number of conjugated C=C bonds for various carotenoids [10]: (a) 8'-apo-β-caroten-8'-al (**482**), (b) neurosporene (**34**), (c) lutein (**133**), (d) spheroidene (**97**), (e) β,β-carotene (**3**), (f) canthaxanthin (**380**), (g) 3,4-dihydrospirilloxanthin (**168**), and (h) spirilloxanthin (**166**). Raman spectra were recorded in tetrahydrofuran at room temperature, *ca.* 24°C. Closed circles indicate carotenoids in which a C=O group is attached to the conjugated C=C system.

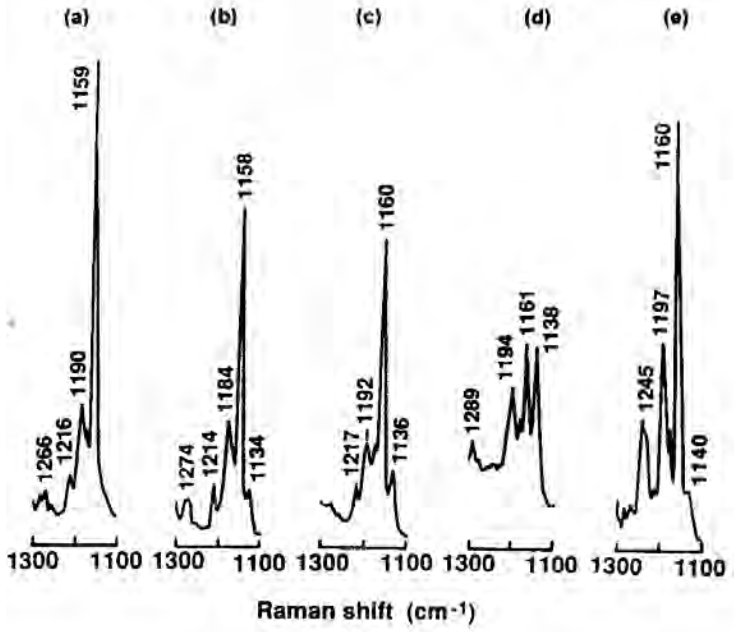


Fig. 5. Unique spectral patterns in the region of 1300 to 1100 cm^{-1} for the (a) all-*E*, (b) 7*Z*, (c) 9*Z*, (d) 13*Z* and (e) 15*Z* isomers of β,β-carotene (**3**) [11]. The Raman spectra were recorded in *n*-hexane at liquid nitrogen temperature. Key Raman lines are at 1160, 1140, 1274 and 1245 cm^{-1}.

the series of mono-*Z* isomers have been determined: for 7*Z*, 1 cm^{-1}; for 9*Z*, 5 cm^{-1}; for 13*Z*, 13 cm^{-1} and for 15*Z*, 10 cm^{-1}. Larger isomerization shifts were seen for di-*cis* and tri-*cis* isomers [11]. The trend may be ascribed to interruption of the conjugation by introducing a *cis* bend in the extended conjugated chain, and to the resultant increase in the bond orders (the force constants).

The Raman spectral pattern in the region of 1300 to 1100 cm^{-1}, where coupled vibrations of the C–H in-plane bendings and the C–C stretchings appear, was found to be unique to each geometrical configuration. Figure 5 shows the spectral patterns for the (a) all-*E*, (b) 7*Z*, (c) 9*Z*, (d) 13*Z*, and (e) 15*Z* isomers of β,β-carotene (3) [11]. The key Raman lines to distinguish the geometrical configurations are as follows.

i) The Raman line at around 1160 cm^{-1} is strongest for the all-*E* isomer. The intensity of this line decreases systematically in the order, all-*E* > 7*Z* > 9*Z* > 13*Z*. (The Raman line for the all-*E* isomer was denoted as υ_2 in Section C.1.).

ii) The Raman line at around 1140 cm^{-1} is absent from the spectrum of the all-*E* isomer, but its intensity increases systematically in the order, all-*E* < 7*Z* < 9*Z* < 13*Z*.

iii) The 7*Z* isomer uniquely gives a Raman line at 1274 cm^{-1}.

iv) The 15*Z* isomer uniquely gives a Raman line at 1245 cm^{-1}.

The normal modes for the above key Raman lines have been determined by calculations of normal vibrations for a carotenoid model which lacks the β rings at both ends [12].

Empirical rules concerning the Raman intensity follow from this study.

i) 'A *trans* mode', which takes place in the extended all-*trans* part of the conjugated chain, gives rise to the highest Raman intensity when the particular mode takes place in the centre of the all-*trans* part and the lowest intensity when peripheral.

ii) 'A *cis* mode', which takes place at the *cis* bend of the conjugated chain, gives rise to medium Raman intensity.

The key Raman lines can be explained in terms of the above normal modes and empirical rules as follows [12].

i) The normal mode which is responsible for the 1160 cm^{-1} Raman line is located in the centre of the all-*trans* part for the all-*E* configuration. The location of the particular mode does not change, but it becomes a peripheral part of the residual all-*trans* chain when the *cis* bend introduced is nearer to the centre. Thus, the decrease in intensity in the order all-*E* > 7*Z* > 9*Z* > 13*Z* can be explained.

ii) For the all-*E* configuration, the normal mode that is responsible for the 1140 cm^{-1} Raman line occurs at both ends of the long all-*trans* chain. For the 13*Z* configuration, however, half of the normal mode occurs in the central part of the residual all-*trans* chain. Thus, the increase in intensity in the order all-*E* < 7*Z* < 9*Z* < 13*Z* is explained.

iii) The normal mode which is responsible for the 1274 cm^{-1} line takes place at the *cis* bend of the 7*Z* configuration.

iv) The normal mode which is responsible for the 1245 cm^{-1} line takes place at the *cis* bend of the 15*Z* configuration. The calculated normal modes support the idea that these key Raman lines are relevant to a variety of carotenoids that have the same type of conjugated backbone.

E. Applications of Resonance Raman Spectroscopy in the Carotenoid Field

Resonance Raman spectroscopy can provide valuable information about geometrical configuration. The ability to obtain specific resonance Raman spectroscopic information about a carotenoid molecule when this is located in a pigment-protein complex or other structural matrix has also been described. The technique has been used to investigate the geometrical configuration of carotenoid molecules in the photosynthetic reaction centre of phototrophic bacteria, and to probe membrane potentials and carotenoid-protein interactions. Such applications [13, 14] are particularly relevant to studies of the functions and actions of carotenoids *in vivo*. Time-resolved (transient) resonance Raman spectroscopy, which has not been dealt with in this Chapter, provides useful information on the structures of carotenoids in the exited states [15].

References

[1] J. Loader, *Basic Laser Raman Spectroscopy*, Heyden, London (1970).
[2] T. R. Gilson and P. J. Hendra, *Laser Raman Spectroscopy*, Wiley, London (1970).
[3] H. A. Szymanski (ed.), *Raman Spectroscopy: Theory and Practice, Vol. 1 and 2*, Plenum Press, New York (1967 and 1970).
[4] D. A. Long, *Raman Spectroscopy*, McGraw-Hill, New York (1977).
[5] P. R. Carey, *Biochemical Applications of Raman and Resonance Raman Spectroscopies*, Academic Press, New York (1982).
[6] A. T. Tu, *Raman Spectroscopy in Biology: Principles and Applications*, Wiley, New York (1982).
[7] F. Inagaki, M. Tasumi and T. Miyazawa, *J. Mol. Spectrosc.*, **50**, 286 (1974).
[8] J. Tang and A. C. Albrecht, in *Raman Spectroscopy: Theory and Practice*, (ed. H. A. Szymanski), Vol. 2, p. 33 (1970).
[9] K. Okada, E. Nishizawa, Y. Fujimoto, Y. Koyama, S. Muraishi and Y. Ozaki, *Appl. Spectrosc.*, **46**, 518 (1992).
[10] H. Hashimoto and Y. Koyama, *Photochem. Photobiol.*, **54**, 67 (1991).
[11] Y. Koyama, T. Takii, K. Saiki and K. Tsukida, *Photobiochem. Photobiophys.*, **5**, 139 (1983).
[12] Y. Koyama, I. Takatsuka, M. Nakata and M. Tasumi, *J. Raman Spectrosc.*, **19**, 37 (1988).
[13] Y. Koyama, *J. Photochem. Photobiol. B: Biol.*, **9**, 265 (1991).
[14] Y. Koyama and H. Hashimoto, in *Carotenoids in Photosynthesis* (ed. A. Young and G. Britton), p. 327, Chapman and Hall, London (1993).
[15] Y. Koyama and Y. Mukai, in *Advances in Spectroscopy, Vol. 21: Biomolecular Spectroscopy Part B* (ed. R. J. H. Clark and R. E. Hester) p. 49, Wiley, Chichester (1993).

Carotenoids
Volume 1 B: Spectroscopy
© 1995 Birkhäuser Verlag Basel

Chapter 6
NMR Spectroscopy

Gerhard Englert

A. Introduction

In the past decade, nuclear magnetic resonance (NMR) spectroscopy has become an even more efficient spectroscopic tool for the identification and structure elucidation of carotenoids. Its increasing importance mainly results from the following factors. First, modern NMR instrumentation, with superconducting magnets of high and very high magnetic field strength corresponding to measuring frequencies of up to 750 MHz, is now available in many laboratories. This increase in the frequency has caused a dramatic increase of the dispersion of chemical shifts, a fact which greatly simplifies the interpretation of the ^{1}H-NMR spectra and hence increases the amount of structural information that can be deduced from the spectra. Moreover, the increase of the measuring frequency was accompanied by a significant improvement in the sensitivity and this alleviated, at least in part, a previous limitation of NMR. A further important reason is the general availability of modern one-dimensional and two-dimensional (1D and 2D) pulse techniques which can now readily be applied in a routine way even by non-experts. As will be seen, the application of these techniques to the elucidation of carotenoid structures is of great benefit and can significantly facilitate the analysis of the partially crowded NMR spectra.

This Chapter is not an overview of the extended literature on the applications of NMR to the elucidation of carotenoid structures. Instead, it is an attempt to characterize the merits and limitations of NMR spectroscopy in this field by selecting a number of practical applications and demonstrations which are solely taken from the work of the author. The same selection principle applies to the comprehensive chemical shift data for ^{1}H-NMR and ^{13}C-NMR that are presented here. These have been accumulated in the author's laboratories over the past twenty years and have only been published in part in previous articles [1-5].

In Section B some relevant instrumental aspects and practical points such as sample requirements will be treated. In this context, the advantage of the pulsed Fourier technique will be discussed briefly and recent progress and present limitations of the technique will be summarized by selecting some examples of ^{1}H-, ^{13}C- and ^{17}O-NMR. Moreover, the meaning

and importance of two NMR parameters, namely the spin-lattice and the spin-spin relaxation times T_1 and T_2 will be emphasized. In Section C a compilation of ^1H and ^{13}C chemical shifts of end groups will be given which will assist in the identification by NMR of known or unknown carotenoids. Section D will give a survey on proton and carbon-13 chemical shifts of selected carotenoids. In addition, some basic features of the NMR spectra of carotenoids will be treated, to provide a first step in the interpretation. In Section E the elucidation of the structure of geometrical isomers of carotenoids by ^1H- and ^{13}C-NMR will be discussed. Section F will outline the general procedure for assigning ^1H and ^{13}C spectra in more complex cases by use of modern 1D and 2D pulse techniques. Since this article addresses the practitioner in the field of carotenoids rather than the NMR specialist, only very limited explanations of these methods are provided. For a deeper understanding of the physical and experimental background, the reader is referred to the pertinent literature [6-9]. This Chapter, particularly Sections C to F, is strongly based on a series of previous publications on the same subject [1-5].

B. Experimental Aspects

1. Measuring frequency

Major progress in NMR during the past decade results from the increase of the measuring frequency and this fact had a particularly important impact on ^1H-NMR. Since the chemical shift difference $\Delta\upsilon$, measured in Hz, between the signals of differently shielded protons, increases proportionally to the measuring frequency, whereas the splittings of the signals caused by mutual spin-spin couplings J (in Hz) are independent of the measuring frequency, the individual multiplets are increasingly separated at higher frequencies. Under this condition ($\Delta\upsilon \gg J$; so-called weak coupling case) the multiplets can easily be identified and chemical shifts and coupling constants are accessible by so-called first-order interpretation, *i.e.* they can be taken with reasonable accuracy direct from the observed positions and splittings of the multiplets.

In the early 1960s only instruments of up to 100 MHz were available. Since the olefinic region between *ca.* 5.5 and 6.5 ppm in the proton spectra of carotenoids is often very crowded, this part of the spectrum did not reveal much relevant information at that time, except a rough estimate of the number of protons contributing to the mostly unresolved jumble of signals. A few olefinic protons were found at the edge of or even outside this region, namely those of isolated double bonds, protons near the end of the conjugated chain, or protons close to functional groups with oxygen or with strong diamagnetic anisotropy, such as triple bonds, carbonyl groups, carboxy groups or phenyl rings. In the high-field part of the spectrum, on the other hand, only a few sharp methyl signals, in general, could be recognized and assigned to help in the identification of the different end groups.

This unfavourable situation changed in the mid 1960s when the first commercial high-field instrument with superconducting magnet operating at 220 MHz became available. During the following years such an instrument was used successfully for the study of numerous ^1H-NMR

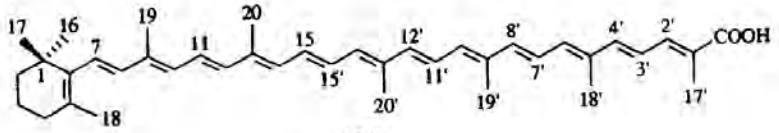
spectra of carotenoids [1, 2]. Even the olefinic part of these spectra now became partly accessible to detailed interpretation.

The advantage of using high-field ^{1}H-NMR spectroscopy is demonstrated in Fig. 1. As an example, the olefinic region of the ^{1}H-NMR spectrum of torularhodin (**428**) measured at 250, 400 and 600 MHz is shown. In all three partial spectra a weak resolution enhancement was applied by multiplication of the FIDs with a Lorentz-to-Gauss window prior to Fourier transformation [7]. For convenience, all the spectra were plotted with the same scale in ppm.cm^{-1}. This means that, in these spectra, the signals of the different protons are centred at the same position on the δ-scale but their apparent splittings and hence their overlapping are reduced in the ratio 250:400:600.

Since torularhodin is poorly soluble in $CDCl_3$ the strongest signal in this region at 7.26 ppm is attributed to the undeuteriated solvent molecules (here < 0.07%). On either side of this signal a weak satellite is found. This pair of signals is caused by the ^{13}C isotopomer occurring in a natural abundance of *ca.* 1%. The doublet splitting is due to the one-bond spin coupling $^1J_{CH}$ of 209 Hz between ^{1}H and ^{13}C. At low concentrations, the intensity of these satellites can often serve as a crude internal standard for estimation of the concentration of the solution, if standard experimental conditions are applied. In the 600 MHz spectrum some additional satellites are seen, caused by field modulation due to the spinning of the sample.

A comparison of the three spectra reveals that, in the 600 MHz spectrum, several individual doublets, and doublets of doublets, are clearly visible. These splittings are caused by the vicinal $J_{H,H}$ couplings of *ca.* 11 and 15 Hz, expected between protons separated by single and double bonds, respectively. Whereas the same observation is still partly valid for the 400 MHz spectrum, the spectrum at 250 MHz is much more complicated. At this frequency, the reduction of the chemical shift differences with respect to the J couplings ($\Delta\upsilon < \sim J$; so-called strong coupling case) resulted in a severe overlap of the individual multiplets and in deviations from simple first-order appearance with strongly distorted signal intensities and complex frequency distributions in the individual multiplets. Although even the 600 MHz spectrum might appear rather complicated, it will be shown in Section F.1.e. for a similar level of complexity (citranaxanthin, **466**) that, with some basic knowledge of the spin couplings, the predicted range of the chemical shifts of the different olefinic protons, the expected appearance of their multiplet patterns, and, most importantly, with the aid of modern 1D and 2D NMR techniques, a complete and reliable assignment of all the protons is clearly feasible.

As a first demonstration, the assignment of 12 out of 18 olefinic multiplets in the spectrum of torularhodin (**428**) is presented in Fig. 1. To avoid overcrowding, the splitting patterns of the remaining six protons [H(11), H(15), H(15'), H(11'), H(7'), and H(4')], which absorb around 6.65 ppm, have not been inserted in Fig. 1 although even these assignments were possible by application of 2D COSY at 400 MHz and by comparison with related compounds. A starting point in this task was the assumption that H(2') can be assigned unambiguously at 7.382 ppm because of its extra downfield shift caused by its β position to the carboxy group, as will be discussed in Section D.1. All other connectivities of the protons of the olefinic chain, and hence their chemical shifts, were eventually obtained from cross peaks in the 2D spectrum. The full set of chemical shifts for torularhodin is reported in Table 3.



428

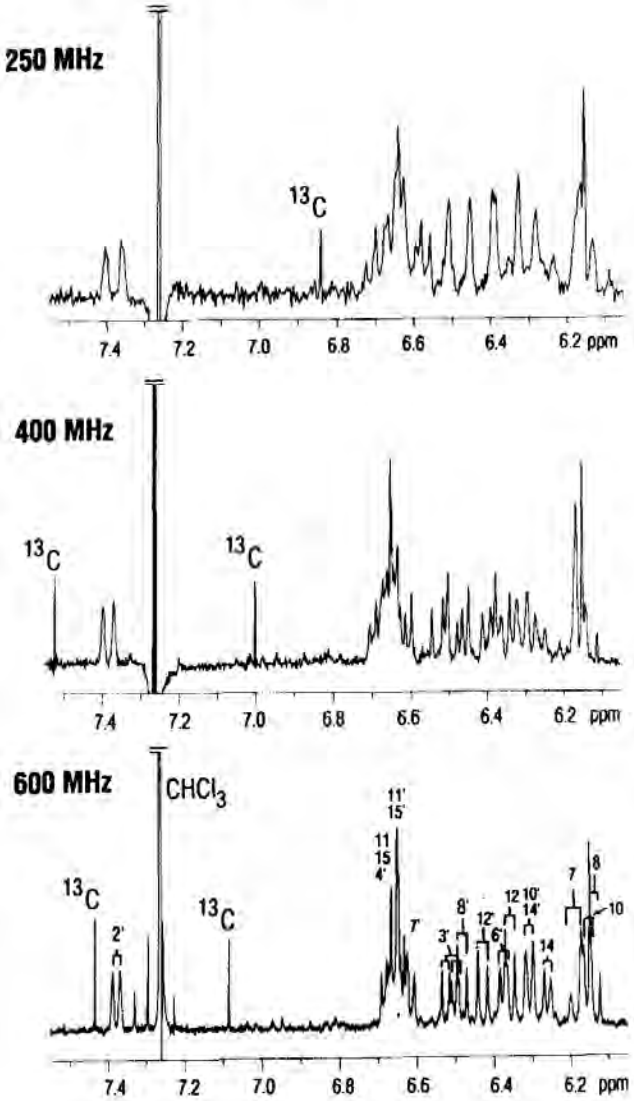


Fig. 1. Olefinic section of the ^{1}H-NMR spectrum of torularhodin (**428**; <0.8 mg in 0.6 ml $CDCl_3$) measured at 250 MHz (top), 400 MHz (centre) and 600 MHz (bottom; courtesy of Spectrospin AG). A Lorentz-to-Gauss resolution enhancement window was applied (LB = -1, GB = 0.1) to all FIDs. Between 100 and 200 scans were acquired using a flip angle of *ca.* 65°. The two satellites of the ^{13}C isotopomer of the solvent are designated by ^{13}C (see text).

2. Sensitivity

a) Pulsed Fourier-transform (FT) spectroscopy

The advent of FT NMR spectroscopy in the early 1970s, and the increasing measuring frequencies, have strongly improved the sensitivity. An additional contributing factor has been the continuous improvement of instrumentation, particularly of the probe heads.

In a pulsed acquisition experiment, a short radiofrequency (rf) pulse (~10 μs) is applied to the nuclear spin system and rotates the equilibrium magnetization by the so-called flip angle away from the z direction along the external magnetic field, resulting in a magnetization component in the perpendicular x,y plane [6, 7]. This transverse magnetization consists of a superposition of the different nuclear magnetization components precessing around the z axis according to their individual precession frequencies. During this process the transverse magnetization slowly decays exponentially by relaxation processes with a time constant called spin-spin or transverse relaxation time, T_2, of the order of one second (see Section B.2.f). The precession of the tranverse magnetization induces in the receiver coil a time-dependent signal which is called free induction decay (FID). This signal is amplified and transferred to the audiofrequency range by the rf electronics of the spectrometer and is finally digitized and stored in the memory of the computer. For this purpose, normally 16K to 32K points or addresses of the computer memory are used. The time during which the FID is measured is called acquisition time t_2. The whole process of pulsing and acquisition is then repeated until a satisfactory signal-to-noise ratio has been achieved. The FID accumulated in the computer is then multiplied with a suitable weighting or window function [6, 7], which may improve the signal-to-noise ratio at the expense of an increase in line-width or, conversely, may improve the resolution at the expense of the signal-to-noise ratio, depending on the choice of the window function. The altered FID is then subjected to a Fourier transformation which typically takes only a few seconds. This converts the time response into a spectrum consisting of the signal intensities as a function of the frequency. The gain in sensitivity of FT spectroscopy compared to previous continuous wave (CW) spectroscopy is due to the fact that all the frequencies of the spin system are excited simultaneously by the rf pulse instead of being excited one after another by slowly varying the irradiation frequency over the full range of chemical shifts. A single FID is hence accumulated in FT spectroscopy in only about 1 s in ^{13}C-NMR and about 2 to 4 s in ^{1}H-NMR, whereas a single scan in CW operation may last several minutes. Therefore, the repetitive accumulation of many FIDs of a typical carotenoid, available in mg quantity, takes only a few minutes. The signal-to-noise ratio increases with the square root of the number of accumulations. Thus, in order to compensate for a reduction in sample quantity by a factor of 100, an increase of the total measuring time by a factor of 100^2 is needed to obtain a spectrum of similar quality. Despite the increase in sensitivity during the past decade, acquisition of the spectrum of a very small sample still requires that a costly instrument can be blocked for a significant time. However, this may be justified in important cases, if larger sample quantities cannot be readily isolated or if the isolation procedure is also time-consuming and hence very costly.

b) ^{1}H-NMR

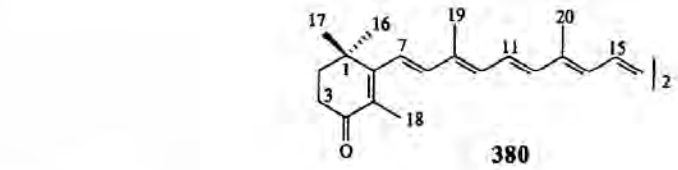
About ten years ago it was demonstrated that the acquisition of ^{1}H-NMR spectra of carotenoids is feasible with sample quantities as low as around 1 μg [3]. Thus, 400 MHz spectra of canthaxanthin (**380**) and lactucaxanthin (**150**) were published from 0.25 and 1.5 μg of sample, respectively. The former spectrum, corresponding to 4.4 x 10^{-10} moles or 3.4 μ*M* concentration, was acquired at that time in about 116 hours, the latter spectrum, with 22 μ*M* concentration, was run in 13 hours total accumulation time. The following practical example will demonstrate that long acquisition times may indeed be justified in important cases if an unknown carotenoid has to be identified unambiguously.

It was found that patients who have been treated by preparations containing carotenoids may suffer from tiny deposits of coloured crystals in the entire retina of the eye [10]. A sample quantity of only a few μg, extracted at autopsy from retinal tissue, was made available for physico-chemical investigation. In a first step the main component of the mixture of carotenoids was isolated by HPLC and then subjected to ^{1}H-NMR investigation. After about one hour of accumulation the first spectrum was inspected. Although the signal-to-noise ratio was still rather poor it became evident that the compound must be canthaxanthin (**380**), one of the components of the preparation that had been administered. The spectrum that was obtained after about 5 hours of accumulation is shown in Fig. 2. The structure was proved unambiguously by comparison with an authentic spectrum. The solution was then investigated by UV/Vis spectrometry and the sample quantity was determined to be 1.4 μg.

In this extremely low concentration range, the handling of the NMR solution and the purity of sample and solvent pose some severe problems. In order to minimize the residual proton signal of the solvent, so-called 100%-deuterium quality solvent should be used despite its higher price. It contains less than 0.07% or, in the best quality available now, less than 0.04% residual protons. Moreover, reduction of the sample volume from about 0.5 ml to 0.12 ml is recommended, although the use of corresponding microcells may introduce some difficulties when the field homogeneity is being optimized.

When very small sample quantities are being investigated, impurity peaks that mainly occur in the high-field range of the spectrum are particularly disturbing. These impurities often accumulate when the excess solvent used during the isolation procedure is evaporated. One of these signals, albeit with relatively low intensity, is seen in Fig. 2 near 1.25 ppm. It is caused by the presence of multiple $(CH_2)_n$ groups in contaminating lipids.

A further problem originates from the unavoidable presence of traces of water which gives rise to a signal near 1.55 ppm even if the solvent is stored under dry conditions with added molecular sieve (0.4 nm, beads of about 2 mm size) and the NMR solution has been prepared under dry conditions. As a rule of thumb, rigorous sample preparation should ensure that the water signal is distinctly smaller than the remaining solvent peak. Even when this is achieved, the undesired signal may hide a sharp signal of a methyl group, and thus seriously influence a structure elucidation. Since the position of the water signal is strongly dependent on temperature (and concentration) it can readily be shifted upfield or downfield by increasing or decreasing the sample temperature by a few degrees, so that any hidden signal can be revealed.



380

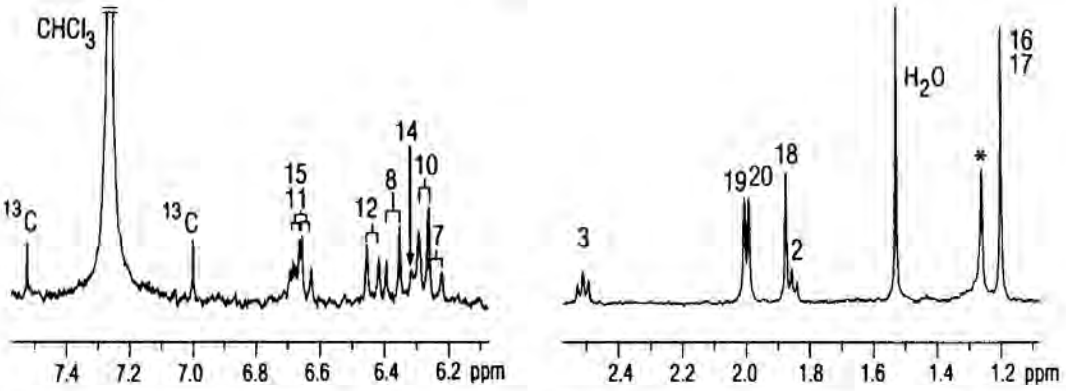


Fig. 2. Olefinic sections (left) and aliphatic sections (right) of the 400 MHz ^{1}H-NMR spectrum of 1.4 µg of canthaxanthin (**380**), dissolved in 0.13 ml of $CDCl_3$ (100% D quality, <0.07% H). Total acquisition time 5 hours, flip angle 65°. The intensity of the left trace was increased by a factor of 3 relative to the right trace. An impurity is marked by an asterisk.

When very small sample quantities are being studied, a further critical point can be the presence of traces of acid which may reduce the chemical stability of carotenoids. Moreover, this can enhance the exchange rate of exchangeable protons so that OH protons may be effectively decoupled from their spin-coupled neighbours. In severe cases it may happen that their signals completely disappear by broadening or by coalescence with the strong water signal. This can often be suppressed by filtering the solvent through a thin layer of alumina before use. Finally it should be mentioned that OH signals are very sensitive to saturation effects due to their long relaxation time T_1 (see Section B.2.e) and this may reduce their measured integrals. A final problem to be mentioned here is that the stability of very small samples is often seriously affected by the presence of dissolved oxygen in the solvent; this can easily be removed, however, by bubbling argon gas through the solution for a few minutes.

c) ^{13}C-NMR

Since the ^{13}C nucleus has a smaller gyromagnetic ratio than the proton by a factor of 4, and since its natural abundance is only 1.1%, the sensitivity of ^{13}C-NMR is significantly lower. In practice, it is reduced by roughly a factor of 500 compared to ^{1}H-NMR. This means that for a

good proton-decoupled ^{13}C spectrum of a typical carotenoid, at least about 0.5 mg of sample should be available, whenever possible. Even then, long accumulation times of about 24 hours are necessary to obtain a spectrum of reasonable quality. Some spectra from even smaller quantities have been presented elsewhere [3, 5] and a further example will be discussed below.

A further reason for the lower sensitivity of ^{13}C is that, in a given molecule, some of the ^{13}C nuclei may have no spatially close protons. This leads to an increase in the spin-lattice or longitudinal relaxation time, T_1 [6, 7]. This characteristic time constant, which can range between 0.2 s and several seconds (see Section B.2.e) for the different carbons of a carotenoid, is a measure of the time the spin system needs for the equilibrium population of the NMR energy levels to be largely restored after distortion by irradiation. This restoration by T_1 relaxation is mainly caused by rapidly fluctuating magnetic fields of spatially close magnetic nuclei (in this case protons and carbon-13) owing to the rapid molecular tumbling of the molecules in the liquid. More precisely, it mainly depends on the existence of molecular rotations at frequencies near the measuring frequency. Therefore, T_1 is not only dependent on the measuring frequency, but also on the molecular size and the viscosity of the solvent.

A long T_1 means that the corresponding nucleus is very sensitive to effects of saturation by repetitive pulsing during acquisition. Hence the signal intensity for this carbon-13 is reduced compared to those of other ^{13}C nuclei with faster relaxation. As a result, the ^{13}C signals in a typical spectrum often have strongly varying intensities at practical repetition rates. This reduction in signal intensity is particularly large in the case of unprotonated quaternary carbons such as carbonyls, the central carbon of allenic groups and others. When small sample quantities are being measured by using relatively fast repetition rates, the signals of slowly relaxing nuclei may become too weak to be detected, *i.e.* they disappear in the background noise. In such cases it is advisable to reduce the flip angle from the usual maximum of about 40° to about 30° by reduction of the duration of the applied rf pulse. This reduces the saturation effects, but also reduces the intensity of all the signals of nuclei with faster relaxation.

A second, though less favourable, possibility is to decrease the repetition rate of the pulses by inserting an extra relaxation delay into the acquisition sequence. This also will work only at the expense of the signal-to-noise ratio of the nuclei with shorter T_1 since the number of accumulations in a given time is correspondingly reduced. It should be mentioned in this context that in ^1H-NMR of carotenoids T_1 is mostly between 0.5 and 1.5 s (see B.2.e). Saturation effects here play a minor role since the time between subsequent pulses is always necessarily longer (3 to 4 s) than in ^{13}C-NMR (*ca.* 1 s) owing to the smaller frequency width of the ^1H-NMR spectral range and the increased digital resolution. Therefore, when extremely small sample quantities are dealt with, optimum pulses with up to 90° flip angle are feasible in ^1H-NMR compared to only 40° in ^{13}C-NMR.

As an example of the sensitivity that is currently achievable and the influence of the spin-lattice relaxation time on the variation of the intensity of the different carbon signals, the proton-decoupled 100 MHz ^{13}C-NMR spectrum of *ca.* 0.2 mg of the heptaacetate of the glycosidic carotenoid P457 (13'-*cis*-7',8'-dihydroneoxanthin-20'-al 3'-β-lactoside (**280.1**), see [5]), dissolved in 0.3 ml $CDCl_3$, is shown in Fig. 3. This quantity was estimated by UV/Vis spectrometry with an assumed $A^{1\%}_{1cm}$ value of 2500 [5]. The spectrum was acquired with a 40° observation pulse and a repetition time of 0.75 s between pulses.

The spectrum shows a huge solvent peak near 77 ppm (actually a 1:1:1 triplet due to coupling between the carbon and the deuterium nucleus with spin I = 1). Due to the favourable fact that, in this case, the relaxation time of the unprotonated carbon of the solvent is relatively long, its signal intensity is only about 100 times stronger (due to its partial saturation) than those of the average signal of the carotenoid. It can be further reduced, where necessary, by using ^{13}C-depleted chloroform as the solvent.

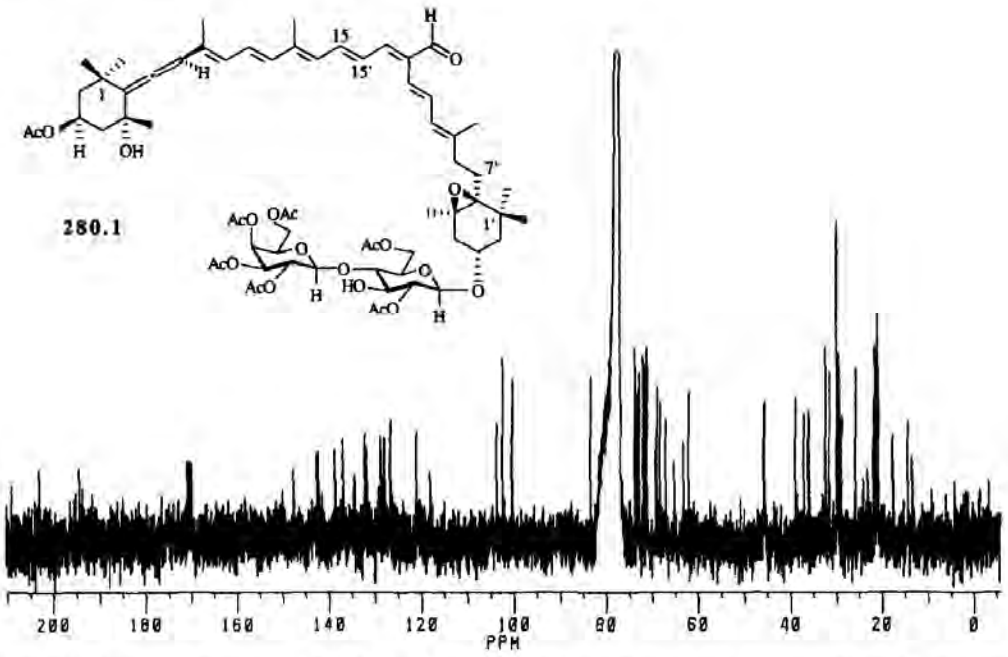


Fig. 3. 100 MHz proton-decoupled ^{13}C-NMR spectrum of *ca.* 0.2 mg of the heptaacetate of the glycosidic carotenoid P457 (**280.1**) dissolved in 0.3 ml of $CDCl_3$ [5]. A flip angle of 40° was used and the pulse repetition time was 0.75 s. Total acquisition time 88 hours.

The strong variation of the signal intensities of the different carbons in this representative example is clearly evident. Despite the extremely long acquisition time of 88 hours that was sacrificed to record the spectrum shown in Fig. 3, not all the expected signals were detected, *i.e.* the signal-to-noise ratio of some was actually too low. An example is the central carbon of the allenic group which is expected to absorb near 200 ppm (see Table 2). In this context it is interesting to note that a proton-detected 2D $^{1}H,^{13}C$-COSY of very good quality was obtained in a shorter time than this 1D ^{13}C spectrum [5]. By this indirect detection technique most of the signals could be assigned and even those ^{13}C signals which were unclear in the 1D spectrum were located from corresponding cross peaks in the 2D spectrum. Thus, partial information on ^{13}C chemical shifts can be obtained indirectly with significantly higher sensitivity by proton detection of the ^{13}C magnetization of ^{13}C isotopomers, as will be shown in Section F.2.d.

This technique is, however, limited to the detection of the signals of those carbons which are coupled to a proton *via* one-bond or multiple-bond coupling. For the former, the present lower limit under these experimental conditions is around 50 to 100 µg of sample, and for the latter about 300 µg. Corresponding spectra were presented recently [5]. These figures refer to a 400 MHz Bruker AM-400 instrument and may be improved by a factor of approximately 2 if an instrument operating at 600 MHz is available.

d) ^{17}O-NMR

Besides hydrogen and carbon-13, many carotenoids contain oxygen-17 as a further magnetic nucleus which is, in principle, accessible by NMR [11]. However, detection of its NMR signal is strongly hampered by two unfortunate properties. First, oxygen-17 has a very low natural abundance of only 0.037%. Second, it has a nuclear quadrupole moment which, together with strong electric-field gradients in covalent bonds, leads to a severe broadening of the signals, and this broadening increases with the molecular mass. In practice, the sensitivity of ^{17}O-NMR is a factor of 10^3 to 10^4 lower than that of ^{13}C-NMR.

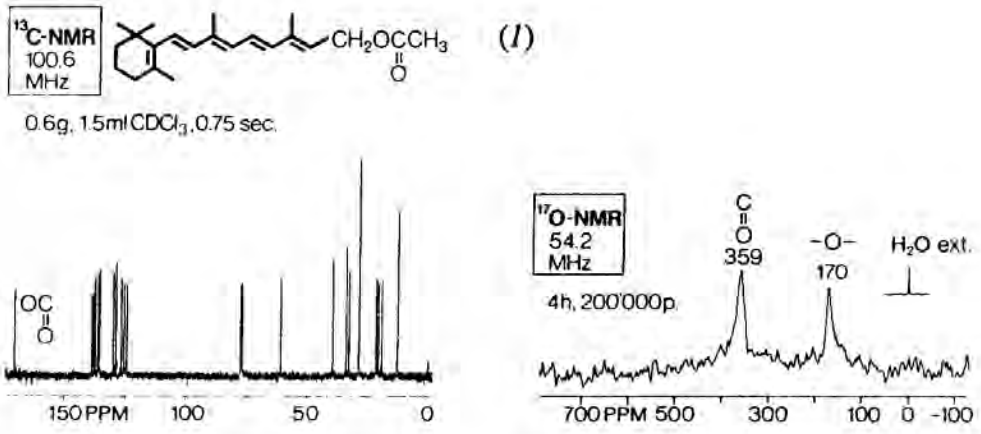


Fig. 4. 100.6 MHz ^{13}C-NMR (left) and 54.2 MHz ^{17}O-NMR (right) spectra of 0.6 g vitamin A acetate (*1*) dissolved in 1.5 ml $CDCl_3$. The left spectrum was obtained by a one pulse experiment, the right spectrum by accumulation of 200000 FIDs. Taken from [3] with permission.

The ^{17}O-NMR spectra of some small reference compounds, some vitamins A and canthaxanthin (**380**) have been studied previously [3]. From this work is presented in Fig. 4, as an example of the reduction in sensitivity, the ^{13}C-NMR and the ^{17}O-NMR spectra of 0.6 g vitamin A acetate (*1*) dissolved in 1.5 ml $CDCl_3$. The same tunable 10 mm probe head was used for both measurements. Whereas the ^{13}C spectrum of this extremely concentrated sample was obtained by a one-pulse experiment, the ^{17}O spectrum required the accumulation of 200 000 FIDs in 4 hours. The line-widths are around 1 KHz. Due to the very short relaxation times T_1 and T_2 the repetition time could be chosen as low as *ca.* 70 ms without the danger of

saturating the signals even though a 90° pulse was applied. As an external reference the signal of water was used (see narrow line in the insert of Fig. 4).

Although the different types of oxygen function can be well distinguished [3, 10] due to the wide chemical-shift range of about 1000 ppm compared to about 250 ppm in ^{13}C-NMR, the increasing line-width of several KHz with compounds of medium or higher molecular masses and the high concentrations needed will certainly strongly hamper routine application of this technique to the elucidation of carotenoid structures.

e) Spin-lattice relaxation time T_1

The spin-lattice relaxation time T_1 at different positions of a molecule is an important parameter in NMR, and contains relevant information on the dynamics of the molecular motion. From a more practical point of view, the expected range of the T_1 values in typical carotenoids should be known approximately in order that optimum experimental conditions can be chosen such as flip-angle, repetition rate and relaxation delays in all types of NMR experiments. The quality of practically all experiments depends critically on the extent to which the equilibrium state is restored before the next scan is started. In all experiments that use 90° and/or 180° pulses (COSY, TOCSY, ROESY, DEPT, *etc.*), the total time allowed for relaxation (relaxation delay plus acquisition time t_2) should be at least $2T_1$ for a quick experiment and about $4T_1$ for a clean experiment without intensity distortions and signal artifacts. These two cases correspond to *ca.* 87% and 98% approach to the equilibrium magnetization, respectively.

Values of T_1 can readily be obtained by a saturation experiment which measures the rate of reappearance of the signals after complete saturation. Another possibility is to exchange the greater population of the lower energy level with the lower population of the upper energy level of the spin system by a so-called 180° pulse. This inverts the magnetization from its equilibrium orientation parallel to the magnetic field (longitudinal z magnetization) to the opposite –z direction. Subsequently the re-approach to the equilibrium population by these relaxation processes is measured as a function of time by a following 90° observation pulse (inversion recovery technique, [6]). From the normally exponential approach of the intensities of the different signals as a function of time towards their equilibrium value, observed after a long delay, T_1 can be calculated by an exponential fit to the measured intensities as a function of time.

i) ^{13}C-NMR. In Fig. 5 are presented ^{13}C-NMR T_1 values for some symmetrical C_{40} carotenoids measured at 22 and 68 MHz by the inversion recovery technique. Relatively high concentrations (*ca.* 100 mg in 0.5 ml) were used in order to reduce the time needed for the measurements. The accuracy of these values, which is estimated to be better than 20% at 68 MHz and better than 30% at 22 MHz, is thought to be sufficient for this qualitative discussion.

It is seen that the values for protonated olefinic carbons are fortunately rather short, in the range 0.2 to 0.4 s, and virtually independent of the measuring frequency. Very similar T_1 values are, therefore, expected at 100 MHz or above. The fact that the T_1 is not increasing with frequency is explained by the assumption that the decreasing dipolar relaxation is compensated by the increasing contribution of the anisotropy of the chemical shift of these carbons at higher

frequency. Since the T_1 values for protonated carbons are so short, an observation pulse up to 90° would give maximum sensitivity, in principle, at the usual repetition time of *ca.* 1 s. This is clearly prohibited, however, by the observation that relatively long T_1 values of several seconds were found for unprotonated carbons, in agreement with expectation, due to the absence of nearby protons. Here, some of the values are significantly shorter at 68 MHz than at 22 MHz, and this can be explained in the same way as before, since the dipolar contribution is expected to be very weak. At still higher frequencies of 100 MHz or above, a further reduction in T_1 of these unprotonated carbons can be expected and this also contributes to the improved sensitivity at higher frequencies.

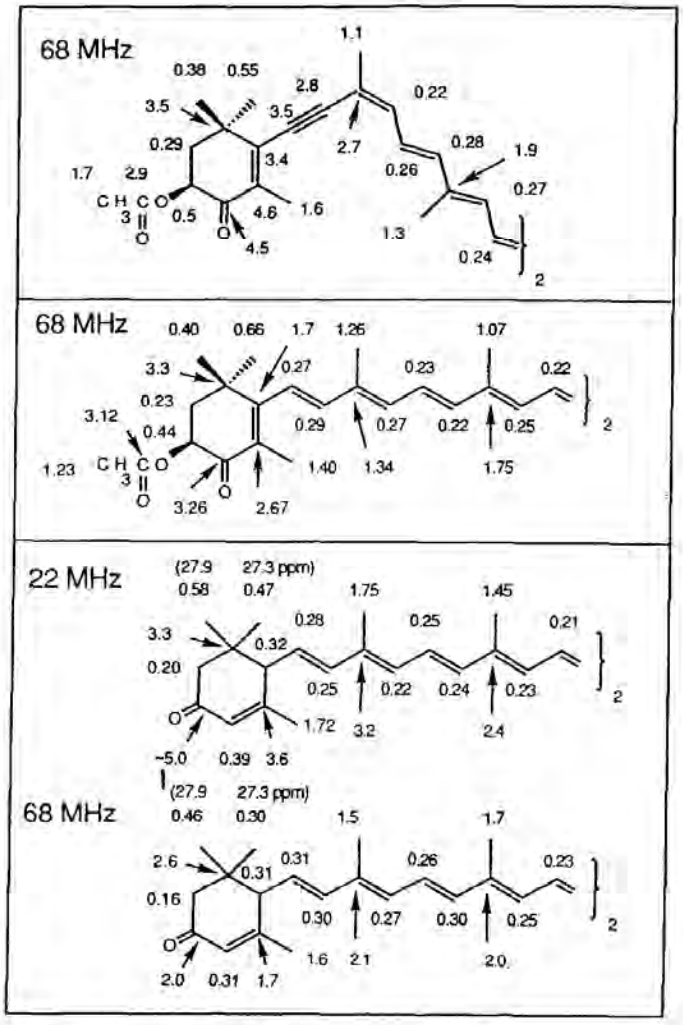


Fig. 5. ^{13}C-NMR spin-lattice relaxation time T_1 in s for the different carbons of some carotenoids measured by inversion recovery at 22 MHz and 68 MHz. The temperature was 39°C for the former and about 25°C for the latter frequency. Relatively high concentrations of *ca.* 100 mg in 0.6 ml $CDCl_3$ were used.

Methyl groups possess relevant additional mobility by internal rotation and their T_1 values vary according to their position and orientation in the molecule. In general, it is found that the axially oriented methyl carbons of end groups have longer T_1 than the equatorial ones. This allows speculative assignment of the two methyl groups of the last compound in Fig. 5. No significant dependence of T_1 of methyl carbons on the measuring frequency is observed.

This general discussion on some typical ^{13}C-NMR T_1 values of carotenoids indicates that the individual relaxation times vary considerably for the different sites in a molecule. Therefore, the optimum experimental conditions that are selected can, in most cases, only be a compromise.

ii) ^{1}H-NMR. In this context it is useful to show for comparison a few selected ^{1}H-NMR spin-lattice relaxation times T_1 of some carotenoids measured in the same way as before by inversion recovery. As shown in Fig. 6 these values, all measured at 400 MHz, are in part significantly longer than in ^{13}C-NMR. Thus values between 0.5 and 1.5 s were observed, in general. Longer values of up to several seconds may be expected only in very rare cases such as for protons with no close neighbours and/or with high mobility. Examples are OH protons which have T_1 values around 5 s. It is concluded that in ^{1}H-NMR of small samples and with typical repetition times of pulsing (3 to 4 s) an observation pulse of up to nearly 90° might be acceptable in critical cases without the danger of significantly saturating most of the signals.

The fact that for carotenoids most T_1 are significantly longer in ^{1}H-NMR than in ^{13}C-NMR must be specifically stressed here since in the literature the opposite statement is frequently repeated [9]. This has some practical consequences when relaxation delays are to be selected for the different multi-pulse experiments that involve protons and carbon-13. Finally, in this context, in heteronuclear experiments, the ^{1}H-NMR T_1 values of the ^{13}C isotopomers are active and not those of the ^{12}C isotopomers given in Fig.6. These values are not known, in general. It can be predicted, however, that the additional magnetic interaction of proton and carbon-13 results in a significant reduction of the corresponding T_1 by a factor of up to about three and this is very advantageous in view of a possible fast repetition of the scans in these experiments.

f) Spin-spin relaxation time T_2

It has already been mentioned briefly that a further relaxation time, called spin-spin or transverse relaxation time, T_2, also plays an important role in NMR. This is a measure of the lifetime of the transverse magnetization in the x,y-plane perpendicular to the external magnetic field. It causes the FID, which is a superimposition of the different frequencies of the differently shielded nuclei, to decay exponentially with time constants T_2. Since this transverse magnetization is detected in the NMR experiment, the value of T_2 determines the natural line width of the measured signals, *i.e.* without taking into account a further possible source of broadening, namely the inhomogeneity of the external magnetic field. A long T_2 with slowly decaying FID corresponds to a narrow line and *vice versa*. Therefore, multiplication of the experimental FID with a weighting or window function can artificially enhance or reduce the

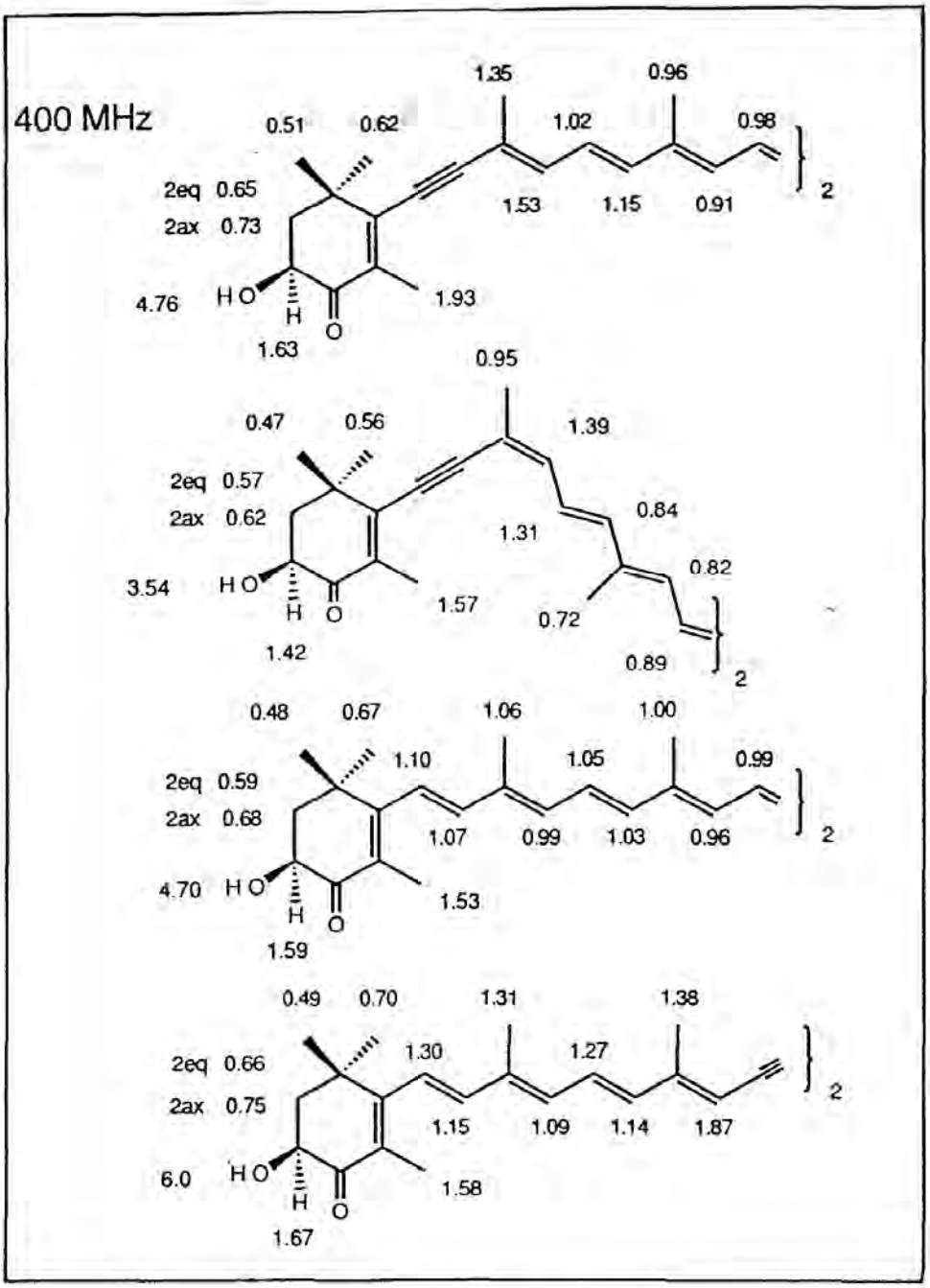


Fig. 6. ^{1}H-NMR spin-lattice relaxation time T_1 in s for some carotenoids measured by inversion recovery at 400 MHz and at about 25°C. Concentrations between 1.5 mg and 6 mg in 0.5 ml $CDCl_3$ were used. The samples were degassed by bubbling argon through the solutions for about 10 minutes.

line widths in the transformed spectrum, depending on the chosen type of window. This procedure is called digital filtering.

In contrast to T_1, T_2 relaxation is essentially determined by fluctuating dipolar interactions between close neighbours in the low-frequency range near zero. This has an important influence on NOE experiments as will be seen in Section F.1.c. It can be expected that, in the mass range of typical carotenoids, $T_2 \sim T_1$ in ^{1}H- and ^{13}C-NMR. Since the line width $\Delta\upsilon_{1/2}$ at half height of a Lorentzian-shaped line is given by $1/(\pi T_2)$, the natural half-width of ^{1}H and ^{13}C signals can be roughly estimated from the T_1 values given above. Thus, in ^{13}C-NMR, with T_1 values between 0.3 and 5 s, the natural line width should be in the range 1 to 0.06 Hz. In practice, the latter value cannot be reached in a routine spectrum since the digital resolution is only about 1 Hz per point. However, if good digital resolution and small flip angles are being used, thus avoiding saturation effects, the quaternary carbon signals appear with highest signal intensities (smallest line width) and can again readily be distinguished. This is in contrast to routine spectroscopy where fast repetitive pulsing leads to a reduction of the signal height of unprotonated carbons due to partial saturation.

In ^{1}H-NMR the corresponding line width is expected to be around 0.3 Hz corresponding to T_1 values around 1 s. It has already been pointed out that most of the actual lines are significantly broader because of unresolved long-range couplings.

C. Chemical Shifts of End Groups

1. ^{1}H-NMR

The characterization or identification of an unknown carotenoid usually involves several steps. Compared to UV/Vis, IR, CD and MS, ^{1}H-NMR spectroscopy often provides the most valuable information on the length and the geometry of the conjugated olefinic chain and, more importantly, on the specific type of end groups present. In addition, the purity of the sample can readily be checked. A corollary of this is that the reliability of NMR results is often more strongly dependent on the purity of the sample than is the case with the other techniques.

In the course of the past twenty years a comprehensive collection has been compiled of ^{1}H and ^{13}C chemical shifts of numerous end groups of synthetic and natural carotenoids and retinoids, based almost exclusively on high-field spectra. These data, some of which have been presented previously [2-4], have been partly revised and extended and are now presented in Tables 1 and 2. As previously, the concept of 'end group' is used in a broad sense. Since the chemical shifts of end groups such as β or ε rings *etc.* do depend on the first few neighbouring atoms and, conversely, the shifts of the latter atoms are influenced by the specific type of end group, these end groups, as defined in Tables 1 and 2, include the relevant first part of the attached side chain. It will be shown later that the chemical shifts of the remaining central part of the conjugated chain are, as expected, less strongly dependent on the end group and, therefore, are predictable from the data for only a relatively small number of selected carotenoids which will be presented in Tables 3 and 4.

In Table 1 are collected ^1H chemical shifts of 140 different end groups (and some *cis* isomers). They were all measured and assigned in the author's laboratories with $CDCl_3$ as solvent. In order not to overload the data the values of coupling constants are only quoted in a few relevant cases. Moreover, in most cases they fall within a normal predictable range and hence do not provide such important information as the chemical shifts. The latter are mostly given as average values extracted from the spectra of more than one related compound. This means that these shifts generally behave in a fairly additive manner if perturbing effects of strongly anisotropic neighbouring groups are absent (see Section D).

Practical experience from numerous applications, further substantiated in Section D, shows that, for the same end group in different compounds, these shift values are reliable in most cases within about ± 0.01 ppm for sharp singlet signals, and about ± 0.02 ppm for more complicated multiplets. In the olefinic region, the multiplets are often significantly broadened by unresolved spin couplings (see Section F.1.e) and in the aliphatic region they may sometimes be partially obscured by strong methyl signals or even the presence of impurities.

Furthermore, it is found that the chemical shifts of protons (and carbons) are, in general, not very sensitive to change in concentration as long as this is not excessive. Concentration effects, however, played a certain role in previous work when very high concentrations (up to 100 to 200 mg in 0.5 ml solvent, compared to only a few mg normally used for ^1H-NMR) were used to record quickly a ^{13}C spectrum. Particularly in $^1H,^{13}C$-correlated 2D experiments, the possibility of minor relative shift changes should be kept in mind if strongly differing concentrations are used for the acquisition of the spectra.

Much more important is the fact that all the data reported throughout this article were obtained, even in cases of low solubility, in the same solvent, namely $CDCl_3$, since relatively large changes are to be expected when other solvents such as dimethyl sulphoxide or benzene are used.

It was previously shown [3, 4] that the chemical shifts of end groups are, as expected, also dependent on the geometry of the first few neighbouring double bonds. Thus, characteristic shift variations are clearly detectable for 7-*cis* and 9-*cis* isomers and therefore, whenever available, the data for these isomers have been included in Tables 1 and 2. Small effects are sometimes also observed with 11-*cis* and even 13-*cis* isomers. Also included in Tables 1 and 2 are a number of chemically modified end groups, such as methylated and acetylated derivatives. In all these cases the corresponding shift changes upon chemical modification are very characteristic for a given end group and hence can help in its identification.

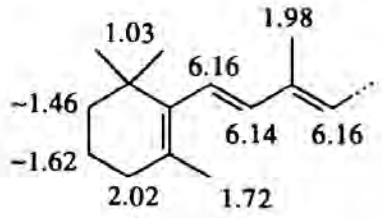
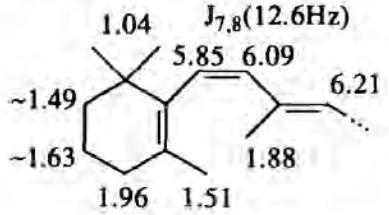
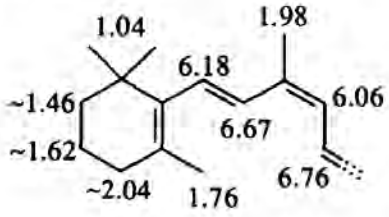
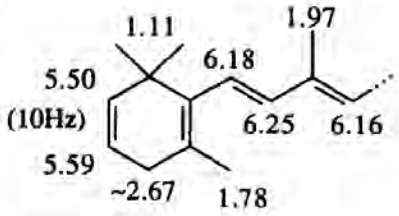
Whenever the absolute configuration of the different end groups is known it is explicitly given in Tables 1 and 2. Other end groups, for which only relative geometries are known, remain in this sense undefined. Since the NMR spectra of enantiomers are strictly identical, this differentiation is in some cases irrelevant here. Whenever possible, however, the equatorial or axial (or α or β) orientation of protons, substituents and methyl groups is specifically enumerated since this gives information on mutual chemical shift effects as well as on the conformation of the end groups. This is particularly true for 6-membered rings where axially oriented protons are readily recognized by their large total splitting. Since spin couplings between axially oriented neighbours have values between 8 and 14 Hz, but those between

equatorially and axially oriented protons only around 4 Hz, the total width of the signals of the two types of protons, given by the sum of all coupling constants, differs strongly.

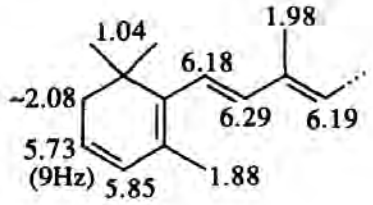
The relative or absolute orientation of protons, methyl groups or substituents and hence their local stereochemical assignment was, therefore, either derived from the spin couplings involved, or from numerous nuclear Overhauser effect experiments (from the author's laboratory, partly unpublished). A representative example, namely the stereochemical assignments by 2D ROESY of the signals of the end group of capsorubin (**413**) diacetate will be discussed in Section F.1.c.

In the context of relative and absolute geometries of end groups the following additional remarks are worthwhile. Although diastereoisomers are normally expected to give different NMR spectra, this is, in practice, not the case if two chiral centres are far apart from each other. Thus, diastereoisomers with the centres located in the two end groups, separated by a typical nonaene system, have not yet been distinguished by ^{1}H- or ^{13}C-NMR [12, 13], although their chromatographic separation can be achieved [13].

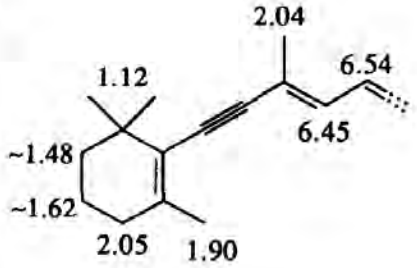
Table 1. Characteristic ^{1}H-NMR data for some end groups of natural and synthetic carotenoids (solvent $CDCl_3$).

e1  	**e1a (7-*cis*)** 
e1b (9-*cis*)  	**e2** 

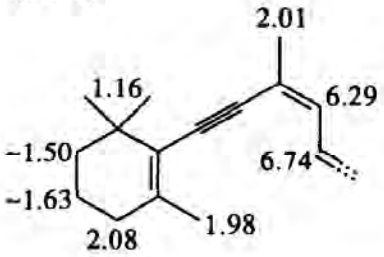
e3



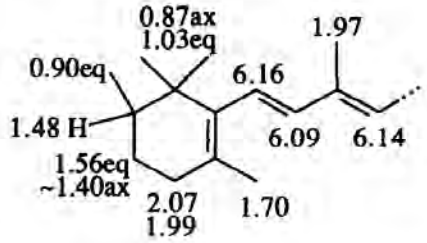
e4



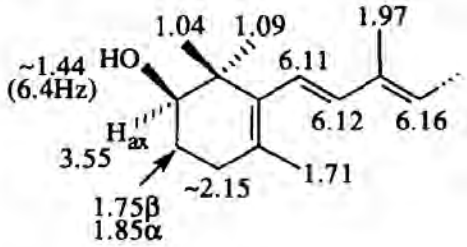
e4a (9-*cis*)



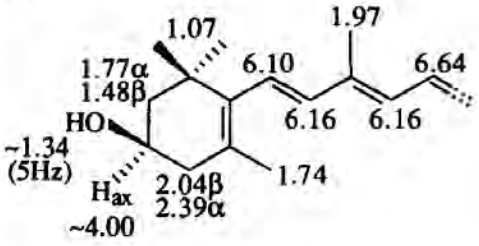
e6



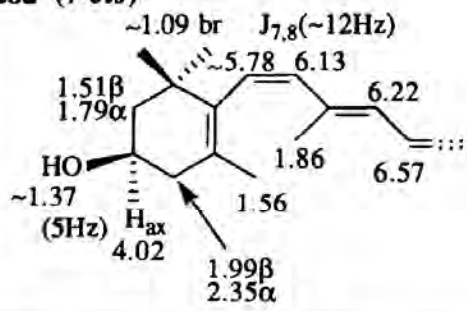
e7



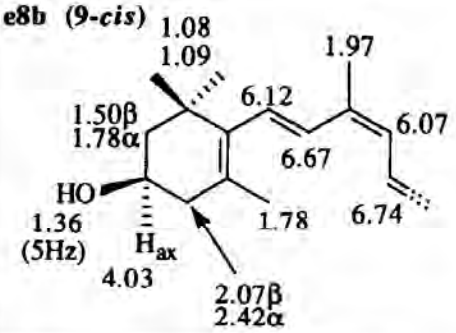
e8



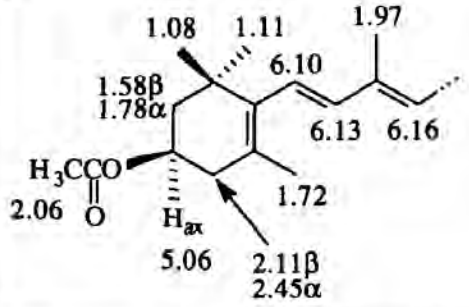
e8a (7-*cis*)



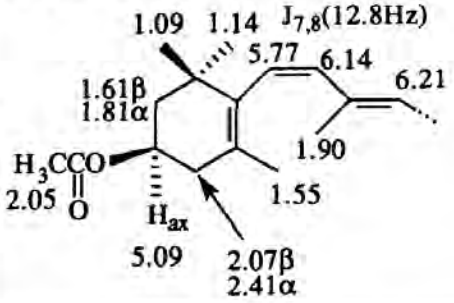
e8b (9-*cis*)



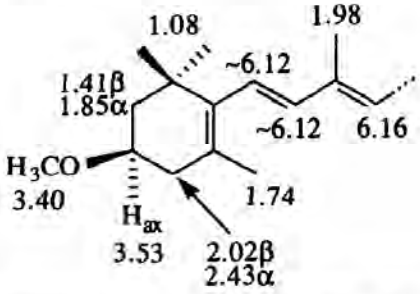
e9



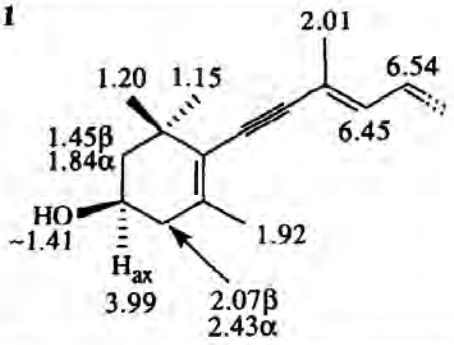
e9a (7-*cis*)



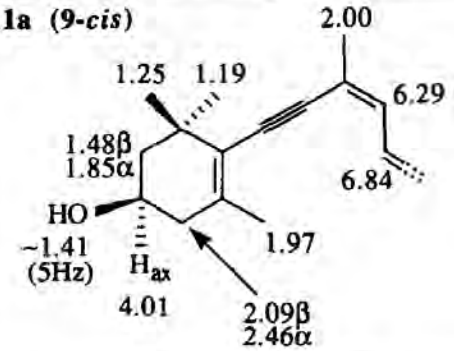
e10



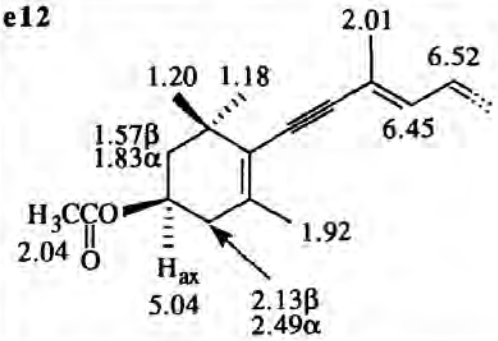
e11



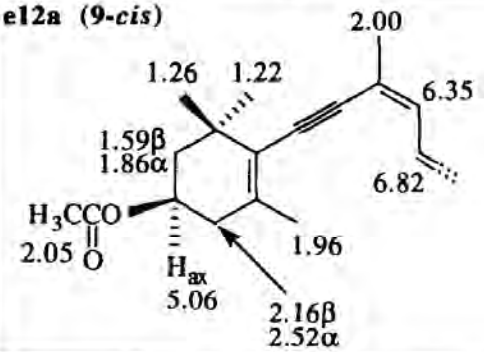
e11a (9-*cis*)



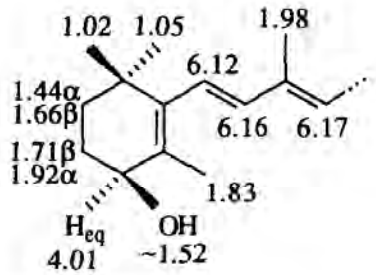
e12



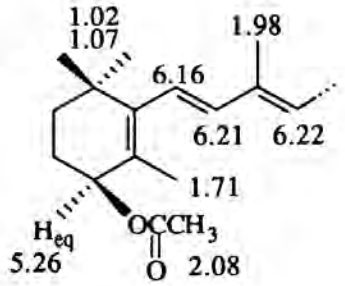
e12a (9-*cis*)



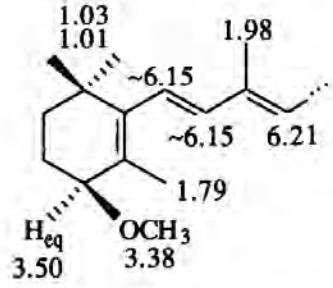
e14



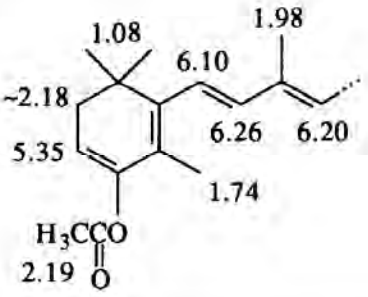
e15



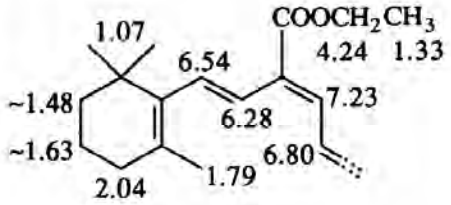
e16



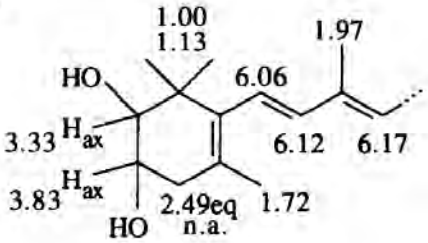
e17



e18

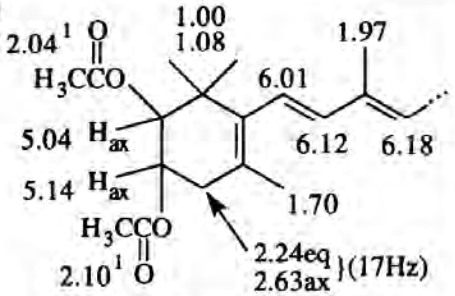


e19



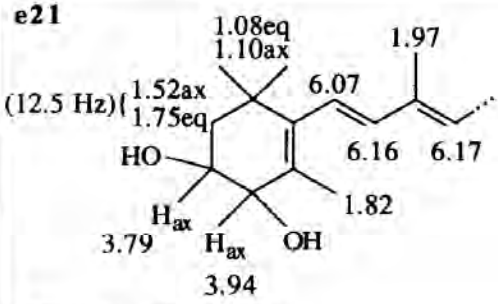
OH *trans* : $J_{2,3}$ = 10Hz

e20



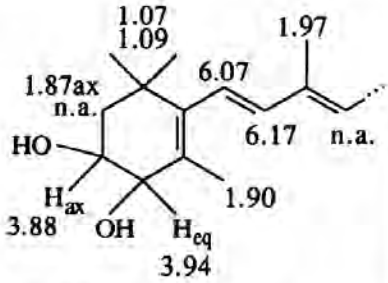
OAc *trans* : $J_{2,3}$ = 12Hz

e21



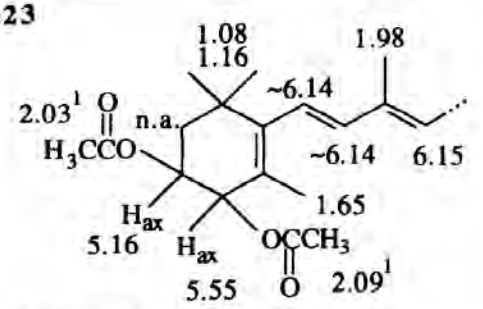
OH *trans* : $J_{3,4}$ ~ 7.5Hz

e22



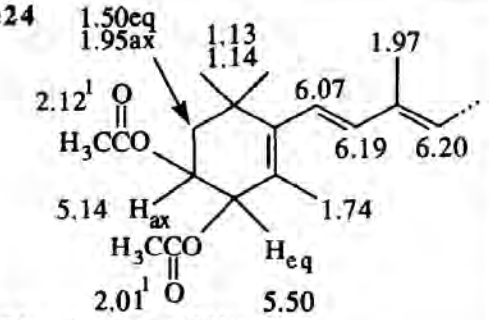
OH *cis* : $J_{3,4}$ ~3.5Hz ; $J_{2a,3a}$ ~12Hz

e23



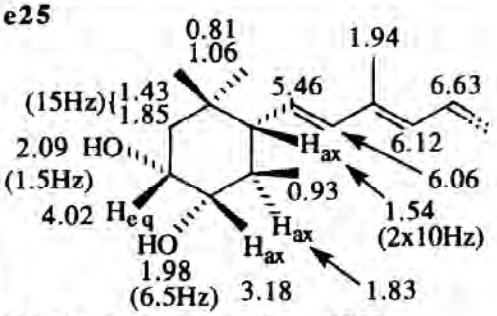
OAc *trans* : $J_{3,4}$ ~ 8Hz

e24



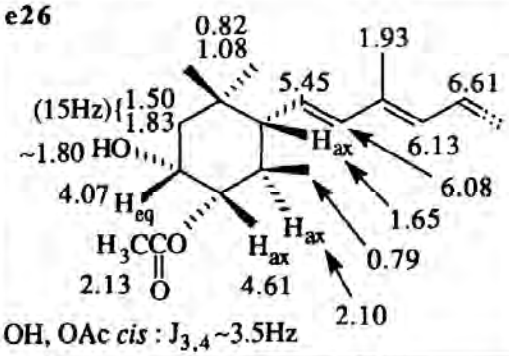
OAc *cis* : $J_{3,4}$ = 3.5Hz

e25



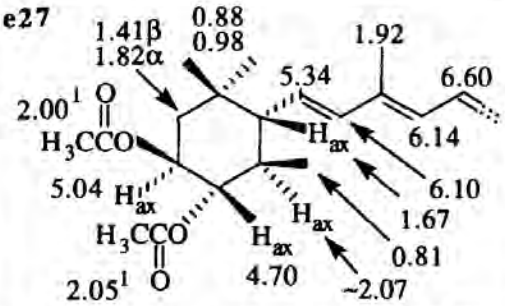
OH *cis* : $J_{3,4}$ = 3.5Hz ; $J_{4,5}$ =10 Hz

e26



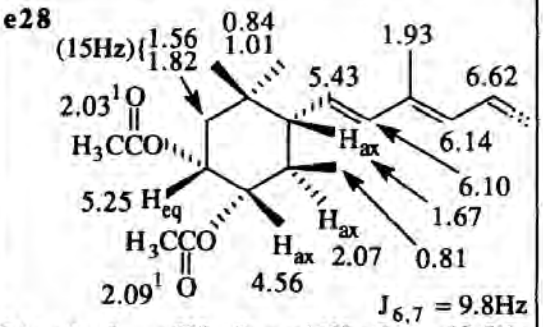
OH, OAc *cis* : $J_{3,4}$ ~3.5Hz

e27



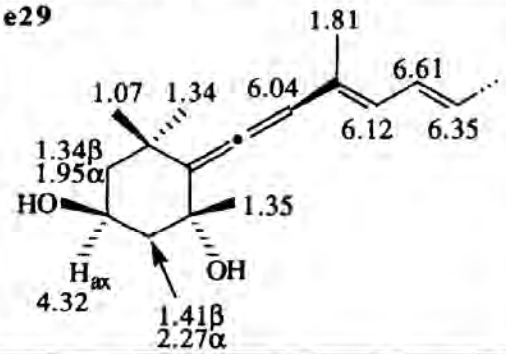
OAc *trans* : $J_{3,4}$ = 10Hz ; $J_{5,6} = J_{6,7}$ = 9.5Hz

e28

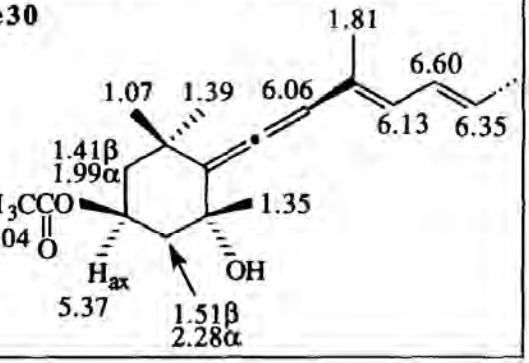


OAc *cis* : $J_{3,4}$ ~3Hz; $J_{4,5}$ ~11Hz; $J_{5,6}$ ~10.5Hz

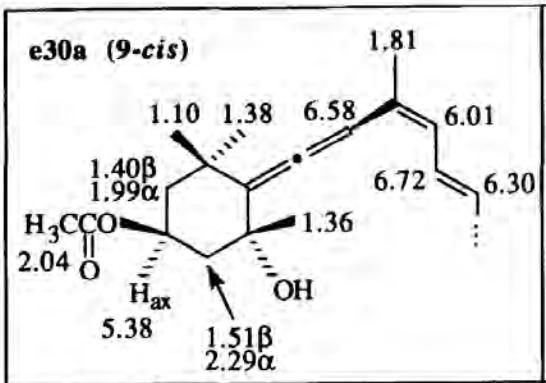
e29



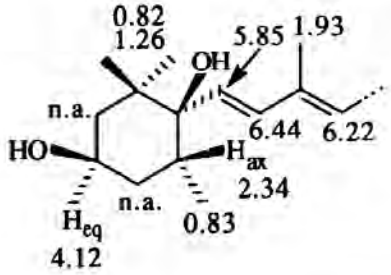
e30



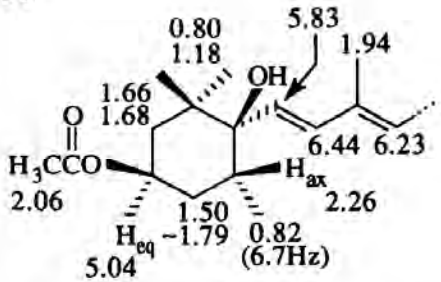
e30a (9-*cis*)



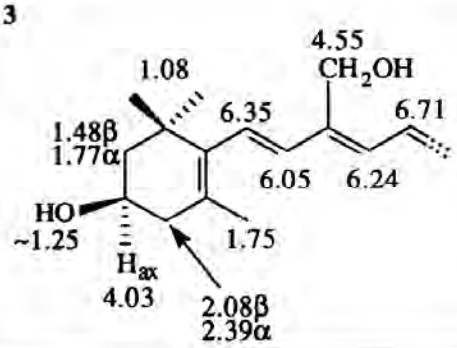
e31



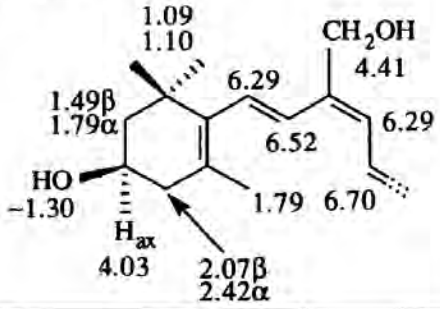
e32



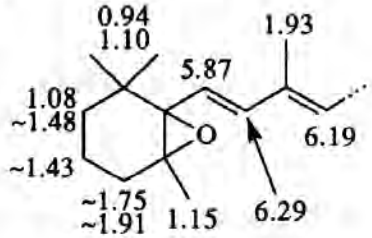
e33



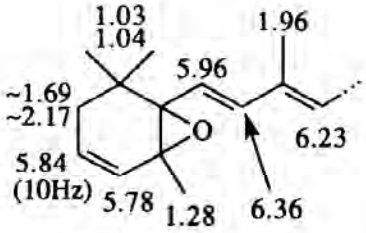
e33a (9-*cis*)



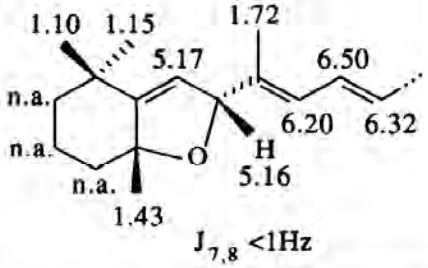
e34



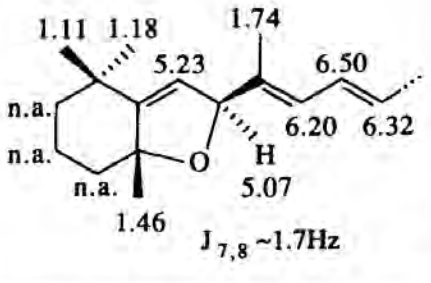
e35



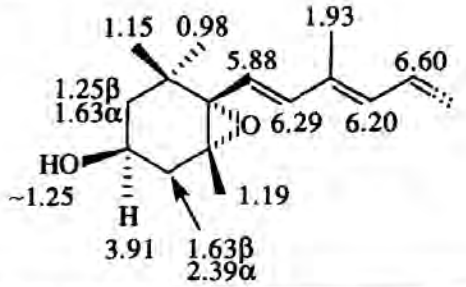
e36



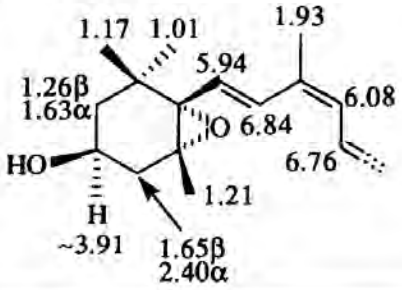
e37



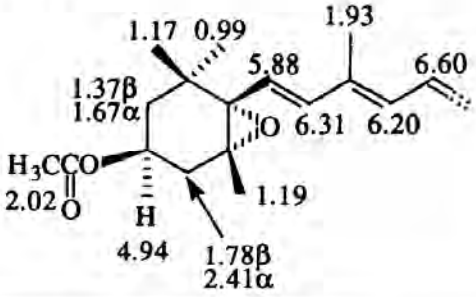
e38



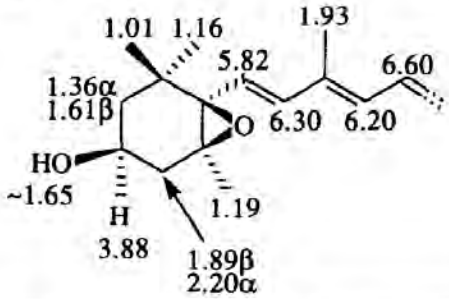
e38a (9-*cis*)



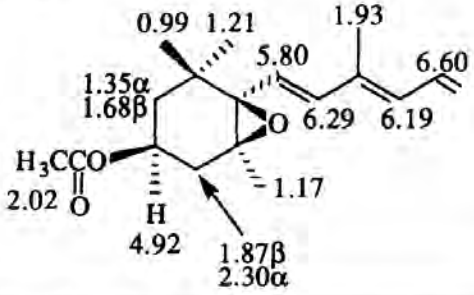
e39



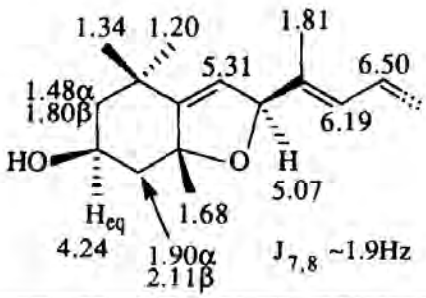
e40



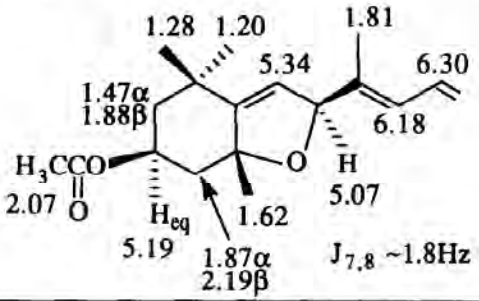
e41



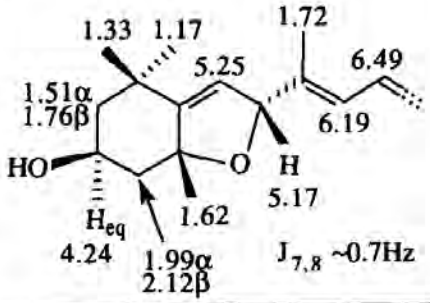
e42



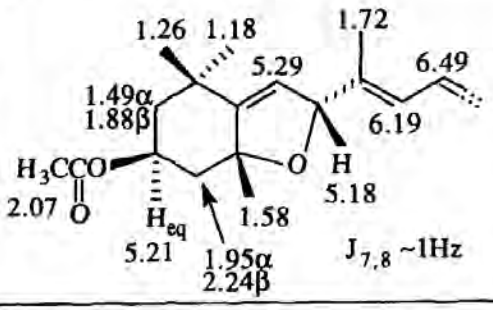
e43



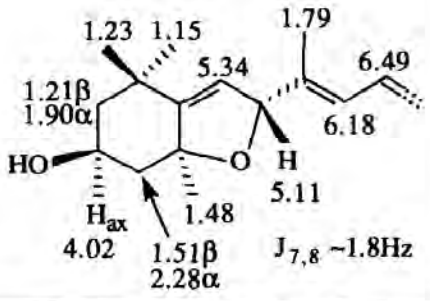
e44



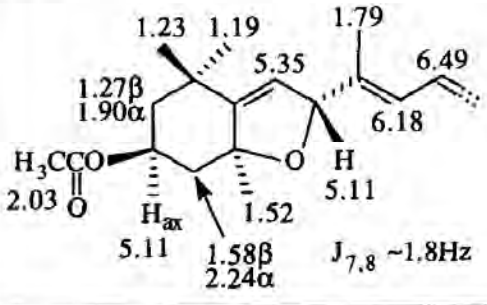
e45



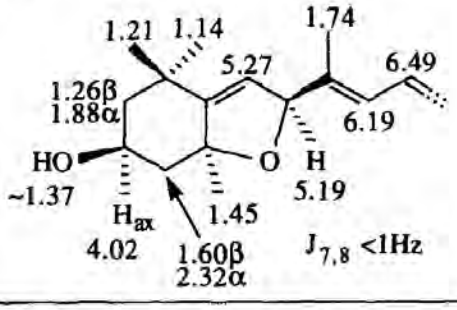
e46



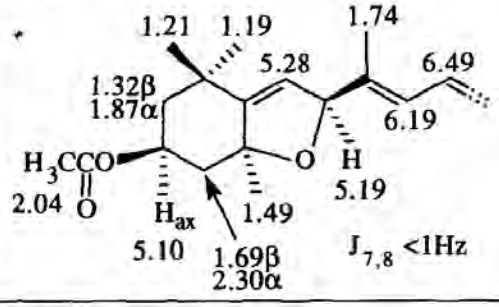
e47



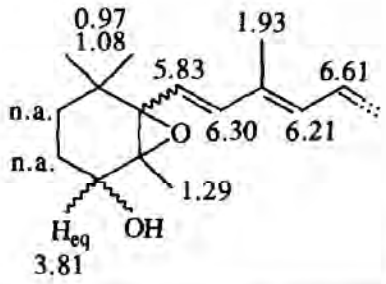
e48



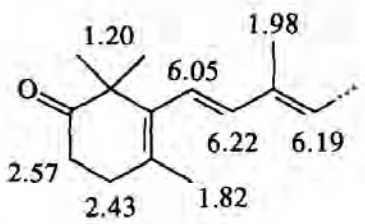
e49



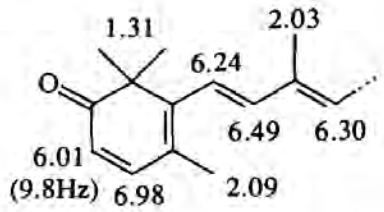
e50



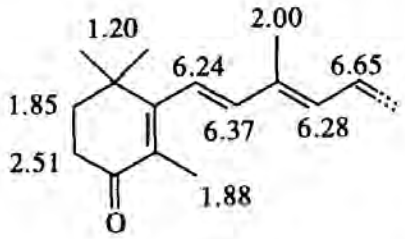
e51



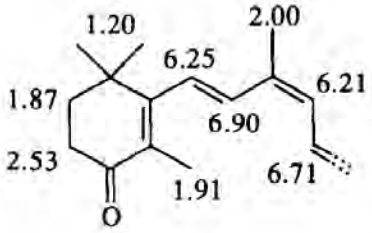
e52



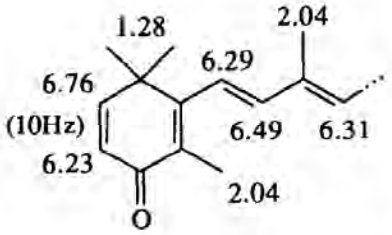
e53



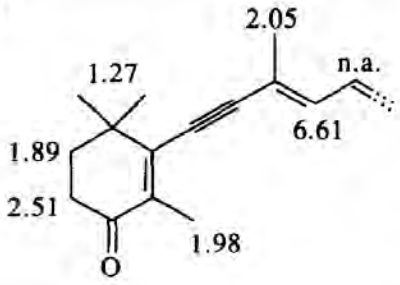
e53b (9-*cis*)



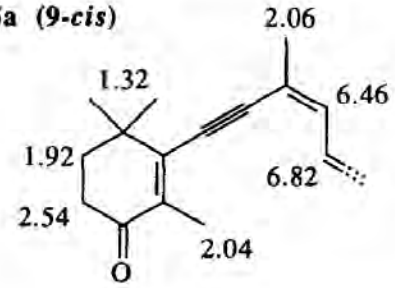
e54



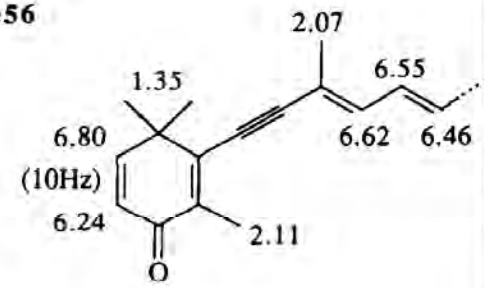
e55



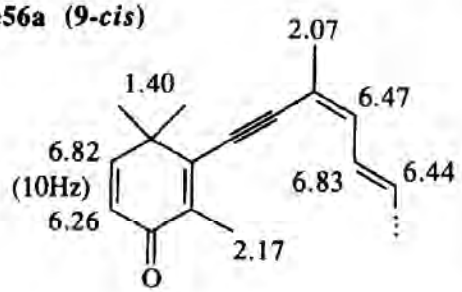
e55a (9-*cis*)



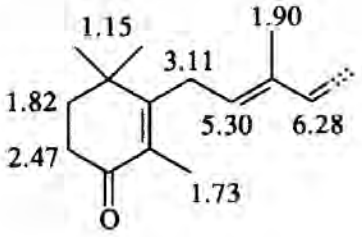
e56



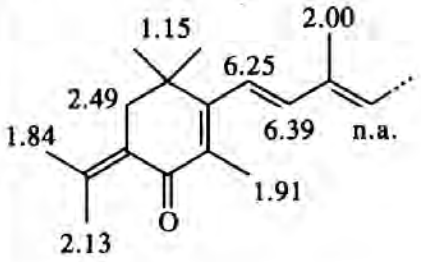
e56a (9-*cis*)



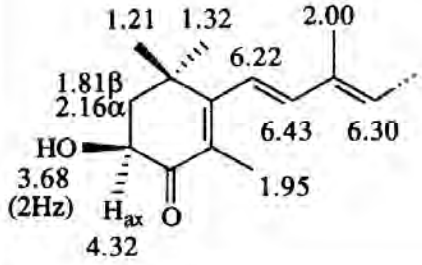
e57



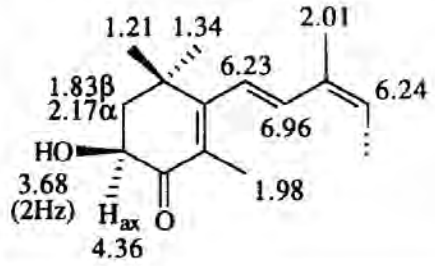
e58



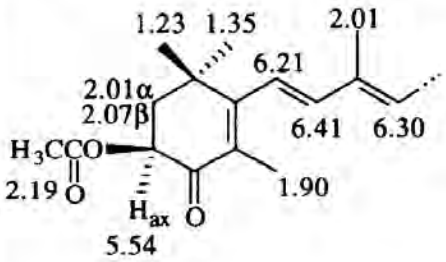
e59



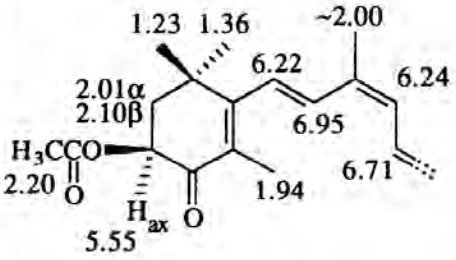
e59a (9-*cis*)



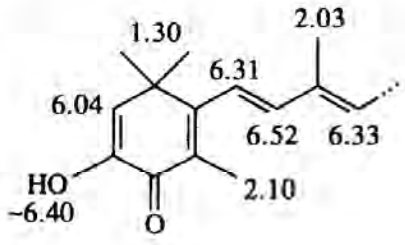
e60



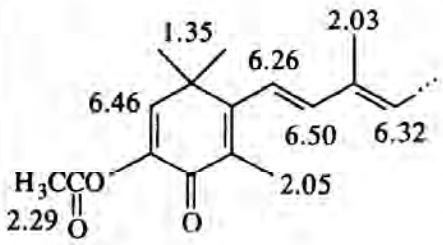
e60a (9-*cis*)



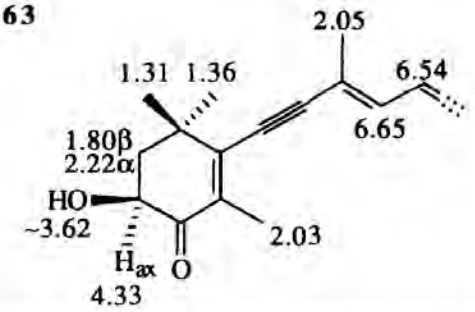
e61



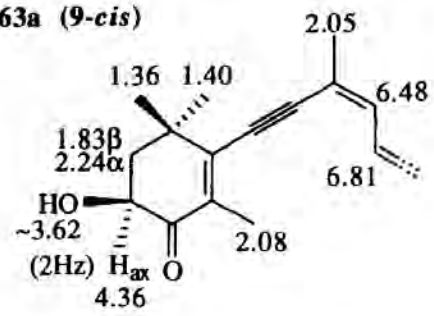
e62



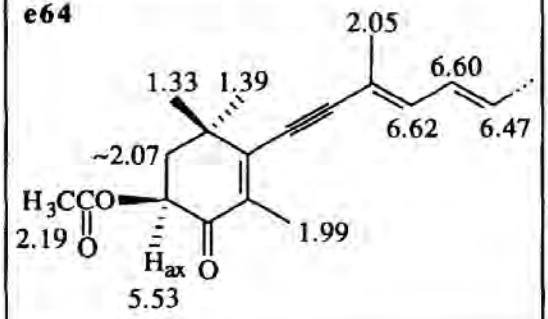
e63



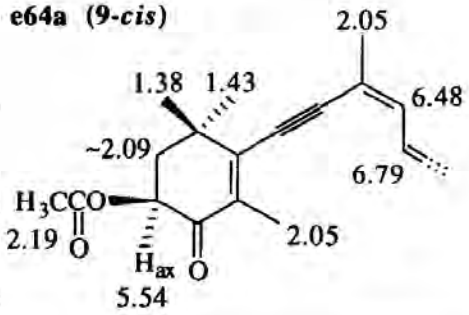
e63a (9-*cis*)



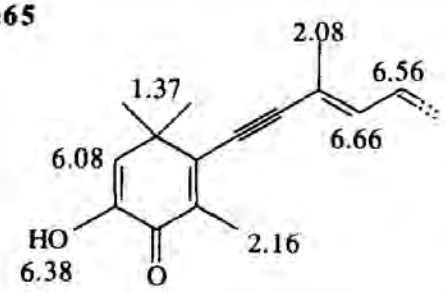
e64



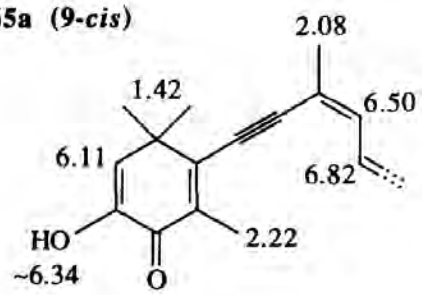
e64a (9-*cis*)



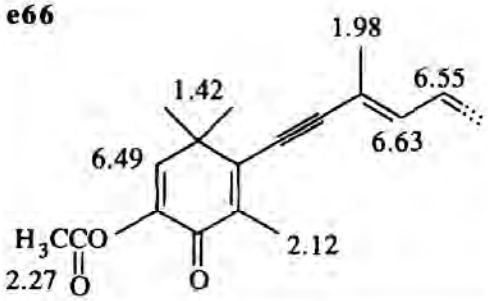
e65



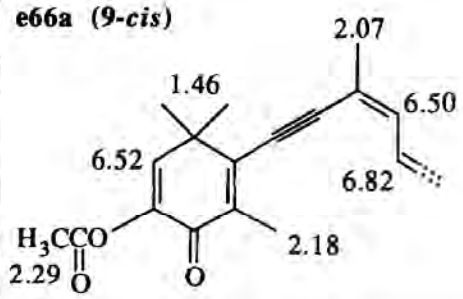
e65a (9-*cis*)



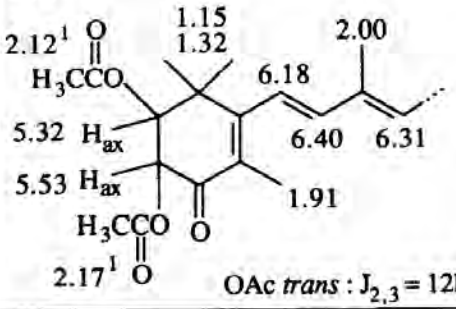
e66



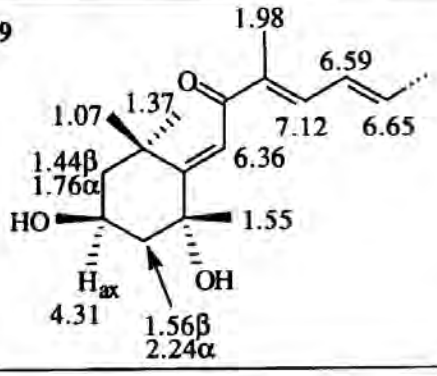
e66a (9-*cis*)



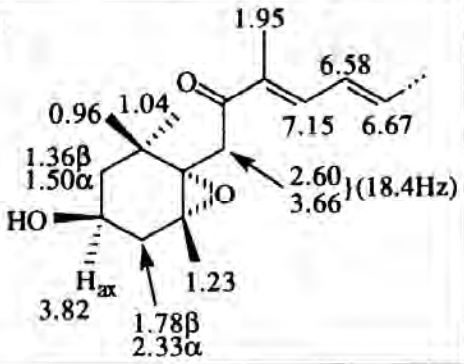
e68



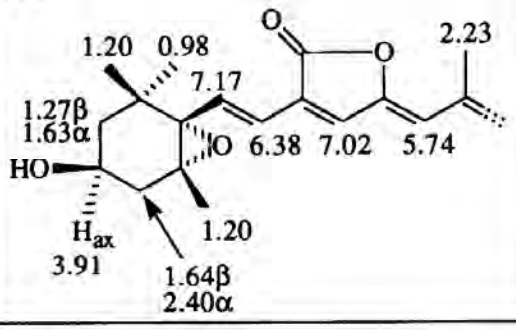
e69



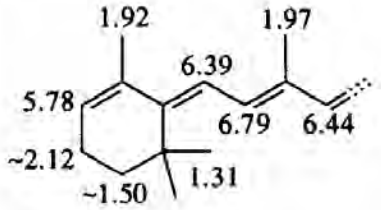
e70



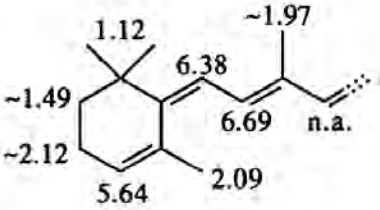
e71



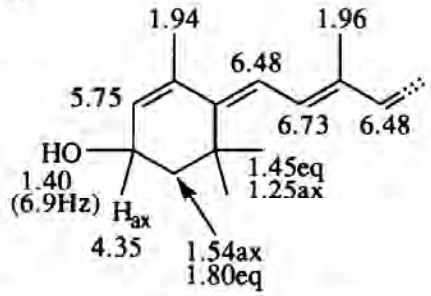
e72



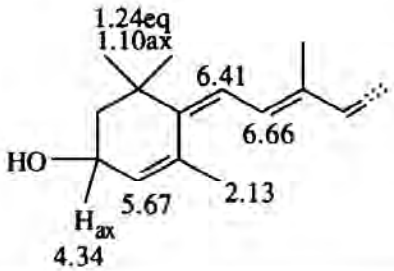
e72a (6-*cis*)



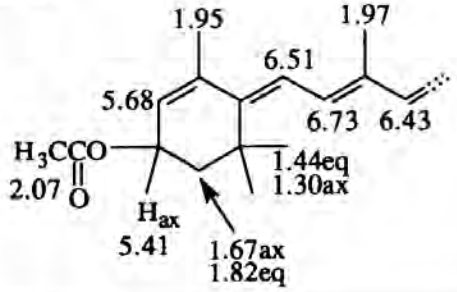
e73



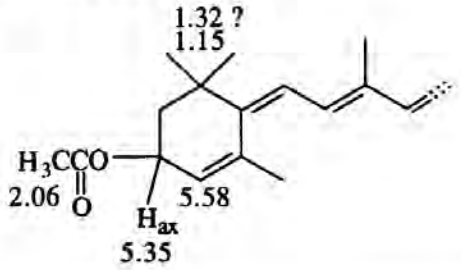
e73a (6-*cis*)



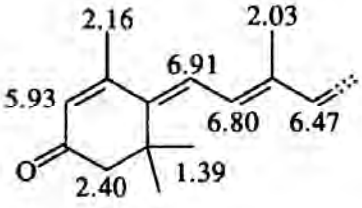
e74



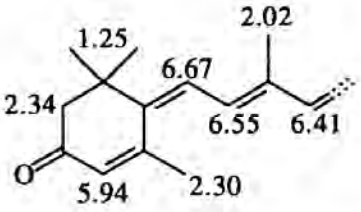
e74a (6-*cis*)



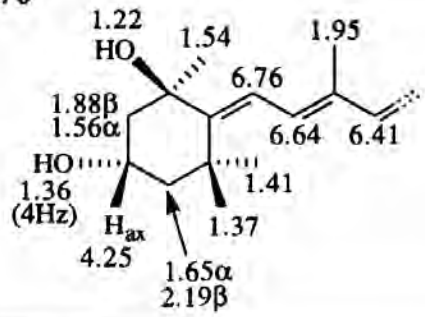
e75



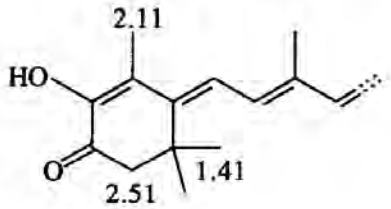
e75a (6-*cis*)



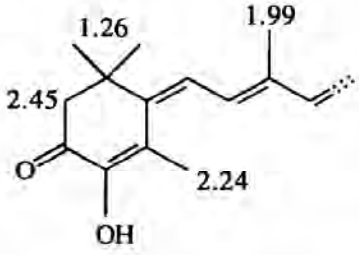
e76



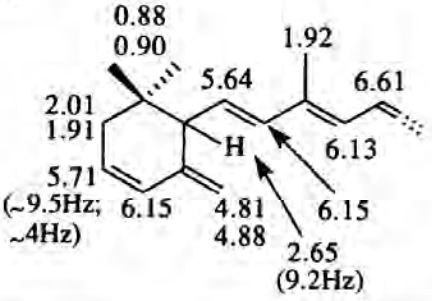
e77



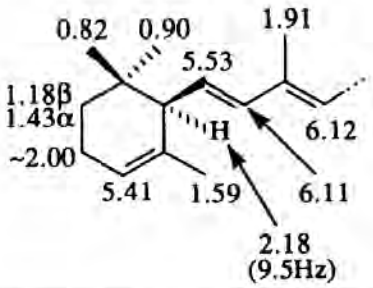
e77a (6-*cis*)



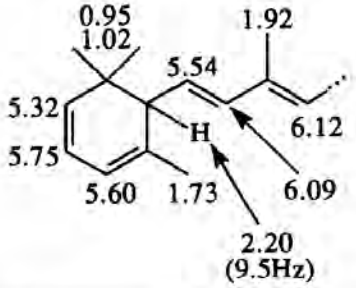
e78



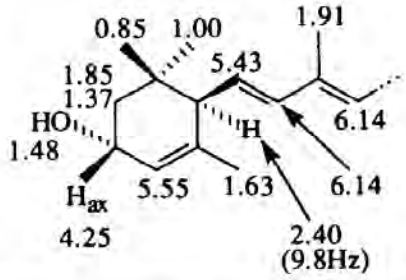
e79



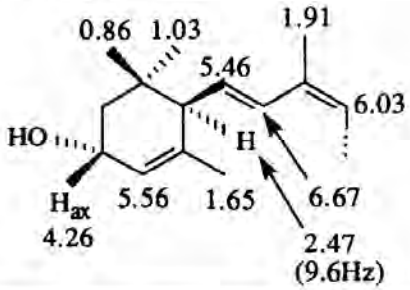
e80



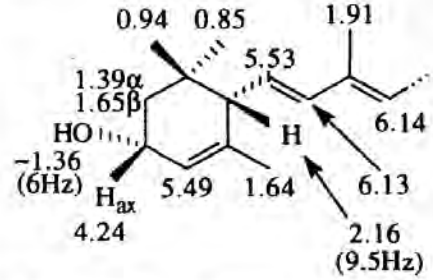
e81



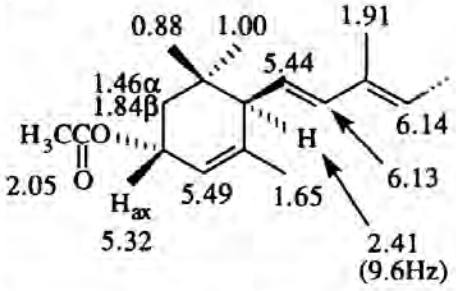
e81a (9-*cis*)



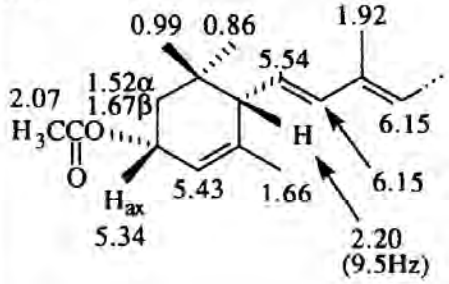
e82



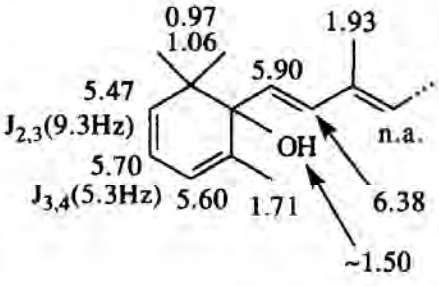
e83



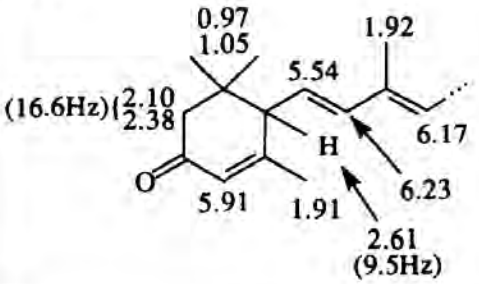
e84



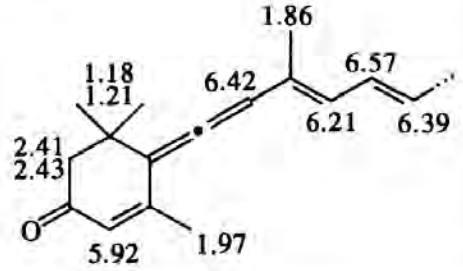
e85



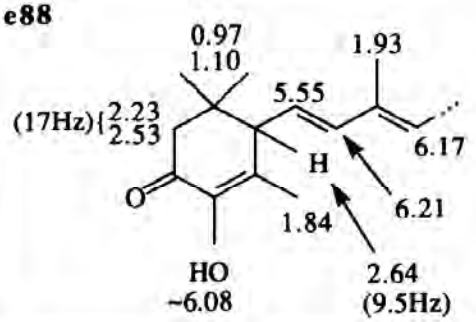
e86



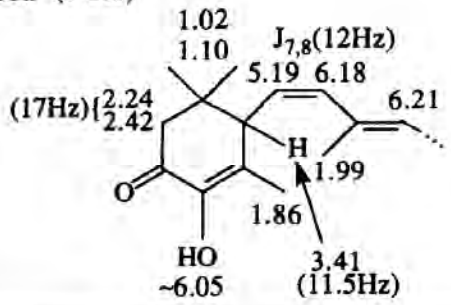
e87



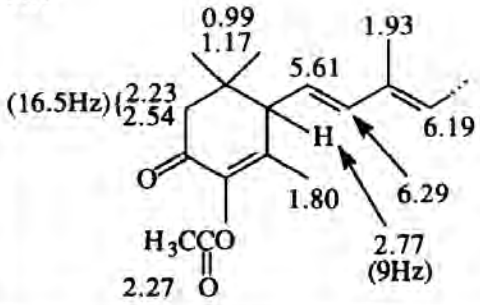
e88



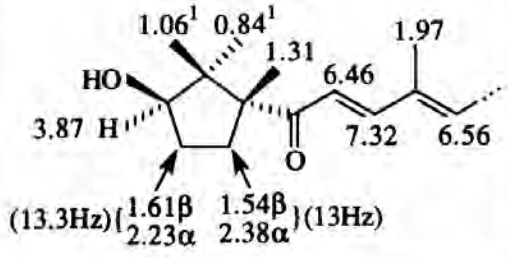
e88a (7-*cis*)



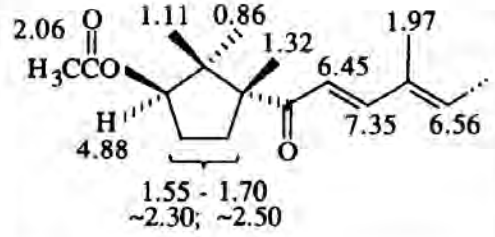
e89



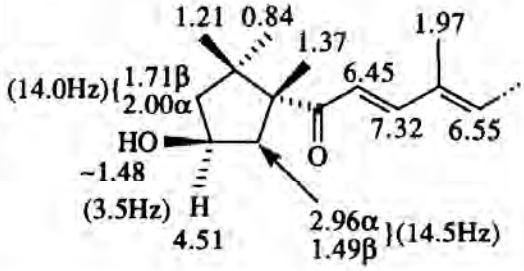
e91



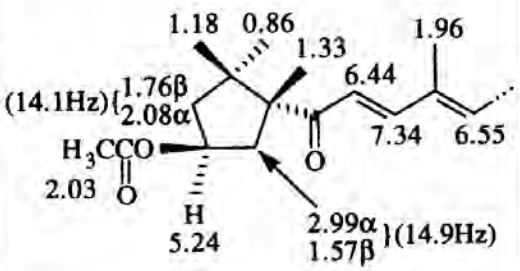
e92



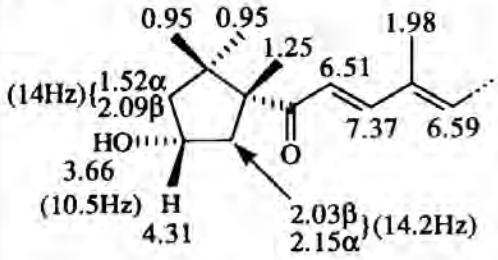
e93



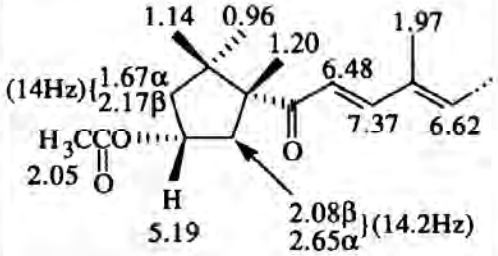
e94



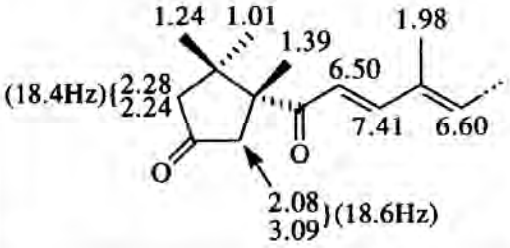
e95



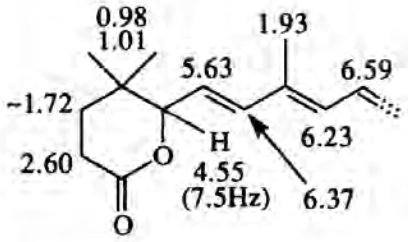
e96



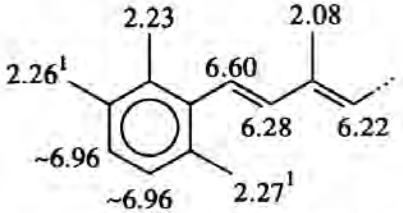
e97



e98

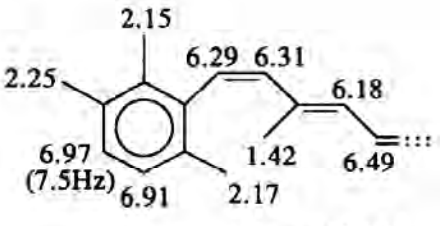


e99



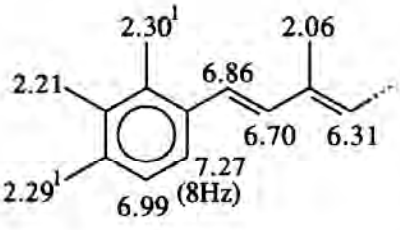
$J_{7,8}$ =16.3Hz

e99a (7-*cis*)

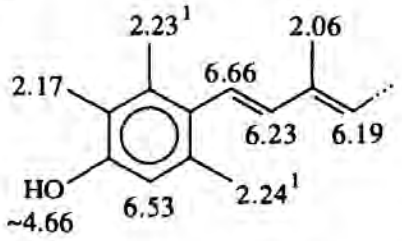


$J_{7,8}$ =12.4Hz

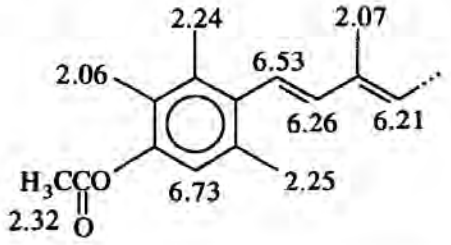
e100



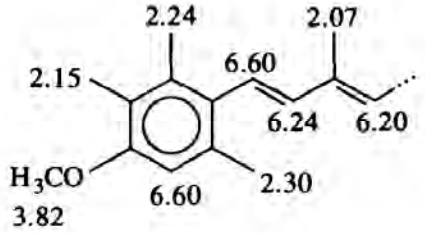
e101



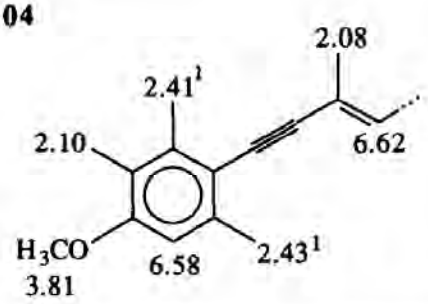
e102



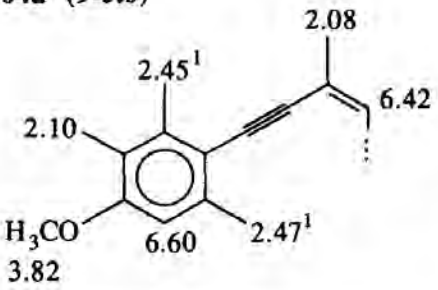
e103



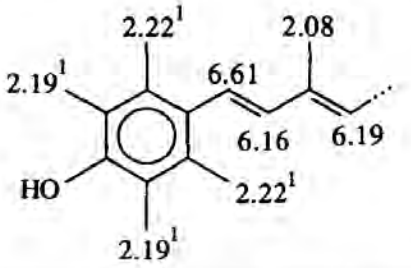
e104



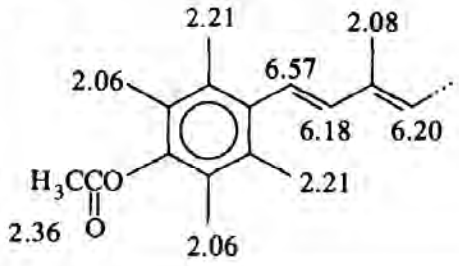
e104a (9-*cis*)



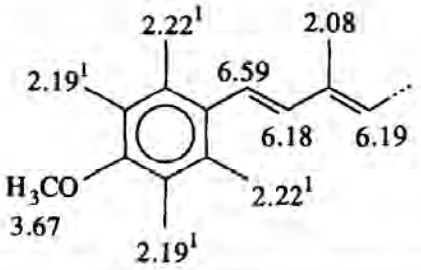
e105



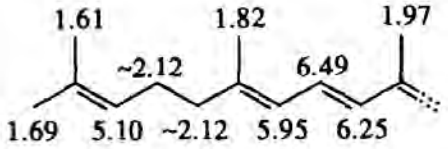
e106



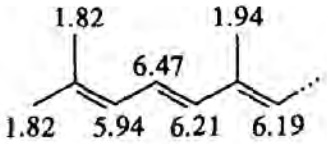
e107



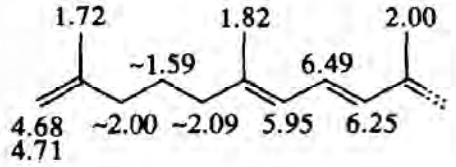
e108



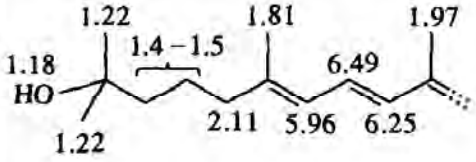
e109



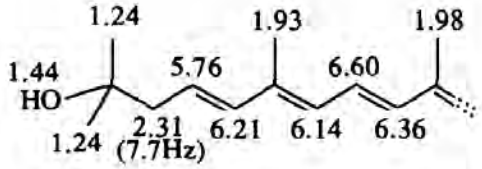
e110



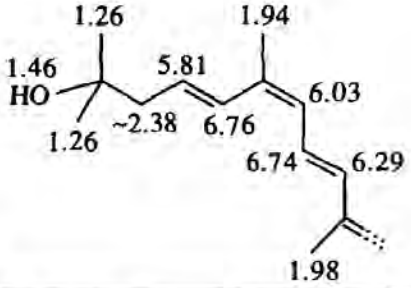
e111



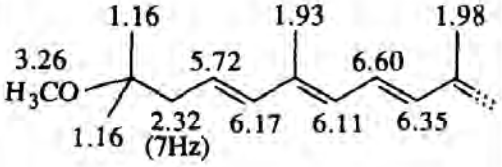
e112



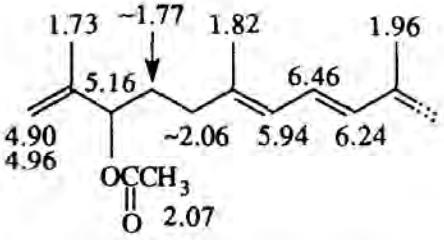
e112a (*5-cis*)



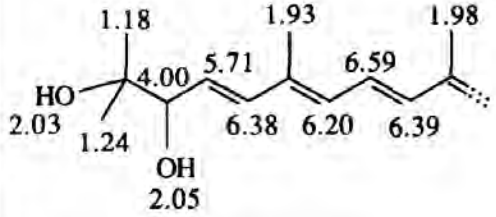
e113



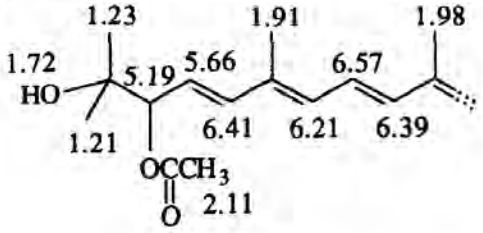
e114



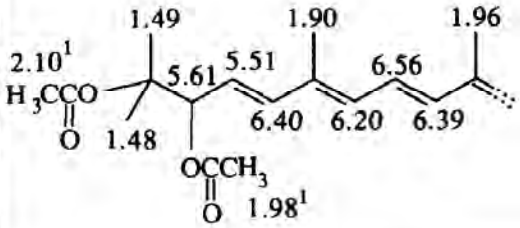
e115



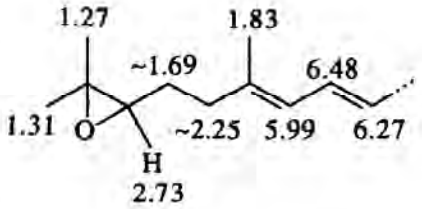
e116



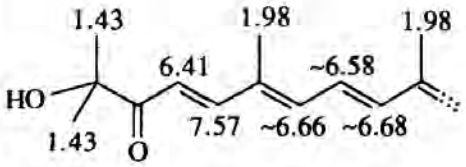
e117



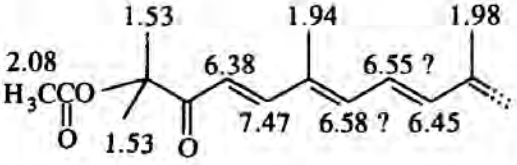
e118



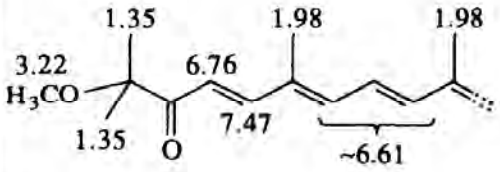
e119



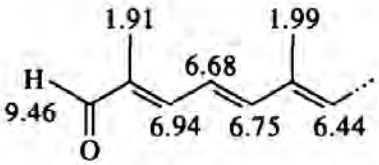
e120



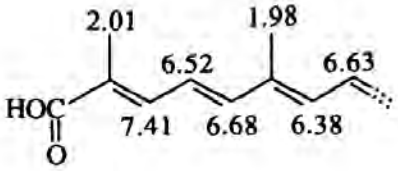
e121



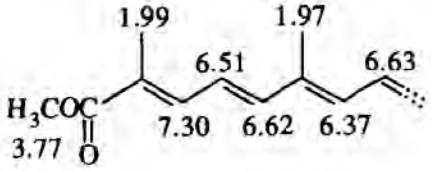
e122



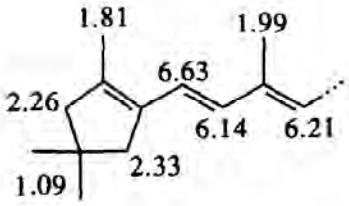
e123



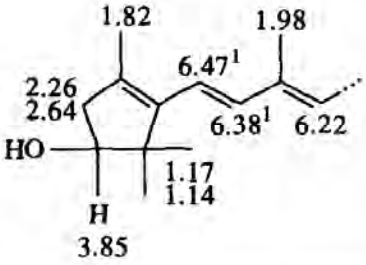
e124



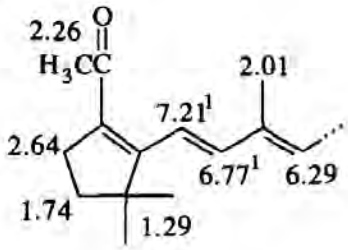
e126



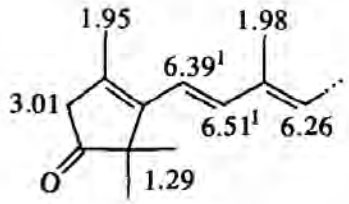
e127



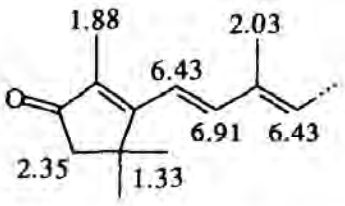
e128



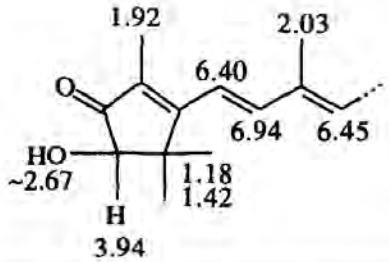
e129



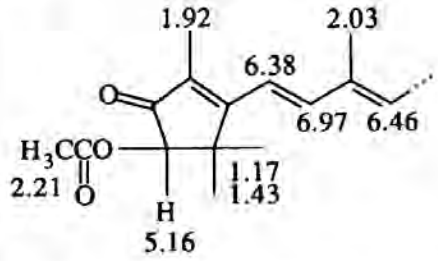
e130



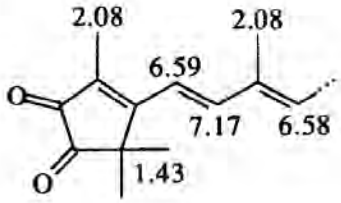
e131



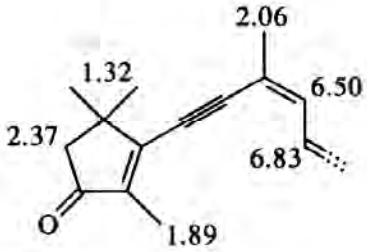
e132



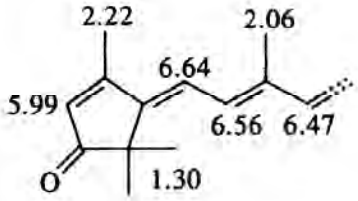
e133



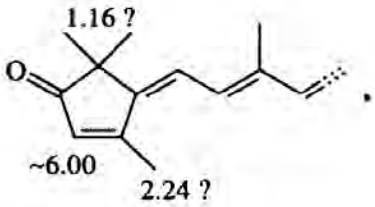
e134 (9-*cis*)



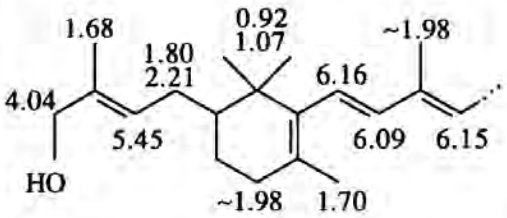
e135



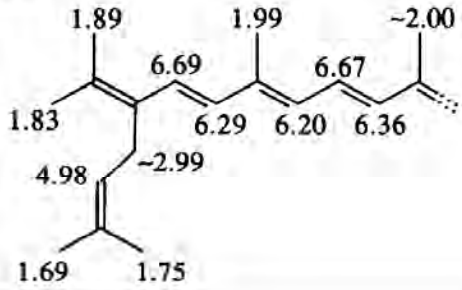
e135a



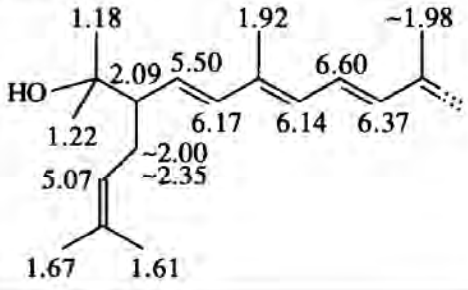
e136



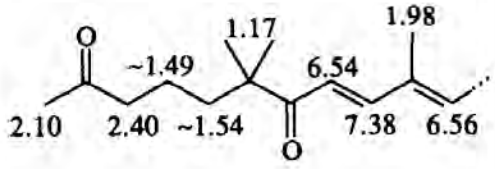
e137



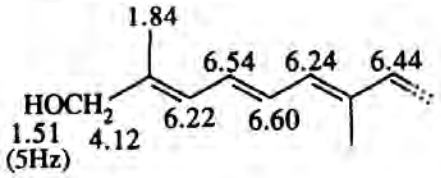
e138



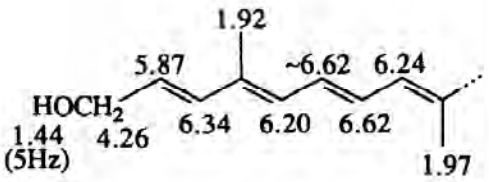
e139



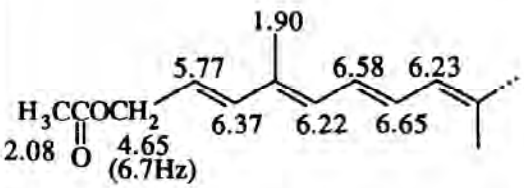
e140



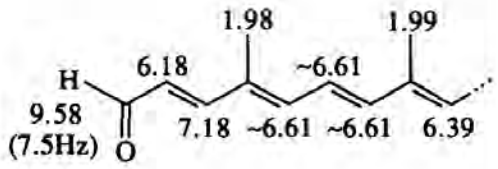
e141



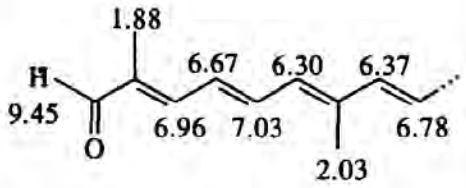
e142



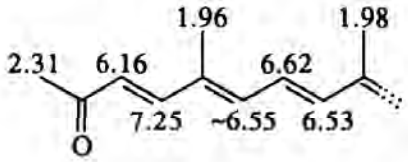
e143



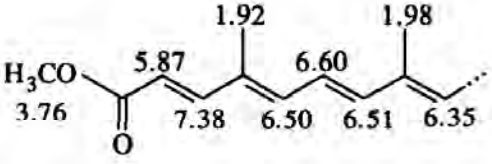
e145



e146



e147



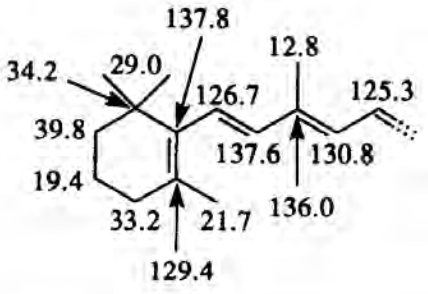
n.a.: not assigned
[1,2] assignments may be reversed

2. ^{13}C-NMR

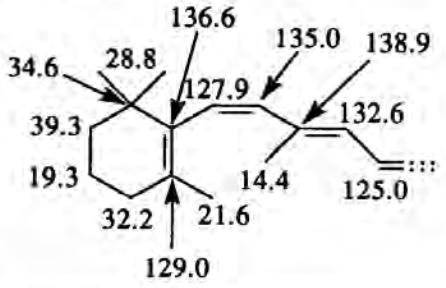
In Table 2 are given the ^{13}C chemical shifts of 90 different end groups; these data represent in part an extension of previous collections [4, 14]. It is important to note that some of the previous assignments were performed at a time when ^{1}H,^{13}C-correlated 2D NMR spectroscopy (heteronuclear COSY), which is now considered to be the most reliable method, was not available. This means that the previous assignments were based solely on 'classical' methods such as comparison of the shifts of related compounds, application of shift reagents, selective on-resonance or CW off-set decoupling, as was previously discussed in detail [14]. In the meantime, a considerable number of these previous assignments, as well as the novel ones, have been supported by extensive applications of modern 1D and 2D techniques and they are considered, therefore, to be very reliable. Based on numerous practical applications it is felt that these data may serve as a promising starting point when known or unknown carotenoids have to be identified. Inevitably, the ^{13}C data bank of Table 2 is smaller than the ^{1}H data bank of Table 1 since the amount of sample needed for the former is much greater and hence the acquisition of ^{13}C spectra has not always been possible.

Table 2. Characteristic ^{13}C-NMR data for some end groups of natural and synthetic carotenoids (solvent $CDCl_3$).

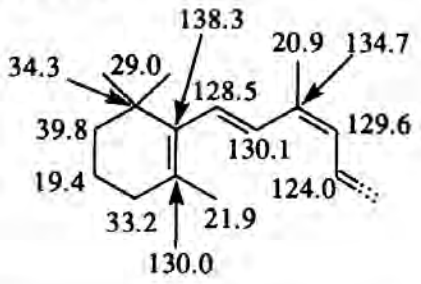
e1



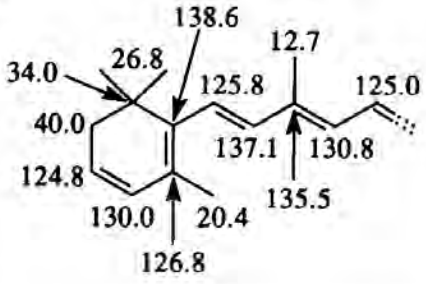
e1a (7-*cis*)



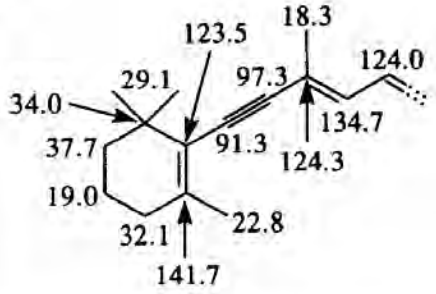
e1b (9-*cis*)



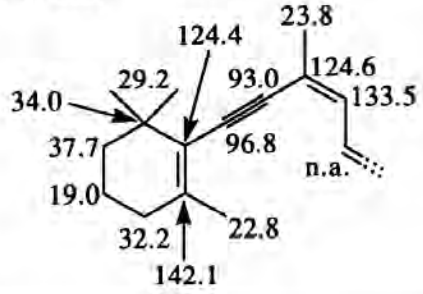
e3



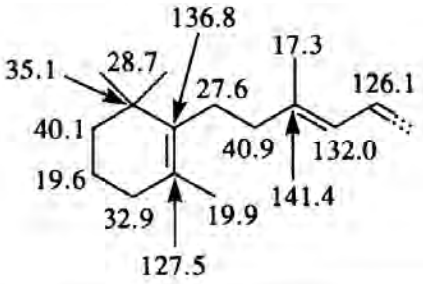
e4



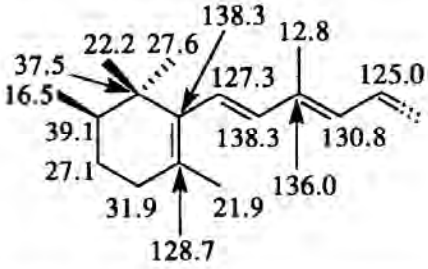
e4a (9-*cis*)



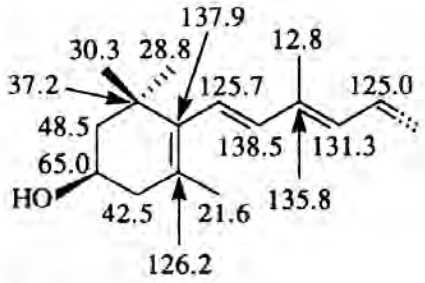
e5



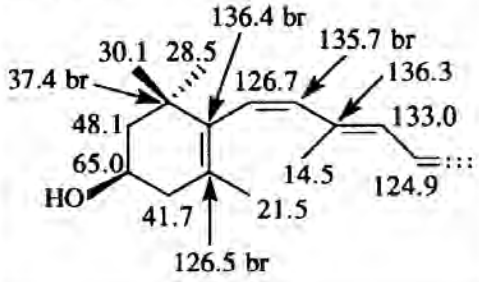
e6



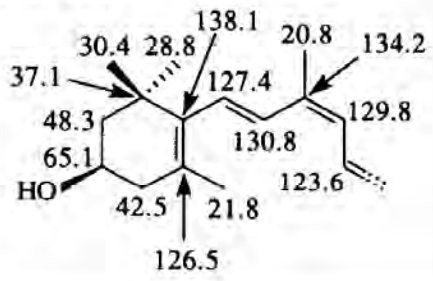
e8



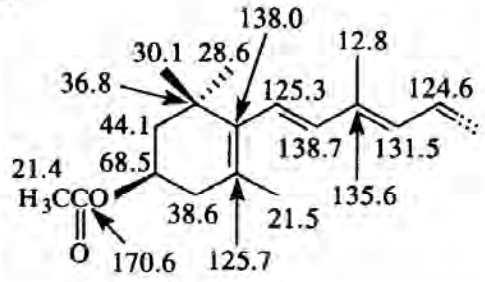
e8a (7-*cis*)



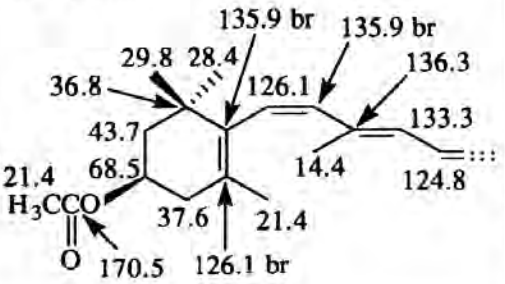
e8b (9-*cis*)



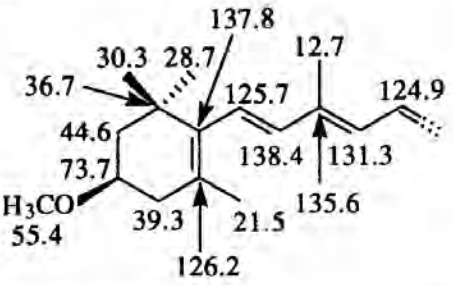
e9



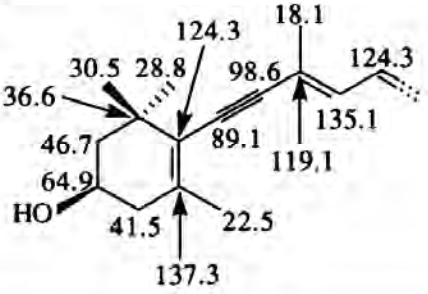
e9a (7-*cis*)



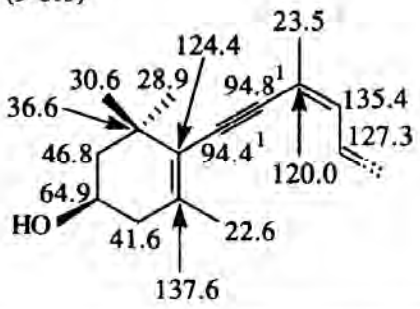
e10



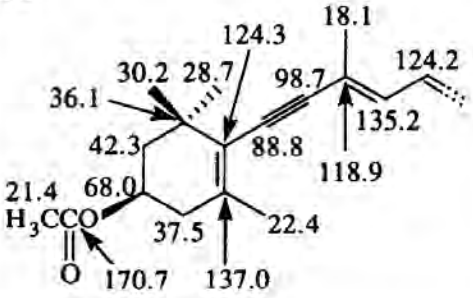
e11



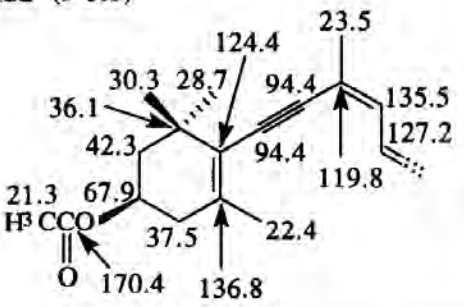
e11a (9-*cis*)



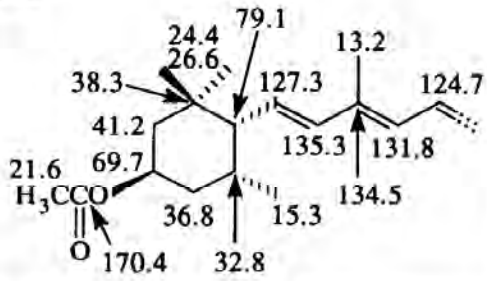
e12



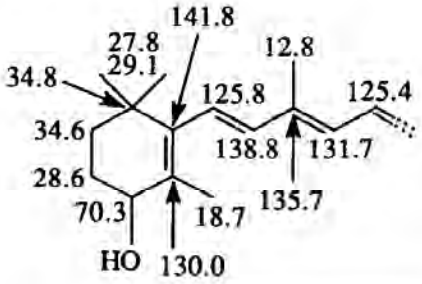
e12a (9-*cis*)



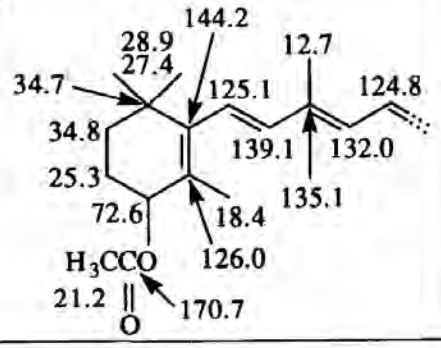
e13



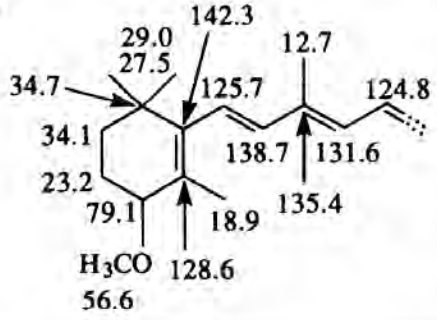
e14



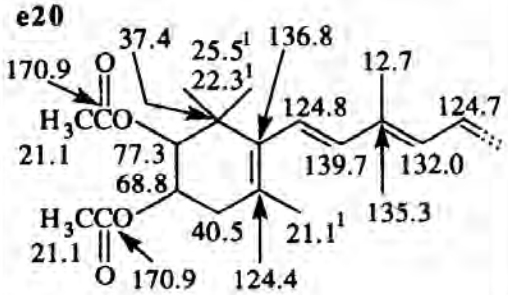
e15



e16

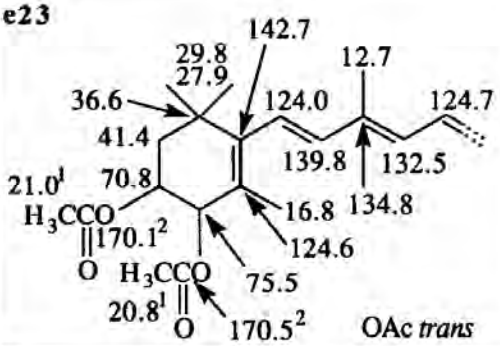


e20



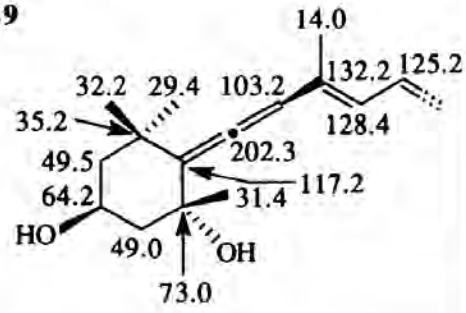
OAc *trans*

e23

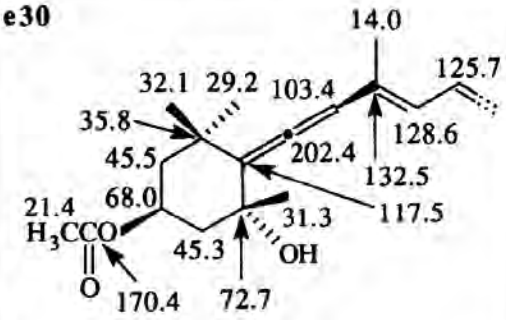


OAc *trans*

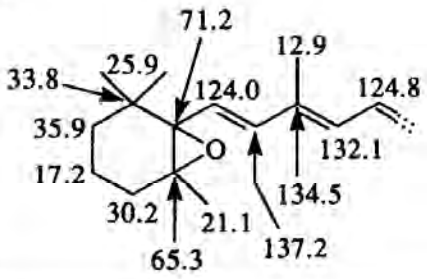
e29



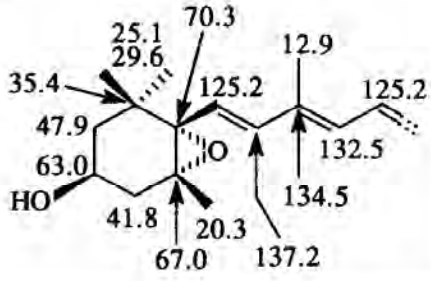
e30



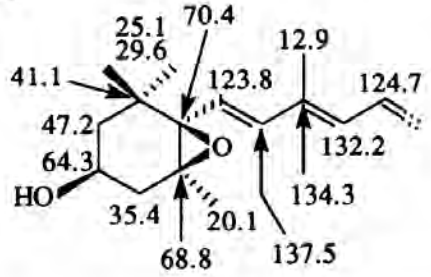
e34



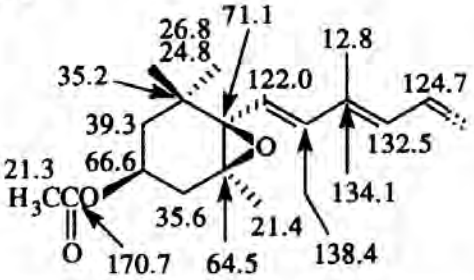
e38



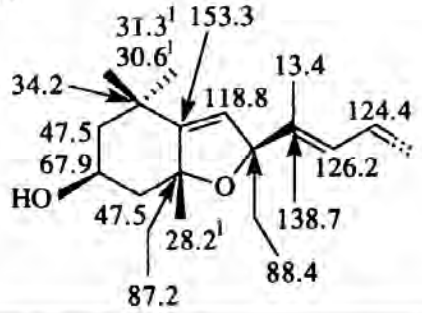
e40



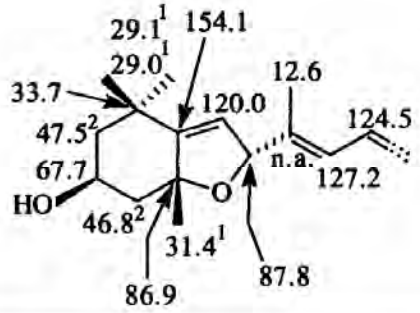
e41



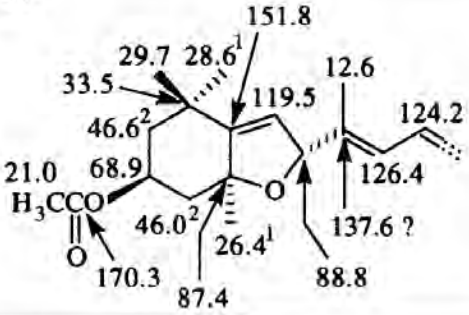
e42



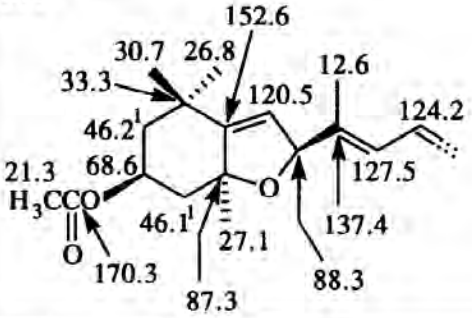
e44



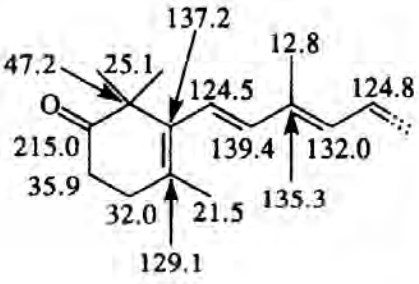
e47



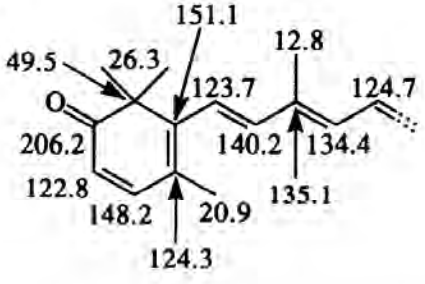
e49



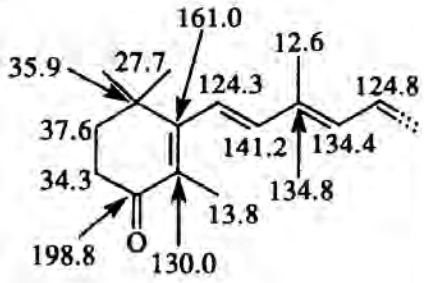
e51



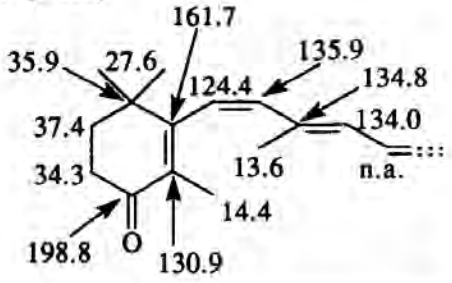
e52



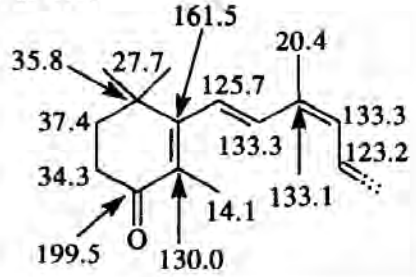
e53



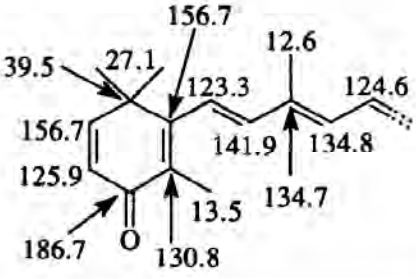
e53a (7-*cis*)



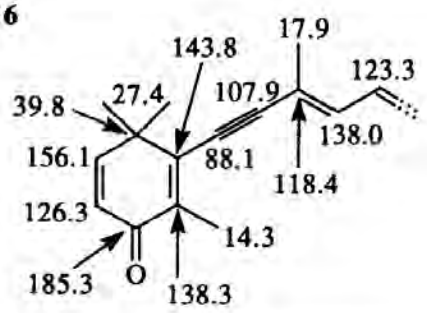
e53b (9-*cis*)



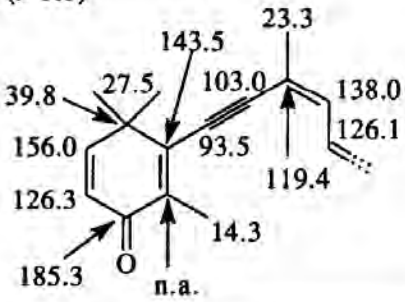
e54



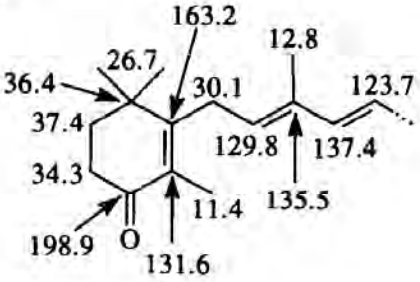
e56



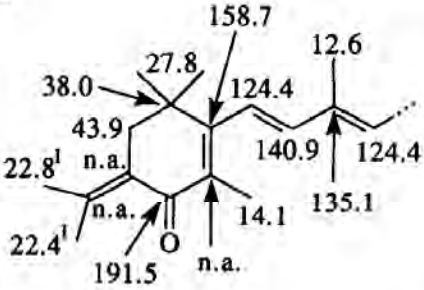
e56a (9-*cis*)



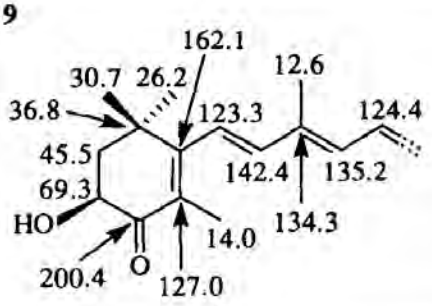
e57



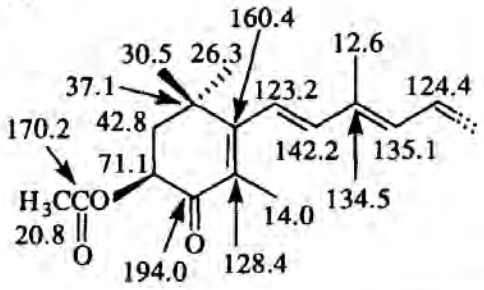
e58



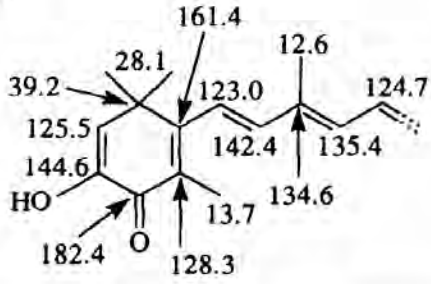
e59



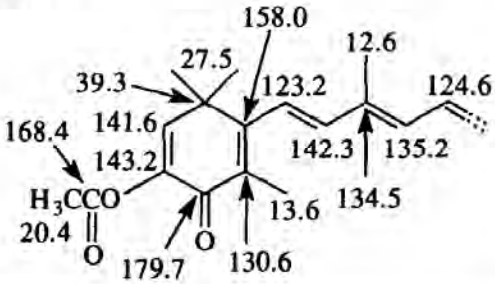
e60



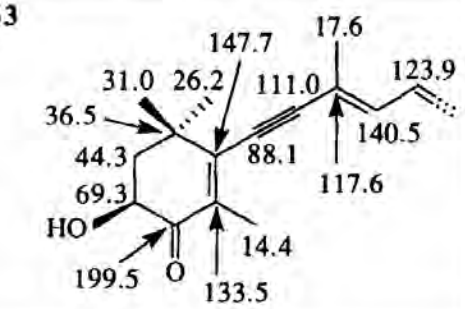
e61



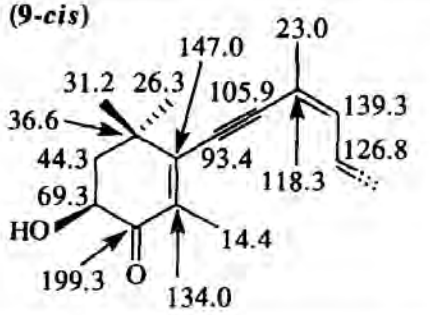
e62



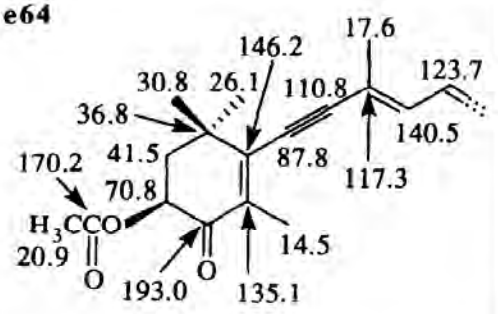
e63



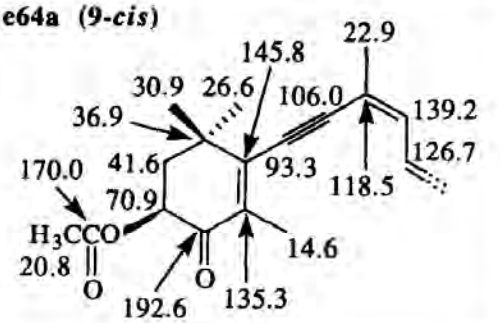
e63a (9-*cis*)



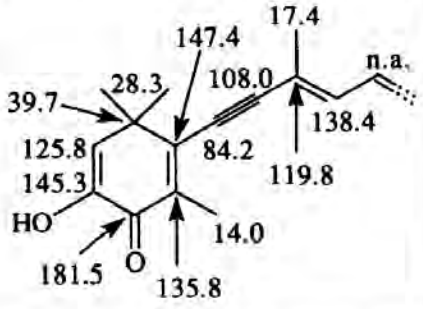
e64



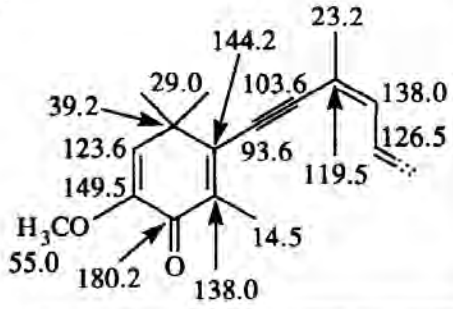
e64a (9-*cis*)



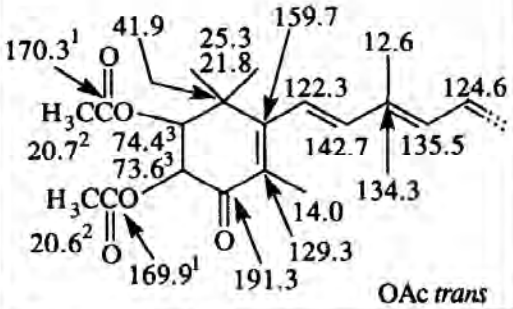
e65



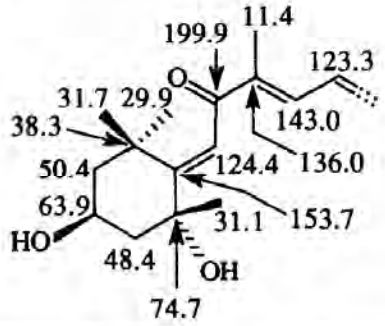
e67



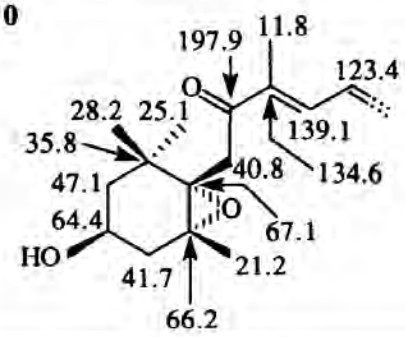
e68



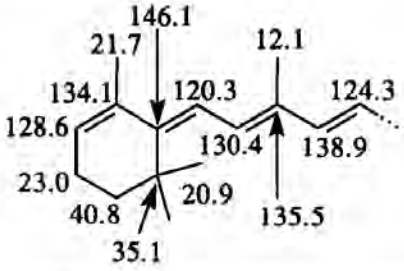
e69



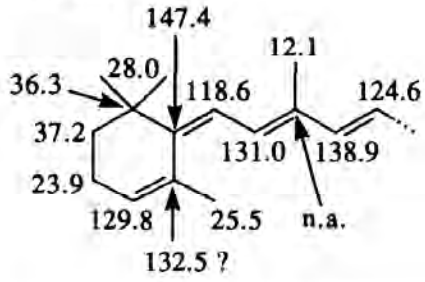
e70



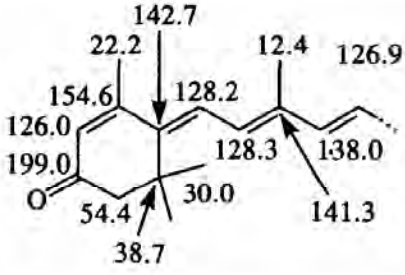
e72



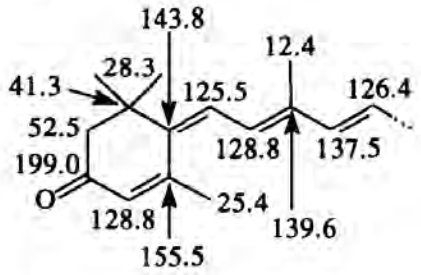
e72a (6-*cis*)



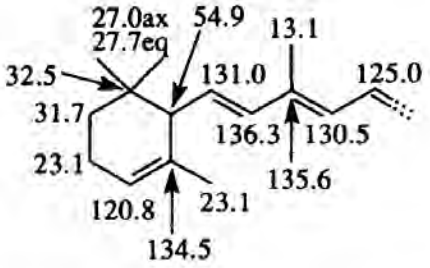
e75



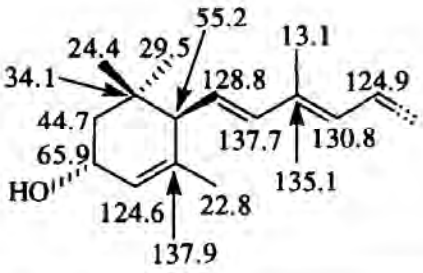
e75a (6-*cis*)



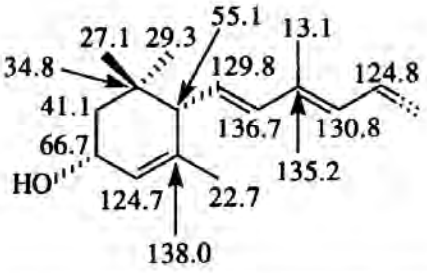
e79



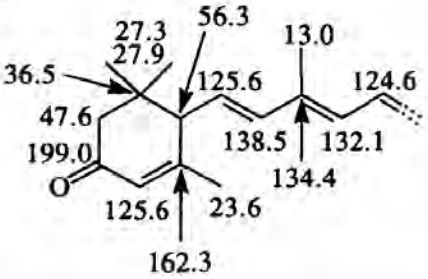
e81



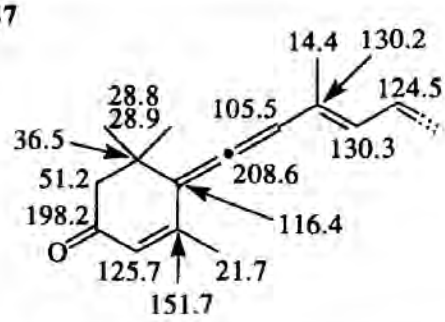
e82



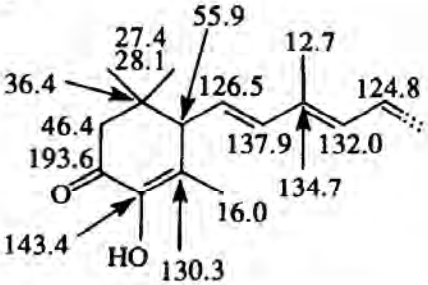
e86



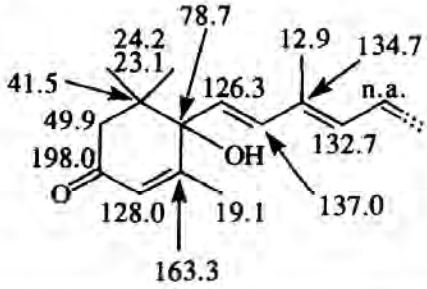
e87



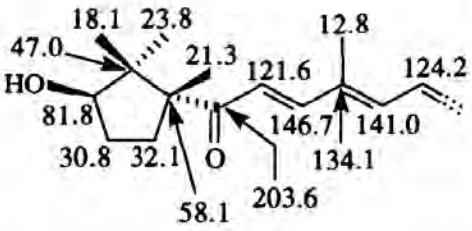
e88



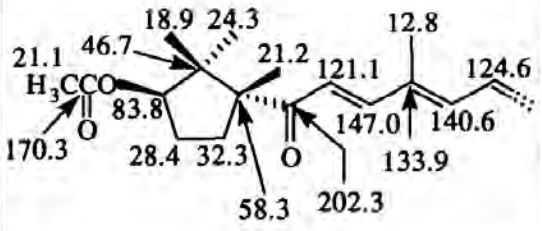
e90



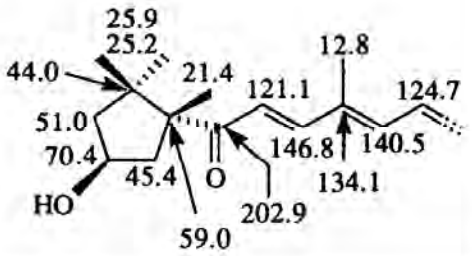
e91



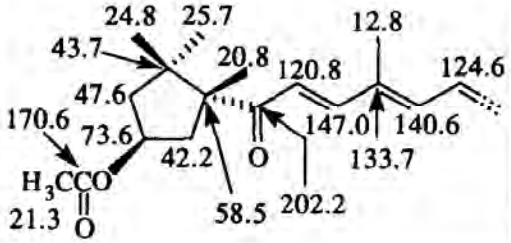
e92



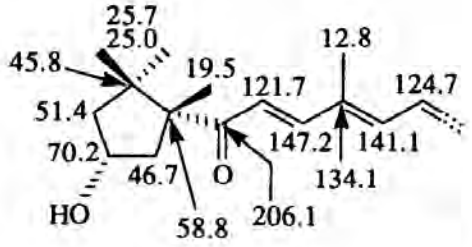
e93



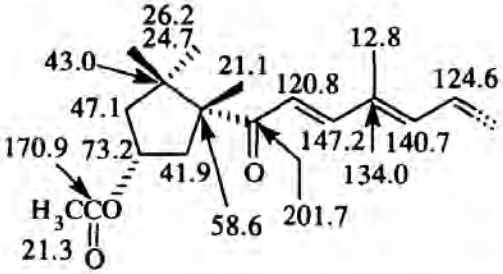
e94



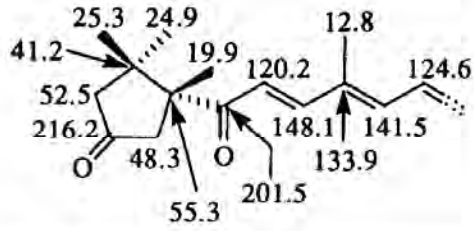
e95



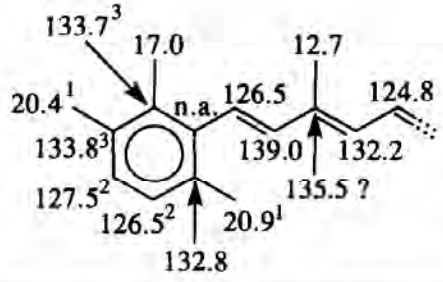
e96



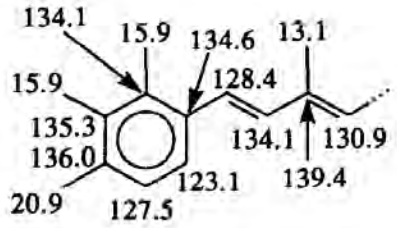
e97



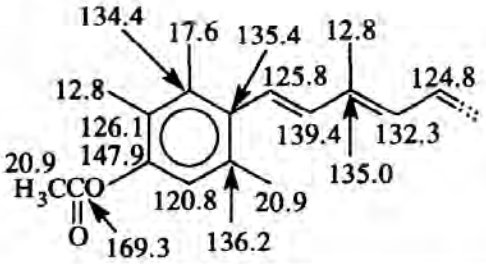
e99



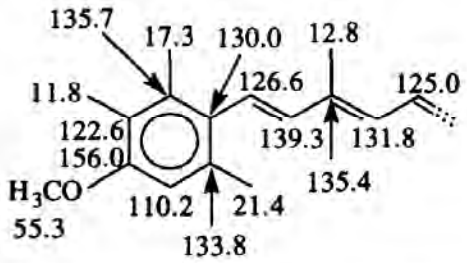
e100



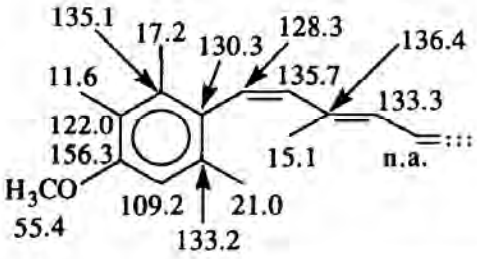
e102



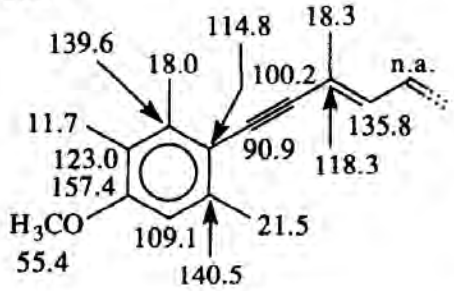
e103



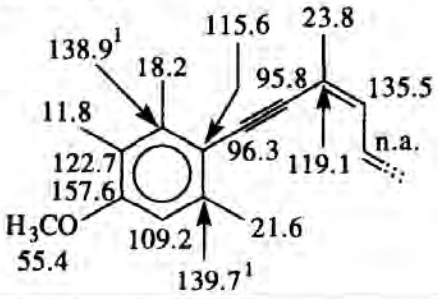
e103a (7-*cis*)



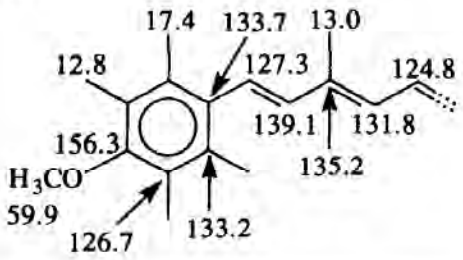
e104



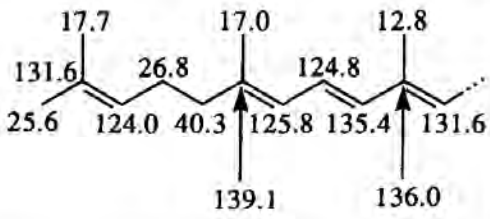
e104a (9-*cis*)



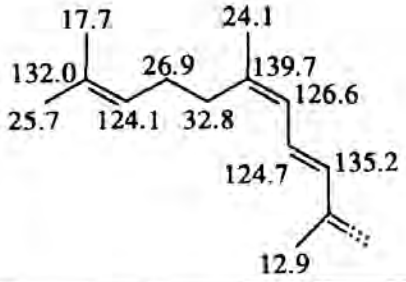
e107



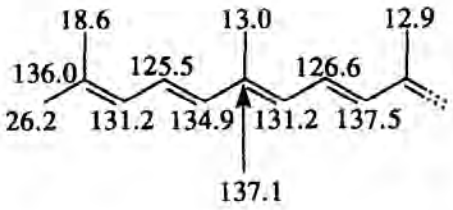
e108



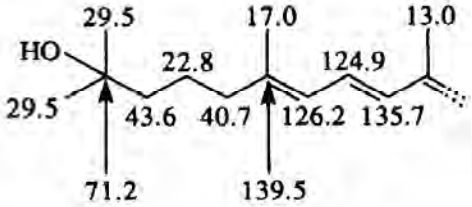
e108a (*9-cis*)



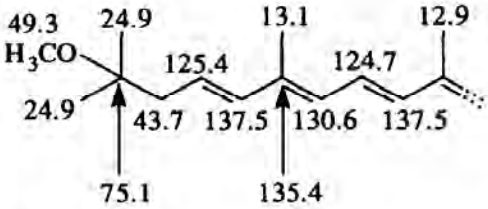
e109



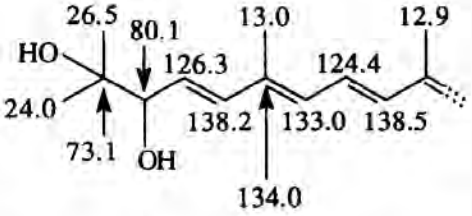
e111



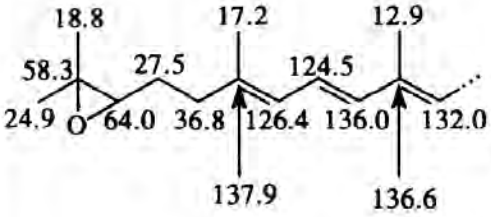
e112



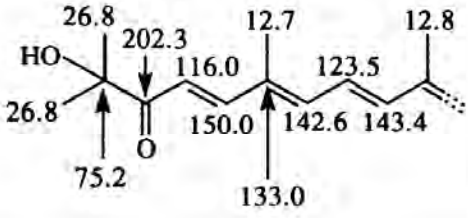
e115



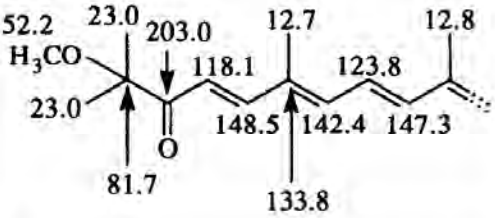
e118



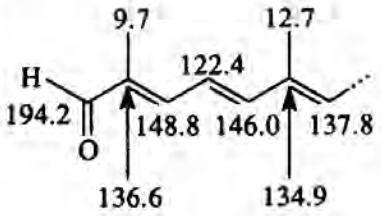
e119



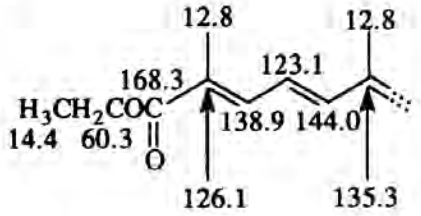
e121



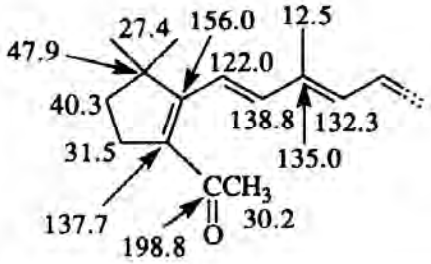
e122



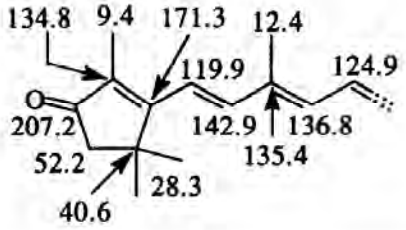
e125



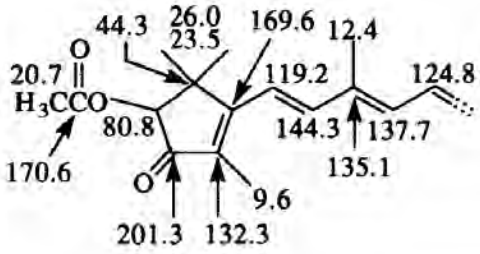
e128



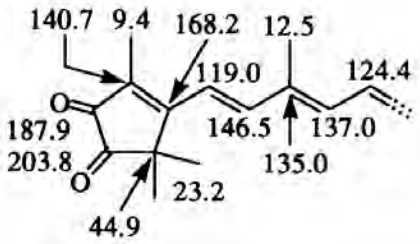
e130



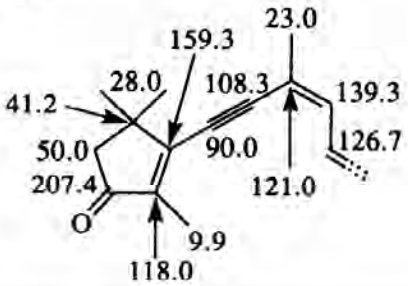
e132



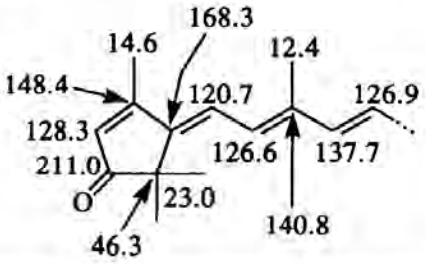
e133



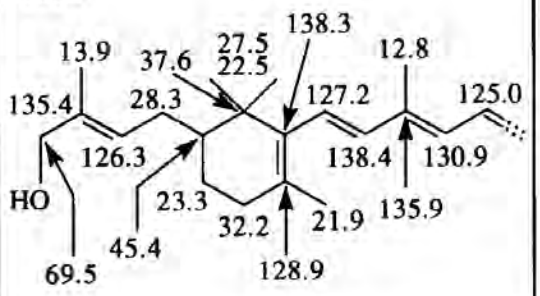
e134



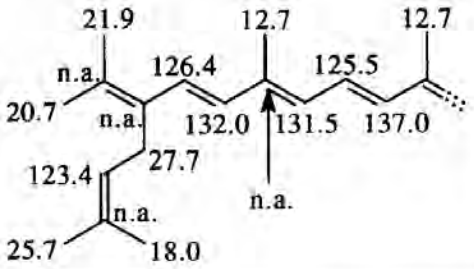
e135



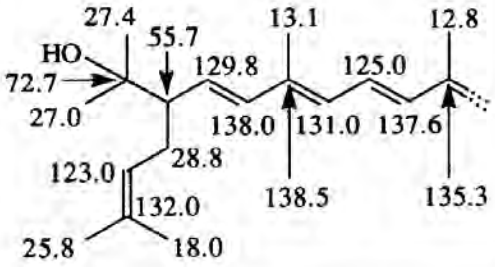
e136



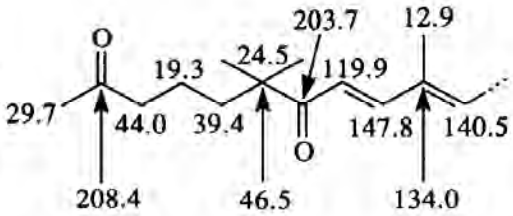
e137



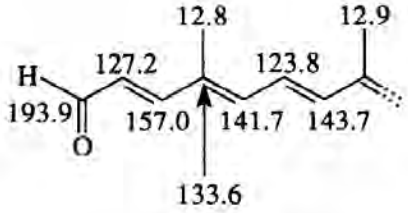
e138



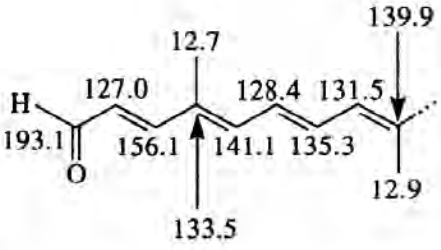
e139



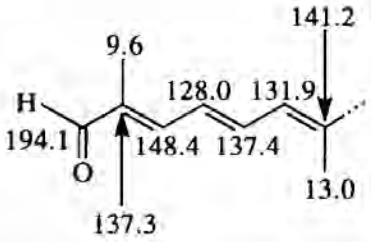
e143



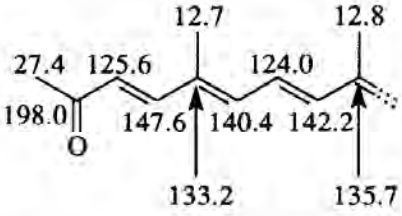
e144



e145



e146



n.a.: not assigned
[1,2] assignments may be reversed

D. Chemical Shifts and Spin Couplings of Carotenoids

In Tables 3 and 4 are presented the ^1H and ^{13}C chemical shifts of some selected symmetrical and unsymmetrical carotenoids with varying length of the conjugated chain. These data provide some supplementary information on those proton and carbon shifts which were not covered in Tables 1 and 2, *i.e.* on positions that are more distant from the end groups. Thus, it will be demonstrated that, in most cases, these shifts are only weakly dependent on the specific type of end group because of the great distance from it. Some compounds with triple bonds, carbonyl or carboxy functions have been included in order to show that, in contrast, these groups cause far-reaching chemical shift effects at other positions and that their influence has to be taken into consideration in the interpretation of spectra of related compounds. With few exceptions, all of the assignments are based on a full sequence of 1D and 2D experiments such as 1D and/or 2D NOE (ROE), double INDOR difference, homonuclear and heteronuclear 2D COSY. These methods and their efficiency will be discussed in Section F.

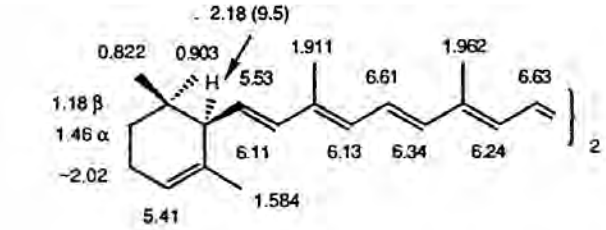
1. ^1H-NMR

One part of Table 3 is devoted to ^1H shifts of some symmetrical C_{40} carotenoids with different end groups. The remaining part deals with some unsymmetrical carotenoids of varying length of the conjugated olefinic chain and containing groups which exert a strong and far-reaching effect on the chemical shifts at other positions. Whereas the shifts reported in Table 1 in most cases actually represent average values from several related carotenoids or retinoids, the shifts in Table 3 are from direct experimental observations and hence are given to 3 decimal digits in the case of sharp singlets, and to 2 digits in all other cases. Again, only a few relevant couplings have been included (in Hz, in brackets).

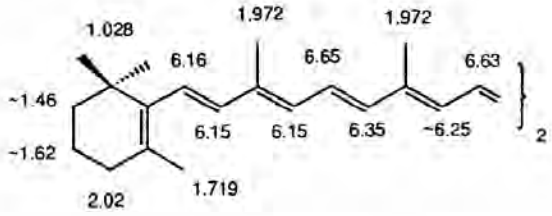
The spectra of symmetrical C_{40} carotenoids are, in general, readily interpreted since the number of signals is smaller and hence the problem of overlapping signals is reduced. For these simple cases an attempt will be made to describe first the different multiplet patterns that are observed in a typical experimental spectrum. This will help later in the discussion of more complex cases where additional information must usually be extracted by application of a number of 1D and 2D techniques.

The procedure for assignment of the different protons of a carotenoid begins advantageously with a search in the expanded spectrum for the multiplets of the different quasi-isolated 2-spin, 3-spin and 4-spin sub-systems, namely of H(7) and H(8), of H(10), H(11) and H(12) (and symmetry-related positions), and of H(14), H(15), H(15') and H(14'), respectively. They can be treated to a good approximation as being isolated since only very small and unresolved couplings are active between the protons of different sub-systems. However, their linkage and hence their relative sequence can be determined in more complex cases by homonuclear 2D COSY from weak cross peaks, caused by these small couplings (see Section F.1.e). A further possibility is to link the different sub-systems by NOE experiments or from cross peaks in the $^1H,^{13}C$-COSY tuned to multiple-bond $^{2,3}J_{CH}$ couplings over two and three bonds (see Section F.2.d).

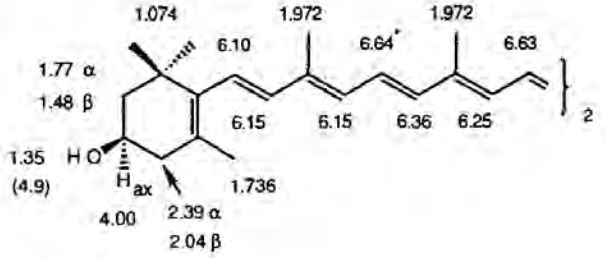
Table 3. ^{1}H-NMR shifts of some selected carotenoids (solvent $CDCl_3$).



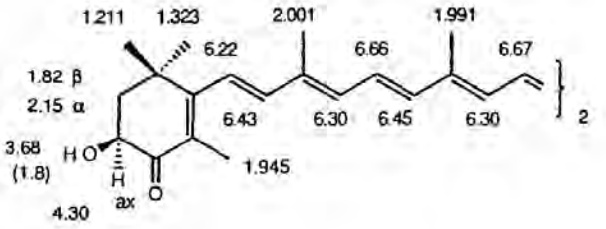
(20)



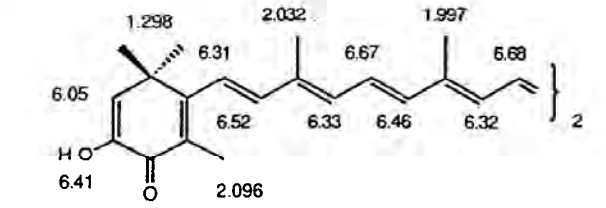
(3)



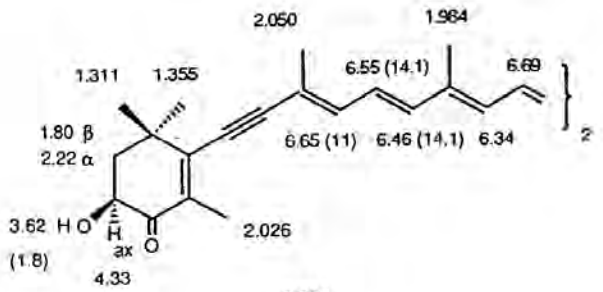
(119)



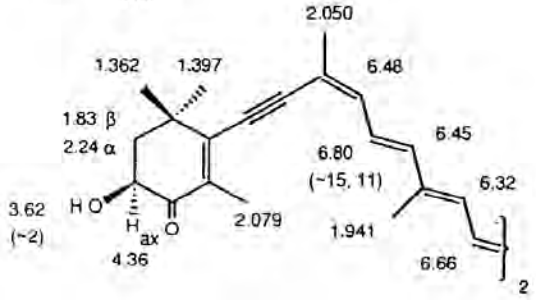
(406)



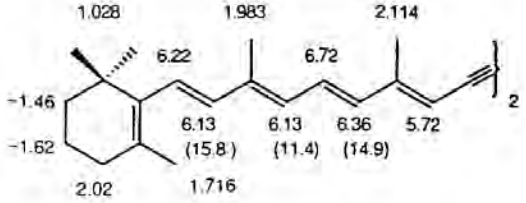
(398)



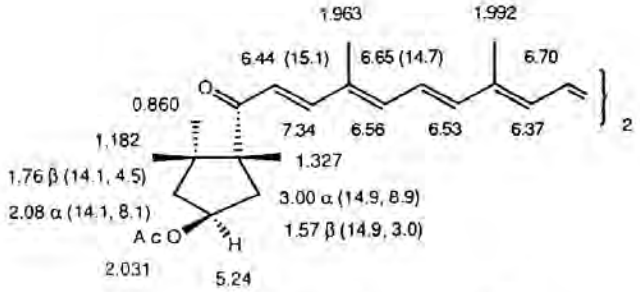
(400)



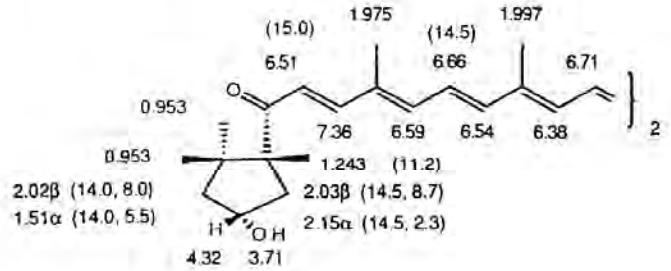
(400, 9Z)



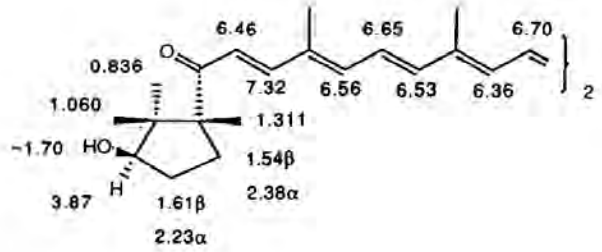
(2)



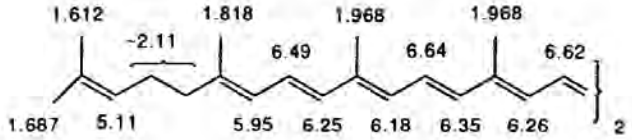
(413, Ac)



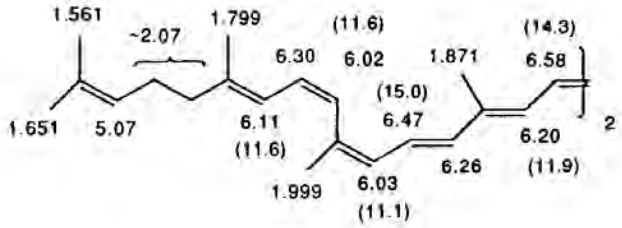
(3)


6.46
6.65
6.70
O
0.836
7.32
6.56
6.53
6.36
2
1.060
1.311
~1.70
HO
1.54β
H
3.87
1.61β
2.38α
2.23α

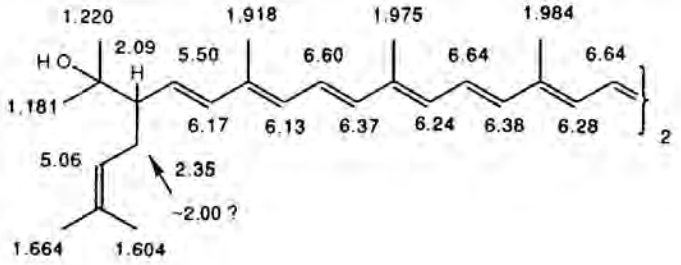
(4)


1.612
1.818
1.968
1.968
~2.11
6.49
6.64
6.62
1.687
5.11
5.95
6.25
6.18
6.35
6.26
2

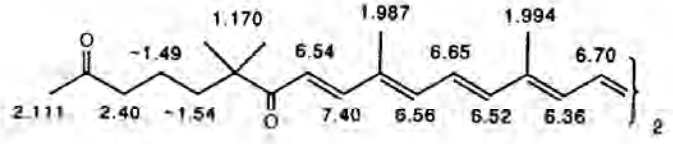
(31)


1.561
1.799
(11.6)
(14.3)
~2.07
6.30
6.02
1.871
6.58
(15.0)
6.47
1.651
5.07
6.11
(11.6)
6.20
2
6.26
(11.9)
1.999
6.03
(11.1)

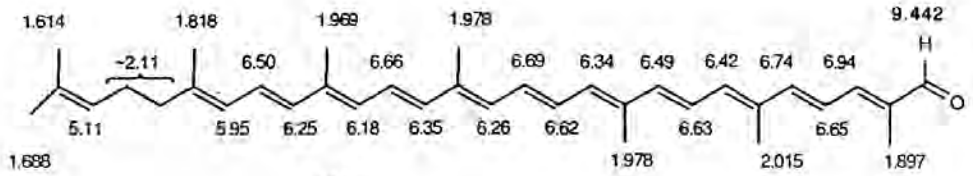
(5)


1.220
1.918
1.975
1.984
2.09
5.50
6.60
6.64
6.64
HO
H
1.181
6.17
6.13
6.37
6.24
6.38
6.28
2
5.06
2.35
~2.00 ?
1.664
1.604

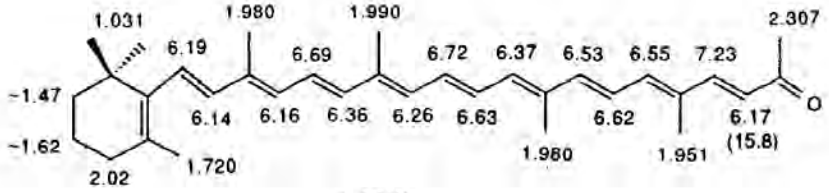
(453)


1.170
1.987
1.994
O
~1.49
6.54
6.65
6.70
2.111
2.40
~1.54
O
7.40
6.56
6.52
6.36
2

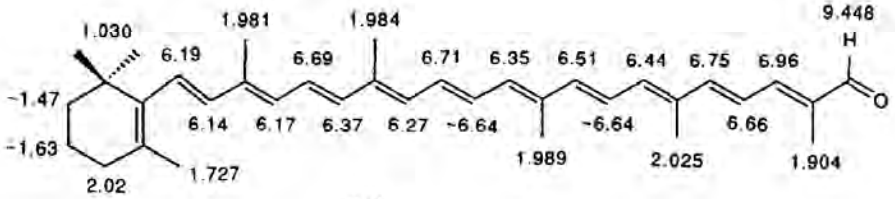
(562)



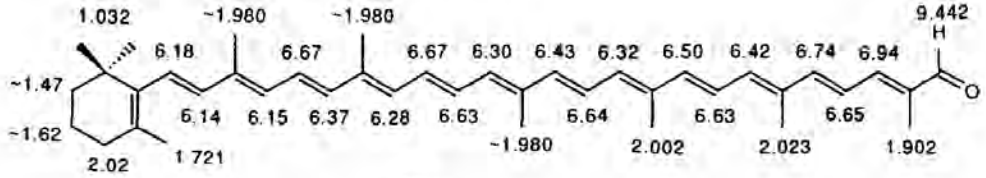
(6)



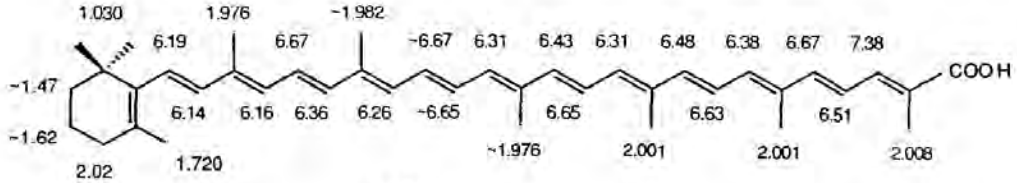
(466)



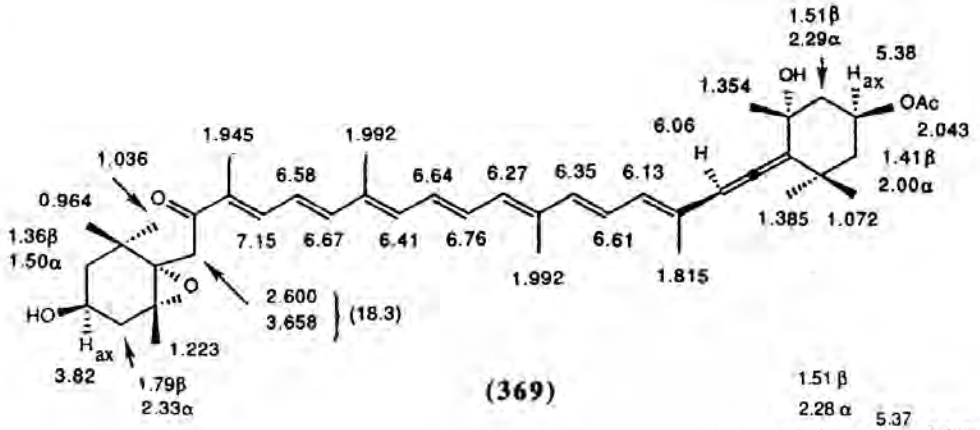
(7)



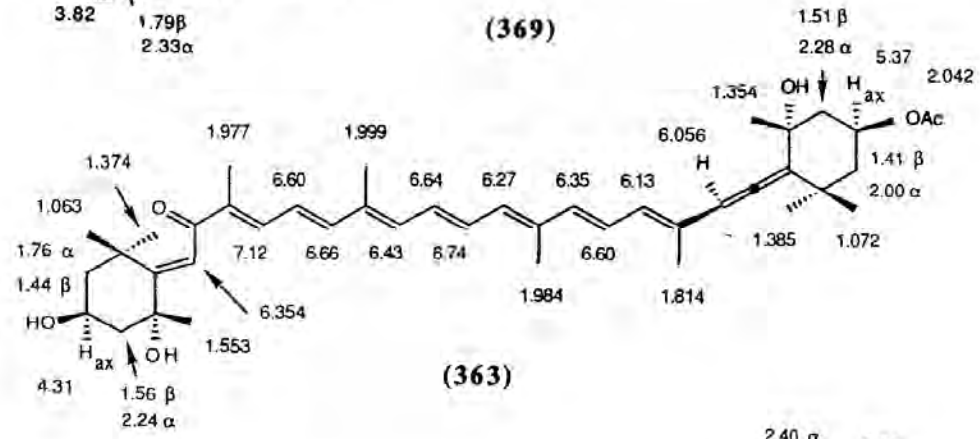
(271)



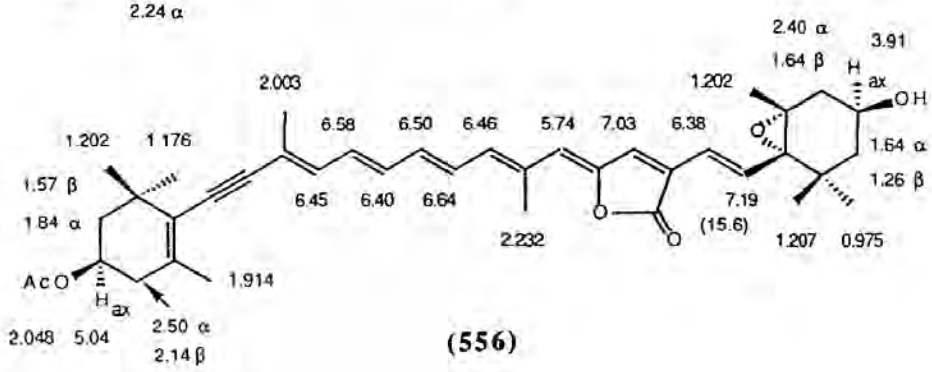
(428)


1.51β
2.29α
5.38
1.354
OH
Hax
OAc
2.043
1.41β
2.00α
6.06
H
1.385
1.072
1.945
1.992
1.036
6.58
6.64
6.27
6.35
6.13
0.964
O
7.15
6.67
6.41
6.76
6.61
1.36β
1.50α
1.992
1.815
2.600
3.658
(18.3)
HO
Hax
1.223
3.82
1.79β
2.33α

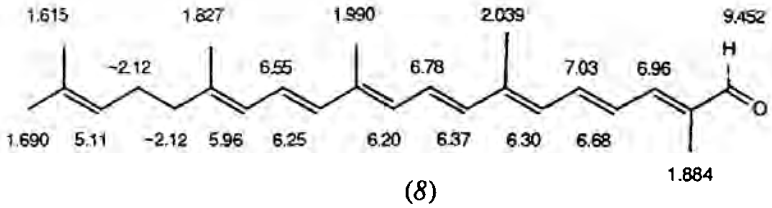
(369)


1.51 β
2.28 α
5.37
2.042
1.354
OH
Hax
OAc
1.41 β
2.00 α
6.056
H
1.385
1.072
1.977
1.999
1.374
6.60
6.64
6.27
6.35
6.13
1.063
O
7.12
6.66
6.43
6.74
6.60
1.76 α
1.44 β
1.984
1.814
6.354
HO
Hax
OH
1.553
4.31
1.56 β
2.24 α

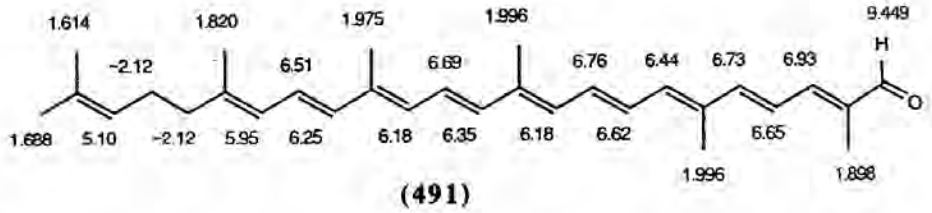
(363)


2.40 α
1.64 β
3.91
H
ax
OH
1.202
2.003
6.58
6.50
6.46
5.74
7.03
6.38
1.202
1.176
1.64 α
1.26 β
1.57 β
1.84 α
6.45
6.40
6.64
7.19
(15.6)
2.232
1.207
0.975
AcO
Hax
1.914
2.048
5.04
2.50 α
2.14 β

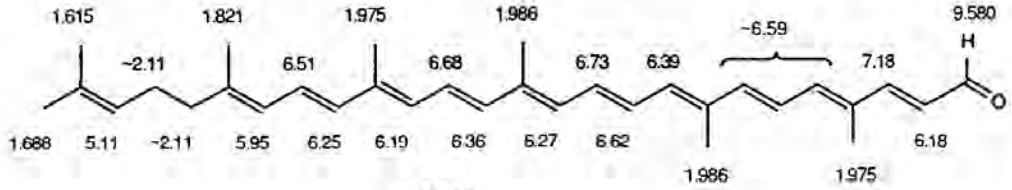
(556)


1.615
1.827
1.990
2.039
9.452
H
-2.12
6.55
6.78
7.03
6.96
O
1.690
5.11
-2.12
5.96
6.25
6.20
6.37
6.30
6.68
1.884

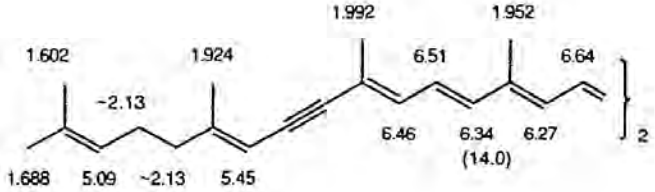
(*8*)



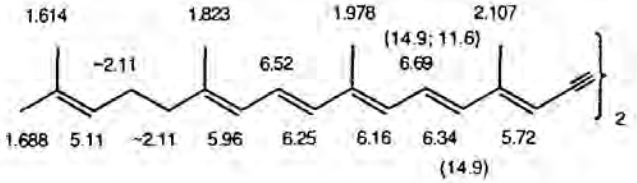
(491)



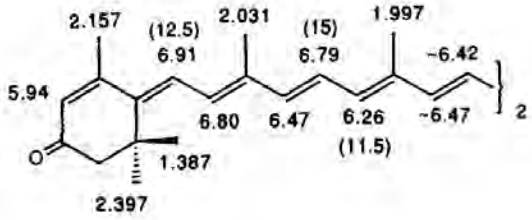
(471)



(9)



(10)



(424)

Normally, the 2-spin system of H(7) and H(8) is readily identified as an AB-type spectrum near the high-field edge of the olefinic range (see Tables 1 and 3) with $J_{7,8}$ of 15.2 to 16.8 Hz, depending on the type of end group. This value is, in general, distinctly greater than that of other *trans* couplings which are normally between 14 and 15 Hz.

In compounds with a β end group, the doublet of H(7) can readily be distinguished from that of H(8) by its larger line width which is caused by unresolved couplings of H(7) to H(18) and H(4). In the spectrum shown in Fig. 1 only the outer lines of the AB-type four-line spectrum of H(7) and H(8) are seen near 6.2 and 6.1 ppm, free from other overlapping signals. Here, the unresolved coupling of H(7) is clearly evident from the larger line width and hence the lower peak height of the low-field component of the H(7) doublet compared to the high-field component of the doublet of H(8). In Fig. 2, the broader doublet of H(7) is distinguished at higher field than that of H(8).

In compounds that possess an ε end group, on the other hand, the signal of H(7) is split by a *trans* coupling of *ca.* 15.4 Hz to H(8) and an additional coupling to H(6) of 9.5 Hz. Therefore, its signal is seen as a doublet of doublets. In other cases, *e.g.* **413** acetate, *3*, *4*, **562** and **424**, the differentiation between H(7) and H(8) is not straightforward and may have to rely on a comparison with related compounds, on NOE measurements [3], or on the observation of cross peaks in the $^{1}H,^{13}C$-COSY spectrum caused by three-bond couplings $^{3}J_{CH}$ such as that between H(19) and C(8).

Due to the general fact that H(11) always absorbs at relatively low field compared to its spin-coupled neighbours, *i.e.* around 6.6 ppm (see Table 3, and Figs. 1, 2 and 7), the chemical shift difference between H(11) and H(10), as well as that between H(11) and H(12), is often much larger than their vicinal couplings [($\Delta\upsilon \gg J$, (weak coupling case; $J_{10,11} \sim 11.3$, $J_{11,12} \sim 14.8$ Hz)]. Hence, this 3-spin sub-spectrum can normally be subjected to a simple first-order interpretation, *i.e.* good estimates for the coupling constants can be derived directly from the observed splittings. Thus, this 3-spin partial spectrum can be readily identified in most cases as doublet [H(10)], doublet of doublets [H(11)], and doublet [H(12)], with the above-mentioned splittings. In a similar manner to that of H(7), the doublet of H(10) is significantly broadened by the normally unresolved coupling of *ca.* 1.4 Hz to the three methyl protons H(19).

Much more difficulty arises when the remaining 4-spin spectrum of protons H(15,15') and H(14,14') has to be identified and analysed in symmetrical carotenoids, since the former protons absorb near 6.6 ppm, an often crowded region (see Figs. 1 and 2). Moreover, in contrast to the 2-spin and 3-spin systems treated above, the spectral parameters of the 4-spin system (particularly the different coupling constants) cannot readily be obtained from the experimentally determined spectrum. This is demonstrated in the lower part of Fig. 7, which shows the olefinic range of the 400 MHz ^{1}H-NMR spectrum of prolycopene (7,9,7',9'-tetra-*cis* lycopene; *5*). The assignments of the different proton signals and the derivation of the structure were mainly based on NOE experiments [15, 16] and this structure was later confirmed by chemical synthesis [17]. This compound has been chosen here since it represents one of the rare cases where the two multiplets of these protons are seen virtually free from other overlapping signals.

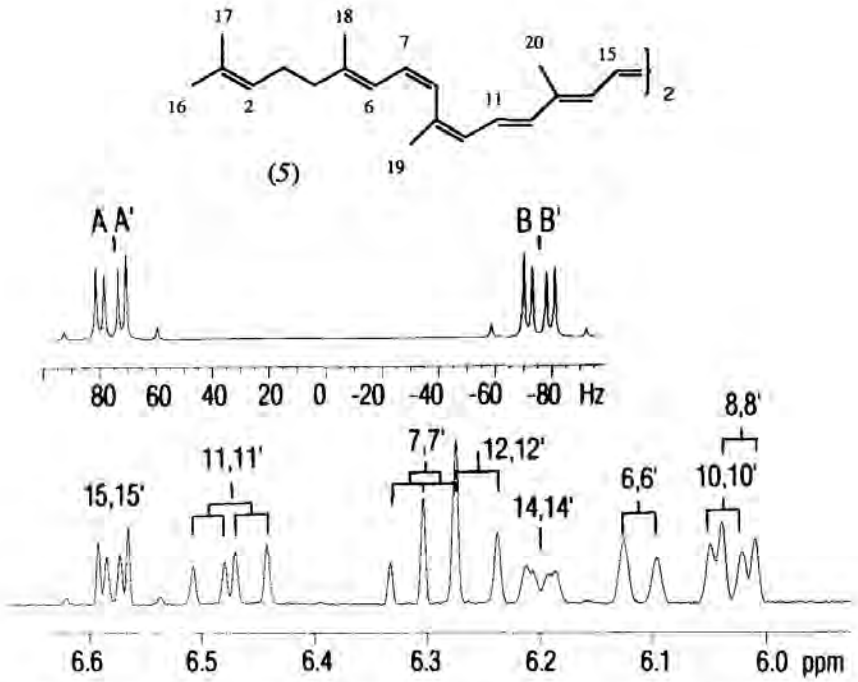


Fig. 7. Olefinic range of the 400 MHz ^{1}H-NMR spectrum of prolycopene (*5* in $CDCl_3$; bottom) and theoretical AA'BB' spectrum (top) of H(15,15') and H(14,14') calculated with a chemical shift difference of 0.381 ppm (152.5 Hz) and the coupling constants $J_{14,15} = J_{14',15'} = 11.85$, $J_{15,15'} = 14.28$, $J_{14,15'} = J_{15,14'} = -1.02$, and $J_{14,14'} = 0.02$ Hz. A line-width of 0.8 Hz for the individual superimposed Lorentzian components was assumed.

In Fig. 7 the signals of H(15,15') and H(14,14') were assigned as symmetrical multiplets at 6.580 and 6.199 ppm, respectively. In NMR textbooks such a 4-spin system is commonly denoted as an AA'XX'-type spectrum. This means that protons A,A' [H(15,15')] and X,X' [H(14,14')] have pairwise identical chemical shifts (with $\Delta\nu(AX) \gg$ all Js), but are said to be magnetically non-equivalent since they have different couplings to either proton of the other pair ($J_{14,15} \neq J_{14,15'}$). This leads to some complications when the couplings have to be extracted from the experimental spectrum. In order to demonstrate the general appearance of this type of spectrum, the upper part of Fig. 7 shows a theoretical 4-spin spectrum which was calculated with the aid of the Bruker NMR simulation program PANIC. This program can be run on the ASPECT 3000 computer of the spectrometer.

In a first step an approximate theoretical spectrum, *i.e.* one containing the frequencies and intensities of the different transitions, was calculated from reasonable starting values for the chemical shifts and the coupling constants. The result was plotted as a superimposition of individual Lorentzian-shaped lines for all the calculated transitions. Here, the individual line width was assumed to be 0.8 Hz in good agreement with the experimental spectrum. After assignment of the experimental to the theoretically calculated transitions, the starting parameters

were improved by iteration until the experimental and theoretical spectra were thought to be identical. This resulted in the theoretical 4-spin spectrum of Fig. 7 (top) obtained from the final coupling constants given in the legend. Here in this final step, the AA'XX' approximation was discarded in favour of the more accurate AA'BB' treatment. In this actual case, the difference between the AA'XX' and AA'BB' treatment is rather small and only visible as a slight decrease in the intensities of the outer parts of the two multiplets (so-called roof effect). As expected, the calculated *trans* coupling $J_{15,15'}$ of 14.3 Hz is relatively small in the central part of the conjugated chain, whereas the coupling across the single bonds is relatively large (11.9 Hz). This seems to be a general trend, as will be discussed below. The remaining coupling constants were $J_{14,15'} = J_{15,14'} = -1.02$, and $J_{14,14'} = 0.02$ Hz.

An AA'BB' sub-spectrum is strictly symmetrical with respect to the common centre of gravity (here at 6.389 ppm) of the two AA' and BB' multiplets. In the experimental spectrum, the half spectrum of H(14,14') is, however, additionally broadened mainly by unresolved coupling ($J \sim 1.4$ Hz) to methyl protons H(20,20'), a fact which immediately allows the assignment of the otherwise indistinguishable two multiplets. The relative order of the two related multiplets is reversed in 15-*cis* carotenoids and this allows a facile recognition of this stereomutation without the need of a spectral simulation (see Section E.1).

The chemical shifts of protons H(15,15') and H(14,14') are taken at the centres of the two approximately symmetrical multiplets. It was shown more than 30 years ago [18] that, in principle, all the coupling constants can be obtained directly as sums or differences from the experimental splittings within the two identical multiplets. Here, and in related carotenoids, this task is, however, considerably hampered by the fact that each of the two half spectra actually consists of 12 transitions (instead of 6 superimpositions as shown in Fig. 7) which are pairwise too close to each other to be resolved experimentally. Moreover, the weak lines at either side of the two multiplets are often difficult to detect in a typical spectrum (see Figs. 1 and 2) and they are needed for the calculation of $J_{15,15'}$ [18].

A further cause of line-broadening, namely the existence of several unresolved long-range couplings (see Section F.1.e), also contributes to the observed line width and hence to the reduced accuracy of the spectral simulation. This fact is supported by the general observation that, in the experimental spectra of carotenoids, even under optimum experimental conditions, the residual line width of olefinic signals is often of the order of 1 Hz, *i.e.* much larger than that of other signals such as that of the reference compound tetramethylsilane, TMS. For all these reasons it is estimated that the given values for the calculated couplings may be in error by up to ± 0.2 Hz. In order to simplify the recognition of this type of AA'XX' or AA'BB' spectrum, in practical applications the approximate distances in Hz in each half spectrum of *trans* carotenoids are specified as follows: between 1st and 6th line *ca.* 34 Hz, between 2nd and 5th *ca.* 11 Hz, between 3rd and 4th *ca.* 5 Hz.

It is evident that, in compounds with distorted symmetry (as in 13-*cis* carotenoids or in compounds with a strongly anisotropic end group), the equivalency of H(15) and H(15') may no longer hold and their spectra can be used to determine typical values of the corresponding coupling constants in a more facile way.

The other couplings measured in the spectrum of prolycopene were $J_{6,7} = 11.6$, $J_{7,8} = 11.6$, a typical value for a *cis* double bond, $J_{10,11} = 11.1$, and $J_{11,12} = 15.0$ Hz. All these

values were obtained by simple first-order interpretation from the measured splittings and are thought to be accurate within ± 0.2 Hz.

As a generalization, based on the interpretation of numerous spectra of carotenoids, it can be expected that vicinal coupling constants across *trans* double bonds have values between about 13.5 and 16.8 Hz with the tendency to decrease towards the central part of the conjugated chain. This decrease is explained by the assumption that the conjugation and hence partial delocalization of the π electrons is slightly stronger near the central part. The possible physical causes and their relative influence on the variation of the values of the coupling constants in β,β-carotene (**3**) and some geometrical isomers have been discussed in detail [19].

Relatively small values for the vicinal *trans* coupling constants were in some cases observed near the triple bond of didehydrocarotenoids. Thus, a small value of only 14.1 Hz was measured for $J_{11,12}$ in all-*E*-7,8,7',8'-tetradehydroastaxanthin (**400**). Interestingly, a regular value near 15 Hz was found in the 9,9'-di-*cis* isomer of (**400**) and in 15,15'-didehydro-β,β-carotene (*2*). Correspondingly, in 7,8,7',8'-tetradehydrolycopene (*9*) the coupling $J_{11,12} = J_{11',12'}$ was 14.0 Hz, whereas a regular value of 14.9 Hz was found in 15,15'-didehydrolycopene (*10*). The smallest coupling of this type observed so far was $J_{11,12}$ = 13.5 Hz in 7,8-didehydrolycopene.

The couplings across single bonds are normally between 10.5 and 12 Hz with the larger values often near the central part of the molecule ($J_{14,15}$=11.9 Hz in prolycopene). Typical couplings across *cis* double bonds are between 11.5 and 12.8 Hz, *i.e.* the *trans* and *cis* ranges obviously do not overlap. Some couplings in 7-*cis* carotenoids are presented in Table 1.

The data of Table 3 show that, in addition to H(11), H(15) also absorbs relatively downfield. In a simple intuitive picture, this extra deshielding of the two types of protons can be explained by the assumption that it is caused by strong steric interaction of their electron clouds with those of H(19) and H(20) of the methyl groups at positions 9 and 13. This view was previously supported by the observation that, in 9-demethyl and 13-demethyl derivatives of some compounds related to vitamin A, the signal of H(11) was shifted upfield [1]. It is known from crystal structures of carotenoids, determined by X-ray diffraction, that hydrogens H(7) and H(11) must indeed have very strong steric interactions with the methyl hydrogens and these interactions are known even to cause a slight curvature of the olefinic chain in its plane. In a very simple intuitive picture, the resulting steric compression causes a small displacement of the interacting electron clouds and hence an additional polarization of the C–H bond, thus slightly decreasing the shielding of the protons involved. In agreement with this explanation is the observation that, in *cis* isomers, any relief of this interaction actually results in an upfield shift of the corresponding proton signals (see Section E.1). In this connection it is interesting to note that the resulting downfield shift of a proton signal is virtually always accompanied by an upfield shift of the signal of the attached carbon-13 nucleus. According to this simple picture this shift reversal is obviously caused by a slight shift of the electron cloud from the proton to the carbon, thus enhancing the shielding of the latter.

Table 3 also contains data for a number of unsymmetrical carotenoids including some apocarotenoids of different chain lengths. The procedure of assignment in these more complex spectra, with the aid of modern pulse techniques, will be demonstrated later. The data for compounds *6*, **466**, *7*, **271**, **428**, **369**, **363**, **556**, *8*, **491** and **471** indicate that the presence

of a carbonyl (or related) group produces very far-reaching effects on the chemical shifts of the olefinic protons. The main effect is thought to arise by participation of mesomeric resonance structures with shifted double bonds and with negatively charged oxygen and positively charged carbons at the alternate β, δ, ζ *etc.* positions. According to this simple picture, an alternating distribution of the electron density at subsequent carbons is present which also affects the charge density at the attached protons in the same way. This explains why the signals of protons at the α, γ, ε *etc.* positions, with slightly enhanced electron density, are at relatively high field, whereas those at the β, δ, ζ *etc.* positions, with decreased electron density, are shifted downfield. This effect is attenuated with increasing number of intervening bonds but it is still clearly effective at positions that are five or more double bonds away. Thus, in compounds *6*, **466**, *7*, **271**, **428**, *8*, **491** and **471**, for example, H(15) and H(15') are differently shielded and only after seven intervening double bonds, as in compounds **271** and **428**, is this difference reduced to a small value, *i.e.* this effect is indeed very far-reaching. Moreover, carbonyl and related groups are also known to exert a direct, through-space effect on the chemical shifts of neighbouring protons due to the fact that these groups (as well as others such as the triple bond and the phenyl ring) possess a strong anisotropy of the diamagnetic susceptibility. This means that, under the influence of the strong external magnetic field, a diamagnetic flow of electrons is induced, thus producing a local magnetic dipolar field. This exerts a small extra magnetic field at the site of neighbouring protons, depending on the distance r (proportional to $1/r^3$) and the relative orientation of anisotropic group and affected proton. This local through-space contribution is not averaged to zero by the molecular tumbling motion. The net effect is a downfield shift of protons in the C–C=O plane and an upfield shift in the spatial zone above or below it. This simple model will be used in the interpretation of some shifts of the end group of capsorubin (**413**) diacetate (Section F.1.c).

In olefinic systems, the qualitative dissection of the observed effects into individual contributions of the mesomeric effect and of the anisotropy effect is hardly possible. However, with **556** it is assumed that the anisotropy effect of the cross-conjugated carboxy group is responsible for the strong deshielding of H(7'). Also mainly caused by the anisotropy effect of the carbonyl function at position 6 of capsorubin (and related compounds) are some unusual shifts of protons of the end group, as will be discussed later.

A completely analogous diamagnetic anisotropy effect is operative in the close vicinity of a phenyl ring. The extra shift caused by the triple bond at neighbouring positions is probably caused mainly by through-space anisotropy effects. The latter are known to result in an upfield shift within a spatial cone parallel to the bond axis and a downfield shift in a spatial cone perpendicular to this axis. In agreement with this naive picture is the downfield shift of H(11) for the 9-*cis* isomer compared to all-*trans*-**400**. It is obvious that the through-space downfield effect in the 9-*cis* isomer overcompensates for the expected upfield shift that is due to the reduction of steric interactions between H(11) and H(19). Comparison of the shifts of H(14) between compounds *2* and *3* or *10* and **31** and that of H(6) in compounds *9* and **31** indicates a strong upfield shift of *ca.* –0.5 ppm at the α position to the triple bond.

This qualitative discussion clearly demonstrates that these sometimes very far-reaching shift effects have to be taken into account when the data of Tables 1 and 3 are combined in order to

predict the shifts of unknown carotenoids. Similar strong effects are also found in ^{13}C-NMR, as will be seen in Section D.2.

Conversely, it is evident that the presence of these groups can readily be detected by their very strong shift effects at neighbouring positions. Moreover, these effects are particularly conclusive in the structure elucidation of geometrical isomers (see Tables 3, 4, 5 and 6).

Additional carotenoids chosen for Table 3 are (3*S*,5*R*,3'*S*,5'*R*)-capsorubin (**413**) diacetate, (3*R*,5*R*,3'*R*,5'*R*)-epicapsorubin (*3*), (2*R*,5*R*,2'*R*,5'*R*)-isocapsorubin (*4*) [20], fucoxanthin (**369**) [21], isofucoxanthin (**363**) [22], and pyrrhoxanthin (**556**) [23], and further chemical shift data for related compounds are given in these references. Other chemical shift data from the general literature, often with only partial assignments, are accessible *via* reference [24].

Finally, most of the generalizations on chemical shifts and coupling constants discussed so far, as expected, do not apply to *retro*-carotenoids in which the positions of the double bonds are shifted. An example, all-*trans*-rhodoxanthin (**424**), is, therefore, included in Table 3. In the *retro*-carotenoids the signals of H(8) and H(12) are significantly broadened by allylic coupling [instead of H(10) and H(14)] and the shifts of H(14,14') and H(15,15') are almost identical. These compounds are often isolated as a mixture of geometrical isomers with the all-*trans* as the main component and minor amounts of the 6-*cis* and 6,6'-di-*cis* isomers [25, 26]. The ^{1}H-NMR data of eschscholtzxanthin (**180**) and its diacetate, of *retro*dehydrocarotene (**48**), and a number of smaller *retro* compounds, have been presented and partly assigned [25]. The chromatographic separation of 6-*cis*-, 6,6'-di-*cis*-, and all-*trans*- rhodoxanthin (**424**) and their ^{1}H- and ^{13}C-NMR data have been discussed [26].

2. ^{13}C-NMR

In Table 4 are collected ^{13}C-NMR chemical shifts of 38 carotenoids. These data supplement those of Table 2 and they should also give an overview of the expected shift ranges of the different carbons farther away from the end groups. Moreover, the very strong effects caused by the anisotropic groups, discussed above for ^{1}H-NMR, will become evident. All the assignments, including the stereochemical ones, are thought to be unambiguous since most were based on a full sequence of homonuclear and heteronuclear 2D experiments. The general procedure of assignment will be discussed in Section F.

Although the chemical shifts of typical routine ^{13}C spectra can be measured to $\pm$ 0.01 ppm, corresponding to a digital resolution of *ca.* 1 Hz per point, the shifts given have been rounded to the nearest 0.1 ppm. This seems to be justified by the observation that the chemical shifts of a given compound, measured several times, possibly on different instruments or in slightly different concentrations, sometimes show variations of several tenths of a ppm. Moreover, the assignment of very closely spaced signals is often difficult to perform and would not contribute, in general, any relevant structural information.

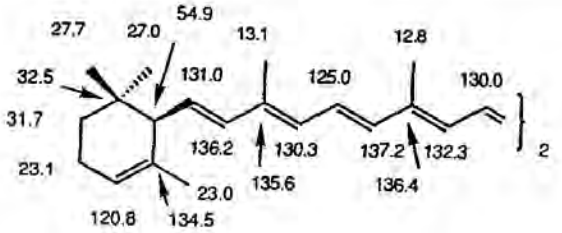
In 'regular' C_{40} carotenoids, the shifts of C(15), C(14), C(13), C(12), and even C(11) are expected to be more or less independent of the type of end group, as is seen by comparison of the data for compounds **20**, **3**, **119**, **406**, **398**, **400** (*trans* and 9-*cis*), **379** and **117**. Due to

the steric reasons discussed above, C(11) and C(15) absorb at relatively high field. Introduction of a carbonyl (or related) group at the end of or in the conjugated chain again produces very far-reaching alternating effects in the same sense as discussed for ^{1}H-NMR. This effect was observed and rationalized many years ago [27] in the ^{13}C-NMR spectra of a number of apocarotenals and this helped at that time also in assigning, by extrapolation, the ^{13}C signals of β,β-carotene (**3**) and axerophthene. From the data of Table 4 it is seen that the shift difference between carbons in the α and β positions to the carbonyl can exceed –20 ppm and that the alternating effect is again attenuated only weakly with increasing number of intervening double bonds. Even after 7 double bonds the difference can still be of the order of 1 ppm, as is observed, for example, with **271** and **428** ester for the shifts of C(15) and C(15').

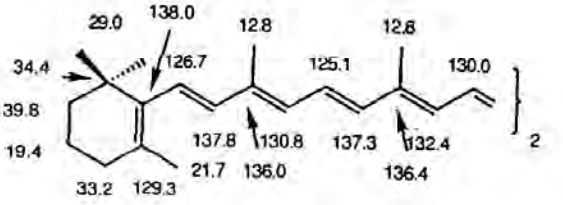
Introduction of a triple bond also leads to strong effects at the α and β positions, as is seen by comparison of the pairs of compounds **119** and **117**, **406** and **400**, or **3** and *2*. Thus the signal of the α-carbon is shifted upfield by *ca.* –16 to –20 ppm, and that of the β-carbon downfield by 4 to 10 ppm, depending on the position of the triple bond in the conjugated chain.

It is clear from this short discussion that the strong effects of these groups have to be taken into consideration when additive predictions of the chemical shifts are made by combination of the reported data of Tables 2 and 4. Further ^{13}C chemical shift data are given in the following references: *adonixanthin* (**328**), *adonirubin* (**391**) *and related compounds* [12]; *capsanthin* (**335**), capsorubin (**413**) and related compounds [20]; more than 100 retinoids and carotenoids [14, 28]; fucoxanthin (**369**) and 19'-butanoyloxyfucoxanthin (**370.2**) [21]; renierapurpurin-20-al [29]. A great number of further references covering older work, often with only partial assignments, can be found in [24].

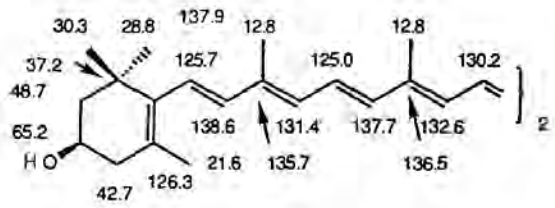
Table 4. ^{13}*C-NMR shifts of some selected carotenoids (solvent* $CDCl_3$*).*



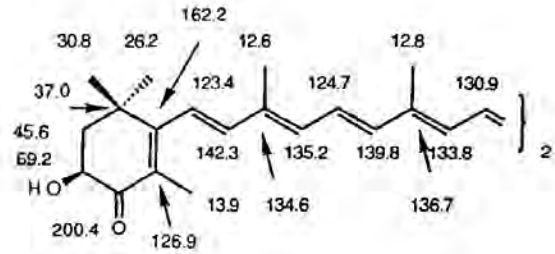
(20)



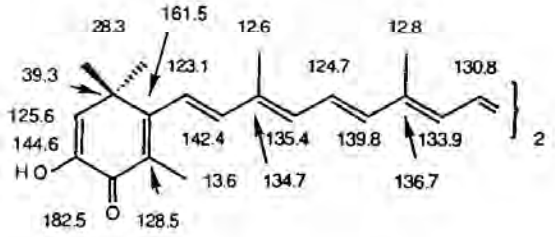
(3)



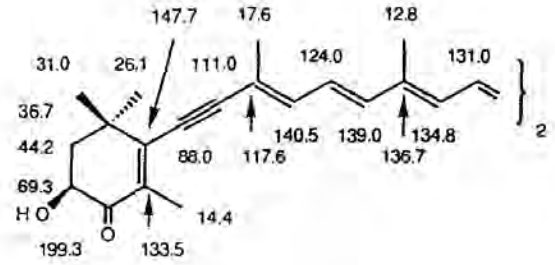
(119)



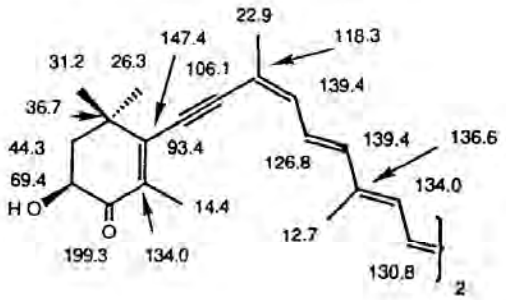
(406)



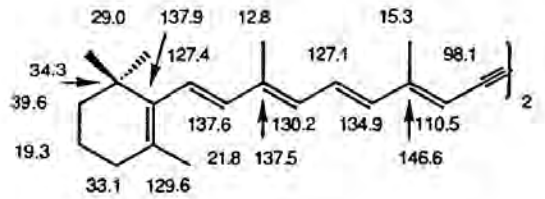
(398)



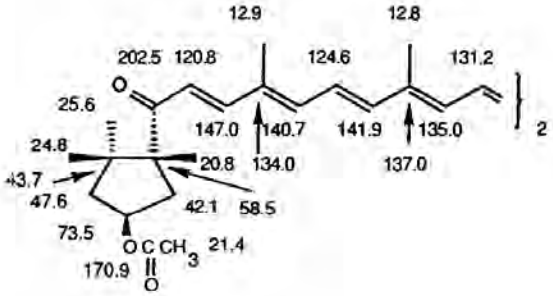
(400)



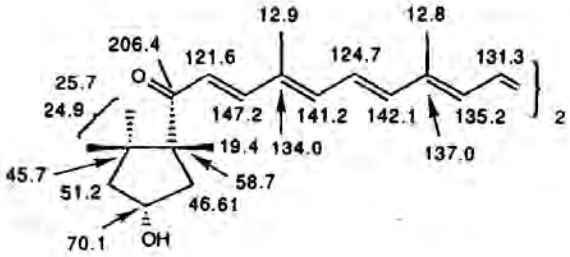
(400, 9Z)


29.0
137.9
12.8
15.3
127.4
127.1
98.1
34.3
39.6
137.6
130.2
134.9
110.5
2
19.3
21.8
137.5
146.6
33.1
129.6

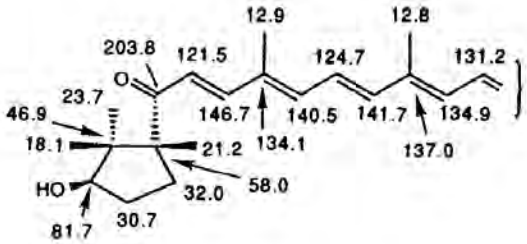
2


12.9
12.8
202.5
120.8
124.6
131.2
O
25.6
147.0
140.7
141.9
135.0
2
24.8
20.8
134.0
137.0
43.7
47.6
42.1
58.5
73.5
O C CH3
21.4
170.9
O

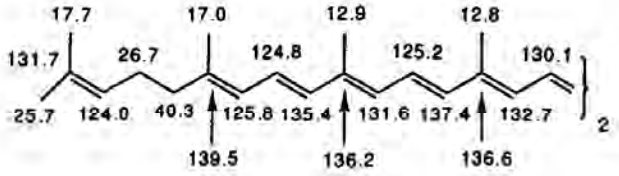
(413, Ac)


12.9
12.8
206.4
121.6
124.7
131.3
O
25.7
24.9
147.2
141.2
142.1
135.2
2
19.4
134.0
137.0
45.7
51.2
58.7
46.61
70.1
OH

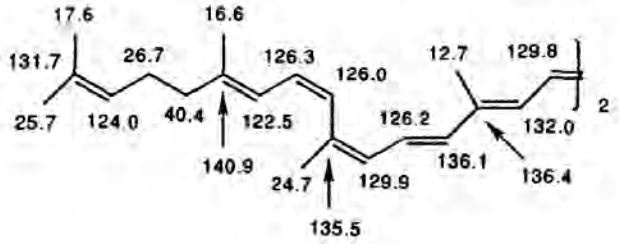
3


12.9
12.8
203.8
121.5
124.7
131.2
O
23.7
46.9
146.7
140.5
141.7
134.9
18.1
21.2
134.1
137.0
HO
32.0
58.0
81.7
30.7

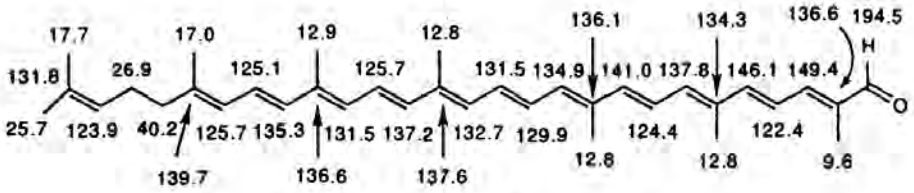
4


17.7
17.0
12.9
12.8
131.7
26.7
124.8
125.2
130.1
25.7
124.0
40.3
125.8
135.4
131.6
137.4
132.7
2
139.5
136.2
136.6

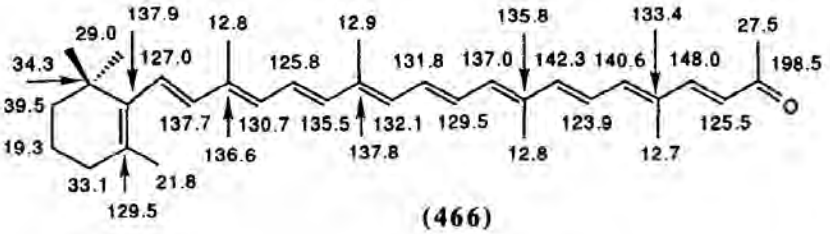
(31)


17.6
16.6
131.7
26.7
126.3
126.0
12.7
129.8
25.7
124.0
40.4
122.5
126.2
132.0
2
140.9
136.1
136.4
24.7
129.9
135.5

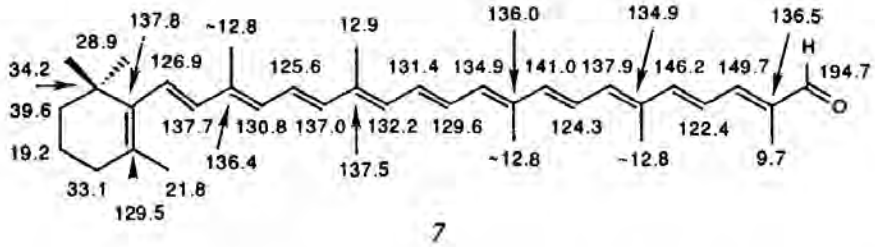
5


17.7
17.0
12.9
12.8
136.1
134.3
136.6
194.5
H
131.8
26.9
125.1
125.7
131.5
134.9
141.0
137.8
146.1
149.4
O
25.7
123.9
40.2
125.7
135.3
131.5
137.2
132.7
129.9
124.4
122.4
139.7
136.6
137.6
12.8
12.8
9.6

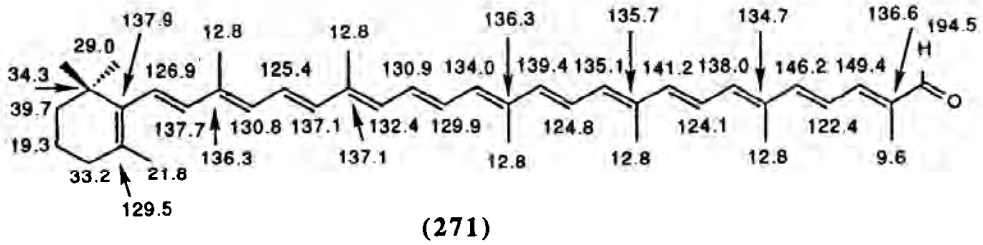
6


137.9
12.8
12.9
135.8
133.4
27.5
29.0
127.0
34.3
125.8
131.8
137.0
142.3
140.6
148.0
198.5
O
39.5
137.7
130.7
135.5
132.1
129.5
123.9
125.5
19.3
136.6
137.8
12.8
12.7
33.1
21.8
129.5

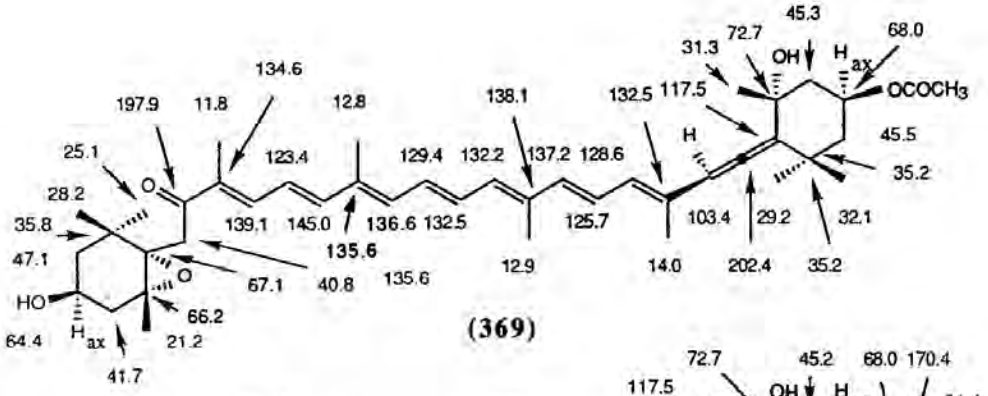
(466)


137.8
~12.8
12.9
136.0
134.9
136.5
28.9
126.9
H
34.2
125.6
131.4
134.9
141.0
137.9
146.2
149.7
194.7
O
39.6
137.7
130.8
137.0
132.2
129.6
124.3
122.4
19.2
136.4
137.5
~12.8
~12.8
9.7
33.1
21.8
129.5

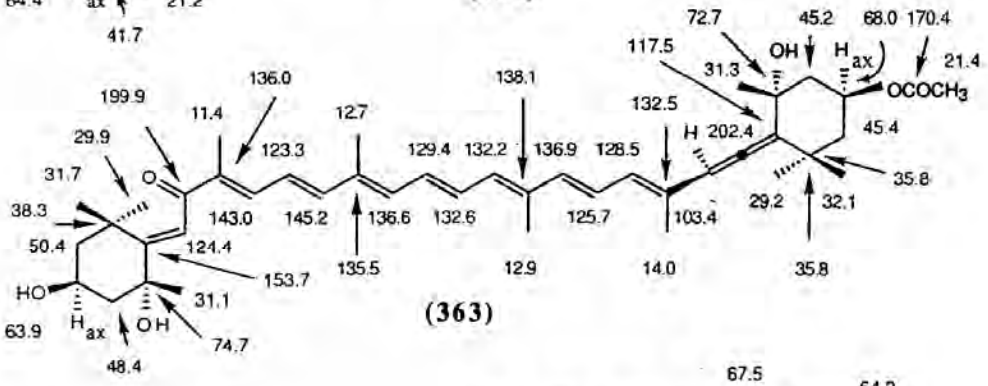
7


137.9
12.8
12.8
136.3
135.7
134.7
136.6
194.5
29.0
H
126.9
34.3
125.4
130.9
134.0
139.4
135.1
141.2
138.0
146.2
149.4
O
39.7
137.7
130.8
137.1
132.4
129.9
124.8
124.1
122.4
19.3
136.3
137.1
12.8
12.8
12.8
9.6
33.2
21.8
129.5

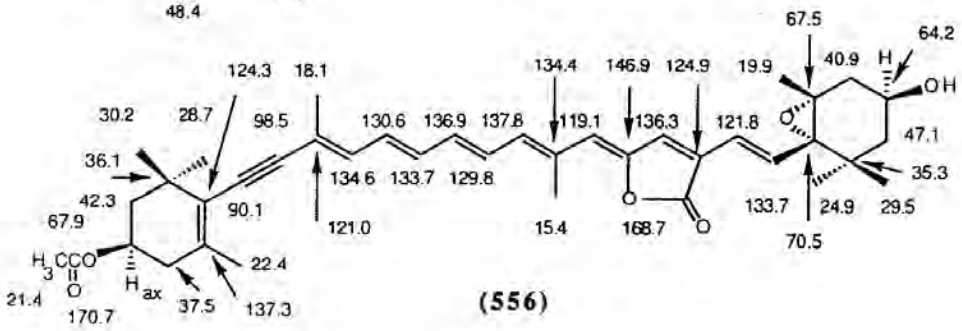
(271)



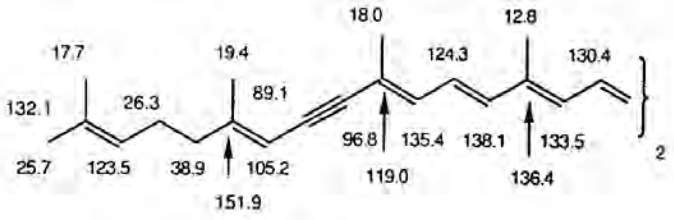
(369)



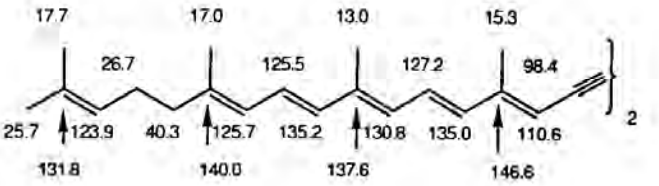
(363)



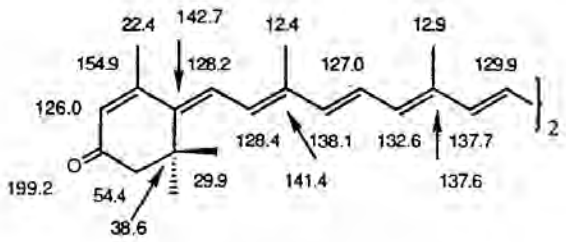
(556)



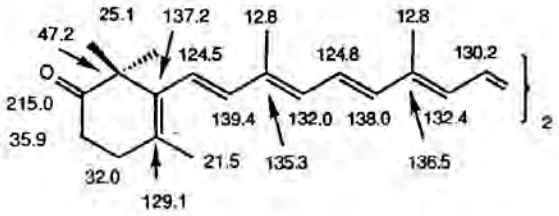
9



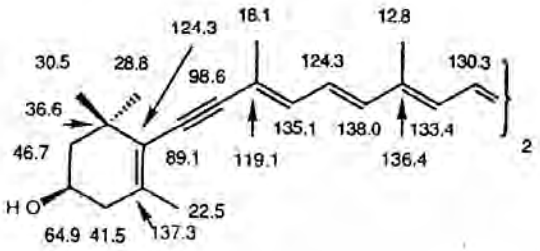
10



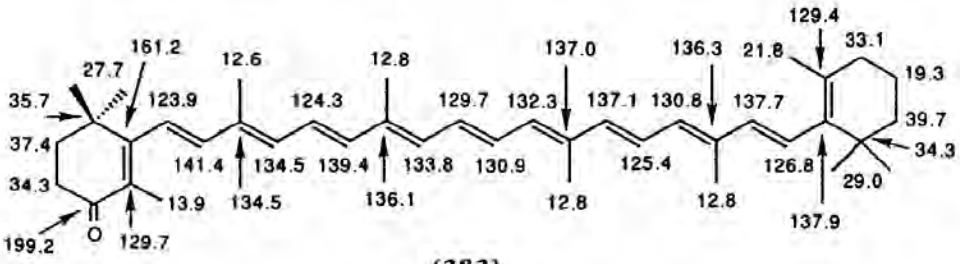
(424)



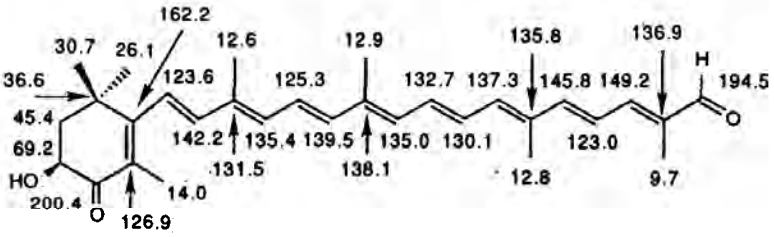
(379)



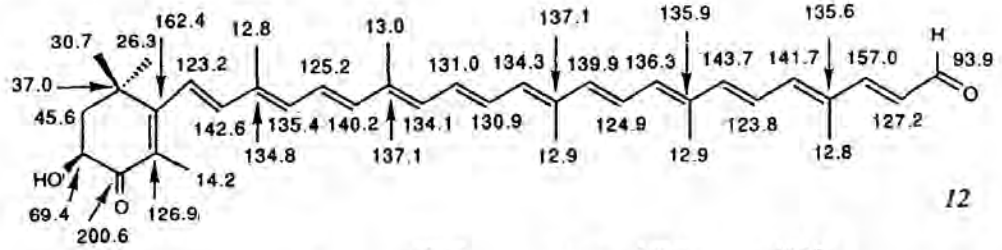
(117)



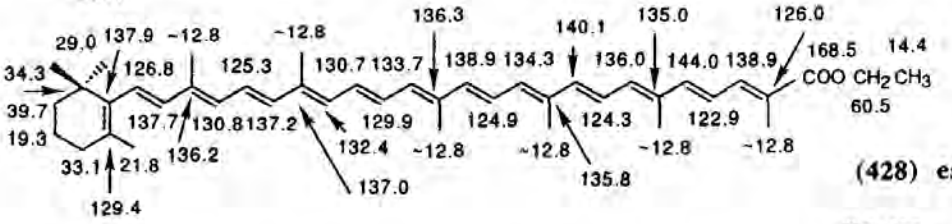
(283)



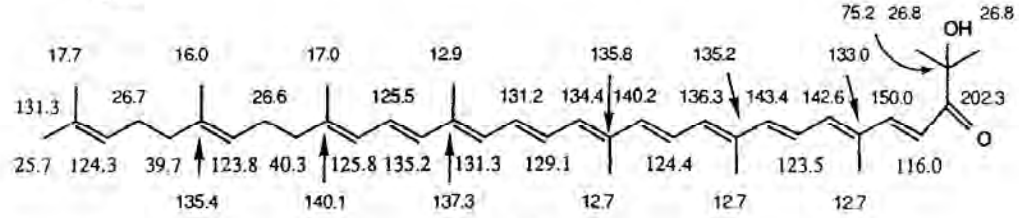
11



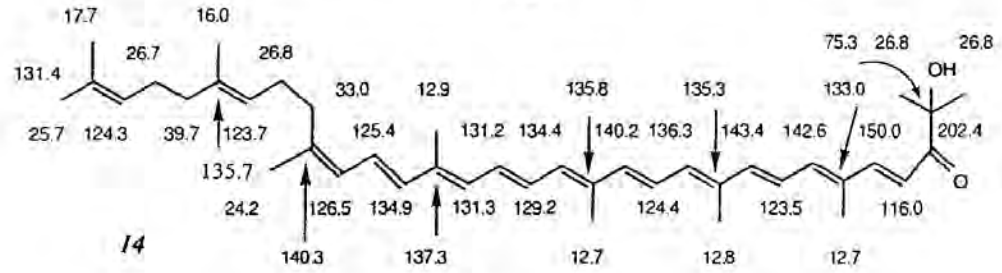
12



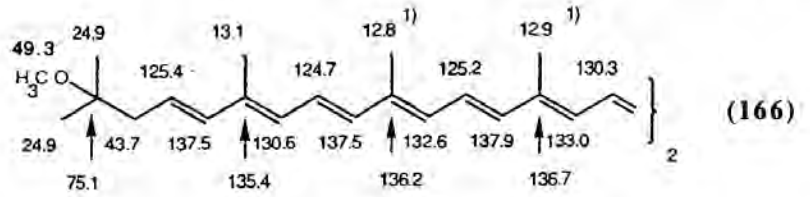
(428) ester



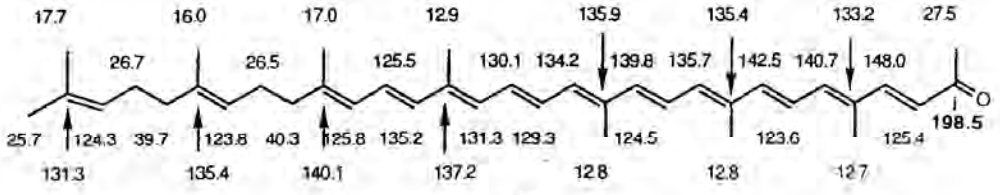
13



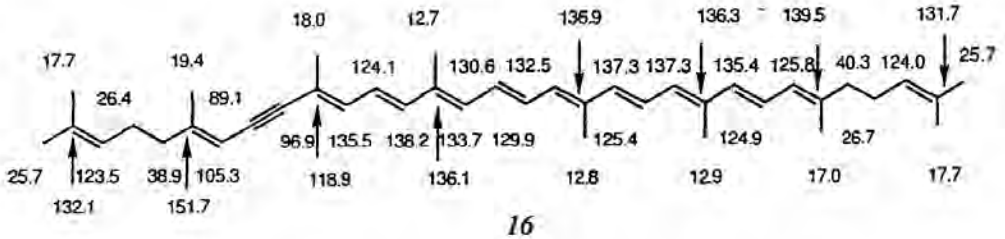
14



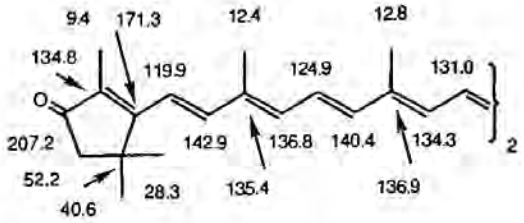
(166)



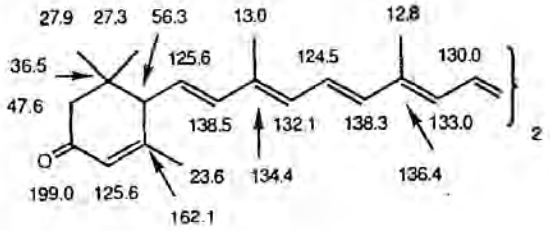
15



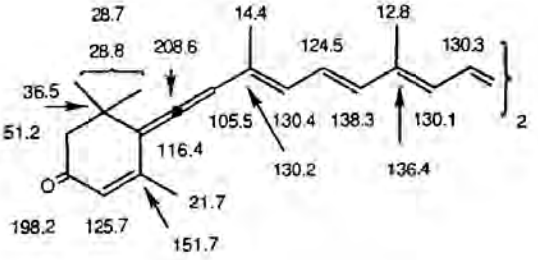
16



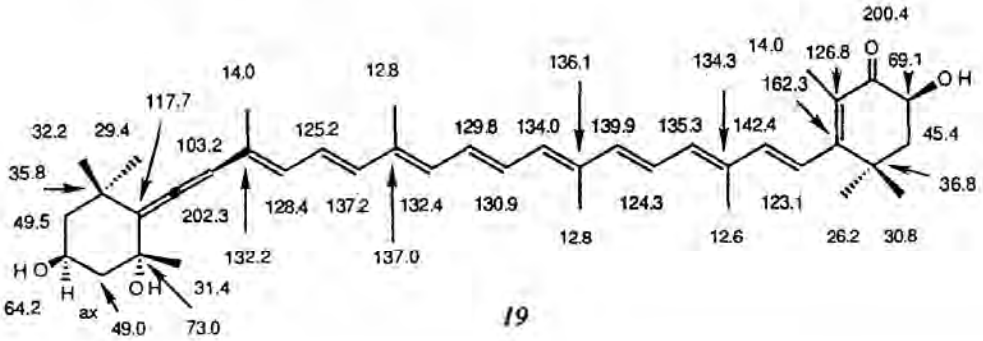
17



(385)



18



19

E. Carotenoid *Cis* Isomers

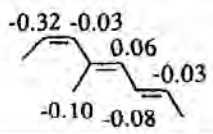
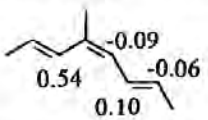
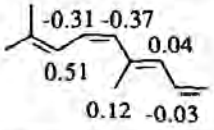
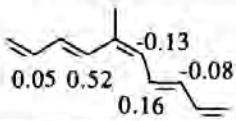
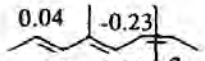
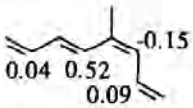
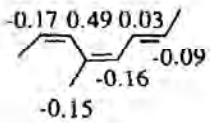
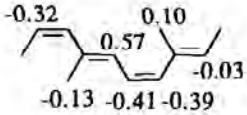
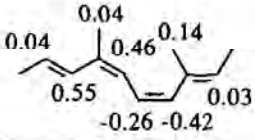
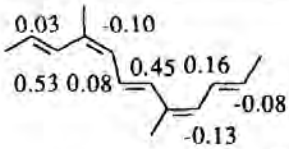
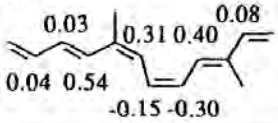
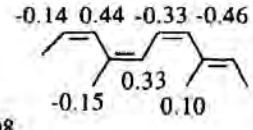
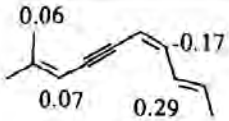
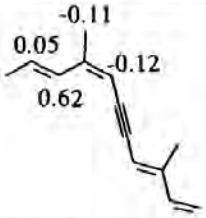
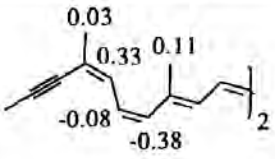
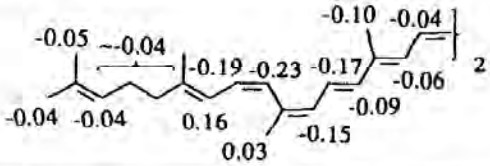
When the end groups and the length of the olefinic chain of a natural or synthetic carotenoid have been determined, a frequent further task is to deduce the geometry of the double bonds. In this context it has already been demonstrated conclusively [1, 3] that the elucidation of the structure of geometrical isomers can be performed very efficiently by ^{1}H-NMR spectroscopy at high magnetic fields. Although ^{13}C-NMR can contribute equally well in principle [14], its application is frequently hampered by the need for much larger quantities of sample, a prerequisite which is, in practice, often not fulfilled if the isomer is obtained as a minor by-product only.

1. ^{1}H-NMR

A first step in the elucidation of the structure of a *cis* isomer is the complete and unambiguous assignment of all the signals by modern NMR techniques, as will be discussed in Section F. The identification of *cis* stereomutation at double bonds Δ(7) or Δ(11) (and related positions) is straightforward and can be achieved by inspection of the value of the corresponding vicinal coupling constants, which is in the range of 11.5 to 12.8 Hz in *cis* isomers compared to 13.5 to 16.8 Hz in *trans* (see Section D.1). The derivation of the position of all other *cis* double bonds can be based very reliably on the observed chemical-shift changes between *cis* and *trans* isomers, although some decisive NOE experiments can be very useful in further supporting the conclusions. It was shown many years ago [1, 3, 14], that these isomerization shifts $\Delta\delta = \delta_{cis} - \delta_{trans}$ (in ppm) of the different protons are indeed very useful for the elucidation of the *cis* structures. Typical average values of this parameter extracted from the spectra of more than 40 mono-*cis* and di-*cis* isomers of several different types of C_{40} carotenoids were presented in [3]. Moreover, a number of further, more detailed studies were published which included data on 9 geometrical isomers of astaxanthin (**406**) diacetate [30], 11 isomers of β,β-carotene (**3**) [19, 31, 32], 11 isomers of zeaxanthin (**119**) [33], 6 isomers of fucoxanthin (**369**) [34], and 10 isomers of canthaxanthin (**380**) [3, 35]. Since then, further isomers have been obtained and identified spectroscopically in the author's laboratories, including 14 lycopene (**31**) isomers and further isomers of related compounds [36].

From these studies an extended list of average Δδ values has been compiled in Table 5 for several different types of mono-*cis*, di-*cis* and tri-*cis* structures. These values can successfully be applied quite generally to the elucidation of the structures of other *cis* isomers of carotenoids. From these studies it is estimated that these average values should be valid in other related cases within *ca.* ± 0.02 ppm. It is assumed here that no strongly anisotropic groups are present close to the *cis* bond(s) which might influence the observed shift changes due to the far-reaching effects that were discussed in Section D.1. Moreover, in all cases, deuteriated chloroform was used as the solvent, since sometimes significantly different Δδ values were reported for some canthaxanthin isomers in deuteriobenzene [35].

Table 5. Average values of the ^{1}H-NMR isomerization shift $|\Delta\delta| = \delta_{cis} - \delta_{trans} > 0.02$ ppm for different types of *cis* isomers (solvent $CDCl_3$).

7-cis and 7,7'-di-cis	9-cis and 9,9'-di-cis	11-cis and 11,11'-di-cis
		
13-cis	15-cis	13,13'-di-cis
		
7,9-di-cis	7,11-di-cis	9,11-di-cis
		
9,13-di-cis	13,15-di-cis	7,9,11-tri-cis
		
9-cis	13-cis	9,11,11',9'-tetra-cis
		
prolycopene (7,9,7',9'-tetra-cis lycopene)		
		

From the data of Table 5 (except prolycopene) some useful practical rules follow:

i) A relevant value of $\Delta\delta$ ($|\Delta\delta| > 0.02$ ppm) is observed, as expected, only for those protons which are close to the stereomutated bond.

ii) As a consequence, the shifts of isomers with two (or more) *cis* bonds behave in a fairly additive manner if the *cis* bonds are sufficiently separated. Strict additivity is hence observed, for instance, in 7,7'-di-*cis*, 9,9'-di-*cis*, 9,13'-di-*cis*, 11,11'-di-*cis* and 9,15-di-*cis* isomers; data for these isomers have, therefore, not been given separately in Table 5.

iii) If two *cis* bonds are separated by only one unchanged *trans* bond, additivity is, in general, still maintained approximately (see 7,11-di-*cis*, 9,13-di-*cis* and 13,13'-di-*cis*). In the case of consecutive *cis* bonds, only the gross features are to some extent predictable by additivity (see 7,9-di-*cis* and 9,11-di-*cis*, and 7,9,11-tri-*cis*).

iv) The isomerization shift of methyl protons is often surprisingly small and hence less indicative. Only in the case of hindered *cis* double bonds, such as 7-*cis* and 11-*cis*, are the observed shifts relatively large and hence characteristic.

v) Due to the limitation of the effects to a small section of the structure, it can be expected that the isomerization shifts can be transferred fairly well to structurally related positions of the same carotenoid or of other carotenoids. Thus, as an example, it has been found that the effects of stereomutation of $\Delta(11)$ are, within the normal deviation of *ca.* $\pm$ 0.02 ppm, virtually identical to those observed for 7-*cis*-lycopene [36].

Inspection of the data of Table 5 reveals that some of the reported isomerization shifts are particularly strong and hence very indicative. Thus, stereomutation of $\Delta(9)$, $\Delta(11)$ or $\Delta(13)$ is revealed unambiguously by strong downfield shifts of about 0.5 ppm for H(8), H(10) or H(12), respectively, caused by the newly introduced steric interactions. Conversely, protons attached to the convex side of the stereomutated bond are shifted upfield, partially due to the relief of steric interactions. A relatively strong effect is also exerted by a neighbouring triple bond, as discussed in Section D.1; three examples are included in Table 5.

It was already mentioned that in 15-*cis* isomers the relative chemical shifts of H(15,15') and H(14,14') are interchanged with respect to those of the *trans* isomer and hence this type of stereomutation is readily identified without the need to calculate $J_{15,15'}$ by a spectral simulation.

Although the values for 7-*cis* isomers are expected to depend to some extent on the specific type of end group, this case has been included in Table 5, since the $\Delta\delta$ values found for zeaxanthin (**119**) [33] were close to those of β,β-carotene (**3**) [19] and some further compounds listed in Table 1. However, this cannot be expected generally for all the shifts near the stereomutated bond, since far-reaching effects from the different end groups may be encountered. An example is renieratene (ϕ, χ-carotene, **26**, end groups **e99** and **e99a** in Table 1) where a strong upfield shift of $\Delta\delta = -0.66$ ppm is observed for H(19) in the 7-*cis* isomer compared to only –0.10 ppm in the examples shown in Table 5. It is obvious that the extra upfield shift with renieratene is caused by the fact that H(19) is now placed in the strong shielding zone above or below the anisotropic aromatic ring. In contrast, the $\Delta\delta$ value of H(19) in end group **e88a** (Table 1) is weakly positive (0.06 ppm). Interestingly, the $\Delta\delta$ values of H(7) and H(8) of both compounds are again virtually identical to those given in Table 5.

Numerous applications of these rules, particularly of rule (i), for the elucidation of the structures of various *cis* isomers, show that they are, in general, extremely useful and widely

applicable. However, one clear exception has been found, namely prolycopene (*5*). Here, all shifts in the ^{1}H-NMR spectrum were significantly ($|\Delta\delta| > 0.02$ ppm) altered compared to those of the all-*trans* compound (see **31** and *5* and last entry of Table 5). This is especially noteworthy for the shifts of H(16), H(17), H(20), H(14) and H(15), since these protons are rather distant from the stereomutated bonds, if a nearly planar structure is assumed. It should be pointed out in this context that previous ^{1}H- and ^{13}C-NMR assignments [15, 16] have been fully confirmed (see Tables 3 and 4) by modern 2D experiments, including ^{1}H,^{1}H- and ^{1}H,^{13}C-COSY ($^1J_{CH}$ and $^{2,3}J_{CH}$). A speculative explanation of the irregular behaviour of prolycopene is that this isomer deviates significantly from planarity as the ends of the molecule are folded back towards the central part. However, this obvious interpretation does not fully explain why the ^{13}C-NMR isomerization shifts obey rule (i) more closely (see below). Moreover, a careful 2D ROESY study [36] did not provide any indication of an irregular conformation. It is also worth mentioning in this context that other isomers of lycopene such as 7-*cis*, 7,7'-di-*cis*, 9-*cis*, and 9,9'-di-*cis* behave in a strictly regular manner both in ^{1}H- and ^{13}C-NMR [36]. Only in the case of 5-*cis* and 5,5'-di-*cis* is a small isomerization shift of $\Delta\delta = 0.04$ detectable at H(2), H(2'). It is evident that a detailed interpretation of the unexpected behaviour of prolycopene needs further experimental and theoretical studies.

2. ^{13}C-NMR

In Table 6 are presented some average isomerization shifts for ^{13}C-NMR which are based partly on previous work [14], partly on more recent, unpublished studies, and cover mainly isomers of β,β-carotene (**3**), zeaxanthin (**119**) and lycopene (**31**) [36].

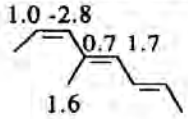
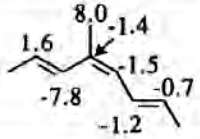
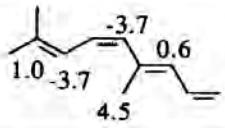
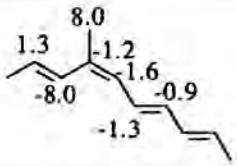
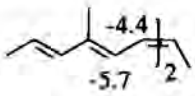
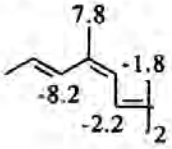
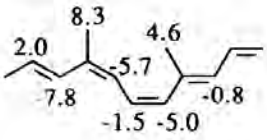
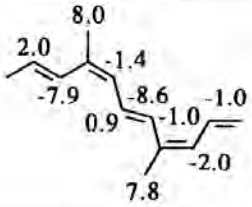
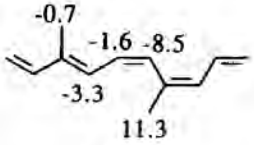
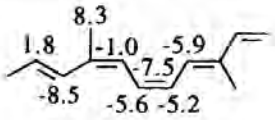
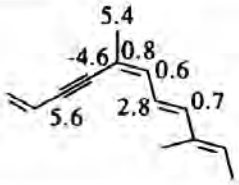
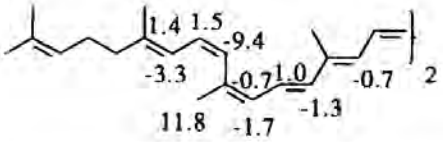
To a good approximation the rules given above for ^{1}H-NMR apply also for ^{13}C-NMR, except rule (iv). Here, the ^{13}C shifts of methyl carbons do show strong variations upon stereomutation of a double bond and their isomerization shifts are, therefore, complementary and very informative. The isomerization shift of C(19) and C(20) is close to 8 ppm in 9-*cis* and 13-*cis*, respectively, and reaches a peak value for C(20) of *ca.* 11 ppm in the hindered 11,13-di-*cis* isomer. Instead of a downfield shift for H(8) and H(12) in 9-*cis* and 13-*cis*, C(8) and C(12) are now shifted upfield by *ca.* –8 ppm. It is evident that at least these major shift effects can be explained qualitatively by the simple model of steric compression, as discussed above. This seems not to be the case for the fine details of the isomerization shifts given in Table 6.

It has already been mentioned that the isomerization shifts of prolycopene (last entry of Table 6) were essentially as expected according to rule (i). This is particularly true for C(1) to C(4), C(16) and C(17), whereas there are thought to be minor deviations at positions close to the central part of the molecule.

In the same way as before, rule (v) also seems to apply to ^{13}C-NMR. Thus, as an example, the isomerization shifts given for 11-*cis* can be fairly well transferred to 7-*cis*-lycopene [36].

In conclusion, it is evident that the use of these ^{13}C-NMR isomerization shifts can contribute in a complementary way to the structure elucidation of a great variety of different *cis* isomeric carotenoids.

Table 6. Average values of the ^{13}C-NMR isomerization shift $|\Delta\delta| = \delta_{cis} - \delta_{trans} > 0.05$ ppm for different types of *cis* isomers (solvent $CDCl_3$).

7-cis and 7,7'-di-cis	9-cis and 9,9'-di-cis	11-cis and 11,11'-di-cis
		
13-cis	**15-cis**	**13,13'-di-cis**
		
9,11-di-cis	**9,13-di-cis**	**11,13-di-cis**
		
13,15-di-cis	**9-cis**	
		
prolycopene (7,9,7',9'-tetra-cis lycopene)		
		

F. Experimental Techniques

A crucial step in the elucidation of the structure of an unknown carotenoid is the unambiguous assignment of (most of) the ^{1}H- and ^{13}C-NMR signals. For this purpose a number of well-proven experimental techniques may be used, ranging from simple 1D methods such as the decoupling (or decoupling difference) experiment in ^{1}H-NMR and the useful DEPT pulse sequence in ^{13}C-NMR, to more sophisticated 2D pulse techniques. In this Section some selected experimental techniques which are of special interest in the field of carotenoids will be discussed briefly. In this context, the relative advantages and drawbacks of these techniques will be summarized by assessing their experimental complexity, the typical acquisition time needed to perform the experiment, and the type of information that becomes accessible. It is clear that the following discussion will be strongly guided by the personal experience and preferences of this author. The physical background of these methods will be discussed briefly. Only some simple intuitive explanations will be used for sophisticated experiments. For a more detailed discussion the reader is referred to selected references from a growing list of monographs and review articles, which are also partly addressed to the non-specialist in the NMR field (see [6, 7] and references therein).

1. ^{1}H-NMR

a) Homonuclear decoupling

The use of the homonuclear decoupling or decoupling difference experiment is widespread in daily routine work. By irradiation of a selected proton multiplet with a second rf source from the decoupler, the signals of spin-coupled protons partly coalesce, since their spin coupling is effectively removed by an enforced precessional motion. In this way the connectivity of different protons by spin couplings can readily be revealed in simple cases.

A serious disadvantage of this experiment is that, for a full decoupling, a relatively strong irradiation field is needed whose intensity $\gamma H_2/2\pi$ (in Hz) must be greater than the total splitting of the signal that is irradiated. In crowded spectra this necessarily means that other closely spaced signals are also disturbed. Moreover, the continuous irradiation leads to small frequency shifts of neighbouring signals, called the Bloch-Siegert shift [6]. Both effects often result in undesired changes in the spectrum. As a consequence, this technique is of limited use with the crowded spectra of carotenoids.

b) Double-INDOR-Difference (DID)

The situation is quite different in this 1D experiment, which was introduced many years ago [37] as a useful variant of the long-known Fourier INDOR technique [38].

In the latter experiment, a very weak and hence selective pre-irradiation rf field ($\gamma H_2/2\pi \sim$ 1Hz) of *ca.* 0.5 s duration is applied to only one selected component of a multiplet. This slightly changes the population of the two energy levels connected by the chosen transition. In

a next step, the normal broad-band excitation pulse is applied to excite simultaneously all lines of the spectrum. Subsequently, the FID is acquired. If the pre-irradiation frequency is now shifted outside the spectral region, a difference FID can be accumulated. In the difference spectrum, obtained upon Fourier transformation of the FID, only those transitions appear which have altered intensities, *i.e.* which start or end on either of the two energy levels that are connected by the irradiated transition. In practical terms this means that, besides the irradiated transition, only those additional signals are retained which belong to the same coupled spin system. Since the population of the lower level has decreased, and that of the upper level has been increased by pre-irradiation, positive and negative signals appear in the difference spectrum. They can all be rendered positive, however, by a subsequent magnitude calculation of the spectrum [6, 7].

In the related DID experiment, two different transitions of a given multiplet are subsequently pre-irradiated (instead of only one and an off-resonance frequency). For this purpose, the first and second components of a doublet, or the first and fourth components of a doublet of doublets, are chosen. It has been shown [37] that, under this experimental condition, in the case of isolated 2-spin and 3-spin systems, the true line form of the signals of the coupled protons is obtained in the difference spectrum. This means that, in these cases, chemical shifts and spin couplings of the coupling partners, which absorb in strongly crowded regions, can be measured directly. This is not necessarily valid for systems with four and more spins; here, only approximate chemical shifts are sometimes accessible since irradiation of only two transitions can be insufficient to delineate the total energy level system so that not all the transitions of these multi-spin systems appear in the spectrum. A special 4-spin system, involving methyl protons, will be discussed below.

Since only very weak irradiation power is needed in DID, the technique is applicable even in overlapping regions, provided that the two components of the irradiated multiplet are sufficiently far away from other signals (preferably > 2 Hz). Concerning the experimental set-up, the same simple and automated procedure (called 'microprogram' in Bruker's terminology) is applicable as is used for a 1D nuclear Overhauser effect difference experiment, except that the duration of pre-irradiation is shorter (0.5 s instead of 3 to 5 s) and the rf intensity is much lower (decoupler power at least 56 db below 0.5 w instead of near 40 db). Since the final magnitude calculation in DID results in an undesired partial broadening of the individual lines, a slight resolution enhancement such as a Lorentz-to-Gauss window is normally applied to the difference FID before Fourier transformation; this partly removes the broadening.

Because of the excellent selectivity and its simplicity, DID has been applied successfully in numerous cases in the author's laboratory for the assignment of signals of carotenoids in cases of low and medium complexity. Some examples have been presented previously [4]. Two further demonstrations of its efficiency are given in Figs. 8 and 9.

In Fig. 8, the olefinic section of the 400 MHz ^{1}H-NMR spectrum of torularhodinaldehyde (**271**) is shown in spectrum A, together with some DID experiments (B to G). In trace B is shown a DID spectrum obtained upon subsequent pre-irradiation of the two components of the doublet at 6.94 ppm (see arrows). This signal is attributed to H(2') in the β position to the aldehyde. Besides the irradiated doublet signal, a doublet of doublets is retained at 6.65 ppm, corresponding to H(3').

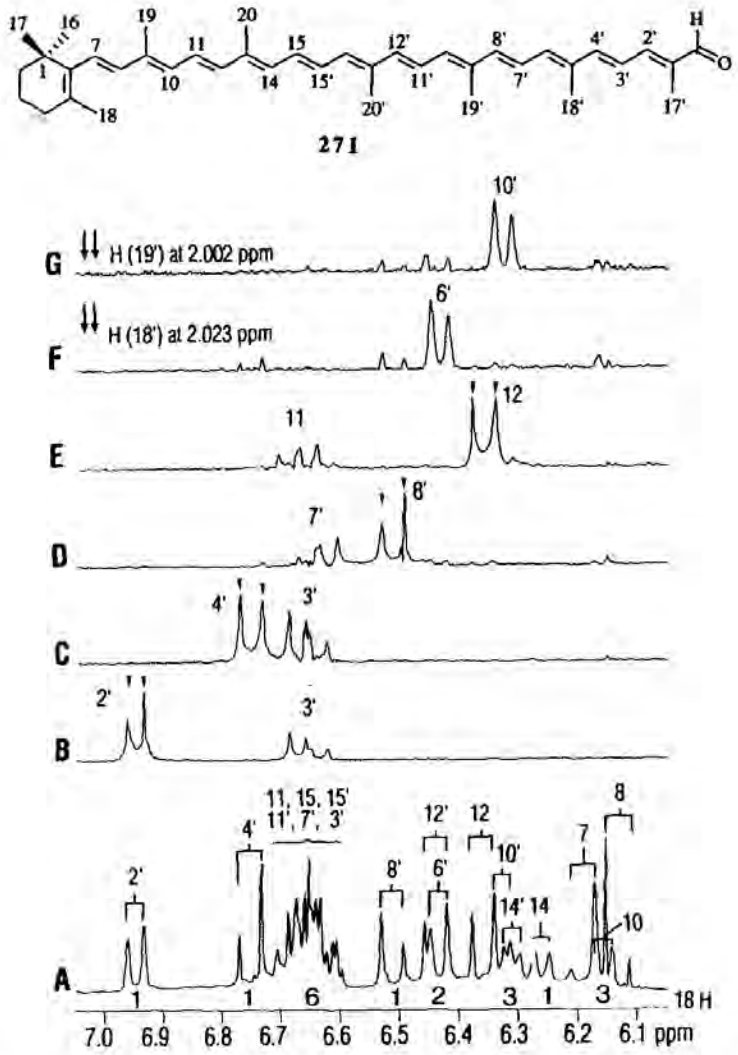


Fig. 8. Olefinic region of the 400 MHz ^{1}H-NMR spectrum of torularhodinaldehyde (**271**) in $CDCl_3$ (A) and a series of double INDOR difference (DID) spectra (B to G). A pre-irradiation of 0.5 s duration was applied at positions indicated by arrows at a decoupler power of 58L below 0.5 W (A to E) and 61L (F and G). The difference FIDs were subjected to a mild resolution enhancement by application of a Lorentz-to-Gauss window (LB = -1.0, GB = 0.15) before Fourier transformation. Eventually a magnitude calculation was performed. Experiments B to E were performed in *ca.* 3 minutes, those of F and G in 8 minutes per experiment.

The excellent selectivity of DID is also seen in trace C, where the two components of the doublet at 6.74 ppm were pre-irradiated, resulting in the same doublet of doublets as before. This second doublet is therefore assigned to H(4') which also absorbs at relatively low field due to the effect of the aldehyde group in the δ position. Similarly, the signals of H(7') and H(8'), as well as those of H(11) and H(12), were linked in experiments D and E. In the latter experiment, the irradiated high-field component of the signal of H(12) is partly overlapped by

the low-field component of the doublet of H(10'). Despite this near degeneracy the resulting DID spectrum can readily be interpreted and this once more demonstrates the high selectivity. It is noteworthy that the total acquisition time per DID experiment was less than 3 minutes, *i.e.* only 2 x 8 scans were needed, each followed by a relaxation delay of 5 s.

Further experiments (not shown) were used to locate the positions of the signals of H(11'), H(15) and H(15') by pre-irradiation of H(12'), H(14) and H(14'), respectively. Although in the first of these experiments some artifacts were present due to a partial overlap of the signals, the results were again unambiguous.

It had previously been shown [4] that even connectivities between methyl and olefinic protons can be revealed by this technique, since the pairs H(19) and H(10), or H(20) and H(14) (or other corresponding protons) are coupled by a small allylic $^4J_{HH}$ coupling of *ca.* 1.4 Hz. Although these methyl signals mostly appear as broad singlets rather than as doublets, due to further, still smaller, long-range couplings [see Section F.1.e], pre-irradiation at two frequencies about ± 0.7 Hz apart from the signal centre makes possible the detection of the signal of the coupled proton in this special 4-spin system. Again, the experiment is very selective and methyl signals that are only a few Hz apart from each other can be irradiated separately and their connectivity to coupled olefinic protons found. This is demonstrated in traces F and G of Fig. 8, linking H(18') at 2.023 ppm with H(6'), as well as H(19') at 2.002 ppm with H(10'). Further experiments (not shown) were performed to link the superimposed signals of H(19), H(20), and H(20') at *ca.* 1.98 ppm with protons H(10), H(14) and H(14'), without distinction by this experiment. Similarly, the connectivity between H(18) and H(7) was readily proven. In experiments based on such small couplings and with very close chemical shifts, it can be useful to decrease the rf intensity of the irradiation further in order to improve the selectivity. Then, a corresponding increase of the number of scans and hence of the acquisition time may be advisable. Therefore, the total acquisition time of experiments F and G was extended to 8 minutes each.

In Fig. 9 a further demonstration of the efficiency of DID is presented. In the upper parts, the different sections of the 400 MHz ^{1}H-NMR spectrum of the apo-8'-carotenal (*20*) derived from bisanhydrobacterioruberin (**453**) (end group **e138** of Table 1) are shown. Traces A to K are DID spectra plotted in three sections in the range 5 to 7 ppm to help in identifying the different spin sub-systems in the olefinic range. As usual, a start can be made from some predictable assignments, namely (from high to low field) of H(2"), H(3), H(6), H(4), H(10), H(14), and, at lowest field, H(10'). The search for the signals of their coupling partners begins in trace A. Here, the two components of the doublet of H(10') were pre-irradiated, resulting in an additional doublet of doublets which must be assigned to H(11'). The latter signal shows a strong roof effect pointing to the fact that the signal of the coupling partner H(12') must be at the left-hand side and very close to it. This is proved in trace B since the signal of H(11') is again detected upon pre-irradiation of the two components of the close doublet corresponding to H(12'). In experiment C, the first and fourth components of a doublet of doublets ($\Sigma J \sim 26$ Hz) in this crowded region were selected for pre-irradiation. This yielded the two doublets of H(8) and H(6) and thus the irradiated signal must correspond to H(7). In experiments D to I, further connectivities between H(14') and H(15'), H(12) and H(11), H(8) and H(7), H(14) and H(15), H(10) and H(11), and H(4) and H(3) are evident. In experiments J and K,

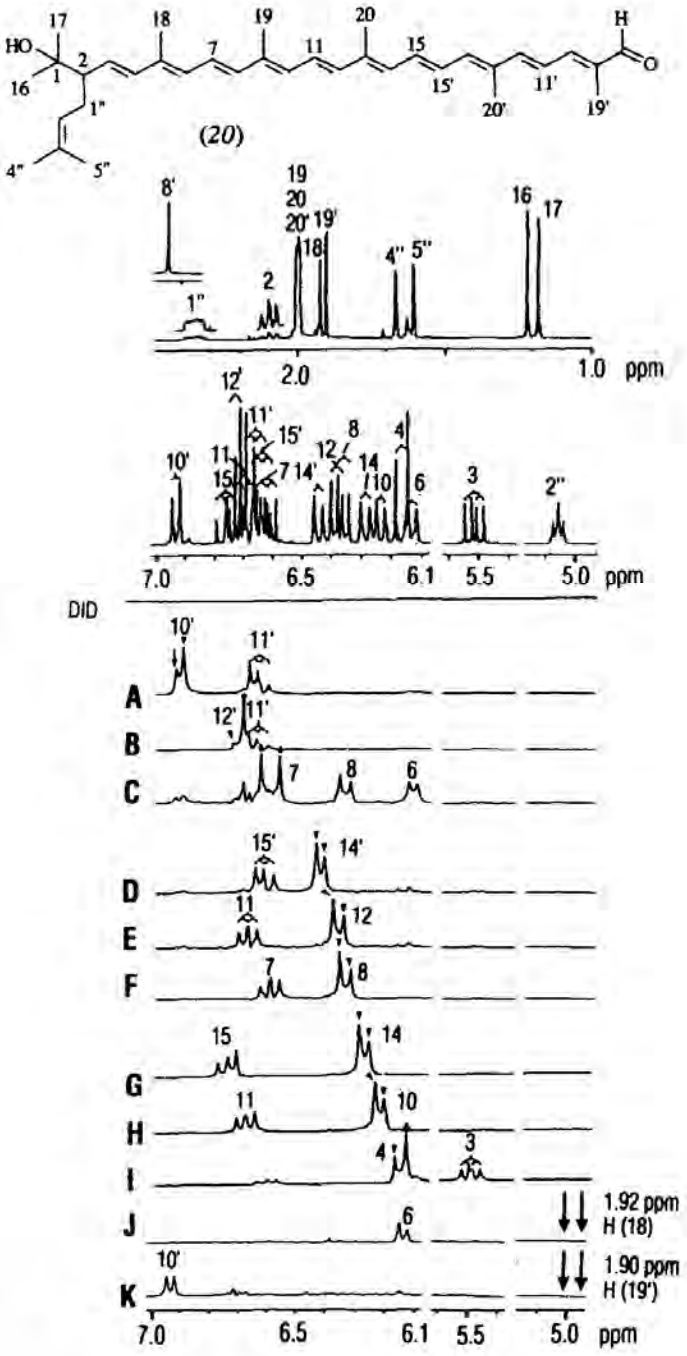


Fig. 9. Top: Sections of the 400 MHz ^{1}H-NMR spectrum of a C_{35} aldehyde (*20*) with bisanhydro bacterioruberin end group (6 mg in 0.4 ml $CDCl_3$). Traces A to K present DID spectra obtained upon pre-irradiation (0.5 s) of the multiplet components labelled by arrows. Each experiment was performed with 2•32 scans with a relaxation delay of 6 s, corresponding to a measuring time of 12 min.

connectivities between the separated methyl signals of H(18) and H(19') and the olefinic protons H(6) and H(10'), respectively, are seen.

Some undesired artifact peaks of low intensity are sometimes found in DID spectra (see Figs. 8 and 9). They can be attributed to four sources. First, a partial overlap of the irradiated components with other nearby signals may occur. An example is seen in trace I of Fig. 9. Here, the high-field component of the doublet of H(4) is very close to the low-field component of the doublet of H(6). As a result, weak additional signals, attributed to H(7), are visible near 6.6 ppm. Secondly, spurious side-band frequencies on either side of the selected irradiation frequencies are present which weakly excite other nearby signals. Thirdly, any minor instability of the spectrometer during acquisition may lead to incomplete subtraction in the difference FID. Finally, the relaxation delay between the scans may have been too short (< 3 s). Despite these minor drawbacks, which are also present to some extent in other 1D difference methods, it is obvious that DID can be applied very efficiently to determine some selected connectivities between coupled protons in crowded spectra of carotenoids. If only a few experiments are needed, a dramatic saving of spectrometer time is possible compared to the typical 2D COSY experiment.

c) Nuclear Overhauser effect (NOE)

i) Longitudinal NOE. A further important experimental technique is based on the NOE [39, 40]. In a typical steady-state 1D NOE difference experiment [39], the sufficiently separated signal of a selected proton is saturated for 3 to 5 s by application of a strong rf field from the decoupler. In the same way as discussed above, the non-selective observation pulse and the accumulation of the FID follow. If the irradiation frequency is then shifted outside the spectral region, a difference FID can be acquired. Upon Fourier transformation, the NOE difference spectrum is obtained which contains, besides the irradiated signal, only those additional signals which belong to spatially close neighbours of the irradiated proton. Since the 1D version of this experiment suffers in the same way as the decoupling experiment from its inherent low selectivity, it can be replaced in complex cases by its more time-consuming 2D version.

In the 1D experiment, selective saturation of a signal leads to a change in the population of all the energy levels involved. As was discussed briefly in Section B.2.e, neighbouring protons are coupled through space by rapidly fluctuating dipolar magnetic fields caused by the molecular tumbling. As a consequence, relaxation processes tend to restore the distorted equilibrium population of the irradiated proton by a spontaneous flow of magnetization between the saturated proton and its neighbours. As a consequence, the population of the energy levels of the neighbouring protons is also affected after a time of the order of the spin-lattice relaxation time T_1. This change of population can be detected by measuring a difference spectrum between on-resonance and off-resonance irradiation. Since it is the longitudinal z magnetization which is transferred in this experiment, the effect is often called longitudinal NOE [39, 40]. In the resulting NOE difference spectrum, only the positive signals of the neighbouring protons are visible besides the negative signal of the irradiated proton.

As in T_1 relaxation, the efficiency of exchange of longitudinal z magnetization is strongly

dependent on the presence of frequency components of the magnetic noise near the measuring frequency and, therefore, on the molecular size of the solute and the viscosity of the solvent. Moreover, since the dipolar fields decay with $1/r^3$, r being the distance between the interacting magnetic nuclei, the interaction between two dipoles, and hence the NOE, rapidly decays proportionally to $1/r^6$. It is, therefore, in practice only measurable for distances below 4 or 5 Å. It is evident that this experiment provides important information about molecular geometry [39, 40].

Steady-state 1D NOE experiments have been applied in numerous cases in the author's work for the assignment of signals and for the deduction of geometrical information. Some examples were presented elsewhere [3, 15] and many of the stereochemical assignments given in Table 3 (and therefore also in Table 4) were based on this experiment. Although a corresponding 2D version called NOESY is available and has found numerous applications in other fields of structural chemistry, this seems not to be the case in the field of carotenoids.

Due to its dependence on measuring frequency and molecular mass, the longitudinal NOE has a substantial disadvantage. Theory and experiment show [40] that this NOE, which is strong and positive for small molecules, becomes small or even completely vanishes for molecular masses around 800 Da at measuring frequencies in the range of 400 to 600 MHz. At still higher masses the longitudinal NOE changes its sign and becomes negative [40]. This means that, in this region, irradiation of a signal results in a decrease (instead of an increase) of the signal intensities of the neighbouring nuclei, and a resulting negative signal in the difference spectrum, *i.e.* with the same sign as the irradiated signal.

The disappearance of the longitudinal NOE in this critical range of molecular mass has often been confirmed experimentally. In an NMR study of the structures of 19'-butanoyloxyfucoxanthin (**370.2**) and its 9'-*cis* isomer which, at 772 Da, are within the critical mass range, it was shown [21] that, within the rigid part of these molecules (the olefinic chain), the NOE was actually zero, whereas a small and still positive effect was detected between protons of the more mobile end groups. The significant decrease or even complete disappearance of the NOE is extremely unfortunate in this mass and frequency range, which is particularly important in the field of carotenoids. However, an efficient and attractive remedy is now available.

ii) Transverse or rotating-frame NOE (ROE). It has been shown [41] that, instead of a transfer of the longitudinal magnetization by cross-relaxation processes, a corresponding exchange is also effective for the transverse x,y components of the magnetization perpendicular to the direction of the external magnetic field. This process has a completely different dependence on the molecular tumbling rate. Here, as in T_2 relaxation, only frequencies of the fluctuating dipolar fields near zero are most effective. In contrast to the longitudinal NOE, the ROE is, as a consequence, always positive and, in the medium molecular mass range, considerably stronger than the former [40, 41]. Therefore, it is a very important substitute in the field of carotenoids.

For the detection of this transverse NOE or ROE (originally termed CAMELSPIN [41]), a slightly different experimental set-up is needed. Again, 1D and 2D variants are available.

In the 2D experiment (called ROESY) a 90° pulse first rotates the equilibrium z magnetization to the transverse y axis of the laboratory system. Subsequently this

magnetization starts to precess around the z axis. After a short time delay, called evolution time, which is incremented in each of the several hundred subsequent FIDs of the full 2D experiment, the transverse magnetization is spin-locked by a strong CW rf field [41] or by a train of 90° pulses [42] which forces the transverse magnetizations into a coherent motion. During this spin-locking or mixing time, which is typically chosen between 0.2 and 0.6 s, transverse magnetization is exchanged between spatially close protons *via* mutual spin flip-flop relaxation processes. Eventually, the FID is acquired.

In a corresponding 1D ROE experiment, a selective 180° pulse is first applied to a selected signal [41]. For this purpose, a train of weak pulses, called a DANTE pulse sequence [6, 7] is preferred. This consists of several hundred short pulses (each of 2 μs) separated by delays of about 70 μs. By careful selection of rf power and number of repetitions, it can be finely tuned to the width of a given multiplet [5]. By this selective DANTE pulse train, the magnetization of the irradiated proton is rotated to the –z axis. Then, a non-selective 90° pulse is applied to all protons, and the mixing pulse train is switched on [42]. When a partial exchange of transverse magnetization has been achieved during the mixing time, the pulse train is switched off and the FID acquired. In a second step, the irradiation frequency of the DANTE sequence is shifted off-resonance and a difference FID is acquired.

Two typical 1D ROESY experiments are depicted in Fig. 10 (traces B and C). They look identical to corresponding longitudinal 1D NOE experiments except that the effect is much stronger here. The pre-irradiated signals have negative intensity; the signals enhanced by ROE are positive. At the bottom, the olefinic region of the 400 MHz ^{1}H-NMR of pyrrhoxanthin (**556**) is presented. As discussed in Section D.1, the 2-spin sub-spectrum of H(7') and H(8') is readily identified (without distinction in the beginning) as two doublets, as indicated in the spectrum. Moreover, the two singlets at 5.74 and 7.03 ppm, later to be assigned to H(12') and H(10'), are immediately seen.

In experiment B of Fig. 10, the low-field singlet was selectively inverted and only the signals of one of the doublets ($J_{7',8'}$ = 15.6 Hz) and of the high-field singlet appear in the ROE difference spectrum. The only possible interpretation is that the irradiated signal corresponds to H(10') with H(8') and H(12') as spatially close neighbours. In experiment C the signal at 5.74 ppm, now to be assigned to H(12'), was inverted and ROEs were seen at H(10') and a broadened doublet at 6.46 ppm which must be assigned to H(14'). These assignments were verified also by 2D ^{1}H,^{13}C-COSY tuned to one-bond and long-range couplings [23].

The 1D ROE experiments of Fig. 10 were performed in 18 min each and it is evident from the excellent signal-to-noise ratio obtained that a reduction of measuring time by a factor of *ca.* 5 to 10 would be feasible without loss of relevant information. The 1D ROE experiment is therefore very time-efficient and it is preferred in those cases where only a few through-space connectivities are needed and the signals of the protons to be irradiated are sufficiently free from overlap.

In contrast, the 2D ROESY experiment is indispensable in more complicated cases, particularly when information is needed from protons which are in crowded spectral regions and are not readily accessible by a selective experiment. In the 2D spectrum, close proximity of protons H(a) and H(b), with chemical shifts δ(a) and δ(b), is revealed by cross peaks that appear at coordinates δ(a), δ(b) and δ(b), δ(a) along the horizontal F_2 and the vertical F_1 shift

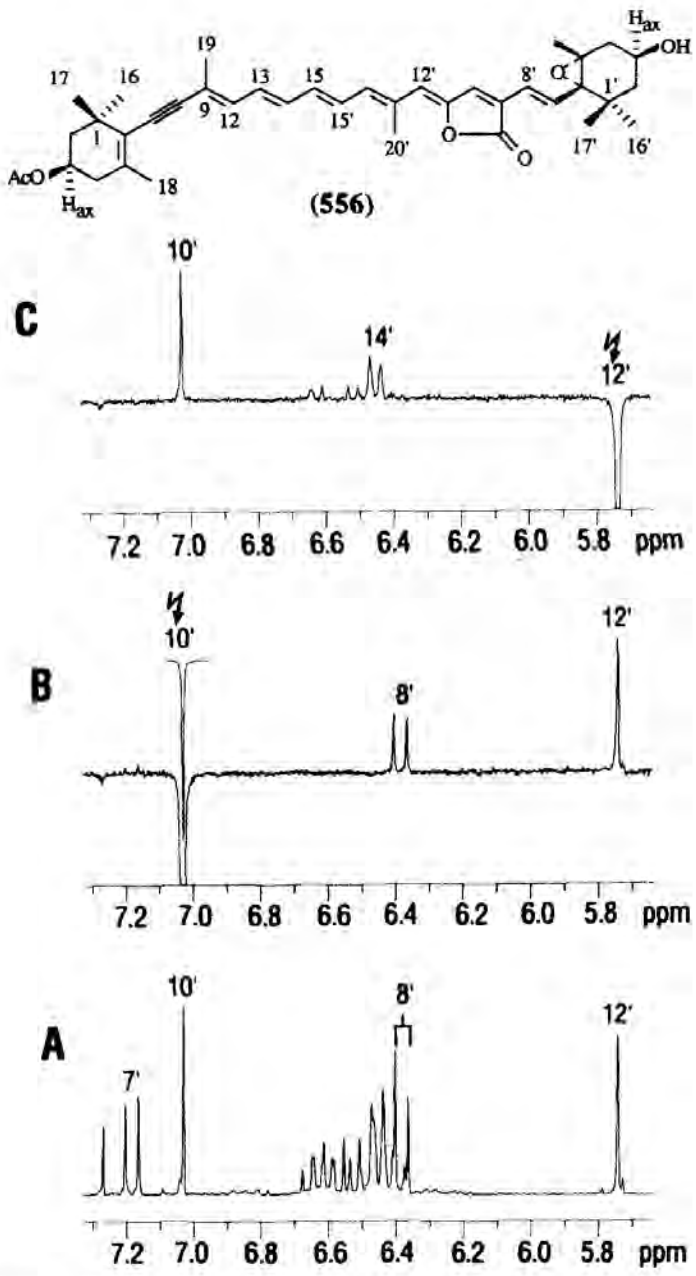


Fig. 10. Olefinic range of the 400 MHz ^{1}H-NMR spectrum of pyrrhoxanthin (**556**) (trace A; 0.9 mg in $CDCl_3$) and 1D ROE difference spectra obtained upon inversion of the magnetization of H(10') (trace B) and of H(12') (trace C) by a train of DANTE pulses (2400 times 2 μs at decoupler power level 19H). Mixing times of 0.3 s and 0.6 s were used and the FIDs added. 160 on-resonance and 160 off-resonance FIDs were accumulated. With a relaxation delay of 3 s, the total accumulation time per experiment was 18 minutes.

axes of the 2D spectrum, *i.e.* at symmetrical positions with respect to the diagonal. The more intense a cross peak is, the more contour levels are shown in the spectrum. It has recently been demonstrated [5, 21] that 2D ROESY provides a wealth of geometrical information; the experimental conditions and some precautions were discussed in detail in these references.

As a further example, Fig. 11 shows a small selected part of the full 2D ROESY spectrum of (3*S*,5*R*,3'*S*,5'*R*)-capsorubin (**413**) diacetate. This region contains cross peaks between protons that absorb between 7.5 and 5.0 ppm along F_2 and between 3.2 and 0.7 ppm along F_1. This range is situated in the upper left corner of the full 2D spectrum and a completely analogous range is found in the lower right part. In Fig. 11, cross peaks are found between H(3α) and the olefinic protons on one side and the remaining signals of the end groups on the other side. It will be shown by this representative example that, by interpretation of the different cross peaks, an unambiguous stereospecific assignment of the methyl signals and of the other ring protons is readily possible.

Starting from the known orientation of H(3α), two strong cross peaks are found with two other ring protons which must be on the same side of the ring, *i.e.* H(2α) and H(4α), without distinction at this stage. The corresponding geminal β protons are readily assigned since the geminal couplings of the two pairs of protons are distinctly different.

In addition, H(3α) has a further cross peak with only one of the three ring methyl groups (the one resonating at 0.86 ppm) which must be on the same side of the ring. This is therefore the 1α-CH_3 [H(16)]. The two pairs of methylene protons can now be distinguished since inspection of molecular models indicates that only those at C(4) are expected to give a strong ROE with H(7). In the same way, only the 5β-CH_3 protons [H(18)] are sufficiently close to H(7) to give a cross peak of strong intensity. A number of further cross peaks in other parts of the spectrum (not shown) clearly support these assignments, particularly those between the two geminal methyl groups at C(1), between the 1β-CH_3 and 5β-CH_3, and between the ring methyl protons and their neighbouring methylene protons on the same side of the ring.

In Fig. 11, a number of further, relatively poorly resolved cross peaks is seen, revealing spatial proximity of H(20) to H(15) and H(11), and of H(19) to H(11) and H(7). Some further, weaker cross peaks, such as those between H(19) and H(10) (given in brackets), probably arise because the shift difference between H(11) and H(10) is relatively small and this causes a partial mixing of the spin states of these protons.

If relatively good resolution is to be obtained, a 2D spectrum of this quality needs a long acquisition time, in this case 15 hours, corresponding to 875 subsequent experiments (see legend of Fig. 11). From the excellent signal-to-noise ratio and from other examples, it is concluded that a reduction of the measuring time by a factor of *ca.* 3 is feasible without relevant loss of cross peaks of medium and strong intensity. The ROESY spectrum shown in Fig. 11 was measured with a relatively large sample quantity of 15 mg, which was also used for $^1H,^{13}C$ correlation. Since the cross peaks in ROESY may have very weak intensities of only a few percent of the diagonal peaks, it was found that for the detection of at least the stronger cross peaks in an overnight acquisition the lower limit is around 25 μg of sample.

A quantitative interpretation of the measured ROE data is, in general, a very sophisticated task. However, qualitative information can readily be extracted with the help of molecular models. The result is condensed in the proposed structure given in the upper part of Fig. 11.

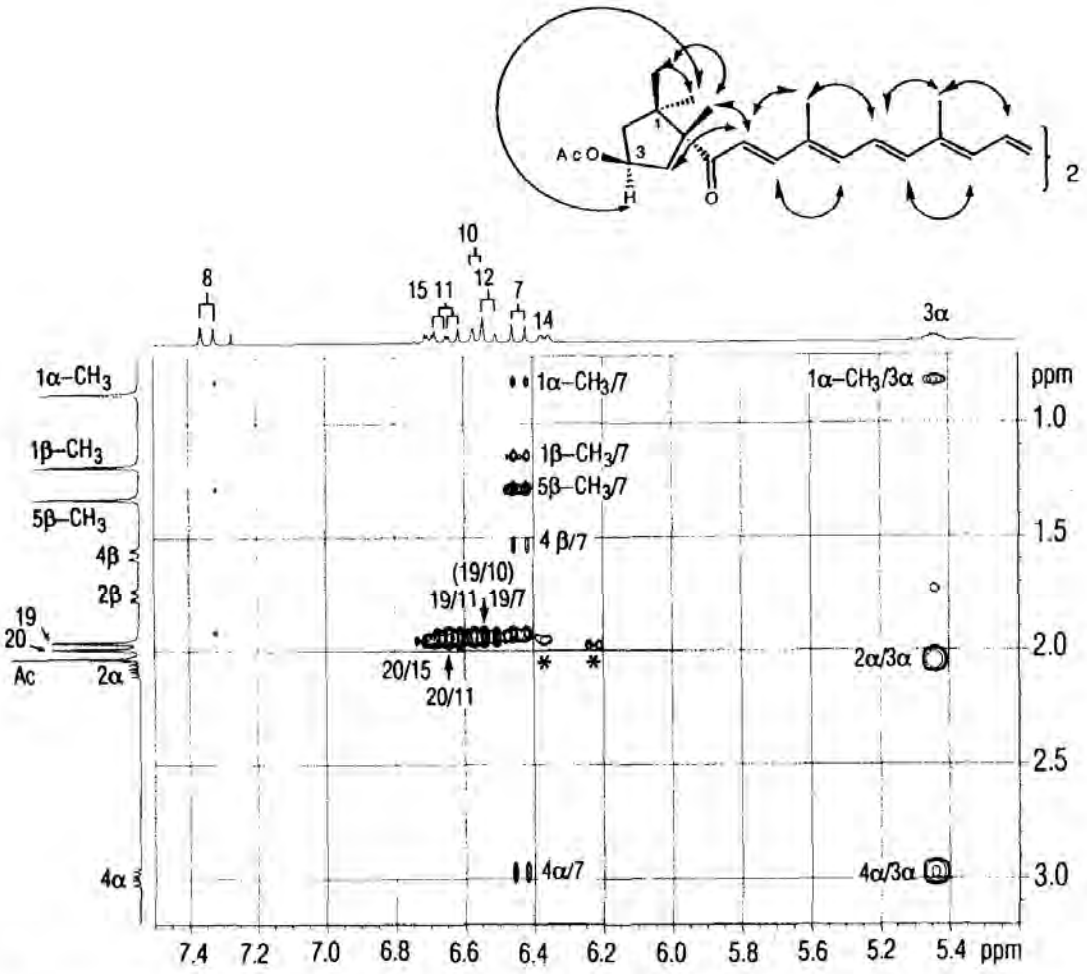


Fig. 11. Part of the 400 MHz phase-sensitive 2D ROESY spectrum of (3*S*,5*R*,3'*S*,5'*R*)-capsorubin (**413**) diacetate (15 mg in 0.5 ml $CDCl_3$). Experimental conditions: time-domain in F_2 4K data points, 875 experiments in F_1, spectral widths 5000 Hz, acquisition t_2 0.41 s, zero-filling to 4K in t_1, cosine-square windows, 16 scans and 2 dummy scans in each experiment, co-addition of the FIDs of 0.3 s and 0.6 s mixing time, 2 s relaxation delay, total measuring time 15 hours. Peaks marked by an asterisk correspond to a small quantity of the stereomutated 13-*cis* isomer formed during storage in solution.

Here, each arrow represents a medium or strong through-space contact observed in the 2D spectrum. Further contacts between the protons of the end group (see above) have been omitted in order not to overload the picture. The data can be explained best by the assumption that the C-6,7 bond is in an s-*cis* configuration. This allows a relatively close approach of H(18) and H(7), in agreement with the high intensity of the corresponding cross peak. Moreover, this explains why no cross peaks are seen between H(8) and other protons of the end group. The strong downfield shift of H(4α) is also explained since this proton is now mainly located in the

plane of the anisotropic carbonyl group and hence in the deshielding zone. Conversely, the high-field shift of the signal of protons H(16) is partly caused by their position in the cone above the carbonyl group which is known to be a shielding region (see Section D.1).

From this discussion it is evident that ROE experiments are very informative and should be preferred in the case of carotenoids in the mass range above about 500 Da. Whether 1D or 2D versions are applied is solely dictated by the information needed and the amount of sample and spectrometer time available. Both versions are extremely useful for the deduction of geometrical information, *e.g.* for the elucidation of the structure of geometrical isomers, and for the stereochemical assignment of protons.

Since proton and carbon shifts can be directly linked by $^{1}H,^{13}C$-correlation spectroscopy, the results can be transferred to the assignment of carbon signals. The shifts of the latter are also known to be very sensitive to steric interactions and their unambiguous assignment will contribute to the understanding of the underlying effects. Further applications of ROE and a discussion of the experimental conditions are available [5, 21].

A cumbersome problem with the previous ROESY experiment was that, besides weak ROESY peaks, some additional, relatively strong TOCSY artifacts with opposite sign were often observed under typical experimental conditions, and these partly obscured the through-space connectivities. It has been shown recently [23] that by application of a special spin-locking sequence (T-ROESY) this disadvantage can be largely removed.

d) Total correlation spectroscopy (TOCSY, or HOHAHA)

The 2D TOCSY experiment was introduced in 1983 [43]. Its experimental set-up is, in principle, very similar to the ROESY experiment. First, a transverse magnetization is produced by a 90° pulse. After the incrementable evolution delay, a CW spin lock or a correspondingly effective composite pulse-decoupling scheme (such as MLEV-17) follows which effectively averages out any z magnetization. This leads to an exchange of the remaining transverse magnetization between spin-coupled protons. Finally the FID is acquired. This process is repeated several hundred times for each of the different incremented delays of the evolution time to result in the full 2D data set.

In 1D TOCSY or HOHAHA (**ho**monuclear **Ha**rtmann-**Ha**hn experiment), as it is frequently called now [44], a selective 180° pulse is applied to an isolated signal. As in 1D ROE a DANTE pulse train is preferred for this purpose because of its ease in experimental handling. After a non-selective 90° pulse which rotates the magnetization of all protons into the transverse plane, the mixing is performed by a special sequence, called MLEV-17 [45]. Finally the FID is acquired. As in 1D ROESY, the irradiation frequency of the DANTE sequence is now shifted off-resonance and a difference FID is accumulated. After Fourier transformation, the only signals retained in the difference spectrum are those which belong to directly or indirectly spin-coupled neighbours of the proton whose signal was inverted.

It is evident that full sub-spectra can be obtained starting from the inverted signal [44, 46]. Their quality can be improved significantly if a so-called z-filter is incorporated into the pulse sequence before acquisition of the FID [46]. It consists of two 90° pulses separated by a variable delay. In practice, co-addition of the FIDs with 10 different delays between a few ms

and about 50 ms is sufficient to reduce admixture of dispersive components completely [21]. An important advantage of 1D TOCSY is the fact that the resolution of the sub-spectrum is as high as in a normal 1D spectrum, *i.e.* it is not limited by the reduced number of data points (low digital resolution) as it is in 2D.

In contrast to the incoherent through-space exchange of transverse magnetization by cross-relaxation processes in ROESY, a coherent exchange of magnetization is active in TOCSY, mediated by through-bond spin-spin couplings. Very similar to the oscillatory exchange of energy between two coupled pendulums, the exchange of magnetization between two (or more) weakly coupled protons is oscillatory with period 1/J, J being the spin coupling between the two protons [43, 44]. Moreover, in contrast to COSY, the transfer is not limited to the next neighbour, but it can propagate by relayed processes through a full sequence of J-coupled spins, provided the duration of the mixing time is sufficiently long. In practice, the duration is chosen at around 25 ms if mainly the first and weakly the second neighbours are to be affected. Longer mixing times of up to *ca.* 0.4 s are used if the magnetization should be relayed through a longer sequence of consecutive coupled protons. In practice, six consecutive relay steps can readily be achieved with these long mixing times in suitable spin systems, provided the subsequent coupling constants are not too small (> 1 Hz).

The TOCSY experiment has some substantial advantages over COSY. First, in its 2D version the diagonal and cross peaks are in pure phase, thus partial cancellation of anti-phase components, as occurs in COSY, is avoided. Secondly, in overlapping regions it might become necessary to supplement a COSY by a relayed (or doubly relayed) COSY, whereas a TOCSY experiment can be adjusted by proper choice of the duration of the mixing time to give directly further information on other protons in a sequence of coupled protons. The intensity of the cross peaks in multi-spin systems often directly reflects the position (or 'distance') in the sequence.

A slight disadvantage of TOCSY is caused by the oscillatory exchange of magnetization and this is particularly disturbing in 2-spin and 3-spin systems. In practice, it can happen that the intensity of the cross peak of a next neighbour (or the signal intensity in the 1D experiment) can be nullified if a mixing time is chosen that is close to 1/J. Fortunately, this problem can often be circumvented by a suitable choice of the mixing time. More importantly, the oscillatory exchange is highly damped and hardly detectable in systems of four and more consecutive spins.

The 2D TOCSY has been applied in some special cases but its 1D version is usually preferable as a really attractive and useful technique for special applications in the field of carotenoids, as illustrated in the following examples.

A particularly interesting application of 1D TOCSY is in the field of carbohydrates where complete sub-spectra of the different rings are readily accessible, starting from the signals of the anomeric protons at C(1), since they are often sufficiently separated. This technique has recently been used to elucidate the structure of the glycosidic part of the carotenoid P457 (13'-*cis*-7',8'-dihydroneoxanthin-20'-al 3'-β-lactoside, **280.1**) and related compounds; a further discussion of the experimental details and of the problems involved is given in [5].

A second interesting application to the structure elucidation of carotenoids is demonstrated in Fig. 12. Here, the aliphatic range of the 400 MHz ^{1}H-NMR spectrum of pyrrhoxanthin

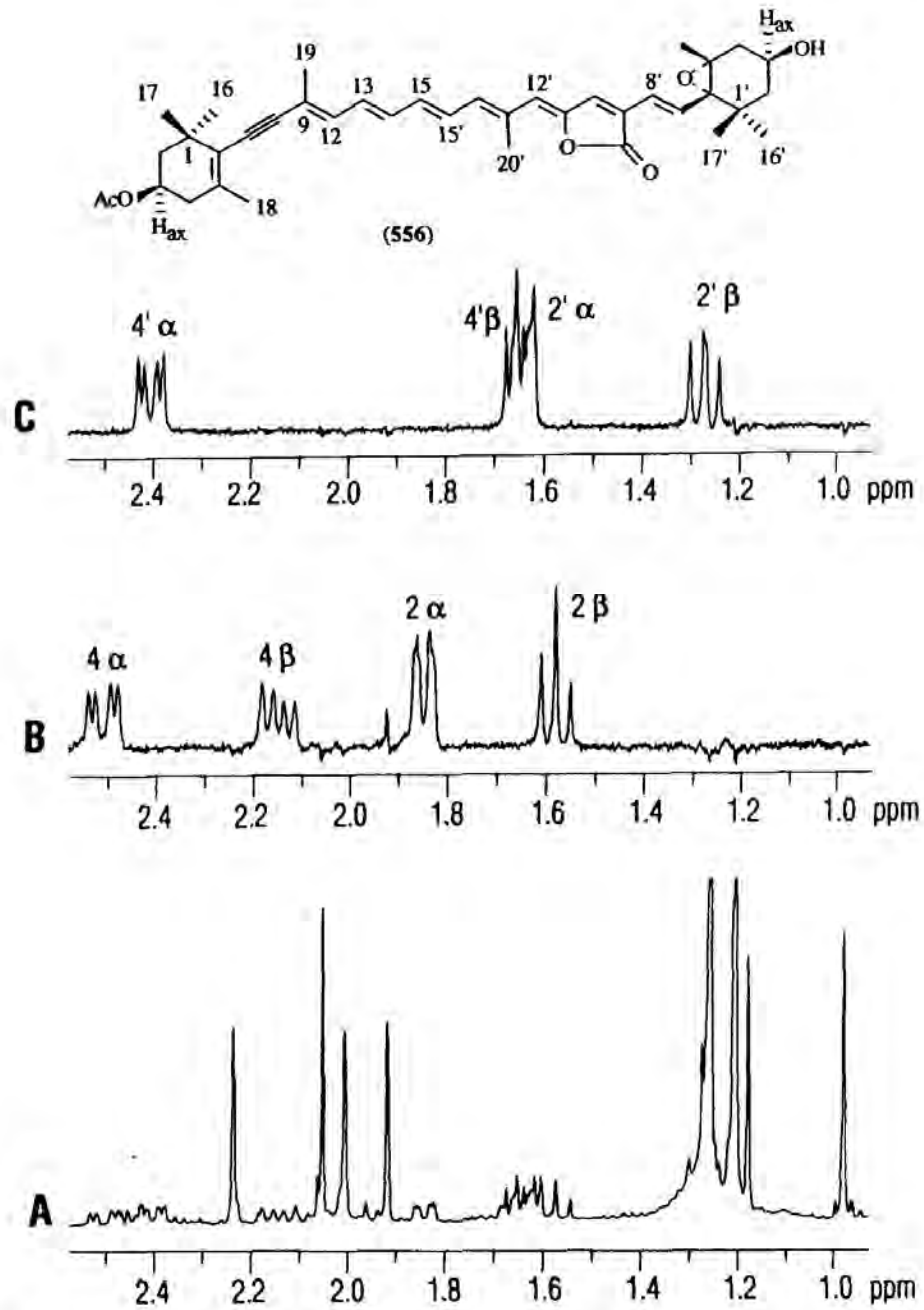


Fig. 12. High-field part of the 400 MHz ^{1}H-NMR spectrum of pyrrhoxanthin (**556**) (trace A; 0.9 mg in $CDCl_3$) and 1D TOCSY difference spectra obtained upon inversion by a 180° DANTE pulse (650 times 2 μs at power level 18H) of the signals of H(3) (trace B) and H(3') (trace C). Mixing was achieved by MLEV-17 with a last pulse of 60° and a total duration of 40 ms. In order to reduce admixture of dispersive components in the signals, a z-filter [45] was used with 10 different delays between 5 and 50 ms. The acquisition time per experiment was 16 min. Further experimental details are found in [5, 21].

(**556**) is shown in the lower trace (A). A frequent task in the interpretation of this spectral range of carotenoids is to identify and to analyse the sub-spectra of the two end groups. This can be done very efficiently by 1D TOCSY.

In the difference spectrum B, the signal of H(3), absorbing outside this region at 5.04 ppm, was inverted by a DANTE pulse train. A mixing time of 40 ms was chosen. In the resulting difference spectrum the complete sub-spectrum of the methylene protons of the 3-substituted β end group is seen. As in the previous example of capsorubin (**413**) diacetate (Fig. 11) the distinction between positions 2 and 4 is not directly evident and must be derived by other experimental techniques. Illustrated in trace C, the same experiment was performed by inverting H(3'). The total acquisition time of each experiment was only 16 min.

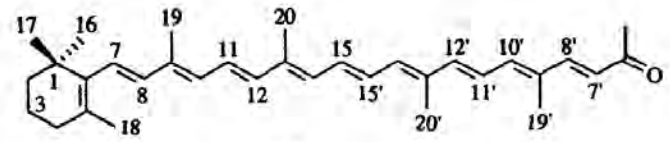
It is evident that in these difference spectra the subtraction even of the strong methyl signals is excellent and that even those signals which are difficult to see in the 1D spectrum [*e.g.* H(2'β)] can be clearly located. This technique is of special interest in cases where the high-field part of the spectrum is very complex or even partly obscured by strong impurity peaks. A further application of this experiment has been reported [21].

This discussion underlines the particular importance and utility of 1D TOCSY in special applications to carotenoids.

e) Homonuclear ^{1}H, ^{1}H-correlated 2D spectroscopy (COSY)

In all but the simplest assignment problems, which can be performed frequently by application of a few selected 1D experiments, the homonuclear ^{1}H,^{1}H-COSY 2D experiment is a routine first resort which has a number of advantages, to be discussed below, and only one minor disadvantage, namely that typically a total measuring time of several hours is needed, in practice, for a 2D spectrum with good signal-to-noise and, more importantly, of sufficiently high resolution. In spite of this limitation, 2D COSY is the most useful technique for the assignment of the NMR signals of carotenoids, particularly in the crowded olefinic range. The 2D COSY partial spectrum of citranaxanthin (**466**) is presented in Fig. 13. This serves as a representative example of medium complexity to illustrate in detail the merits and limitations of this pulse experiment and particularly to show the kind of structural information that becomes available.

A standard COSY pulse sequence starts with a 90° pulse, followed by an incrementable delay called evolution time t_1. Then, a second 90° pulse follows, called the mixing pulse (COSY-90). Subsequently the FID is acquired during acquisition time t_2. This cycle is repeated a number of times until a good signal-to-noise ratio is obtained. Subsequently the evolution time t_1 is incremented and the second FID is accumulated and stored separately. The full time-domain 2D data set finally consists of several hundred FIDs corresponding to the chosen number of incremented evolution times [6-9]. The FIDs are then multiplied by suitable window functions which improve the signal-to-noise or the resolution in the same way as in 1D spectroscopy. Moreover, the choice of the window function opens the possibility to enhance or to reduce the intensities of cross peaks caused by very small couplings. The final resolution increases with the number of data points acquired during t_2 and the number of experiments (number of data points in t_1). The time domains are normally enlarged advantageously by so-called zero-filling, which can considerably improve the digital resolution at the expense of an



466

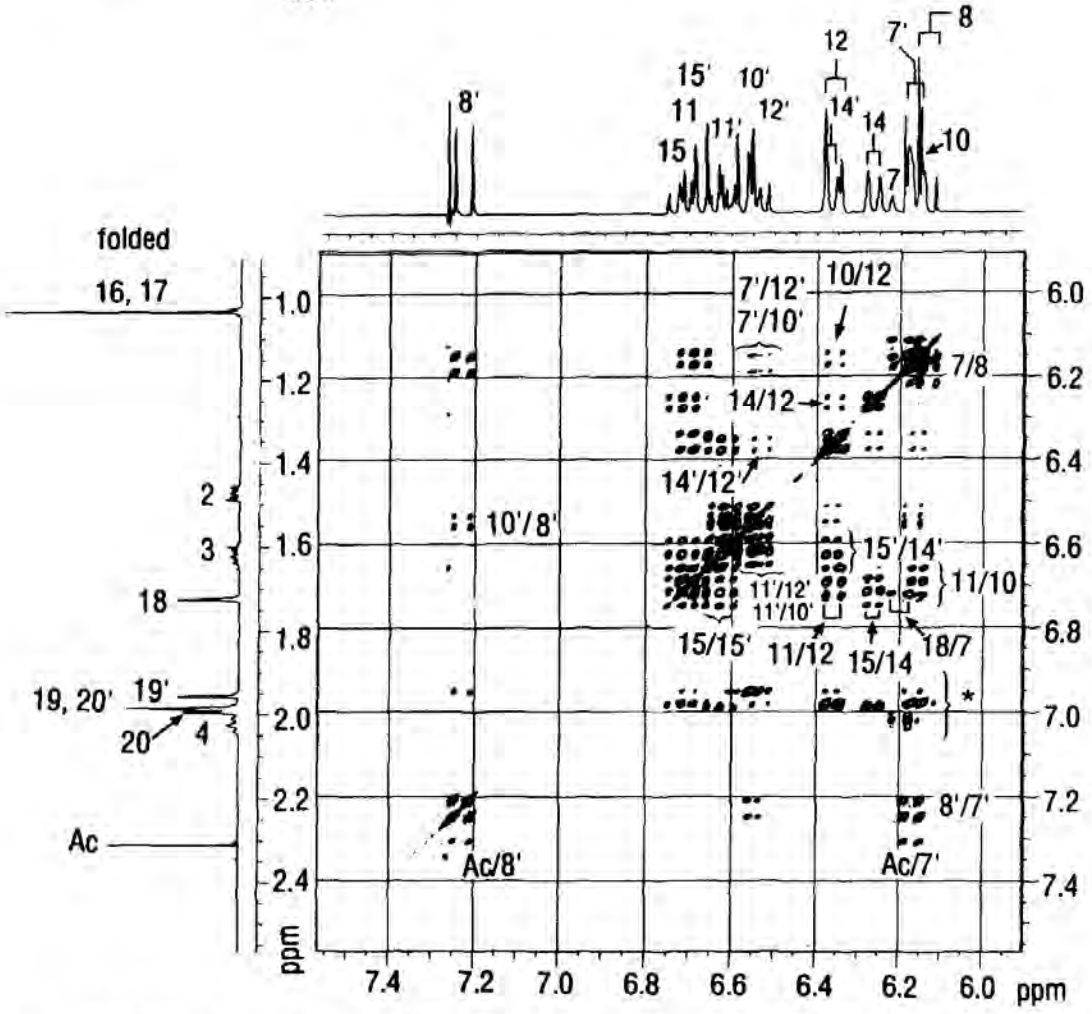


Fig. 13. 400 MHz (absolute-value) 2D COSY spectrum of citranaxanthin (**466**; 10 mg in 0.6 ml $CDCl_3$). Experimental conditions: 1K data points in t_2, 800 experiments in t_1, transmitter frequency at 6.73 ppm, spectral widths 666.7 Hz in F_1 and F_2, acquisition time in t_2 0.77 s, relaxation delay 1.07 s, 16 scans and 2 dummy scans per experiment, zero-filling to 4K and 2K in t_2 and t_1, sine-bell windows in t_1 and t_2, total measuring time *ca.* 8h.

On top the olefinic part of the 400 MHz ^{1}H-NMR spectrum of the measured range is plotted to simplify the recognition of the fine structure of the cross peaks. On the left margin the aliphatic range of the 1D spectrum is seen as it would appear after three-fold folding along the perpendicular F_1 axis. Cross peaks between these folded signals and olefinic protons appear on horizontal rows at positions of the coupled olefinic protons. The range marked by an asterisk is expanded in Fig. 15.

increase of the size of the data files. Upon 2D Fourier transformation, the frequency-domain data set is obtained which consists of intensities as a function of two frequency axes F_2 and F_1. In the same way as was discussed briefly for ROESY, this 2D spectrum is normally represented as an intensity contour plot where each level corresponds to a selected intensity of the peaks [6, 7].

The mixing pulse of the COSY pulse sequence partly transfers magnetization, that is initially associated *e.g.* with proton H(a) at chemical shift δ(a), to its spin-coupled neighbour H(b) at shift δ(b) and *vice versa*. As a consequence, the intensity of the signal of H(a) is modulated during t_1 by the shift of H(b), and *vice versa*. Upon Fourier transformation this modulation is transformed into a frequency and hence into cross peaks at positions δ(a), δ(b) and δ(b), δ(a) along the horizontal F_2 and the vertical F_1 axes, respectively. The two cross peaks, which are symmetrically positioned with respect to the diagonal (see below), thus reveal that the two protons H(a) and H(b) are spin-coupled. In a highly resolved 2D spectrum the fine structure of a cross peak represents the complete multiplet structure of the two coupling partners since a cross peak between two doublets consists of four components (two in either direction), a cross peak between a doublet and a doublet of doublets consists of eight components, and so on. As a result, the structure of a cross peak defines the positions and the multiplet structures of the signals of the two coupled protons which often cannot be resolved in the 1D spectrum in overlapping regions.

A homonuclear COSY 2D spectrum also possesses a diagonal (see Fig. 13) which arises from all magnetization components which were unaffected during t_1, *i.e.* these peaks represent the normal 1D spectrum. Close to the diagonal are further peaks that arise by magnetization exchange between the multiplet components of a given proton.

Several different variants of the basic COSY pulse sequence are known [6-9]. As will be demonstrated in the following discussion, the simplest version, called absolute-value or magnitude COSY, yields excellent results provided the experimental parameters are properly chosen for application to carotenoids. Based on numerous applications it is felt that the long-range COSY or the phase-sensitive COSY and its different variants have only marginal advantages here. Particularly in the latter case the slightly improved resolution and the additional information on active and passive couplings, revealed by positive and negative intensities of cross peaks, are in general outweighed in routine applications by the need to perform a phase correction in both directions. A further practical advantage of the absolute-value COSY is the fact that sine-bell windows can be used advantageously and this enhances cross peaks due to long-range couplings [9], thus providing important structural information.

Application of COSY to carotenoids is greatly hampered by the fact that at least one region of the spectrum, namely the olefinic part, is often heavily crowded. Therefore, the derivation of a sequence of consecutive coupled protons is only possible in this range if excellent digital resolution can be achieved in order to represent correctly and to resolve the overlapping multiplets. This can be obtained, in principle, in two ways. First, the number of data points (including zero-filling) of the FID and hence of the transformed spectrum is increased such that at least 0.5 Hz per point digital resolution is obtained in both directions for a typical frequency width of about 3000 Hz. In practice, this is not a good choice since it would generate impracticably large data files that would need to be stored and processed by the computer.

Moreover, the increasing number of experiments would increase the total acquisition time to an unacceptable degree. The second and preferable possibility is to reduce the measured spectral range in F_1 and F_2 to about 1 to 2 ppm, *i.e.* to acquire only the olefinic part of the spectrum. An important consequence of this is that, by reduction of the frequency width, the acquisition time t_2 is prolonged. As a result, observation of cross peaks caused by small or even very small long-range couplings becomes possible [6]. As will be seen, this gives important structural information on the linkage of the different spin sub-systems. This remedy has been applied to the study of carotenoids, and the excellent resolution and the existence of cross peaks caused by extremely small long-range couplings have been demonstrated [4, 29].

Although only the olefinic part is acquired in both directions, the 2D spectrum shows, besides the highly resolved cross peaks between coupled olefinic protons, further connectivities to protons that absorb outside this region. This arises from the fact that, in pulsed Fourier-transform spectroscopy, signals from outside the acquisition range are folded back by the digitization process into the measured region; this principle also applies to the cross peaks between olefinic protons and other coupled partners [6, 7]. Along F_2 this folding is vastly suppressed, as in normal 1D spectroscopy, by suitable audiofrequency filters. This also helps to suppress noise which would otherwise be folded from outside into the measured region. Along F_1, on the other hand, this suppression is not possible. Cross peaks between aliphatic and olefinic protons, which would appear in the upper left-hand part of a spectrum measured with the full spectral width, are folded along F_1 and appear at defined positions in the 2D spectrum measured with reduced spectral width. Therefore, the spectrum given in Fig. 13 shows, in addition to the symmetrically placed cross peaks between coupled olefinic protons, a number of additional peaks that reveal connectivities to protons absorbing outside this range. These peaks have no symmetrical counterparts and can, therefore, readily be distinguished from the regular cross peaks. Moreover, they can be removed, where necessary, by symmetrization of the 2D file [6].

The 2D spectrum shown in Fig. 13 was acquired in magnitude mode with spectral widths of 1.667 ppm (666.7 Hz) in both dimensions with the transmitter placed at 6.73 ppm. Hence, the range acquired extends from 7.57 to 5.90 ppm. After zero-filling, a very fine digital spectral resolution of 0.33 Hz per point was achieved in both directions. In the upper part of Fig. 13, the 1D spectrum of the same range was plotted. A corresponding spectrum should, in principle, also run along F_1 (see scale at the right-hand side of the 2D spectrum). Cross peaks between olefinic and aliphatic protons absorbing around 2 ppm appear after three-fold folding, $3 \times 1.667 = 5$ ppm downfield, *i.e.* at about 7 ppm along F_1. For convenience the corresponding region has been plotted on the left-hand side of the 2D spectrum. The experimental conditions were chosen such that most of the folded cross peaks appear in the horizontal range free from other unfolded cross peaks. In magnitude mode, the folded spectral part preserves its direction from high to low field, whereas in phase-sensitive mode the direction in consecutive foldings is reversed. This might introduce some minor complications in the interpretation of this type of COSY.

i) Regular cross peaks. In order to demonstrate the general procedure for assigning the olefinic signals, the first step is to interpret the unfolded cross peaks between olefinic protons. In order

to simplify the overview and the following discussion, all relevant cross peaks in Fig. 13 are denoted according to their origin at the two coupled protons. Here, the first number refers to the proton on the diagonal, the second to its coupled partner. In the upper-left triangle the designations of long-range connectivities, corresponding to couplings over more than three bonds, have been inserted. In the lower-right triangle those corresponding to vicinal ^3J couplings have been labelled, although both types of cross peaks appear in a symmetrical fashion in both triangles.

For citranaxanthin (**466**), the doublet at lowest field (7.23 ppm) is assigned to H(8') at the β position to the carbonyl group. All other assignments of the olefinic protons can then readily be obtained from a sequence of cross peaks in the 2D spectrum. Thus, the location of the coupling partner H(7') is obvious from strong cross peaks (2 x 2 multiplet) with H(8') along F_1 and F_2 at positions near 6.17 ppm. Other, much weaker cross peaks at 6.55 ppm define the position of a further doublet which is assigned to H(10'). This coupling, $J_{8',10'}$, is estimated to be of the order of 1 Hz and is not resolved in the 1D spectrum. From the signal of H(10') the signals of H(11') and then of H(12') can be localized by corresponding strong cross peaks in the crowded region near 6.6 ppm. From H(12'), weak cross peaks provide a linkage to H(14') and from there again strong cross peaks help to assign, in subsequent steps, the remaining protons of this 4-spin sub-system, namely H(15'), H(15), and H(14). Weak cross peaks from H(14) to H(12) help to identify the H(12) signal which serves as a starting point for the next 3-spin system with H(11) and H(10). Finally, the remaining 2-spin system of H(8) and H(7) is readily detected as the only remaining signals near 6.16 ppm, although the weak cross peaks to be expected between H(10) and H(8) are not visible because their chemical shifts are so close.

So far, only connectivities by ^3J and ^4J couplings have been used. Under the experimental conditions chosen in this experiment (see legend of Fig. 13), further cross peaks are found which correspond to couplings that extend over even more intervening bonds. Examples are those between H(12') and H(7'), over seven bonds, and between H(10') and H(7'), over five bonds. Other examples have been reported [4]. Fortunately, these peaks have much smaller intensity and can therefore be distinguished from those which arise from three-bond couplings and are structurally more relevant. Some further long-range connectivities will be discussed below.

Since the sequence of assignments is not always readily seen in this contour plot, a slightly different way of presentation is used in Fig. 14. Here, some horizontal rows along the horizontal F_2 axis are plotted at selected chemical shifts, namely at the position of one of the multiplet components of the underlined protons. This way of presentation reveals much better the relative intensities of the different cross peaks. Thus, protons which are coupled by large vicinal spin couplings show approximately the same intensities as the corresponding diagonal peak. In contrast, those cross peaks corresponding to smaller couplings show much smaller intensities.

In trace B is presented the selected row through the low-field component of the H(8') doublet at 7.251 ppm on the diagonal. As a result it is possible to obtain the 2-spin spectrum of H(8') and H(7') and the much weaker signal of H(10') due to the long-range coupling $J_{8',10'}$. In trace C the signals of H(12') and H(11') are seen with further connectivities to H(14') and H(7'). The connectivity between H(12') and H(7') corresponds, as was already noted, to a

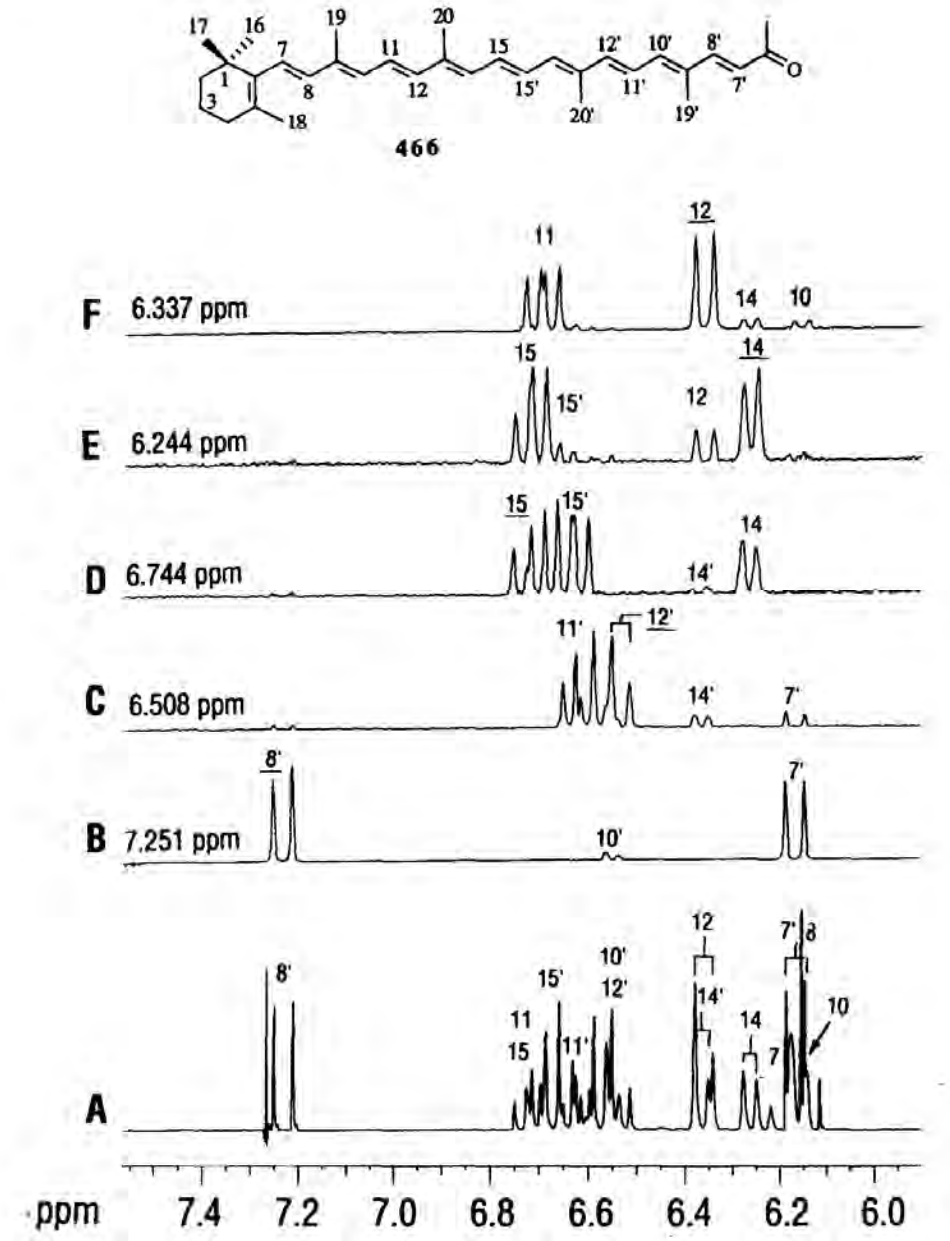


Fig. 14. Trace A: olefinic part of the 400 MHz ^{1}H-NMR spectrum of citranaxanthin (**466**). Traces B to G give selected rows from the 2D COSY of Fig. 13 chosen at the chemical shift positions on the diagonal as indicated. The designation of the corresponding proton is underlined. The rows represent the different sub-spectra of coupled protons. The intensities reflect the magnitude of the involved spin couplings with strong intensities due to vicinal couplings between 11 Hz and 15 Hz and weak peaks caused by small multiple-bond couplings. Trace C shows, besides the intense sub-spectrum of H(12') and H(11'), weak connectivity between H(12') and H(14') and H(7'). The latter is caused by a long-range coupling over seven intervening bonds. Arbitrary scale factors were used in the different spectra.

long-range coupling over seven bonds which must have a similar magnitude to the coupling $^4J_{12',14'}$, as indicated by the relative intensities of both cross peaks. Because of the high digital resolution of the experiment and the fact that the row was chosen at the high-field component of the doublet of H(12') with no other close signals, the presence of this long-range coupling is clearly proven. Other connectivities are delineated in traces D to F, in agreement with the results of Fig. 13.

From this discussion it is evident that a COSY spectrum of good resolution is extremely informative. Not only can the different olefinic sub-spin systems readily be assigned and identified, but their linkage can be deduced from a number of small, long-range couplings. From corresponding plots of selected rows (or columns), well-resolved 1D sub-spectra can be obtained. These can be used to determine chemical shifts and coupling constants which are often not accessible in the 1D spectrum.

ii) Folded cross peaks. Figure 13 also contains some folded cross peaks between aliphatic protons and olefinic protons (see the folded spectrum at the left-hand side). They appear in horizontal rows through the folded aliphatic signals at the F_2 position of the coupled olefinic proton. A very interesting observation is that even the acetyl protons, whose signal is commonly denoted as being very narrow, must have very weak long-range couplings to H(7') and even H(8') as indicated by the corresponding cross peaks. This connectivity might be informative in other cases if the shifts of the immediate neighbours cannot be predicted solely by consideration of their expected chemical shifts. Further expected connectivities are seen between H(18) at 1.72 ppm (folded to 6.72 ppm) and H(7).

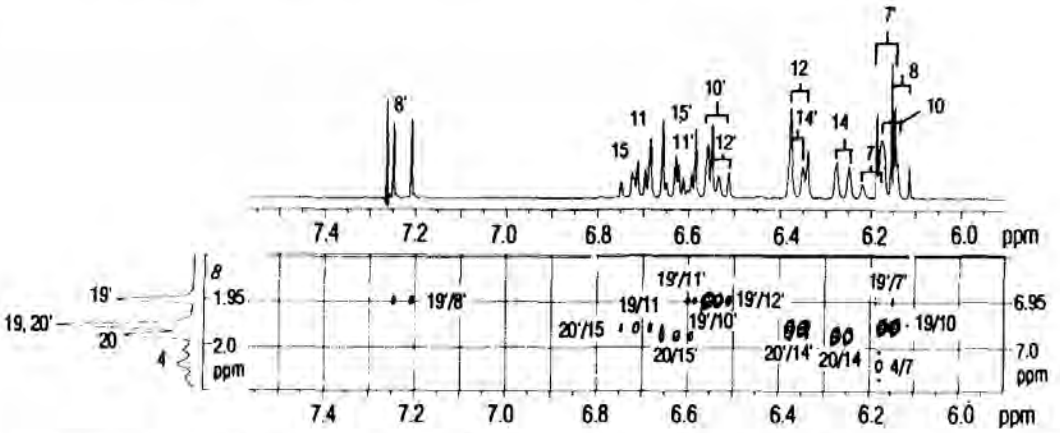


Fig. 15. Expanded part of the COSY spectrum of Fig. 13 showing cross peaks between folded aliphatic protons and olefinic protons. Strong cross peaks correspond to couplings over four bonds (~1.4 Hz); other much weaker cross peaks are caused by very small and unresolved couplings over up to six bonds.

Since the part of the spectrum containing cross peaks between the olefinic and in-chain methyl protons is slightly overloaded in Fig. 13, Fig. 15 shows this interesting region as an expanded plot. Connectivities between methyl protons and olefinic protons are readily obtained

from the four pairs of strong cross peaks which are caused by relatively large ^4J couplings of about 1.4 Hz such as $J_{19,10}$, $J_{20,14}$ *etc*. After the four methyl signals have been assigned in this way, some further much weaker cross peaks to other protons can be used to link the different olefinic sub-spectra in the same way as before, by using some long-range connectivities between olefinic protons. Thus, as an example, H(19') has, besides a strong cross peak to H(10'), further weak cross peaks to olefinic protons such as H(8') and H(7') on one side and H(12') and even H(11') on the other side. This again links together the consecutive 2-spin and 3-spin systems. Further cross peaks between the triplet of the two equivalent methylene protons H(4) and the doublet of H(7) are also clearly identified.

This partial 2D spectrum is again better visualized in Fig. 16, which depicts some selected rows of the same data set (traces B to E) indicating the relative intensities of the different cross peaks in a much clearer way. These examples demonstrate the excellent signal-to-noise ratio of this 2D experiment, pointing again to the fact that a considerable reduction in sample concentration or in measuring time would be feasible without loss of relevant information.

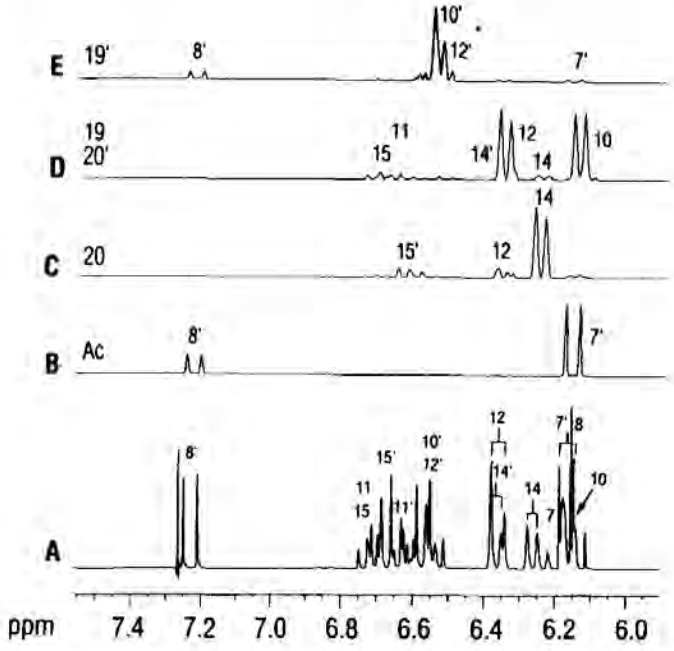


Fig. 16 Selected rows of the COSY spectrum of Fig. 13 showing connectivities between folded methyl signals of citranaxanthin and some olefinic protons. Arbitrary intensity scale factors were used for the different traces.

In conclusion, it has been demonstrated that a 2D COSY experiment leads to a complete and reliable assignment of the proton signals of carotenoids. This is mainly due to the fact that connectivities caused by very small couplings are detectable under properly chosen experimental conditions. These long-range couplings provide a wealth of structural information which has not yet been fully explored. It has already been mentioned in Section D.1 that the

presence of long-range couplings with a magnitude of the order of 1 Hz has to be taken into consideration when precise calculations of coupling constants are being made either by spectral simulation or directly from the experimental spectrum.

For the COSY spectrum shown in Fig. 13 a relatively large sample quantity was used (10 mg). It should be emphasized that spectra of reduced quality but still containing useful information have been recorded from quantities around 10 μg, although part of the long-range information in particular was lost in the noise background.

Related structural information can also be deduced by other techniques such as ROESY or $^{1}H,^{13}C$ multiple-bond COSY. However, the absolute-value COSY with reduced spectral range should be the method of choice at the beginning of the spectral interpretation because of the ease of experimental implementation and high information content.

It is worth mentioning in this context that virtually all the assignments given in Table 3 were made in this way. Only in a few cases were the phase-sensitive and double-quantum filtered variant or other techniques such as double-quantum 2D applied [6-8, 36].

A minor drawback of the reduction in spectral width is that connectivities between coupled protons which both absorb outside the acquired range cannot be detected. However, as has been demonstrated before, this information can readily be obtained by some selected 1D TOCSY experiments. In cases where the full frequency width is measured, the application of the long-range version of COSY [9] with an extra delay of up to 0.2 s before acquisition of the FID is recommended; this partly retains the long-range information but is, in general, unable to resolve connectivities in the crowded olefinic regions because of its poor digital resolution.

2. ^{13}C-NMR

a) ^{1}H-decoupled ^{13}C-NMR

The reduced sensitivity of ^{13}C-NMR by a factor of about 500 has already been mentioned. This refers to the standard spectrum which is measured under simultaneous ^{1}H decoupling over the full range of proton chemical shifts of about 15 ppm. This results in a singlet signal for each of the differently shielded carbons in the molecule. For the decoupling, one of the optimum composite pulse decoupling sequences such as WALTZ-16 is normally used [6, 9]. This gives excellent decoupling to sharp lines over a wide range of proton shifts at relatively low rf power. This ensures that there is no excessive heating of the sample and hence no problems arise with the field homogeneity and with the deuterium lock. If solubility is not a limiting factor it is advantageous, in practice, to measure the solution in a 5 mm sample tube since the corresponding probe head is superior in sensitivity to the 10 mm probe head.

b) ^{1}H-coupled ^{13}C-NMR

This type of spectrum can provide useful information on the different couplings between protons and carbons. However, its acquisition is greatly hampered by the considerable loss in sensitivity compared to the decoupled spectrum. Since each carbon is often coupled to several

different protons over one to three (rarely over four) bonds, most of the signals are split into multiplets and/or are broadened by unresolved multiple-bond couplings. In practice, acquisition of a good ^{1}H-coupled spectrum therefore needs measuring times which are at least a factor of 20 longer than those for decoupled spectra. This is in most cases unacceptable unless large sample quantities are available. A further disadvantage is that, in crowded regions, it is often impossible to disentangle the overlapping multiplets even at higher measuring frequencies. Moreover, the most valuable information on the multiplicity of the different carbon signals is obtained much faster by DEPT (see Section 2.c, below).

However, to enable optimum choice to be made of the delays in a number of multi-pulse sequences such as DEPT and ^{1}H,^{13}C-COSY, some average values are presented of typical coupling constants between protons and carbons as measured from some ^{1}H-coupled ^{13}C spectra of a number of carotenoids. Because of the problems mentioned before, only a relatively coarse overview of the expected range of the different couplings can be given here.

In agreement with expectation, the couplings depend on the hybridization of the carbons involved. Protonated olefinic carbons show typically $^1J_{CH}$ couplings between 148 and 160 Hz. An aldehyde carbon at the end of the conjugated chain has a considerably larger coupling of around 172 Hz. In-chain methyl carbons show couplings at the lower end of the $^1J_{CH}$ range near 128 Hz with further multiple-bond couplings of about 7.5 and 5 Hz over three bonds. As an example, C(19) is coupled to H(10) and H(8), and C(20) is coupled to H(14) and H(12). These multiple-bond couplings and their cross peaks in the long-range variant of the ^{1}H,^{13}C-COSY are particularly informative. Similar couplings are to be expected between the protons of the methyl groups such as H(19) and the three carbons C(8), C(10) (three bonds) and C(9) (two bonds) and similarly between H(20) and C(12), C(14) and C(13). These couplings also give rise to informative cross peaks in this experiment. Couplings over four and more bonds are very rarely detected.

One-bond couplings of aliphatic methyl carbons in end groups are normally between 126 and 130 Hz and, again, there may be a characteristic difference between axial and equatorial orientation. Carbons with substituted oxygen functions such as C(3) in astaxanthin (**406**) diacetate have slightly greater $^1J_{CH}$ values near 145 Hz, whereas the value for C(2) in these compounds is around 132 Hz.

An important feature of multiple-bond couplings between olefinic protons and carbons is that three-bond couplings are normally much greater than those over two bonds which are, in most cases, too small to be resolved. Thus C(11) and related carbons appear solely as a doublet by $^1J_{CH}$ with no further splittings by H(10) or H(12). In contrast, C(15) and C(15') have, besides one-bond couplings, also three-bond couplings of roughly 5 Hz to H(14') and H(14), respectively, and thus their signals can readily be distinguished. In many cases these empirical rules have considerably simplified previous assignments [14] and they are also very helpful in the interpretation of multiple-bond heteronuclear 2D COSY spectra.

In summary, ^{1}H-coupled ^{13}C spectra contain important structural information which can be useful for the assignment of carbon signals and for the optimum set-up and interpretation of heteronuclear COSY spectra. Despite these advantages, these spectra are only rarely used in present ^{13}C-NMR experiments because of their low sensitivity and the severe problems caused by the strong overlap of the different closely spaced signals.

c) Distortionless enhancement by polarization transfer (DEPT)

One of the first tasks in the analysis of a ^{13}C-NMR spectrum of an unknown carotenoid is to determine the multiplicities of the different signals, *i.e.* to divide them into groups according to the number of attached protons. Whereas the signals of unprotonated carbons are often immediately visible by their reduced intensities due to their partial saturation by rapid pulsing, the correct and unambiguous identification of the number of CH, CH_2 and CH_3 carbons is an important prerequisite for the structure elucidation.

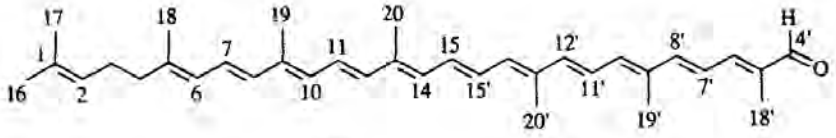
The method of choice is the ^1H, ^{13}C multi-pulse experiment DEPT which is known to have some substantial advantages over other related pulse sequences [6, 7, 9]. As the name indicates this sequence, which consists of three ^1H and two ^{13}C pulses, is based on the transfer of polarization (or excess population) from the more sensitive proton to the less sensitive ^{13}C nucleus. This results in a gain in sensitivity of the detected ^{13}C signal by up to a factor of 4. The transfer occurs after a delay D which is set equal to $1/(2\ ^1J_{CH})$. Although, as was noted above, one-bond couplings involved can vary between 130 and 170 Hz, a choice of D = 3.6 ms corresponding to an average value of $^1J_{CH}$ of 140 Hz gives good results since the DEPT sequence is relatively insensitive to variations of the coupling constants.

The information on the multiplicity is obtained as phase information (positive or negative intensities) in the final ^1H-decoupled DEPT spectra by selecting the duration of the last proton pulse in the sequence in such a way that the flip angle is 45°, 90° and 135° in three successive experiments. As a result, three different ^{13}C spectra are obtained showing CH, CH_2 and CH_3 as positive singlet signals in the first, CH only with positive intensity in the second, and CH and CH_3 with positive, CH_2 with negative intensity in the third experiment. In all these experiments, the signals of quaternary carbons are suppressed and can thus be identified. The three different DEPT spectra of astaxanthin (**406**) diacetate have recently been presented [4]. It has also been demonstrated that, by suitable linear combinations of the three spectra, three so-called edited DEPT spectra can be calculated which are pure sub-spectra of the three groups of carbons, namely of CH, CH_2 and CH_3 [9].

It is evident that, for daily routine practice, it suffices, in general, to acquire solely a single DEPT-135 spectrum since this normally gives all the information that is needed. Only in rare cases might it be desirable to distinguish additionally between CH and CH_3 signals by acquisition of a DEPT-90 spectrum.

An example of a 100 MHz DEPT-135 spectrum, of apo-4'-lycopenal (*6*), is shown in Fig. 17 (upper) together with the ^1H-decoupled spectrum (lower). The DEPT spectrum has been phased so that CH and CH_3 have positive signals and CH_2 negative signals. Owing to the sharp signals, the multiplicity of closely spaced signals can readily be distinguished. It is important to note that, because of the gain in sensitivity, the number of scans (but not the total measuring time) can be reduced in DEPT compared to the normal ^{13}C spectrum. In the latter a flip angle of around 40° and an acquisition time of 0.7 s per scan were used, whereas the DEPT sequence consists of 90° and 180° pulses and this needs some special precautions. The DEPT spectrum shown in Fig. 17 was obtained by accumulation of 1500 FIDs compared to 5000 FIDs needed for the normal ^{13}C spectrum. Since the polarization transfer from ^1H to ^{13}C can only work properly if the proton and carbon equilibrium magnetizations are nearly restored

before the next scan is started, a suitable relaxation delay of at least 1.5 s must be added between scans in order to allow for relaxation. Together with the acquisition time t_2 of 0.7 s this results in a scan repetition time of *ca.* 2.2 s. Hence the minimum requirement of $2T_1$ is nearly fulfilled since the proton T_1 are of the order of 1 s and longer than the T_1 of protonated carbons. Therefore the total accumulation times of DEPT and ^{1}H-decoupled spectra are normally about the same despite the increased sensitivity of the former. This compares very favourably with the long total acquisition time needed for ^{1}H-coupled or CW off-resonance decoupled spectra which were previously used to determine the multiplicity.



(*6*)

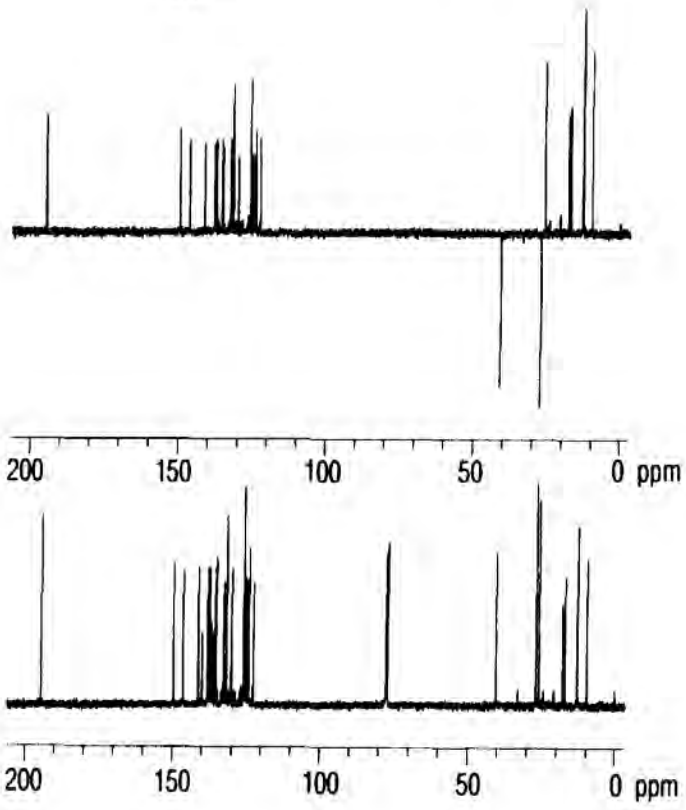


Fig. 17. Bottom: 100 MHz ^{1}H-decoupled ^{13}C-NMR spectrum of apo-4'-lycopenal (*6*, 20 mg in 0.6 ml $CDCl_3$). Top: DEPT-135 ^{13}C-NMR showing CH and CH_3 carbons with positive intensity, CH_2 with negative intensity. Signals of unprotonated carbons are eliminated. A delay of 3.6 ms was used to select polarization transfer by $^1J_{CH}$ couplings of about 140 Hz. A relaxation delay of 1.5 s was applied in the DEPT experiment.

d) ^{1}H, ^{13}C-Correlated 2D spectroscopy (hetero-COSY)

This class of 2D multi-pulse experiments is extremely useful since it correlates ^{1}H and ^{13}C chemical shifts. Thus, the two shift axes now correspond to ^{1}H and ^{13}C instead of solely ^{1}H as in homonuclear COSY. A cross peak at coordinates $\delta(^{1}H)$ along the proton axis and $\delta(^{13}C)$ along the ^{13}C axis indicates that proton and carbon are spin-coupled to each other. Therefore, if the assignment of either nucleus is known, the assignment of the other is directly deducible.

A great variety of different pulse sequences is available [6-9]. Some rely on polarization transfer methods from the more sensitive proton to the less sensitive carbon as in DEPT. Other sequences use so-called single quantum or multiple quantum coherence evolving during t_1. In all of them, there is a certain delay between pulses of the sequence. This delay is set to $D = 1/(2J_{CH})$, *i.e.* the experiments are tuned to the average value of the involved heteronuclear couplings, to obtain optimum sensitivity.

It was explained in Section F.2.b that there are two well-separated classes of couplings, namely one-bond and multiple-bond couplings, with values around 140 Hz and between 0 and *ca.* 12 Hz (absolute values), respectively. According to this separation, two different variants of $^{1}H,^{13}C$-COSY are possible, namely one in which the delay is tuned to one-bond couplings (D = 3.6 ms), and the second with a longer delay tuned to the much smaller multiple-bond couplings. Here, a delay of 70 ms is frequently chosen, which assumes an average coupling of about 7 Hz.

The two variants provide different information. The former directly links a given carbon with its directly attached protons and thus mainly supports the assignment of the signals of protonated carbons. The multiple-bond version, on the other hand, has some interesting features. First, it allows the assignment of unprotonated carbons, an otherwise difficult task. More importantly, a given proton is normally linked to several neighbouring carbons and, conversely, a given carbon is often linked to several protons in its vicinity. All these couplings give rise to observable cross peaks in the 2D spectrum, provided the coupling constants are in the range covered by the polarization transfer delay.

A great help in the interpretation of these spectra is the experimentally found rule that, in general, only two-bond and three-bond couplings are sufficiently large (> 2 Hz) to produce observable cross peaks. Therefore, this experiment provides important structural information, as will be seen below.

The two types of $^{1}H,^{13}C$-COSY can be distinguished further according to the nucleus, ^{13}C or ^{1}H, which is detected during acquisition time t_2.

i) ^{13}C-Detected $^{1}H,^{13}C$-COSY. The previously described standard $^{1}H,^{13}C$-COSY 2D pulse sequence relied on polarization transfer from the more sensitive proton to the less sensitive carbon with the final detection of the ^{13}C magnetization during acquisition time t_2 under simultaneous decoupling of the protons [6-8]. The information on the chemical shift of protons arises from modulation of the ^{13}C magnetization during the evolution time t_1. It is evident that the sensitivity of this experiment must be rather low. The one-bond and the multiple-bond experiments with the polarization transfer delay D tuned to 140 and 8 Hz, respectively, have recently been applied to (5'*R*)-cryptocapsone (**382**) and the experimental conditions,

advantages and drawbacks of this technique when applied to carotenoids have been discussed briefly [4]. As a rule of thumb, based on numerous experiments of this type, it is concluded that at least 20 mg of sample should be available in order for a one-bond and a multiple-bond experiment of acceptable quality to be acquired in a typical overnight run of 15 h.

In this context it should be noted that the multiple-bond version has much poorer sensitivity since the original magnetization is normally distributed over several cross peaks. Moreover, the polarization transfer delay is optimally active only within a narrow range of a few Hz and not over the full range of couplings between about 2 and 12 Hz. Therefore, some of the potential cross peaks are weak and lost in the background noise. If sufficient instrument time is available, a second experiment with a longer delay may be advantageous in important cases to cover a second range of smaller couplings.

To compensate for the loss in sensitivity, it is advisable to use at least four times as many scans per FID of the 2D experiment in the multiple-bond than in the one-bond experiment. As will be seen, the $^{1}H,^{13}C$-COSY with detection of ^{1}H magnetization during t_2 is far superior and therefore necessary in cases where less than about 20 mg of sample is available.

ii) ^{1}H-Detected $^{1}H,^{13}C$-COSY. This novel multi-pulse experiment offers a substantial gain in sensitivity over the old 2D heteronuclear correlation with ^{13}C detection. It starts with the magnetization of the more sensitive proton and ends by acquisition of proton magnetization during time t_2. The information on the chemical shift of ^{13}C is produced by modulation of the ^{1}H magnetization during the evolution time t_1. In this experiment, the assignment of the F_1 and F_2 axes to the two types of nucleus is therefore interchanged compared to the old version and hence the experiment is often called inverse or reverse $^{1}H,^{13}C$-COSY. Moreover, this ^{1}H-detected experiment is performed on older spectrometers in the so-called reverse mode with the ^{1}H-decoupler as the source for the proton pulses. This needs some hardware changes in the set-up of the spectrometer.

It is important to note that it is the ^{1}H signals of isotopomers with ^{13}C that are detected, *i.e.* the much stronger ^{1}H signals of the 99% of protons that are attached to ^{12}C must be efficiently suppressed. This problem has largely been solved in recent years by modern multi-pulse techniques and improvement in instrumentation.

Of the two different classes of pulse sequences of the one-bond version available now, namely the so-called heteronuclear single-quantum and the multiple-quantum coherence experiment, the former is particularly useful for application to carotenoids [47, 48]. In recent years, this multi-pulse experiment has been favoured over the multiple quantum version since, in the former, the ^{1}H–^{12}C magnetization is better suppressed and, moreover, the cross peaks are not broadened along F_1 by the mostly unresolved ^{1}H–^{1}H couplings [48, 49]. A theoretical discussion of the relative advantages and drawbacks of the two versions was presented recently [49].

Further improvement of sensitivity is possible if simultaneous ^{13}C-decoupling is applied during acquisition time t_2. This leads to a coalescence of the doublet components along F_2 that are caused by heteronuclear one-bond coupling and hence to a gain in signal intensity by a factor of up to 2. A composite pulse-decoupling scheme called GARP-1 [50] is frequently used

which allows the decoupling of ^{13}C over the wide chemical shift range of *ca.* 200 ppm (about 20 KHz at 100 MHz) without the use of excessive power.

A representative one-bond $^{1}H,^{13}C$-COSY spectrum with ^{1}H-detection at 400 MHz and ^{13}C-decoupling is shown in Fig. 18; it was measured in 3.5 hours from 4 mg of echinenone (**283**, see assignment in Table 4). As was discussed before, the ^{1}H shift axis now runs horizontally (F_2), whereas the 100 MHz ^{13}C axis is along the vertical axis F_1 as indicated by the 1D spectra of these nuclei along the top and on the left-hand side of the 2D contour plot. Each cross peak between given ^{1}H and ^{13}C signals shows essentially the same multiplet structure along F_2 (singlet, doublet *etc.*) as in the 1D ^{1}H spectrum and appears at a given ^{13}C position along the F_1 axis, thus revealing the connectivity of the two nuclei.

As can be seen, the signals of the ^{12}C isotopomers are indeed completely suppressed. Their signals would give rise to strong ridges along F_1 mainly at positions of strong ^{1}H signals such as the methyl singlets. From suitable expansions of this contour plot the assignments of all the protonated carbons are readily derived from the known assignments of the protons. The signal-to-noise ratio is excellent despite the relatively short total acquisition time. As in previous examples, reduction of the number of scans per experiment from 16 to 8 would clearly be feasible.

A few general remarks about the one-bond $^{1}H,^{13}C$-COSY experiment may be useful here. First, since the ^{1}H magnetization of ^{13}C isotopomers is acquired, it may happen in some cases that two carbons give, at the same time, two cross peaks each with two protons, and *vice versa*. This ambiguity can be explained in the following way. If ^{13}C is present at a given position, *e.g.* at C(11), then in 50% of these isotopomeric molecules the corresponding ^{13}C spin is oriented parallel to the external field; in the other 50% it has an antiparallel orientation. This gives rise to two ^{1}H satellite multiplets for H(11) which are $^{1}J_{C,H}$ ~150 Hz apart from each other. Since H(11) is coupled to H(12) [and H(10)] it may happen that in 50% of the molecules the frequency difference between H(11) and H(12) [or H(10)] in this isotopomer becomes smaller than the mutual proton coupling $J_{11,12}$ (or $J_{11,10}$). This corresponds to the strong coupling case, as was discussed in Section D.1, and it results in mixing of the two proton spin functions. This means that C(11) may 'see' two different protons instead of only one, *i.e.* it may have cross peaks with H(11) and H(12) [or H(10)]. In the isotopomer with ^{13}C at C(12), H(12) and H(11) are also strongly coupled in 50% of the molecules and hence both give cross peaks with C(12). In many cases the 'wrong' cross peaks have lower intensity than the regular ones but, in certain cases, differentiation and hence the assignment may remain ambiguous. This situation can occur in ^{1}H-detected and in ^{13}C-detected hetero-COSY and may need further information on the predicted range of the two chemical shifts or, preferably, additional information from a long-range hetero-COSY experiment to solve this remaining ambiguity.

The opposite may also occur. It can happen that two or three protons have nearly identical chemical shifts, such as H(12'), H(11') and H(10') in the spectrum of the ^{12}C isotopomer of **471**. This 3-spin sub-system is thus strongly coupled and the individual multiplets are grossly degenerate. This accidental degeneracy is, however, partly lifted in the three ^{13}C isotopomers with ^{13}C in positions C(12'), C(11') and C(10'). This means that their cross peaks in the 2D spectrum with H(12'), H(11') and H(10') may have the correct and expected multiplet form

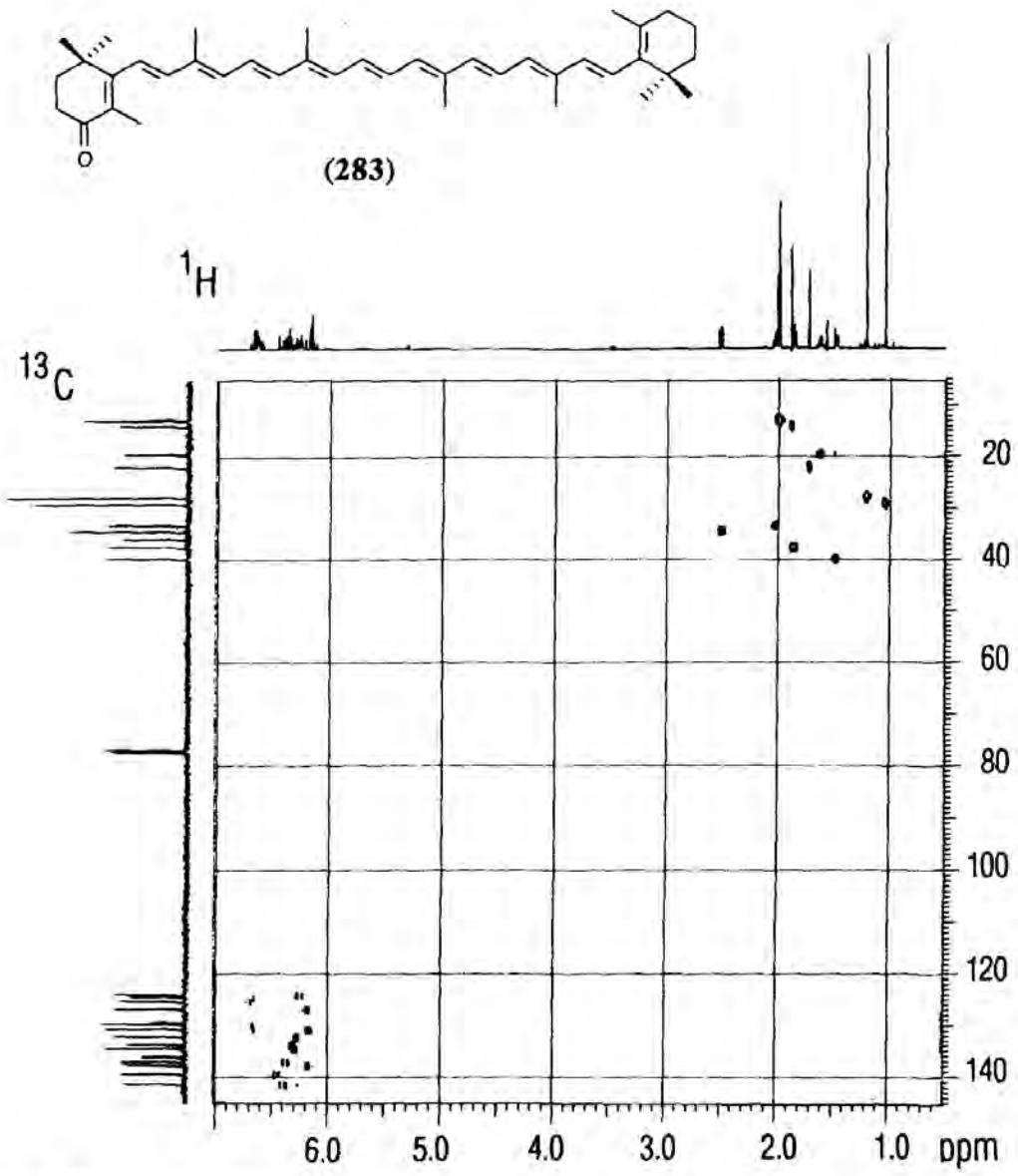
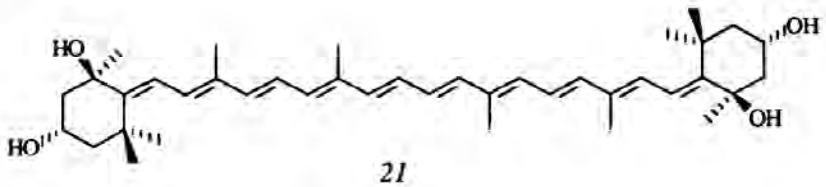


Fig. 18. Phase-sensitive 400 MHz ^{1}H-detected one-bond $^1J_{CH}$ ^{1}H,^{13}C-COSY spectrum of 4 mg echinenone (**283**) in 0.6 ml $CDCl_3$, ^{13}C decoupled during acquisition in t_2 by GARP. Only positive levels are shown. Top: ^{1}H-NMR; left side: 100 MHz ^{13}C-NMR. Experimental conditions of 2D: 1500*400 data points in t_2 and t_1, zero-filling to 2K and 1K, cosine-square windows in both directions, 4000 Hz and 22726 Hz spectral width, 3.9 Hz and 44.4 Hz per point digital resolution, delay for polarization transfer 3.6 ms, trim pulses of 2 ms, 90° pulse for GARP 48 ms, relaxation delay 1s, 16 scans per experiment, total acquisition time 3.5 h.

and this often allows determination of the approximate chemical shifts of the protons involved, in addition to the assignment of the ^{13}C signals.

In practice, the ^{1}H-detected one-bond hetero-COSY is roughly a factor of 20 to 60 times more sensitive than the ^{13}C-detected variant. The three-fold range arises from the fact that 1, 2 or 3 equivalent protons in methine, methylene and methyl groups are attached to the same carbon and they all contribute to the detected signal.

This multi-pulse sequence has been applied successfully to carotenoids in numerous cases and two representative examples, *i.e.* fucoxanthin (**369**) (0.8 mg, total acquisition time 20 h) [21] and a novel symmetrical C_{40} *retro*-carotenoid (*21*, 75 µg, 36 h) [5] have been presented recently. In this context it is important to note that below *ca.* 0.5 mg of sample the acquisition of a good ^{13}C spectrum is severely hampered by the excessive acquisition time needed. However, approximate chemical shifts of protonated carbons can be obtained much faster with lower sample quantities from the positions of the cross peaks on the ^{13}C axis of a ^{1}H-detected 2D hetero-COSY.



21

The multiple-bond, ^{1}H-detected version of 2D $^{1}H,^{13}C$-COSY is also much more sensitive than the ^{13}C-detected version and this brings down the minimum amount of sample needed to the 1 mg range. There is only one well-proven pulse sequence available [51], which is based on multiple-quantum coherence evolving during evolution time t_1 thus introducing a modulation of the ^{1}H magnetization by the chemical shifts of ^{13}C. During acquisition time t_2 no ^{13}C-decoupling is needed.

The sequence contains two delays. The first one of duration $1/(2^{1}J_{C,H}) = 3.6$ ms is needed to suppress one-bond correlations which otherwise might be confusing in some parts of the spectrum. This suppression is achieved by alternating the phase of the first ^{13}C pulse, resulting in a subtraction of the one-bond cross peaks. Since this often does not work completely, some weak one-bond correlation cross peaks may be found in the multiple-bond contour plot. An example often found is the doublet cross peak of $CHCl_3$ at 7.26 and 77 ppm with a $^{1}J_{CH}$ of about 209 Hz which is too far outside the assumed value.

The second delay of the pulse sequence is set to about 60 ms to optimize cross peaks due to multiple-bond heteronuclear couplings around 8 Hz. For reasons discussed in [51], the 2D data can only be processed in absolute-value mode.

A representative example, measured from 0.8 mg of 9,9'-di-*cis*-7,8,7',8'-tetra-dehydrolycopene (*9*) at 500 MHz (125 MHz ^{13}C) in 20.5 hours total acquisition time will be discussed. The full assignment of the ^{1}H and ^{13}C signals is given in [36]. Instead of a less clear overview 2D contour plot, two enlarged interesting sections are shown, namely the aliphatic-olefinic range (Fig. 19) and the olefinic-olefinic range (Fig. 20). The assignments of

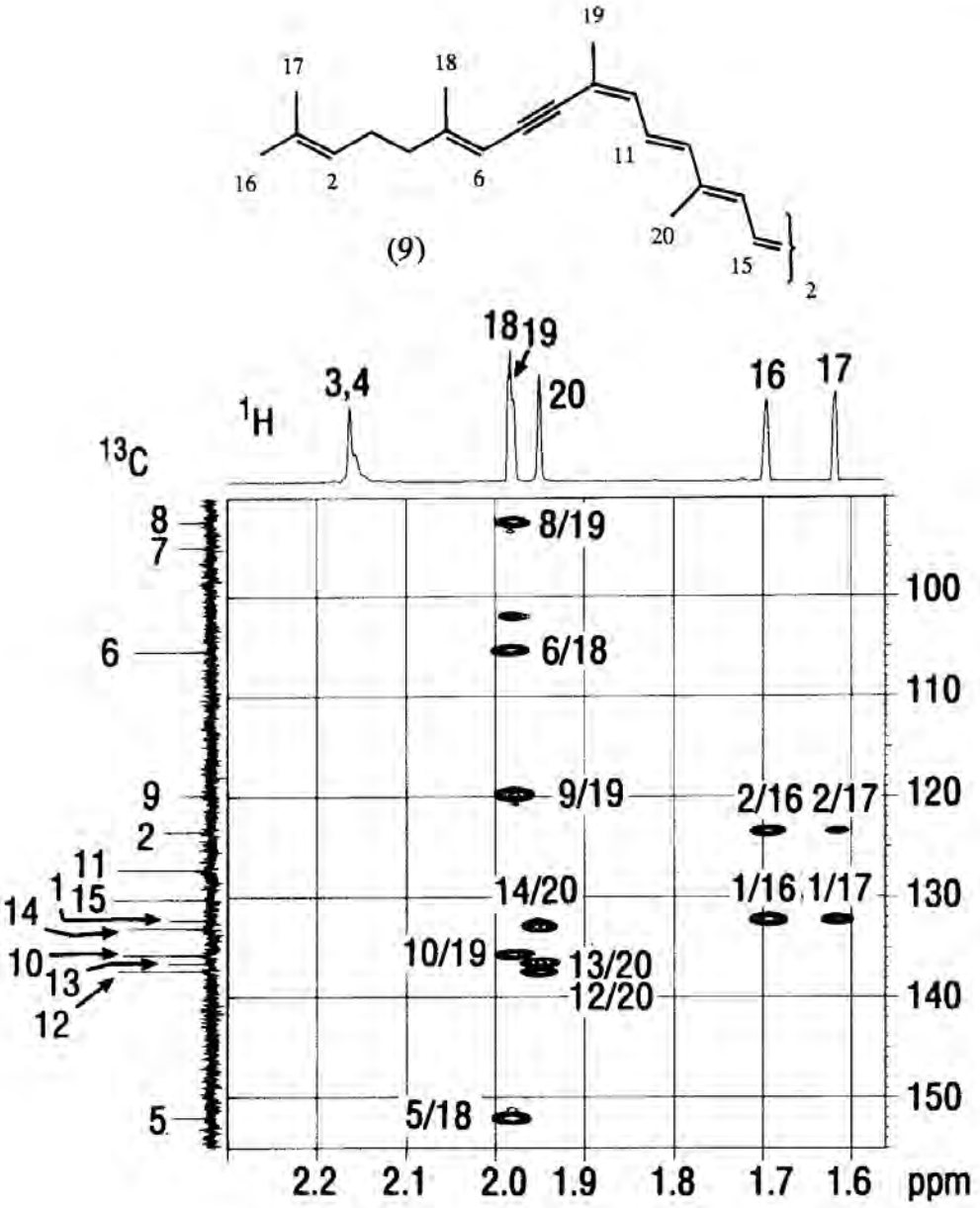


Fig. 19. Aliphatic-olefinic section of the 500 MHz ^{1}H-detected multiple-bond 2D ^{1}H,^{13}C-COSY of 0.8 mg 9,9'-di-*cis* -7,8,7',8'-tetadehydrolycopene (*9*) in 0.5 ml $CDCl_3$. Cross peaks are caused by two-bond and three-bond ^{1}H,^{13}C-couplings. The sections of the 500 MHz ^{1}H and 125 MHz ^{13}C 1D NMR spectra are plotted along F_2 and F_1.

Experimental conditions: time domain 1K in t_2, 312 experiments in t_1, zero-filling to 4K and 1K, sine-bell windows in both directions, spectral widths 4504 Hz and 22727 Hz, 160 scans and 4 dummy scans per experiment, 1.3 s relaxation delay, pulse delays 3.3 ms (151 Hz) and 60 ms (8 Hz), total acquisition time 20.5 h.

the protonated carbons are already known from the one-bond correlation experiment [36]. They were inserted, together with the proton assignments, into the corresponding 1D spectra plotted along the F_1 and F_2 axes. The cross peaks of the 2D contour plot were designated according to the connectivities between ^{13}C and ^{1}H.

In Fig. 19 are shown connectivities between protons that absorb in the aliphatic range, 1.6 to 2.3 ppm, and ^{13}C in the olefinic range, 90 to 155 ppm. Thus, H(16) and H(17) show cross peaks with C(2) and C(1); the latter has already been identified as a quaternary carbon by DEPT and from the missing cross peak in the one-bond experiment. Proton H(20) has cross peaks with C(14) and C(12), as well as with the quaternary C(13); the two-bond and three-bond cross peaks are of similar intensity. This means that the two types of coupling must have similar values (see F.2.b).

In the 1D ^{1}H spectrum, the signals of H(18) and H(19) are very close to each other, but several cross peaks of these signals allow H(18) to be identified at slightly lower field than H(19). Thus, cross peaks of H(18) to C(6) and C(5) have their centres slightly downfield compared to cross peaks between H(19) and C(8), C(9) and C(10). Carbons C(7) and C(8) can now be distinguished since only the latter is expected to have a cross peak to H(19) by three-bond heteronuclear coupling.

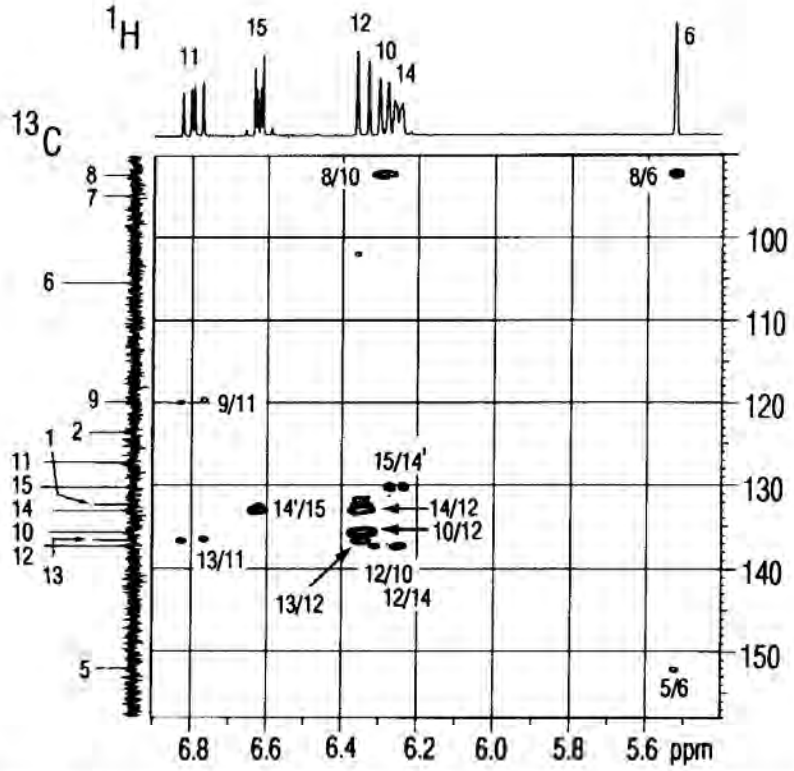


Fig. 20. Olefinic-olefinic section of the 500 MHz ^{1}H-detected multiple-bond $^{1}H,^{13}C$ 2D COSY of Fig. 19.

In Fig. 20 are seen cross peaks between H(6) and C(8) and (very weakly) C(5), pointing to the fact that, in this case, two-bond couplings are normally much smaller. Therefore, it is assumed that H(14') and not H(14) has cross peaks with C(15) *via* three-bond coupling. This interpretation is supported by the interpretation of further cross peaks seen in Fig. 20.

In the two remaining sections of the 2D spectrum (not shown) further connectivities were detected, such as those between H(6) and C(18) and C(4), H(10) and C(19), H(12) and C(20), H(16) and C(17), and H(17) and C(16). The latter connectivity is often particularly useful since it allows, quite generally, the recognition of geminal methyl groups at C(1) of end groups and their differentiation from the methyl group at C(5). Finally, a further cross peak between H(18) and C(4) helps to distinguish the methylene carbons C(4) and C(3).

Further applications of the ^{1}H-detected multiple-bond ^{1}H,^{13}C-COSY, to the 9'-*cis* isomer of 19'-butanoyloxyfucoxanthin (**370.2**, 1.5 mg, total measuring time 60 h) and to the octaacetate of the glycosidic carotenoid 13'-*cis*-7',8'-dihydroneoxanthin β-lactoside (**280.1**) (*ca.* 0.4 mg, 65 h), both measured at 400 MHz, were recently reported [21, 5]. It should be mentioned that, in the latter case, some weak connectivities over four bonds involving the allenic group were found.

These results clearly indicate that the multiple-bond experiment provides a wealth of structural information which can make an essential contribution to the elucidation of the structure of a novel carotenoid. The examples mentioned so far show that the minimum sample quantity needed for this multiple-bond experiment is around 0.5 mg, *i.e.* about a factor of five higher than for the corresponding one-bond experiment.

G. Experimental

All the spectra illustrated or discussed in this chapter were recorded on Bruker FT spectrometers of the type AC-250, AM-400 and AM-500 with ASPECT 3000 computer, with process controller and 160 Mbyte disk. Deuteriated chloroform was used as solvent, with tetramethylsilane (TMS) as internal reference. Standard Bruker software (DISNMR versions 87 to 90) and Bruker microprograms for the different experiments were applied except in the case of TOCSY, ROESY and ^{1}H-detected hetero-COSY which were used as recently described [21]. The one-bond version of the ^{1}H-detected hetero-COSY corresponded exactly to sequence E of [48]; the multiple-bond version was described in [51]. The DANTE pulse train consisted of 2 μs pulses separated by delays of 70 μs and number of repetitions as given in the legends of the Figures. These latter experiments were all performed in the reverse mode of the spectrometer with the decoupler as source of ^{1}H excitation. Many of the spectra were recorded by Ph. Cron, W. Grunauer, Y. Mercadal, and D. Travella.

The work described here owes a great debt to numerous colleagues who have synthesized, isolated and purified all the compounds used for the spectroscopic investigations that are reported. Major contributions were made by Drs. K. Bernhard, U. Hengartner, H. Mayer, R. K. Müller, A. Rüttimann, K. Schiedt, E. Widmer, R. Zell, and Mr. E. Glinz, all of Hoffmann-La Roche, and the groups of Professors S. Liaaen-Jensen (Trondheim), H. Kleinig (Freiburg i. Br.) and H. Pfander (Bern).

H. Concluding Remarks

In the past ten years or so there has been dramatic progress in the ability to assign and analyse the ^{1}H- and ^{13}C-NMR spectra of carotenoids. This overview is an attempt to discuss the necessary basic tools and facts in order to enable the practitioner to begin to interpret these spectra by using the given comprehensive collection of chemical-shift data of end groups and of a number of selected carotenoids of variable levels of complexity.

From the numerous experimental techniques now available only those were treated here which are thought to be of special interest and use for the elucidation of the structure of a carotenoid. Their relative merits and drawbacks were briefly discussed by selecting some representative examples. A number of further elegant multi-pulse experiments such as phase-sensitive COSY [36] and its variants, double-quantum 2D for protons and INADEQUATE [3] for ^{13}C and others were omitted here since it is thought that they are of less importance in the context of this Chapter.

In the past two years, further very interesting progress has been achieved in the general field of NMR measuring techniques. By incorporation of pulsed magnetic field z-gradients (PFG; [52]) into various pulse experiments, the measuring time of several experiments such as 2D COSY and 2D hetero-COSY can be significantly reduced and, at the same time, the quality of the spectra can be partly improved, mainly by removing undesired artifacts. Some promising results have been obtained in the author's laboratory when these techniques were applied to carotenoids.

References

[1] W. Vetter, G. Englert, N. Rigassi and U. Schwieter, in *Carotenoids* (ed. O. Isler), p. 189, Birkhäuser, Basel (1971).

[2] U. Schwieter, G. Englert, N. Rigassi and W. Vetter, *Pure Appl. Chem.*, **20**, 365 (1969).

[3] G. Englert, in *Carotenoid Chemistry and Biochemistry* (ed. G. Britton and T. W. Goodwin), p.107, Pergamon, Oxford (1982).

[4] G. Englert, *Pure Appl. Chem.*, **57**, 801 (1985).

[5] G. Englert, *Pure Appl. Chem.*, **63**, 59 (1991).

[6] A. E. Derome, *Modern NMR Techniques for Chemistry Research*, (Organic Chemistry Series, Vol. 6), Pergamon, Oxford (1987).

[7] G. E. Martin and A. S. Zektzer, *Two-Dimensional NMR Methods for Establishing Molecular Connectivity*, VCH Publishers, Weinheim (1988).

[8] H. Kessler, M. Gehrke and H. Griesinger, *Angew. Chem. Int. Edn. Engl.*, **27**, 490 (1988).

[9] G. A. Morris, *Magn. Reson. Chem.*, **24**, 371 (1986).

[10] B. Daicker, K. Schiedt, J. J. Adnet and P. Bernond, *Graefe's Arch. Clin. Exp. Ophthalmol.*, **225**, 189 (1987).

[11] J.-P. Kintzinger, in *NMR, Basic Principles and Progress, Vol. 17* (ed. P. Diehl, E. Fluck and R. Kosfeld), p. 1, Springer-Verlag, Berlin (1981).

[12] K. Bernhard, G. Englert, H. Mayer, R. K. Müller, A. Rüttimann, M. Vecchi, E. Widmer and R. Zell, *Helv. Chim. Acta*, **64**, 2469 (1981).

[13] M. Vecchi, G. Englert and H. Mayer, *Helv. Chim. Acta*, **65**, 1050 (1982).

[14] G. Englert, *Helv. Chim. Acta*, **58**, 2367 (1975).

[15] G. Englert, *Helv. Chim. Acta*, **62**, 1497 (1979).
[16] G. Englert, B. O. Brown, G. P. Moss, B. C. L. Weedon, G. Britton, T. W. Goodwin, K. L. Simpson and R. J. H. Williams, *J. Chem. Soc., Chem. Commun.*, **1979**, 545.
[17] G. Pattenden and D. C. Robson, *Tetrahedron Lett.*, **28**, 5751 (1987).
[18] B. Dischler and G. Englert, *Z. Naturforsch.*, **16a**, 1180 (1961).
[19] Y. Koyama, M. Hosomi, H. Hashimoto and T. Shimamura, *J. Molec. Struct.*, **193**, 185 (1989).
[20] A. Rüttimann, G. Englert, H. Mayer, G. P. Moss and B. C. L. Weedon, *Helv. Chim. Acta*, **66**, 1939 (1983).
[21] G. Englert, T. Bjørnland and S. Liaaen-Jensen, *Magn. Reson. Chem.*, **28**, 519 (1990).
[22] J. A. Haugan, G. Englert and S. Liaaen-Jensen, *Acta Chem. Scand.*, **46**, 614 (1992).
[23] G. Englert, T. Aakermann and S. Liaaen-Jensen, *Magn. Reson. Chem.*, **31**, 910 (1993).
[24] O. Straub, *Key to Carotenoids, 2nd Edition* (ed. H. Pfander), Birkhäuser, Basel (1987).
[25] A. G. Andrewes, G. Englert, G. Borch, H. H. Strain and S. Liaaen-Jensen, *Phytochem.*, **18**, 303 (1979).
[26] G. Englert and M. Vecchi, *J. Chromatogr.*, **235**, 197 (1982).
[27] W. Bremser and J. Paust, *Org. Magn. Reson.*, **6**, 433 (1974).
[28] G. P. Moss, *Pure Appl. Chem.*, **47**, 97 (1976).
[29] G. Englert, E. Glinz and S. Liaaen-Jensen, *Magn. Reson. Chem.*, **26**, 55 (1988).
[30] G. Englert and M. Vecchi, *Helv. Chim. Acta*, **63**, 1711 (1980).
[31] M. Vecchi, G. Englert, R. Maurer and V. Meduna, *Helv. Chim. Acta*, **64**, 2746 (1981).
[32] Y. Koyama, M. Hosomi, A. Miyata, H. Hashimoto, S. A. Reames, K. Nagayama, T. Kato-Jippo and T. Shimamura, *J. Chromatogr.*, **439**, 417 (1988).
[33] G. Englert, K. Noack, E. A. Broger, E. Glinz, M. Vecchi and R. Zell, *Helv. Chim. Acta*, **74**, 969 (1991).
[34] J. A. Haugan, G. Englert, E. Glinz and S. Liaaen-Jensen, *Acta Chem. Scand.*, **46**, 389 (1992).
[35] H. Hashimoto, Y. Koyama and T. Shimamura, *J. Chromatogr.*, **448**, 182 (1988).
[36] U. Hengartner, K. Bernhard, K. Meyer, E. Glinz and G. Englert, *Helv. Chim. Acta*, **75**, 1848 (1992).
[37] H. Kessler, G. Krack and G. Zimmermann, *J. Magn. Reson.*, **44**, 208 (1981).
[38] K. G. R. Pachler and P. L. Wessels, *J. Chem. Soc., Chem. Commun.*, **1981**, 1038.
[39] J. H. Noggle and R. E. Schirmer, *The Nuclear Overhauser Effect, Chemical Applications*, Academic Press, New York (1971).
[40] D. Neuhaus and M. P. Williamson, *The Nuclear Overhauser Effect in Structural and Conformational Analysis*, VCH Publishers, Weinheim and New York (1989).
[41] A. A. Bothner-By, R. L. Stevens, J. Lee, C. D. Warren and R. W. Jeanloz, *J. Amer. Chem. Soc.*, **106**, 811 (1984).
[42] C. Griesinger and R. R. Ernst, *J. Magn. Reson.*, **75**, 261 (1987).
[43] L. Braunschweiler and R. R. Ernst, *J. Magn. Reson.*, **53**, 521 (1983).
[44] D. G. Davis and A. Bax, *J. Amer. Chem. Soc.*, **107**, 7197 (1985).
[45] A. Bax and D. G. Davis, *J. Magn. Reson.*, **65**, 355 (1985).
[46] S. Subramanian and A. Bax, *J. Magn. Reson.*, **71**, 325 (1987).
[47] G. Bodenhausen and D. J. Ruben, *Chem. Phys. Lett.*, **69**, 185 (1980).
[48] G. Otting and K. Wüthrich, *J. Magn. Reson.*, **76**, 569 (1988).
[49] A. Bax, M. Ikura, L. E. Kay, D. A. Torchia and R. Tschudin, *J. Magn. Reson.*, **86**, 304 (1990).
[50] A. J. Shaka, P. B. Barker and R. Freeman, *J. Magn. Reson.*, **64**, 547 (1985).
[51] A. Bax and M. F. Summers, *J. Amer. Chem. Soc.*, **108**, 2093 (1986).
[52] R. E. Hurd, *J. Magn. Reson.*, **87**, 422 (1990).

Carotenoids
Volume 1 B: Spectroscopy
© 1995 Birkhäuser Verlag Basel

Chapter 7

Mass Spectrometry

Curt R. Enzell and Susanne Back

A. Introduction

Since the survey in 1971 [1], several reviews in the field of mass spectrometry (MS) of carotenoids have appeared which reflect the importance of the technique in both analytical work and structure elucidation [2-8]. The power of MS for structural studies on carotenoids was already apparent in 1971. High resolution, accurate mass measurements could provide not only molecular masses but also unequivocal molecular formulae for the carotenoids and for important fragment ions in the spectra. Mechanisms were discussed for the fragmentations that lead to losses of toluene and xylene from the polyene chain, and the possible structural significance of the intensity ratio of the $[M-92]^{+\cdot}$ and $[M-106]^{+\cdot}$ ions was considered. In addition to the standard fragmentations such as the elimination of water from alcohols, acetic acid from acetates and methanol from methyl ethers, some of the most important end-group fragmentations were also described. In particular the diagnostic value of the following ions was recognized and mechanisms for some of these reactions were described:

i) *m/z* 133 and $[M-133]^+$ for arylcarotenoids,
ii) *m/z* 73 and $[M-73]^+$ for methoxycarotenoids such as spirilloxanthin (**166**),
iii) *m/z* 165 and 205 (181 and 221 if a C-3 hydroxy group is also present) and $[M-80]^{+\cdot}$ for 5,6-epoxides and 5,8-epoxides,
iv) $[M-56]^{+\cdot}$ for ε-ring carotenoids,
v) the $[M-69]^+$, $[M-137]^+$ and $[M-205]^+$ ions produced by bis-allylic cleavage of the C-3,4, C-7,8 and C-11,12 single bonds adjacent to the chromophore of the acyclic carotenes.

In this Chapter, this survey has been greatly extended, and tabulated data for 170 different carotenoid end groups are presented.

The use of MS data as part of a combined spectroscopic and chemical approach to structure elucidation is given in Chapter 9. Over the past two decades, structures of many new carotenoids, including those with a triterpenoid skeleton, and carotenoid conjugates such as glycosides, have been established with the aid of mass spectrometry.

The important reactions that lead to the elimination of in-chain fragments with production of the $[M-92]^{+\cdot}$, $[M-106]^{+\cdot}$, and $[M-158]^{+\cdot}$ ions under electron impact, and the use of the intensity ratio of the $[M-92]^{+\cdot}$ and $[M-106]^{+\cdot}$ peaks to provide structural information, have been studied in considerable detail.

Although the traditional method of ionization by electron impact (EI) is still used most commonly, some of the newer mass spectrometric ionization techniques, especially fast atom bombardment (FAB) and chemical ionization (CI), have been applied recently in studies of carotenoids.

Analysis of metastable ions by tandem mass spectrometry and mass-analysed ion kinetic energy (MIKE) spectra have been used to obtain diagnostic structural information.

Applications of combined chromatography–mass spectrometry techniques in the carotenoid field are limited, but the applicability of HPLC–MS and SFC–MS is now being explored.

B. Ionization Techniques

1. Electron impact

In 1971 the only ionization technique available was electron impact (EI). Even today, this is the technique most commonly used for routine recording of carotenoid mass spectra.

In this method, electrons, obtained from a heated filament *in vacuo*, are accelerated and directed at the sample. Impact of an electron with a sample molecule generates the positively charged molecular ion $M^{+\cdot}$. As involatile substances, carotenoids are introduced directly into the electron beam by means of a direct insertion probe. This is heated to a temperature (usually 180 to 220°C) which causes the carotenoid to be vaporized at the very low pressures that are maintained in the system. Most routine spectra are obtained at an ion source potential of 70 eV, but the use of an appreciably lower voltage (10 to 20 eV) can be advantageous, as this reduces fragmentation and so gives simpler spectra, usually with a prominent molecular ion. Relative intensities of ions in a spectrum are highly dependent on the conditions used, especially on factors such as temperature and ionizing voltage.

2. Fast atom bombardment

Fast atom bombardment (FAB) mass spectrometry is the commonly preferred soft ionization technique for structure elucidation of involatile and thermally labile compounds. FAB MS uses a beam of high-energy atoms, commonly xenon or caesium, produced by accelerating Xe^+ or Cs^+ ions through an electric field, to bombard a solution of the analyte dissolved in a relatively involatile matrix (*e.g.* glycerol). Dissipation of the kinetic energy of the bombarding atom beam (primary beam) induces volatilization and ionization of the analyte and matrix molecules. Although positive ion FAB normally yields even-electron protonated molecular ions, a recent detailed study [9], following an examination of β,β-carotene (**3**) [10], has shown that carotenoids, like some aromatic compounds, furnish odd-electron molecular ions. These

molecular ions dominate the spectra in all cases and the formation of ions by cleavage of acyclic or cyclic end groups is very limited. The ionization efficiency has been shown to be very high, which is an obvious advantage since β,β-carotene (**3**) is a hydrocarbon, and is therefore practically insoluble in all solvents commonly used for FAB [10].

Table 1. The molecular ion region of the positive FAB mass spectra of some carotenoids[a,b] [9].

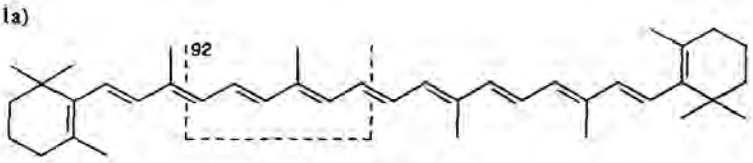
Compound	$M^{+\cdot}$	$[M+1]^{+}$	$[M+2]^{+\cdot}$
β,ε-Carotene (**7**)	100 (100)	45 (45)	10 (10)
β,β-Carotene (**3**)	100 (100)	45 (45)	10 (10)
Lycopene (**31**)	100 (100)	45 (45)	10 (10)
Zeaxanthin (**119**)	100 (100)	46 (45)	14 (10)
Lutein (**133**)	100 (100)	46 (45)	11 (10)
Canthaxanthin (**380**)	100 (100)	63 (45)	21 (10)
8'-Apo-β-caroten-8'-al (**482**)	100 (100)	48 (34)	12 (6)

[a] Intensities rounded to nearest integral value expressed as a percentage of the base peak $M^{+\cdot}$.

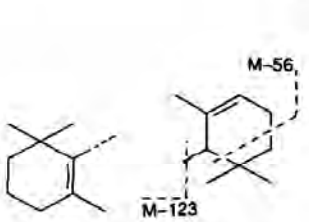
[b] Values in parentheses are the calculated isotopic distributions normalized to $M^{+\cdot}$.

It follows from a study [9] of seven carotenoids (Table 1), that the molecular-ion region in the spectra of hydrocarbons consists exclusively of the radical ion $M^{+\cdot}$. The reason for this is related to an easy electron transfer from the molecule to the matrix because of the low ionization potentials (< 7 eV) of these hydrocarbons. Accordingly, the usual protonation of the substrate from the matrix does not occur, because of delocalization of the charge in the extended conjugated system.

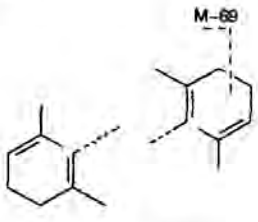
Fig. 1a)



β,β-Carotene (**3**)

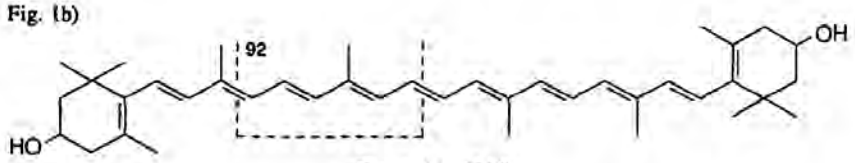


β,ε-Carotene (**7**)

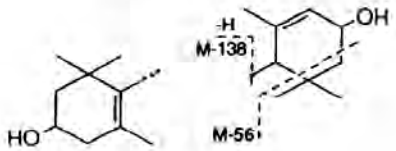


Lycopene (**31**)

Fig. 1(b)

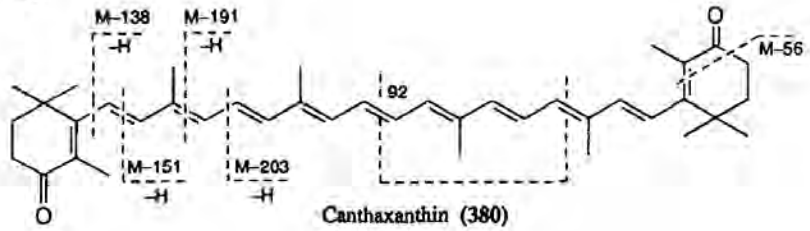


Zeaxanthin (119)



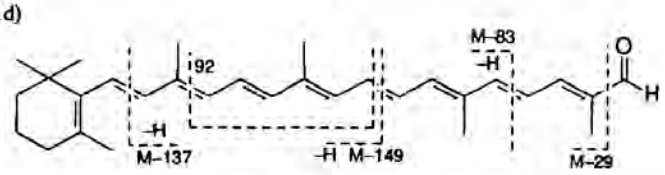
Lutein (133)

Fig. 1(c)



Canthaxanthin (380)

Fig. 1(d)



8'-Apo-β-caroten-8'-al (482)

Fig. 1. Main fragmentations of the molecular ion, studied by B/E linked-scan positive-ion FAB for a series of carotenoids: (a) comparison of β,β-carotene (3), β,ε-carotene (7), lycopene (31), (b) comparison of zeaxanthin (119) and lutein (133), (c) canthaxanthin (380) and (d) 8'-apo-β-caroten-8'-al (482) [9].

In the case of canthaxanthin (**380**) and 8'-apo-β-caroten-8'-al (**482**), $[M+H]^+$ ions are formed to a slight extent, perhaps because of the higher ionization potential of these compounds and the presence of polar hydroxy or carbonyl groups in which the oxygen provides a good site for protonation.

In addition to the peaks in the molecular-ion region, only a few low-intensity fragments were observed above *m/z* 400 for a range of carotenoids (Fig. 1) [9]. β,β-Carotene (**3**) did not exhibit any intense ions in this region, whereas lycopene (**31**) displayed a weak $[M-69]^+$ ion (3%), and β,ε-carotene (**7**) underwent *retro*-Diels-Alder (RDA) fragmentation and abstraction of toluene to produce $[M-56]^{+\cdot}$ (10%) and $[M-92]^{+\cdot}$ (4%) ions, respectively. Lutein (**133**) also gave rise to an RDA fragment (1%) but, as expected, zeaxanthin (**119**) did not. Canthaxanthin (**380**) and 8'-apo-β-caroten-8'-al (**482**) did not show any peaks with relative intensity higher than 1% in their spectra above *m/z* 300, except in the molecular-ion region.

Unless it is stated to the contrary, the percentage figures given in this Chapter refer to the observed intensity expressed as a percentage of the strongest peak in the spectrum. In this particular case, the relative intensities reported were computed after subtraction of the contribution from the matrix, and represent averages of five added mass spectra.

In this work [9], B/E linked-scan positive-ion FAB studies were used to differentiate between isomers (Fig. 1). Under these conditions, lutein (**133**) showed intense $[M-138]^{+\cdot}$, $[M-92]^{+\cdot}$ and $[M-56]^{+\cdot}$ daughter ions derived from the $M^{+\cdot}$ species, whilst the zeaxanthin (**119**) $M^{+\cdot}$ ion gave rise only to an $[M-92]^{+\cdot}$ ion. Similarly, the β,ε-carotene (**7**) molecular ion furnished $[M-123]^+$ and $[M-56]^{+\cdot}$ daughter ions, which were absent from the β,β-carotene (**3**) spectrum, and the lycopene (**31**) $M^{+\cdot}$ ion furnished an $[M-69]^+$ species. The B/E linked-scan FAB spectra of canthaxanthin (**380**) and 8'-apo-β-caroten-8'-al (**482**) contained further peaks (Fig. 1).

An advantage of FAB mass spectrometry is the elimination of thermal interference, since the ion source is not heated. This reduces the reaction that leads to the extrusion of xylene. In fact, the $[M-106]^{+\cdot}$ ion was observed only in the spectrum of β,ε-carotene (**7**), and then only as a very minor peak (0.4%). FAB mass spectrometry has also proved useful in studies of highly polar synthetic intermediates such as triphenylphosphonium chloride derivatives [11].

3. Chemical ionization

Chemical ionization (CI) is used to generate mass spectra by means of ionic reactions rather than electron bombardment. Typically a reagent gas, *e.g.* methane, ammonia or isobutane, is introduced into the ion source at a pressure of around 1 torr. Bombardment of the gas with electrons yields a population of ions and neutral molecules. The reagent gas molecules will take part in ion-molecule reactions with the sample molecules that vaporize into the source. Fragmentation is less and CI spectra are simpler than EI spectra, the most abundant ions generated usually being the quasimolecular ion $[M+H]^+$ and molecular adduct ions with the reagent gas, *e.g.* $[M\pm CH_5]^+$.

The degree of fragmentation is dependent upon the ionizing gas used and usually increases with the protonating power of its predominating species, *i.e.* $[H_3]^+ > [C_4H_{11}]^+ > [NH_4]^+$.

Thus hydrogen CI spectra exhibit a somewhat more extensive fragmentation pattern, especially in the lower mass region, than do isobutane CI spectra [12]. When ammonia is used as the reagent gas, the diagnostic ions normally observed are the $[MH]^+$ and $[M+NH_4]^+$ species, and daughter ions arising from these through elimination of water from hydroxycarotenoids or of acids from carotenoid esters [13-15]. The difference between an EI and an isobutane CI spectrum of capsanthin (**335**) is illustrated in Fig. 2.

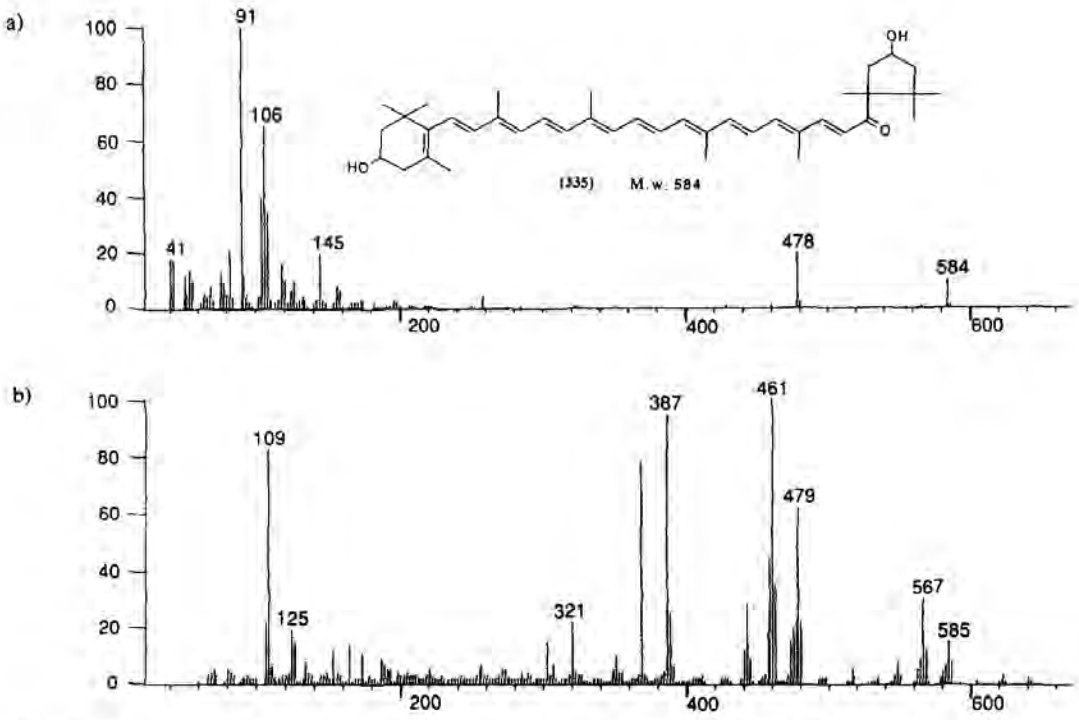


Fig. 2. EI spectrum (a) and isobutane CI spectrum (b) of capsanthin (**335**) (MW = 584).

Sensitivity comparison of the intensity of the $[MH]^+$ ion in hydrogen and isobutane CI and the $M^{+\cdot}$ ion in EI made on β,β-carotene (**3**) and on canthaxanthin (**380**) [12], shows the response of the $[MH]^+$ ion to be much greater in each case and the intensity ratios $CI[MH]^+/EI[M]^{+\cdot}$ to be in the range 20 to 200. The sensitivity comparisons were performed by examination of equal amounts of compounds, dissolved in chloroform and introduced *via* a capillary tube into the ion source. Although the greater sensitivity of the CI technique could readily be demonstrated, the precision was not sufficient to differentiate between the sensitivities when different reagent gases (hydrogen and isobutane) were used. Characteristic peaks in the hydrogen or isobutane CI spectra of seven representative carotenoids, and the relative intensities of these peaks, are given in Table 2 [12].

Studies [12] of metastable transitions of ions from β,β-carotene (**3**), lycopene (**31**) and capsanthin (**335**) indicate that fission occurs at every carbon along the polyene chain under CI with hydrogen or isobutane as reagent gas. Thus, these CI spectra, as distinct from the corresponding EI spectra, show abundant ions in the middle mass range and exhibit a simpler and more useful pattern in the low mass region. The CI spectra of all compounds that were examined exhibited fragmentation patterns characterized by multiple fissions, as illustrated for β,β-carotene (**3**) in Fig. 3.

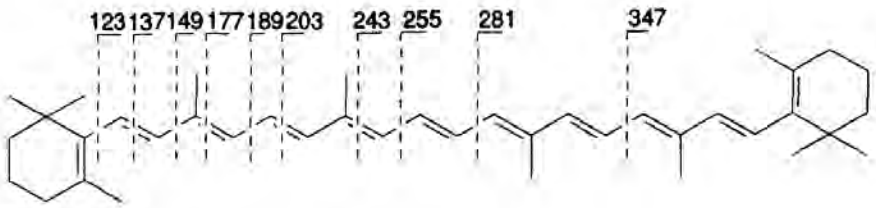


Fig. 3. The CI fragmentation pattern of β,β-carotene (**3**) [12].

Table 2. Intensities of characteristic peaks in CI spectra of some carotenoids.

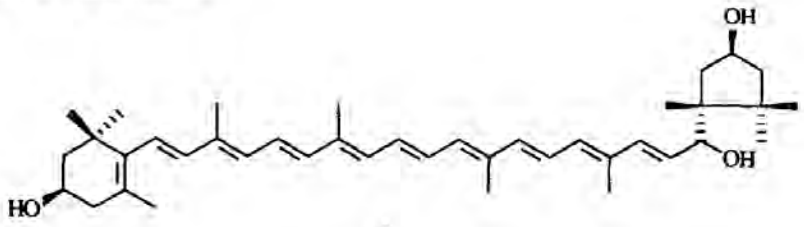
	Relative intensity at *m/z* (% base peak)												
	93	107	109	127	M-137	M-153	M-193	M+1 -198 -H_2O	M+1 -198	M+1 -106 -$2H_2O$	M+1 -92 -$2H_2O$	M+1 -106 -H_2O	M+1 -92 -H_2O
Lycopene[a] (**31**)	28	100	10	3	<1	-	-	-	<1	-	-	-	-
β,β-Carotene[b] (**3**)	35	30	12	20	3	-	-	-	1	-	-	-	-
β,β-Carotene[a] (**3**)	5	14	7	4	3	-	-	-	2	-	-	-	-
Canthaxanthin[a] (**380**)	71	42	7	5	1	-	-	-	2	-	-	-	-
Isozeaxanthin[a] (**129**)	36	28	16	3	-	3	4	-	-	4	3	5	12
Capsanthin[b] (**335**)	3	21	85	14	1	1	7	78	95	22	12	100	16
Capsanthol[a] (*1*)	73	100	39	9	-	1	1	10	1	13	5	37	6
Bistrimethylsilyl capsanthin[b]	62	64	21	-	-	-	-	-	51	-	-	-	-

Table 2 (part 2)

	M+1 -106	M+1 -92	M+1 $-2H_2O$	M+1 $-H_2O$	M+1	Others
Lycopene[a] (31)	20	6	-	-	18	M(30), M-1(12), M-106-69(6), M-92-69(2), 69(44), 43(55)
β,β-Carotene[b] (3)	6	16	-	-	100	M+57(43), M+57-92(7), M+57-106(2), M(56), M-1(22), M-92(12), M-106(5), 347(6), 281(5), 255(6), 243(5), 203(14), 189(20), 177(23), 149(4), 137(18), 123(14)
β,β-Carotene[a] (3)	7	13	-	-	100	M(26), M-1(31), 347(19), 281(15), 255(11), 243(10), 203(17), 189(23), 177(42), 149(9), 137(42), 123(12)
Canthaxanthin[a] (380)	12	18	-	-	100	M+1-16(3), M+1-18(2), M-203(7), M-217(3), M-191(1), M-151(3), 203(32), 189(9)
Isozeaxanthin[a] (129)	2	12	38	62	40	M(76), M-1(17), M-H_2O(53), M-1-H_2O(28), M-$2H_2O$(8), 361(5), 347(4), 269(5), 257(12), 203(13), 201(10), 189(14), 149(20), 139(13), 123(19)
Capsanthin[b] (335)	59	3	82	26	14	M+57(2), M+57-H_2O(3), M+57-92(9), M+57-106(5), M-H_2O(17), M-1-H_2O-92(40), M+1-198-$2H_2O$(10), M-155(3), 155(4), 153(13), 139(3)
Capsanthol[a] (1)	9	2	12	29	10	M+1-$3H_2O$(1), M-1-$3H_2O$(2), M-157(4), M+1-198-$2H_2O$(13), M+1-198-$3H_2O$(4), 281(24), 257(37), 223(46), 207(63), 187(11), 157(13), 149(21), 139(32)
Bistrimethylsilyl capsanthin[b]	100	5	-	-	15	M+57(2), M+57-90(3), M+57-106(4), M+1-90(16), M+1-180(3), M+1-92-90(4), M+1-106-90(59), M+1-198-90(25), M-227(2), 227(3), 199(5)

[a] Hydrogen CI mass spectrum.

[b] Isobutane CI mass spectrum.



1

Losses of 92 (toluene) and 106 mass units (xylene) from the $[M+1]^+$ ion give rise to fairly abundant ions in the hydrogen and isobutane CI spectra (see Section E). These losses also occur from the $[M]^{+\cdot}$ and $[M-1]^+$ ions and, when isobutane is the reagent gas, from the $[M+57]^+$ ion. Their intensities vary widely, but they are much more abundant than the $[M-92]^{+\cdot}$ and $[M-106]^{+\cdot}$ ions that appear in the EI spectra. The intensity ratio for $[M-92]^{+\cdot}/[M-106]^{+\cdot}$ encountered in the EI spectra is similar to the $[(M\pm1)-92]^+/[(M\pm1)-106]^+$ ratio observed in the hydrogen and isobutane CI spectra.

All compounds listed in Table 2 gave rise to the series of $[M+1]^+$, $[M]^{+\cdot}$ and $[M-1]^+$ ions, of which the $[M+1]^+$ ion was the most intense of the group, except with isozeaxanthin (**129**) and lycopene (**31**), where the $[M]^{+\cdot}$ ion predominated. In most cases the $[M\pm1]^+$ and/or $[M]^{+\cdot}$ ions in the CI spectra were of greater intensity than the $[M]^{+\cdot}$ ion in EI spectra.

A feature of the hydrogen CI spectrum of lycopene (**31**) is the appearance of the $[M-69]^+$, $[M-92-69]^+$ and $[M-106-69]^+$ ions as well as abundant *m/z* 69 and *m/z* 43 ions. It is noteworthy that the diagnostically important $[M-69]^+$ species, whose formation is consistent with scission of the doubly allylic C-3,4 bond, is of higher abundance in the CI than in the EI spectrum.

The end group of β,β-carotene (**3**) shows no special fragmentation features in the CI spectrum, but significant ions at *m/z* 347, 281, 255, 243, 203, 189, 177, 149, 137 and 123, due to successive cleavages of the polyene chain, are observed, and the intensities of them are greater than those of the corresponding peaks in the EI spectrum (Fig. 3).

Except for small peaks corresponding to the loss of 16 and 18 mass units from the $[M+1]^+$ ion, the fragmentation pattern of canthaxanthin (**380**) does not show any special features. Prominent peaks at *m/z* M–217, M–203, M–191, M–151, 203 and 189, that have been shown to be characteristic of this end group in the EI spectrum, are also seen in the CI spectrum [12].

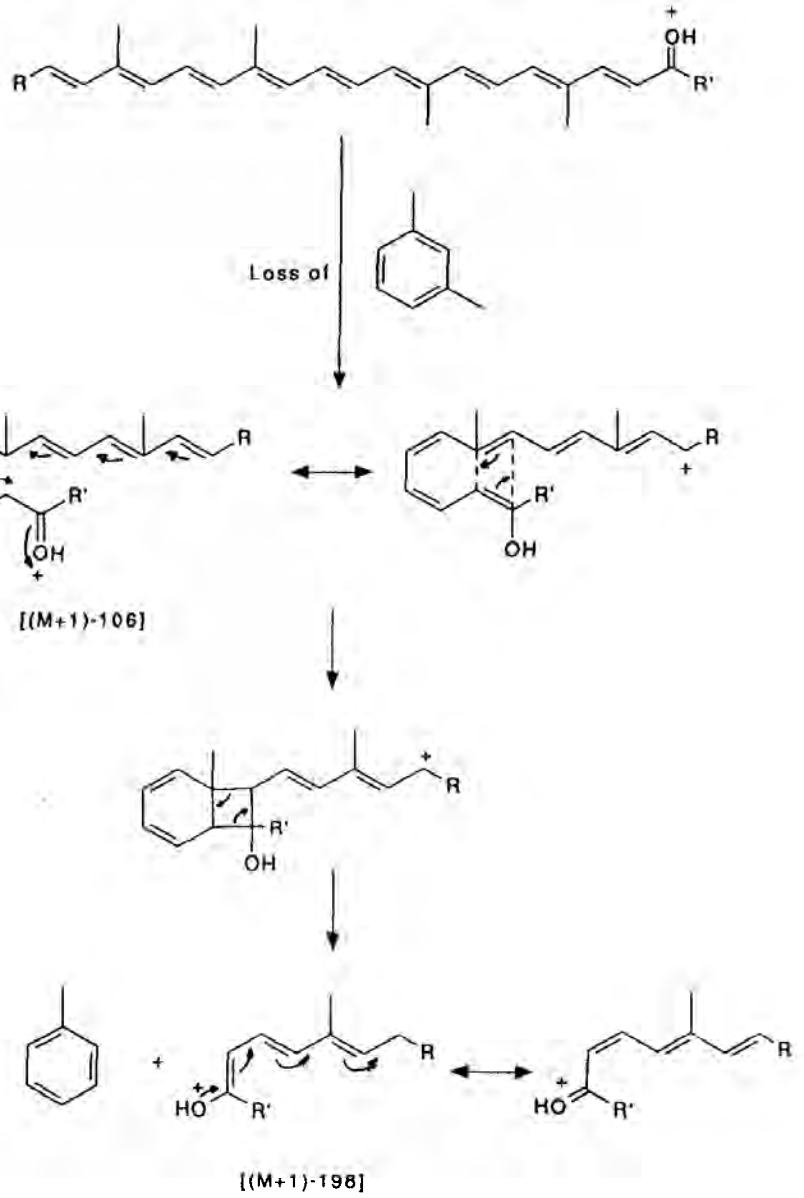
Carotenoids that possess hydroxylated end groups (*cf.* Table 2) are characterized by a predominant fragmentation pattern that can be ascribed to loss of water from the ions $[M\pm1]^+$, $[M]^{+\cdot}$, $[M\pm1-92]^+$, and $[M\pm1-106]^+$, which are much more abundant in the CI than in the EI spectra. Similarly, when the carotenoid contains two or more (*n*) hydroxy groups, intense peaks corresponding to $[M\pm1-n H_2O]^+$, $[M\pm1-92-n H_2O]^+$ and $[M\pm1-106-n H_2O]^+$ ions are usually observed. It is also noteworthy that, after initial losses of water from isozeaxanthin (**129**), degradation leads to significant peaks at *m/z* 361, 347, 269, 203, 201, 189, 149 and 123, which are characteristic of β,β-carotene (**3**). These peaks are not distinctive in the EI spectrum.

The isobutane CI spectrum of the bistrimethylsilyl ether of capsanthin (**335**) is characterized by abundant ions due to losses of 90 mass units (trimethylsilanol) from the $[M+1]^+$, $[M+1-92]^+$ and $[M+1-106]^+$ ions, whereas the EI spectrum does not show $[M-90]^{+\cdot}$, $[M-180]^{+\cdot}$ or corresponding ions derived by additional loss of toluene or xylene, but exhibits the base peak at *m/z* 197 due to the trimethylsilylcyclopentyl group ($C_{11}H_{21}OSi$). Moreover, the bistrimethylsilyl ether exhibits characteristic peaks at *m/z* M–227, 227 and 199, which are analogues of the M–155, 155 and 127 peaks in the spectrum of capsanthin (**335**) itself [12].

Examination of carotenol fatty acid esters [13, 14] by ammonia desorption chemical ionization (DCI) mass spectrometry has revealed that information can be obtained not only about the molecular mass of the carotenoid but also about the molecular mass of the fatty acids. Thus, for instance, the ammonia DCI spectrum of isozeaxanthin (**129**) dipelargonate exhibits major ions at *m/z* 866 (41%, $[M+NH_4]^{+\cdot}$), 883 (7%, $[M+(NH_3)_2H]^+$), 690 (44%, $[M-C_9H_{18}O_2]^{+\cdot}$), 708 (29%, $[M-C_9H_{18}O_2+NH_4]^{+\cdot}$), 725 (8%, $[M-C_9H_{18}O_2+(NH_3)_2H]^+$), 532 (100%, $[M-(C_9H_{18}O_2)_2]^{+\cdot}$), 550 (12%, $[M-(C_9H_{18}O_2)_2+NH_4]^{+\cdot}$). 567 (3%, $[M-(C_9H_{18}O_2)_2+(NH_3)_2H]^+$).

Metastable defocusing studies on capsanthin (**335**) revealed that the *m/z* 387 ion arises through consecutive losses of xylene and toluene from the $[M+1]^+$ ion, and that this *m/z* 387

ion in turn eliminates water to give the *m/z* 369 ion [12]. This consecutive loss of xylene and toluene is also observed in the spectra of capsanthin (**335**) bistrimethylsilyl ether and of capsanthol (*1*), but is not encountered in the EI spectrum. Scheme 1 shows a mechanism that has been proposed [12] for the subsequent elimination of toluene from the $[(M+1)-106]^+$ ion that is derived through loss of xylene from capsanthin (**335**).



Scheme 1

4. Particle desorption

Particle-desorption mass spectrometry, which is based on desorption of secondary ions that are induced by bombardment with high-energy heavy ions, has been used to examine a mixture of carotenoids obtained from carrots, in order to evaluate the utility of the method for multi-component assays without separation of the components [16]. The sample was electro-sprayed onto aluminized mylar and the desorbed secondary ions, which were generated through impact by ^{252}Cf-derived primary ions, were analysed by time-of-flight mass spectrometry. The information obtained was limited to three peaks in the high-mass region at *m/z* 537, 569 and 551 which, since β,ε-carotene (**7**) and β,β-carotene (**3**) constitute about 50% of the carotenes and lutein (**133**) about 60% of the xanthophylls in carrots, were considered to be associated, respectively, with the $[M+1]^+$ ion from carotene and the $[M+1]^+$ and $[M+1-H_2O]^+$ ions from lutein. A high background was observed in the higher mass regions as a result of metastable decompositions of the desorbed ions. It was concluded that the differences in peak intensities in a given spectrum cannot be used for quantitative purposes since several factors, including desorption efficiencies, determine the ion abundances.

C. Tandem Mass Spectrometry

1. Linked scanning

Linked scanning of the magnetic field and the electric sector voltage of a conventional double-focusing mass spectrometer provides a means of analysing metastable ions derived from any given precursor ion, and has been shown [17] to be a convenient way of identifying carotenoids when it is applied to the molecular ion. The major advantages over regular EI spectra are that carotenoids can be detected even in the presence of gross contamination and that ions that are characteristic of the end groups but of low abundance are more readily recognized, since all but the selected metastable ions are 'defocused' and do not contribute to the spectrum. The individual isomeric carotenes ($M^{+\cdot}$ = *m/z* 536) are readily differentiated by their linked-scan spectra as shown in Fig. 4.

Thus, β,β-carotene (**3**) displayed the expected $[M-137]^+$ ion (Fig. 4a), whilst β,ε-carotene (**7**) (Fig. 4b) showed the losses of 56, 123 and 148 (56 + 92) mass units from $M^{+\cdot}$ characteristic of the ε end group. The distinction between β,ε-carotene (**7**) and ε,ε-carotene (**20**) (Fig. 4c) is readily made on the basis of the abundances of their $[M-56]^{+\cdot}$ and $[M-138]^{+\cdot}$ ions, notably when the intensity ratios $[M-56]^{+\cdot}/[M-92]^{+\cdot}$ are compared, *i.e.* 0.11 for β,ε-carotene (**7**) and 0.44 for ε,ε-carotene (**20**). All the isomers that contain the ψ end group, namely β,ψ-carotene (**12**) (Fig. 4d), ε,ψ-carotene (**21**) (Fig. 4e) and ψ,ψ-carotene (lycopene) (**31**) (Fig. 4f), give rise to prominent $[M-69]^+$ ions, which constitute the base peak in the spectrum of lycopene. It is obvious from Fig. 4 that the spectra are readily amenable to interpretation and that all six isomers can be distinguished. It is noteworthy that all spectra show apparent losses of 91 mass units. This is likely to be because the resolution of the instrument used was insufficient in the region of the precursor to exclude completely the ^{13}C-derived $[M+1]^+$ ions.

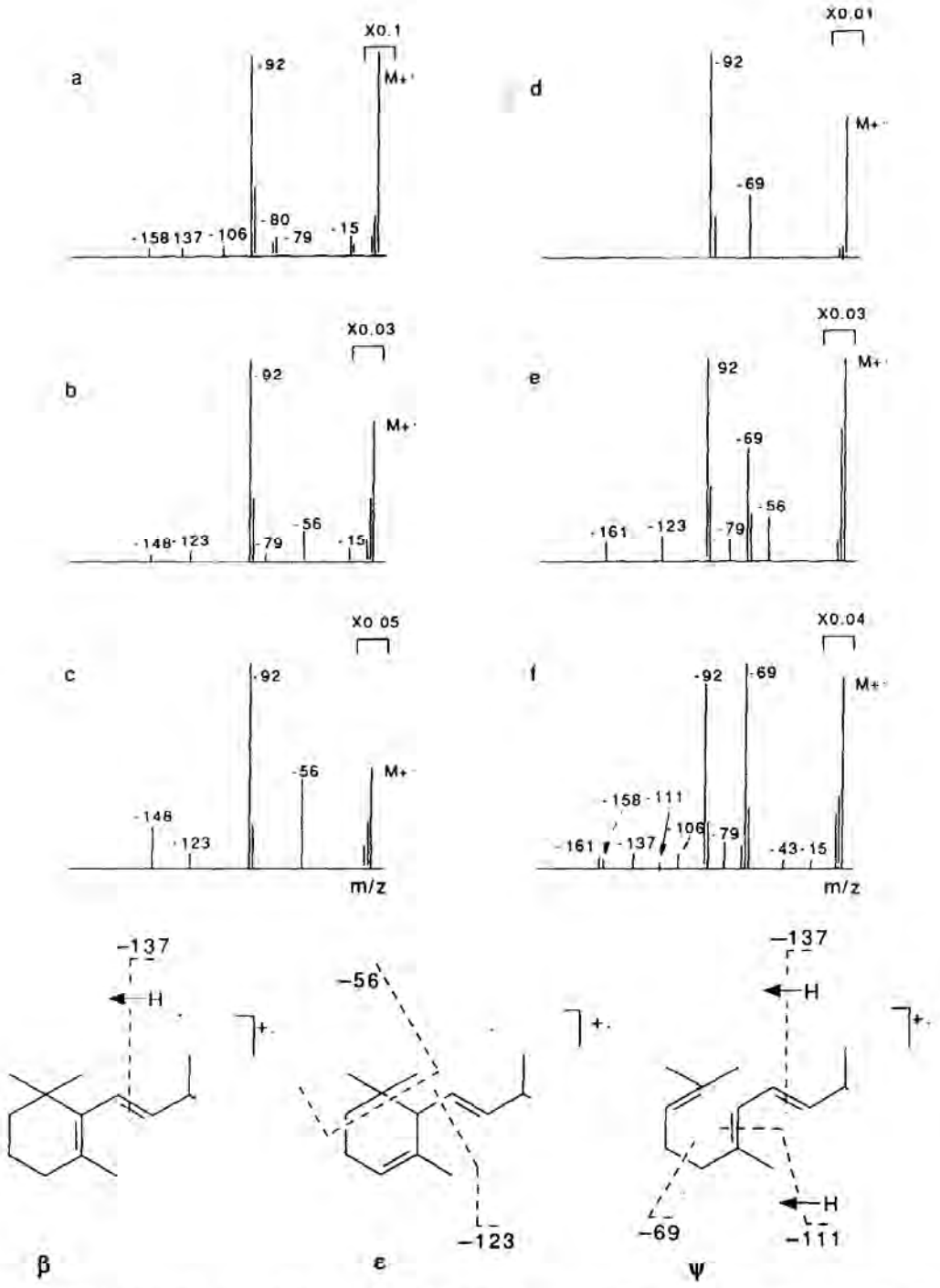


Fig. 4. B/E linked-scan spectra of molecular ions of (a) β,β-carotene (3), (b) β,ε-carotene (7), (c) ε,ε-carotene (20), (d) β,ψ-carotene (12), (e) ε,ψ-carotene (21) and (f) ψ,ψ-carotene (lycopene, 31) [17].

Similar examination of zeaxanthin (**119**) and lutein (**133**) by B/E linked scanning mass spectrometry [17] showed that the molecular ions of both substances undergo losses of 15 and 206 mass units, in addition to the losses of 18, 79, 92 and 153 mass units expected from regular EI spectra. Zeaxanthin (**119**) also exhibits an $[M-106]^{+\cdot}$ ion, and lutein (**133**) $[M-56]^{+\cdot}$, $[M-138]^{+\cdot}$, $[M-148]^{+\cdot}$, $[M-153]^{+}$ and $[M-230]^{+\cdot}$ ions.

2. MIKE Scanning

When pre-selected molecular precursors which dissociate spontaneously in the second field-free region of a reversed-geometry double-focusing instrument exhibit identical mass-analysed ion kinetic energy (MIKE) spectra, the dissociating molecular ions must have not only identical structures but also identical internal energy distributions. The result is achieved only by ionization of the same compound under identical conditions. This kind of analysis of metastable ions derived from molecular ions that are generated by electron impact has recently been used to confirm the structural assignment of two carotenoids, semi-β-carotenone (**559**) [18] and 5-hydroxy-5,6-seco-β,β-caroten-6-one (**558.4**) [19]. The metastable ion MIKE spectrum of semi-β-carotenone (**559**) (Fig. 5) shows a much greater abundance of $[M-92]^{+\cdot}$ ions than of $[M-106]^{+\cdot}$ ions, *i.e.* a ratio that is reversed relative to that seen in normal EI spectra.

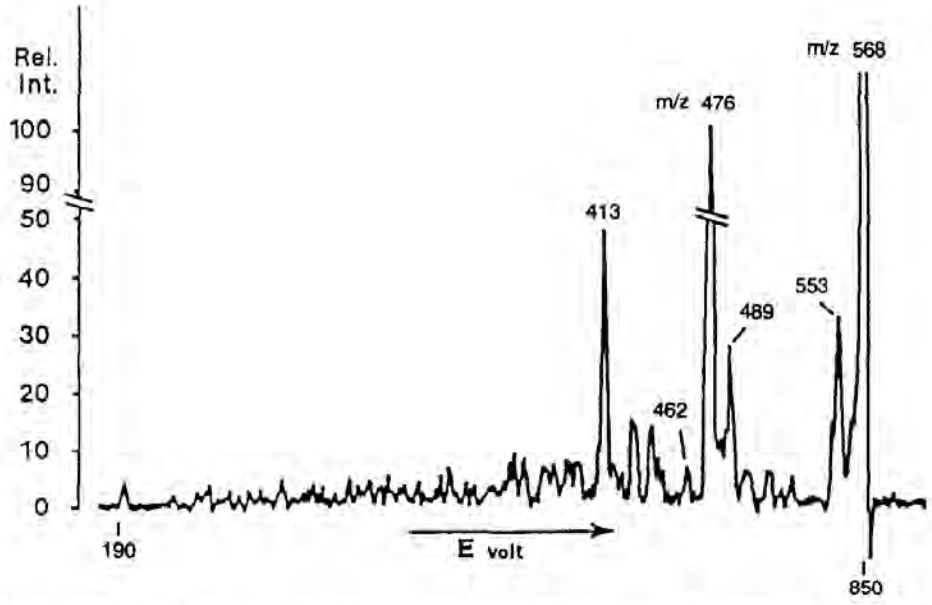


Fig. 5. Metastable ion (MI) mass-analysed ion kinetic energy (MIKE) spectrum of $[M]^{+\cdot}$ (*m/z* 568) of semi-β-carotenone (**559**) from *Ceratozamia fuscoviridis*, upon electron impact ionization (EI) at 70eV [18].

D. Combined Chromatography-Mass Spectrometry

1. GC-MS and LC-MS

Little work has been published on combined on-line chromatography–mass spectrometry of carotenoids. Gas chromatography–mass spectrometry (GC-MS) is unsuitable for analysis of mixtures of carotenoids because of the involatility and thermal lability of most of these compounds, but a study has been reported [20] in which the carotenoids were perhydrogenated and their hydroxy groups acetylated or silylated prior to analysis. The GC-MS technique is rapid and technically simple, but the pre-treatments are laborious and the available structural information is limited, *i.e.* data are obtained only about the molecular size, some specific structural features, and the functional groups present.

All reports on combined liquid chromatography and mass spectrometry of carotenoids are off-line studies in which the carotenoids have first been separated and collected and then introducted into the mass spectrometer. However, there has been one on-line LC-MS study of the 11*E* and 11*Z* isomers of retinyl acetate, that introduced and evaluated an improved monodisperse aerosol generation interface, a technique which should be applicable also to carotenoids. The interface is designated MAGIC-LC/MS and consists of a momentum separator, which allows generation of electron impact spectra of searchable quality under typical LC separation conditions, including reversed-phase and gradient elution [21]. Developments in this area are expected in the near future.

2. SFC-MS

Apparent reasons for the more elaborate studies of on-line supercritical fluid chromatography–mass spectrometry (SFC-MS) of carotenoids [22, 23] are that the hardware modifications required are considerably less extensive than with LC-MS and that on-line SFC is compatible with several common MS ionization modes such as electron impact (EI), chemical ionization (CI) and charge-exchange (CE). Conversion between GC-MS and SFC-MS is also simplified and involves only an injector substitution and a column change.

An exploratory study [22] of a set of selected carotenoids comprising β,β-carotene (**3**), echinenone (**283**), canthaxanthin (**380**), astacene (**398**), fucoxanthin (**369**), fucoxanthin 3-acetate, isofucoxanthin (**363**), zeaxanthin (**119**), and zeaxanthin diacetate, has demonstrated that the most promising stationary phases for capillary SFC of complex natural mixtures of carotenoids appear to be cyanopropyl polysiloxane and polyethylene glycol. All the carotenoids listed, as well as several related isomers, were sufficiently soluble in supercritical CO_2 to allow chromatographic elution from the stationary phases tested. The use of polar modifiers (*e.g.* 2 to 5% methanol), which was required in some cases when longer columns (10 and 20 m) were used, showed that certain stationary phases were unstable, and caused dissolution of the column coating, leading to plugging of the capillary restrictor. Plugging problems were also observed with straight capillary restrictors, but could be avoided by using jet-type restrictors (Guthrie type [24]), which constitute an integral part of the column and are easily interfaced

with the mass spectrometer, thereby essentially eliminating dead volumes and active surfaces.

A simple carotenoid test mixture has been used to explore the potential of SFC-MS. An ion chromatogram obtained in this work is shown in Fig. 6. Although the ion-source pressure changes are substantial, they are within the limits acceptable for chemical ionization, and CO_2 clusters above the tetramer are not significant. The use of an adequate restrictor, for SFC pressure programming up to 400 bar, is compatible with normal mass spectrometer operating pressures, and particle formation during decompression seems to be minimized by avoiding additional heating of the restrictor. This also leads to increased sensitivity.

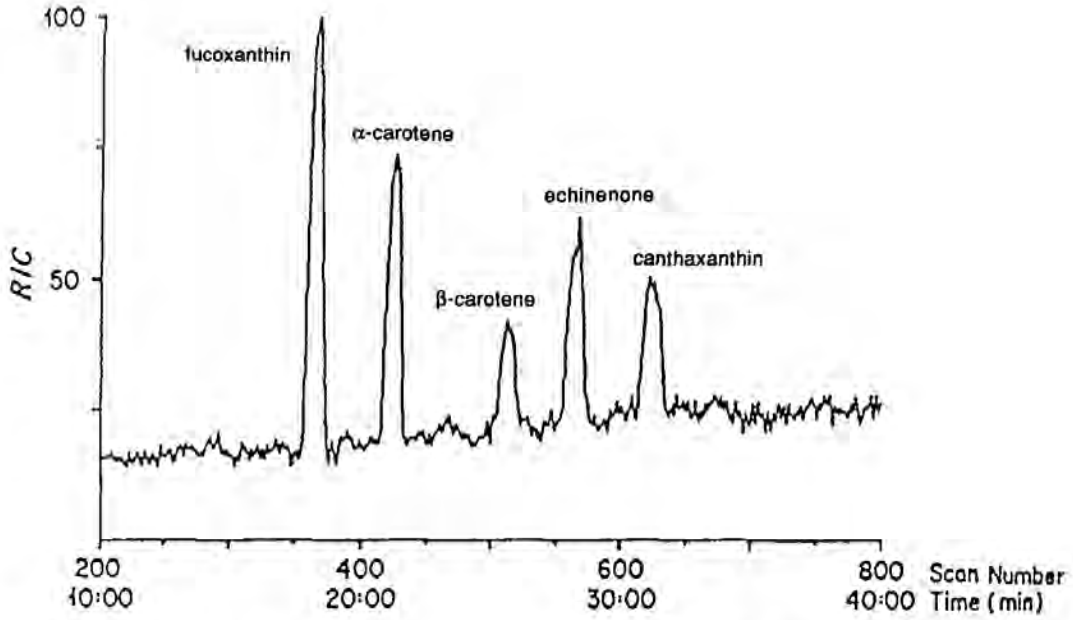


Fig. 6. SFC-MS total ion chromatogram obtained for a carotenoid test mixture: fucoxanthin (**369**), β,ε-carotene (**7**), β,β-carotene (**3**), echinenone (**283**) and canthaxanthin (**380**) [22]. *Column*: OV-17, 20 m x 100 μm i. d. *Mobile phase*: CO_2 at 70°C. *Pressure*: injection at 80 bar; fast ramp to 200 bar; program 200 to 320 bar at 4 bar.min^{-1}.

The methane-CI mass spectra of β,β-carotene (**3**), echinenone (**283**), canthaxanthin (**380**) and astacene (**398**) consist primarily of $[M+1]^+$ ions, the usual $[M+29]^+$ and $[M+41]^+$ adduct ions being of very low intensity. A small $[M+H+CO_2]^+$ ion is also observed for some of these compounds. In addition to the $[M+1]^+$ ion, which furnishes the base peak, zeaxanthin (**119**) exhibits a prominent $[M+1-H_2O]^+$ ion, but no peaks that reveal the presence of two hydroxy groups. The diol structure, however, follows from the 84 dalton shift of the $[M+1]^+$ peak in the spectrum of the corresponding diacetate, which also shows two sequential losses of acetic acid. Similar structural information has been obtained on chemical ionization with heated direct insertion probes [12].

Increased fragmentation, leading to more information about structure, can be obtained by using more energetic ionization conditions, *e.g.* higher source temperatures, replacing methane by hydrogen as reagent gas, and mixed CI-CE ionization. Increase in the CO_2 pressure also leads to increased fragmentation, probably because charge-exchange reactions are favoured. It is noteworthy that minimal fragmentation is advantageous in the case of tandem mass spectrometry, since collisional activation of the molecular ion prior to the second analyser provides the necessary structural information.

A standard Kratos thermospray source equipped with a discharge ionization electrode linked *via* a length of fused silica capillary tubing to a conventional packed LC column (silica, 2 mm i. d.) mounted in the GC oven of a Kratos MS25 GC-MS system, has been used to obtain SFC-MS results that show excellent chromatographic resolution and peak shape [23]. The silica line was passed through a resistively heated stainless steel capillary housed within the probe, directly into the thermospray source. An additional feature was a miniature T-piece located at the inlet to the steel capillary, allowing an additional co-axial flow to be introduced into the thermospray source. During chromatography of carotenoid hydrocarbons with CO_2 as mobile phase, a considerably enhanced response in the positive ion operation was observed [23] from the separated hydrocarbons if an additional low flow (approximately 20 $\mu l.min^{-1}$) of a solvent such as dichloromethane was introduced *via* the T-piece. The presence of dichloromethane had no obvious effect on the quality of the spectra, which showed intense molecular ions and little fragmentation (Fig. 7) but, in contrast to the SFC-(methane-CI)MS spectra, exhibited M–92, M–106 and M–158 peaks. Another application of this interface is the addition, *via* the T-piece, of chemical ionization reagents which modify the spectrum that is obtained.

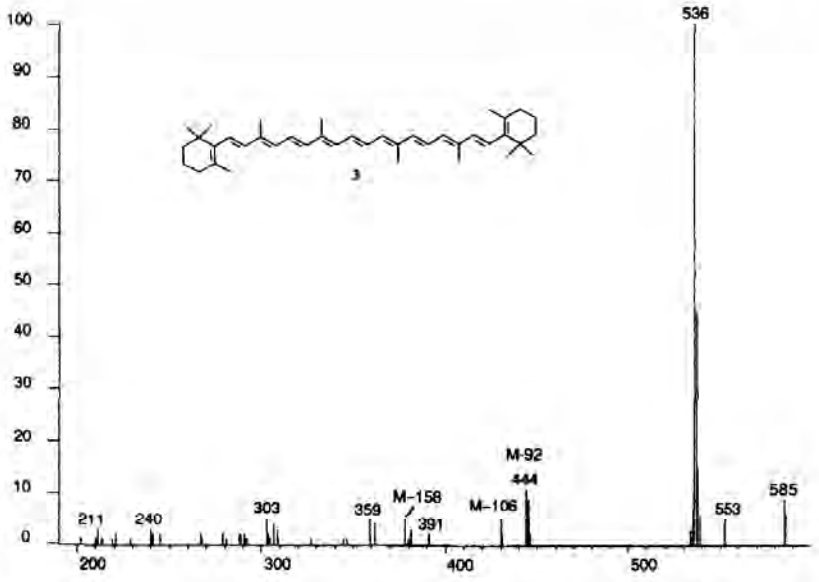


Fig. 7. Spectrum of β,β-carotene (3) obtained by SFC-MS in the presence of dichloromethane [23].

Some carotenoids, notably fucoxanthin (**369**) and related compounds, undergo considerable fragmentation under SFC-(methane-CI)MS conditions [22]. Thus, SFC-MS analysis of fucoxanthin (100 ng) produced a sharp chromatographic peak and a spectrum that exhibited, besides an intense protonated molecular peak at *m/z* 659, several diagnostically valuable peaks (Fig. 8), which were not due to ions formed by extrusion of toluene or xylene.

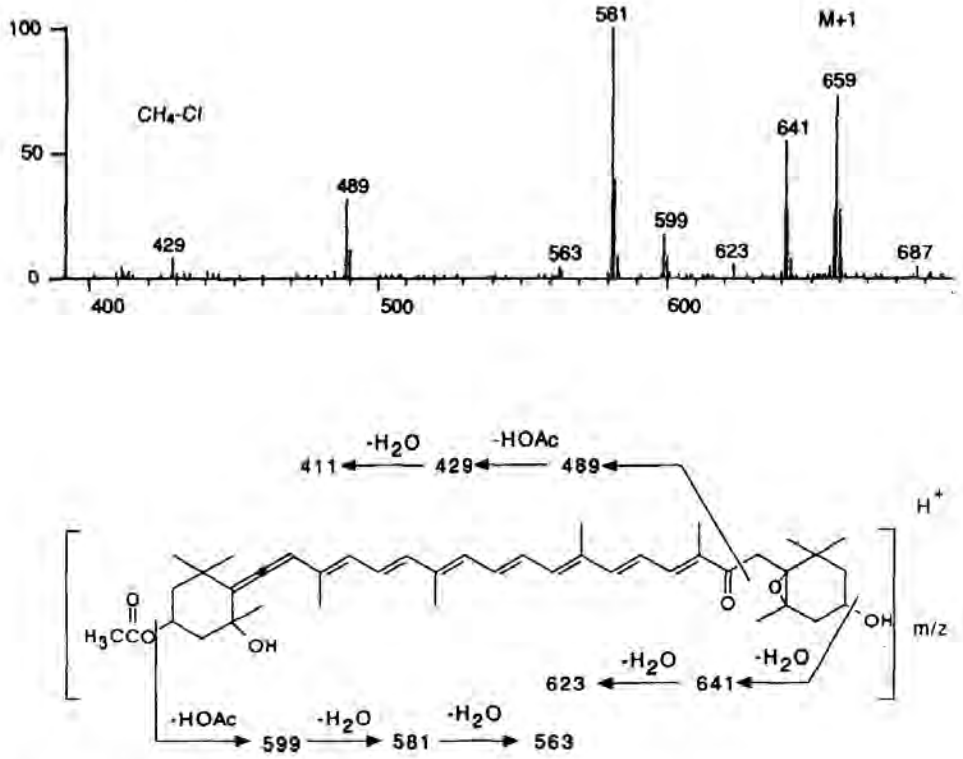


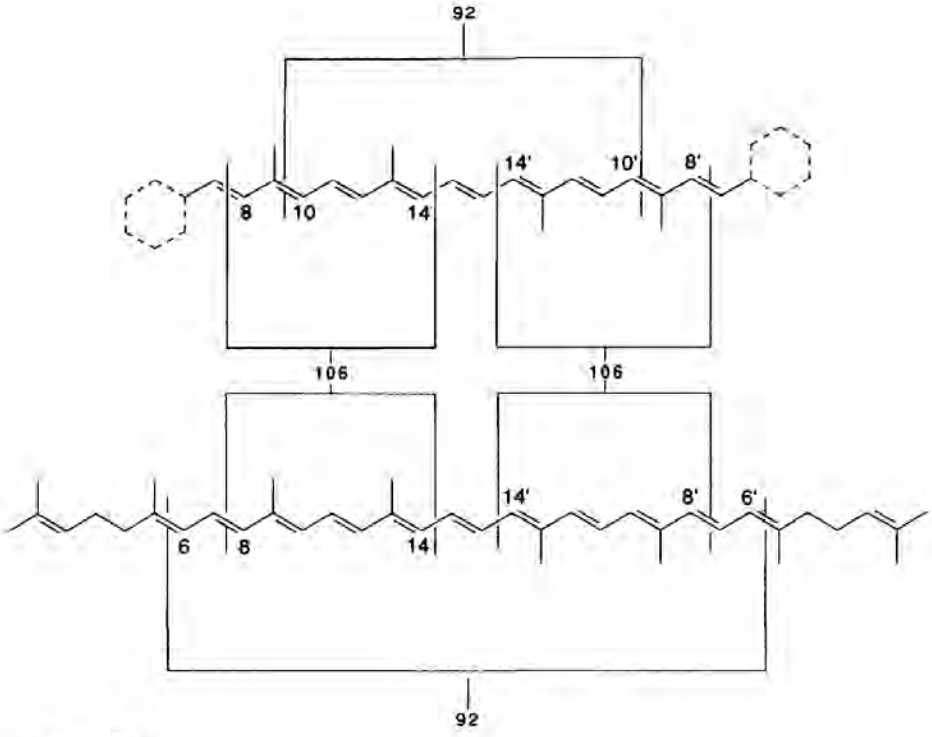
Fig. 8. Fragmentation of fucoxanthin (**369**) under SFC-(methane-CI)MS conditions [22].

E. Elimination of In-Chain Units

1. Mechanisms for the major reactions

Over the past two decades, considerable interest has been focused on the elimination of in-chain fragments from carotenoids, notably the formation of the almost ubiquitous $[M-92]^{+\cdot}$ and $[M-106]^{+\cdot}$ species, and the less abundant but frequently occurring $[M-158]^{+\cdot}$ ions. More recently, investigations employing labelled compounds [25], especially an extensive study [26]

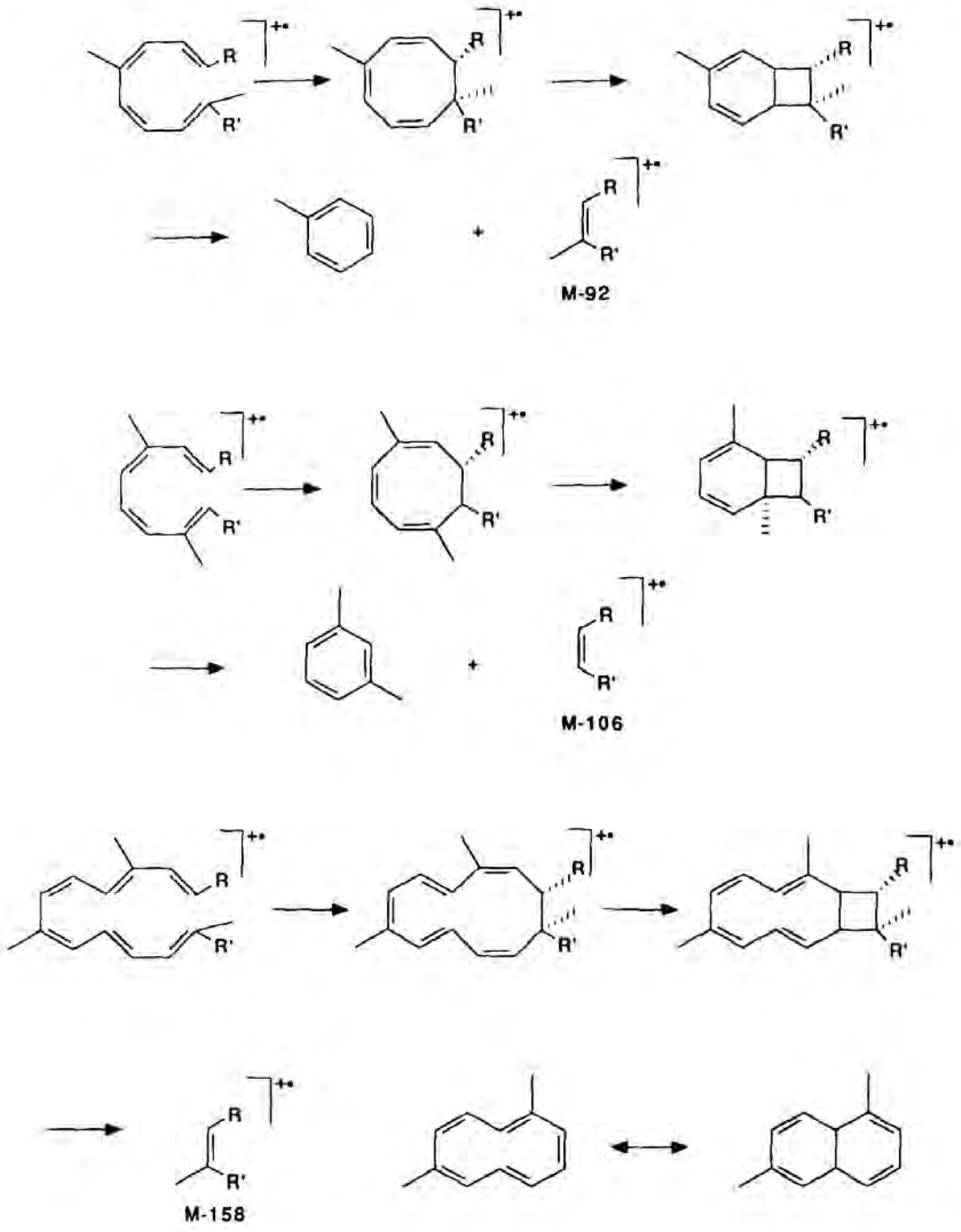
covering 19 different deuteriated species of dicyclic carotenoids with labels in positions 4, 7, 8, 10, 11, 12, 14, 15, 19 and 20, have confirmed earlier results which showed that elimination of toluene and xylene (92 and 106 mass units, respectively) is limited to certain parts of the polyene chain, as illustrated in Scheme 2. Moreover, the $C_{10}H_8(CH_3)_2$ fragment (dimethylcyclodecapentaene/dimethyldihydronaphthalene, 158 mass units) is derived from the same parts of the polyene chain as is toluene [26].



Scheme 2

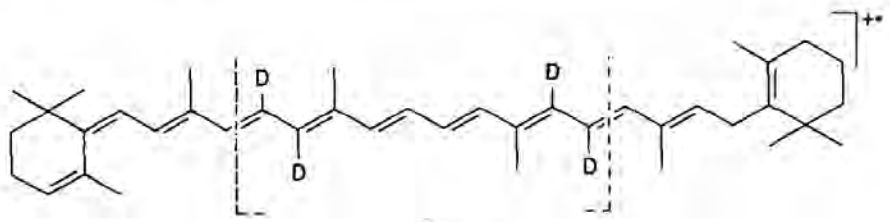
These studies [26] also demonstrated that the in-chain reactions occur without hydrogen shifts and follow the Edmunds-Johnstone mechanism, as previously proposed [27], and hence formally involve scission of double bonds only. A modified version of this mechanism, [1, 28], adapted to conform to the Woodward-Hoffmann rules and to accommodate results encountered in studies on cyclization of polyolefins, explains the formation of toluene, xylene, and dimethylcyclodecapentaene/dimethyldihydronaphthalene (Scheme 3).

This mechanism, if stereochemical implications are disregarded, is applicable to EI as well as to thermally induced reactions. This is satisfactory since the extent to which isomerization of the original molecule and thermal elimination of in-chain units precede ionization is unknown [1, 29]. However, studies of metastable ion transitions, which require a special technique in the case of the formation of the $[M-106]^{+\cdot}$ and $[M-158]^{+\cdot}$ species, have shown that these ions, at least in part, are formed from $M^{+\cdot}$ [1, 3, 17].



Scheme 3

The same mechanism also applies to *retro*-carotenoids, in which the displacement of the double bonds alters the cleavages correspondingly so that the formation of toluene and xylene still formally occurs only by rupture of carbon–carbon double bonds [26]. This is well illustrated by [11,12,11',12'-$^2H_4$]-6',7-*retro*-β,ε-carotene (*2*), which exhibits an $[M-162]^{+\cdot}$ ion that is explicable only by the cleavages indicated in Scheme 4 [26].



2

Scheme 4

15,15'-Didehydrocarotenoids also fragment by the same mechanism but, since fission of the triple bond does not take place in these compounds, the $[M-92]^{+\cdot}$ ion is replaced by an $[M-90]^{+\cdot}$ ion, which is formed by elimination of methylbenzyne through breakage of the 11,12 and 13',14' bonds, or of the 13,14 and 11',12' bonds [1, 30].

2. Intensity ratio of the $[M-92]^{+\cdot}$ and $[M-106]^{+\cdot}$ peaks

a) Regular carotenoids

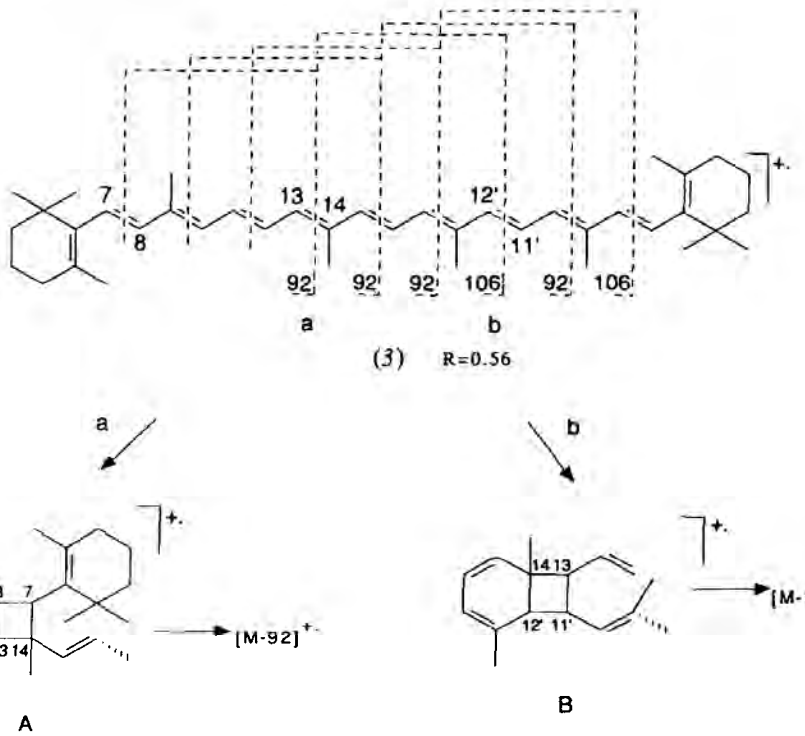
The inverse relationship (Table 3, [31]) that was encountered between the abundance ratio R of the $[M-92]^{+\cdot}$ and $[M-106]^{+\cdot}$ ions ($R = I_{M-92}/I_{M-106}$) and the number of conjugated double bonds in the acyclic polyene chain, when the end groups do not contain multiple oxygen functions, has been confirmed in subsequent investigations [26, 32]. Attempts to rationalize this relationship in terms of differences in steric congestion in the various intermediates have proved fruitful [3-5]. Thus the fact that R is altered from 12.9 to 0.56 when the methyl group at C-13 in β,β-carotene (**3**) is transferred to C-14 (compound *3*) is readily explained as the result of altered steric congestion in some of the intermediates that lead to the elimination of toluene and xylene [33]. Since the number of structurally possible ways of eliminating these fragments remains unchanged (*cf.* compounds *3* and **3** in Scheme 5), it can be inferred that the altered ratio is due to two factors, *i.e.* (i) elimination of toluene *via* intermediate A (path a) is suppressed or inhibited because of steric repulsion on formation of the 7,14-bond and, (ii) more important, elimination of xylene *via* intermediate B (path b) is favoured since, in this intermediate, both non-bridging carbons of the four-membered ring (C-13 and C-11') carry acyclic substituents, whereas one of these carbons in the corresponding intermediate, C, from normally substituted compounds carries a more space-demanding cyclohexene substituent [33].

Table 3. Relationship between the intensity radio R (= I_{M-92}/I_{M-106}) and the number of conjugated double bonds in the acyclic polyene chain [31].

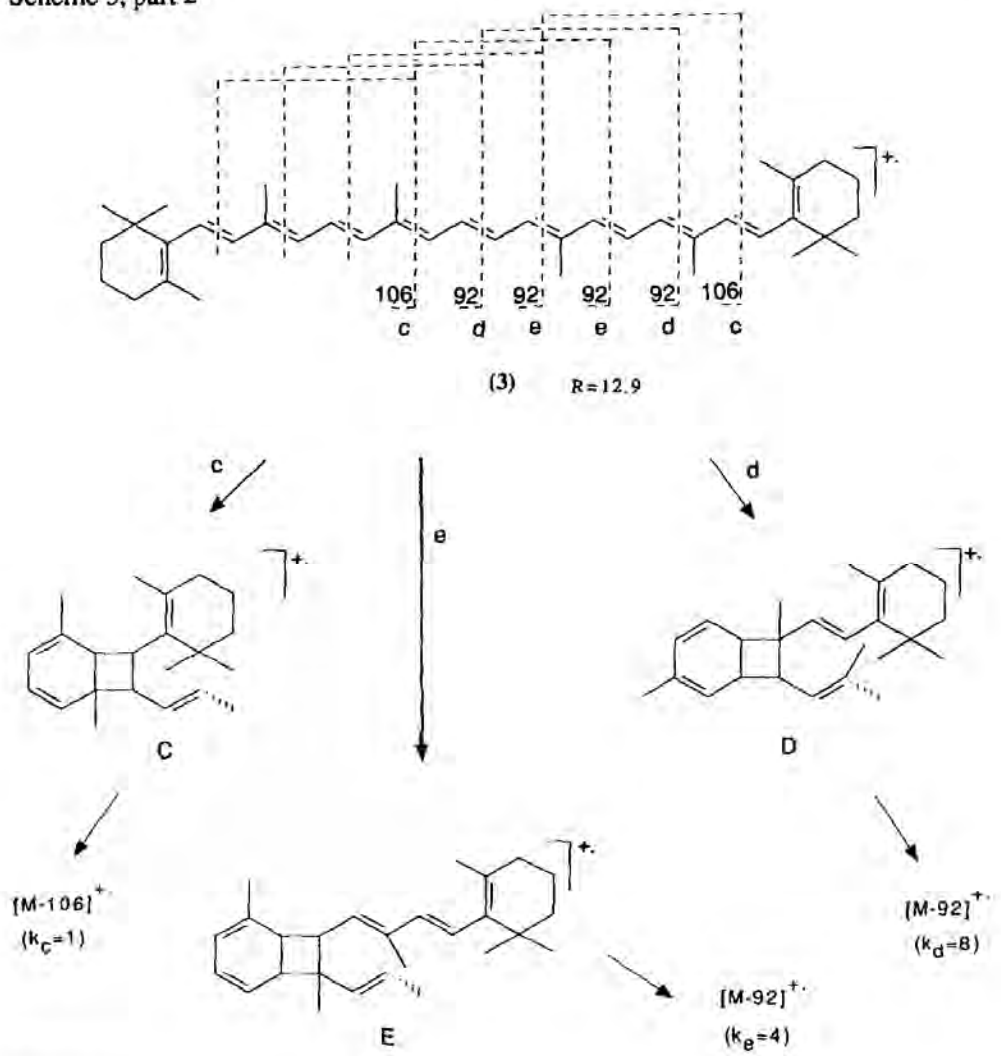
R (= I_{M-92}/I_{M-106})	Double bonds
12.9-1.59	9
1.00-0.44	10
0.36-0.26	11
0.068-0.057	12
0.029-0.018	13

Approximate values for the overall relative rate constants for the in-chain reactions of normal dicyclic carotenoids such as β,β-carotene (**3**) can be calculated from deuterium labelling data and R-values, if the assumption is made that the further fragmentations of the $[M-92]^{+\cdot}$ and $[M-106]^{+\cdot}$ species occur at a similar rate. It has been shown [26], for several labelled derivatives of β,β-carotene (**3**) and zeaxanthin (**119**), that the abundance of the $[M-92]^{+\cdot}$ species formed by path d is about twice that of the $[M-92]^{+\cdot}$ ions generated by path e (Scheme 5), a result which suggests that the rate constant for reaction e is about half that for reaction d.

Scheme 5, part 1



Scheme 5, part 2



Scheme 5

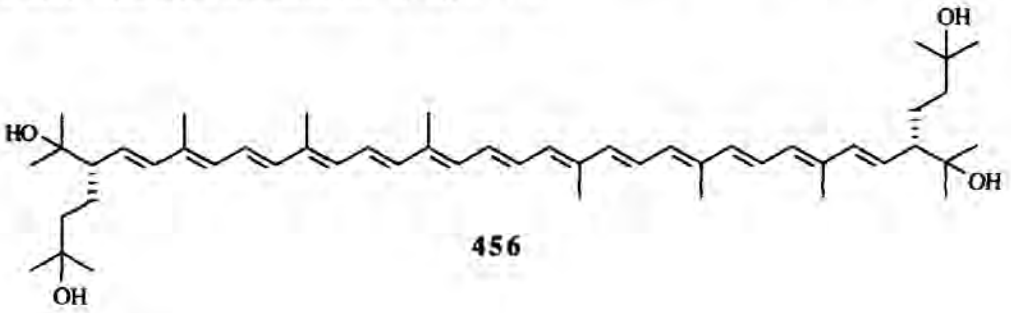
If the rate constant for reaction c leading to the $[M-106]^{+\cdot}$ ion is designated k_c and arbitrarily assigned the value 1, it can be inferred, since R for β,β-carotene (3) is about 12, that the rate constants for reactions d (k_d) and e (k_e) are 8 and 4 respectively, *i.e.*

$$(2k_d+2k_e)/2k_c = 12;\ k_d = 2k_e;\ k_c = 1.$$

The reduction of R (Table 3) when the number of conjugated double bonds of the polyene chain is increased can be accounted for in a similar way [33].

b) Acyclic C_{50} carotenoids

Steric arguments have been used [34] to explain the fact that the extension of an undecaene chromophore by the introduction of a double bond between C-3 and C-4 in acyclic C_{50} carotenoids does not alter the original value of *R*. The obvious reason is that the formation of $[M-106]^{+\cdot}$ ions from bacterioruberin (**456**) is slow.



456

c) Aromatic carotenoids

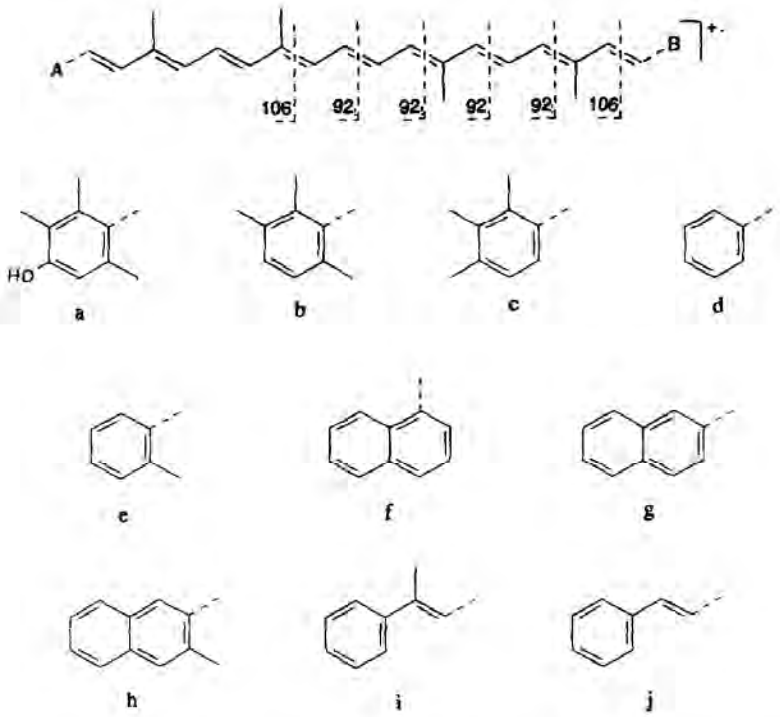
Carotenoids that possess aromatic end groups or carbonyl functions conjugated to the acyclic chromophore sometimes exhibit irregular values of *R*, which might be due to electronic factors [28], although it is unclear how the effect operates. It follows from Table 4 [6] that the values of *R* for the aromatic compounds fall within the expected range (1.69 to 12.9) only when the aromatic rings are substituted in the 1 and 5 positions (carotenoid numbering) (carotenoids **24, 87, 161**), whilst the ratio is reduced in the absence of either or both of these substituents. It was therefore inferred that conjugation (coplanarity) of the aromatic nucleus with the polyene chain, which is suppressed in carotenoids **24, 26, 87** and **161** or counteracted sterically in compound *9*, favours migration of the double bond closest to the aromatic chromophore, and that this is the cause of the observed reduction in *R*. The same rationale was used to explain the decreased ratios encountered for 10 out of 13 compounds that have carbonyl groups directly conjugated to the acyclic chromophore [28].

The compounds that possess a monocyclic end group (**26**, **28**, *4*, *5*, *9*, *10*), however, furnish results which, with fair precision, can also be accounted for on the basis of the steric concepts mentioned above and outlined in detail elsewhere [3]. Thus, calculations gave for compound **26** $R = 0.4$, for *4*, **28**, and *5* $R = 0.2$, for *9* $R = 0.3$, and for *10* $R = 1.2$.

d) Oxocarotenoids

Introduction of an oxo function conjugated with the olefinic chain tends to increase *R* [3]. If the effect is local, as proposed [28], and hence primarily affects the in-chain reaction that involves the olefinic bond closest to the carbonyl group, the rate constants for the elimination by this path should be reduced when xylene is lost but increased when toluene is extruded. It is difficult, however, to associate available results with a specific electronic or steric effect,

Table 4. Values of the abundance ratio R ($= I_{M-92}/I_{M-106}$) in the mass spectra of aromatic carotenoids and model compounds [6].



Compound	End groups A	B	Ratio R
87	a	b	3.5
6	f	f	0.074
7	g	g	0.071
24	b	b	3.4
161	a	a	1.8
26	b	c	0.95
4	d	d	0.40
28	c	c	0.33
5	e	e	0.23
8	h	h	0.071
9	i	i	0.37
10	j	j	2.42

especially since the outcome of conjugating an oxo group with the polyolefinic chain is usually small when compared with the effects on *R* of the major site-dependent variations of the rate constants discussed above [3].

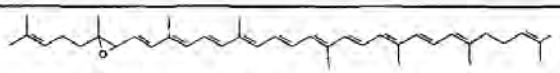
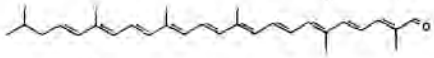
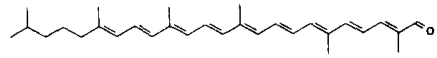
e) Carotenoids substituted at C-20

The variations of *R* that are observed following alterations to C-20 (the methyl substituent at C-13) are of considerable theoretical and diagnostic interest. A comparison of experimental data [35-37] for values for the in-chain eliminations shows that introduction of an oxygen function apparently enhances the elimination of C_6H_5CHX and $C_6H_4(CH_3)CHX$ relative to that of toluene and xylene (X = H, OH; X = O *etc.*) [3].

f) Acyclic carotenoids with fewer than 11 conjugated double bonds

Experimentally observed and calculated values of *R* for some acyclic compounds that possess ten (**222**, *11*) or nine (**35**, **515**, **520**, **521**, **523**, *12*) conjugated double bonds are given in Table 5 [3]. In most cases the agreement is fair. Carotenoids which possess fewer than nine conjugated double bonds do not usually give rise to $[M-106]^{+\cdot}$ species, whereas $[M-92]^{+\cdot}$ ions are frequently encountered [1]. Exceptions are found, however, among triterpenoid carotenes that have seven conjugated double bonds, *e.g.* compounds **516** and **517** [40]. Although compound **517** theoretically should give rise only to $[M-92]^{+\cdot}$ ions and **516** should have *R* = 0.3, both compounds exhibit *R* = 1.3.

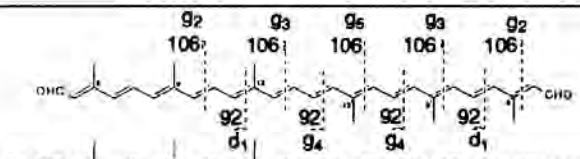
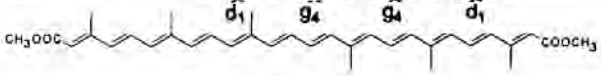
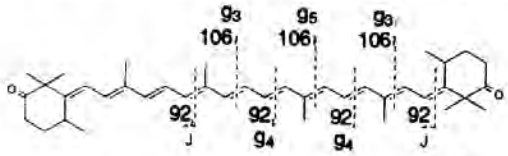
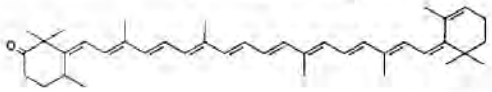
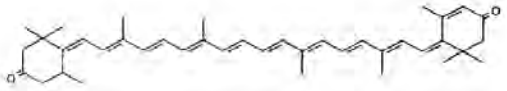
Table 5. Comparison of observed and calculated values of the abundance ratio *R* (= I_{M-92}/I_{M-106}) for some acyclic carotenoids with a chromophore of ten or nine conjugated double bonds [3].

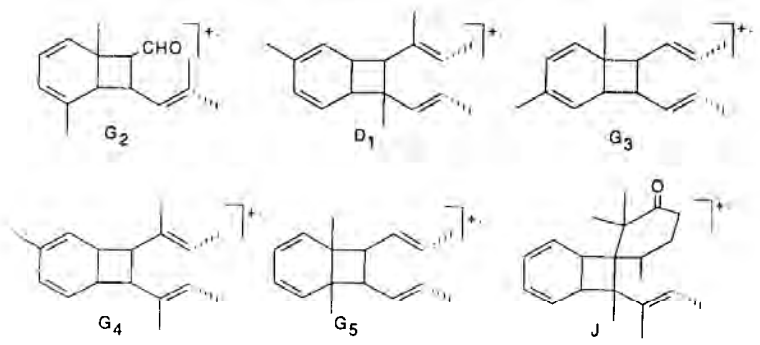
Double bonds	Compound		Ratio *R* Found	Calc.	Ref.
10		(**222**)	0.21	0.25	38
9		*11*	0.047	0.045	39
9		(**35**)	1.3	0.50	39
9		(**515**) X=H_2	0.60	0.50	40
		(**520**) X=H,OH	0.60		41
		(**521**) X=H,glucopyranosyl	0.19		41
		(**523**) X=O	0.33		42
9		*12*	2.3	0.50	39

g) *Retro*-carotenoids

Retro-carotenoids also undergo in-chain eliminations; available intermediates for the loss of xylene and toluene from known representatives which comprise 12 or 10 conjugated double bonds (*13-17*) are shown in Table 6 [3, 43-45]. None of these intermediates is identical to those mentioned earlier [3].

Table 6. Comparison of observed and calculated values of the abundance ratio R (= I_{M-92}/I_{M-106}) for some *retro*-carotenoids.

Double bonds	Compound		Ratio *R* Found	Calc.	Ref.
12		*13*	0.5	0.45	1
12		*14*	0.13		1
10		*15*	0.60	0.67	43
10		*16*	0.75		44
10		*17*	0.55		45



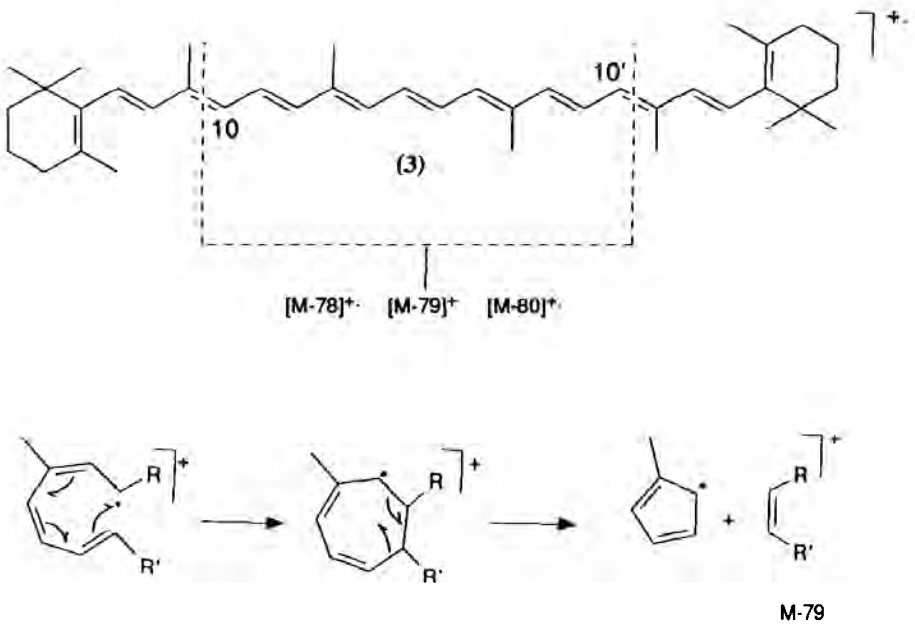
h) Irregular carotenoids

When the results of a study [46] of a series of deuterium-labelled, mainly irregular carotenoids were examined in the same manner as those above, a fair agreement between observed and calculated values for R was encountered for all regular carotenoids, except a C_{30} compound which, like some of the other triterpenoid carotenoids discussed above, gave unexpected results [3].

3. Other reactions

a) Formation of $[M-78]^{+\cdot}$, $[M-79]^{+}$, and $[M-80]^{+\cdot}$ ions

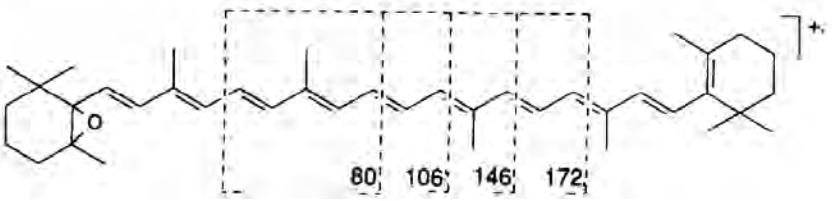
A mechanism has been presented [47] for the elimination of in-chain fragments leading to the formation of the $[M-78]^{+\cdot}$, $[M-79]^{+}$, and $[M-80]^{+\cdot}$ ions *via* a common seven-membered-ring transition state. This mechanism is outlined in Scheme 6 for the loss of 79 mass units from β,β-carotene (**3**). Since these ions, which are found in many carotenoid mass spectra, are of low abundance, the mechanism proposed could not be confirmed in a study of the labelled dicyclic carotenoids [26]. It was established, however, that the loss of C_6H_6, C_6H_7, and C_6H_8 occurs from the same part of the polyene chain as the loss of dimethyldihydronaphthalene and toluene (*i.e.* the C-10 to C-10' range).



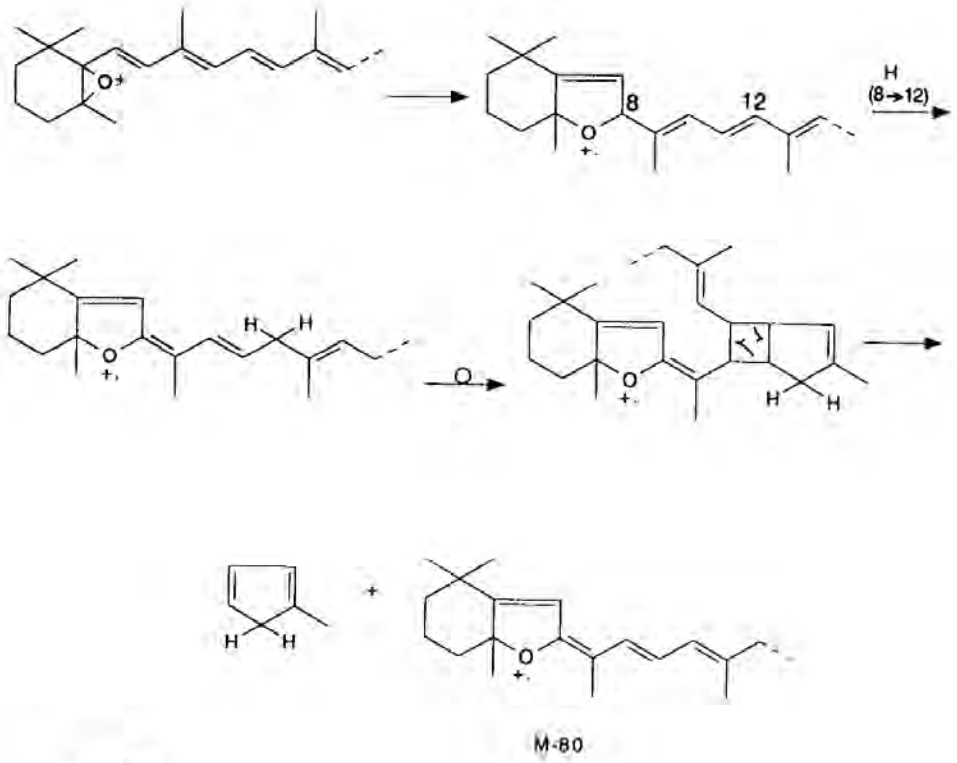
Scheme 6

b) 5,6-Epoxides and 5,8-epoxides

Both 5,6-epoxides and 5,8-epoxides can furnish $[M-106]^{+\cdot}$ ions, as well as $[M-80]^{+\cdot}$, $[M-146]^{+\cdot}$, and $[M-172]^{+\cdot}$ ions, by non-conventional in-chain elimination reactions, which involve breaking of the bonds indicated in Scheme 7 for β,β-carotene-5,6-epoxide (**213**). On the basis of extensive deuterium-labelling studies, which invalidated earlier proposed mechanisms, the mechanism shown in Scheme 7 has been invoked [26] for the formation of the $[M-80]^{+\cdot}$ species that is diagnostic of carotenoid epoxides, and this mechanism is applicable also to the analogously formed $[M-106]^{+\cdot}$ and $[M-146]^{+\cdot}$ species; the $[M-172]^{+\cdot}$ ions arise by a different mechanism.



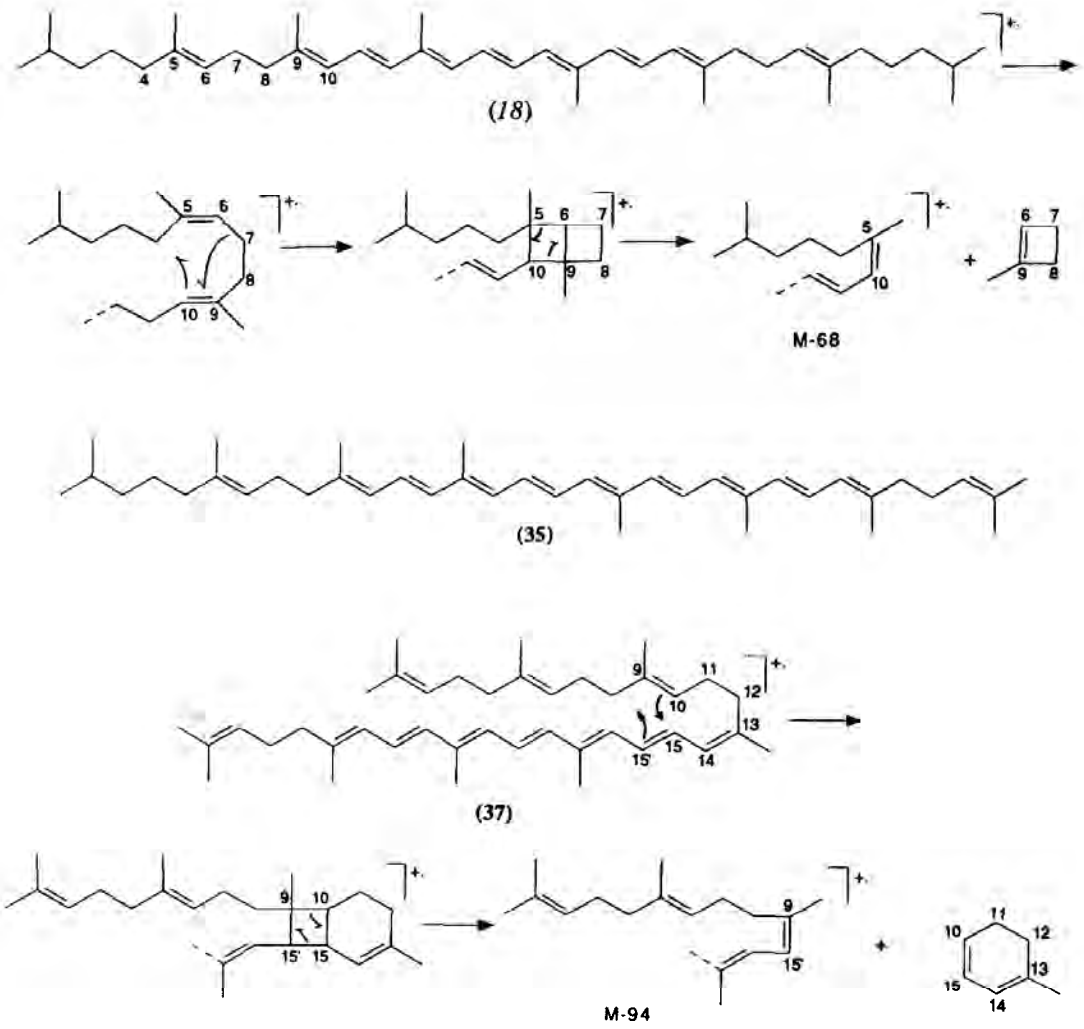
(213)



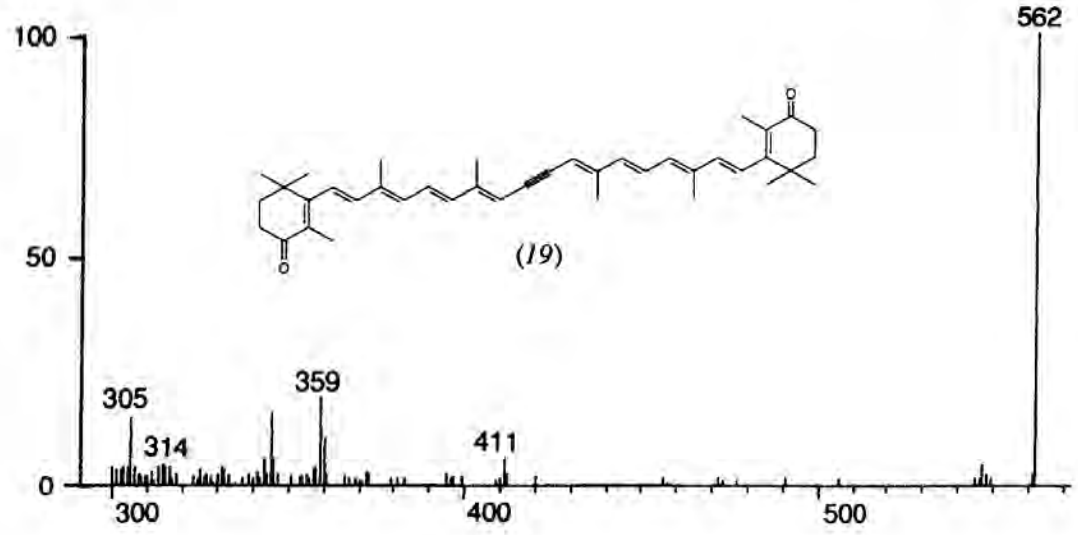
Scheme 7

c) Acyclic 7,8-dihydrocarotenoids and 7,8,11,12-tetrahydrocarotenoids

Some 7,8-dihydrocarotenoids and 7,8,11,12-tetrahydrocarotenoids have been found to undergo other in-chain elimination reactions. Thus, 1,2,7,8,1',2',7',8'-octahydro-ψ,ψ-carotene (*18*) and 1,2,7,8-tetrahydro-ψ,ψ-carotene (**35**) give rise to prominent $[M-68]^{+\cdot}$ ions (15% and 12%, respectively), the formation of which has been proposed to occur by the mechanism shown for compound *18* in Scheme 8 [39]. A related mechanism, also given in Scheme 8, has been suggested [48] for the formation of the $[M-94]^{+\cdot}$ species that is encountered in the spectrum of 7,8,11,12-tetrahydrolycopene (**37**).



Scheme 8



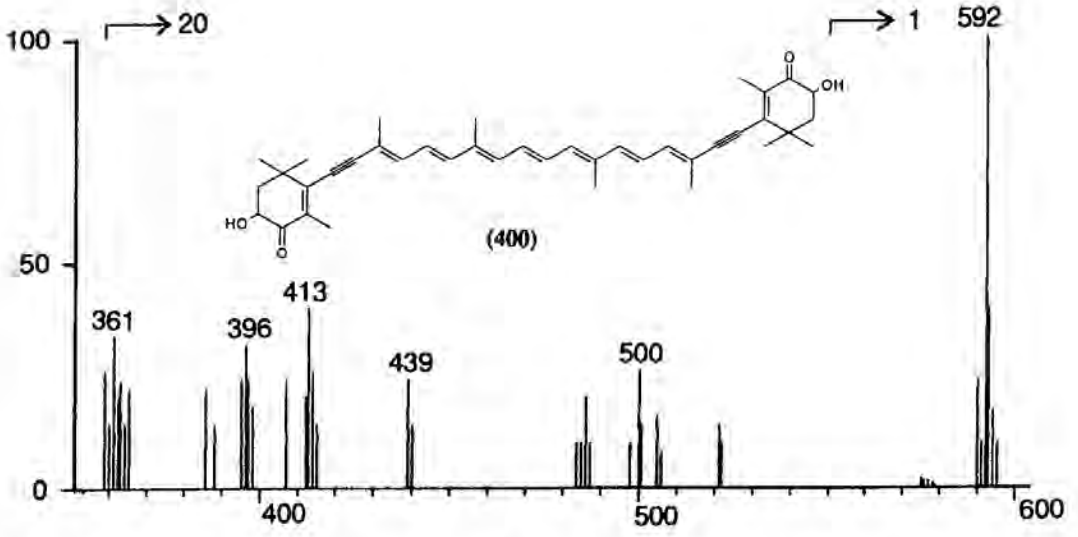


Fig. 9. Elimination of in-chain fragments from acetylenic carotenoids. EI spectra (70eV) of 15,15'-didehydrocanthaxanthin (*19*) and 7,8,7',8'-tetradehydroastaxanthin (**400**).

d) Acetylenic carotenoids

Substitution of an olefinic by an acetylenic bond in the acyclic polyolefinic chain prevents fission of the bond between the two sp-hybridized carbons. Thus, when a triple bond is present between C-15 and C-15', $[M-90]^{+\cdot}$ ions are encountered instead of $[M-92]^{+\cdot}$ species [1, 25]. Comparison of the *R*-value (2.6) for canthaxanthin (**380**) with the equivalent ratio (1.5) of the $[M-90]^{+\cdot}$ and $[M-106]^{+\cdot}$ peaks for 15,15'-didehydrocanthaxanthin (*19*) implies that elimination of methylbenzyne is a reasonably favoured reaction, particularly since, for steric reasons, extrusion of xylene might have a somewhat greater probability in the acetylenic compound *19* than in canthaxanthin (Fig. 9).

Elimination of xylene by excision of the fragment C-8 to C-13 is prevented in dicyclic carotenoids that possess an acetylenic bond in the 7,8-position. When there is either an additional acetylenic bond in the 7',8'-position or considerable steric congestion at C-6', as in heteroxanthin (**198**), no $[M-106]^{+\cdot}$ ion is observed [49]. It may be noted, however, that 7,8,7',8'-tetradehydroastaxanthin (**400**) does give rise to an $[M-106]^{+\cdot}$ peak (Fig. 9). It is unclear at present whether the presence of the peak is due to the elimination of an in-chain fragment by a non-conventional mechanism or to the loss of part of the terminal groups [50], although this question could readily be settled by high-resolution or deuterium-exchange studies.

e) Allenic carotenoids

All allenic carotenoids known to date are fairly heavily oxygenated, which makes the upper mass region of their spectra quite complex. Ions formed by in-chain elimination reactions are, therefore, less dominant and less easy to distinguish. The presence of an allenic moiety, so far always encountered in the C-6 to C-8 (C-6' to C-8')-position and exocyclic to a six-membered ring, inhibits the formation of $[M-106]^{+\cdot}$ ions by extrusion of the C-8 to C-13 (C-8' to C-13') unit [1, 32, 51]. The $[M-92]^{+\cdot}$ ions are observed, however.

F. Elimination Reactions of Terminal Groups

Mass spectral data for selected end groups, designated **e1** to **e170**, are summarized in Table 7. Acyclic and cyclic end groups are listed separately and in order of decreasing number of conjugated olefinic bonds. The fragmentation pathways that result from the presence of a particular end group in a carotenoid are not normally affected by the length of the conjugated chain or by the other end group. However, large differences in stability between two different end groups in a carotenoid can sometimes make it difficult to detect peaks that are associated with the more stable end group.

Table 7. Peaks of diagnostic value in the mass spectra of carotenoids.

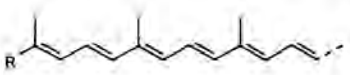
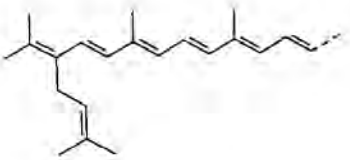
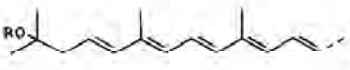
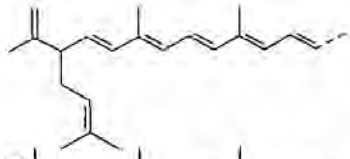
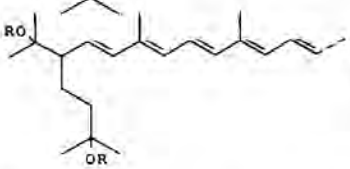
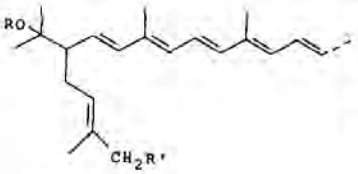
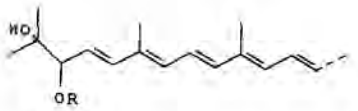
End group		Number	Characteristic peaks	Ref.
	R=CH_3	e1	M-69,M-82,M-122,M-135, M-148,M-175	45
	R=CH_2OH	e2	M-2,M-18,M-31	52
	R=$CH(OCH_3)_2$	e3	M-31	53
	R=CHO	e4	M-15	53
		e5	M-69,69	54
	R=H	e6	M-18,M-58	45
	R=CH_3	e7	M-32,M-73,73	45
	R=TMS	e8	M-131,131	55
		e9	M-69,69	54,56
	R=H	e10	M-18,M-58	57
	R=TMS	e11	M-90,M-131,131	57
	R=H,R'=H	e12	M-18,M-58,M-69,69	58
	R=TMS,R'=H	e13	M-72,M-90,M-131,131	58
	R=H,R'=OH	e14	M-18,M-58,M-87	58
	R=H,R'=OAc	e15	M-18,M-42,M-58,M-60	58
	R=TMS,R'=OAc	e16	M-42,M-60,M-72,M-90, M-131,131	58
	R=H	e17	M-16,M-18,M-58,M-59,M-60, M-88,M-90	45
	R=Ac	e18	M-60,M-76,M-156	59
	R=Rham (tetraacetate)	e19	M-58	60

Table 7. contd

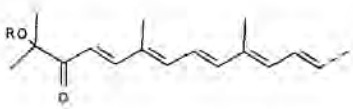
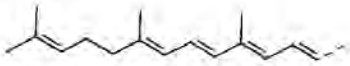
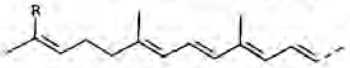
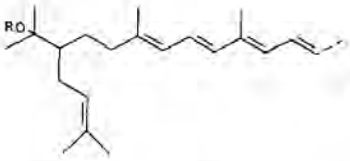
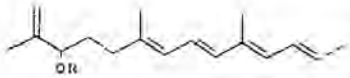
End group		Number	Characteristic peaks	Ref.
	R=H	e20	M-16,M-18,M-59,M-87,M-88	45
	$R=CH_3$	e21	M-30,M-32,M-60,M-73, M-101,73	45
	$R=COCH_3$	e22	M-43,M-187	45
	R=CHO	e23	M-18,M-28,M-29	45
	R=COOH	e24	M-44,M-99	45
	$R=COOCH_3$	e25	M-31,M-59,M-113	45
	R=COOEt	e26	M-45,M-73,M-127	61
		e27	M-69,69	45
	$R=CH_2OH$	e28	M-16,M-18,M-85,M-153	45
	R=CHO	e29	M-28,M-29,M-83,M-151	45
		e30	M-71	62
	R=H	e31	M-18	45
	$R=CH_3$	e32	M-30,M-32,M-73	45
		e33	M-85	38
	R=H	e34	69	63
	R=TMS	e35	131	63
	R=H	e36	M-29,M-42,M-43,M-57,M-71, M-85	64,65
	R=Ac	e37	M-42,M-43,M-60	64,65

Table 7. contd

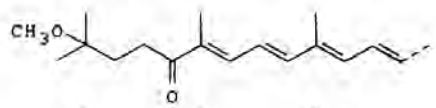
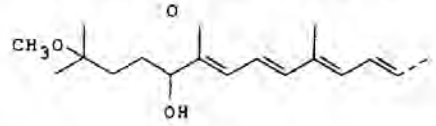
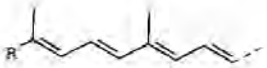
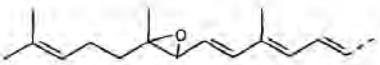
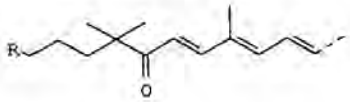
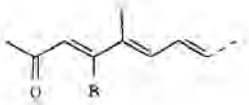
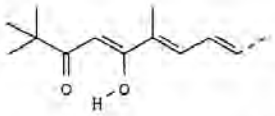
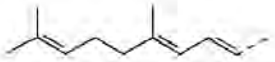
End group		Number	Characteristic peaks	Ref.
		e38	M-32,M-101,M-129,73	45
		e39	M-18,M-32,M-73	66
	R=CH_3	e40	M-81,81	40-42
	R=CH_2OH	e41	M-16,M-18	41
	R=CHO	e42	M-18,M-28,M-29	45
	R=COOH	e43	M-44,M-99	45
	R=$COOCH_3$	e44	M-31,M-59,M-113	45
	R=COOEt	e45	M-45,M-73,M-127	61
		e46	M-69	38
	R=CH_3CO	e47	M-43,M-155,127,109,43	38,67
	R=$CH(OH)CH_3$	e48	M-18,M-157	18
	R=H	e49	M-16,M-18,M-43,M-187,M-43	67
	R=OH	e50	M-15,M-43,M-85,85	68
		e51	M-15,M-57,M-85, M-127,127,85,57	68
		e52	M-69,M-137,69	45
		e53	M-153	38
		e54	M-69,M-83,83,69	40
		e55	73	69

Table 7. contd

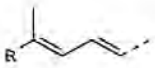
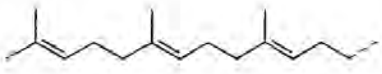
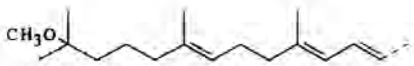
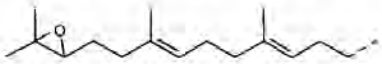
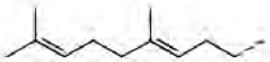
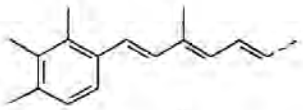
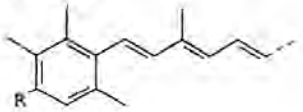
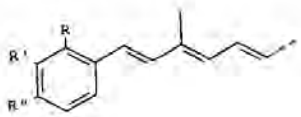
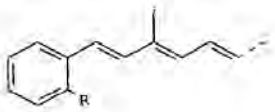
End group		Number	Characteristic peaks	Ref.
	R=CH_2OAc	e56	M-44,M-58,M-60	70
	R=CHO	e57	M-40,M-66	66
		e58	M-69,M-137,M-205,69	45
		e59	73	69
		e60	M-85,M-153,M-221	71
		e61	M-69,M-137,69	40,72
		e62	M-43,109,43	73
		e63	M-133,133	45
	R=H	e64	M-133,133	45
	R=OH	e65	149	74
	R+R'+R"= $2CH_3+CO_2CH_3$	e66	177	66
	R+R'+R"= $2CH_3+CH_2OH$	e67	149	66
	R=H	e68	M-91,M-131,M-144, M-157,131,91	75
	$R=CH_3$	e69	M-105,M-145,M-171,145,105	75

Table 7. contd

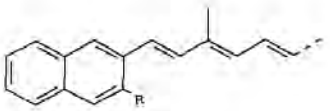
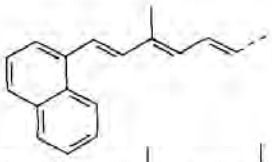
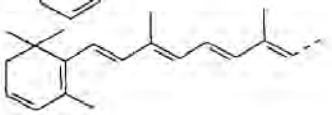
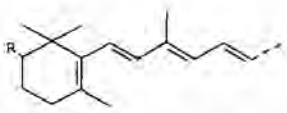
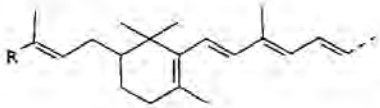
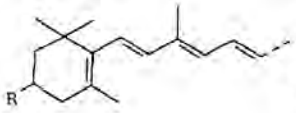
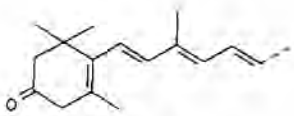
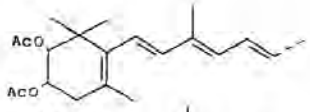
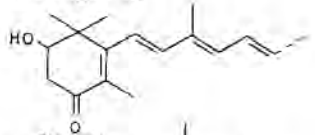
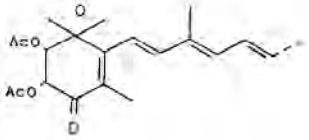
End group		Number	Characteristic peaks	Ref.
	R=H	e70	M-141,M-181,M-194, M-207,141	75
	R=CH_3	e71	M-155,155	75
		e72	M-141,M-194,M-207,141	75
		e73	M-15,M-121	76
	R=H	e74	M-137	33
	R=CH_3	e75	M-149	77
	R=OH	e76	M-18,M-153	43,78
	R=CH_2OH	e77	M-18,M-58	79,80
	R=OH	e78	M-18,M-153,M-193	45
	R=OAc	e79	M-60,M-195,M-235	45
	R=CH_3COS	e80	M-75,M-76,M-151	81
		e81	M-138,M-151,M-191,M-204	45
		e82	M-60,M-120,M-152,M-212	82
		e83	M-18,M-166	83
		e84	M-60,M-102,M-254,254,203	82

Table 7. contd

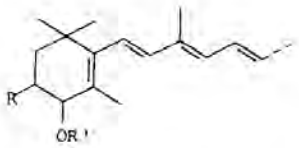
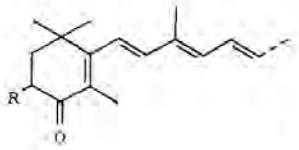
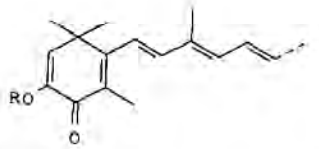
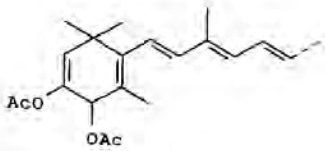
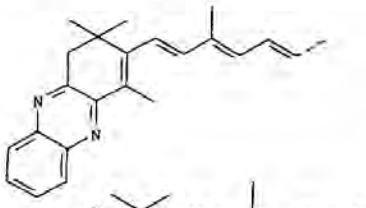
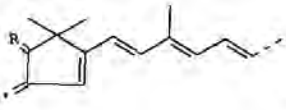
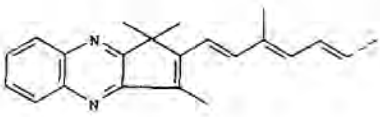
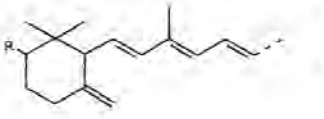
End group		Number	Characteristic peaks	Ref.
	R=H,R'=H	e85	M-18	1
	R=H, R'=t-Bu$(CH_3)_2$Si	e86	119	53
	R=OH,R'=H	e87	M-2,M-18	84
	R=H	e88	M-28,M-138,M-151,M-191	45
	R=OH	e89	M-16,M-154,M-M-167, M-203,152,137	45,85
	R=OAc	e90	M-44,M-58,M-60,245	85,86
	R=H	e91	M-152,203,152,137	85
	R=Ac	e92	M-42,M-58,M-194,245,203	85,86
		e93	M-60,M-120	59
		e94	M-237,M-303,M-315,M-343, M-355	86
	R=H,R'=OH	e95	M-18,M-34	1
	R=O,R'=O	e96	M-28,M-58,M-60	1
		e97	M-210,M-223,M-263,M-275, M-289,M-329	86
	R=H	e98	M-123,M-177,M-190,M-203	87,88
	R=CH_3	e99	M-137,M-204,M-217	89

Table 7. contd

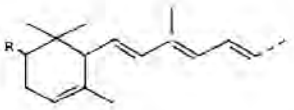
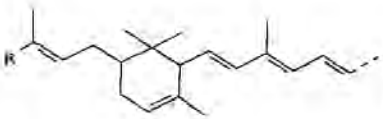
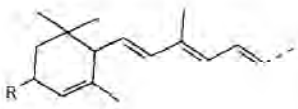
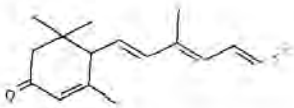
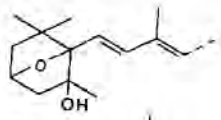
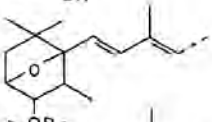
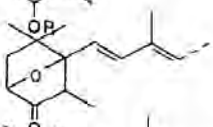
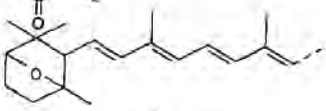
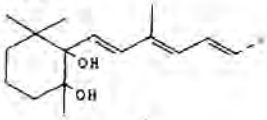
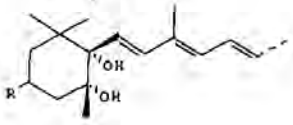
End group		Number	Characteristic peaks	Ref.
	R=H	e100	M-56,M-123	90
	R=CH_3	e101	M-70,M-137	1
	R=CH_3	e102	M-124	1
	R=CH_2OH	e103	M-16,M-140	1,91
	R=CH_2OAc	e104	M-42,M-182	91,92
	R=OH	e105	M-18,M-56,M-138,M-153	45
	R=CH_3COO	e106	M-158,M-60,M-180,M-195	45
	R=CH_3O	e107	M-32,M-56,M-152,M-167	45
	R=SH	e108	M-34	81
		e109	M-56,M-138,M-151,M-204	45
		e110	M-18	92,93
	R=H	e111	M-15	94
	R=Ac	e112	M-15,M-59,M-75	94
		e113	M-15,M-56,M-71	94,95
		e114	incomplete info.	96
		e115	M-18,M-98,M-127,M-155,109	75
	R=OH	e116	M-18,M-36,M-98,221,181	97
	R=OAc	e117	M-18,M-78,M-98,263,223	97

Table 7. contd

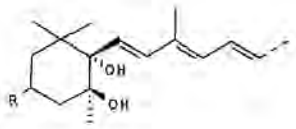
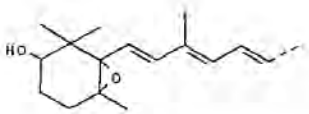
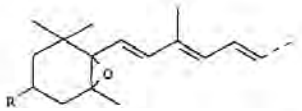
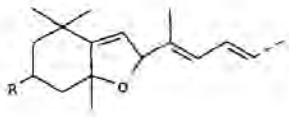
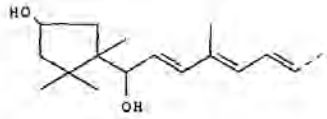
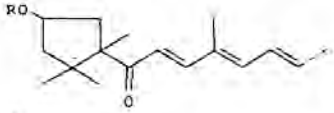
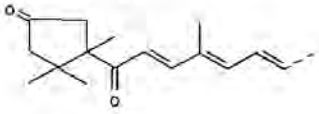
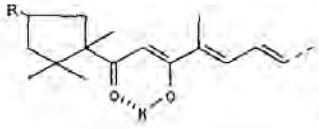
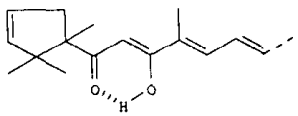
End group		Number	Characteristic peaks	Ref.
	R=OH	e118	M-18,M-98,M-143,M-186, M-199,M-226,221	49,97
	R=OAc	e119	M-60,M-80,M-241,263,223	97
		e120	M-16,M-80,221,181	98
	R=H	e121	M-80,M-146,M-172,205,165	32,99
	R=OH	e122	M-18,M-80,M-146,M-172 ,221,181	99
	R=OAc	e123	M-60,M-80,M-146,M-172,263	99
	R=H	e124	M-80,M-146,M-172,205,165	99
	R=OH	e125	M-60,M-80,M-146,M-172, 221,181	99
		e126	M-18,M-127	32
	R=H	e127	M-16,M-18,M-155,127,109	67
	R=CH_3CO	e128	M-60,M-197,109	67
		e129	125,83	85
	R=H_2	e130	M-111,M-139,181,111	68,100
	R=H,OH	e131	M-127,M-155,M-197,197	55,101
	R=H,OAc	e132	M-42,M-60,M-169,M-197,239	102
	R=H,$(CH_3)_3SiO$	e133	M-72	68
	R=O	e134	M-125,M-195,195,125	103
		e135	M-109	68,100

Table 7. contd

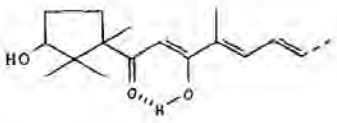
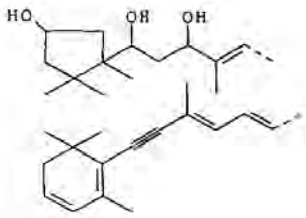
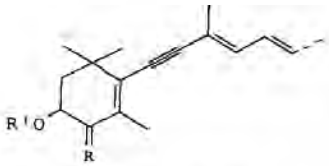
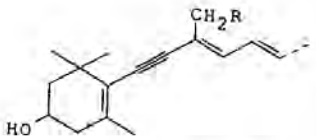
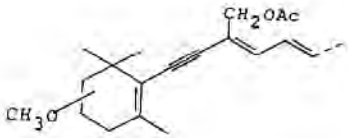
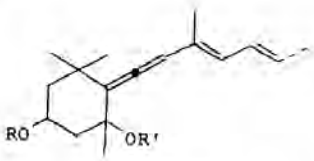
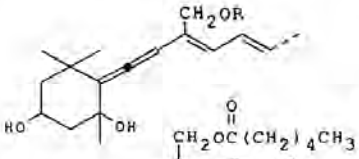
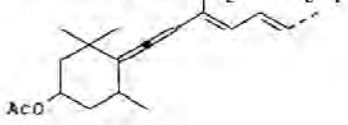
End group		Number	Characteristic peaks	Ref.
		e136	M-18,127	68,100
		e137	incomplete info.	103
		e138	M-2,M-15	94
	R=H$_2$,R'=H	e139	M-2,M-18,M-58,M-139	1,84
	R=H$_2$,R'=Ac	e140	M-2,M-15,M-60,M-75	100,104
	R=O,R'=H	e141	M-17,M-87,M-153,M-205, M-231	50
	R=OH	e142	incomplete info.	84
	R= $OCO(CH_2)_4CH_3$	e143	M-18,281	84
		e144	M-15,M-32	102
	R=H,R'=H	e145	M-18	32
	R=Ac,R'=H	e146	M-18,M-60	32
	R=Ac, R'=$(CH_3)_3Si$	e147	M-2,M-60,M-75,M-90,M-150,263,223	105
	R=H	e148	M-18,M-36,M-225, 254,227,213,189	106
	R= $CO(CH_2)_4CH_3$	e149	M-18,M-132,M-150,M-152	107
		e150	M-18	84

Table 7. contd

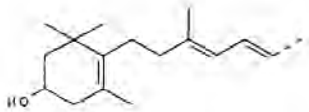
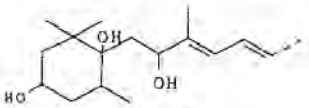
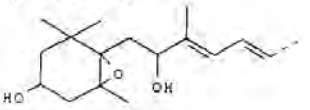
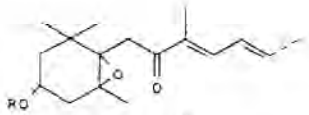
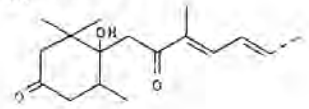
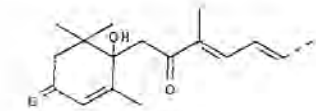
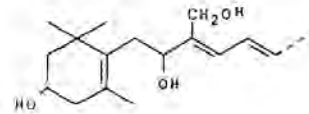
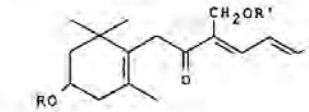
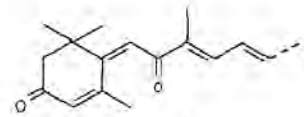
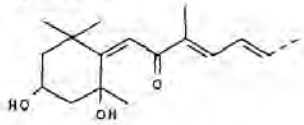
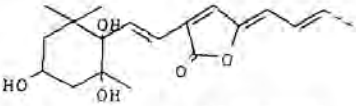
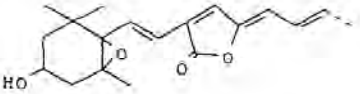
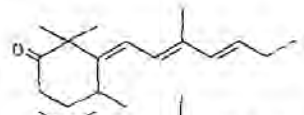
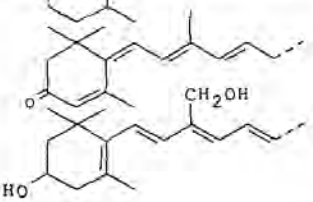
End group		Number	Characteristic peaks	Ref.
		e151	M-18,M-153	108
		e152	M-18,M-36	104
		e153	M-18,M-170	32,109
	R=H	e154	M-18,368	32,109
	R=Ac	e155	M-60	109
		e156	M-154,M-169,M-197, 197,164,155	101
		e157	M-18	84
		e158	M-18,M-36,M-46,M-48,M-54, M-64,M-157,M-171,M-171, M-182	110,111
	R=H,R'=H	e159	M-18,M-36,M-44,M-62, M-153,M-171,M-181,M-199	110,111
	R=H,R'=CH_3	e160	M-18,M-32,M-153,M-185, M-213	110,111
	R=H, R'=$CH_3(CH_2)_8$-CH=CHCO	e161	M-18,M-180,M-198,M-216	94
	R=H, R'=$C_{11}H_{23}CO$	e162	M-18,M-180,M-198	112
	R=Ac,R'=Ac	e163	M-60,M-120,M-195,M-241, M-255,M-223,MM-283	110,111

Table 7. contd

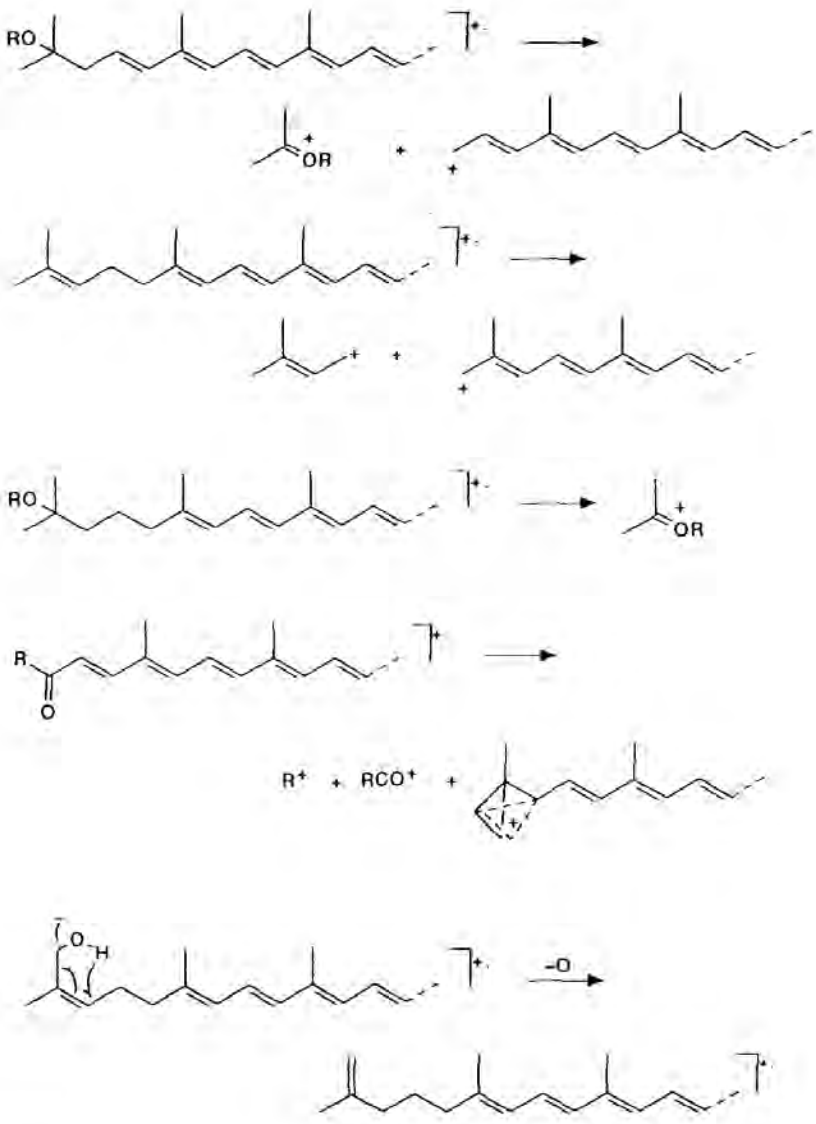
End group	Number	Characteristic peaks	Ref.
	e164	M-58	84
	e165	M-18,368	32
	e166	M-18	84
	e167	M-18	84
	e168	M-18,M-165,M-205	43
	e169	M-56,M-137,M-150,M-163, M-190,M-203,M-216	45
	e170	M-2,M-20	94

1. Acyclic end groups

Most acyclic end groups fragment predominantly by rupture of appropriately activated bonds and by elimination of functional groups, with hydrogen transfer to or from the larger fragment, as exemplified in Scheme 9 [1, 45].

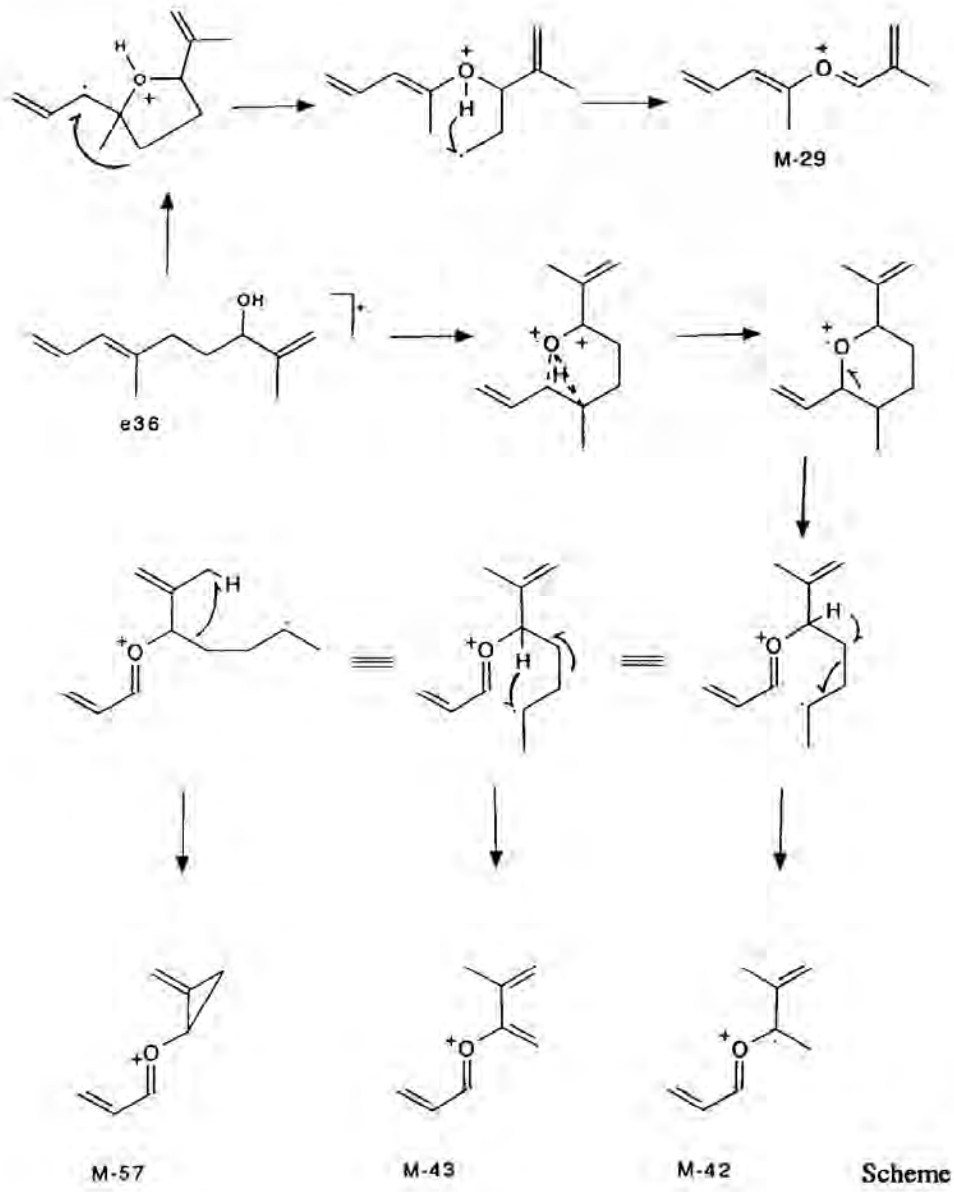
Rupture of in-chain bonds, with or without hydrogen transfer, is also encountered, not only for highly stable end groups such as **e1**, but occasionally also for end groups that can undergo reactions that are more favoured energetically. Thus, end groups **e28** and **e29** suffer scission of bonds other than the doubly allylic ones.

Several of the end groups, namely **e10** to **e16**, **e34** and **e35**, differ from their simpler relatives only by the presence of an extra prenyl unit at C-2. This substituent does not alter the fragmentation materially, although cleavages within the additional prenyl moiety contribute alternative fragmentation modes [57, 58].



Scheme 9

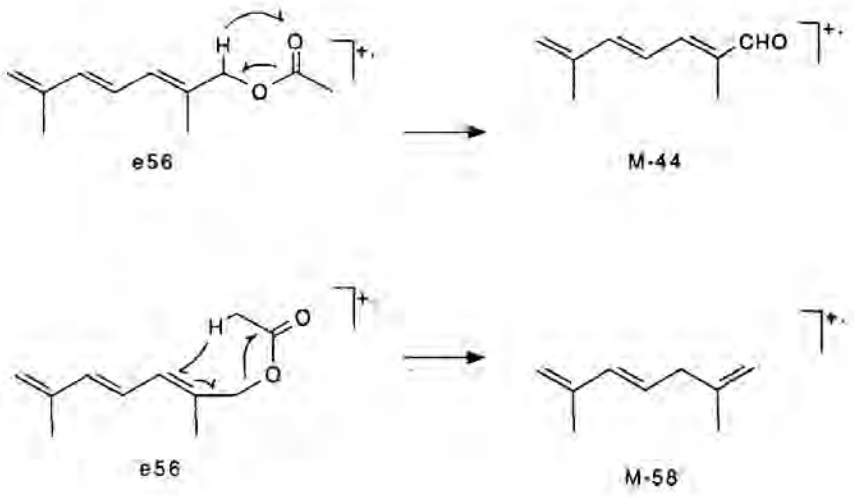
In addition to the $[M-71]^+$ and $[M-85]^+$ ions, which are generated by simple allylic cleavage, end group **e36**, first encountered in aleuriaxanthin (**81**), furnishes several ions whose formation requires rearrangement reactions, *i.e.* $[M-29]^+$, $[M-42]^{+\cdot}$, $[M-43]^+$, and $[M-57]^+$ [64, 65]. In contrast to some of the fragmentation pathways proposed originally [64], the reactions shown in Scheme 10 do not involve an allylic rearrangement leading to end group **e28** as an intermediate, since this end group is known not to give rise to $[M-29]^+$, $[M-42]^{+\cdot}$, $[M-43]^+$, and $[M-57]^+$ ions.



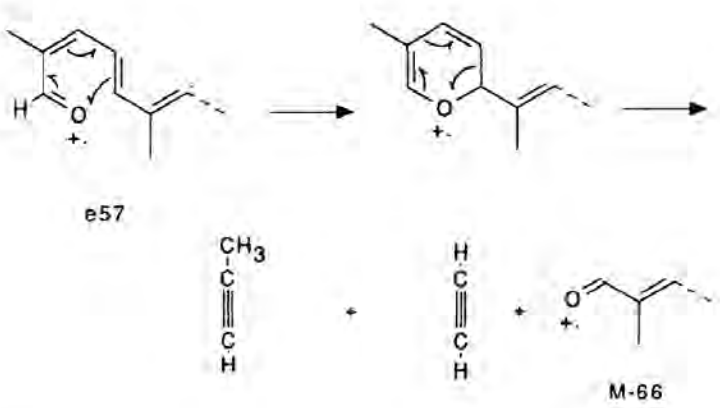
Scheme 10

Compounds that contain end group **e56** eliminate C_2H_4O and $C_2H_2O_2$, in addition to acetic acid. Although probably largely thermal, these reactions may be depicted as shown in Scheme 11 [78]. End group **e57**, which contains an aldehyde group instead of an acetoxy group, gives rise to $[M-40]^{+\cdot}$ and $[M-66]^{+\cdot}$ peaks, the latter of which has been assigned to a species generated as depicted in Scheme 12 [66].

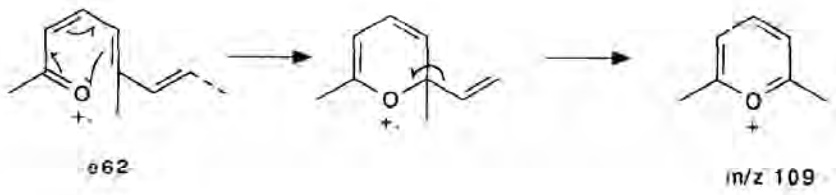
End group **e62** has also been proposed to cyclize when ionized. In this case, however, the cyclic intermediate suffers α-cleavage to yield a low-mass ion as illustrated in Scheme 13 [73].



Scheme 11



Scheme 12



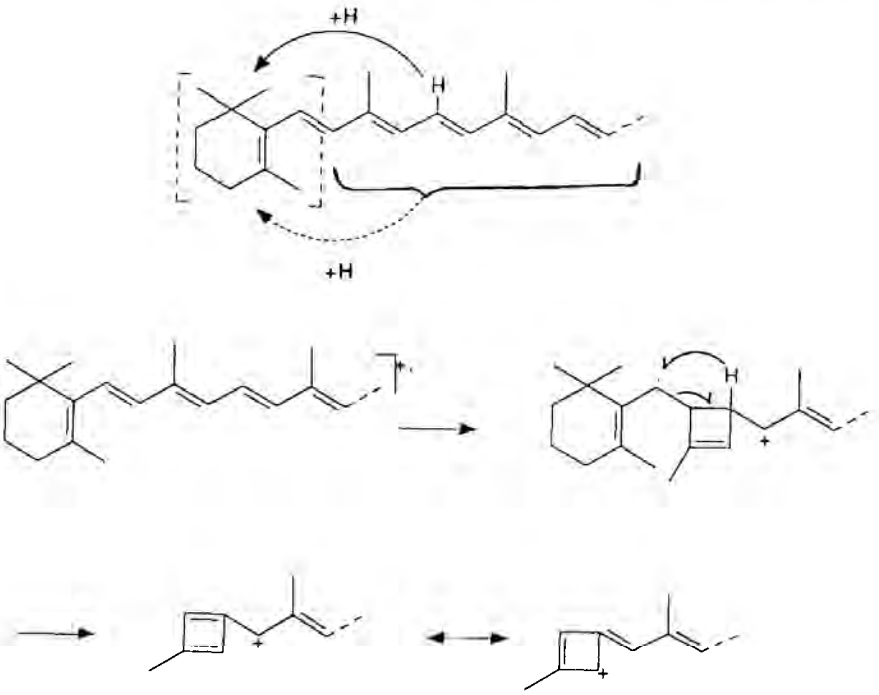
Scheme 13

2. Cyclic end groups

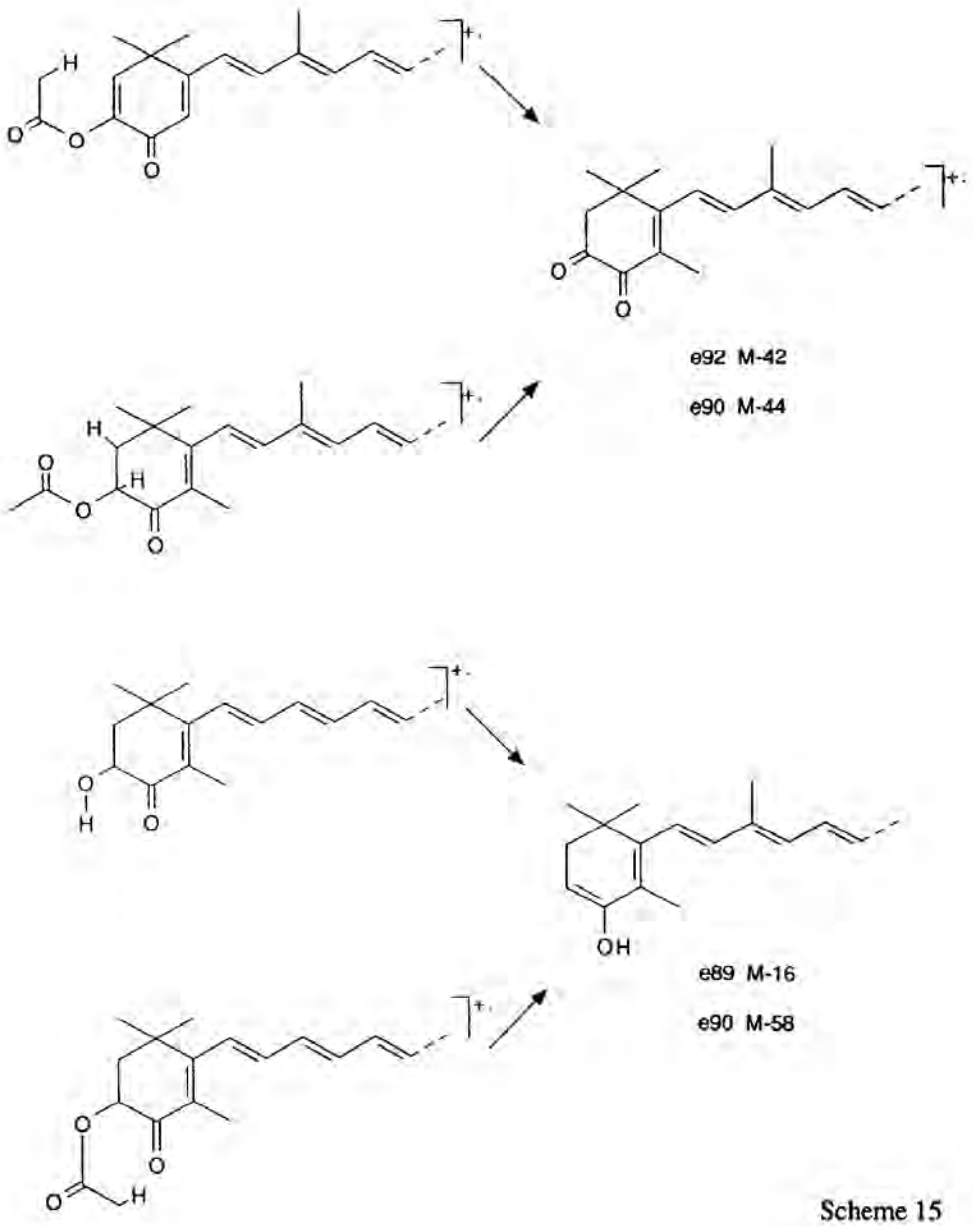
Most cyclic end groups are remarkably stable and the carotenoids that contain them decompose predominantly by cleavage of in-chain bonds, notably by rupture of the 7, 8, 9, 10, and 11 bonds, with transfer of a hydrogen atom to the smaller fragment. Labelling studies [26] have shown that the mechanism proposed initially for these reactions [45] requires modification, since hydrogen transfer does not occur specifically from C-14 but from several sites, especially from C-11 (40%). The reactions leading to the cleavage of the 7,8-bond may therefore be summarized as shown in Scheme 14, which also includes a plausible mechanism for the reaction that represents the main pathway.

The set of end groups that contain an aromatic nucleus, **e63** to **e72**, now includes naphthalenic as well as oxygenated entities, but only ions due to in-chain cleavages have been found to be of significance [6].

Most of the end groups that have a 5,6-double bond, **e74** to **e97**, give rise to characteristic ions at high mass, predominantly by in-chain cleavages or elimination reactions that are related to the presence of an oxygen function. Thus, when such an end group contains only one hydroxy or one acetoxy function, $[M-18]^{+\cdot}$ and $[M-60]^{+\cdot}$ ions are observed, whilst when two or more oxygen functions are present, formation of $[M-16]^{+\cdot}$, $[M-42]^{+\cdot}$, $[M-44]^{+\cdot}$, and $[M-58]^{+\cdot}$ species becomes feasible and may occur by processes such as those outlined in Scheme 15 [45, 85, 86].

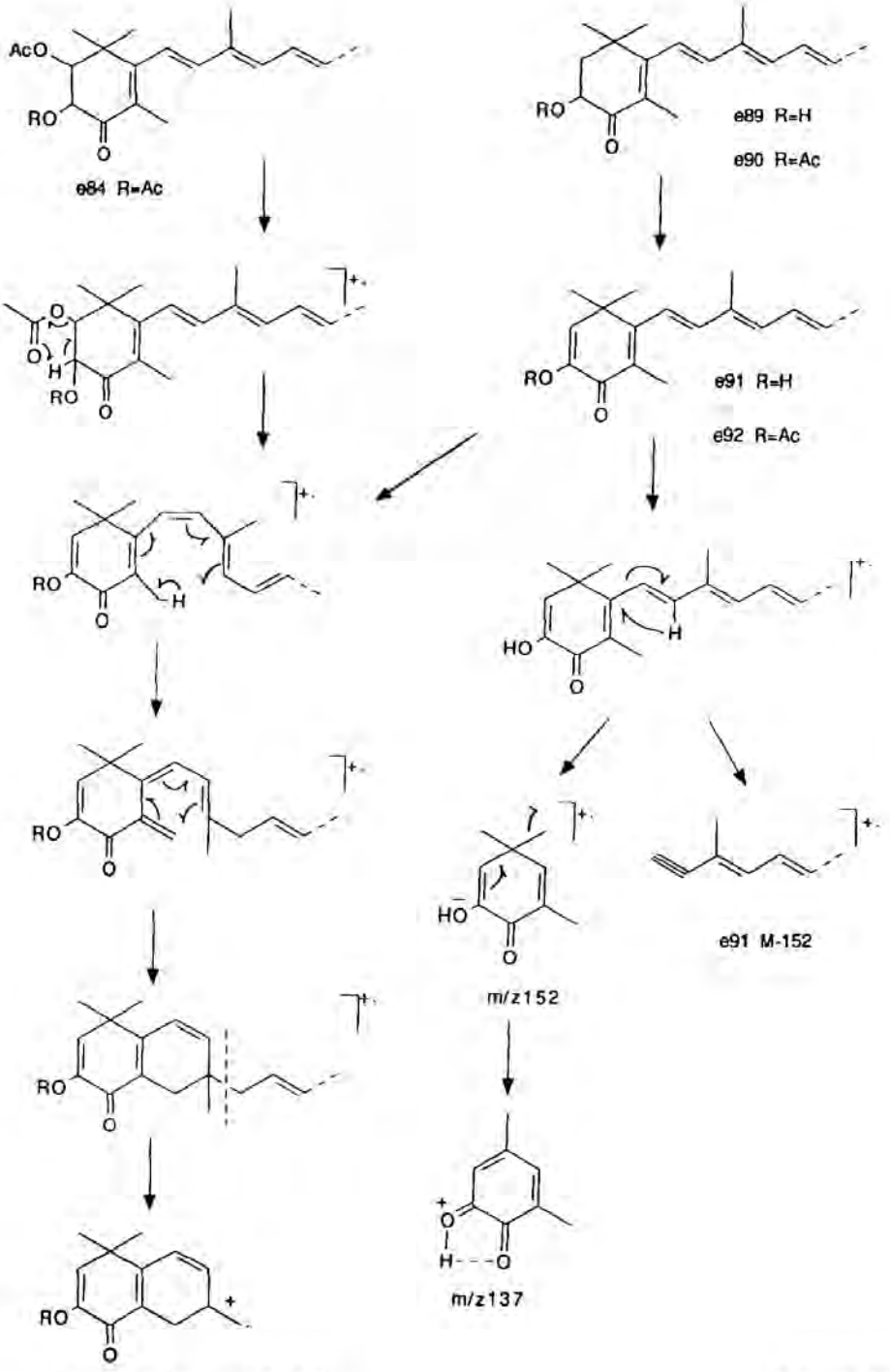


Scheme 14



Scheme 15

Reverse or *retro*-Diels-Alder (RDA) ring opening of the β-type end groups, **e74** to **e94**, would not normally increase conjugation substantially and is accordingly not observed. However, high-resolution studies have shown that loss of C-2 and C-3 does occur by such a reaction in the case of end group **e88** [32]. This implies that the $[M-56]^{+\cdot}$ ion encountered in the spectrum of canthaxanthin (**380**) is due to two such losses of 28 mass units consecutively, rather than to the fragmentation of one of the end groups, as invoked previously [45].

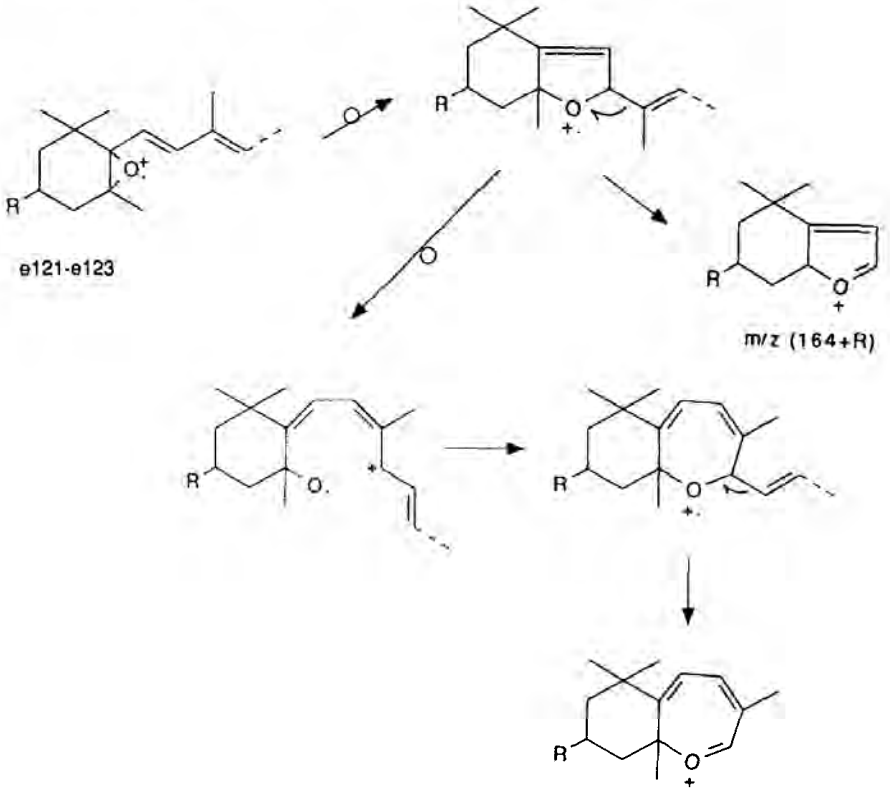

AcO
RO
O
e84 R=Ac
e89 R=H
e90 R=Ac
e91 R=H
e92 R=Ac
HO
H
e91 M-152
m/z152
m/z137
m/z203 R=H m/z245 R=Ac

Scheme 16

In addition to significant high-mass ions, end groups **e84** and **e89** to **e92** furnish some highly stable low-mass ions, whose formation has been proposed to occur by the routes shown in Scheme 16 [85].

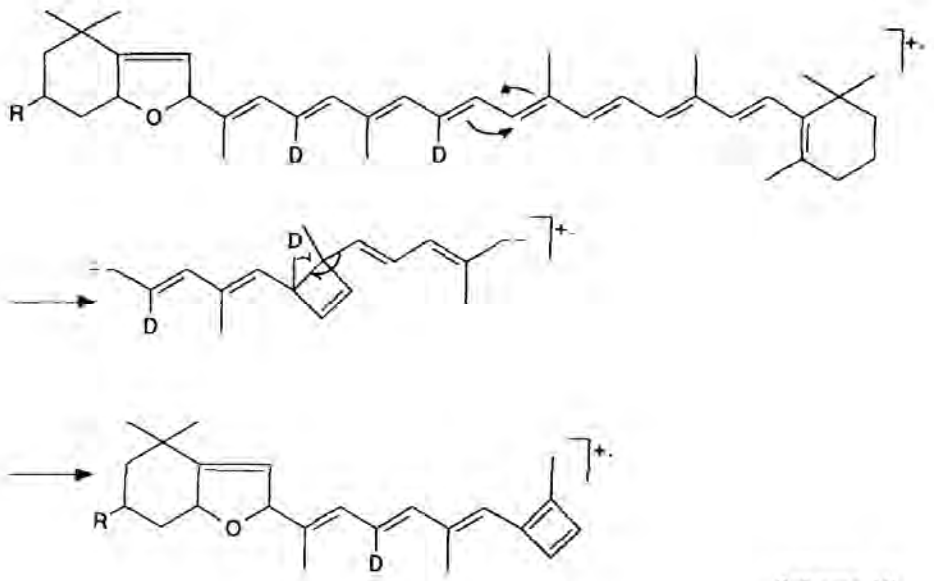
End groups **e98** and **e99**, which have an exocyclic double bond, give significant high-mass ions by rupture of the allylic 6,7-bond and of the 9,10-bond, 10,11-bond, and 11,12-bond [87-91]. This fragmentation is thus similar to that of the end groups that possess a 4,5-double bond, notably end groups **e104** to **e107**. The latter end groups also undergo RDA degradation readily, leading to extrusion of C-1 and C-2 with their substituents [45].

Of the end groups that are oxygenated at C-5 and C-6 and linked to a normal polyene chain (**e115** to **e123**), the 5,6-epoxides **e121** to **e123**, together with the corresponding 5,8-epoxides **e124** and **e125**, have been studied in great detail [26, 32]. In addition to $[M-80]^{+\cdot}$, $[M-106]^{+\cdot}$, $[M-146]^{+\cdot}$, and $[M-172]^{+\cdot}$ ions produced by the in-chain elimination reactions discussed above, these compounds give rise to many abundant fragments at lower masses, that contain the epoxide ring and part of the polyene chain. Mechanisms have been proposed [99] for the formation of the abundant $[164+R]^{+}$ and $[204+R]^{+}$ species. The former mechanism has been verified, whilst the latter was found to require some modification, because there is an exchange of the hydrogens on C-8 and C-15/C-15', which involves participation of the hydrogen at C-11 and presumably also that at C-12 [26], (Scheme 17).



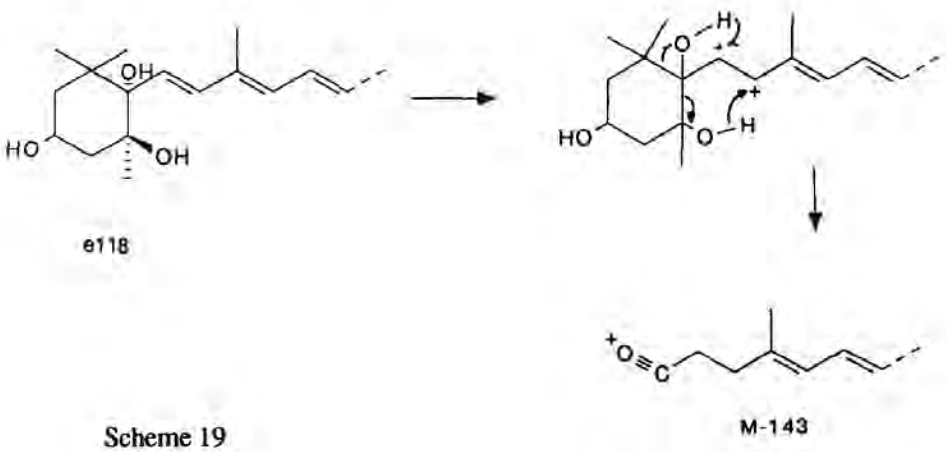
Scheme 17

In the generation of some of the ions of still higher masses, which retain the epoxide group, chain cleavage is accompanied by extrusion of a hydrogen radical. A mechanism for the formation of one of these ions, $[336+R-H]^{+\cdot}$, has been suggested [39] on the basis of extensive deuterium labelling, and is shown in Scheme 18.



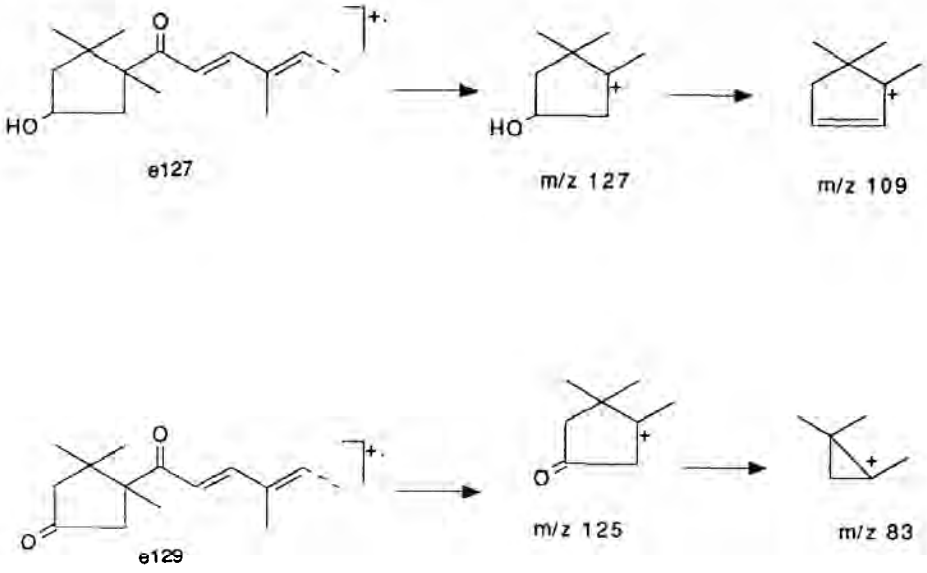
Scheme 18

Available data suggest that end group **e120**, which contains both 2-hydroxy and 5,6-epoxy functions, fragments in a similar fashion [98]. The 3,5,6-triols, **e116** and **e118**, and the corresponding 3-monoacetates, **e117** and **e119**, like the 5,6-epoxides and 5,8-epoxides, give high-mass ions by elimination of C_6H_8 from the polyolefinic part, and low-mass ions (*m/z* 164+R and *m/z* 204+R) by rupture of the 8,9-bond and 10,11-bond [97]. Differences in fragmentation between the epimeric triols, **e116** and **e118**, are also observed [49, 97], and may be related to the configurational differences. Thus, only the (5*S*)-epimer, **e118**, which has the 5-hydroxy group *cis* to the polyolefinic chain, gives rise to an $[M-143]^+$ ion. The formation of this ion may be accounted for by the mechanism shown in Scheme 19, which differs only with respect to concertedness from that previously invoked [45] for the formation of the $[M-127]^+$ species from compounds with end group **e115**. Moreover, both the (5*R*)-triol, **e116**, and its 3-monoacetate, **e117**, eliminate one molecule of water more than the corresponding (5*S*)-epimers, **e118** and **e119** [97]. This may be associated with the fact that the (5*R*)-compounds can lose water by an additional route that involves the hydrogen at C-3 and the 5-hydroxy group.



Scheme 19

In several of the carotenoids that have a cyclic end group, the ring is not linked directly to an olefinic carbon of the conjugated polyene chain; this may influence the fragmentation considerably. Thus the end groups which contain a cyclopentane entity, **e126 to e137**, nearly all give rise to characteristic ions that are formed by breaking of the bond which links the ring to the chain [55, 67, 85, 101]. The smaller fragments, when retaining the charge, suffer subsequent fragmentation to give daughter ions as depicted in Scheme 20 [67].

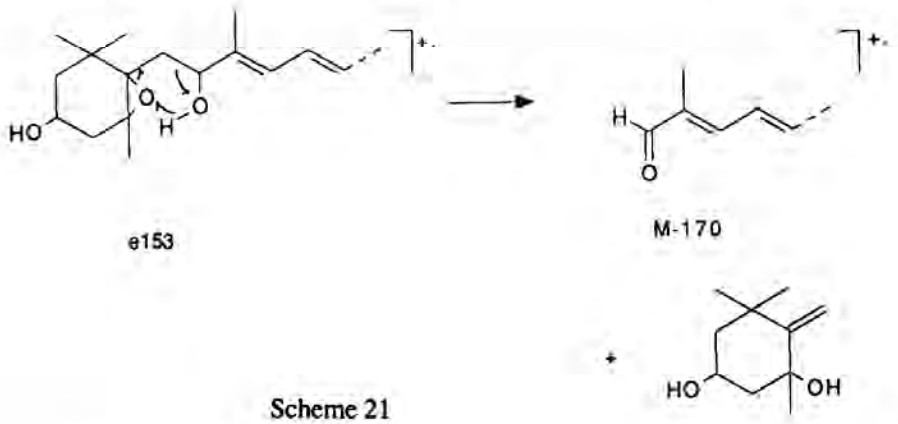


Scheme 20

Of the end groups that have a 7,8-acetylenic bond, **e141** gives abundant ions formed by cleavage of the 6,7-bond, 9,10-bond, and 11,12-bond and by elimination of C-1 to C-3 with substituents, whilst $[M-18]^{+\cdot}$ is the only significant peak reported for end group **e139** [1, 50].

It is noteworthy that compounds that have the allenic end groups **e145** and **e146** give rise to characteristic ions at high masses by cleavage at the 8,9-bond and by elimination of water and acetic acid [33, 109]. Of the corresponding 19-oxygenated end groups, **e148** furnishes several important ions at low mass, whilst significant ions associated with end group **e149** arise by elimination of water or of the ester group, accompanied by hydrogen transfer to or from the larger charged fragment.

A number of end groups, **e159 to e162**, have either two methylene groups or one methylene group and a hydroxymethylene or carbonyl group in place of the olefinic methine groups in positions 7 and 8. Most of these end groups give diagnostic high-mass ions by breakage of the 7,8-bond, a reaction which, in the case of end group **e153**, is accompanied by hydrogen transfer, and probably occurs by the mechanism shown in Scheme 21 [33, 109].

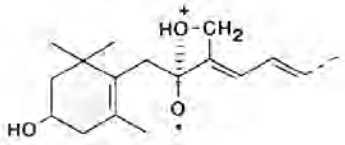


e153 M-170

Scheme 21

Several of the 8-oxo representatives also furnish high-mass ions by scission of the 8,9-bond. When both a 1-hydroxy group and an 8-oxo or 8-hydroxy group are present, further rather unusual fragmentation reactions are encountered. The former combination of oxygen functions, present in **e159**, leads to the loss of CO_2 from $[M]^{+\cdot}$, a reaction that was proposed [66] to occur *via* the intermediate shown in Scheme 22 and to involve union of C-1 and C-7 or of C-9 and C-7, accompanied by a transfer of oxygen prior to extrusion of CO_2. When there is a hydroxy group at C-8, as in end group **e158**, excision of CO and of CH_2O, together with water, occurs and $[M-CO-H_2O]^{+\cdot}$, $[M-CH_2O-H_2O]^{+\cdot}$, and $[M-CO-2H_2O]^{+\cdot}$ ions are observed [110].

Despite the structural differences, end group **e165** exhibits essentially the same fragmentation as **e154** [32]. Of the two end groups that have *retro* structures, **e168** and **e169**, the latter is more extensively conjugated and displays the larger number of significant high-mass ions due to both ring and chain cleavages.



Scheme 22

G. Carotenoid Conjugates

1. Fatty acid and retinoic acid esters

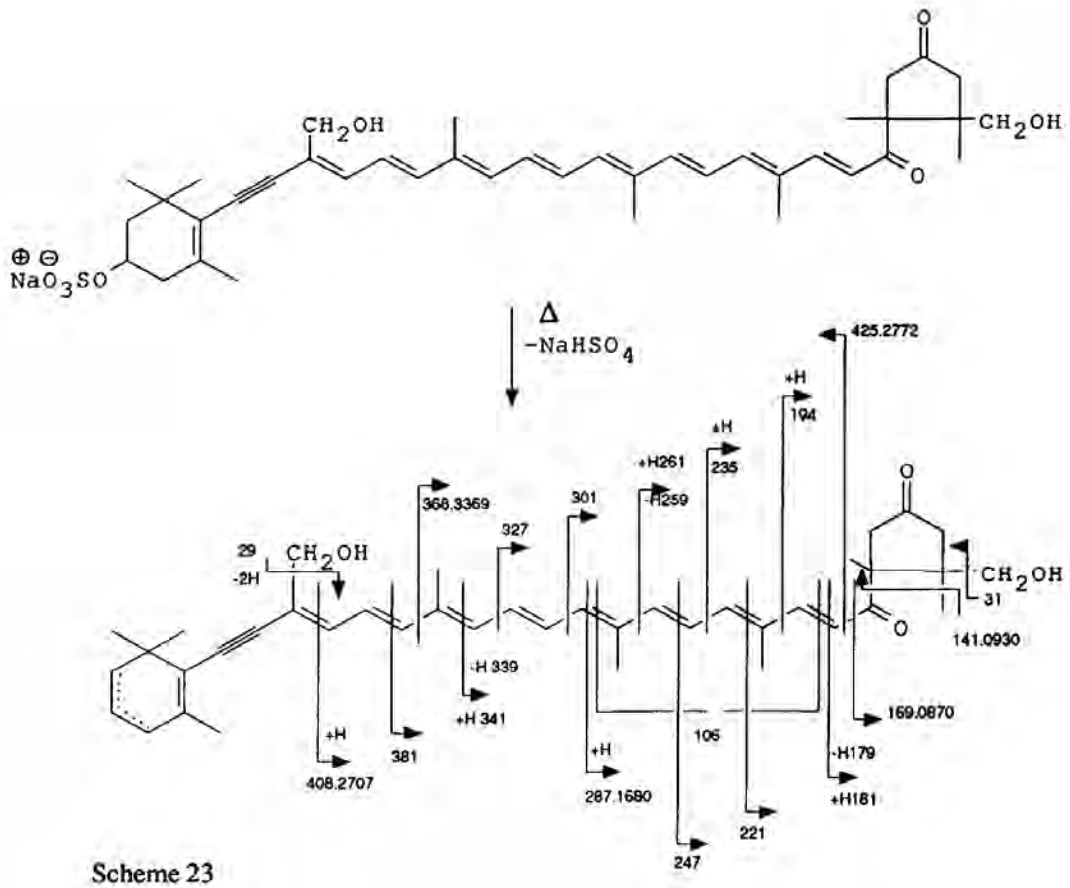
Fatty acid esters of xanthophylls (mainly lutein, **133**) from marigold flowers (*Tagetes erecta*) have been separated by HPLC, and then identified by their mass spectra, which are characterized by their simplicity. Only six significant types of ions appeared above *m/z* 200 in the spectra of the diol diesters that were encountered (dimyristate, myristate palmitate, dipalmitate, palmitate stearate, distearate). These are $[M]^{+\cdot}$, $[M-R_1COOH]^{+\cdot}$, $[M-R_2COOH]^{+\cdot}$, $[M-R_1COOH-R_2COOH]^{+\cdot}$, $[R_1COOH]^{+\cdot}$, and $[R_2COOH]^{+\cdot}$, and the dominating reaction is obviously, therefore, the McLafferty rearrangement in which both fragments formed are able to retain the charge [113].

Carotenoid retinoates show a similar fragmentation pattern in that $[M-300]^{+\cdot}$ and *m/z* $300^{+\cdot}$ (retinoic acid) ions are observed for monoretinoates and also $[M-600]^{+\cdot}$ ions for diretinoates. In addition, both groups of compounds display the common fragmentations of the polyene chain and the underivatized end group [114].

2. Sulphates

Lycoxanthin (**109**) sulphate and zeaxanthin (**119**) disulphate have been prepared and examined spectroscopically [115] to facilitate structure elucidation of more complex natural carotenoid sulphates, notably bastaxanthin c (**420**) [116]. The mass spectra of the sodium salts of the first two synthetic compounds were obtained with some difficulty, but they suggest that $NaHSO_4$ is eliminated thermally in the ion source and that the resulting carotenoid products fragment in a conventional manner under electron impact. In agreement with this, the mass spectrum of bastaxanthin c (**420**) not only shows the characteristic $[M-92]^{+\cdot}$ and $[M-106]^{+\cdot}$ ions, but can be interpreted as shown in Scheme 23 [116].

Mass spectrometry proved useful in the structure elucidation of the recently isolated acetylenic carotenoid sulphate, dehydroophioxanthin (**204.1**), since the FAB negative ion spectrum exhibited parent peaks at *m/z* 761, 783 (major) and 799 corresponding to the molecular ions $[M(SO_3H)SO_3]^-$, $[M(SO_3Na)SO_3]^-$ and $[M(SO_3K)SO_3]^-$, respectively. Intense peaks at *m/z* 681 and 663 were assigned to monosulphate ions. Moreover, dehydro-ophioxanthol, which was obtained on removal of the sulphate groups by mild acid hydrolysis, showed in the EI spectrum a molecular ion at *m/z* 602, compatible with the expected molecular formula $C_{40}H_{58}O_4$ [117].



Scheme 23

3. Glycosides

Carotenoid glycosides are usually examined after derivatization, when they often give mass spectra which afford considerable structural information. Peracetylated carotenoid glycosides normally provide intense molecular ions and a series of ions resulting from multiple losses of 60 mass unit fragments (acetic acid). Additionally, cleavage of bonds in the aglycone situated close to the sugar moiety often gives rise to peaks in the high-mass region of the spectrum. The low-mass region of the spectrum always shows a series of relatively intense peaks that allow identification of the type of sugar present, when results obtained in a study [118] of peracetyl pentoses and hexoses are applied.

Even high molecular mass representatives such as C_{50}-carotenyl diglycosides, after acetylation, not only display molecular peaks but also exhibit readily interpretable and highly informative fragmentation patterns [119]. The situation is illustrated more conveniently,

however, by results obtained for a simpler representative (**493**) [120]. In this case both the natural methyl ester and its tetraacetate (*20*) gave highly informative spectra, as shown in Fig. 10. The formation of the $[M-81]^+$ ion from the natural ester (**493**) and of the $[M-56]^{+\cdot}$ ion from the tetraacetate (*20*) have been explained as shown in Scheme 24, which also accounts for the major ions derived from the sugar moiety, and shows that *20* is a hexoside with four acetoxy groups [120].

Mass spectrometry has also been used in the structure elucidation of C_{30}-carotenoic acid glucosyl esters [121, 122].

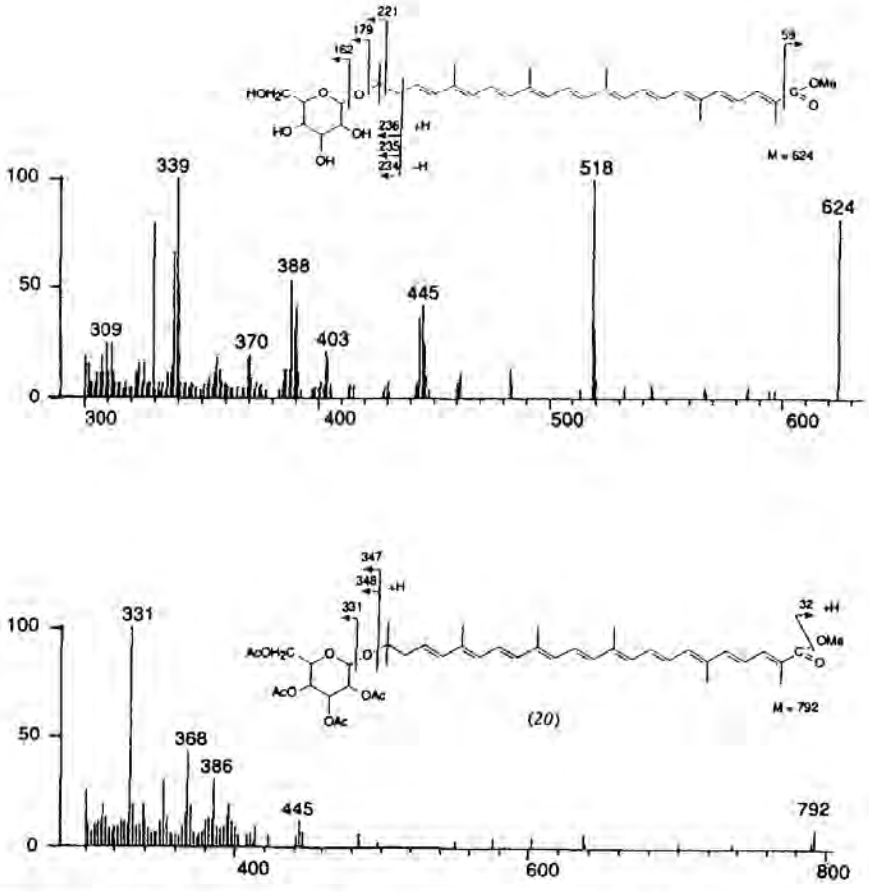
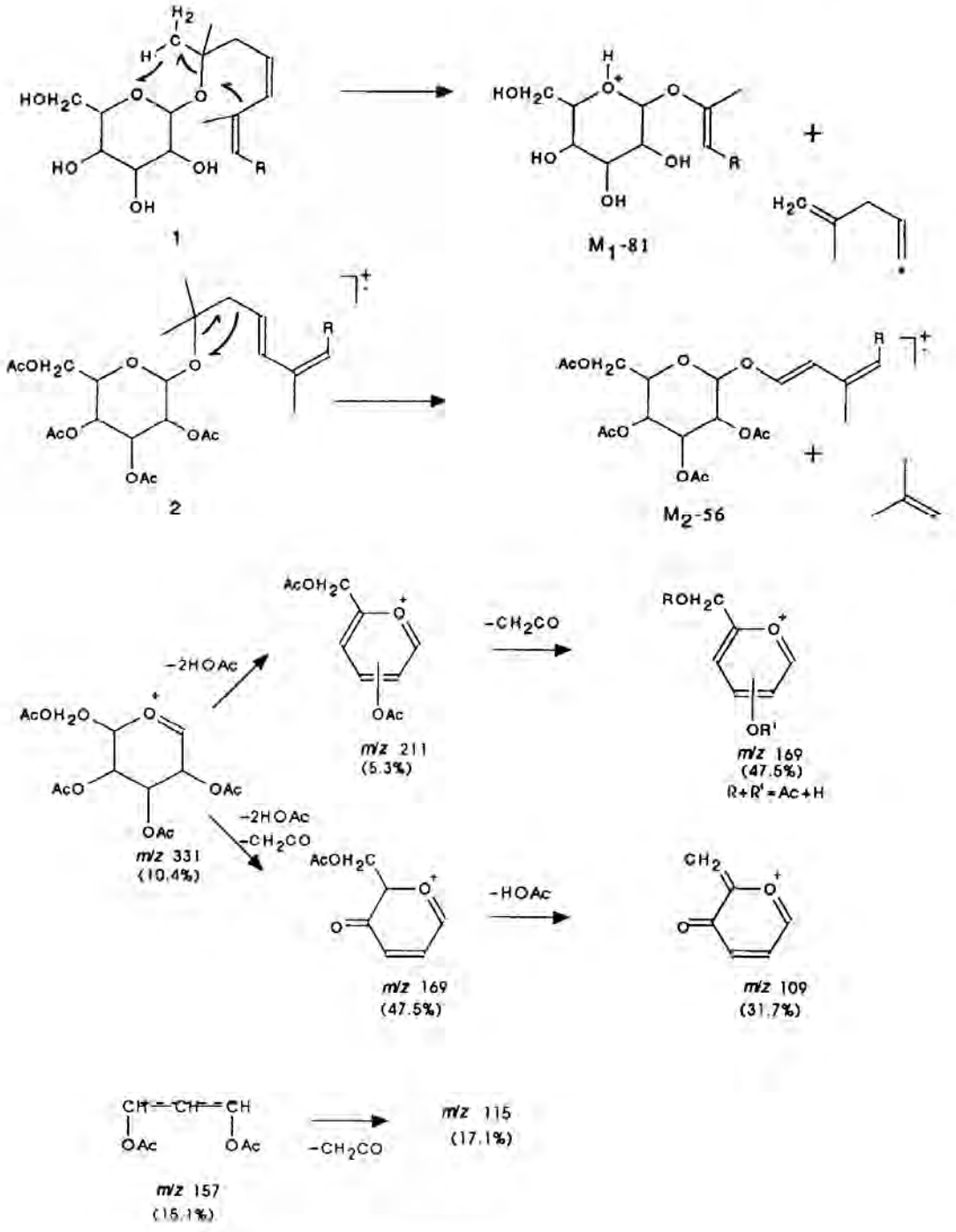


Fig. 10. Mass spectra of the natural ester methyl 1-mannosyloxy-3,4-didehydro-1,2-dihydro-8'-apo-ψ-caroten-8'-oate (**493**) and its tetraacetate (*20*) [120].


1
M1-81
2
M2-56
-2HOAc
-CH2CO
m/z 211
(5.3%)
m/z 331
(10.4%)
-CH2CO
m/z 169
(47.5%)
R+R'=Ac+H
-2HOAc
-CH2CO
m/z 169
(47.5%)
-HOAc
m/z 109
(31.7%)
m/z 157
(15.1%)
-CH2CO
m/z 115
(17.1%)

Scheme 24

H. Conclusions

It follows from the above discussion that the fragmentation of the central polyene chain and of the end groups of carotenoids can be treated as two essentially independent processes. The first of these processes, which leads to the losses of toluene, xylene and dimethylcyclodecapentaene, is experimentally well-founded and the mechanisms involved have a sound theoretical basis. The relative importance of steric *versus* electronic factors on the outcome of these reactions is still uncertain, however, and further insight into the factors that govern the abundance ratio for the ions derived from the molecular ion by loss of toluene and xylene is needed.

The number of end groups that have been studied by MS has increased dramatically over the past two decades and this has improved the chances of identifying an unknown compound with the aid of mass spectrometry. It is clear, however, that systematic studies of the relative MS stability and fragmentation characteristics of these end groups would improve the situation further. It would also be of considerable interest to create a software program for computer recognition/identification of carotenoids on the basis of the mass spectrometric data now at hand. This would increase the usefulness of mass spectrometry and narrow down considerably the number of possible structures for an unknown, thereby reducing the amounts of material and time required for the identification or structure elucidation.

Although electron impact is, and obviously will remain, the ionization method of choice, additional information can often be obtained through the use of several of the newer soft ionization techniques [123], some of which offer advantages such as reduced thermal interference, increased abundance of certain ions, especially molecular ions, and simplified recognition of the number of carotenoid components in complex mixtures.

Whilst metastable-ion scanning techniques have been used and have proved informative in the carotenoid field, no collisional activation spectra of carotenoids seem to have been reported, although this method offers advantages in that the fragmentation of virtually any pre-selected ion can be analysed, and further structural information thus obtained.

Although GC-MS is hardly useful in the analysis of carotenoids, several of the more recent combined liquid chromatography-mass spectrometry techniques [124] are exceptionally well suited for this purpose. Whether SFC-MS or LC-MS will become the more important technique will be related to a number of factors such as improvements of inlet systems, availability of suitable and stable stationary phases and developments in the areas of ionization and ion-handling techniques. In the analysis of complex mixtures of carotenoids, however, SFC-MS has a major advantage over LC-MS, because of the greater compatibility of SFC with mass spectrometry, and a key factor will probably be the accessibility of stable polar chromatographic phases.

References

[1] W. Vetter, G. Englert, N. Rigassi and U. Schwieter, in *Carotenoids* (ed. O. Isler), p. 189, Birkhäuser, Basel (1971).

[2] H. Budzikiewicz, *Adv. Mass Spectrom.*, **6**, 163 (1974).
[3] C. R. Enzell and I. Wahlberg, in *Biochemical Applications of Mass Spectrometry* (ed. G. Waller), Vol. 2, p. 407, Wiley, New York (1980).
[4] C. R. Enzell, I. Wahlberg and R. Ryhage, *Mass Spectrom. Rev.*, **3**, 395 (1984).
[5] C. R. Enzell, R. A. Appleton and I. Wahlberg, in *Biochemical Applications of Mass Spectrometry* (ed. G. Waller), p. 351, Wiley, New York (1972).
[6] G. W. Francis, Thesis, University of Stockholm (1973).
[7] S. Liaaen-Jensen, *Planta Med.*, **23**, 251 (1973).
[8] S. Liaaen-Jensen, *Pure Appl. Chem.*, **35**, 81 (1973).
[9] O. Caccamese and D. Garozzo, *Org. Mass. Spectrom.*, **25**, 137 (1990).
[10] W. Vetter and W. Meister, *Org. Mass. Spectrom.*, **20**, 266 (1985).
[11] G. Englert, K. Noack, E.A. Broger, E. Glinz, M. Vecchi and R. Zell, *Helv. Chim. Acta*, **74**, 969 (1991).
[12] J. Carnevale, E. R. Cole, D. Nelson and J. S. Shannon, *Biomed. Mass Spectrom.*, **5**, 641 (1978).
[13] F. Khachik and G. R. Beecher, *J. Agr. Food Chem.*, **36**, 929 (1988).
[14] F. Khachik, G. R Beecher and W. R. Lusby, *J. Agr. Food Chem.*, **36**, 938 (1988).
[15] C. Marty and C. Berset, *Analysis*, **14**, 32 (1986).
[16] M. U. D. Beug-Deeb, J. A. Bennett, M. E. Inman and E. A. Schweikert, *Anal. Chim. Acta*, **218**, 85 (1989).
[17] M. E. Rose, in *Carotenoid Chemistry and Biochemistry* (ed. G. Britton and T. W. Goodwin), p. 167, Pergamon, Oxford (1982).
[18] F. Cardini, G. Britton and A. Selva, *Phytochem.*, **28**, 2793 (1989).
[19] F. Cardini, M. Ginanneschi, A. Selva and M. Chelli, *Phytochem.*, **26**, 2029 (1987).
[20] R. F. Taylor and M. Ikawa, *Meth. Enzymol.*, **67**, 233 (1980).
[21] P. C. Winkler, D. D. Perkins, W. K. Williams and R. F. Browner, *Anal. Chem.*, **60**, 489 (1988).
[22] N. M. Frew, C. G. Johnson and R. H. Bromund, *ACS Symp. Ser.*, **366**, 208 (1988).
[23] R. H. Chapman, *Rapid Commun. Mass Spectrom.*, **2**, 67 (1988).
[24] E. J. Guthrie and H. E. Schwartz, *J. Chromatogr. Sci.*, **24**, 236 (1986).
[25] J. E. Johansen, Å. Eidem and S. Liaaen-Jensen, *Acta Chem. Scand.*, **B28**, 385, (1974).
[26] B. Johannes, H. Brzezinka and H. Budzikiewicz, *Org. Mass Spectrom.*, **9**, 1095 (1974).
[27] U. Schwieter, G. Englert, N. Rigassi and W. Vetter, *Pure Appl. Chem.*, **20**, 365 (1969).
[28] G. W. Francis, *Acta Chem. Scand.*, **26**, 1443 (1972).
[29] P. N. Onyewu, C.-T. Ho and H. Daun, *J. Amer. Oil Chem. Soc.*, **63**, 1437 (1986).
[30] G. W. Francis, R. R. Upadhyay, S. Liaaen-Jensen and P. Karrer, *Acta Chem. Scand.*, **24**, 3053 (1970).
[31] C. Enzell, G. Francis and S. Liaaen-Jensen, *Acta Chem. Scand.*, **22**, 1054 (1968).
[32] H. Budzikiewicz, H. Brzezinka and B. Johannes, *Monatsh. Chem.*, **101**, 579 (1970).
[33] C. Enzell and S. Liaaen-Jensen, *Acta Chem. Scand.*, **25**, 271 (1971).
[34] G. W. Francis, S. Norgård and S. Liaaen-Jensen, *Acta Chem. Scand.*, **B28**, 244 (1974).
[35] K. Schmidt, G. W. Francis and S. Liaaen-Jensen, *Acta Chem. Scand.*, **25**, 2476 (1971).
[36] G. W. Francis and S. Liaaen-Jensen, *Acta Chem. Scand.*, **24**, 2705 (1970).
[37] G. Britton, H. C. Malhotra, R. K. Singh and A. Ben-Aziz, *Phytochem.*, **12**, 1971 (1976).
[38] A. Ben-Aziz, G. Britton and T. W. Goodwin, *Phytochem.*, **12**, 2759 (1973).
[39] Å. Eidem, R. Buchecker, H. Kjøsen and S. Liaaen-Jensen, *Acta Chem. Scand.*, **B29**, 1015 (1975).
[40] R. Taylor and B. H. Davies, *Biochem. J.*, **139**, 751 (1974).
[41] R. Taylor and B. H. Davies, *Biochem. J.*, **139**, 761 (1974).
[42] R. Taylor and B. H. Davies, *Biochem. J.*, **153**, 233 (1976).
[43] H. Kayser, *Z. Naturforsch.*, **31c**, 646 (1976).
[44] H. Kayser, *Z. Naturforsch.*, **31c**, 121 (1976).
[45] C. Enzell, G. Francis and S. Liaaen-Jensen, *Acta Chem. Scand.*, **23**, 727 (1969).

[46] B. Johannes, H. Brzezinka and H. Budzikiewicz, *Z. Naturforsch.*, **34b**, 300 (1979).
[47] H. Kjøsen, Thesis, University of Trondheim (1972).
[48] B. H. Davies, C. J. Hallett, R. A. London and A. F. Rees, *Phytochem.*, **13**, 1209 (1974).
[49] H. H. Strain, K. Aitzetmüller, W. A. Svec, and J. J. Katz, *J. Chem. Soc., Chem. Commun.*, **1970**, 867.
[50] G. W. Francis, R. R. Upadhyay and S. Liaaen-Jensen, *Acta Chem. Scand.*, **24**, 3050 (1970).
[51] H. Kjøsen, S. Norgård, S. Liaaen-Jensen, W. A. Svec, H. H. Strain, P. Wegfahrt, H. Rapoport and F. T. Haxo, *Acta Chem. Scand.*, **B30**, 157 (1976).
[52] J. Gross and G. Eckhardt, *Phytochem.*, **20**, 2267 (1981).
[53] A. Haag and C. H. Eugster, *Helv. Chim. Acta*, **68**, 1897 (1985).
[54] J. E. Johansen and S. Liaaen-Jensen, *Acta Chem. Scand.*, **B33**, 551 (1979).
[55] M. Aguilar-Martinez and S. Liaaen-Jensen, *Acta Chem. Scand.*, **26**, 2528 (1972).
[56] A. G. Andrewes, G. Borch and S. Liaaen-Jensen, *Acta Chem. Scand.*, **B38**, 871 (1984).
[57] M. Kelly, S. Norgård and S. Liaaen-Jensen, *Acta Chem. Scand.*, **24**, 2169 (1970).
[58] S. Norgård, Thesis, University of Trondheim, (1972).
[59] A. G. Andrewes, P. Foss, G. Borch and S. Liaaen-Jensen, *Acta Chem. Scand.*, **B38**, 337 (1984).
[60] H. Rønneberg, A. G. Andrewes, G. Borch, R. Berger and S. Liaaen-Jensen, *Phytochem.*, **24**, 309 (1985).
[61] U. Schwieter, H. Gutmann, H. Lindlar, R. Marbet, N. Rigassi, R. Rüegg, S. Schaeren and O. Isler, *Helv. Chim. Acta*, **49**, 369 (1966).
[62] H. Kjøsen and S. Liaaen-Jensen, *Acta Chem. Scand.*, **24**, 2259 (1970).
[63] S. Norgård, A. J. Aasen and S. Liaaen-Jensen, *Acta Chem. Scand.*, **24**, 2183 (1970).
[64] H. Kjøsen and S. Liaaen-Jensen, *Acta Chem. Scand.*, **27**, 2495 (1973).
[65] N. Arpin, H. Kjøsen, G. W. Francis and S. Liaaen-Jensen, *Phytochem.*, **12**, 2751 (1973).
[66] A. G. Andrewes and S. Liaaen-Jensen, *Acta Chem. Scand.*, **26**, 2194 (1972).
[67] G. Francis, *Acta Chem. Scand.*, **25**, 2916 (1969).
[68] A. K. Chopra, G. P. Moss and B. C. L. Weedon, *J. Chem. Soc., Perkin Trans. 1*, **1988**, 1371.
[69] R. Gebhard, J. T. M. van Dijk, E. van Ouwerkerk, M. V. T. J. Boza and J. Lugtenburg, *Recl. Trav. Chim. Pays-Bas*, **110**, 459 (1991).
[70] U. Leuenberger, I. Stewart and R. W. King, *J. Org. Chem.*, **41**, 891 (1976).
[71] T. W. Goodwin, *Biochem. J.*, **123**, 293 (1971).
[72] S. C. Kushwaha, E. L. Pugh, J. K. G. Kramer and M. Kates, *Biochim. Biophys. Acta*, **260**, 492 (1972).
[73] A. F. Thomas, B. Willhalm and R. Muller, *Org. Mass Spectrom.*, **2**, 223 (1969).
[74] G. Nybraaten and S. Liaaen-Jensen, *Acta Chem. Scand.*, **25**, 370 (1972).
[75] G. W. Francis, *Acta Chem. Scand.*, **26**, 2969 (1972).
[76] Y. Tanaka, *C. Mem. Fac. Fish., Kagoshima Univ.*, **27**, 355 (1978).
[77] A. G. Andrewes, S. Liaaen-Jensen and G. Borch, *Acta Chem. Scand.*, **B28**, 737 (1974).
[78] R. R. Upadhyay and S. Liaaen-Jensen, *Acta Chem. Scand.*, **24**, 3055 (1970).
[79] G. Britton, A. P. Mundy and G. Englert, *J. Chem. Soc., Perkin Trans. 1*, **1985**, 601.
[80] A. G. Andrewes and S. Liaaen-Jensen, *Tetrahedron Lett.*, **25**, 1191 (1984).
[81] H.-R. Sliwka and S. Liaaen-Jensen, *Acta Chem. Scand.*, **B44**, 61 (1990).
[82] H. Kleinig, W. Heumann, W. Meister and G. Englert, *Helv. Chim. Acta*, **60**, 254 (1977).
[83] P. Foss, V. Partali, Y. Olsen, G. Borch, and S. Liaaen-Jensen, *Acta Chem. Scand.*, **B40**, 157 (1986).
[84] S. Hertzberg, V. Partali and S. Liaaen-Jensen, *Acta Chem. Scand.*, **B42**, 495 (1988).
[85] J. Baldas, Q. Porter, A. Leftwick, A. Holzel and B. Weedon, *Chem. Commun.*, **1969**, 415.
[86] G. W. Francis, S. Hertzberg, R. R. Upadhyay and S. Liaaen-Jensen, *Acta Chem. Scand.*, **26**, 1097 (1972).
[87] A. G. Andrewes and S. Liaaen-Jensen, *Acta Chem. Scand.*, **27**, 1401 (1973).

[88] N. Arpin, J.-L. Fiasson, M. P. Bouchez-Dangye-Caye, G. W. Francis and S. Liaaen-Jensen, *Phytochem.*, **10**, 1595 (1971).
[89] A. G. Andrewes, G. Borch and S. Liaaen-Jensen, *Acta Chem. Scand.*, **B31**, 212 (1977).
[90] U. Schwieter, H. Bolliger, L. Chopard-dit-Jean, G Englert, M. Kofler, A. König, C. von Planta, R. Rüegg, W. Vetter and O. Isler, *Chimia*, **19**, 294 (1965).
[91] S. Liaaen-Jensen, S. Hertzberg, O. B. Weeks and U. Schwieter, *Acta Chem. Scand.*, **22**, 1171 (1968).
[92] T. Matsuno, Y. Tani, T. Maoka, K. Matsuno and T. Komori, *Phytochem.*, **25**, 2837 (1986).
[93] J. Deli, P. Molnar, G. Tóth, A. Baumeler and C. H. Eugster, *Helv. Chim. Acta*, **74**, 819 (1991).
[94] A. Fiksdahl, T. Bjørnland and S. Liaaen-Jensen, *Phytochem.*, **23**, 649 (1984).
[95] T. Bjørnland, G. Borch and S. Liaaen-Jensen, *Phytochem.*, **25**, 201 (1986).
[96] M. P. Gmünder and C. H. Eugster, *Helv. Chim. Acta*, **73**, 2190 (1990).
[97] R. Buchecker and S. Liaaen-Jensen, *Phytochem.*, **16**, 729 (1977).
[98] G. Nybraaten and S. Liaaen-Jensen, *Acta Chem. Scand.*, **B28**, 483 (1974).
[99] J. Baldas, Q. N. Porter, L. Cholnoky, J. Szabolcs and B. C. L. Weedon, *Chem. Commun.*, **1966**, 852.
[100] A. K. Chopra, A. Khare, G. P. Moss and B. C. L. Weedon, *J. Chem. Soc., Perkin Trans. 1*, **1988**, 1383.
[101] A. Khare, G. P. Moss and B. C. L. Weedon, *Tetrahedron Lett.*, **1973**, 3921.
[102] R. Buchecker, C. H. Eugster and C. Litchfield, *Helv. Chim. Acta*, **60**, 2780 (1977).
[103] T. Matsuno, M. Ookubo, T. Nishizawa and I. Shimizu, *Chem. Pharm. Bull.*, **32**, 4309 (1984).
[104] A. Khare, G. P. Moss and B. C. L. Weedon, *J. Chem. Soc., Perkin Trans. 1*, **1988**, 1389.
[105] T. Bjørnland, *Phytochem.*, **21**, 1715 (1982).
[106] N. Arpin, W. A. Svec and S. Liaaen-Jensen, *Phytochem.*, **15**, 529 (1976).
[107] S. Hertzberg, T. Mortensen, G. Borch, H. W. Siegelman and S. Liaaen-Jensen, *Phytochem.*, **16**, 587 (1977).
[108] T. Matsuno, S. Nagata and K. Kitamura, *Tetrahedron Lett.*, **1976**, 4601.
[109] R. Bonnett, A. K. Mallams, A. A. Spark, J. L. Tee, B. C. L. Weedon and A. McCormick, *J. Chem. Soc. C*, **1969**, 429.
[110] H. H. Strain, W. A. Svec, K. Aitzetmüller, B. T. Cope, A. L. Harkness and J. J. Katz, *Org. Mass Spectrom.*, **5**, 565 (1971).
[111] T. J. Walton, G. Britton, T. W. Goodwin, B. Diner and S. Moshier, *Phytochem.*, **9**, 2545 (1970).
[112] A. Fiksdahl and S. Liaaen-Jensen, *Phytochem.*, **27**, 1447 (1988).
[113] W. Gau, H. J. Ploschke and C. Wünsche, *J. Chromatogr.*, **262**, 277 (1983).
[114] S. Hertzberg and S. Liaaen-Jensen, unpublished work.
[115] T. Ramdahl and S. Liaaen-Jensen, *Acta Chem. Scand.*, **34**, 773 (1980).
[116] S. Hertzberg, T. Ramdahl, J. E. Johansen and S. Liaaen-Jensen, *Acta Chem. Scand.*, **B37**, 267 (1983).
[117] M. V. D'Auria, L. Minale, R. Riccio and E. Uriarte, *J. Nat. Prod.*, **54**, 606 (1991).
[118] K. Biemann, D. C. De Jongh and H. K. Schnoes, *J. Amer. Chem. Soc.*, **85**, 1763 (1963).
[119] S. Norgård, G. W. Francis, A. Jensen and S. Liaaen-Jensen, *Acta Chem. Scand.*, **24**, 1460 (1970).
[120] A. J. Aasen., G. W. Francis and S. Liaaen-Jensen, *Acta Chem. Scand.*, **23**, 2605 (1969).
[121] H. Kleinig, R. Schmitt, W. Meister, G. Englert and H. Thommen, *Z. Naturforsch.*, **34c**, 181 (1979).
[122] H. Kleinig and R. Z. Schmitt, *Z. Naturforsch.*, **37c**, 758 (1982).
[123] J. R. Chapman, *Practical Organic Mass Spectrometry*, Wiley, Chichester (1982).
[124] A. L. Yergey, C. G. Edmonds, I. A. S. Lewis and M. L. Vestal, *Liquid Chromatography/Mass Spectrometry*, Plenum Press, New York (1990).

Carotenoids
Volume 1 B: Spectroscopy
© 1995 Birkhäuser Verlag Basel

Chapter 8

X-Ray Crystallographic Studies

Frode Mo

A. Introduction

In the 1971 edition of *Carotenoids* the crystallographic work in this field was presented briefly in an article on stereochemistry [1]. By 1970, five carotenoid crystal structures had been reported in the literature. Over the ensuing two decades a similar number of new carotenoids have been studied successfully by diffraction methods. This rather modest accomplishment contrasts with the developments in many other fields in the physical, chemical and life sciences, where X-ray crystallography has played a central role in the elucidation of structure on the atomic scale. In addition to a review of structural features, this fact will be addressed, some probable causes discussed and the present standing examined in view of the advances that have been made in crystallographic methods and technology.

The present overview will concentrate on carotenoids as defined by the IUPAC rules (Vol. 1A, Chapter 3). A brief review of structural work on degraded carotenoids, carotenoid synthons and analogues will be given at the end of the Chapter.

B. Experimental

1. X-ray diffraction and determination of structure

X-rays are scattered on the electrons. In the scattering process a diffraction pattern is created, which is the Fourier transform of the 3-dimensional electron density of the object. For a true crystal, which is characterized by a high degree of internal periodicity, the transform consists of a large number of discrete diffraction maxima. The geometry and relative intensities of this set of maxima relate specifically to the shape of the crystal unit cell and the spatial distribution of electron density within this cell. The experimental part of a crystal structure analysis involves measurement of the diffracted intensities from a crystal with physical dimensions typically a few tenths of a mm. Even for a small structure there will normally be several

thousand reflection intensities accessible for measurement. Several different types of detectors are currently in use, ranging from photographic film to sophisticated position-sensitive electronic devices.

Diffraction of X-rays in a crystal is geometrically very similar to diffraction of visible light from a periodic object. The diffracted intensities are proportional to the squares of the magnitudes of the corresponding wave amplitudes, which are generally complex in the case of X-rays. However, in contrast to the optical experiment, it is not possible, with the X-ray wavelengths commonly employed for diffraction studies (*ca.* 1 Å), to recreate directly a picture of the scattering structure. The back-transformation must be made by computation, in a separate operation. Unfortunately, the phases required for these computations are generally lost in the experiment. This is the origin of the phase problem in crystallography. Several methods have been devised and refined to resolve this problem. If the crystal is of good quality, the powerful direct methods are capable of providing a solution for light-atom structures with up to about 150 independent nonhydrogen atoms. However, quite often crystalline substances of prime interest form crystals of inferior quality. Poor crystallinity may imply strong mosaicity, defects of different kinds, twinning, large atomic displacements including disorder of static or dynamic origin, even partial liquefaction. All these factors, as well as high internal molecular symmetry, notably pseudotranslational symmetry, may seriously impede the *a posteriori* determination of phase angles and subsequent refinement of the structure. Research aimed at improving existing methods for solving crystal structures or developing alternative techniques is still in a very active state.

Assuming that it has been possible by some method to assign or retrieve approximate phase values, ϕ_{hkl}, for at least a subset of the diffracted waves, a 3-dimensional electron distribution $\rho(xyz)$ in real space can be calculated by Fourier summation:

$$\rho(xyz) = 1/V \sum_h \sum_k \sum_l K\, F_{hkl,\,obs} \exp(-2\pi i(hx + ky + lz)) \qquad (1)$$

where the coefficients

$$F_{hkl,\,obs} = |F_{hkl}|_{obs} \exp(i\phi_{hkl}) \qquad (2)$$

are the generally complex structure factors for which only magnitudes have been measured. In equation (1), V = unit cell volume, K = scale factor, and h, k, l are the Laue indices relating in a well known manner to any $|F_{hkl}|_{obs}$. Several factors of geometrical or physical origin will affect the measurements, and appropriate corrections must be made at some stage. However, their interference is not a matter of concern here. Then calculation according to equation (1) gives a spatial distribution of electron density which represents the structure or, in the initial stages, more commonly a partial structure. As a good approximation, atomic positions can be defined in the maxima of electron density.

The complex structure factor can be rewritten as in equation (3)

$$|F_{hkl}|_{calc} \exp(i\phi_{hkl})_{calc} = \sum_{j=1}^{N} f_{j(hkl)} \exp(T_{j(hkl)}) \exp(2\pi i(hx_j + ky_j + lz_j)) \quad (3)$$

which shows explicitly how an F_{hkl} contains the scattering contribution from all atoms (N) in the unit cell. In equation (3), f_j = atomic scattering factor, a known function for each element, varying with $\sin\theta/\lambda$, where θ = scattering angle and λ = wavelength of the radiation; $x_j y_j z_j$ = positional parameters of the jth atom, and $T_{j(hkl)}$ = expression for the generally anisotropic displacements of the jth atom.

The structure parameters are refined in an iterative process. Several methods exist. For structures like carotenoids, the common method is based on some type of least-squares minimization, usually of the quantity

$$\Delta = \sum_h \sum_k \sum_l w_{hkl} (|F_{hkl}|_{obs} - 1/K|F_{hkl}|_{calc})^2 \quad (4)$$

As a measure of the agreement between observed and calculated structure factors, crystallographic residuals can be computed, for instance

$$R = \frac{\sum \left| |F_{hkl}|_{obs} - 1/K|F_{hkl}|_{calc} \right|}{\sum |F_{hkl}|_{obs}} \quad (5)$$

or related indices, based on the squared amplitudes, $|F_{hkl}|^2$, with or without weights w_{hkl}. In modern structure studies of small molecules, final R factors are frequently in the range 0.02 to 0.04. A value of $R > 0.05$ usually indicates some problem or problems in defining a good model of the structure. Such difficulties can arise for a variety of reasons.

Under favourable conditions a properly executed single-crystal diffraction study can provide a precise 3-dimensional picture of the structure. With R factors in the range given above, estimated standard deviations in bond lengths are typically between 1×10^{-3} and 2×10^{-3} Å, and in bond angles 10^{-1} deg. This level of precision is often more than adequate to solve a structural problem. In many cases this information is essential for the interpretation of other types of physical measurements.

2. Determination of absolute configuration

X-Ray crystallography provides a unique means for determining the absolute configuration of a chiral molecule. The traditional method, first demonstrated in 1949 [2, 3] makes use of a resonance phenomenon which can be optimized in the scattering process. If the energy of the incident X-ray beam is slightly larger than that of an absorption edge of an element in the structure, the scattering factor of this element becomes complex. In a non-centrosymmetric

crystal containing both normal (f_j real) and anomalous (f_j complex) scatterers, the intensities of inversely related reflections become generally unequal, $I_{hkl} \neq I_{-h-k-l}$.

The equality, $I_{hkl} \neq I_{-h-k-l}$, known as Friedel's law, holds if anomalous scattering is absent (or negligible) and is always satisfied in the centrosymmetric case. The breakdown of Friedel's law is illustrated in Fig. 1.

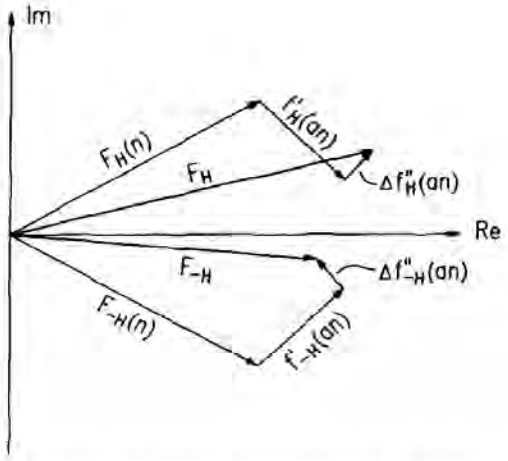


Fig. 1. The breakdown of Friedel's law in a non-centrosymmetric structure with several normal (n) and one anomalous (an) scatterer. The imaginary part of the contribution from the anomalous scatterer, $i\Delta f''_H(an)$, involves a phase shift of $+\pi/2$ relative to the real part, $f'_H(an)$. As a general result $|F_H| \neq |F_{-H}|$; H denotes hkl.

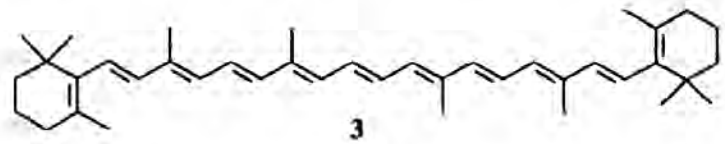
In practice, the determination of absolute configuration is deferred until the end of the structure refinement. Then Friedel pairs of reflections with large $\Delta I_{hkl} = I_{hkl} - I_{-h-k-l}$ can be reexamined, each I_{hkl} now being related in a known way to the refined structure and its inverted image. In principle, the correct handedness can be inferred unambiguously from the observation of a single significant ΔI_{hkl}.

The real and imaginary corrections, $\Delta f'$ and $\Delta f''$, respectively, to the uncorrected scattering factor of the anomalous scatterer, are generally much larger for heavy elements than for light ones. Thus, with CuKα radiation at $\sin\theta/\lambda = 0$ Å^{-1}, $\Delta f'$ and $\Delta f''$ for iodine are –0.326 and 6.836 electrons, respectively, whereas the corresponding values for oxygen are 0.049 and 0.032 electrons [4]. The ratio between the two $\Delta f''$ values is about 215. For many years, preparation of heavy atom derivatives of light atom structures was a well established method to initiate solution of the phase problem. This strategy is made almost completely obsolete in modern small structure crystallography. On the other hand, the use of heavy atoms continues to be the preferred approach for the determination of absolute configuration. However, it was demonstrated repeatedly more than 20 years ago that the chirality of light-atom structures can be determined from the very small anomalous scattering of CuKα radiation on oxygen, [5, 6], even in cases of poorly refined structures [7].

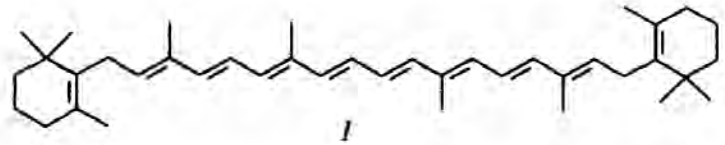
C. Studies of Carotenoid Structure

1. Structural studies before 1970

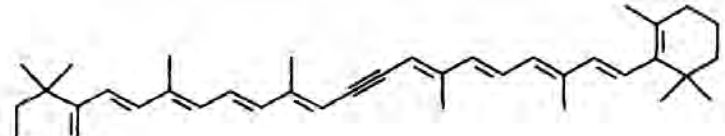
Before 1970, X-ray diffraction (XRD) studies were reported for β,β-carotene (**3**) [8], and its 7,7'-dihydro derivative (*1*) [9] and 15,15'-didehydro derivative (*2*) [10], and for canthaxanthin (**380**) [11] and its 15,15'-didehydro derivative (*3*) [12]. All these compounds crystallize in centrosymmetric space groups. With the exception of canthaxanthin they have a crystallographic inversion centre in the central bond. The asymmetric unit, which is the smallest structural entity devoid of any crystallographic symmetry element is one molecule for canthaxanthin, one half molecule for the other compounds.



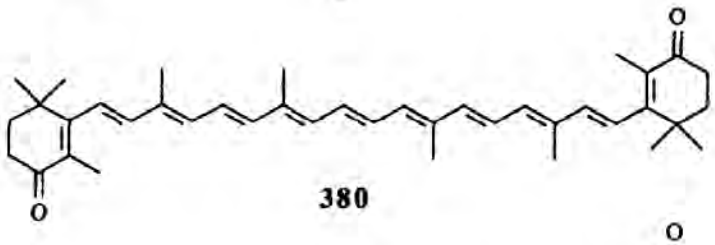
3



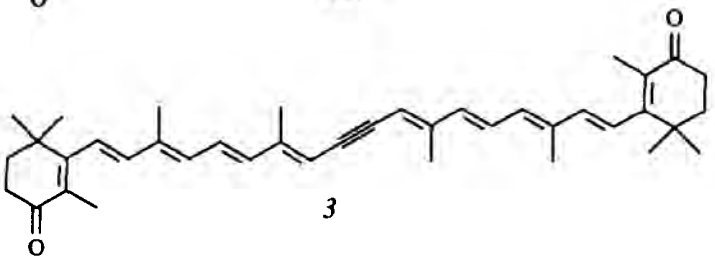
1



2



380



3

Before the main structural findings in the pre-1970 studies are discussed some common crystallographic characteristics will be pointed out. The number of reflections observed and thus available for the refinement is generally small but varies greatly among the five structures, from about 850 for β,β-carotene (**3**) and its 7,7'-dihydro derivative (*1*), to about 2200 for 15,15'-didehydrocanthaxanthin (*3*). The numbers are normalized to correspond to one half molecule. The crystallographic R-factors are high in all the studies, in the range 0.17 to 0.19 for β,β-carotene (**3**) and 7,7'-dihydro-β,β-carotene (*1*) and 0.095 to 0.115 for the other three structures. The scarcity of data and the high R-factors must be attributed primarily to the loose molecular packing in the crystals, as indicated by generally high atomic displacement parameters (adps, also known as thermal parameters), in particular in the cyclohexene and cyclohexenone rings. The calculated densities confirm this picture. They are in the range 1.02 to 1.04 $Mg.m^{-3}$ for β,β-carotene (**3**) and its two derivatives (*1*, *2*), and slightly higher, 1.06 to 1.08 $Mg.m^{-3}$ for canthaxanthin (**380**) and its 15,15'-didehydro derivative (*3*).

The studies have established some important and consistent structural features in these carotenoids. The conjugated chain is all-*trans* (all-*E*) and has a pronounced S-shape which has been ascribed to steric requirements of the methyl groups along the chain. The chain can also be slightly bent out of the main plane due to small twists about the single bonds. The three most accurate studies [10-12] indicate that the central part of the chain is quite planar.

Another point of interest has been the alternation of bond lengths along the chain. Early theoretical analyses of linear polyenes had predicted that single and double bonds would tend to attain a common value, 1.395 Å, in a chain of increasing length [13]. In contrast, later studies based on the band theory for solids [14], free electron MO theory [15], or LCAO theory at different levels of approximation [16, 17] had independently concluded that a bond-length alternation will persist since it corresponds to a lower total energy. The difference between single and double bonds was predicted to decrease very little from short polyenes (5 to 10 double bonds) to long ones [15]. In three of the X-ray studies a systematic decrease was observed in the alternate character of single and double bonds towards the centre of the chain [9, 10, 12]. This trend was not significant in β,β-carotene (**3**) [8] and canthaxanthin (**380**) [11]. However, reliable studies of such subtle effects on bond lengths require more data of better quality than were actually available. Corrections for apparent bond shortening due to rigid-body motion [18] would be necessary as well. The problems associated with vibrational shortening have been discussed [10, 11].

The attachment of the β-ring to the chain is *gauche* (s-*cis*) about the C(6)–C(7) single bond in all four structures with a through-conjugated chain. Steric interactions between the methyl groups of the ring and the hydrogen atoms bonded to the chain atoms C(7) and C(8) prevent coplanarity between the best planes through the double bond systems of the ring and the chain. Differences in crystal packing may also contribute to the observed range of *gauche* conformations. It was noted [11] that the introduction of a keto function in the ring did not promote an appreciably higher degree of conjugation. All the cyclohexene rings are puckered in the half-chair conformation. The largest torsion angle is about the C(2)–C(3) bond which is opposite the double bond in the ring. The keto group at position C(4) in the canthaxanthin structures restricts the puckering of the ring, changing the type of conformation to 'sofa' at C(2). A detailed analysis of the conformation angles at the ring/chain junction and about the

ring bonds in these and some related molecules has been published [19].

The large atomic displacement parameters, particularly in the rings, are a recurrent feature in all the structures studied. Excessive values for some of the ring atoms indicate partial disorder. It has been pointed out that both half-chair conformations of the cyclohexene ring may coexist in the crystal [20]. The preponderance of one form over the other is determined by the difference in the corresponding intramolecular and intermolecular interaction energies. Since the activation energy for conversion is less than 7 kcal.mol^{-1} [21], dynamic interconversion between the two forms could also take place to some extent with increasing temperature in these loosely packed crystals. In the sofa conformation of the cyclohexenone rings in canthaxanthin (**380**), atom C(2) is displaced from a plane defined approximately by the other ring carbon atoms and the oxygen atom. A change of conformation would also involve a flip-over of the two methyl groups at C(1) to new positions. The possibility for conformational disorder has been recognized [11, 12]. In the studies of the canthaxanthin structures three additional carbon atoms with partial occupancy were included in positions corresponding to the alternative conformation which was indicated by significant maxima of electron density in the Fourier maps. Refinement suggested the presence of about 10 to 20% of the minor conformation.

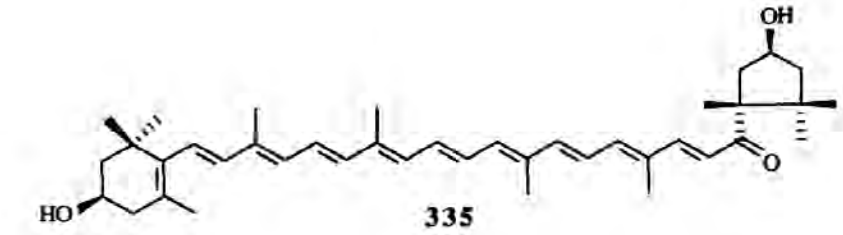
2. Structural studies after 1970

The structures studied after 1970 can be divided in two subgroups: a) carotenoids and apocarotenoids with at least one terminal ring, and b) the carotenoid conjugated chain.

Note that in this Section the numbering of atoms in the discussion of crystal structures does not correspond to the normal carotenoid numbering scheme. In some cases, carotenoid numbering is also given, for comparison.

a) Carotenoids and apocarotenoids

The crystal structure of capsanthin (**335**) as the bis(*p*-bromobenzoate) was reported [22]. This appears to be the first successful crystallographic study of a carotenoid with unequal end groups. The bromo derivative crystallizes in the monoclinic polar space group $P2_1$ with two distinct molecules in the asymmetric unit. The structure analysis therefore involved solution and refinement of a bimolecular structure comprising 124 non-hydrogen atoms. As usual for carotenoids, a rapid fall-off in scattering power was observed and the crystals were reported to suffer radiation damage. Nearly 3000 reflections were recorded above threshold with film, corresponding to about 750 reflections per half molecule. The crystallographic refinement, which was in the isotropic mode for the carbon and oxygen atoms and anisotropic for Br, converged at an R-factor = 0.174. Figure 2 shows the two molecules in projection; the characteristic S-shape of the all-*trans* chains is clearly seen. Independent determination of two molecular units confirmed the identity and attachment of the end groups to the chain. In this derivative, the esterified hydroxy group on the cyclopentane ring and the attached terminal carbon atom of the chain are oriented *trans*. Large errors in the atomic positions were the cause



335

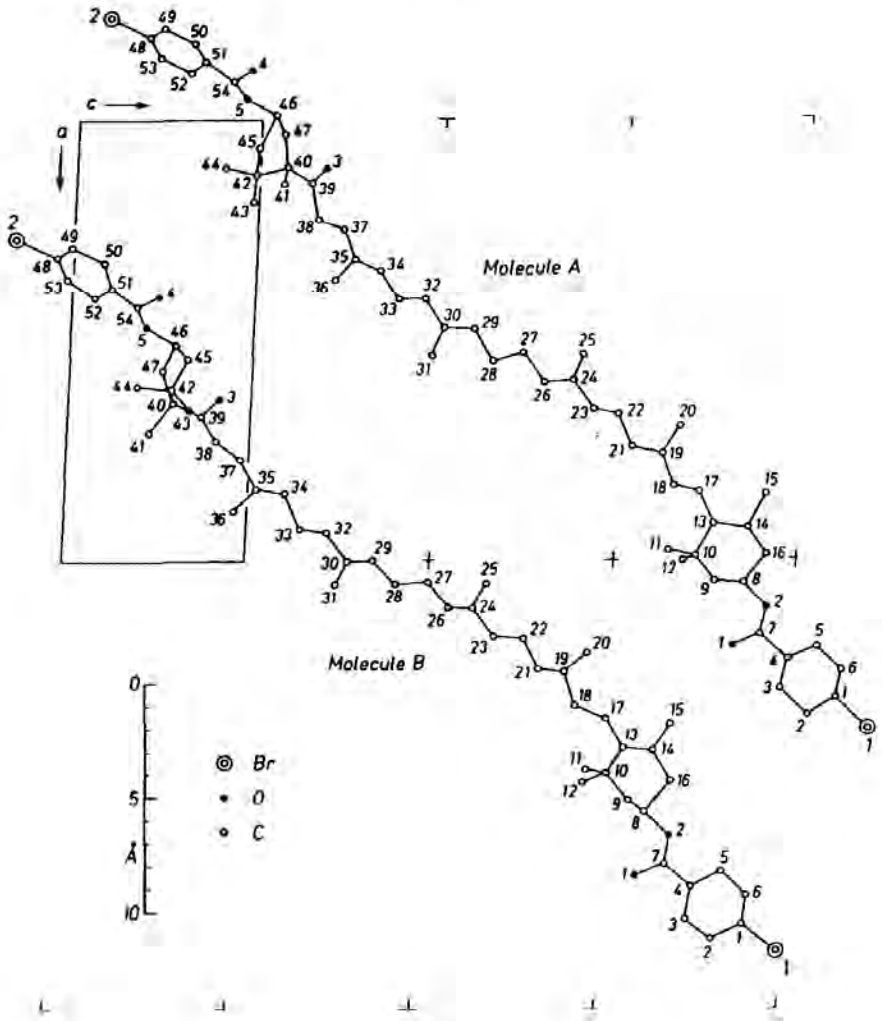
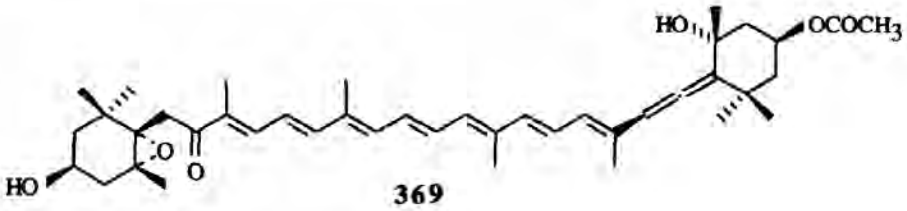


Fig. 2. Conformation of two independent molecules of capsanthin bis(*p*-bromobenzoate). (Reproduced by permission of *Z. Kristallogr.*, R. Oldenbourg Verlag GmbH).

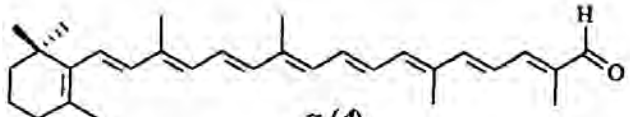
of several anomalous values for bond lengths, and an analysis of bond character was not possible.

A preliminary study of fucoxanthin (**369**) has been published [23]. The carotenoid crystallizes in space group P1 with two molecules in the asymmetric unit, corresponding to 96 independent C and O atoms. At R = 0.25, individual atoms of the chains and the end groups could barely be resolved, and there was evidence of partial disorder. The conformation deduced for the allenic end group was reported to be in agreement with that derived from X-ray studies of smaller synthetic products [24].

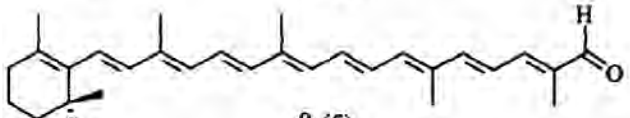


369

8'-Apo-β-caroten-8'-al or APC (**482**) crystallizes in two different monoclinic forms. One form, α-APC, belongs to the non-centrosymmetric space group $P2_1$, the other, β-APC, is centrosymmetric $P2_1/a$ [25]. Both structures have one molecule in the asymmetric unit. For the α-form, averaging over a large number of multiple (counter) measurements and symmetry-equivalent reflections yielded a unique set of 2538 F^2_{obs}, of which 1993 were larger than the chosen threshold, $2\sigma(F^2_{obs})$. The parent numbers for β-APC were 2460 F^2_{obs}, with 1372 exceeding the threshold. The carbon and oxygen atoms, but not hydrogen, were refined anisotropically. Final R-factors based on F^2_{obs} were 0.063 (α) and 0.068 (β).



α (*4*)



β (*5*)

The main conformational difference between the two forms lies in the orientation of the cyclohexene ring. In α-APC the orientation is *gauche* (*s-cis*) relative to the chain (*4*), whereas it is *antiperiplanar* (*s-trans*) in β-APC (*5*). The torsion angle for the atomic sequence C(5)C(6)C(7)C(8), which describes the twist about the C(6)–C(7) single bond (carotenoid numbering) is + 46° in α-APC and ±158° in β-APC. The former value is within the range

defined by β,β-carotene (**3**), (±39°), 15,15'-didehydro-β,β-carotene (*2*), (±49°), canthaxanthin (**380**), (±52 and ±54°), and 15,15'-didehydrocanthaxanthin (*3*), (±43°) [19]. The ring orientation in β-APC is similar to that calculated for *trans*-β-ionylidenecrotonic acid (±169°) [20] and for the monoclinic form of retinoic acid (±166°) [26].

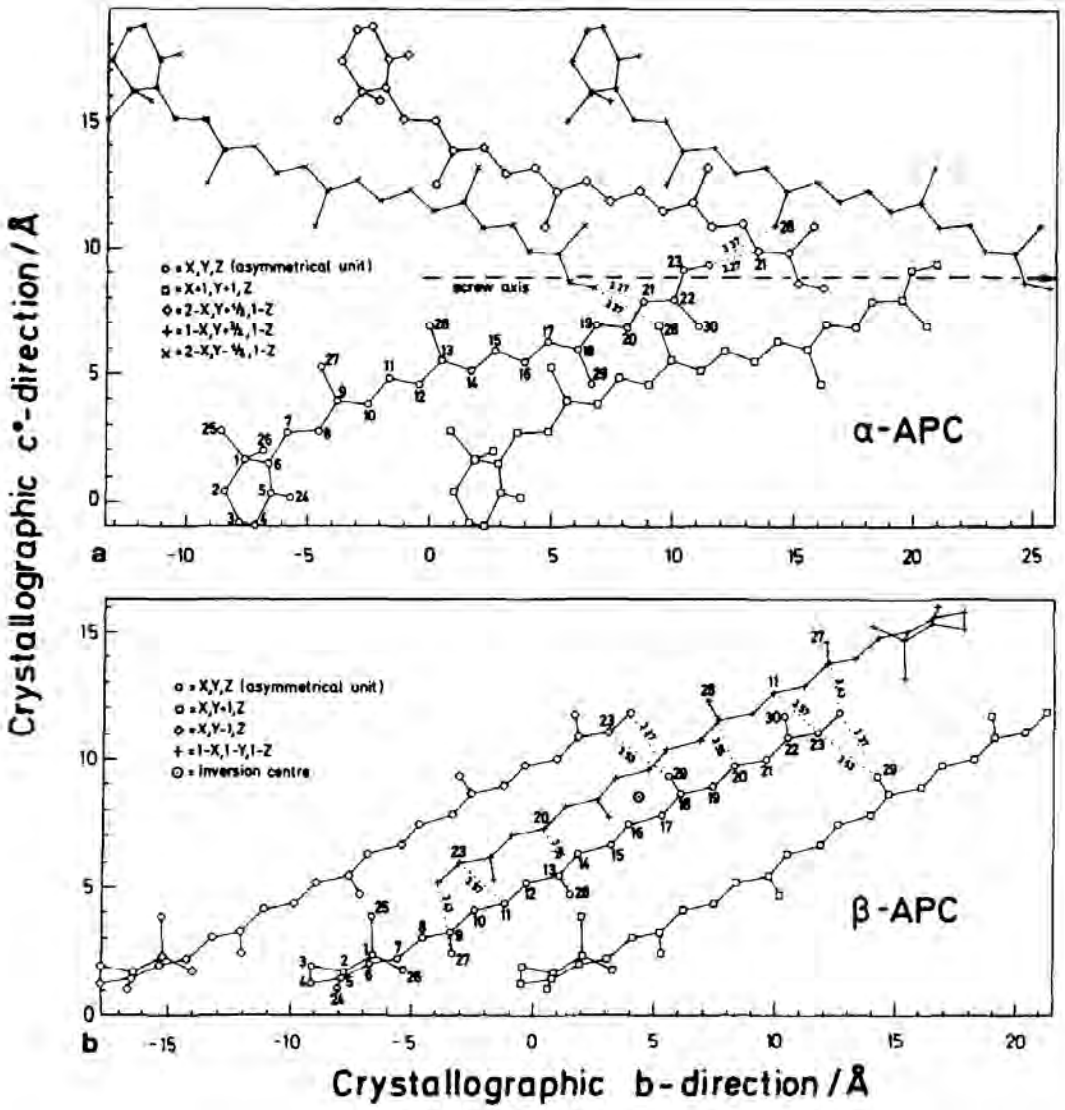


Fig. 3. The crystal structures of α-APC (*4*) and β-APC (*5*). (Reproduced by permission of *Eur. Biophys. J.*, Springer-Verlag)

The α-APC has a non-planar conjugated chain, the root-mean-square (rms) deviation from a common best plane being 0.238 Å. A central portion including the atoms C(11) to C(21) has a rms deviation from planarity of only 0.016 Å. Within this part the double bonds are significantly lengthened and the single bonds are shortened. The chain of the β-form has a better overall planarity; the rms deviation is 0.120 Å. For the fragment C(11) to C(21) the parent rms value is 0.040 Å. The data for this form were not of sufficient quality to allow a reliable analysis of bond-length variations.

The molecules of the α-form adopt a polar packing with the C=O groups close to the 2-fold screw axis. Coulomb interactions involving the aldehyde groups appear to be important for the molecular cohesion; the packing in other regions is rather loose as indicated by generally high adps and a low density, 1.02 $Mg.m^{-3}$. The β-form is packed in an antiparallel fashion, as is found commonly among the carotenoids. The density is 1.05 $Mg.m^{-3}$. Figure 3 shows both crystal structures in the same projection.

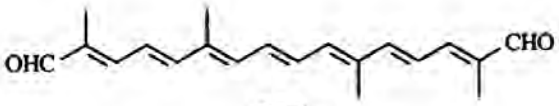
A recent reinvestigation of the crystal structure of β,β-carotene (**3**) was carried out at reduced temperature, 130K [27]. Of 3956 measured intensities, 3848 were independent; only 1671 of these were larger than the chosen threshold, 2.5 σ(I). All non-hydrogen atoms were refined anisotropically, and the hydrogen atoms were then included in a riding model with fixed C–H distances and one common isotropic adp. Strong disorder involving the C(2) and C(3) atoms was analysed by applying an unconstrained split-atom refinement for the multiple sites. The refinement converged at R = 0.071. The final structure is in agreement with a model in which both half-chair conformations of the ring are present in a 50/50 ratio. The overall structure corroborates the main results from the original work [8], but several bond lengths that were anomalous from the 1964 study could be corrected.

The new set of atomic positions shows that the chain is significantly non-planar. For the central 10-atom fragment C(12) to C(12') [carotenoid numbering C(11) to C(11')] the rms deviation from planarity for the carbon atoms involved, 0.058 Å with the range –0.080 to 0.067 Å, can be calculated from the published data. Both methyl groups are displaced from this plane; the largest displacement (0.36 Å) is seen for the central C(15). A better conformational description, perhaps, is given by the torsion angles about the sequence of bonds C(7)–C(8)–C(9)–C(11)–C(12)–C(13), which starts with a C=C double bond. The angles determined are –176.2, –175.2, 177.7, –174.9 and 175.8°; the estimated standard deviation (esd) in these angles is about 0.4°. The set of angles corresponds to an average deviation of 4° from exact antiperiplanarity. The revised torsion angle C(5)C(6)C(7)C(8) is ±42°. The correction of the previous value (±39°) narrows slightly the range of conformation angles for rings attached *gauche* to the carotenoid chain. The new study did not show a diminishing difference between single and double bond lengths towards the centre of the chain. This observation testifies to the influence of non-planarity on the conjugation.

b) The carotenoid chain

Crocetindialdehyde (**536**) crystallizes in the triclinic, centrosymmetric space group $P\bar{1}$, with one half molecule in the asymmetric unit [28]. Unconstrained refinement with anisotropic adps for the carbon and oxygen atoms, and isotropic ones for the hydrogen atoms was based on

1142 reflections with intensities $I > 2\sigma(I)$. At the end of the refinement R = 0.047, and esds in bond lengths and angles (excluding H) are 0.003 Å and 0.2 to 0.25°, respectively. This well refined structure is an interesting model since its conformation is not influenced by steric interactions with terminal rings.



536

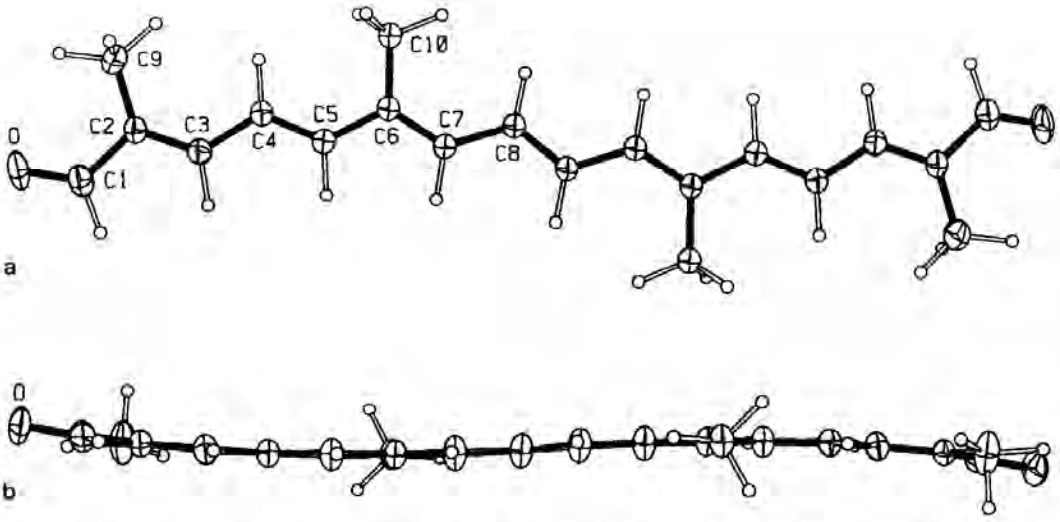


Fig. 4. Molecular conformation of crocetindialdehyde (**536**) with labelling of the non-hydrogen atoms. Displacement ellipsoids correspond to a 25% probability; *a*) view down on the main chain plane, and *b*) view along this plane. (Drawings produced from data published in *Acta Crystallogr.*; reproduced by permission of the International Union of Crystallography).

Figure 4a shows the all-*trans* chain in the familiar S-shape. In order to assess more reliably the effects of steric crowding, all intramolecular contacts have been recalculated with C–H bond lengths normalized to 1.10 Å [29, 30]. Both uncorrected and corrected interatomic distances are given in Table 1. Along either edge of the molecule there is a string of short contacts, including O ••• H(91) at 2.50 Å, which manifests the importance of intramolecular contacts for the conformation of the carotenoid chain. The chain deviates from planarity as well. A fragment containing the central ten chain carbon atoms C(4) to C(4') [carotenoid numbering C(11) to C(11')], including the central methyls C(10) and C(10'), has a rms deviation from planarity of 0.034°. The range of distances is −0.051 to 0.047 Å. The remaining carbon and oxygen atoms are displaced from this plane with increasing magnitude

towards the ends of the chain. The resulting out-of-plane S-bend is illustrated in Figure 4b. The torsion angles about the sequence of bonds C(1)–C(2)–C(3)–C(4)–C(5), which starts with a C–C single bond, are 174.6, –176.5, 175.2 and –176.6°, respectively, with an esd of about 0.15°. The average magnitude of deviation from 180° is 4.25°.

Table 1. Short intramolecular contacts in crocetindialdehyde (**536**). Esds are in parentheses.

	I[a]	II[b]
O ••• H(91)	2.53(3) Å	2.50 Å
H(1) ••• H(3)	2.20(3)	2.17
H(3) ••• H(5)	2.34(3)	2.32
H(4) ••• H(92)	2.31(4)	2.18
H(4) ••• H(103)	2.34(3)	2.29
H(5) ••• H(7)	2.20(2)	2.18
H(8) ••• H(101)	2.13(2)	2.03

[a] Calculated with coordinates from [28]. [b] Calculated with C–H bond lengths normalized to 1.10 Å.

The central chain fragment of crocetindialdehyde (**536**) is more planar than that in β,β-carotene (**3**), and contains the central methyl carbon atoms. The observed differences δ between alternate single and double bonds in sequence from the terminal towards the central carbon atom are: δ = 0.115, 0.093, 0.087 and 0.067. This is a systematic and significant decrease.

The molecular chains are packed end-to-end in the crystal with the aldehyde and the terminal methyl groups positioned around centres of symmetry. The central methyl groups of a chain fill the space between chain ends in adjacent layers. It is likely that the slight out-of-plane bending is effected to accomodate the methyl groups [28]. From the mode of packing which features several short O ••• H contacts it is inferred that the chain ends are partially polarized and are involved in Coulomb interactions. The calculated density of the crystals, 1.11 $Mg.m^{-3}$, is higher than for any of the other carotenoids studied by X-ray diffraction.

Crocetindialdehyde (**536**) reacts with the triamine $N(CH_2CH_2NH_2)_3$ to form a solid macrobicyclic hexaimine. Trigonal crystals belonging to the non-centrosymmetric space group R3 have been studied by XRD [31]. From a set of 3348 independent reflections, 1526 had $I > 3\sigma(I)$ and were used in the crystallographic refinement. Anisotropic adps were assigned to the non-hydrogen atoms, isotropic hydrogen atoms were included in calculated positions. The final R was 0.069. The complex has three carotenoid chains strung between two $N(CH_2CH_2NH_2)_3$ tripods as shown in Fig. 5. The central N–N' axis is a crystallographic three-fold axis, thus the asymmetric unit contains one complete strand. Each strand is all-*trans* but twisted, torsion angles about the single C–C bonds are in the range –166 to –178°, and the range for the double bonds is –174.5 to +178.5°. The average values, –174 and –178°, respectively, show that there is a consistent right-handed twist along the chain resulting in a

total end-to-end torsion of about 65°. This novel chain conformation is no doubt caused primarily by the close proximity of two other chains bonded to the same tripod. The lateral accommodation of methyl groups appears to be an important constraint for the molecular packing.

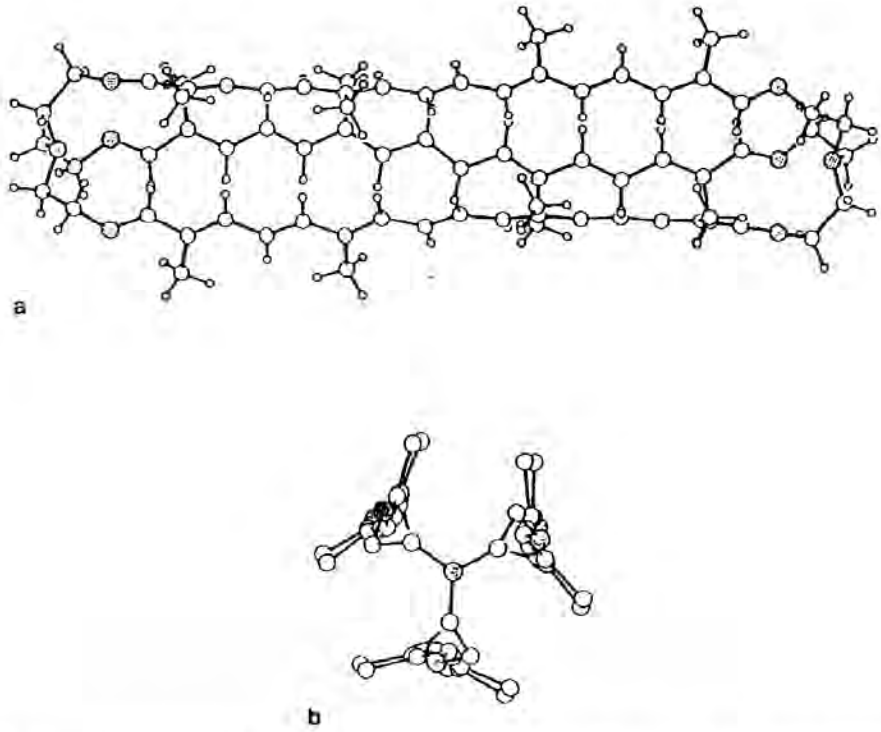


Fig. 5. Two representations of the crystal structure of the macrobicyclic cryptand of crocetindialdehyde and $N(CH_2CH_2NH_2)_3$; *a*) sideview, and *b*) view along the N,N' bridgehead axis. (Reproduced by permission of *Helv. Chim. Acta*, Verlag Helvetica Chimica Acta).

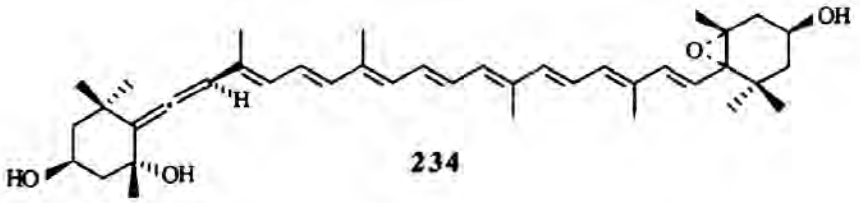
D. Structures of Degraded Carotenoids, Synthons and Analogues

The methods most commonly employed for determining absolute configuration are based on optical properties of the chiral compound. However, the spectra from optical rotatory dispersion (ORD) or circular dichroism (CD) measurements (Chapter 3) must be correlated with those from known absolute standards to allow assignment of the absolute configuration.

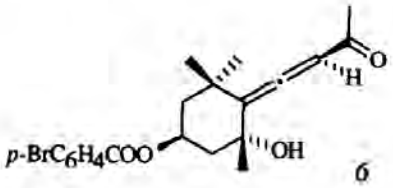
As yet there is no example of the use of XRD on a chiral carotenoid to determine its absolute structure, but diffraction methods have been used in many cases to determine the relative or absolute configuration of degradation products or synthetic intermediates. These smaller fragments usually comprise only the end group and its stereospecific attachment to the chain. Important XRD studies of carotenoid fragments or analogues after 1968 will be reviewed here.

X-Ray structure analysis of a degradation product (*6*) of fucoxanthin (**369**) provided the absolute configuration of the allenic end group in fucoxanthin, neoxanthin (**234**) and related carotenoids [24, 32]. The C(5)-hydroxyl group is *trans* to the oxygen function on C(3) and *cis* to the allenic hydrogen.

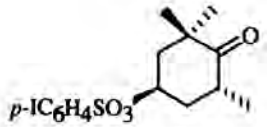
Two different optical isomers of astaxanthin can be synthesized in high optical purity *via* several different pathways starting from suitable derivatives of 6-oxoisophorone. The absolute configuration of the (3*S*,3'*S*) isomer (**406**), previously deduced from ORD data, was verified from an X-ray study of the derivative *7* [33]. Confirmatory evidence of the absolute configuration of the enantiomer (3*R*,3'*R*) (**404**) was secured through X-ray analyses of the two *cis*/*trans* related intermediates *8* and *9* [34].



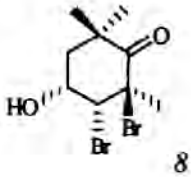
234



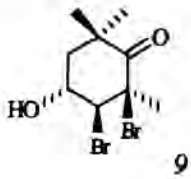
6



7

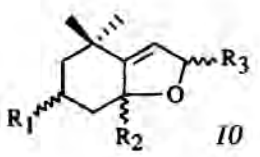


8

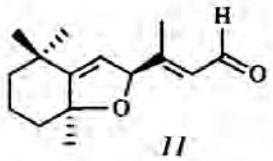


9

The substituted 7-oxabicyclo[4.3.0]nona-9-ene unit *10* is the end group in several furanoid carotenoids (carotenoid 5,8-epoxides). Spectroscopic assignments relating the relative orientation of the substituents at C(5) and C(8) were substantiated by an XRD study of the *trans* isomer (±) *11* [35].

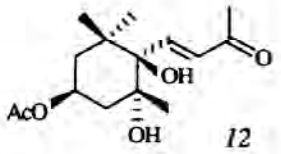


10

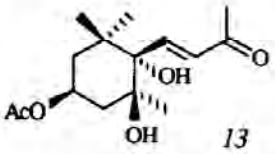


11

The naturally occurring carotenoids with 3,5,6-trihydroxy-5,6-dihydro-β end groups may be regarded as hydrolysis products of the corresponding 5,6-epoxy-5,6-dihydro species. In order to establish the relative and absolute configuration of carotenoids belonging to the former class, several ionone derivatives with the trihydroxy end group were synthesized [36]. Acid-catalysed ring opening of the (3*S*,5*S*,6*R*) and (3*S*,5*R*,6*S*) isomers of 3-acetoxy-5,6-epoxy-5,6-dihydro-β-ionone gave crystalline diols, with structures (±) *12* and (±) *13* respectively, as determined from XRD. The structures show that hydrolysis under strong acid conditions involves exclusive inversion at C(5). It was also found that under mild conditions hydrolysis of the 5,6-epoxide may proceed with or without inversion of the configuration at C(6).

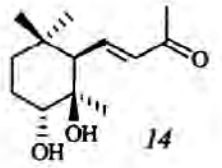


12

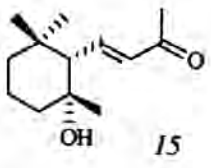


13

A related study pertains to the stereochemistry of the symmetrical 4,5:4',5'-diepoxy-4,5,4',5'-tetrahydro-ε,ε-carotenes. Epoxidation of α-ionone with peracid gives a mixture of epoxides, of which the major component was shown to have the epoxide ring *cis* relative to the side chain [37]. Acid hydrolysis of both isomers gave a single 4,5-diol [38]. Its molecular structure (±) *14* shows that the epoxy ring of the *cis* isomer is opened with inversion at C(4). The *cis* conformation was confirmed by the structure determination of (–)-(*S*)-5-hydroxy-4,5-dihydro-α-ionone, (*15*), which was obtained from (–)-(*S*)-α-ionone through epoxidation and reduction followed by MnO_2 oxidation [38].

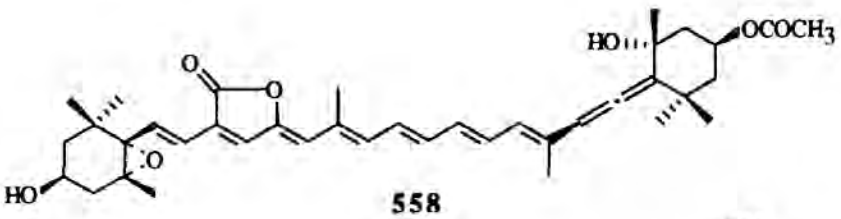


14

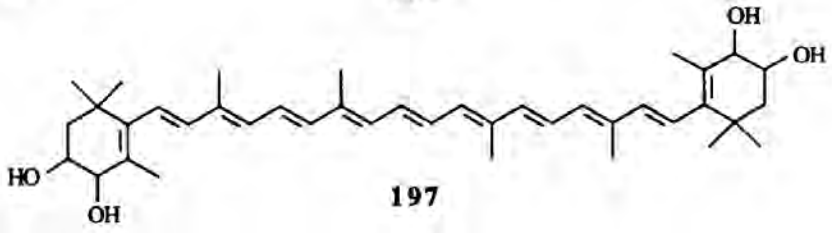


15

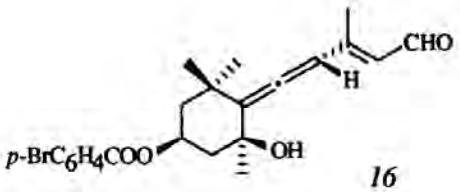
Stereochemical studies of C_{37}-norcarotenoids related to peridinin (**558**) required the preparation of some C_{22} acetylenic and allenic conjugated apocarotenals with the same unusual methylation pattern in the chain [39]. The stereochemistry of one of the chiral allenic synthons was determined as its *p*-bromobenzoate (±) *16* by XRD. In the solid-state structure the C(3) and C(5) oxygen functions are both equatorial and *cis* to the allenic hydrogen.



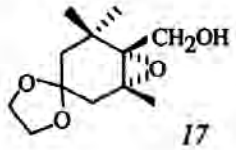
558



197

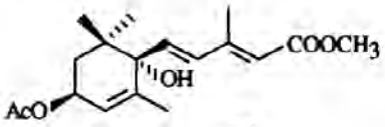


16

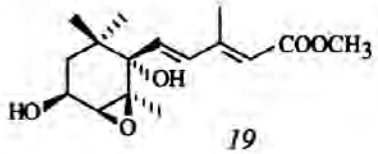


17

The pure diastereoisomers (3*S*,4*R*,3'*S*,4'*R*)- and (3*S*,4*S*,3'*S*,4'*S*)-crustaxanthin (**197**) were synthesized from the chiral epoxide *17*. As part of the configurational assignment the crystal structure of the intermediate *cis* isomer (+) *18* was determined [40]. Chirally pure 3,6:4,5:3',6':4',5'-tetraepoxy-4,5,4',5'-tetrahydro-ε,ε-carotene could be synthesized in several steps from the enantiomeric aldehyde of *17* [41]. One of the intermediates is (+) *18*. The relative configuration of its epoxide (+) *19*, together with chiroptical data, served to establish the absolute structure of other key intermediates.

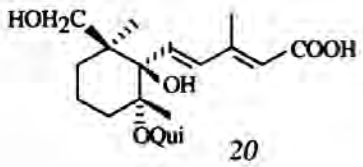


18

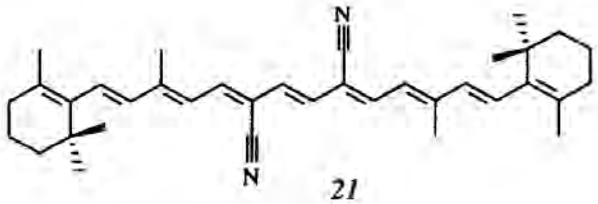


19

The relative configuration of jiocarotenoside A_1, a new norcarotenoid glycoside with *D*-quinovose as the sugar residue was resolved by XRD, as (+) *20*, [42]. Finally, in this section is included the structure of the carotenoid analogue *21* which has the cyclohexene ring antiperiplanar to the all-*trans* chain [43].



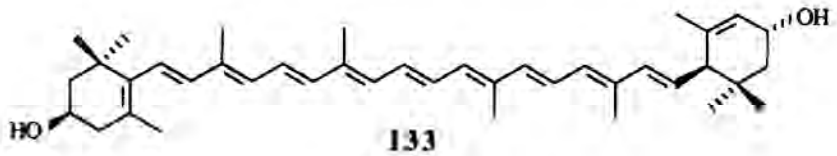
20



21

E. Concluding Remarks

The pioneering X-ray studies of carotenoids and related retinoid structures that were carried out in the late 1950s and continued in the following 15 years provided basic structural elements which are common to a great majority of these compounds. In 1963/64 there was a breakthrough in the application of new methods for solving the crystallographic phase problem [44, 45]; the methods were based on fundamental work that had been done nearly 15 years earlier [46, 47]. The strong development of these direct methods that began in the late 1960s and still continues has revolutionized the power of diffraction methods for the study of solid-state structures in a wide range of scientific fields. Carotenoid crystallography apparently was not much affected by the changes. There are several reasons for this. The typical carotenoid molecule consists of a conjugated chain with two terminal groups, which are often rings. The presence of bulky methyl groups along the chain and usually also in the end groups implies severe steric strain. This causes the chain to adopt a pronounced in-plane S-shape, as a rule also with out-of-plane twists, and rings and chain deviate significantly from coplanarity. A unit of such peculiar topology is not compatible with the requirements for efficient three-dimensional packing. In addition, the major, if not the total, contribution to intermolecular cohesion comes from weak van der Waals or dispersive forces. One consequence of this is a general inability of these compounds to form crystals. The crystals that have been grown are characterized by poor packing as reflected in large atomic displacement parameters, sometimes involving partial disorder, and in low calculated densities. Weak and unspecific intermolecular forces also provide the environment for a carotenoid with different, yet sufficiently similar, end groups to pack these end groups in a random fashion, as was reported for lutein (**133**) [23]. With problems of this type being the rule it is understandable that analyses of complete carotenoid structures remain a rarity. Instead, degradation products and synthons containing end group and a short chain segment have been studied, and proved adequate for resolving specific questions of conformation and chirality.



133

Modern crystallography offers several possibilities to advance the use of X-ray diffraction for studies of carotenoid structures. Some of these will be addressed in the following. The choice of solvent for crystallization can be important. Sometimes the medium will promote decisively the desired preference of one minimum-energy conformation over several others. Such directive properties of the solvent may be assessed from NMR studies of the compound in different solutions. The method has been used successfully in work involving crystallization of highly flexible molecules like oligosaccharides and oligonucleotides (A. Segre, personal communication).

From the accumulated knowledge of the crystallography of carotenoids, it is observed that the compounds containing oxygen functions, in particular carbonyl groups, are packed more densely and apparently also diffract a little better than the parent pure hydrocarbons. (One exception to this rule is α-APC [25] which has a rather unique mode of packing.) It is concluded that Coulomb attraction realized by the polar character of the C=O group may stabilize the crystal structure significantly. A similar, and even stronger, contribution may be effected by hydroxy groups through their ability to form hydrogen bonds. Therefore, if there is a choice, the carotenoid with oxygen-containing functional groups would be preferable for the X-ray study.

The large atomic displacements in carotenoids are usually both of a dynamic (thermal) and a static nature (disorder, defects). The diffraction study should be carried out at low temperature to reduce the contribution from thermal vibrations. With a gas-flow liquid nitrogen cryostat the temperature of the crystal can easily be reduced to 85 to 90 K, with a He cryostat to about 10 K. The effect of reduced temperature in X-ray studies of organic compounds is usually a remarkable increase both in quality and in the number of measurable intensities. This can improve greatly the final description of the structure model. The benefits of low temperature are clearly demonstrated in the two structure analyses of β,β-carotene (3) [8, 27].

Lack of crystals or of sufficiently large crystals of carotenoid compounds has limited the use of diffraction methods in the past. This problem has been greatly reduced with the advent of new and more powerful radiation sources, in particular the synchrotron sources. The beam from a wiggler device at a modern synchrotron facility has a brilliance about 10^8 times higher than that from a conventional X-ray tube. This enormous increase in beam 'intensity' has made crystals with dimensions < 10 μm amenable to diffraction studies. Some crystalline carotenoids are easily damaged in air or on exposure to light or X-rays. With synchrotron light and modern detectors available it is now possible to accumulate the necessary diffraction data in a very short time. Thus, with polychromatic radiation and position-sensitive area detectors several thousand reflections can be excited simultaneously in a protein crystal and recorded during exposure times of the order of 1 ms [48, 49]. Microcrystallography combined with the use of area detectors is expected to enhance very strongly the analytical power of crystallography in chemistry.

It was stated in Section B that the phases of the diffracted waves are generally lost in the X-ray diffraction experiment. When more than two beams are excited simultaneously, however, the beams will interact on passing through the crystal and, as a result, information on the parent phases can be transmitted and recorded, in a manner similar to a holographic

experiment. In the case of three interacting beams, the sum of the corresponding three phases can be estimated approximately from a careful mapping of the profile of the primary diffracted intensity in and close to the exact 3-beam diffraction situation. The phase signals which arise under multiple diffraction conditions are most easily observed with perfect crystals but can be significant for imperfect or mosaic (common) crystals as well. However, crystal mosaicity is a limiting factor, and increasing mosaic character tends to eliminate the phase signals. Triplet phases have been estimated even with crystals of very complex structures like proteins [50, 51, 52]. This new method for phase estimation, which is still in the development stage, suggests several interesting applications. It can be used to acquire a starting set of triplet phases to initiate a complete structure solution by other methods [53]. This may be very useful in special cases, for instance with molecules that show pseudo-translational symmetry, or with complex structures like proteins [54].

Another interesting field for application is the determination of absolute configuration. A phase ϕ_{hkl} for a non-centrosymmetric structure will be $-\phi_{hkl}$ for the inverted structure. Therefore, a triplet sum of phases Φ_3 which happens to be $+\pi/2$, will be $-\pi/2$ for the enantiomer structure. In practice, phase triplets with values calculated near $+\pi/2$ or $-\pi/2$ at the end of the refinement can be examined in a multiple diffraction experiment. Since the phase signature on the intensity profile is different for the two extreme cases $+\pi/2$ or $-\pi/2$, the absolute configuration can be established. This method, which does not require anomalous scattering, has been used successfully with at least one organic light-atom structure [55].

The two decades following the last edition of *Carotenoids* have seen a strong development in crystallography. The theory has been refined and extended. Experimental techniques have become more sophisticated and specialized to address specific problems, and new promising methods are under development. Last but not least, new and extremely powerful technology opens up for structure studies that were not feasible in the past. It appears that the tools for solving some of the solid-state structure problems in the carotenoid field now exist.

References

[1] B. C. L. Weedon, in *Carotenoids* (ed. O. Isler), p. 267, Birkhäuser, Basel (1971).
[2] J. M. Bijvoet, *Proc. Koninkl. Ned. Akad. Wetenschap.*, **B52**, 313 (1949).
[3] J. M. Bijvoet, A. F. Peerdeman and A. J. van Bommel, *Nature*, **168**, 271 (1951).
[4] *Int. Tables for Crystallography, Vol. C*, p. 219, Klüver, Dordrecht, Netherlands (1992).
[5] H. Hope and U. de la Camp, *Nature*, **221**, 54 (1969).
[6] J. W. Moncrief and S. P. Sims, *J. Chem. Soc., Chem. Commun.*, **1969**, 914.
[7] D. W. Engel, *Acta Crystallogr.*, **B28**, 1496 (1972).
[8] C. Sterling, *Acta Crystallogr.*, **17**, 1224 (1964).
[9] C. Sterling, *Acta Crystallogr.*, **17**, 500 (1964).
[10] W. G. Sly, *Acta Crystallogr.*, **17**, 511 ((1964).
[11] J. C. J. Bart and C. H. MacGillavry, *Acta Crystallogr.*, **B24**, 1587 (1968).
[12] J. C. J. Bart and C. H. MacGillavry, *Acta Crystallogr.*, **B24**, 1569 (1968).
[13] C. A. Coulson, *J. Chem. Phys.*, **7**, 1069 (1939).
[14] R. E. Peierls, in *Quantum Theory of Solids*, p. 108, Clarendon Press, Oxford (1955).

[15] H. Labhart, *J. Chem. Phys.*, **27**, 957 (1957).
[16] Y. Ooshika, *J. Phys. Soc. Jpn.*, **12**, 1246 (1957).
[17] H. C. Longuet-Higgins and L. Salem, *Proc. Roy. Soc.*, **A251**, 172 (1959).
[18] V. Schomaker and K. N. Trueblood, *Acta Crystallogr.*, **B24**, 63 (1968).
[19] M. Sundaralingam and C. Beddell, *Proc. Nat. Acad. Sci. USA*, **69**, 1569 (1972).
[20] B. Koch, *Acta Crystallogr.*, **B28**, 1151 (1972).
[21] R. Bucourt and D. Hainaut, *Bull. Soc. Chim. Fr.*, **12**, 4562 (1967).
[22] I. Ueda and W. Nowacki, *Z. Kristallogr.*, **140**, 190 (1974).
[23] G. P. Moss, *Pure Appl. Chem.*, **51**, 507 (1979).
[24] T. E. DeVille, M. B. Hursthouse, S. W. Russell and B. C. L. Weedon, *J. Chem. Soc., Chem. Commun.*, **1969**, 1311.
[25] G. Drikos, H. Dietrich and H. Rüppel, *Eur. Biophys. J.*, **16**, 193 (1988).
[26] C. H. Stam, *Acta Crystallogr.*, **B28**, 2936 (1972).
[27] M. O. Senge, H. Hope and K. M. Smith, *Z. Naturforsch.* **47c**, 474 (1992).
[28] J. Hjortås, *Acta Crystallogr.*, **B28**, 2252 (1972).
[29] T. F. Koetzle, M. S. Lehmann, J. J. Verbist and W. C. Hamilton, *Acta Crystallogr.*, **B28**, 3207 (1972).
[30] G. M. Brown and H. A. Levy, *Acta Crystallogr.*, **B29**, 790 (1973).
[31] J.-M. Lehn, J.-P. Vigneron, I. Bkouche-Waksman, J. Guilhem and C. Pascard, *Helv. Chim. Acta*, **75**, 1069 (1992).
[32] T. E. DeVille, M. B. Hursthouse, S. W. Russell and B. C. L. Weedon, *J. Chem. Soc., Chem. Commun.*, **1969**, 754.
[33] E. Widmer, R. Zell, T. Lukác, M. Casadei, P. Schönholzer and E. A. Broger, *Helv. Chim. Acta*, **64**, 2405 (1981).
[34] R. Zell, E. Widmer, T. Lukác, H. G. W. Leuenberger, P. Schönholzer and E. A. Broger, *Helv. Chim. Acta*, **64**, 2447 (1981).
[35] M. Acemoglu, R. Prewo, J. H. Bieri and C. H. Eugster, *Helv. Chim. Acta*, **67**, 175 (1984).
[36] R. Buchecker, U. Marti and C. H. Eugster, *Helv. Chim. Acta*, **67**, 2043 (1984).
[37] A. Haag, W. Eschenmoser and C. H. Eugster, *Helv. Chim. Acta*, **63**, 10 (1980).
[38] P. Uebelhart, A. Baumeler, A. Haag, R. Prewo, J. H. Bieri and C. H. Eugster, *Helv. Chim. Acta*, **69**, 816 (1986).
[39] M. Ito, Y. Hirata, K. Tsukida, N. Tanaka, K. Hamada, R. Hino and T. Fujiwara, *Chem. Pharm. Bull. Jpn.*, **36**, 3328 (1988).
[40] D. J. Buschor and C. H. Eugster, *Helv. Chim. Acta*, **73**, 1002 (1990).
[41] M. P. Gmünder and C. H. Eugster, *Helv. Chim. Acta*, **73**, 1954 (1990).
[42] H. Sasaki, H. Nishimura, T. Morota, T. Katsuhara, M. Chin and H. Mitsuhashi, *Phytochem.*, **30**, 1639 (1991).
[43] P. B. Braun, J. Hornstra and J. I. Leenhouts, *Acta Crystallogr.*, **B27**, 90 (1971).
[44] I. L. Karle and J. Karle, *Acta Crystallogr.*, **16**, 969 (1963).
[45] I. L. Karle and J. Karle, *Acta Crystallogr.*, **17**, 835 (1964).
[46] J. Karle and H. Hauptman, *Acta Crystallogr.*, **3**, 181 (1950).
[47] H. Hauptman and J. Karle, *The Solution of the Phase Problem. I. The Centrosymmetric Crystal.* ACA Monograph No. 3, Polycrystal Book Service, New York (1953).
[48] H. D. Bartunik, in *Handbook on Synchrotron Radiation, Vol. 4* (ed. S. Ebashi, M. Koch and E. Rubenstein), p. 147, North-Holland, Amsterdam (1991).
[49] E. F. Pai, *Current Opinion in Struct. Biol.*, **2**, 821 (1992).
[50] K. Hümmer, W. Schwegle and E. Weckert, *Acta Crystallogr.*, **A47**, 60 (1991).
[51] S. L. Chang, H. E. King, Jr., M. T. Huang and Y. Gao, *Phys. Rev. Lett.*, **67**, 3113 (1991).

[52] E. Weckert, W. Schwegle, I. Bauscher, F. Edler and K. Hümmer, *Abstr. 14th Eur. Crystallogr. Meeting*, Enschede (*ECM-14*), 1992, p. 258.
[53] F. Mo, B. C. Hauback and G. Thorkildsen, *Acta Chem. Scand.*, **A42**, 130 (1988).
[54] F. Mo and R. Mathiesen, *Abstr. 14th Eur. Crystallogr. Meeting*, Enschede (*ECM-14*), 1992, p. 244.
[55] H. Burzlaff, K. Hümmer, W. Rothammel, G. Schäfer, E. Weckert, H. J. Bestmann and D. Roth, *Acta Crystallogr.*, **B45**, 303 (1989).

Carotenoids
Volume 1 B: Spectroscopy
© 1995 Birkhäuser Verlag Basel

Chapter 9

Combined Approach: Identification and Structure Elucidation of Carotenoids

Synnøve Liaaen-Jensen

A. Introduction

The identification of a known, naturally occurring carotenoid, or the elucidation of the structure of a previously unknown carotenoid, requires the application of a variety of physical and chemical methods. Details of these methods are presented in other Chapters of this book. In this Chapter, a brief outline of the structural information that can be obtained from each method is given, but the main objective is to show, with examples, how the combined application of all the methods leads to the elucidation of a carotenoid structure. The appropriate Chapters in Vol 1A and 1B should be consulted for details of each method and its application. Note: The term 'structure' includes full details of stereochemistry. If the stereochemistry is not established, the term 'constitution' should be used.

B. Polarity: Evidence from Chromatography

Chromatographic purification is an essential step that precedes characterization of an unknown carotenoid. Chromatographic behaviour, preferably in two different systems by TLC and/or HPLC, provides information about the polarity of the carotenoid in question relative to one or more carotenoids of known structure, so that tentative assignment as a carotene, monool, diol or more polar carotenoid may be made. Partition data provide supplementary information on polarity.

As hydrocarbons, carotenes are non-polar. Increasing polarity may be attributed to the presence of oxygen functions, the strongest influence being from hydroxy groups, glycosyl groups, acidic functions such as carboxy groups, enolized α-diketones or β-diketones, phenols or ionized functions such as sulphate.

The presence of acidic functions may be revealed by strong adsorption on alkaline adsorbents *e.g.* alumina, and by hypophasic behaviour upon partition at alkaline pH.

C. Spectroscopic Data

The application of spectroscopic methods is imperative for identification and structure elucidation. Detailed treatment of each spectroscopic technique is given in this Volume. In the following Section the key information provided by each method will be summarized. The methods are treated in the order recommended to give maximum information from a limited sample. One or more tentative identifications can usually be made from the UV/Vis spectrum and mass spectrum, together with chromatographic evidence of relative polarity. The *Key to Carotenoids* [1] and the Appendix (Vol. 1A, Chapter 8) should then be consulted to see if any of these structures have been reported previously. Co-chromatography with authentic samples is then essential to substantiate the tentative identification. The identification is confirmed by MS fragmentation pattern, NMR, IR, and CD spectra, in comparison with published data or with data obtained from an authentic standard.

1. Key information provided

a) UV/Vis spectra

The UV/Vis spectrum of a carotenoid is always examined first, since it provides useful information about the chromophore present.

Thus the number of conjugated C=C double bonds in an aliphatic, monocyclic or dicyclic carotenoid may be assigned from the position of the λ_{max} (usually three) of the main absorption band in a common solvent and by consideration of the spectral fine structure. Conjugated carbonyl functions normally cause bathochromic shifts and reduced spectral fine structure, *i.e.* rounded spectral shape, particularly in methanol or ethanol. Reduction with complex metal hydrides serves to reduce carbonyl functions so that the polyene chromophore can be identified.

A UV/Vis spectrum of good quality can easily be obtained from 1 to 2 μg of isolated carotenoid. During HPLC with photodiode-array detection, an acceptable spectrum can be obtained on-line from as little as a few nanograms of carotenoid.

For any carotenoid, *cis* isomers usually show characteristic hypsochromic shifts of the main absorption bands and a *cis*-peak appears at *ca.* 142 nm lower wavelength, in hexane, than the λ_{max} at longest wavelength for the all-*trans* isomer. A double *cis*-peak is compatible with an aliphatic or monocyclic chromophore. The relative intensity of the *cis*-peak is greatest when the *cis* double bond is located at or near the centre of the chromophore.

If the UV/Vis spectrum indicates a *cis* isomer, I_2-catalysed stereomutation may serve to identify the parent all-*trans* isomer at an early stage. However, *cis* isomers are frequently produced as artifacts during isolation.

b) Mass spectra

The most important information obtained from the MS is the molecular mass of the carotenoid, provided the molecular ion is unequivocally identified. Most carotenoids provide molecular ions upon electron impact. Suspected glycosides (very high polarity) should be methylated or acetylated in order to increase their volatility. Characteristic fragmentations, *e.g.* M–92, M–106, serve to confirm the identification of the molecular ion and to give information about the functional groups present. Losses characteristic of particular functional groups, *e.g.* 18 mass units (water) from alcohols, 32 mass units (methanol) from methyl ethers, serve to identify the functional groups. Confirmation is obtained from the changes in molecular mass following derivatization, *e.g.* an increase of 42 mass units for acetylation of a hydroxy group. High-precision measurement gives the elementary composition of the molecular ion and fragment ions.

Sample requirements for MS are small. A routine spectrum can be obtained from only a few μg of pure compound, though a somewhat larger sample may be required for high-precision measurements.

c) ^{1}H-NMR and ^{13}C-NMR spectra

NMR is the most powerful technique for structure elucidation. The ^{1}H-NMR spectrum serves to identify the structural surroundings of each hydrogen atom in the carotenoid. ^{13}C-NMR spectra require more sample and serve to identify the type of each carbon atom (sp^3, sp^2, sp) and its structural surroundings.

Thus NMR spectra substantiate the identification of a known carotenoid, and are essential in the structure elucidation of a new carotenoid. Detailed ^{1}H-NMR and ^{13}C-NMR analysis may prove a carotenoid structure beyond doubt, including the geometry of carbon–carbon double bonds and relative stereochemistry. A routine ^{1}H-NMR spectrum requires about 100 to 200 μg sample, a ^{13}C spectrum 0.5 to 1 mg, but more material is needed for some sophisticated 2-dimensional methods.

d) IR spectra

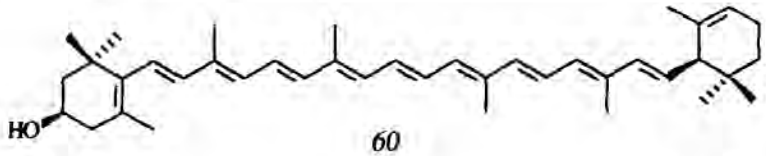
IR spectra are useful for revealing the presence of particular functional groups such as allene, acetylene, various types of carbonyl functions, or sulphate.

The commonly used KBr disc method requires around 0.2 mg sample which may be recovered by solvent extraction immediately after the spectrum is recorded.

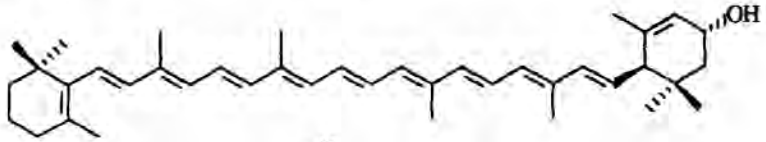
e) CD spectra

Since the CD properties of several carotenoids of established chirality are known, comparative CD spectroscopy may provide information about the absolute configuration of other chiral carotenoids. In this context CD is particularly useful for chiral carotenoids with conjugated β rings. Thus discrimination between, for example, β,ε-caroten-3-ol (**60**) and β,ε-

caroten-3'-ol (**62**) is possible from the Cotton effect, because the 3'-OH group in the ε ring does not contribute significantly to the CD.



60



62

In other carotenoids with several chiral centres, not every centre may contribute to the CD spectrum. Consideration of ^{1}H-NMR spectra may give the relative configuration, and the CD of the carotenoid in comparison with that of relevant model carotenoids of known chirality is then used to establish the absolute configuration.

For CD spectra, the carotenoids used must be devoid of contaminating geometrical isomers. The sample requirement is low (5 to 50 μg), but CD facilities are not so commonly available.

D. Chemical Derivatization

1. Key information obtained

Chemical derivatization is used to confirm the presence of certain functional groups or structural elements in carotenoids. The reactions may be carried out on the μg scale, and the products characterized by chromatography and spectroscopy (Vol. 1A, Chapter 4).

The following functional groups are particularly amenable to derivatizations:

i) Carotenol esters: Alkaline hydrolysis provides the free carotenol, which has unchanged UV/Vis spectrum but higher polarity.

ii) Hydroxy groups: Primary or secondary hydroxy groups are readily acetylated, silylated or methylated. Tertiary hydroxy groups are not acetylated under standard conditions, but are readily silylated. These derivatives are less polar than the parent carotenol, but exhibit the same UV/Vis spectra.

iii) Conjugated carbonyl groups: Reduction with complex metal hydrides provides a primary or secondary carotenol with shorter chromophore and higher polarity.

iv) 5,6-Epoxides: In the presence of acid these undergo rearrangement to the 5,8-epoxide (furanoid) with a shorter chromophore.

Tests (iii) and (iv) can be carried out in a spectrophotometer cuvette, and changes in the UV/Vis spectrum followed directly. In all cases, changes in molecular mass resulting from derivatization can be determined by MS, thus confirming, for example, the number of primary and secondary hydroxy groups in the carotenoid.

E. Recommended Procedure

1. Identification

For identification, the three minimum criteria, *i.e.* co-chromatography with an authentic sample, UV/Vis spectrum, and mass spectrum of a quality that allows identification of the molecular ion, must be fulfilled.

If these criteria are only partly met, a term such as 'zeaxanthin-like' is recommended.

Additional spectroscopic criteria which strengthen the identification are then: (i) detailed MS fragmentation, (ii) ^{1}H-NMR, (iii) ^{13}C-NMR, (iv) IR (if special functional groups are present) and (v) CD (for chiral carotenoids).

Chemical derivatizations on the micro scale may provide additional support.

For secondary carotenols the optical purity should in special cases be determined by the camphanate [2] or carbamate [3] methods (Vol. 1A, Chapter 4) or by chromatographic separation on chiral adsorbents (Vol. 1A, Chapter 6, Part IV).

2. Structure elucidation

Modern methodology permits the structure elucidation of any natural carotenoid by a combination of these physical and chemical methods. All structural information provided by each spectroscopic method must be carefully evaluated, and chemical derivatizations are recommended to provide supporting evidence.

The available amount of pure sample is usually the limiting factor in the structure elucidation of a new, naturally occurring carotenoid.

A recommended general approach on the 0.1 to 3 mg scale is as follows.

i) Identification of the chromophore from the UV/Vis spectrum.

ii) Estimation of the polarity from chromatographic behaviour.

iii) Determination of the molecular mass by MS. *N.B.* Not all carotenoids are C_{40} compounds. High-resolution peak matching of $M^{+\cdot}$ is undertaken, if possible, to establish the molecular formula. From the number of oxygen atoms and the chromatographic polarity, an indication of the functional groups present is obtained. From the molecular formula, the number of double-bond equivalents in the molecule is obtained. As a reference, $C_n H_{2n+2} O_x$ corresponds to a saturated aliphatic structure. By making allowance for the number of conjugated double bonds in the chromophore, the number of rings plus isolated double bonds can be calculated. The shape of the UV/Vis spectrum may confirm the presence of cyclic end groups.

iv) Identification of functional groups. The MS fragmentation pattern will indicate the presence of functional groups such as hydroxyl, acetate, methoxyl, 5,6-epoxide. Peak matching is preferable to confirm the conclusions. The presence of some functional groups, *e.g.* OH, C=O, is also shown by IR spectroscopy, which is particularly useful for identifying the presence of acetylenic and allenic groups. Derivatization or chemical reactions can be used to confirm the presence of hydroxy or carbonyl groups, 5,6-epoxy groups or esters.

v) At this stage, plausible structures may be drawn. The *Key to Carotenoids* [1] and the Appendix (Vol. 1A, Chapter 8) should be checked to see if any of these plausible structures have been described previously.

vi) Detailed structural analysis is undertaken by ^{1}H-NMR and ^{13}C-NMR, including 2D COSY and DEPT, and special NMR techniques, including TOCSY, are applied when appropriate. This study should establish the constitution of the carotenoid unequivocally.

vii) The stereochemistry is determined. The geometrical configuration of double bonds is established from the UV/Vis spectrum and by ^{1}H-NMR. The chirality is established by ^{1}H-NMR, including 2D ROESY, and by CD correlations.

viii) As a final step, the structure may be confirmed by unambiguous synthesis.

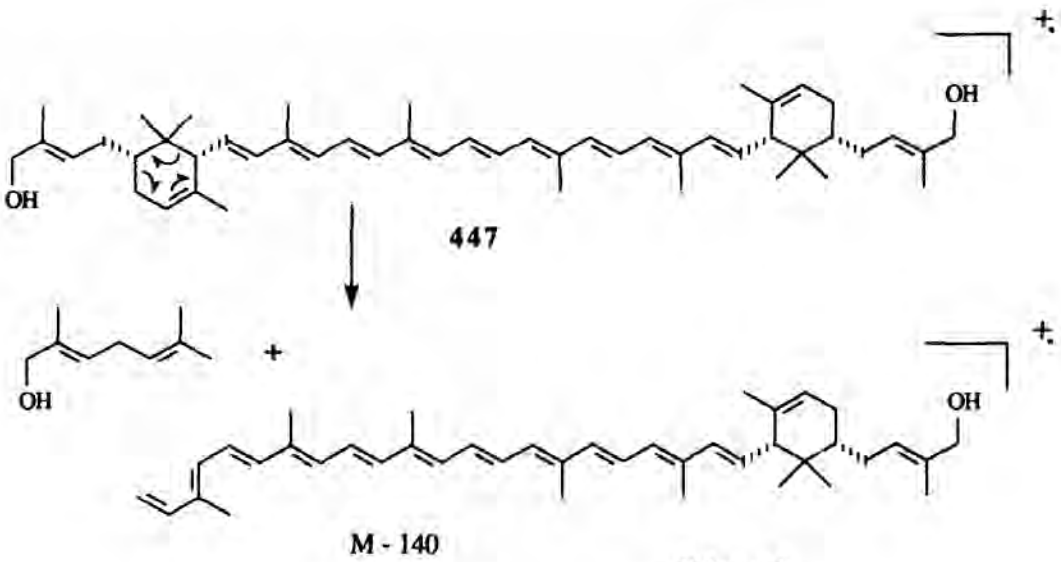
F. Examples of Structure Elucidation

Following the above outline of the information available from each of the essential methods, and the general strategy recommended, the application of this combined approach is now illustrated by some selected examples from the author's laboratory. Emphasis is placed on the key information that led to the breakthrough in each structure elucidation. The oldest example dates back to 1965 and the others follow in chronological order. Although in the two earliest cases the methods available were limited, such limitations may still apply in many laboratories where all modern facilities are not readily available. The historical aspect also demonstrates how the field has progressed. Further details may be obtained from the original literature cited.

1. Decaprenoxanthin (C_{50})

Decaprenoxanthin (**447**, first designated *dehydrogenans*-P439) was the first naturally occurring C_{50} carotenoid encountered [4]. The unexpected C_{50} structure was clearly revealed by MS. It was natural first to consider a linearly extended head-to-tail coupled skeleton of ten isoprene units, but characteristic *retro*-Diels-Alder fragmentation upon electron impact, resulting in a loss of 140 mass units from the molecular ion, provided the clue to the C_5 substitution at C-2 and C-2' (Scheme 1).

The aliphatic nonaene chromophore and the symmetrical structure were clear from UV/Vis and ^{1}H-NMR data, respectively [4-6].



Scheme 1

Acetylation to a diacetate and allylic oxidation to a monoaldehyde and dialdehyde [5, 6] showed the two oxygen functions to be primary, allylic hydroxy groups, separated from the polyene chain. The *E* configuration of the C_5 substituent followed from ^{1}H-NMR data of the dialdehyde [7]. Subsequently, in 1975, the chiral assignment 2*R*,6*R*,2'*R*,6'*R* with 2,6 (2',6')-*cis*-configuration was made by comparison of ^{1}H-NMR and CD data with those of (2*S*,2'*S*)-dimethyl-ε,ε-carotene (C_{42}) obtained by total synthesis [8].

The structure was later confirmed when other research groups synthesized first the optically inactive decaprenoxanthin models with 2,6-*trans* and 2',6'-*trans* geometry [9] and subsequently the racemic (2,6-*cis*, 2',6'-*cis*)-decaprenoxanthin (**447**) [10].

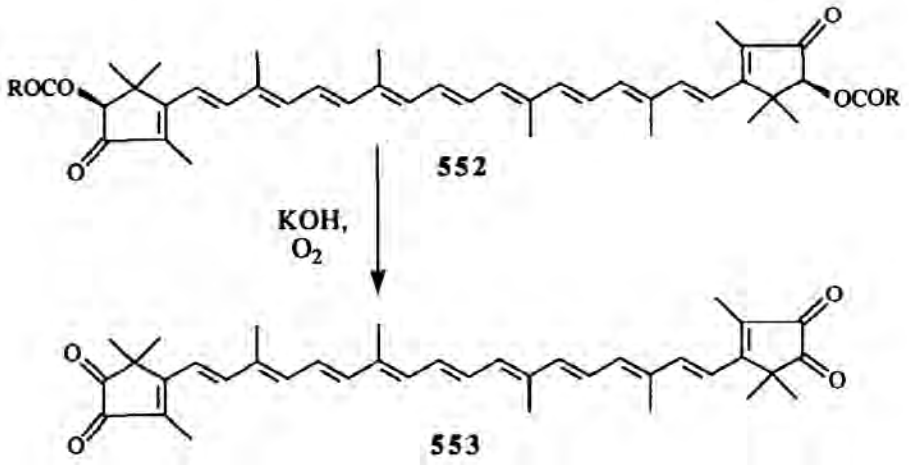
2. Actinioerythrin (C_{38})

Actinioerythrin (**552**), a pigment known since the classical period, was shown in 1969 to be a natural diester of the 2,2'-dinor-α-ketol actinioerythrol [11] (Scheme 2).

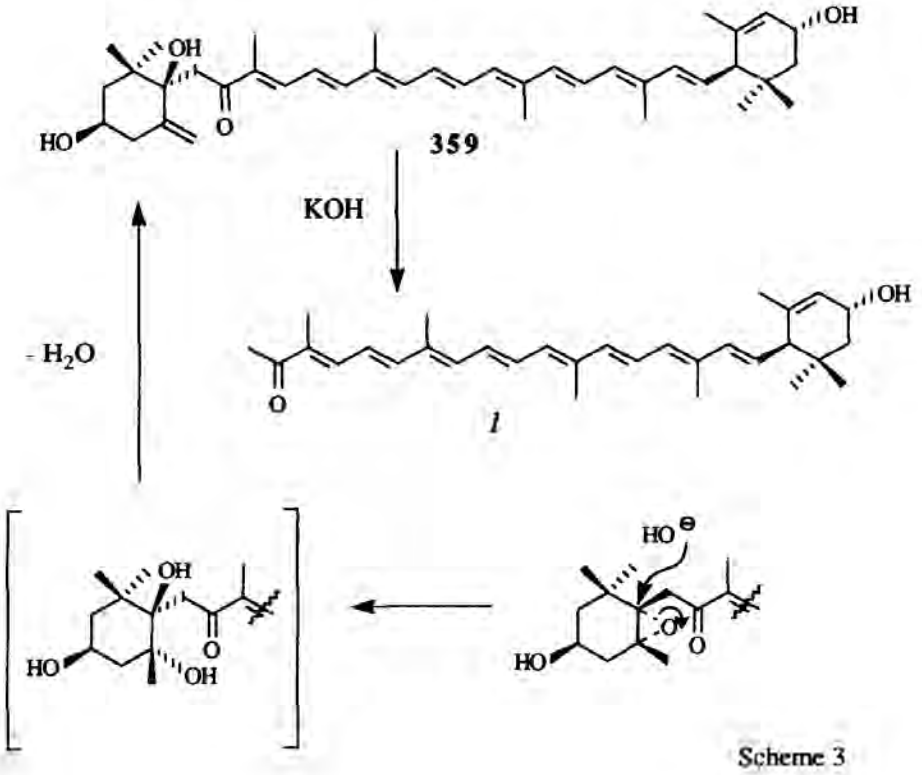
A key feature was the reaction with alkali, which yielded violerythin (**553**), the striking blue colour of which could be associated with the cyclopentenedione structural elements in conjugation with the polyene chain. Detailed chemical derivatizations and MS fragmentation patterns were consistent with the structure assigned [11].

A mixture of fatty acids was released by alkaline hydrolysis, and these were identified by GC of their methyl esters [12].

The chirality could not be determined by CD spectroscopy of actinioerythrin itself, but followed in 1978 by CD correlation with synthetic (3*S*,3'*S*)-actinioerythrol diacetate [13].



Scheme 2



Scheme 3

3. Prasinoxanthin (C_{40})

A more recent example (1983) of a new C_{40} carotenoid is prasinoxanthin (**359**) [14, 15].

Retro-aldol cleavage in the presence of alkali to give the methyl ketone micronone (*1*), Scheme 3, was compatible with the β-hydroxyketone structure assigned. The unusual γ end group was presumed to be formed biosynthetically from a 5,6-epoxy-8-keto-β end group as illustrated in Scheme 3. Indeed, the hypothetical intermediate has recently been isolated from other prasinoxanthin-producing microalgae [16].

Detailed spectroscopic characterization (UV/Vis, MS, IR, 2D ^{1}H-NMR and CD) and chemical derivatization were consistent with the structure assigned. The 3,6-*cis* configuration revealed by NMR [15] for the two hydroxy groups in the γ ring is consistent with a modified biosynthetic route [16] (Scheme 3).

4. Bastaxanthin (carotenoid sulphate)

Bastaxanthin *c* (**420**) was the first carotenoid sulphate to be characterized, in 1983 [17], Scheme 4. The general characterization of carotenoid sulphates and the isolation of bastaxanthin are described in Vol. 1A, Chapter 7, Example 11.

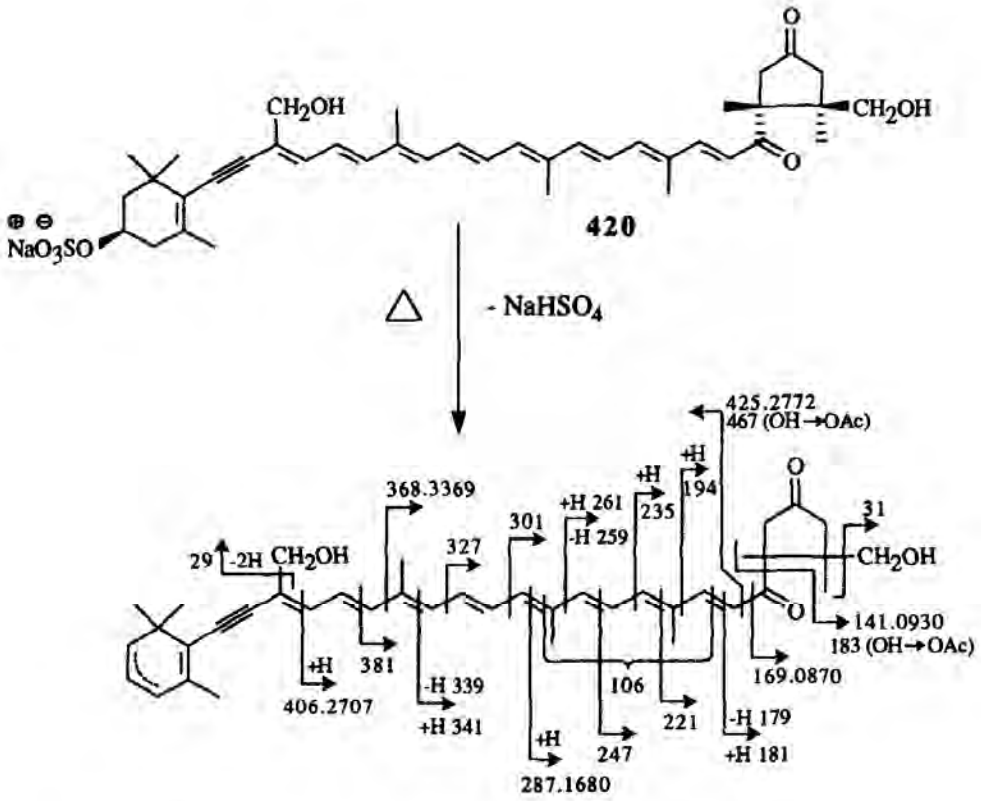
Recognition of the sulphate function was not straightforward. By EI-MS an apparent molecular ion at *m/z* 594.3709, compatible with $C_{40}H_{50}O_4$, was obtained. Only when the nature of the four oxygen functions was established did it become obvious that another functional group, not evident from MS and ^{1}H-NMR spectra, had to be present in order to account for the high polarity of bastaxanthin. In this case IR absorption at 1240 cm^{-1} for sulphate offered the clue. The apparent molecular ion seen in the mass spectrum corresponded to a thermal elimination product (Scheme 4).

Detailed spectroscopic studies (UV/Vis, IR, ^{1}H-NMR, ^{13}C-NMR, CD and MS) of bastaxanthin c and of several derivatives desulphated by enzymic hydrolysis provided the basis for assignment of the 3,19,17'-trihydroxy-7,8-didehydro-β,κ-carotene-3',6'-dione 3-sulphate structure (**420**).

The presence of a disubstituted triple bond followed from IR absorption at 2170 cm^{-1} (KBr) and ^{13}C-NMR signals at δ 91.7 and 98.1 ppm (in CD_3OD). The UV/Vis spectra of natural bastaxanthin, and of its reduction product with $NaBH_4$ and allylic oxidation product with NiO_2 were consistent with the monocyclic enyn-octaenone chromophore assigned. Location of the allylic primary hydroxy group at C-19 followed from ^{1}H-NMR, ^{13}C-NMR and MS data and was compatible with the ease of isomerization to 9-*cis*.

Allocation of the 3'-keto function to a cyclopentanone ring and of the second hydroxy function at C-17' rested on IR (1735 cm^{-1}), ^{1}H-NMR and ^{13}C-NMR data and chemical derivatizations. The acidic character of the four α-hydrogen atoms at C-2' and C-4' caused facile deuterium exchange of these protons.

The absolute configuration of the three chiral centres was discussed and the evidence considered to be in favour of the 3*R*,1'*R*,5'*R* configuration [17].



Scheme 4

5. P457 (glycoside)

This final example illustrates the latest state of the art. This compound was first partly characterized in 1974 [18], and subsequently further examined [19, 20], but improved isolation procedure and advanced NMR techniques were required to solve the structure, 13'-*cis*-7',8'-dihydroneoxanthin-20'-al 3'-β-D-lactoside (**280.1**) [21, 22], Scheme 5.

Even after acetylation this disaccharide derivative did not provide a molecular ion by EI-MS. Eventually molecular ions were obtained for the nonamethyl ether by EI-MS and for the octaacetate by FAB-MS.

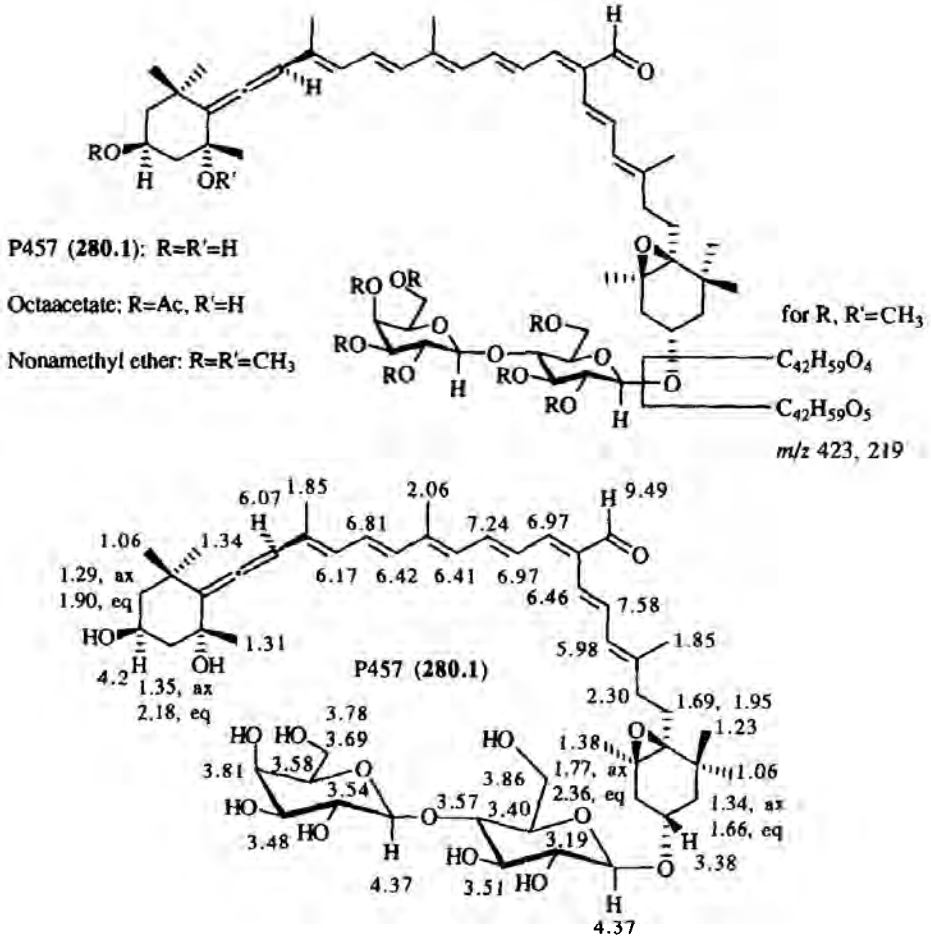
The sugar entity of P457 was shown to consist of glucose and galactose in a 1:1 ratio by acidic methanolysis followed by GLC analysis of the silylated methyl glycosides. This finding was consistent with subsequent ^{1}H-NMR assigments as a β-D-lactoside.

The cross-conjugated 20'-al structure was recognized early [18] from UV/Vis and ^{1}H-NMR data in comparison with related carotenals and from the result of $LiAlH_4$ reduction. The 13'-*cis* configuration is thermodynamically favoured for such carotenals.

Whereas the allenic end group was readily revealed by ^{1}H-NMR (allenic H at δ 6.07 *ppm*) and IR (1931 cm^{-1}), the second end group caused more difficulties. However, from consideration of the molecular formula and the other structural elements, the presence of an epoxidic end group with a saturated C(7')–C(8') bond was inferred. Confirmation of this was obtained by detailed NMR studies of P457 itself (see Chapter 5) [21, 23].

If the usual Δ7' double bond had been present the structure determination would have been considerably simplified, because an epoxide–furanoid rearrangement would have been seen on treatment with weak acid.

Whereas the relative configuration of the allenic end group was, according to NMR data, the same as for other allenic carotenoids, the chirality of the epoxidic end group was suggested tentatively from biosynthetic analogy, and has recently been confirmed by synthesis of a model compound [22, 24].



Scheme 5

References

[1] O. Straub, *Key to Carotenoids, 2nd Edition* (ed. H. Pfander), Birkhäuser, Basel (1987).
[2] M. Vecchi and R. K. Müller, *J. High Res. Chromatogr., Chromatogr. Commun.*, **2**, 195 (1972).
[3] A. Rüttimann, K. Schiedt and M. Vecchi, *J. High Res. Chromatogr., Chromatogr. Commun.*, **6**, 612 (1983).
[4] S. Liaaen-Jensen and O. B. Weeks, *Tidskr. Kjemi Bergv., Metallurgi*, **26**, 130 (1966).
[5] S. Liaaen-Jensen, *Acta Chem. Scand.*, **21**, 1972 (1967).
[6] S. Liaaen-Jensen, S. Hertzberg, O. B. Weeks and U. Schwieter, *Acta Chem. Scand.*, **22**, 1171 (1968).
[7] U. Schwieter and S. Liaaen-Jensen, *Acta Chem. Scand.*, **23**, 1057 (1969).
[8] A. G. Andrewes, S. Liaaen-Jensen and O. B. Weeks, *Acta Chem. Scand.*, **B29**, 884 (1975).
[9] A. K. Chopra, B. P. S. Khambay, H. Madden, G. P. Moss and B. C. L. Weedon, *J. Chem. Soc., Chem. Commun.*, **1977**, 357.
[10] J. P. Ferezou and M. Julia, *Tetrahedron*, **41**, 1277 (1985).
[11] S. Hertzberg, S. Liaaen-Jensen, C. Enzell and G. W. Francis, *Acta Chem. Scand.*, **23**, 3290 (1969).
[12] B. Renstrøm and S. Liaaen-Jensen, *Comp. Biochem. Physiol.*, **69B**, 625 (1981).
[13] R. K. Müller, H. J. Mayer, K. Noack, J. P. Daly, J. P. Tauber and S. Liaaen-Jensen, *Helv. Chim. Acta*, **61**, 2881 (1978).
[14] P. Foss, R. R. L. Guillard and S. Liaaen-Jensen, *Phytochem.*, **23**, 1629 (1984).
[15] P. Foss, T. Skjetne and S. Liaaen-Jensen, *Acta Chem. Scand.*, **B40**, 172 (1986).
[16] E. S. Egeland and S. Liaaen-Jensen, unpublished work.
[17] S. Hertzberg, T. Ramdahl, J. E. Johansen and S. Liaaen-Jensen, *Acta Chem. Scand.*, **B37**, 267 (1983).
[18] J. E. Johansen, W. A. Svec, S. Liaaen-Jensen and F. T. Haxo, *Phytochem.*, **13**, 2261 (1974).
[19] T. Skjenstad, F. T. Haxo and S. Liaaen-Jensen, *Biochem. Syst. Ecol.*, **12**, 149 (1984).
[20] A. G. Andrewes and S. Liaaen-Jensen, *Abstr. 7th Int. Symp. Carotenoids*, Munich, 1984, P39.
[21] G. Englert, *Pure Appl. Chem.*, **63**, 59 (1991).
[22] T. Aakermann, R. R. L. Guillard and S. Liaaen-Jensen, *Acta Chem. Scand.*, **47**, 1207 (1993).
[23] G. Englert, T. Aakermann, K. Schiedt and S. Liaaen-Jensen, *Magn. Res. Chem.*, in preparation.
[24] T. Aakermann and S. Liaaen-Jensen, *Abstr. 10th Int. Symp. on Carotenoids*, Trondheim, 1993, P2-1.

Index

Absorbance A 16, 119
Absorption 2, 6
  coefficient ($A^{1\%}_{1\,cm}$) 13, 56
  coefficient, molar (ε_{mol}) 56, 74
  intensity of see Absorbance
  maximum, wavelength of (λ_{max}) 16
Absorption band 117
  lowest energy 9
  main 16
Absorptivity (ε_{mol}) 56
Abundance ratio ($R = I_{M\cdot92}/I_{M\cdot106}$) 280, 281, 283
Additivity rule 67, 93, 94, 97, 105
Angle of rotation α 63
Anisotropy
  diamagnetic 148
  effect 210, 211, 220
$2\,^1A_g$ state 8, 9, 12
Asymmetric carbon atom 64
Atomic displacement parameters (adps) 326, 327
  anisotropic 331, 333
  isotropic 331
Atomic scattering factor 323
Axis of rotation 65

Baseline, instability of (CD) 74
Beer-Lambert law 13, 56, 119
Bloch-Siegert shift 225
Bond
  alternation of length 2, 326
  angles 2, 117, 323
  length 323, 331
  order 137
  stretching of 117

C.d.b. = number of conjugated double bonds 18
Carotenoprotein 44
CE = Charge-exchange 274, 276
Chain length 18
Chemical shift
  dispersion of 147
  difference of 148
Chirality 63
  chiral molecules 63, 65
  chiral environment 63
  chiral light 63
Chromophore 13, 17, 18
  inherently chiral 67
  intrinsically achiral 67
  intrinsically chiral 65
CI = Chemical ionization 262, 265, 274
Circular dichroism (CD) Chapter 3, 63, 66
cis-Band see *cis*-Peak
cis-Isomers 162, 211, 220, 222
cis-Peak 9, 15, 20, 21,99
  double 21
  intensity of (% A_B/A_{II} or % D_B/D_{II}) 21, 22
Concentration, sample
  CD 105
  IR 119
  Raman 136, 138, 139
  NMR 162
Configuration
  absolute 66, 71, 74, 80, 81,82, 162, 323, 324, 335
  relative 335
Conformation 9, 23, 45, 67, 68, 70, 76, 80
  boat 90
  chair 87
  flexibility of 91
  equilibrium 68, 73, 76, 79, 80, 84, 92, 105
  gauche (s-*cis*) 326, 331
  half-chair 67, 80, 326, 331
  heterogeneity of 11
  'sofa' 326, 327
  S-shape 326, 332, 338
  twisted 69
  rule 80
  s-*cis* 3, 67, 68, 69, 70, 71
  s-*trans* 3, 67, 68, 69, 70, 71
Conjugated backbone, distortion of 137
Conservative CD spectra 67, 76, 81, 90, 91, 92, 96, 97
Contamination 138, 271
Continuous wave (CW) NMR spectroscopy 151
Coplanarity 23, 25, 27, 31, 67

COSY: ^{1}H, ^{13}C-correlated = Heteronuclear
2D spectroscopy 251
^{13}C-detected ^{1}H, ^{13}C-COSY 251
^{1}H-detected ^{1}H, ^{13}C-COSY 252
inverse 252
reverse 252
COSY: ^{1}H, ^{1}H-correlated = Homonuclear
2D spectroscopy 149, 237, 239
absolute value 241, 247
intensity contour plot 241
long-range 241
magnitude 241
phase-sensitive 241
pulse sequence of 241
Cotton effect 80, 81, 82, 83, 87, 88, 90, 91, 92, 96, 102
Coulomb
interaction 333
attraction 339
Coupling 199
across single bond 209
in 6-membered ring 162
$^1J_{CH}$ 248, 249
strong 149
vicinal J_{HH} 149, 209, 220
weak 148
Cross peaks 241, 242, 245, 246, 248
fine structure of 241
folded 242
regular 242, 245
Crystal
density of 333
formation of 338
unit cell 321
van der Waals forces 338
Crystallinity 322

DANTE pulse sequence 232, 236
DCI = Desorption chemical ionization 269
Degradation products 138
DEPT = Distortionless enhancement by polarization
transfer 249
Detection
Raman 137
selective (IR) 118
thermal (IR) 118
UV/Vis 14
X-ray 322
Deuterium labelling 278, 280, 281, 288, 305
Diamagnetic anisotropy effect 210
Diastereoisomers (Diastereomers) 163
Diffraction
intensity 321
maxima 321
pattern 321
Dispersion 63
Double-focusing mass spectrometer 271
Double-INDOR-Difference (DID) 225

EI = Electron impact 262, 274
Electrospray 271
Electron
density 321
transfer 263
π-Electrons, delocalized 2
Electronic configuration 3
ground state configuration ($1\,^1A_g$) 5
lowest-energy excited state ($1\,^1B_u$) 5
Electronic structure Chapter 1, 1
Ellipticity, molecular 66
Emission 2, 6
Empirical rules (CD) 64
Enantiomeric purity 74
End groups, effect of (CD) 64
Equivalency, magnetic 207
Evolution time 232, 239
Excitation energy 3, 11
$1\,^1B_u$ state 6, 7, 8
$2\,^1A_g$ state 6, 7, 8
cis-isomer 3
trans-isomer 3
Excited single state 8
lowest energy 1, 3
Excited state (high-energy state) 1, 15, 18, 136
energy of 18
Exciton splitting 105
Extra relaxation delay 154

FAB = Fast atom bombardment 262
B/E Linked scan 265
FID (Free induction decay) 149, 151, 159, 226
'Fingerprint' region 120
Flip angle 151, 157, 161, 249
Fluorescence 1, 6, 11, 138
Fourier transform
infrared spectroscopy (FTIR) 118, 119
NMR spectroscopy 149, 151, 242
summation (X-ray) 321, 322

Frequency 117, 135
  measuring 147, 148
Functional groups
  identification of 117
  region (IR) 120
  test for 46

GARP-1 252
GC-MS = Gas chromatography-mass spectrometry 274
Geometrical isomers see Isomers, *cis/trans*-
Ground state 15, 136
Gyromagnetic ratio 153

Heterodichiral compounds 64, 93, 94, 96
High-field ^{1}H-NMR spectroscopy 149
HOHAHA (homonuclear Hartmann-Hahn-experiment) 236
HOMO (highest-energy occupied molecular orbital) 5
Homodichiral carotenoids 64, 67, 76, 83, 87, 89, 90
Homonuclear decoupling 225
Hückel resonance integral β 5
Hückel theory 3

Impurity 117, 152, 161
In situ measurement 136, 138, 139
In vivo measurement 13
In-chain reactions 277, 278
Infrared spectroscopy Chapter 4, 117
  absorption 135
Inhomogeneity
  of initial-state energy 10
  environmental 10
  due to s-*cis* conformers 10
Insertion probe, direct 262
Intensity
  contour plot (NMR) 241
  m (medium) 121
  MS 271
  IR 121
  relative (MS) 262, 265, 280
  s (strong) 121
  vs (very strong) 121
  w (weak) 121
Interference filter 137
Interferogram 118

Ionization
  conditions 276
  efficiency 263
  potential 265
IR see infrared spectroscopy
Irradiation
  on-resonance 230
  off-resonance 230
Isomerization 278
  cis/trans see *E/Z*
  E/Z 2, 8, 137, 138, 139, 143
  photoisomerization 2, 8
  shift 143, 220, 222
  shift additivity 222
  thermodynamic barrier of 8
Isomers
  all-*trans* 15, 20, 143, 326
  cis 15, 20
  cis/trans see *E/Z*
  di-*cis* 21
  di-*Z* 67
  E/Z 2, 3, 9, 20, 67, 97, 99, 102
  geometrical see *E/Z*
  mono-*Z* 91, 145
  optical 63
  poly-*cis* 21
Isotopomer 159
  ^{12}C- 151
  ^{13}C- 149, 253

KBr disc (pellet) 119
  experimental procedure 120

Laser beam 137, 138
Lateral methyl group 18, 22
Laue indices 322
LC-MS = Liquid chromatography-mass spectrometry 274
LCAO-MO theory 6
Lifetime, radiative 6
Light
  circularly polarized 63, 65, 66
  linearly polarized 63
  polarized 63
Line width 161, 208
Line broadening 208
Linked scanning 271
Long-range coupling 243, 245, 246, 247
Lorentz-to-Gauss window 149, 226

Lorentzian-shaped line 161, 207
Low mass region 267
LUMO (lowest-energy unoccupied molecular orbital) 5

Magnetization, transverse 151
Mass spectrometry (MS) Chapter 7, 261
Matrix 262, 263, 265
McLafferty rearrangement 313
Meso form 71
Metastable ions 262, 271, 273
Michelson interferometer 118
Microcells 152
Middle mass region 267
MIKE = Mass-analysed ion kinetic energy spectra 262, 273
Mixing pulse (COSY-90) 239
MLEV-17 236
Molecular environment 16
Molecular ion 262, 263, 271, 273, 276
  adduct ion 265
  even-electron protonated 262
  odd-electron 262
  quasimolecular ion 265
  region 263, 265
Molecular tumbling 230, 231
MOLOC forcefield 69
Monochiral carotenoids 64, 76, 87, 90
Monochromators 118
MS see mass spectrometry
Mulls 119
Multiple diffraction conditions 340

NMR spectroscopy Chapter 6, 147
  ^{1}H- 152, 225
  ^{13}C- 153, 211, 223, 247
  ^{1}H-decoupled 247
  ^{1}H-coupled 247
  ^{17}O- 156
NMR-spectrum
  AA'BB'-type 208
  AA'XX'-type 207
  AB-type 206
NOE (Nuclear Overhauser Effect) 161, 230
  longitudinal 230
  transverse (or rotating frame) (= ROE) 231
Non-centrosymmetric crystal 323
Non-conservative CD spectra 67, 73, 83, 88, 89, 90, 96, 99
Nuclear quadrupole moment 156
Nucleus, natural abundance of 153, 156
Nujol 119

Olefinic region 148
One-dimensional pulse technique (1D) 147, 148
Optical rotatory dispersion (ORD) 63
Orbital
  molecular 4, 5
  2 p (= 2p - π) 3
Overlap integral 140

Particle-desorption mass spectrometry 271
Phase problem 322
Photodiode-array detector (PDA) 14
Photon excitation spectroscopy 6
Polarizability 136
Polyene
  conjugated 2, 3
  linear 1, 2, 3
Potential
  energy curves 69, 70, 73
  energy surface 8
  source 262
Pre-irradiation 225, 226, 227, 228, 232
Probe head 151
Protein, effect of 44
Protons, exchangeable 153
Pseudotranslational symmetry 322
Pulse, 180° 157

Quantitative analysis 13, 14, 16, 56, 137
Quantity of sample 151, 152, 154, 162, 247, 252, 255, 258

R factor (X-ray) 323, 326, 327, 329, 332, 333
Racemic mixture 71
Radiation source 118, 339
Radiofrequency (rf) pulse 151, 154
Rayleigh scattering 135, 137
Raman lines (ν_1, ν_2) 139
Raman process
  'off-resonance' 135, 136
  'pre-resonance' 135, 136
  'rigorous-resonance' 135, 136

Raman scattering 135
anti-Stokes Raman scattering 135
Stokes Raman scattering 135
RDA = *Retro*-Diels-Alder 265, 309
Reflections, number of 326
Relaxation time
delay 157, 159
^{13}C-NMR 157
^{1}H-NMR 159
spin-lattice T_1 148, 154, 157, 230
spin-spin T_2 148, 151, 159
transverse see spin-spin

Repetition rate 157
Representative spectra (IR) 124
Resonance Raman spectroscopy Chapter 5, 135
excitation profile 139, 140
Ring double bond
conjugated 23
endocyclic 23
isolated 22
ROESY 231
Root-mean-square deviation (rms) 331

S_1 state 1, 3, 8
energy 6, 8
S_2 state 3
energy 6, 8
Satellite 149
Saturation experiment 157
Scatterer
anomalous 324
normal 324
Scattering
process 321
angle 323
factor 323, 324
Schrödinger equation 3
Sensitivity 266
SFC-MS = Supercritical-fluid chromatography-Mass
spectrometry 274
Shift
accuracy of (NMR) 162, 211
bathochromic 16, 80, 96
chemical 147
dependence on solvent 162
hyperchromic 16, 20
hypochromic 16, 21
hypsochromic 16, 20, 21
values 162
Signal
broadening 156
intensity, ^{13}C-nuclei 154, 155
-to-noise ratio 74, 151
Single-crystal diffraction 323
Solvent
CD 75, 96
crystallisation (X-ray) 339
deuterium quality (NMR) 152
electronic structure 6
environmental shift 6, 7
EPA (CD) 75
influence of (UV/Vis) 13, 31, 43
oxygen in (NMR) 153
polarizability of (UV/Vis) 43
refractive index of (UV/Vis) 43
Soret absorption 141
Space group
centrosymmetric 325
P1 329, 331
$P2_1$ 327, 329
$P2_{1/a}$ 329
R3 333
Spectral broadening 10
Spin-spin coupling J 148
Steric
congestion 280, 291
hindrance 67, 68
interaction 209
Stretch mode 11
Sub-system 199
2-spin 206
3-spin 206
4-spin 206, 208
Substituent, position of 79
Superconducting magnet 147, 148
Supercritical CO_2 274, 275
Symmetry 15
B_u 6
A_g 6
selection rules 15
plane 65
Synchrotron sources 339

Tandem mass spectrometry 262, 271
Temperature
  dependence 68, 69, 73, 74, 81, 96, 105, 152
  low 10, 11, 45, 75, 99, 101, 105, 139, 331, 339
Thermal
  interference 265
  parameters (X-ray) 326
Thermospray 276
Time-of-flight mass spectrometry 271
Time-resolved resonance Raman spectroscopy 146
TOCSY: Total correlation spectroscopy 236, 237
Transition dipole moment
  electric 65, 66
  magnetic 65, 66
Transitions
  $1\ ^1A_g \rightarrow 1\ ^1B_u$ 5, 6, 11, 20, 43
  $1\ ^1A_g \leftarrow 2\ ^1A_g$ 11
  electronic 15
  $\pi \rightarrow \pi^*$ 15
  $S_0 \rightarrow S_2$ see $1\ ^1A_g \rightarrow 1\ ^1B_u$
  $S_0 \leftarrow S_1$ see $1\ ^1A_g \leftarrow 2\ ^1A_g$
Transmittance 119
Triplet phases 340
Two-dimensional pulse technique (2D) 147, 148

UV region 14
UV/Vis spectra 9
UV/Vis spectrophotometer 14
  cell 15
  detector 14
  double-beam instrument 14
  light source 14
  means of dispersing light 14
  single-beam instrument 14
UV/Vis spectrum 13
  cis-peak intensity 21, 22
  fine structure, % III/II 13, 16, 20, 24, 27, 31, 39, 44, 45
  position of absorption maxima 13, 47
UV/Visible spectroscopy Chapter 2, 13

Vibrational
  degree of freedom 135
  fine structure 6, 9, 10, 11
  spectroscopy 135
Vibration modes 117, 120
Vibrations
  C–C stretching 143, 145
  C=C stretching 143
  C=C torsion 143
  C–H in-plane bending 143, 145
  C–H out-of-plane bending 143
  '*cis*-mode' 145
  finger-print 136
  in-plane rocking 143
  normal modes of 143, 145
  overall 136
  '*trans*-mode' 145
Visible region 14

Water, effect of (UV/Vis) 44
Wave amplitude 322
Wavelength
  Na/Hg/HgC/Cd line (CD) 63
  of radiation 323
  UV range 74
  visible range 74
  IR range 117
Wavenumbers 117
Weighting function 151
Window function 151, 239

X-ray crystallography Chapter 8, 321

z-Filter 236
Zero-filling 239

Document generated by Anna’s Archive around 2023-2024 as part of the DuXiu collection (https://annas-blog.org/duxiu-exclusive.html).

Images have been losslessly embedded. Information about the original file can be found in PDF attachments. Some stats (more in the PDF attachments):

{
  "filename": "NDAxMTkxMDAuemlw",
  "filename_decoded": "40119100.zip",
  "filesize": 22144173,
  "md5": "35a5da15d5466e6b01e0db6f754cec1e",
  "header_md5": "fede37763663022043a538df20b34ee3",
  "sha1": "53865a850645e9ffb9d5a00c9d8741af3bcbea72",
  "sha256": "065ce64c2c43f3494d7771a7ca1d6eb56b79f93f573186f90e94093a659e68d9",
  "crc32": 1282853779,
  "zip_password": "",
  "uncompressed_size": 23366942,
  "pdg_dir_name": "CAROTENOIDS VOLUME 1B_SPECTROSCOPY_40119100",
  "pdg_main_pages_found": 360,
  "pdg_main_pages_max": 360,
  "total_pages": 375,
  "total_pixels": 1903104000,
  "pdf_generation_missing_pages": false
}